Dissertation zur Erlangung des Doktorgrades

der Fakultät für Chemie und Pharmazie

der Ludwig-Maximilians-Universität München

Reactivities of Heteroatomic Nucleophiles Towards Carbon Electrophiles

von

Patrick Maximilian Jüstel

aus

München, Deutschland

2021

Erklärung

Diese Dissertation wurde im Sinne von §7 der Promotionsordnung vom 28. November 2011 von Herrn PD Dr. Armin R. Ofial betreut.

Eidesstattliche Versicherung

Diese Dissertation wurde selbstständig und ohne unerlaubte Hilfe erarbeitet.

München, den 09.07.2021

_____

Patrick M. Jüstel

Dissertation eingereicht am: 19.08.2021

1. Gutachter: PD. Dr. Armin R. Ofial

2. Gutachter: Prof. Dr. Hendrik Zipse

Mündliche Prüfung am: 20.09.2021

Acknowledgement

First, I would like to express my deepest gratitude to PD Dr. Armin Ofial, who enabled this thesis by offering me a place in his research group. Whenever I had questions or needed counseling, Dr. Ofial always had the time to support me. I appreciated his diligent supervision. Furthermore, I would like to thank Prof. Dr. Herbert Mayr, for being my de facto second supervisor. I am grateful for the luxury of having two highly experienced physical organic chemists as supervisors and everything they have taught me.

I would like to thank Prof. Dr. Hendrick Zipse for reviewing this thesis as well as the other professors on my defense committee: Prof. Dr. Thomas Klapötke, Prof. Dr. Anja Hoffmann-Röder, and Prof. Dr. Paul Knochel.

There was always a pleasant atmosphere within the Mayr/Ofial group and I would like to thank all present and former group members for this. The lab has been an enjoyable working environment due to its accommodating members.

In addition, I would like to thank my interns, Alexandra Stan and Cedric Pignot, both of whom have done a great job and helped me considerably.

Finally, I would like to thank my partner, family, and friends for their continuous support during the last five years. Special thanks go to the lab-mates that have become my friends during my time in the group.

Publications

P. M. Jüstel, C. D. Pignot, A. R. Ofial,
"Nucleophilic Reactivities of Thiophenolates"
J. Org. Chem., **2021**, *86*, 5965−5972.

B. Maji, X.-H. Duan, P. M. Jüstel, P. A. Byrne, A. R. Ofial, H. Mayr,
"Nucleophilicities and Nucleofugalities of Thio- and Selenoethers"
Chem. Eur. J., **2021**, *27*, 11367−11376.

P. M. Jüstel, P. Rovó, H. Mayr, A. R. Ofial,
"Dynamics of the Dimethyl Sulfide Exchange of
(1,3-Diphenylallyl)dimethylsulfonium Ions"
J. Phys. Org. Chem., **2021**, e4270.

P. M. Jüstel, A. Stan, C. D. Pignot, A. R. Ofial,
"Inherent Reactivity of Spiro-Activated Electrophilic Cyclopropanes"
Chem. Eur. J., **2021**, *Accepted Article:* doi: 10.1002/chem.202103027

Contributions to Conferences

Parts of this thesis were presented as posters at the following conferences:

October 2017	SFB 749 Workshop at Kloster Irsee Poster title: "Concurrent S_N1 and S_N2 Mechanisms in Solvolysis reactions"
July 2018	24th IUPAC International Conference on Physical Organic Chemistry, Faro, Portugal Poster title: "Concurrent S_N1 and S_N2 Mechanisms in Solvolysis reactions"
March 2019	SFB 749 Meeting at Venice International University, Venice, Italy Poster title: "Equilibration of Dialkylsulfides, Carbocations and their Adducts: Dynamic NMR Spectroscopy for Investigating Kinetics"
September 2019	European Symposium on Organic Reactivity, Dubrovnik, Croatia Poster title: "Kinetics of Ring-Opening Reactions of Electrophilic Cyclopropanes"

Table of Contents

Chapter 0. Summary

Nucleophilic Reactivities of Thiophenolates

The kinetics of the reactions of 10 differently substituted thiophenolates with *p*-quinone methides (*p*QMs) were investigated in DMSO at 20 °C (Chart 1, Figure 1a). The previously characterized, colored *p*-quinone methides with known Mayr *E* parameters of the Mayr-Patz equation (log k_2 = $s_N(N + E)$) served as reference electrophiles to determine the *N* and s_N parameters of the thiophenolates.

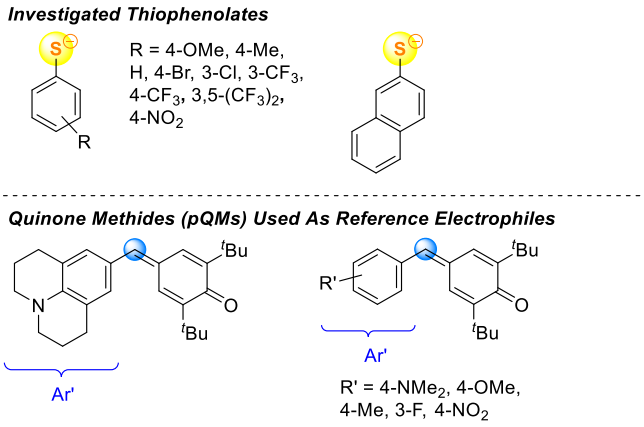

Chart 1. Structures of thiophenolates and *p*QMs used in this work.

However, the reactions were found to be highly reversible, because the formed phenolates have a higher pK_a in DMSO than the thiophenolates. The reactions were driven to completion by addition of thiophenols, which protonated the emerging phenolates to shift the equilibrium to the product side (Figure 1a).

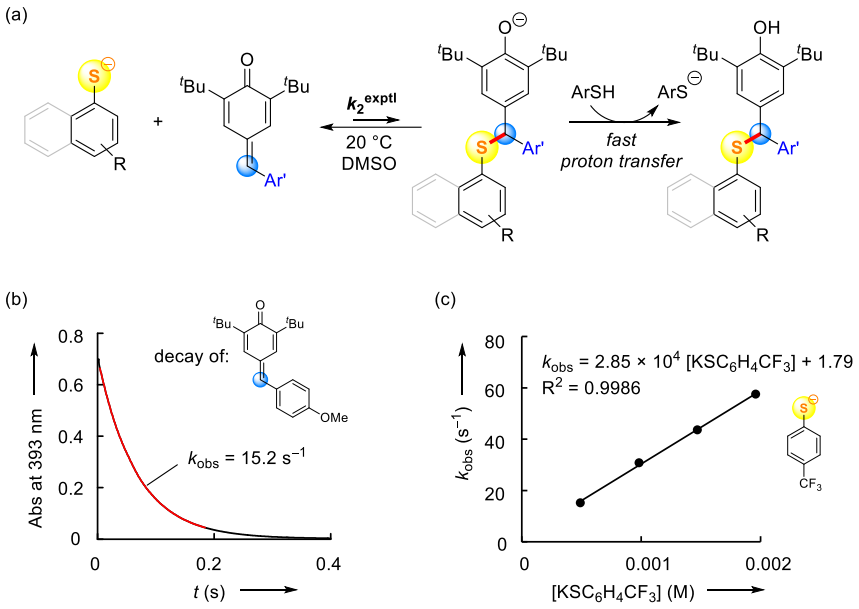

Figure 1. (a) Reactions of substituted thiophenolates with *p*QMs. (b) Monoexponential decay of the absorbance *A* (at 393 nm) during the reaction of 4-(trifluoromethyl)thiophenolate (c = 0.49 mM, counterion: K^+) with the depicted *p*QM. (c) Linear dependence of the first-order rate constant k_{obs} on [4-(trifluoromethyl)thiophenolate].

The decay of the *p*-quinone methide concentrations was followed with stopped-flow UV-Vis spectrometry to monitor the kinetics, and second-order rate constants were obtained by plotting k_{obs} against thiophenolate concentration (Figure 1b, c). Plotting the logarithm of these second-order rate constants against the electrophilicity parameters *E* of the employed *p*-quinone methides gave the nucleophile-dependent parameters *N* and s_N of the thiophenolates as slope and intercept of the linear correlations, respectively (Figure 2). The rate constants of the reactions of thiophenolates with the *p*-quinone methides were shown to correlate linearly with the rate constants of phenolates with the same *p*-quinone methides. Furthermore, the determined *N* parameters of the thiophenolates correlated linearly with Hammett σ constants and the pK_{aH} of the thiophenolates in DMSO. Bordwell reported the rate constants of reactions of *n*-butyl chloride with substituted thiophenolates in DMSO in the past and these correlated linearly with the *N* parameters of the thiophenolates, too. The UV-Vis spectra of the thiophenolates were recorded, with λ_{max} ranging from 302 nm to 501 nm. The high nucleophilicity, the absorption in the UV-Vis spectrum, and the big range of nucleophilic reactivity make thiophenolates promising reference nucleophiles.

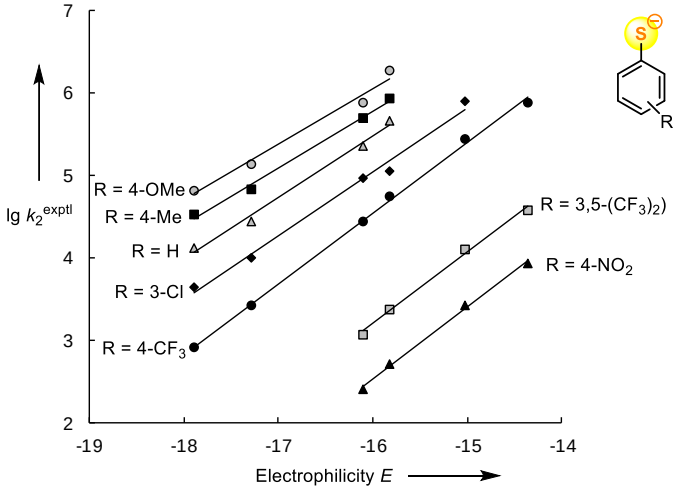

Figure 2. Determination of N/s_N for ArS^- from the linear correlations of log k_2^{exptl} with the electrophilicities *E* of the *p*QMs.

Electrophilicities of Acceptor and Donor-Acceptor Cyclopropanes

The electrophilic reactivities of 10 acceptor substituted cyclopropanes were quantified by following the kinetics of the ring-opening reactions with substituted thiophenolates, C-nucleophiles and sodium azide in DMSO as well as with substituted pyridines in acetonitrile at 20 °C (Chart 2, Figure 3a). UV-Vis spectroscopy was employed to either monitor the decay of the thiophenolates (Figure 3b) or the emergence of the colored carbanions in the case of indandione derivatives. Second-order rate constants were obtained by plotting k_{obs} against cyclopropane concentration (Figure 3c). The second-order rate constants for the reactions of thiophenolates with the electrophilic cyclopropanes correlated linearly with the *N* parameters of the thiophenolates. Consequently, the parameters *E* and s_E of the extended Mayr-Patz equation ($\log k_2 = s_E s_N(N + E)$) were determined for the electrophilic cyclopropanes (Figure 3d).

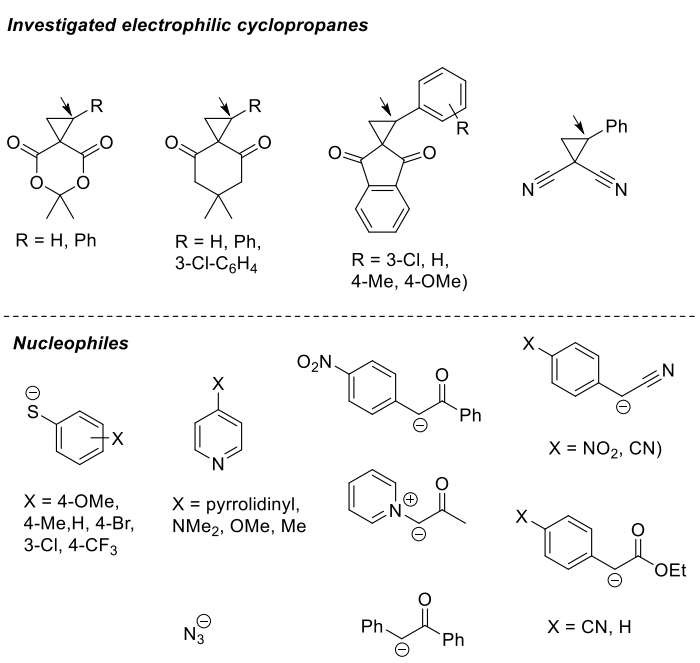

Chart 2. Investigated electrophilic cyclopropanes in this work (top) and reference nucleophiles (bottom).

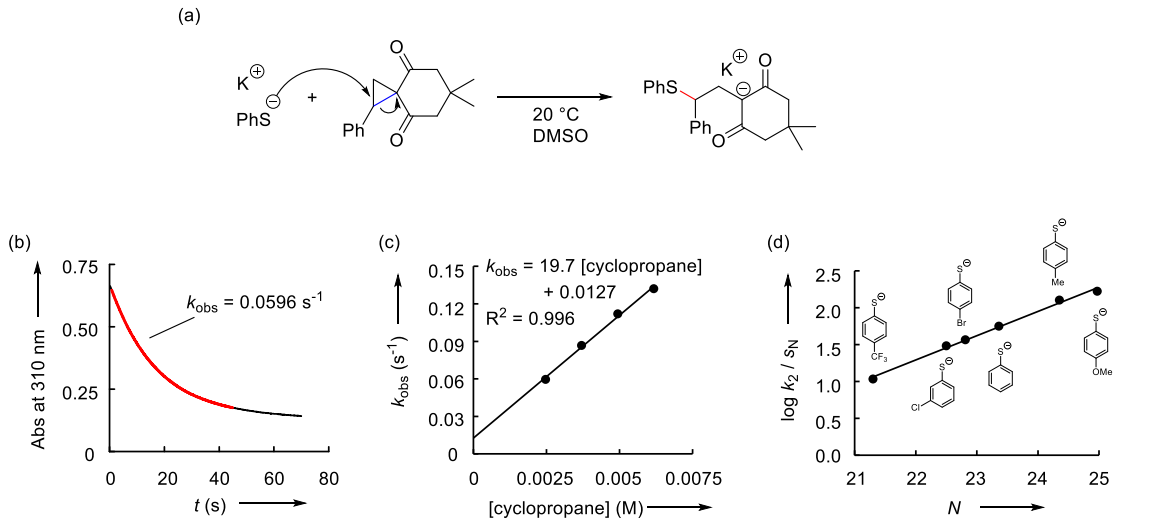

Figure 3. (a) Ring-opening reaction of a donor-acceptor cyclopropane with potassium thiophenolate. (b) Monoexponential decay of the absorbance *A* at 310 nm over the course of the reaction of thiophenolate (0.247 mM) with the dimedone-derived cyclopropane depicted in (a) (2.47 mM). (c) Linear correlation of the observed rate constant k_{obs} versus the concentration of the cyclopropane depicted in (a). (d) Correlation of *N* against $\log k_2/s_N$ to determine *E* and s_E of the cyclopropane depicted in (a).

All investigated cyclopropanes had an s_E between 0.50 and 0.35, indicating low susceptibility towards nucleophiles. Correlation of rate constants k_2 of the reactions of cyclopropanes with thiophenolates with Hammett σ constant for the substitution of the electrophiles' aryl moiety resulted in an unusual U-shaped plot (Figure 4a). Variation of the thiophenolate substituents resulted in a linear correlation in the Hammett plot (Figure 4a).

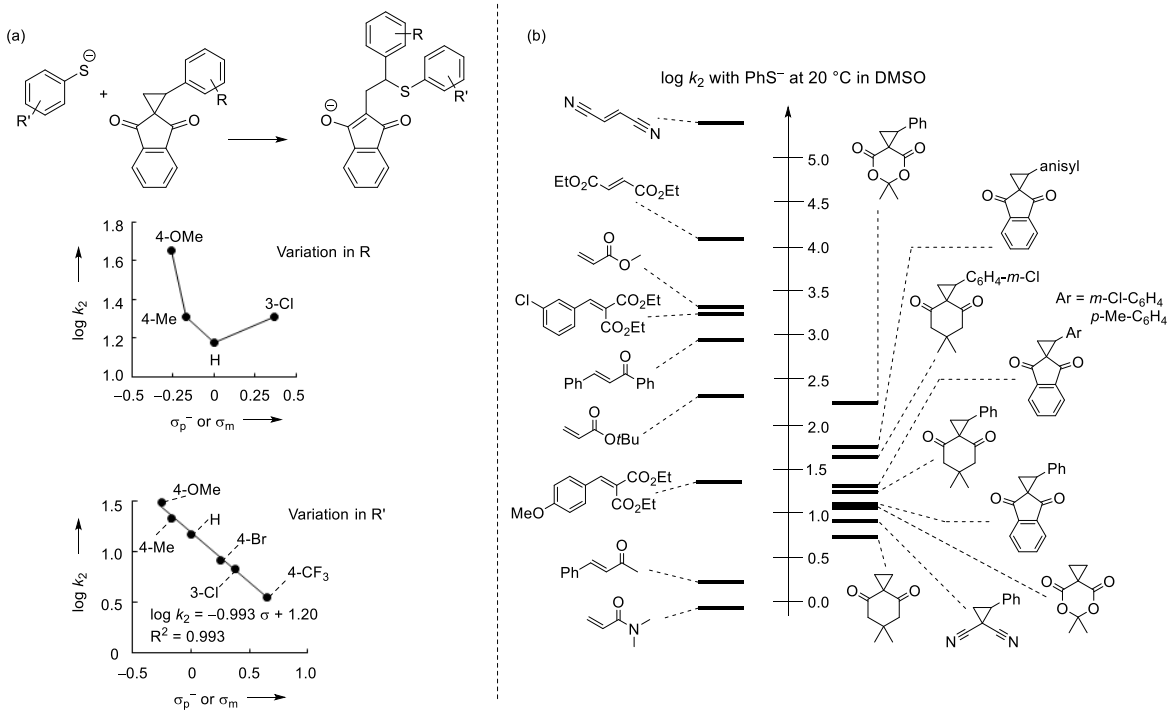

Figure 4. (a) Hammett plots of log k_2 of the reactions of the depicted substituted cyclopropanes with substituted thiophenolates versus Hammett σ_p^- and σ_m constants of the substituted thiophenolates. All reactions were performed in DMSO at 20 °C. (b) Comparison of log k_2 for the reaction of Michael-acceptors with thiophenolate (left side, calculated with the Mayr-Patz equation) with the ring-opening reaction of electrophilic cyclopropanes with thiophenolate.

Interestingly, the acceptor moieties and the substituted aryl donor moiety had little effect on the reactivity of electrophilic cyclopropanes, with the least reactive cyclopropane only one order of magnitude less reactive than the most reactive cyclopropane. This is unlike Michael-acceptors, that span a significantly bigger range of reactivity (Figure 4b). Cyclopropanes were found to be around 7-9 orders of magnitude less reactive than comparable Michael-acceptors towards thiophenolate.

Further reference nucleophiles were employed to confirm the validity of the determined E and s_E parameters calibrated for the reactions of electrophilic cyclopropanes with thiophenolates. However, the reactions of cyclopropanes with C-nucleophiles resulted in a different linear correlation in a plot of log k_2/s_N against N (Figure 5a, black line). This deviation however, was still within the error limits of the Mayr scale, that aims to predict rate constants with an error of 2 orders of magnitude or less. It is presumed that the sterically crowded environment of the reactive carbon center on the cyclopropanes

is the reason for this deviation, since the employed C-nucleophiles were sterically more demanding than the thiophenolates (Chart 2). Furthermore, the C-nucleophiles (black line) showed significantly more scattering in the plot of log k_2/s_N against N (Figure 5a) than the thiophenolates (red line), which also indicates variable steric effects.

The kinetics of the reactions of one indandione-derived cyclopropane with *para* substituted pyridines in acetonitrile at 20 °C were investigated. The linear correlation of log k_2/s_N against N (Figure 5b) was found to differ from the linear correlations found with thiophenolates and C-nucleophiles in DMSO.

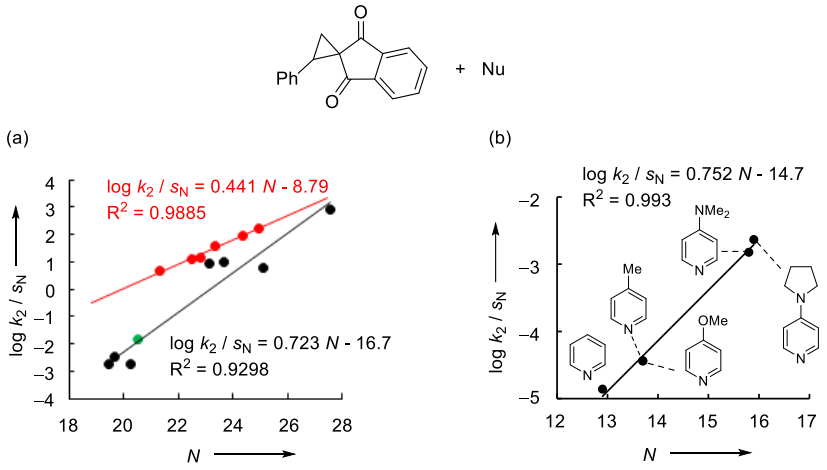

Figure 5. (a) Linear correlation of log k_2/s_N versus N for the reactions of the carbon nucleophiles with the depicted electrophilic cyclopropane (black dots and black correlation line). The red dots and red correlation line represent the reaction of the same cyclopropane with the substituted potassium thiophenolates. The green dot represents the reaction of the same cyclopropane with sodium azide. All reactions were performed in DMSO at 20 °C. (b) Linear correlation of log k_2/s_N versus N for the reactions of the substituted pyridines with the depicted electrophilic cyclopropane. All reactions were performed in acetonitrile at 20 °C.

The linear correlations differed from each other (Figure 5a) due to the increased steric demand of the employed C-nucleophiles, which resulted in smaller rate constants, in comparison to the thiophenolates. Despite this deviation, the determined E and s_E parameters for the reaction of electrophilic cyclopropanes with thiophenolates enable the semi-quantitative prediction of rate constants with other nucleophiles, as long as they are not too sterically demanding.

Kinetic Investigations of Concomitant S_N1 and S_N2 Mechanisms in Menschutkin Reactions

The kinetics of the Menschutkin reactions of eleven benzylic halides or tosylates with five amines were determined in acetonitrile or acetonitrile/methanol mixtures at 20 °C (Figure 1). Butyl halides and tosylate were also employed as electrophiles to investigate the effects of different leaving groups in S_N2 reactions. Conductivity measurements were used to monitor the kinetics.

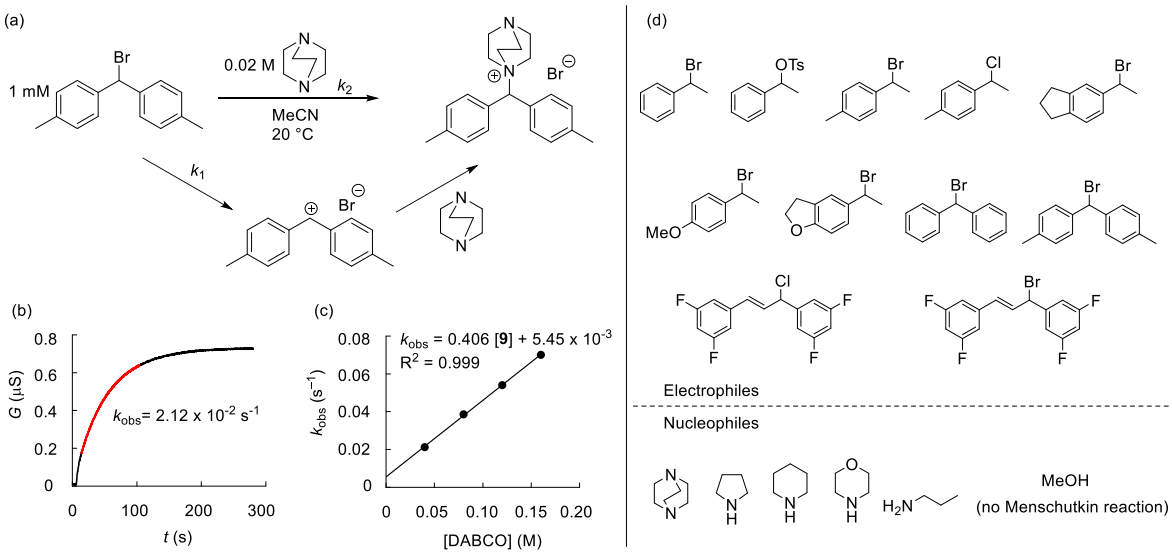

Figure 1. (a) Concurrent S_N1 and S_N2 reaction of 4,4'-bis(*p*-methyl)benzhydryl bromide with DABCO at 20 °C in acetonitrile. (b) Plot of conductance *G* versus time *t* for the reaction in (a). (c) Linear correlation of k_{obs} versus nucleophile concentration. The intercept represents the nucleophile independent rate constant k_1 and the slope represents the nucleophile dependent rate constant k_2. (d) Chart of the employed benzylic halides and tosylate electrophiles and amine and methanol nucleophiles.

The effect of structural changes in the substrate on the rate constants of concomitant S_N1 and S_N2 reactions was investigated. Electron donating groups (EDG) in the electrophile accelerated both S_N1 and S_N2 reactions. However, the rates of S_N1 reactions were affected linearly by stronger EDG, while the rates of S_N2 reactions accelerated exponentially.

The solvent effect was investigated with acetonitrile and acetonitrile/methanol mixtures. With increasing content of the protic solvent (methanol) in acetonitrile, S_N1 reactions became faster while S_N2 reactions was slowed down. The ratio k_2/k_1 decreased by around 3 orders of magnitude when changing the solvent from acetonitrile to 50% (v/v) methanol in acetonitrile.

The rate constants k_2 of the reactions of the employed amines with organic halides did not correlate with Mayr *N* parameters. The ratio k_2/k_1 was shown to decrease with increasing temperature. Furthermore, activation parameters for a concomitant S_N1 and S_N2 reaction were determined, which demonstrated, that the S_N1 mechanism proceeds through an entropically more favorable and an

enthalpically less favorable transition state than the S_N2 mechanism. The leaving group tosylate was shown to be as reactive as bromide in S_N2 reactions but around 3 orders of magnitude more reactive in S_N1 reactions. This is due to tosylate being the thermodynamically more favorable leaving group, but bromide reacts equally fast in S_N2 reactions due to lower intrinsic barriers, as supported by computational considerations. The nucleofuge chloride was less reactive than bromide by about one order of magnitude in S_N1 reactions and by about two orders of magnitude in S_N2 reactions. A guide is depicted in Figure 2 to summarize how to control the ratio k_2/k_1. The parameters N_f and s_f of the Mayr-Kronja equation were determined for bromide in acetonitrile.

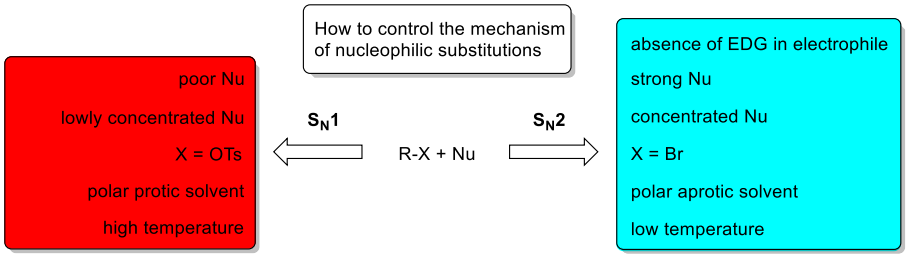

Figure 2. How to control the mechanism of nucleophilic substitutions. Factors that favour S_N1 are on the left (red box), while factors that favour S_N2 are on the right (blue box).

Intrinsic Barriers, an Unsolved Limitation for LFER

Dynamics of the Dimethyl Sulfide Exchange of (1,3-Diphenylallyl)dimethylsulfonium Ions

In Chapter 5.1 the dynamics of the allylic rearrangement of (1,3-diphenylallyl)dimethylsulfonium triflate in dichloromethane, which proceeds through intermediate 1,3-diphenylallylium ions, was investigated with dynamic ^{1}H-NMR spectroscopy (Figure 6). Recent studies have indicated that the nucleofugality parameters in the Mayr-Kronja equation (log k_{het} = $s_f(N_f + E_f)$) may depend on whether the reverse recombination is proceeding under activation-control or diffusion-control. For example, two different sets of parameters N_f and s_f were calculated for dimethyl sulfide when two different sets of reference benzhydrylium electrofuges were used (Figure 7). One set of benzhydryl sulfonium ions was substituted with strong electron donating groups (EDG) (red line in Figure 7), while the other set was substituted with electron withdrawing groups (EWG) or weakly EDG. As a consequence, after heterolysis the first set would form weak electrophiles (EDG substituted benzhydrylium ions) that recombined with the nucleofuge (dimethyl sulfide) under activation-control. However, the heterolysis of the second set of benzhydryl sulfonium ions results in significantly more electrophilic benzhydrylium ions (without strong EDG) that recombine with dimethyl sulfide under diffusion-control.

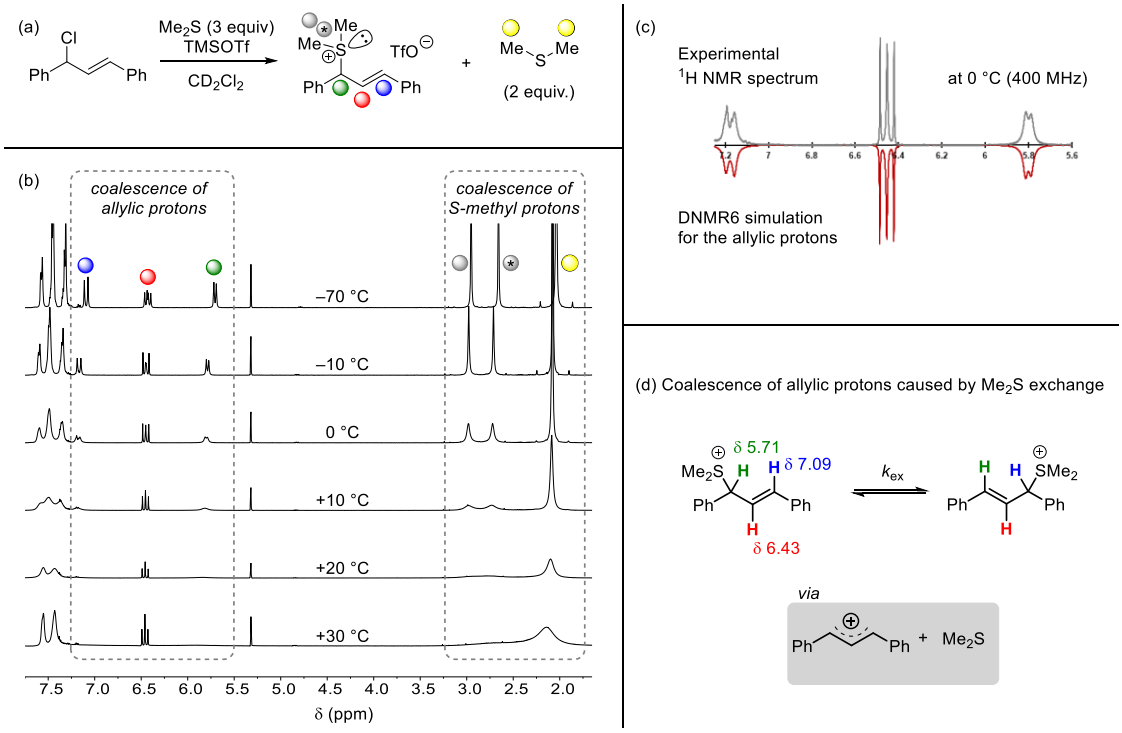

Figure 6. (a) Synthesis of (1,3-diphenylallyl)dimethylsulfonium triflate with excess Me_2S. (b) ^{1}H NMR spectra (400 MHz) of a mixture of (1,3-diphenylallyl)dimethylsulfonium triflate with Me_2S (2 equiv) in CD_2Cl_2 at variable temperatures. Protons used for line shape analysis are marked by colored circles. (c) Experimental and simulated ^{1}H NMR (400 MHz) spectra at 0 °C used to determine k_{ex} from resonances of allylic protons. (d) Mutual exchange reaction observed in the DNMR studies of (1,3-diphenylallyl)dimethylsulfonium triflate mixtures in CD_2Cl_2 (chemical shifts refer to –70 °C).

The (1,3-diphenylallyl)dimethylsulfonium ion was considered to be a suitable probe to further investigate this phenomenon, as it is as good an electrofuge as benzhydrylium ions with strong EDG (equal E_f). However, it is also more electrophilic than the aforementioned benzhydrylium ions (higher E), which results in rate constants close to the diffusion limit for the recombination of the 1,3-diphenylallylium ion with dimethyl sulfide, as estimated with the Mayr-Patz equation ($\log k_2 = s_N(N + E)$). Multiple ^{1}H-NMR spectra at different temperatures were recorded and the allylic proton signals manually fitted in a line-shape analysis (LSA) by using the DNMR6 algorithm (Figure 6b, c, d).

The thus determined rate constant for the heterolytic carbon-sulfur cleavage corroborated that the prediction of rate constants with the Kronja-Mayr equation will depend on whether the reactions of the reverse recombination reaction are activation or diffusion-controlled and consequently different N_f and s_f heterolysis parameters are obtained (Figure 7).

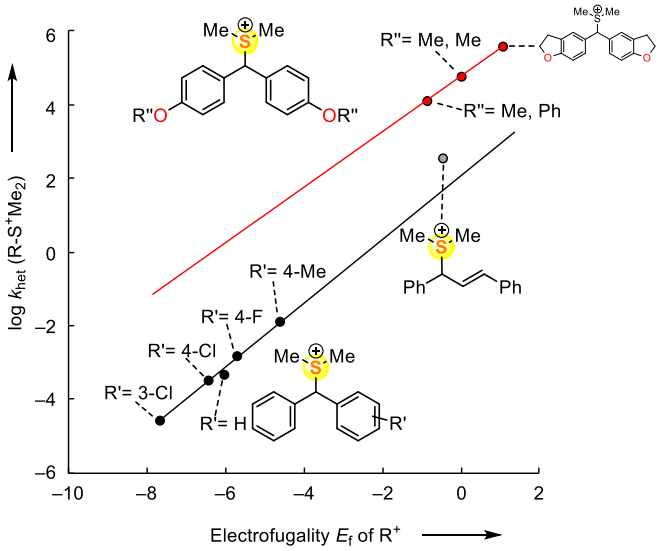

Figure 7. Correlation of the heterolysis rate constants of benzhydryl dimethylsulfonium ions and the (1,3-diphenylallyl)dimethylsulfonium ion with the electrofugality parameters E_f of the resulting carbenium ions.

The Diffusion Limit and LFER

With the published kinetic and thermodynamic data on the reactions of chloride ions with benzhydrylium ions and the reverse heterolysis reactions of benzhydryl chlorides a large data set was identified to investigate the connections between the Mayr-Patz equation ($\log k_2 = s_N(N + E)$), the Mayr-Kronja equation ($\log k_{het} = s_f(N_f + E_f)$), and the equation $\log K = LA + LB$. The data set included rate constants of activation-controlled addition reactions and rate constants of diffusion-controlled addition reactions. Extrapolation on the basis of the known s_N, N, s_f, N_f and LB parameters of chloride

and the known E, E_f and LA parameters of the benzhydrylium ions extended the experimentally accessible range of the three aforementioned equations.

It had been reported before, that correlations of E against E_f are linear for some of the benzhydrylium ions, but not for others. The cause for this collapse of correlation has already been identified: the E_f parameters of benzhydrylium ions correlate linearly with E if the reverse addition reactions are diffusion-controlled, while the E_f parameters of benzhydrylium ions did not correlate linearly with E if the reverse addition reactions were activation-controlled.

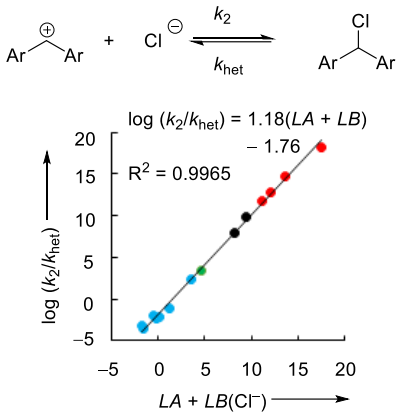

Figure 8. Linear correlation of log (k_2/k_{het}) versus $LA + LB(Cl^-)$ in acetonitrile. Double logarithmic plot of two different ways to predict equilibrium constants. Black dots represent data points with measured rate constants for k_2 and k_{het}. Red dots have reached the diffusion limit (k_2 = const.). The green dot has only an experimentally measured rate constant k_2, k_{het} has been calculated with the Mayr-Kronja equation. Blue dots consist only of calculated data for k_2 (calculated with Mayr-Patz equation) and k_{het} (calculated with Mayr-Kronja equation). There are only 3 variables in this plot: E, E_f, and LA.

A correlation of log (k_2/k_{het}) against log K was found to be linear with good accuracy for the entire data set, including the range of the predicted rate constants (Figure 8). The data set also comprises the crossover from activation-controlled to diffusion-controlled addition reactions. At this point the rate constant k_2 does no longer increase in reactions with even more electrophilic benzhydrylium ions, because diffusion is limiting the rate constant of the reaction (at around log k_2 = 10). Since the correlation remains to be linear beyond that point, the rate constant k_{het} has to compensate the now invariable k_2. This implies that k_{het} can only be predicted by LFERs, like the Mayr-Kronja equation, for reactions with activation-controlled reverse recombination reactions or for reactions with diffusion-controlled reverse recombination reactions. This further corroborates the results in Chapter 5.1. Furthermore, the origin of this phenomenon has also become clear: changes in intrinsic barriers of addition reactions influence a set of reactions proportionally to the changes in the Gibbs reaction energy ($\Delta\Delta G_0$) of these reactions. Due to the principle of microscopic reversibility, the same is also true for the reverse heterolysis reactions. At the diffusion limit intrinsic barriers for addition reactions become irrelevant for reverse heterolysis reactions because $\Delta G^0 = \Delta G^{\ddagger}$ (Figure 9). With intrinsic barriers

irrelevant, only the Gibbs reaction energies need to be known to predict heterolysis rate constants k_{het}. This explains the two different linear correlations found in Chapter 5.1 (Figure 7), the red linear correlation stems from a series of reactions where rate constants are influenced by changes of the Gibbs reaction energy and changes of intrinsic barriers, whereas the black linear correlation stems from a series of reactions where rate constants are influenced only by changes to the Gibbs reaction energy because intrinsic barriers are irrelevant.

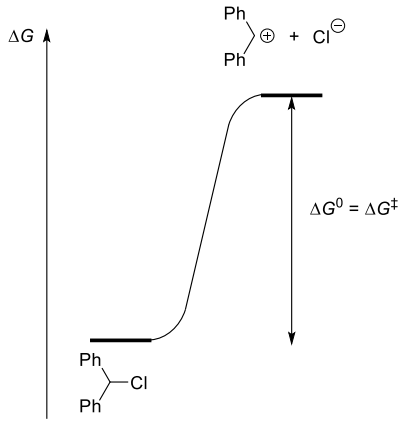

Figure 9. Qualitative energy diagram of the heterolysis of benzhydryl chloride. The reverse recombination reaction is barrierless and thus diffusion-controlled. As a consequence: $\Delta G^0 = \Delta G^{\ddagger}$.

Chapter 1. Introduction and Objectives

1.1 The Chemistry of Thiols

Thiols are alcohols, where the oxygen atom has been replaced with a sulfur atom. The prefix thio- derives from the Greek word for sulfur: θεῖον (*theîon*). Many thiols share similar attributes: toxicicity,[1] strong odor,[2] relatively high acidity when compared to the corresponding alcohols (ethanol pK_a = 15.9,[3] ethanethiol pK_a = 10.25,[4] both in water), high nucleophilicity[5] and they are easily oxidized.[6] Furthermore, since sulfur is less electronegative than oxygen, thiols form less polarized bonds with hydrogen. As a consequence, thiols form weaker hydrogen bridges and are less soluble in water than related alcohols. For example, ethanethiol does only mix with water to a very limited extent, unlike ethanol. Another consequence of weaker intermolecular forces are lower boiling points.[2] Ethanol boils at 78 °C, while ethanethiol boils at 35 °C.[7] Also S-H and O-H bond dissociation energies (BDE) differ significantly, with 440 kJ mol^{-1} (MeO-H)[8] and 366 kJ mol^{-1} (MeS-H).[9]

The receptor in the human nose responsible for the detection of low molecular weight thiols is olfactory receptor 2T11 (OR2T11).[10] Thiols have been used since the late 19th century as malodorant additive for combustible gases.[2] For example, ethanethiol is the odorant used in propane and 2-propanethiol is one of the odorants in natural gas.[2,11] Thiols are chosen for this task because the level of perception is remarkably low for humans. Most low molecular weight thiols can be perceived at concentrations of about 0.12 ppb to 1.70 ppb.[2] Some thiols have even lower perception thresholds, for example thioterpineol (Scheme 1), which is found in grapefruit, can still be perceived at concentrations of 1.1 × 10^{-7} ppb in the air by the human nose.[12] Another member of the family of natural gas odorants, 2-methyl-2-propanethiol (Scheme 4), has an odor-threshold of 0.029 ppb.[13]

Being able to perceive thiols even at low concentrations is advantageous, as rotten food, oxygen depleted areas and predators (through carnivore excretions) can be identified early.[10] Furthermore, thiols have another important sensory impact, as thiols in wine,[14] beer,[15] cheese,[16] onions,[17] grapefruit,[12] durian,[18] roasted coffee[19] and sesame seeds[20] are trace aroma components. The skunk has exploited the low odor threshold of thiols found in many mammals and weaponized them in its skunk spray.[21] Humans are also a source of unpleasant thiol related odors, such as garlic breath[22], armpit odor[23] and the methanethiol found in human flatus.[24]

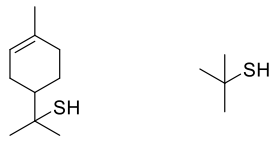

Thioterpineol 2-methyl-2-propanethiol

Scheme 1. Structures of thioterpineol and 2-methyl-2propanethiol.

The synthesis of thiols can be achieved in many different ways (Scheme 2).[2] In industry, the addition of hydrogen sulfide to alkenes under acidic conditions is an often used approach (Scheme 2a). For example, sulfuric acid, phosphoric acid or solid phase catalysts, like alumina-silica gel can be used as acidic catalysts, for example.[2,25] This Markovnikov type addition is most suitable to produce tertiary thiols. Instead of alkenes, alcohols may also be used as feedstock. However, due to the higher relative cost, only methanethiol and cyclohexanethiol are commercially produced from methanol and cyclohexanol, respectively.[2]

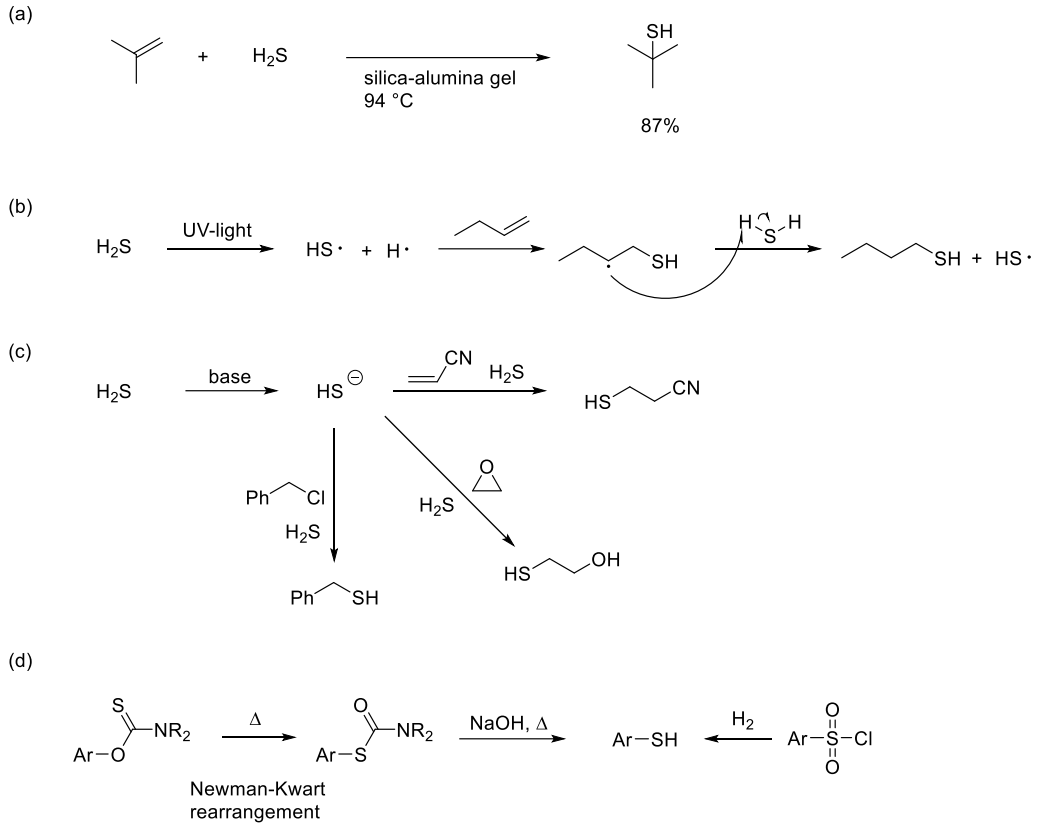

Scheme 2. (a) Synthesis of thiols starting from hydrogen sulfide using either an acid, (b) radical or (c) base mediated pathway.[2] (d) Aromatic thiols can be prepared with the Newman-Kwart rearrangement.[26]

Primary thiols are often prepared *via* free radical initiated synthesis (Scheme 2b) and thousands of metric tons of thiols are produced per year in this way.[2] UV-light is used to homolytically cleave one of the bonds in hydrogen sulfide to form a hydrosulfuryl radical, which subsequently adds to an alkene. Hydrogen atom transfer from the hydrogen sulfide to the resulting carbon centered radical generates the primary thiol as well as another hydrosulfuryl radical, which enter into the next cycle of radical reactions (Scheme 2b). Hydrogen sulfide can be readily deprotonated and can then act as strong nucleophile that undergoes Michael additions, epoxide ring-opening reactions or halide substitutions (Scheme 2c). Syntheses involving the hydrogensulfide anion have the issue of over-alkylation, which results in the formation of mixtures of thiols and dialkyl sulfides. Aromatic thiols are prepared in

different ways, with the Newman-Kwart rearrangement[26] and reduction of arenesulfonyl chlorides being the most frequently used routes (Scheme 2d).[2]

The chemistry of thiols is quite diverse and very similar to the chemistry of hydrogen sulfide. Thiols can react as nucleophiles with strong electrophiles, like an acylium ion (Scheme 3a).[2,27]

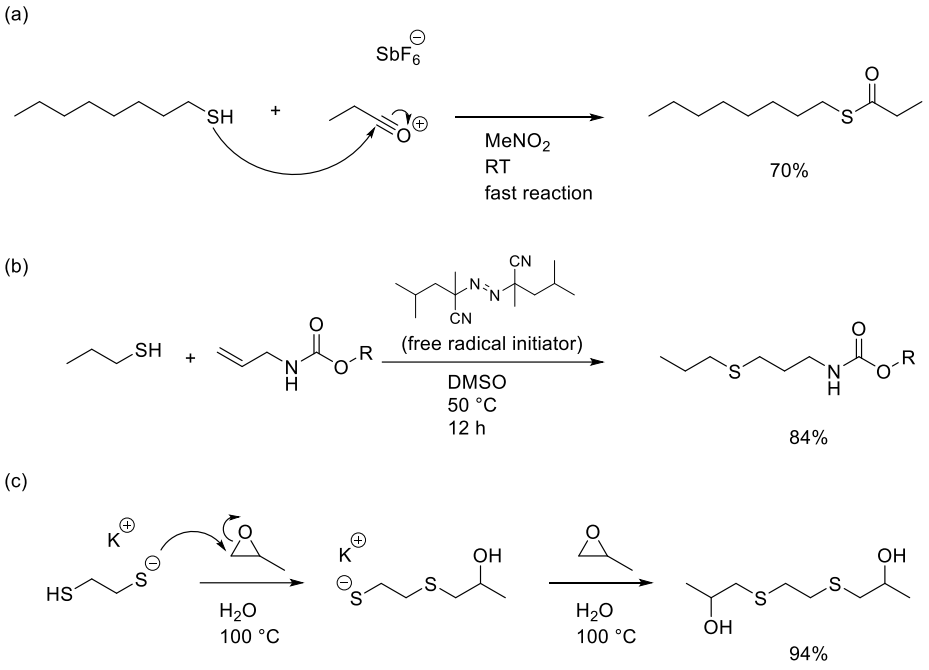

Scheme 3. Examples for the reactions of a nucleophilic thiol with an acylium cation (a),[27] the addition of a thiyl radical to an alkene (b)[28] and the nucleophilic ring-opening reaction of an epoxide mediated by a thiolate anion (c).[29]

Homolytic bond cleavage with radical starters or UV light generates reactive thiyl radicals, that add to alkenes (Scheme 3b).[28,30] The resulting carbon-centered radical abstracts a hydrogen radical from a thiol function and the radical cycle starts again. Deprotonation of thiols gives nucleophilic thiolate ions that can attack epoxides in ring-opening reactions (Scheme 3c).[5,29-31]

The chemistry of thiols has many useful applications in industry and everyday life. For example, thiols have been used since the early 1940 in synthetic rubber production.[2] Thiols act as chain transfer agents in radical polymerization of styrene-butadiene rubbers.[2] They first donate a hydrogen radical and terminate the growth of the polymer chain. Afterwards, the newly formed thiyl radical reacts with a monomer and starts the growth of another polymer chain. As a consequence, higher concentrations of thiols in polymerization reactions lead to shorter average chain lengths. Shorter polymer chains result in a softer rubber material.[2]

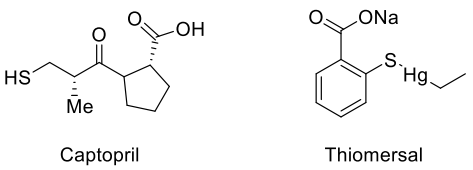

Captopril Thiomersal

Scheme 4. Pharmaceutical thiols Captopril and Thiomersal.

Thiols are also used in pharmaceuticals, like Captopril and Thiomersal (Scheme 4). Captopril acts as an inhibitor to the angiotensin-converting enzyme (ACE) and is used to treat hypertension and certain types of congestive heart failure. Thiomersal is used as an antiseptic and antifungal pharmaceutical, as well as a preservative in skin test antigens, vaccines, nasal products etc.[32] In Thiomersal the inherent, strong affinity of thiolates towards mercury is exploited. Ethylmercury, which is bound to the thiolate, is the reason for the toxicity of Thiomersal.[32] This property of thiols is the reason for another common name for organic R-SH compounds: mercaptan, which was derived from the Latin "mercurium captans" (capturing mercury).[33]

Glutathione (GSH) (Scheme 5) is found in the cytosol and organelles of animal cells in high concentrations of 0.5 mM to 10 mM.[34] GSH is a tripeptide consisting of the thiol bearing amino acid cysteine, glycine and glutamine, which is linked with its γ amino group, unusual for peptide bonds. GSH protects the cells from xenobiotics, oxidative species and radicals.[35] This is mainly achieved by its deprotonated and much more nucleophilic thiolate form of GSH, which is present at a level of 1-10% of the total GSH concentration in cells at physiological pH.[31]

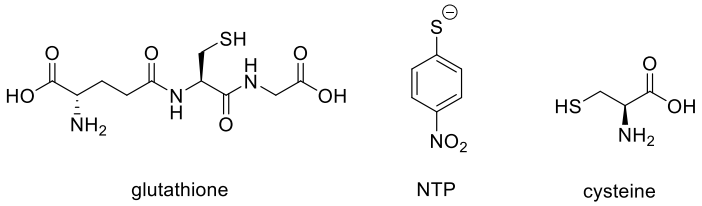

Scheme 5. Thiols and thiolates glutathione (GSH), 4-nitrothiophenolate (NTP), and cysteine.

The amino acid cysteine forms disulfide bridges, which are important for protein folding and structure.[36] The amount of oxidized disulfide bridges and reduced cysteine is controlled by GSH. In the cell, GSH is in an equilibrium with its oxidized, dimeric, disulfide-bridged version (Scheme 6). The position of this equilibrium can be a measure for the oxidative stress. In a normal cell, 90% of GSH is in the reduced state.[37]

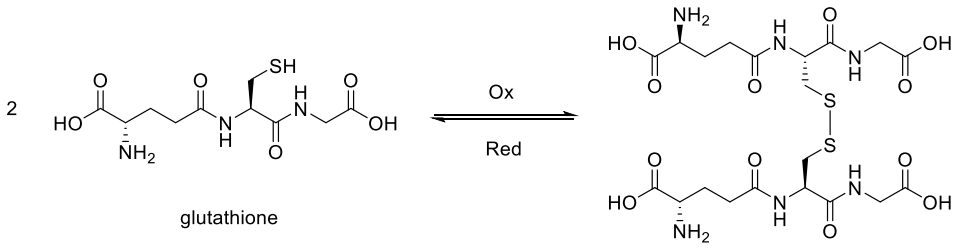

Scheme 6. Glutathione (GSH) forms a disulfide bridge with another molecule of glutathione when oxidized.

Several thiols function as chemical probes in chemoassays. Since the reactivity of GSH towards electrophiles is known to correlate with the electrophiles' toxicity,[38] GSH is one of the standard probes

in chemoassays. However, it can only be monitored indirectly in combination with utilizing Ellman's reagent.[39] This indirect detection method complicates the analysis, as no precise kinetics can be determined.[40] The dark red 4-nitrothiophenolate (NTP) (Scheme 5) has a strong absorption in the visible spectrum. NTP can, thus, be monitored directly and continuously over the course of a reaction by photometric methods, unlike the colorless GSH. Because of this fact, Siegel *et al*. screened the kinetics of the reaction of electrophilic dermal sensitizers with NTP.[40] They showed that the logarithm of the second-order rate constant of the reaction of NTP with electrophiles correlates linearly with the skin sensitizing potential of the same electrophiles. This indicates a possible use to predict toxic effects with the probe NTP. Furthermore, Cheh and Carlson employed NTP as marker for spectral detection and quantification of electrophiles stemming from environmental samples.[41]

Klopman and Hudson investigated the kinetics of the reactions of substituted benzyl bromides with substituted thiophenolates in methanol.[42] Interestingly, thiophenolates showed a minimum of reactivity towards the parent benzyl bromide. Electron-donating or electron-withdrawing substituents at the electrophile significantly increased rate constants when the same nucleophile was used. This resulted in unusual U-shaped Hammett plots of the rate constants log k_2 against the Hammett σ parameters of the substituted benzyl bromides.

Though knowledge of the reactivities of thiolates would be relevant in the context of many applications, there is a lack of data that would allow chemists to calibrate thiolate reactivities towards common reference electrophiles which would make it possible to compare their nucleophilic reactivities with those of other classes of nucleophiles. The nucleophile specific parameter *N* and the nucleophile specific sensitivity parameter s_N, combined with the electrophile specific parameter *E* in the Mayr-Patz equation (1) allow for the prediction of second-order rate constants at 20 °C:

$$\log k_2\ (20\ °C) = s_N(N + E) \qquad (1)$$

One of the goals of this thesis is to quantify the nucleophilicity parameters *N* and s_N of NTP and further substituted thiophenolates in DMSO. The previously characterized, aryl substituted, *para*-quinone methides with known *E* parameters are intended to be used as carbon-centered reference electrophiles. Due to their absorption of visible light or near-UV light ($\lambda_{max} > 300$ nm), the consumption of thiophenolates in a reaction can be readily monitored with UV-Vis spectrometry. Furthermore, thiophenolate ions are strong nucleophiles and will react even with weak electrophiles in a reasonable timespan. It is anticipated that aryl substitution on thiophenolates will give access to a considerable range of reactivity, while keeping the steric demand at the reacting sulfur center and its vicinity unchanged. The corresponding studies are presented in Chapter 2 of this thesis.

Given their high reactivity and straightforward photometric detection in reaction mixtures, thiophenolates may be potentially useful reference nucleophiles. In this thesis their application as

reference nucleophiles will be investigated in ring opening reactions of electrophilic cyclopropanes (Chapter 3).

1.2 Cyclopropanes

Cyclopropane was synthesized for the first time in 1882 by August Freund by treating 1,3-dibromopropane with sodium (Scheme 7).[43] Given its special structure, it has some unique properties. For example, the unusually low C-C bond angles of 60° in cyclopropane,[44] which deviate significantly from the tetrahedral angle of 109.5° that is usually found at sp^3 hybridized carbon.[45] Interestingly, the two hybrid orbitals of carbon facing inwards found in cyclopropane have more *p* character than a standard sp^3 hybridized carbon, with only about 17% *s* character. These orbitals may be called sp^5 orbitals.[45-46] As a consequence, the amount of strain is reduced, because the deviation in preferred angle towards *p* orbitals is smaller: *p* orbitals have a preferred angle of 90°, which is closer to 60° than the tetrahedral angle of sp^3 orbitals (109.5°). Furthermore, more *s* character is found for the two hydrogen facing hybrid orbitals, about 33%, resulting in sp^2 hybridized orbitals. An angle of 115.1° was found between the two hydrogens of a carbon, significantly larger than a tetrahedral angle.[47] The bond between two carbons in cyclopropane is formed by the overlap of the sp^5 orbitals, which causes an unusual phenomenon: "bent bonds".[48] The area of the highest electron density (black dot in Figure 1) was not found directly between the two carbon atoms, but instead this area is shifted off the direct line, at an angle of 21°, causing the bond to appear "bent" (Figure 1).[45,48] This analysis of cyclopropane bonds according to valence bond theory is also called the Coulson-Moffit model.[49] The bent bonds are considerably weaker than normal σ bonds found between sp^3 hybridized carbon. A strain energy of 115.5 kJ mol^{-1} is found in cyclopropane, which is released upon ring-opening reactions. This explains the relatively high reactivity of cyclopropanes and similar compounds like epoxides, when compared to linear alkanes and ethers, respectively.

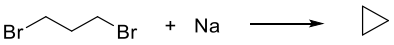

Scheme 7. Synthesis of cyclopropane by A. Freund (1882).

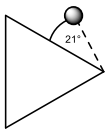

Figure 1. "Bent bond" of cyclopropane.

The pioneers of cyclopropane chemistry were Danishefsky,[50] Stork,[51] and Corey[52] in the late 60s and early 70s. Later Wenkert[53] and Reissig[54] developed donor-acceptor (D-A) cyclopropanes with a substituent controlled C-C bond polarization. Over the last two decades cyclopropanes experienced a renaissance and interest in these intriguing compounds is still on the rise with numerous recent publications and reviews on their applications.[55] Nowadays cyclopropanes are regularly employed as precursors for carbo-[56] and heterocycles.[57] Ring-opening reactions[55e], (formal) cycloadditions[58] and

rearrangements[59] (Scheme 8) offer access to a multitude of building blocks. Over the past decades many asymmetric procedures have been developed, which made cyclopropanes, and particularly D-A cyclopropanes, an even more useful tool for the synthetic chemist.[60]

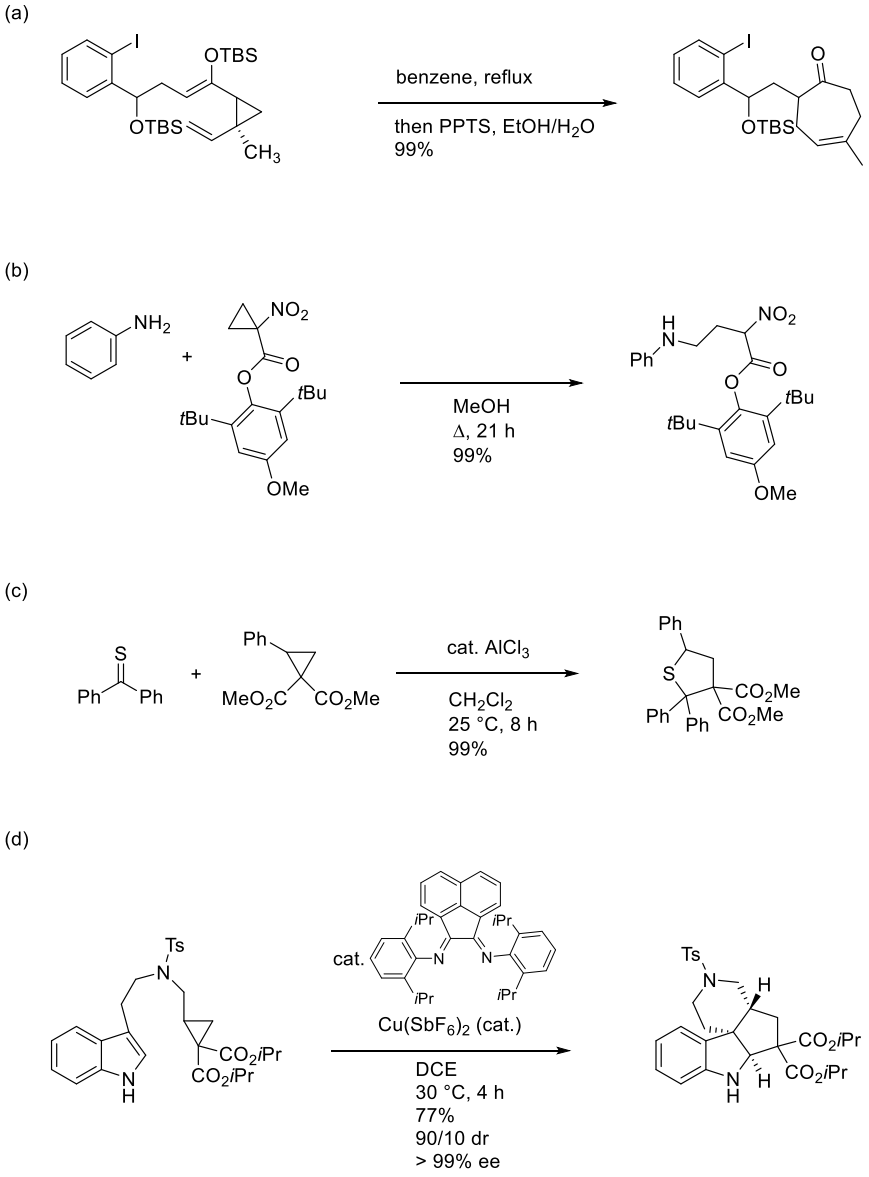

Scheme 8. Examples for a cyclopropane rearrangement (a),[61] a ring-opening reaction (b),[62] a formal cycloaddition (c)[58b] and an asymmetric (3+2) annulation (d).[63]

While the synthetic possibilities have been well explored, there is an astounding lack in systematic kinetic investigations into this topic. McKinney *et al*. published rate constants and activation parameters for the reactions of two Meldrum's acid derived spirocyclopropanes with pyridine in 1984 (Scheme 9a).[64] Hanafusa *et al*. reported rate constants of two cyclopropane derivatives with substituted pyridines (Scheme 9b).[65] More recently, Werz *et al*. published a study on the effect of

different donors on the reactivity in a common D-A cyclopropane with the Lewis acid catalyst $SnCl_4$ in formal (3+2) cycloadditions with *p*-fluorobenzaldehyde (Scheme 9c).[66]

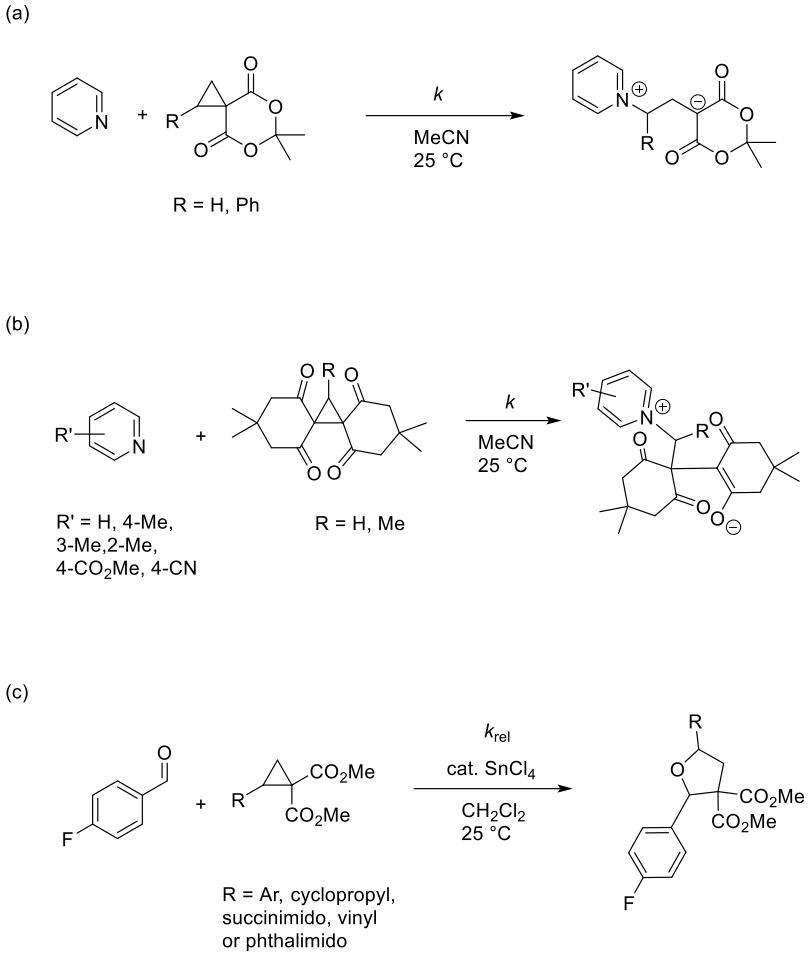

Scheme 9. Kinetic investigations of cyclopropane reactivities by McKinney (a),[64] Hanafusa (b),[65] and Werz (b).[66]

To the best of my knowledge, no further publications exist that quantify the reactivity of cyclopropanes in polar reactions. **As a consequence, it is a goal of this thesis to investigate the electrophilicity of a set of cyclopropanes.** Electrophilicity of S_N2 substrates may be described by the electrophilicity parameter *E* and the electrophile-specific slope s_E of the extended Mayr-Patz equation (1):[67]

$$\log k_2(20\ °C) = s_E s_N(N + E) \qquad (2)$$

The nucleophilicity parameter *N* and the nucleophile-specific slope s_N are specific to the employed nucleophile and solvent. Thiophenolates, characterized in this work (Chapter 2), will be used as reference nucleophiles. Their UV-Vis absorption, sterically unhindered reaction center as well as the high and easily tuneable nucleophilicity should make them ideal reference nucleophiles for this task.

The effect of different acceptor groups on the reactivity of cyclopropanes will be investigated. Furthermore, substitution of one hydrogen at the cyclopropane ring by differently substituted aryl

groups should enable a Hammett analysis, which is also intended for the differently substituted thiophenolates. The results of these kinetic studies are presented in Chapter 3.

1.3 Nucleophilic Substitutions

Nucleophilic substitutions are fundamental reactions in organic chemistry. Hughes and Ingold were the first to recognize, that nucleophilic substitutions can proceed by more than a single mechanism.[68] They investigated the reaction of alkyl ammonium ions and their reaction with alkoxides and subsequently distinguished between substitution via ionization (S_N1) or direct displacement (S_N2). S_N1 is an abbreviation for substitution, nucleophilic, unimolecular, while S_N2 stands for substitution, nucleophilic, bimolecular. General energy diagrams for the S_N1 and S_N2 mechanisms are depicted in Figure 2.

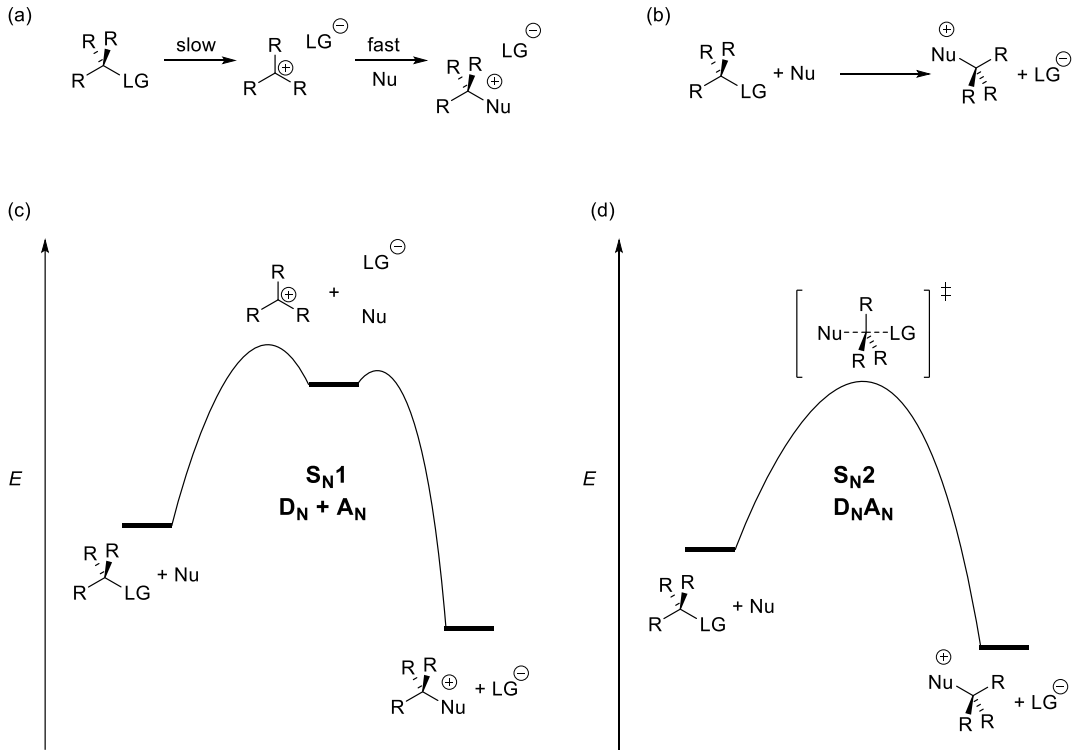

Figure 2: (a) Stepwise mechanism of the S_N1 reaction and (c) corresponding energy diagram. (b) Concerted mechanism of the S_N2 reaction and (d) corresponding energy diagram.

The S_N1 reaction begins with a slow ionization step, followed by a much faster addition reaction. The result is a first-order rate law for S_N1 reactions. The reaction rate is independent of the nucleophile type and concentration: $v = k[R_3C\text{-}LG]$. This a generalization, however, and while many common ionization reactions exhibit this rate law, there are exceptions. If the reaction of the ionized species with the nucleophile is not significantly faster than the ionization, then the rate law changes to second order.[69] As a result, nucleophile type and concentration do matter for such S_N2C^+ ionization reactions.

To avoid confusion of S_N2C^+ reactions with the mechanistically different classical S_N2 reactions one may use the nomenclature recommendations of the IUPAC[70] and call S_N2C^+ reactions and the classical S_N1 reactions $D_N + A_N$, which implies stepwise mechanisms beginning with dissociation followed by a nucleophilic association.

The classical S_N2 reaction is represented by the term D_NA_N, emphasizing the concerted formation and cleavage of the respective bonds in a single step. The transition state of the S_N2 mechanism is trigonal bipyramidal (Figure 1). A second-order rate law is always found in this case: $v = k[R_3C\text{-}LG][Nu]$.

Hughes and Ingold considered S_N1 and S_N2 as two discrete mechanisms, an idea that was later challenged by Winstein *et al.*[71] and Sneen *et al.*[72], who considered a mechanistic continuum more likely. The presence of multiple acting mechanisms in nucleophilic substitution reactions at *N*-substituted pyridinium ions was demonstrated by Katritzky.[73] Furthermore, in 2009 the Mayr group published a detailed kinetic study of concurrent S_N1 and S_N2 mechanisms in reactions of benzhydryl bromides with amines, supporting the interpretation of two independent mechanisms suggested by Hughes and Ingold.[74]

Distinguishing between the stepwise S_N1 mechanism and the concerted S_N2 mechanism can be difficult, in particular in borderline cases. Two of the most important tools to identify the mechanism operating in nucleophilic substitutions are investigations of the kinetics and the stereochemistry of a reaction. However, both of these tools have limits. As mentioned above, stepwise nucleophilic substitutions are often, but not always obeying a first order rate law, which makes kinetics of a reaction an uncertain tool if used alone.

Another problem for the kinetic analysis appears at trivalent (sp^2 hybridized) or bivalent (*sp* hybridized) carbon, here an addition-elimination ($A_N + D_N$) mechanism is possible (Scheme 10), because increasing the coordination number can result in stable intermediates. Dissociation occurs in a following, separate step to complete the nucleophilic substitution.

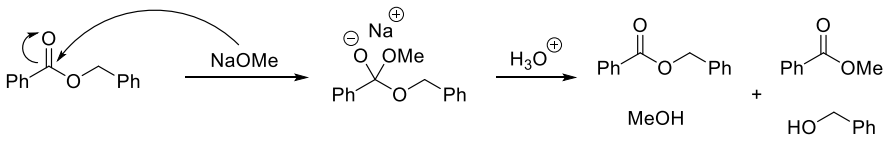

Scheme 10: Stepwise addition-elimination mechanism of benzyl benzoate with sodium methoxide, discovered by Claisen.[75]

The addition-elimination reaction depicted in Scheme 1 was first observed by Claisen in 1887.[75] Claisen noticed a colorless solid precipitate during the reaction, which he correctly identified as the salt resulting from the addition step of benzyl benzoate and sodium methoxide. By isotope labeling ester carbonyl oxygen and subsequent alkaline hydrolysis Bender could prove the interpretation of Claisen in 1951.[76] However, not all nucleophilic substitutions on acyl compounds proceed with an addition-

elimination mechanism, the classical S_N1 mechanism is also found.[77] This mechanism is not only found on carbonyls, but also on aromatic carbon, where this sequence of elementary reaction steps is known as S_NAr. Not only the mechanism of this special addition-elimination reaction has a unique name, but also the addition products, which are known as Meisenheimer or sigma complex. In 1902 Meisenheimer was the first to identify the reaction product of trinitroanisol and potassium ethoxide (Scheme 11).[78]

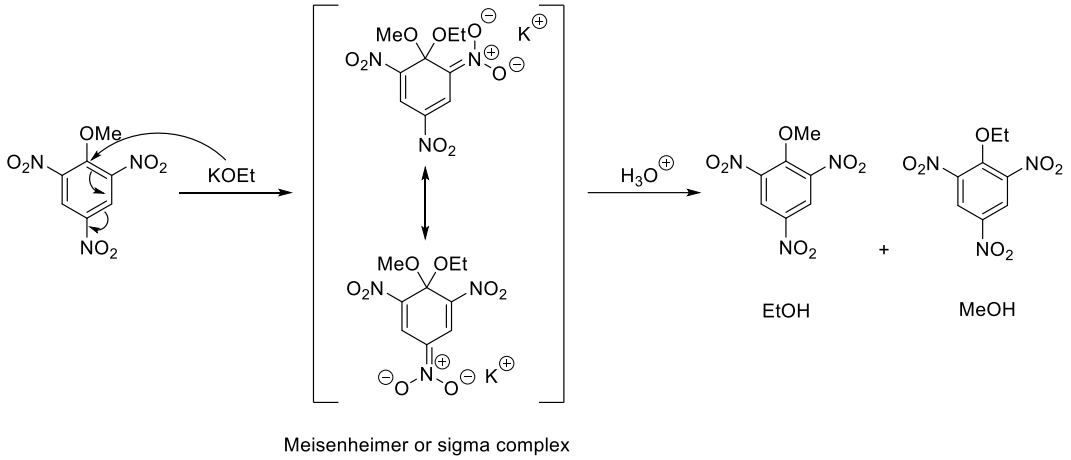

Scheme 11: Addition-Elimination reaction of trinitroanisol and potassium ethoxide and the intermediate Meisenheimer complex.

Addition of acid eliminates either ethanol or methanol from the red Meisenheimer complex and completes the nucleophilic aromatic substitution. However, nucleophilic aromatic substitutions do not necessarily occur stepwise, the concerted variant is also common.[79]

One way to gain information about the mechanism of a reaction is stereochemistry. The stepwise S_N1 mechanism loses the stereoinformation of a chiral, sp^3 hybridized carbon over the course of the reaction, due to the planar sp^2 hybridized carbon in the intermediate carbocation. However there are exceptions to this rule, for example in select cases stereoinformation is retained if, instead of complete dissociation, the carbocation and the leaving group form a close contact or solvent separated ion pair[80] and thus block one of the sides at the planar carbocation for the attacking nucleophile.[81] This would then lead to a partial or complete inversion of the stereocenter in question. Retention of configuration in S_N1 reactions has also been reported.[82] The stereochemical behavior of the concerted S_N2 reaction is different, because the mechanism at hand allows only for inversion at the electrophilic center. This phenomenon is also called Walden inversion,[83] named after Paul Walden who discovered the inversion of configuration when treating a chiral alcohol with PCl_5. For a retention of configuration a frontside attack of the nucleophile on the reactive carbon would be required, but such an attack is hindered by

a much higher activation barrier when compared to the backside attack.[84] As a consequence, nucleophilic frontside attack has yet to be observed.

Fortunately, even when the operating mechanism of a nucleophilic substitution reaction cannot be clearly determined by either kinetic or stereochemical methods due to the shortcomings mentioned above, then there are further tools for elucidating the mechanism, such as kinetic isotope effects, positional isotopic exchange or polar substituent effects.[85]

Nucleophilic substitution reactions are useful and common reactions in chemistry.[86] While many facets of nucleophilic substitutions are well understood nowadays, it is often not clear whether the reaction proceeds *via* the S_N1 or the S_N2 mechanism and there have been many experimental[73-74,86a,87] and theoretical[84a,88] studies to elucidate this question. In particular, it is still unclear which parameters make the concerted S_N2 pathway more or less favorable compared to the stepwise S_N1 pathway.

While S_N1[89] and S_N2[67,87h,88c,88d,90] processes individually have been subject of research in many studies for almost a century, investigations that allow to learn about trends in both reaction mechanisms concurrently and at the same substrate molecules[73-74,91] are comparatively rare. S_N1 and S_N2 do not follow the same trends when solvent[92], leaving group[93] or carbocation stabilization[91a,91b] are varied.

Primary, aliphatic alkyl halides are known to react by the S_N2 mechanism exclusively and tertiary, bulky alkyl halides only by the S_N1 mechanism. It is less clear cut for electrophilic molecules in between these extremes.[94] Depending on the reaction conditions, secondary alkyl halides and tosylates can react *via* S_N1 or S_N2 or both of these mechanisms concurrently.

S_N1 permits the use of very weak nucleophiles, as the generated carbocation is highly reactive (Figure 1).[94] Even poor nucleophiles will react with secondary, benzylic carbocations, e.g. the phenethyl cation $Ph(CH^+)CH_3$, under diffusion control. Because of the high reactivity strong and weak nucleophiles will react both under diffusion control and it is possible to selectively attach weaker nucleophiles at carbocationic centers though much stronger nucleophiles are present if the concentration of the more reactive nucleophile is sufficiently low. With activation-controlled reactions the difference in concentrations would need to be higher to achieve the same effect.

Secondary benzyl halides or tosylates only react with comparatively strong nucleophiles in S_N2 reactions.

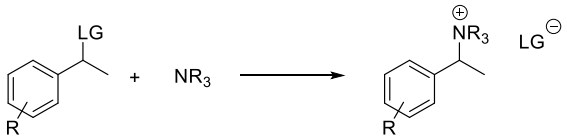

Scheme 12. Menschutkin reaction of substituted phenethyl halides and tosylates with primary, secondary and tertiary amines.

To investigate the effects of substrate structure, solvent, nucleophile type and concentration and temperature on the kinetics of concurrent S_N1 and S_N2 reactions, Menschutkin reactions (Scheme 12) have been investigated in Chapter 4 (Chart 1). With selected substrates these reactions allow to study are all borderline cases that offer the potential to control the mechanism by modifying the reaction conditions. To further investigate leaving group effects in well-defined S_N2 reactions, 1-butyl halides and 1-butyl tosylate will also be employed as electrophiles. Amines will be used as the nucleophiles, because they are nucleophilic enough to react reasonably quickly even with weak electrophiles.

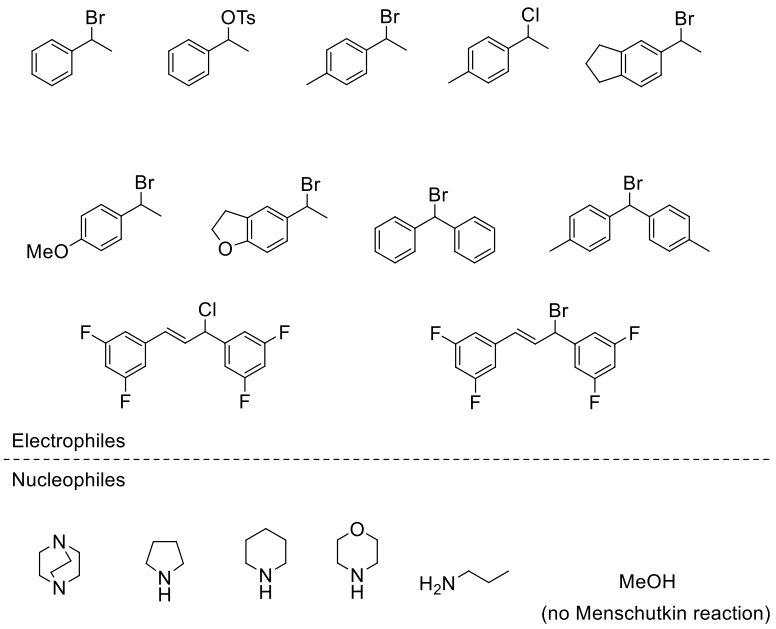

Chart 1. Electrophiles and nucleophiles.

1.4 Intrinsic Barriers, an Unsolved Limitation for LFERs

Linear free energy relationships (LFER) are useful tools to predict rate constants of reactions. The Brønsted relation (1928)[95] has connected the rate constants of closely related reactions with the acidity or basicity of one reaction partner. The notion of the link between equilibrium constants and rate constants was then picked up by Hammett,[96] who introduced equation (3) in 1937.[97] Either equilibrium constants or rate constants can be predicted with the Hammett equation (3) for a related set of reactions with differently substituted arenes. Each substituent is attributed a σ value, depending on the position in the aromatic ring and the development of charge during the reaction. Many hundreds of σ constants have already been reported.[98] The constant ρ is specific for the investigated reaction and indicative for the influence of the substituents. The equilibrium of benzoic acid and benzoate in water is used to define ρ as unity and σ is set to 0.

$$\log \frac{K}{K_0} \quad \text{or} \quad \log \frac{k}{k_0} = \rho \cdot \sigma \qquad (3)$$

Inspired by the Hammett equation (1), in 1948 Grunwald and Winstein[99] established equation (4) that allows for the prediction of heterolysis rate constants in protic solvents. The structures of the Hammett (3) and the Grunwald-Winstein equation (4) are related. However, in equation (4) the solvent is varied instead of the arene substituent in equation (3). The parameter *Y* is describing the solvent ionizing power, and *m* is the sensitivity factor of solvolysis and comparable to the sensitivity parameter ρ in equation (3). The solvent ionizing power of 80% aqueous ethanol was defined as 0 and *m* equals unity for *tert*-butyl chloride. The rate constant *k* represents the solvolysis of one substrate in a certain solvent and the rate-constant k_{80E} represents the solvolysis of the same substrate in 80% aqueous ethanol.

$$\log \frac{k}{k_{80E}} = m \cdot Y \qquad (4)$$

In the 1950s the Swain-Scott Equation[100] and the Edwards Equation[101] were published, trying to quantify nucleophilicity. The Swain-Scott Equation (5) predicts second-order rate constants with an electrophile-specific sensitivity constant *s* and a nucleophile-specific nucleophilicity constant *n*. As reference points Swain and Scott chose *s* = 1 for methyl bromide and *n* = 0 for the reaction of water with methyl bromide in water at 25 °C. The rate constant *k* is for the reaction of an electrophile/nucleophile combination and k_0 is for the reaction of the same electrophile with water.

$$\log \frac{k}{k_0} = s \cdot n \qquad (5)$$

While this method was successful at first, in 1968 Pearson reported severe limitations of the Swain-Scott equation (5) and as a consequence stated that it was not possible at that time to quantitatively predict rate constants for a diverse range of reaction partners.[102]

Surprisingly, Ritchie then published another LFER in 1972,[103] which could predict the rate constants of organic cations with nucleophiles. To achieve this, the Ritchie equation (6) used only the rate constant k of the reaction of a nucleophile with an organic cation, the rate constant k_0 of the reaction of the same cation with water in water, and the nucleophilicity parameter N_+ of the nucleophile.

$$\log \frac{k}{k_0} = N_+ \qquad (6)$$

In 1994 Mayr and Patz marked the beginning of the most extensive and general reactivity scale to date with the Mayr-Patz equation (1).[104] More than 1200 nucleophiles and more than 300 electrophiles have been characterized so far.[105] Nucleophiles are characterized by a solvent dependent nucleophilicity parameter N and a solvent dependent sensitivity parameter s_N. Electrophiles are characterized by the electrophilicity parameter E, which is solvent independent. E for the bis(*p*-methoxyphenyl)methyl cation was arbitrarily set to 0 and s_N for 2-methyl-1-pentene was set to 1. Later it was shown, that the extended Mayr-Patz equation (1) could also predict rate constants for S_N2 reactions and that the Swain-Scott equation (5) and the Ritchie equation (6) are special cases of the (extended) Mayr-Patz equation.[67,106] The solvent independent, electrophile specific sensitivity parameter s_E, analogous to the s_N parameter, is introduced. But there are still limitations, for example at least one of the nuclei, where the new bond is formed, must be carbon. However, equation (2) has not yet been tested for a wider range of reactions.

$$\log k_2\ (20\ ^\circ\mathrm{C}) = s_N(N + E) \qquad (1)$$

$$\log k_2\ (20\ ^\circ\mathrm{C}) = s_N s_E(N + E) \qquad (2)$$

Substituted benzhydrylium ions served as reference electrophiles for establishing equation (1), due to their huge range of reactivity, color and constant steric environment. The color is important for monitoring the kinetics of reactions, although alternative ways of following the concentration of a species during a reaction exist, such as time-resolved conductivity, IR spectroscopy or NMR spectroscopy. UV-Vis spectroscopy has the least limitations of these variants, as long as a disappearing or appearing absorption band can be unequivocally assigned to a reactant or product of the investigated reaction. The Mayr group used these benzhydrylium ions also as reference compounds for the construction of a Lewis acidity/basicity scale.[107] In equation (7), the equilibrium constant K of a Lewis base and a Lewis acid can be described with the Lewis base specific parameter LB and the Lewis acid specific parameter LA.

Unlike the equations (1) and (2), equation (7) can only be applied in dichloromethane and acetonitrile solutions. The reason for this is, that the *LA* parameters are solvent dependent and have only been determined in these solvents so far. Also, the resulting Lewis basicity scales are only valid toward carbon centered Lewis acids. Again, the bis(*p*-methoxyphenyl)methyl cation served as reference point with a *LA* parameter of 0.

$$\log K\ (20\ ^\circ\mathrm{C}) = LA + LB \qquad (7)$$

Furthermore, Mayr and Kronja developed a reactivity scale for nucleofuges and electrofuges.[89c,108] In essence, the rate constants of the reverse reaction of equation (1) are predicted with the Mayr-Kronja equation (8) for heterolysis reactions. The nucleofuge specific parameters s_f and N_f are solvent dependent, the electrofuge specific parameter E_f is not. As reference points served the electrofuge bis(*p*-methoxyphenyl)methyl cation ($E_f = 0$) and the nucleofuge chloride in ethanol ($s_f = 1$).

$$\log k_{het}\ (25\ ^\circ\mathrm{C}) = s_f(N_f + E_f) \qquad (8)$$

Now with the LFERs in equations 1, 7 and 8 at hand, one can analyze the mutual relationships between the reactivity parameters to find intriguing connections between kinetics and thermodynamics (Scheme 13).

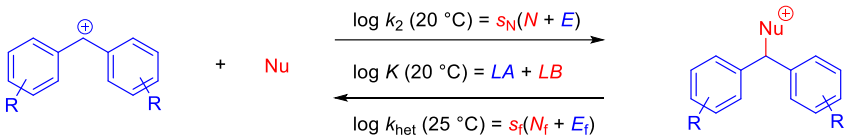

Scheme 13. The reaction of reference benzhydrylium ions electrophiles/Lewis acids with nucleophiles/Lewis bases. Color coding indicates the origin of the individual parameters. Equations employed are: (1), (7) and (8) (top to bottom).

Mayr and Ofial[109] found that the logarithm of the rate constants of a set of reactions involving substituted benzhydrylium ions correlates linearly with the Lewis acidity parameter *LA* of equation (7). Kinetics correlate with thermodynamics in this case. Interestingly, the same rate constants did not correlate with Lewis basicity parameter *LB* of equation (7). Intrinsic barriers as defined by the Marcus equation,[110] were shown by Mayr and Ofial to be important factors for defining the scope of equation (8). For example, they found that DABCO was not only a better nucleophile than DMAP, but also a better nucleofuge. Intuitively, one would expect a strong nucleophile to be a weak nucleofuge and *vice versa*. On the other hand, iodide ions,[109a] are known to be good nucleophiles and good leaving groups (nucleofuges). As a consequence, the thermodynamics of a series of reactions can only correlate with the kinetics, when intrinsic barriers change proportionally with thermodynamics ($\Delta\Delta G^0$) or not at all.

Mayr and Ofial also reported about the correlation of the logarithm of heterolysis rate constants ($\log k_{het}$) with *LA*, which was linear with little scatter for benzhydrylium ions with weak electron donating groups (EDG) ($E > -2$), but had a poor quality for benzhydrylium ions with strong EDG

($E < -2$).[109a] As reason the method of determination of E_f parameters was identified: While the benzhydrylium group with good linear correlations had its E_f parameters determined with chloride as nucleofuge, carboxylates were used to determine E_f for the poorly correlating subset of benzhydrylium ions. The problem is best explained with the reverse, addition reaction: Chloride will recombine with its benzhydrylium partners in a diffusion-controlled reaction. These reactions are barrierless and, as a consequence, the transition states correspond to the benzhydrylium ions. Due to the principle of microscopic reversibility, the transition states for recombination and heterolysis are the same. Carboxylates on the other hand recombine with their less electrophilic benzhydrylium partners with activation control. Consequently, the transition states only resemble the benzhydrylium ions in this case, causing the discrepancy in linear correlations against *LA*.

Because the Gibbs energy equals the activation barrier ($\Delta G^0 = \Delta G^{\ddagger}$) for heterolysis reactions of the reverse, diffusion-controlled addition reactions, activation barriers become independent of the effects of intrinsic barriers. Due to the principle of microscopic reversibility, this is true for addition and heterolysis reactions. Again, correlations of rate constants with thermodynamics are only linear, when the effects of intrinsic barriers do not change in a series of reactions.

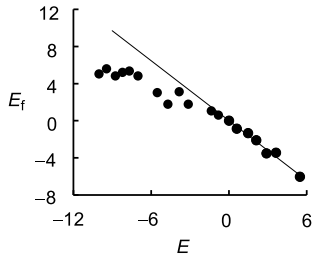

Figure 3. Correlation of E_f (equation 8) against E (equation 1).

Another consequence of this is the collapse in the linear correlation of E_f versus E (Figure 3). The collapse marks the position ($E = -2$), where the transition from E_f parameters that were acquired under activation-control (of the reverse recombination reaction) to E_f parameters that were acquired under diffusion-control (of the reverse recombination reaction) occurs.

In the light of recent results[111] it appears that not all problems in applications of the Mayr-Kronja equation (8) have been recognized so far (Figure 4). For example, different N_f and s_f parameters for the same leaving group (nucleofuge) are obtained, depending on whether the investigated reactions have activation-controlled (red line Figure 4) or diffusion-controlled reverse recombination reactions (black line Figure 4) of dimethylsulfide with the carbenium ions, which are released in the heterolysis reactions.

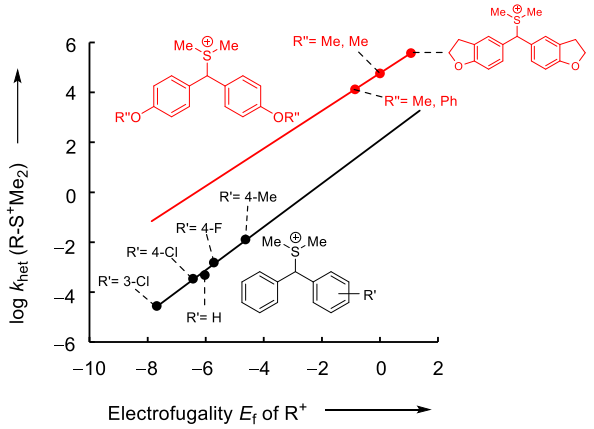

Figure 4. Plot of the logarithm of the rate constant k_{het} for the heterolysis of benzhydryl sulfonium ions against the electrofugality parameter E_f. The red line consists of reactions (in CH_2Cl_2) with activation-controlled reverse recombination reactions and the black line consists of reactions (in ethanol) with diffusion-controlled reverse recombination reactions.

It has to be mentioned, that the solvents are not the same, the black data[111b,111c] points were measured in ethanol, while the red data[111a] points were obtained in dichloromethane. However, the discrepancy of the two data sets seems to be too big to be caused only by the change in solvent, as changing the solvent was reported to have only a minor effect on the rate constants of the heterolysis reactions of sulfonium ions.[111b,111c]

As part of this thesis it was intended to investigate the heterolysis of the 1,3-diphenylallyl dimethylsulfonium ion with dynamic NMR spectroscopy (Scheme 14). The reactivity parameters E[112] and E_f[113] for the 1,3-diphenylallylium ion have already been reported, enabling the estimation of k_{het} by using equation (8). The corresponding dimethylsulfonium ion is expected to undergo the heterolysis reaction with a rate constant k_{het} that follows the correlation of the red data points in Figure 1. At the same time, heterolysis of this sulfonium ion results in a highly electrophilic carbocation (Scheme 14), which should recombine with dimethylsulfide under diffusion-control, as estimated with equation (1). Whether the rate constant k_{het} acquired for the reaction in Scheme 2 correlates with the red or the black data set in Figure 1 will bring significant insight into the problem at hand. The performed studies will be presented in Chapter 5.1.

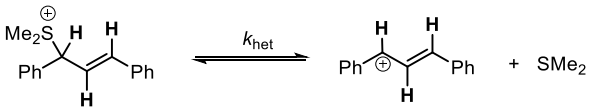

Scheme 14. Heterolysis of the 1,3-diarylallyl dimethylsulfonium ion and recombination of the resulting allylium ion with dimethylsulfide.

Intrinsic barriers and how they affect rate constants in a series of reactions are poorly understood. **To achieve further insights into the impact of intrinsic barriers on reactivity and subsequent**

consequences for correlation analysis, identifying a fitting and sufficiently large set of rate constants to be able to correlate log *k* divided by log k_{het} against *LA* is a goal of this thesis. This correlation should be undisturbed by the influence of variable intrinsic barriers. The behavior or possible collapse of this correlation once log *k* becomes constant at the diffusion limit (log k_{diff} = 10) is of particular interest. Insights into the differences in the influences of intrinsic barriers in activation-controlled combination reactions and diffusion-controlled combination reactions and the resulting ramifications for the reverse heterolysis reactions and the Mayr-Kronja equation (8) may also be gained from this investigation. The results of such attempts of correlation analysis will be presented in Chapter 5.2.

1.5 References

(1) Munday, R., *Free Radic. Biol. Med.* **1989,** *7*, 659−673.

(2) Roberts, J. S., Thiols. In *Kirk‐Othmer Encyclopedia of Chemical Technology*, Wiley & Sons Ltd.: 2000.

(3) Ballinger, P.; Long, F. A., *J. Am. Chem. Soc.* **1960,** *82*, 795−798.

(4) Guthrie, J. P., *J. Am. Chem. Soc.* **1978,** *100*, 5892−5904.

(5) (a) Sardi, F.; Manta, B.; Portillo-Ledesma, S.; Knoops, B.; Comini, M. A.; Ferrer-Sueta, G., *Anal. Biochem.* **2013,** *435*, 74−82. (b) Baidya, M.; Kobayashi, S.; Mayr, H., *J. Am. Chem. Soc.* **2010,** *132*, 4796−4805. (c) Duan, X.-H.; Maji, B.; Mayr, H., *Org. Biomol. Chem.* **2011,** *9*, 8046−8050.

(6) Poole, L. B., *Free Radic. Biol. Med.* **2015,** *80*, 148−157.

(7) Chary, K. P.; Rajaram, S.; Iyengar, D., *Synth. Commun.* **2000,** *30*, 3905−3911.

(8) Reed, D. R.; Hare, M. C.; Fattahi, A.; Chung, G.; Gordon, M. S.; Kass, S. R., *J. Am. Chem. Soc.* **2003,** *125*, 4643−4651.

(9) Berkowitz, J.; Ellison, G. B.; Gutman, D., *J. Phys. Chem.* **1994,** *98*, 2744−2765.

(10) Li, S.; Ahmed, L.; Zhang, R.; Pan, Y.; Matsunami, H.; Burger, J. L.; Block, E.; Batista, V. S.; Zhuang, H., *J. Am. Chem. Soc.* **2016,** *138*, 13281−13288.

(11) Sela, L.; Sobel, N., *Exp. Brain. Res.* **2010,** *205*, 13−29.

(12) Schoenauer, S.; Schieberle, P., *J. Agric. Food Chem.* **2016,** *64*, 3849−3861.

(13) Nagata, Y.; Takeuchi, N., *Odor measurement review* **2003,** *118*, 118−127.

(14) Pavez, C.; Agosin, E.; Steinhaus, M., *J. Agric. Food Chem.* **2016,** *64*, 3417−3421.

(15) (a) Gros, J.; Peeters, F.; Collin, S., *J. Agric. Food Chem.* **2012,** *60*, 7805−7816. (b) Vermeulen, C.; Lejeune, I.; Tran, T.; Collin, S., *J. Agric. Food Chem.* **2006,** *54*, 5061−5068.

(16) Sourabié, A. M.; Spinnler, H.-E.; Bonnarme, P.; Saint-Eve, A.; Landaud, S., *J. Agric. Food Chem.* **2008,** *56*, 4674−4680.

(17) Granvogl, M.; Christlbauer, M.; Schieberle, P., *J. Agric. Food Chem.* **2004,** *52*, 2797−2802.

(18) Li, J.-X.; Schieberle, P.; Steinhaus, M., *J. Agric. Food Chem.* **2012,** *60*, 11253−11262.

(19) Dulsat-Serra, N.; Quintanilla-Casas, B.; Vichi, S., *Food Res. Int.* **2016,** *89*, 982−988.

(20) Tamura, H.; Fujita, A.; Steinhaus, M.; Takahisa, E.; Watanabe, H.; Schieberle, P., *J. Agric. Food Chem.* **2011,** *59*, 10211−10218.

(21) (a) Aldrich, T. B., *J. Exp. Med.* **1896,** *1*, 323–340. (b) Andersen, K. K.; Bernstien, D. T.; Caret, R. L.; Romanczyk Jr, L. J., *Tetrahedron* **1982,** *38*, 1965−1970.

(22) Cai, X.-J.; Block, E.; Uden, P. C.; Quimby, B. D.; Sullivan, J. J., *J. Agric. Food Chem.* **1995,** *43*, 1751−1753.

(23) Kraft, P.; Mannschreck, A., *J. Chem. Educ.* **2010,** *87*, 598−603.

(24) Suarez, F.; Springfield, J.; Levitt, M., *Gut* **1998,** *43*, 100−104.

(25) Schulze, W. A.; Lyon, J.; Short, G., *Ind. Eng. Chem.* **1948,** *40*, 2308−2313.

(26) (a) Newman, M. S.; Karnes, H. A., *J. Org. Chem.* **1966,** *31*, 3980−3984. (b) Kwart, H.; Evans, E. R., *J. Org. Chem.* **1966,** *31*, 410−413.

(27) Olah, G. A.; Tolgyesi, W. S.; Kuhn, S. J.; Moffatt, M. E.; Bastien, I. J.; Baker, E. B., *J. Am. Chem. Soc.* **1963,** *85*, 1328−1334.

(28) Flores, J. D.; Treat, N. J.; York, A. W.; McCormick, C. L., *Polym. Chem.* **2011,** *2*, 1976−1985.

(29) Seyedi, S. M.; Sadeghian, H.; Rezai, M., *Phosphorus Sulfur Silicon Relat. Elem.* **2007,** *182*, 1709−1716.

(30) Nair, D. P.; Podgórski, M.; Chatani, S.; Gong, T.; Xi, W.; Fenoli, C. R.; Bowman, C. N., *Chem. Mat.* **2014,** *26*, 724−744.

(31) Mayer, R. J.; Ofial, A. R., *Angew. Chem., Int. Ed.* **2019,** *58*, 17704−17708.

(32) Sharpe, M. A.; Livingston, A. D.; Baskin, D. S., *J. Toxicol.* **2012,** *2012*, 373678.

(33) Diergart, P., *J. Prakt. Chem.* **1919,** *99*, 281−292.

(34) Wu, G.; Fang, Y.-Z.; Yang, S.; Lupton, J. R.; Turner, N. D., *J. Nutr.* **2004,** *134*, 489−492.

(35) (a) Weerapana, E.; Wang, C.; Simon, G. M.; Richter, F.; Khare, S.; Dillon, M. B.; Bachovchin, D. A.; Mowen, K.; Baker, D.; Cravatt, B. F., *Nature* **2010,** *468*, 790−795. (b) Wang, C.; Weerapana, E.; Blewett, M. M.; Cravatt, B. F., *Nat. Methods* **2014,** *11*, 79−85. (c) Perjési, P., *Glutathione: Biosynthesis, Functions and Biological Implications*. Nova Science Publishers: 2019.

(36) Sevier, C. S.; Kaiser, C. A., *Nat. Rev. Mol. Cell Biol.* **2002,** *3*, 836−847.

(37) (a) Halprin, K. M.; Ohkawara, A., *J. Investig. Dermatol.* **1967,** *48*, 149−152. (b) Lu, S. C., *Biochim. Biophys. Acta Gen. Subj.* **2013,** *1830*, 3143−3153. (c) Pastore, A.; Piemonte, F.; Locatelli, M.; Lo Russo, A.; Gaeta, L. M.; Tozzi, G.; Federici, G., *Clin. Chem.* **2001,** *47*, 1467−1469.

(38) Böhme, A.; Thaens, D.; Schramm, F.; Paschke, A.; Schüürmann, G., *Chem. Res. Toxicol.* **2010,** *23*, 1905−1912.

(39) (a) Ellman, G. L., *Arch. Biochem. Biophys.* **1958,** *74*, 443−450. (b) Ellman, G. L., *Arch. Biochem. Biophys.* **1959,** *82*, 70−77.

(40) Chipinda, I.; Ajibola, R. O.; Morakinyo, M. K.; Ruwona, T. B.; Simoyi, R. H.; Siegel, P. D., *Chem. Res. Toxicol.* **2010,** *23*, 918−925.

(41) Cheh, A. M.; Carlson, R. E., *Anal. Chem.* **1981,** *53*, 1001−1006.

(42) Hudson, R. F.; Klopman, G., *J. Chem. Soc.* **1962**, 1062−1067.

(43) Freund, A., *J. Prakt. Chem.* **1882,** *26*, 367−377.

(44) Allen, F. H.; Kennard, O.; Watson, D. G.; Brammer, L.; Orpen, A. G.; Taylor, R., *J. Chem. Soc., Perkin Trans. 2* **1987**, 1−19.

(45) Smith, M. B.; March, J., March's Advanced Organic Chemistry (6th ed.). John Wiley & Sons, Inc.: Hoboken, New Jersey, 2007; p 216−219.

(46) Randić, M.; Maksić, Z., *Theor. Chim. Acta* **1965,** *3*, 59−68.

(47) Bastiansen, O.; Fritsch, F. N.; Hedberg, K., *Acta Crystallogr,* **1964,** *17*, 538−543.

(48) Wiberg, K. B., *Acc. Chem. Res.* **1996,** *29*, 229−234.

(49) (a) Förster, T., *Z. Phys. Chem.* **1939,** *43*, 58−78. (b) Coulson, C. A.; Moffitt, W. E., *J. Chem. Phys.* **1947,** *15*, 151−151.

(50) (a) Danishefsky, S., *Acc. Chem. Res.* **1979,** *12*, 66−72. (b) Danishefsky, S.; Rovnyak, G.; Cavanaugh, R., *J. Chem. Soc. D: Chem. Commun.* **1969**, 636−636. (c) Danishefsky, S.; Rovnyak, G., *J. Chem. Soc., Chem. Commun.* **1972**, 821−822. (d) Danishefsky, S.; Rovnyak, G., *J. Chem. Soc., Chem. Commun.* **1972**, 820−821. (e) Danishefsky, S.; Singh, R., *J. Am. Chem. Soc.* **1975,** *97*, 3239−3241. (f) Singh, R. K.; Danishefsky, S., *J. Org. Chem.* **1975,** *40*, 2969−2970. (g) Dolfini, J. E.; Menich, K.; Corliss, P.; Cavanaugh, R.; Danishefsky, S.; Chakrabartty, S., *Tetrahedron Lett.* **1966,** *7*, 4421−4426.

(51) (a) Stork, G.; Gregson, M., *J. Am. Chem. Soc.* **1969,** *91*, 2373−2374. (b) Stork, G.; Grieco, P. A., *Tetrahedron Lett.* **1971,** *12*, 1807−1810.

(52) Corey, E.; Balanson, R., *Tetrahedron Lett.* **1973,** *14*, 3153−3156.

(53) (a) Wenkert, E.; Alonso, M. E.; Buckwalter, B. L.; Chou, K. J., *J. Am. Chem. Soc.* **1977,** *99*, 4778−4782. (b) Wenkert, E., *Acc. Chem. Res.* **1980,** *13*, 27−31.

(54) (a) Reissig, H. U.; Hirsch, E., *Angew. Chem., Int. Ed.* **1980,** *19*, 813−814. (b) Brückner, C.; Reissig, H. U., *Angew. Chem., Int. Ed.* **1985,** *24*, 588−589. (c) Reissig, H.-U.; Zimmer, R., *Chem. Rev.* **2003,** *103*, 1151−1196.

(55) (a) Pirenne, V.; Muriel, B.; Waser, J., *Chem. Rev.* **2020**. (b) Liu, J.; Liu, R.; Wei, Y.; Shi, M., *Trends Chem.* **2019,** *1*, 779−793. (c) Liu, Y.; Wang, Q.-L.; Chen, Z.; Zhou, C.-S.; Xiong, B.-Q.; Zhang, P.-L.; Yang, C.-A.; Zhou, Q., *Beilstein J. Org. Chem.* **2019,** *15*, 256−278. (d) Talukdar, R.; Saha, A.; Ghorai, M. K., *Isr. J. Chem.* **2016,** *56*, 445−453. (e) Budynina, E. M.; Ivanov, K. L.; Sorokin, I. D.; Melnikov, M. Y., *Synthesis* **2017,** *49*, 3035−3068. (f) Cavitt, M. A.; Phun, L. H.; France, S., *Chem. Soc. Rev.* **2014,** *43*, 804−818. (g) Craig, A. J.; Hawkins, B. C., *Synthesis* **2020,** *52*, 27−39. (h) Augustin, A. U.; Werz, D. B., *Acc. Chem. Res.* **2021,** *54*, 1528−1541. (i) Ghosh, K.; Das, S., *Org. Biomol. Chem.* **2021,** *19*, 965−982.

(56) Grover, H. K.; Emmett, M. R.; Kerr, M. A., *Org. Biomol. Chem.* **2015,** *13*, 655−671.

(57) (a) Reiser, O., *Isr. J. Chem.* **2016,** *56*, 531−539. (b) Carson, C. A.; Kerr, M. A., *Chem. Soc. Rev.* **2009,** *38*, 3051−3060.

(58) (a) Garve, L. K.; Pawliczek, M.; Wallbaum, J.; Jones, P. G.; Werz, D. B., *Chem. Eur. J.* **2016,** *22*, 521−525. (b) Augustin, A. U.; Sensse, M.; Jones, P. G.; Werz, D. B., *Angew. Chem., Int. Ed.* **2017,** *56*, 14293−14296. (c) Garve, L. K.; Petzold, M.; Jones, P. G.; Werz, D. B., *Org. Lett.* **2016,** *18*, 564−567. (d) Young, I. S.; Kerr, M. A., *Angew. Chem., Int. Ed.* **2003,** *42*, 3023−3026.

(59) (a) Krüger, S.; Gaich, T., *Beilstein J. Org. Chem.* **2014,** *10*, 163−193. (b) Hudlický, T.; Kutchan, T. M.; Naqvi, S. M., *Org. React.* **2004,** *33*, 247−335.

(60) (a) Wang, L.; Tang, Y., *Isr. J. Chem.* **2016,** *56*, 463−475. (b) Pellissier, H., *Tetrahedron* **2008,** *64*, 7041−7095.

(61) Overman, L. E.; Ricca, D. J.; Tran, V. D., *J. Am. Chem. Soc.* **1993,** *115*, 2042−2044.

(62) Seebach, D.; Häner, R.; Vettiger, T., *Helv. Chim. Acta* **1987,** *70*, 1507−1515.

(63) Zhu, J.; Liang, Y.; Wang, L.; Zheng, Z.-B.; Houk, K. N.; Tang, Y., *J. Am. Chem. Soc.* **2014,** *136*, 6900−6903.

(64) McKinney, M. A.; Kremer, K. G.; Aicher, T., *Tetrahedron Lett.* **1984,** *25*, 5477−5480.

(65) Ohkata, K.; Nagai, T.; Tamaru, A.; Nandate, M.-a.; Hanafusa, T., *J. Chem. Soc., Perkin Trans. 2* **1982**, 1255−1259.

(66) Kreft, A.; Lücht, A.; Grunenberg, J.; Jones, P. G.; Werz, D. B., *Angew. Chem., Int. Ed.* **2019,** *58*, 1955−1959.

(67) Phan, T. B.; Breugst, M.; Mayr, H., *Angew. Chem., Int. Ed.* **2006,** *45*, 3869−3874.

(68) (a) Hughes, E. D.; Ingold, C. K., *Nature* **1933,** *132*, 933−934. (b) Hughes, E. D.; Ingold, C. K.; Patel, C. S., *J. Chem. Soc.* **1933**, 526−530.

(69) Mayr, H.; Ofial, A. R., *Pure Appl. Chem.* **2009,** *81*, 667−683.

(70) Guthrie, R. D.; Jencks, W. P., *Acc. Chem. Res.* **1989,** *22*, 343−349.

(71) Winstein, S.; Grunwald, E.; Jones, H. W., *J. Am. Chem. Soc.* **1951,** *73*, 2700−2707.

(72) (a) Sneen, R. A., *Acc. Chem. Res.* **1973,** *6*, 46−53. (b) Sneen, R. A.; Larsen, J. W., *J. Am. Chem. Soc.* **1969,** *91*, 6031−6035. (c) Sneen, R. A.; Larsen, J. W., *J. Am. Chem. Soc.* **1969,** *91*, 362−366.

(73) Katritzky, A. R.; Musumarra, G., *Chem. Soc. Rev.* **1984,** *13*, 47−68.

(74) Phan, T. B.; Nolte, C.; Kobayashi, S.; Ofial, A. R.; Mayr, H., *J. Am. Chem. Soc.* **2009,** *131*, 11392−11401.

(75) Claisen, L., *Ber. Dtsch. Chem. Ges.* **1887,** *20*, 646−650.

(76) Bender, M. L., *J. Am. Chem. Soc.* **1951,** *73*, 1626−1629.

(77) Cleland, W.; Hengge, A. C., *FASEB J.* **1995,** *9*, 1585−1594.

(78) Meisenheimer, J., *Liebigs Ann. Chem.* **1902,** *323*, 205−246.

(79) (a) Lennox, A. J. J., *Angew. Chem., Int. Ed.* **2018,** *57*, 14686−14688. (b) Neumann, C. N.; Hooker, J. M.; Ritter, T., *Nature* **2016,** *534*, 369−373.

(80) Winstein, S.; Clippinger, E.; Fainberg, A. H.; Heck, R.; Robinson, G. C., *J. Am. Chem. Soc.* **1956,** *78*, 328−335.

(81) Cowdrey, W. A.; Hughes, E. D.; Ingold, C. K.; Masterman, S.; Scott, A. D., *J. Chem. Soc.* **1937**, 1252−1271.

(82) (a) Okamoto, K.; Hayashi, M.; Shingu, H., *Bull. Chem. Soc. Jpn.* **1966,** *39*, 408−408. (b) Goering, H. L.; Levy, J. F., *J. Am. Chem. Soc.* **1964,** *86*, 120−121.

(83) Walden, P., *Ber. Dtsch. Chem. Ges.* **1896,** *29*, 133−138.

(84) (a) Bento, A. P.; Bickelhaupt, F. M., *J. Org. Chem.* **2008,** *73*, 7290−7299. (b) Bento, A. P.; Bickelhaupt, F. M., *Chem. Asian J.* **2008,** *3*, 1783−1792.

(85) Williams, A., *Chem. Soc. Rev.* **1994,** *23*, 93−100.

(86) (a) Westaway, K. C.; Ali, S. F., *Can. J. Chem.* **1979,** *57*, 1354−1367. (b) Peters, K. S., *Chem. Rev.* **2007,** *107*, 859−873. (c) Katritzky, A. R.; Brycki, B. E., *Chem. Soc. Rev.* **1990,** *19*, 83−105. (d) Robiette, R.; Trieu-Van, T.; Aggarwal, V. K.; Harvey, J. N., *J. Am. Chem. Soc.* **2016,** *138*, 734−737. (e) Uggerud, E., Chapter One - The Factors Determining Reactivity in Nucleophilic Substitution. In *Advances in Physical Organic Chemistry*, Williams, I. H.; Williams, N. H., Eds. Academic Press: 2017; Vol. 51, p 1−57.

(87) (a) Parker, A., Rates of bimolecular substitution reactions in protic and dipolar aprotic solvents. In *Advances in Physical Organic Chemistry*, Elsevier: 1967; Vol. 5, p 173−235. (b) Pienta, N. J.; Kessler, R. J., *J. Am. Chem. Soc.* **1993,** *115*, 8330−8339. (c) Wang, T.-T.; Iou, Q.-L., *Chem. Eng. J.* **2002,** *87*, 197−206. (d) Meng, Q.; Thibblin, A., *J. Am. Chem. Soc.* **1995,** *117*, 9399−9407. (e) Vlasov, V. M., *J. Phys. Org. Chem.* **2010,** *23*, 468−476. (f) Bentley, T.; Choi, H.; Koo, I. S.; Kevill, D. N., *J. Phys. Org. Chem.* **2017,** *30*, e3585. (g) Xie, J.; Hase, W. L., *Science* **2016,** *352*, 32−33. (h) Stei, M.; Carrascosa, E.; Kainz, M. A.; Kelkar, A. H.; Meyer, J.; Szabó, I.; Czakó, G.; Wester, R., *Nat. Chem.* **2016,** *8*, 151−156.

(88) (a) Uggerud, E., *J. Phys. Org. Chem.* **2006,** *19*, 461−466. (b) Liu, X.; Zhang, J.; Yang, L.; Hase, W. L., *J. Am. Chem. Soc.* **2018,** *140*, 10995−11005. (c) Fernández, I.; Frenking, G.; Uggerud, E., *Chem. Eur. J.* **2009,** *15*, 2166−2175. (d) Kim, Y.; Cramer, C. J.; Truhlar, D. G., *J. Phys. Chem. A* **2009,** *113*, 9109−9114.

(89) (a) Yutaka, T.; Mizue, F.; Yuho, T., *Bull. Chem. Soc. Jpn.* **1990,** *63*, 856−866. (b) Mizue, F.; Toshihiro, S.; Ken-ichi, Y.; Yoshihiro, S.; Mutsuo, G.; Hong, K. S.; Yutaka, T.; Zvi, R.; Yuho, T., *Bull. Chem. Soc. Jpn.* **1995,** *68*, 2619−2628. (c) Denegri, B.; Ofial, A. R.; Jurić, S.; Streiter, A.; Kronja, O.; Mayr, H., *Chem. Eur. J.* **2006,** *12*, 1657−1666. (d) Streidl, N.; Denegri, B.; Kronja, O.; Mayr, H., *Acc. Chem. Res.* **2010,** *43*, 1537−1549. (e) Keaveney, S. T.; White, B. P.; Haines, R. S.; Harper, J. B., *Org. Biomol. Chem.* **2016,** *14*, 2572−2580. (f) Fainberg, A. H.; Winstein, S., *J. Am. Chem. Soc.* **1956,** *78*, 2770−2777.

(90) Flores, A. E.; Gronert, S., *J. Am. Chem. Soc.* **1999,** *121*, 2627−2628.

(91) (a) Yoh, S. D.; Cheong, D. Y.; Lee, C. H.; Kim, S. H.; Park, J. H.; Fujio, M.; Tsuno, Y., *J. Phys. Org. Chem.* **2001,** *14*, 123−130. (b) Lim, C.; Kim, S.-H.; Yoh, S.-D.; Fujio, M.; Tsuno, Y., *Tetrahedron Lett.* **1997,** *38*, 3243−3246. (c) Kim, S. H.; Yoh, S.-D.; Lim, C.; Mishima, M.; Fujio, M.; Tsuno, Y., *J. Phys. Org. Chem.* **1998,** *11*, 254−260.

(92) Abraham, M. H., *J. Chem. Soc. B.* **1971**, 299−308.

(93) Carey, F. A.; Sundberg, R. J., Advanced organic chemistry: part A: structure and mechanisms (5th ed.). Springer Science & Business Media: 2007; p 414.

(94) Carey, F. A.; Sundberg, R. J., Advanced organic chemistry: part A: structure and mechanisms (5th ed.). Springer Science & Business Media: 2007; p 389−405.

(95) Bronsted, J., *Chem. Rev.* **1928,** *5*, 231−338.

(96) Hammett, L. P., *Chem. Rev.* **1935,** *17*, 125−136.

(97) Hammett, L. P., *J. Am. Chem. Soc.* **1937,** *59*, 96−103.

(98) Hansch, C.; Leo, A.; Taft, R., *Chem. Rev.* **1991,** *91*, 165−195.

(99) Grunwald, E.; Winstein, S., *J. Am. Chem. Soc.* **1948,** *70*, 846−854.

(100) Swain, C. G.; Scott, C. B., *J. Am. Chem. Soc.* **1953,** *75*, 141−147.

(101) (a) Edwards, J. O., *J. Am. Chem. Soc.* **1954,** *76*, 1540−1547. (b) Edwards, J. O., *J. Am. Chem. Soc.* **1956,** *78*, 1819−1820.

(102) Pearson, R. G.; Sobel, H. R.; Songstad, J., *J. Am. Chem. Soc.* **1968,** *90*, 319−326.

(103) (a) Ritchie, C. D., *Acc. Chem. Res.* **1972,** *5*, 348−354. (b) Ritchie, C. D.; Virtanen, P., *J. Am. Chem. Soc.* **1972,** *94*, 4966−4971.

(104) (a) Mayr, H.; Patz, M., *Angew. Chem., Int. Ed.* **1994,** *33*, 938−957. (b) Mayr, H.; Bug, T.; Gotta, M. F.; Hering, N.; Irrgang, B.; Janker, B.; Kempf, B.; Loos, R.; Ofial, A. R.; Remennikov, G.; Schimmel, H., *J. Am. Chem. Soc.* **2001,** *123*, 9500−9512. (c) Mayr, H.; Kempf, B.; Ofial, A. R., *Acc. Chem. Res.* **2003,** *36*, 66−77. (d) Mayr, H., *Tetrahedron* **2015,** *32*, 5095−5111.

(105) A database for reactivity parameters *E*, *N*,and s_N is freely accessible via http://www.cup.lmu.de/oc/mayr/DBintro.html.

(106) Minegishi, S.; Mayr, H., *J. Am. Chem. Soc.* **2003,** *125*, 286−295.

(107) Mayr, H.; Ammer, J.; Baidya, M.; Maji, B.; Nigst, T. A.; Ofial, A. R.; Singer, T., *J. Am. Chem. Soc.* **2015,** *137*, 2580−2599.

(108) (a) Denegri, B.; Streiter, A.; Jurić, S.; Ofial, A. R.; Kronja, O.; Mayr, H., *Chem. Eur. J.* **2006,** *12*, 1648−1656. (b) Streidl, N.; Denegri, B.; Kronja, O.; Mayr, H., *Acc. Chem. Res.* **2010,** *43*, 1537−1549.

(109) (a) Mayr, H.; Ofial, A. R., *Acc. Chem. Res.* **2016,** *49*, 952−965. (b) Mayr, H.; Ofial, A. R., *Pure Appl. Chem.* **2017,** *89*, 729−744.

(110) (a) Marcus, R. A., *Annu. Rev. Phys. Chem.* **1964,** *15*, 155−196. (b) Albery, W. J., *Annu. Rev. Phys. Chem.* **1980,** *31*, 227−263. (c) Marcus, R. A., *Pure Appl. Chem.* **1997,** *69*, 13−30.

(111) (a) Maji, B.; Duan, X.-H.; Jüstel, P. M.; Byrne, P. A.; Ofial, A. R.; Mayr, H., *Chem. Eur. J.* **2021**, *27*, 11367−11376. (b) Jurić, S.; Denegri, B.; Kronja, O., *J. Phys. Org. Chem.* **2012,** *25*, 147−152. (c) Jurić, S.; Denegri, B.; Kronja, O., *J. Org. Chem.* **2010,** *75*, 3851−3854.

(112) Troshin, K.; Schindele, C.; Mayr, H., *J. Org. Chem.* **2011,** *76*, 9391−9408.

(113) Troshin, K.; Mayr, H., *J. Org. Chem.* **2013,** *78*, 2649−2660.

Chapter 2. Nucleophilic Reactivities of Thiophenolates

Patrick M. Jüstel, Cedric D. Pignot, Armin R. Ofial, *J. Org. Chem.* **2021**, 86, 8 5965–5972.

Author Contributions

All experiments were performed by Patrick M. Jüstel or by Cedric D. Pignot under the supervision of Patrick M. Jüstel. The manuscript was written jointly by Patrick M. Jüstel and Armin R. Ofial.

2.1 Nucleophilic Reactivities of Thiophenolates

JOC The Journal of Organic Chemistry

pubs.acs.org/joc Note

Nucleophilic Reactivities of Thiophenolates

Patrick M. Jüstel, Cedric D. Pignot, and Armin R. Ofial*

Cite This: J. Org. Chem. 2021, 86, 5965–5972 Read Online

ACCESS | Metrics & More | Article Recommendations | Supporting Information

ABSTRACT: The nucleophilic reactivities of substituted thiophenolates were determined by following the kinetics of their reactions with a series of quinone methides (reference electrophiles) in DMSO at 20 °C. The experimentally determined second-order rate constants were analyzed according to the Mayr–Patz equation $\log k = s_N(N + E)$ to derive the nucleophile-specific reactivity parameters N and s_N for ten thiophenolate ions.

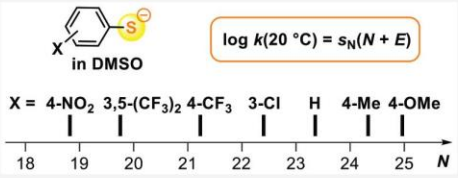

Sulfur nucleophiles are considered to be among the most reactive nucleophilic species. Importantly, the thiol moieties of cysteine (Cys) in proteins or in glutathione (GSH) are the reactive sites to trap xenobiotic Michael acceptors in cells.[1,2] Also the concept for the use of targeted covalent inhibitor drugs relies on the high reactivity of SH groups in peptides.[3−5] The nucleophilic reactivities of some aliphatic thiolates,[6] including Cys[7] and GSH[8] in aqueous solution, have recently been characterized utilizing Mayr's benzhydrylium methodology.[9]

It is common knowledge that also *aromatic* thiolates, that is, thiophenolates (ArS^-), are potent nucleophiles given that several Michael addition reactions to weak electrophiles have been reported.[10−14] Depletion kinetics of *p*-nitrothiophenolate (NBT) by electrophilic allergens were suggested as models to replace skin sensitization tests that use animals.[14] In addition, numerous kinetic studies of S_N2 reactions of ArS^- with $C(sp^3)$-centered electrophiles have been carried out to assess, for example, the effect of β-halogen atoms on the S_N2 reactivity of alkyl bromides,[15] the change in charge density at the electrophilic reaction center of substituted benzyl bromides,[16] and the susceptibility of the transition state structure on changes in the leaving group.[17] To characterize substituent effects on ArS^- reactivity, Bordwell and Hughes determined the rate constants for the reactions of several thiophenolates with *n*-butyl chloride in DMSO.[18] The influence of ion pairing on the reactivity of alkali metal thiophenolates toward *n*-butyl chloride in aq diglyme solutions was investigated by Fang and Westaway.[19]

Despite the fact that such quantitative data on the nucleophilic reactivity of ArS^- are at hand, the comparison of ArS^- with other types of nucleophiles, even with analogously substituted phenolates (ArO^-),[20] is hampered by a lack of kinetic data about ArS^- reactivity toward common reference electrophiles.

As we planned to use the UV-active thiophenolates ArS^- to investigate the reactivity of colorless electrophiles in future studies, we set out to calibrate their reactivity within the framework of Mayr's reactivity scales for polar reactions. The aryl-substituted *p*-quinone methides (*p*QMs) have repeatedly been used as reference electrophiles for reactions with anionic nucleophiles in DMSO,[21] a polar, non hydrogen bond donor solvent.[18b] We intended, therefore, to follow the kinetics of the 1,6-additions[22,23] of the X-substituted ArS^- **1a−j** (in DMSO) to the *p*QMs **2a−f** whose Mayr electrophilicity parameters E are known (Chart 1).[24]

Chart 1. Structures of Thiophenolates and *p*QMs Used in This Work

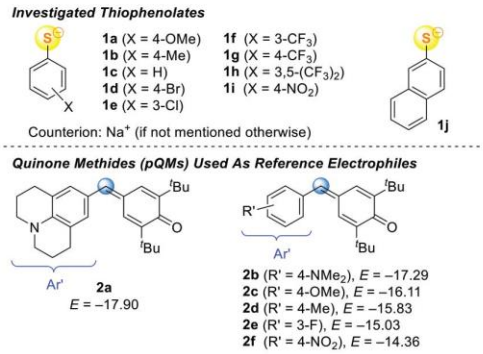

In a first step, we investigated the outcome of selected conjugate additions of ArS^- **1** to *p*QMs **2** (Scheme 1) in DMSO-d_6 by NMR spectroscopy and HRMS. Exclusive carbon−sulfur bond-formation was observed for the reactions of **1a−j** with the *p*QM **2d** to yield the adducts **4a−j**, and analogous thioethers **4k−o** resulted from the reactions of **1b**

Received: January 18, 2021
Published: April 2, 2021

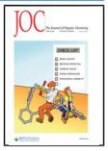

https://doi.org/10.1021/acs.joc.1c00025
J. Org. Chem. 2021, 86, 5965–5972

The Journal of Organic Chemistry pubs.acs.org/joc Note

Scheme 1. Reactions of Thiophenolates 1 with *p*QMs 2

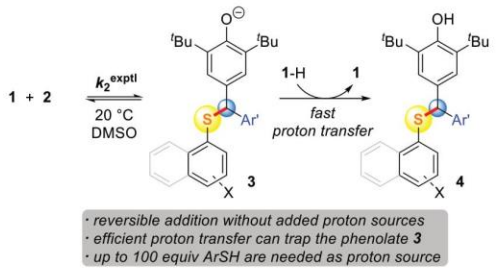

with a series of *p*QMs **2**. The reaction of **1b** with **2c** was performed at a 1 mmol scale and furnished **4m** in 88% yield after purification by column chromatography.

Analyzing the kinetics for the adduct formation with the Mayr–Patz eq 1 should allow one to assign the nucleophile-specific reactivity parameters N and s_N for the ArS^- ions **1** in DMSO solution.

$$\log k_2(20°C) = s_N(N + E) \quad (1)$$

Accordingly, the conjugate additions of the ArS^- **1** to the *p*QMs **2** were followed by using stopped-flow photometry to detect the absorption changes at or close to the *p*QMs' absorption maxima (λ_{max}) in DMSO at 20 °C.[25] Initial kinetic experiments indicated that the reactions did not go to completion but soon reached an equilibrium owing to reversible formation of the phenolate species **3** in the first step of the reaction (Scheme 1).

The relative Brønsted acidities of 2,6-di-*tert*-butylphenol (pK_a 17.3 in DMSO)[26] and thiophenols (pK_a 11.2 for the least acidic **1a**-H)[18] show that thiophenols **1**-H are capable to efficiently protonate the emerging phenolates **3**. In this way, **3** is removed from the equilibrium with the starting materials **1** and **2** and generates the phenols **4** in a fast, thermodynamically favorable step.

To define conditions under which protonation of **3** proceeds faster than the backward reaction to the educts **1** and **2**, we kept the ArS^-/*p*QM ratio in reactions of **1a** or **1c** with **2c** constant and varied the concentrations of the thiophenol additives **1**-H. Fitting the exponential decay function $A = A_0 \cdot \exp(-k_{obs}t) + C$ to the decrease of the absorbance of **2** furnished the first-order rate constants k_{obs} (s^{-1}). The rate constants k_{obs} steadily increased with increasing concentration of ArSH (**1**-H) and reached a plateau (within experimental error) when more than 100 equiv of **1a**-H or 40 equiv of **1c**-H were added to the reaction mixture (Supporting Information, Tables S2 and S3). This suggests that the first step in Scheme 1 becomes rate determining when >100 equiv of **1**-H are added to the reaction mixtures.

Trapping the phenolates **3** by a sufficient amount of **1**-H allowed us, therefore, to reliably determine the rate for the 1,6-conjugate addition of thiophenolate ions **1** to *p*QMs **2** (Figure 1a). By utilizing this procedure, the second-order rate constants k_2^{exptl} (M^{-1} s^{-1}) were obtained as the slopes of the linear correlations of k_{obs} with [**1**] (Figure 1b). The k_2^{exptl} values are gathered in Table 1 for all investigated reactions of **1** with the reference electrophiles **2**.

Changing the counterion for ArS^- from sodium to potassium or the addition of crown ethers affected the reactivity of ArS^- only insignificantly (Table 2 and Tables S36 and S37, Supporting Information,). We, therefore, used

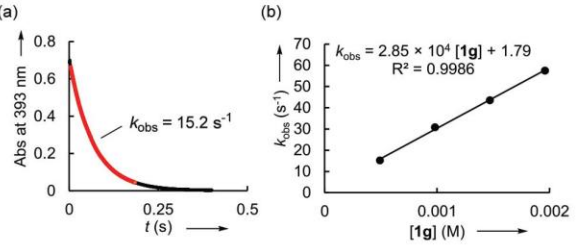

Figure 1. (a) Monoexponential decay of the absorbance A (at 393 nm) during the reaction of **1g** (c = 0.49 mM, counterion: K^+) with **2c** (c = 0.050 mM) in DMSO at 20 °C ($[\mathbf{1g}\text{-H}]_0$ = 5.0 mM). (b) Linear dependence of the first-order rate constant k_{obs} on [**1g**].

kinetic data originating from Na-**1** and K-**1** side by side in the following analysis.

Figure 2 illustrates that the rate constants log k_2^{exptl} for the reactions of the thiophenolates **1** with the *p*QMs **2** correlate linearly with the known electrophilicities E of **2**. As a consequence, the nucleophile-specific reactivity parameters N (and s_N) were determined for the thiophenolates **1** and listed in the second column of Table 1.

Reported kinetic and thermodynamic data on substituted thiophenolates are compiled in Table S1 (Supporting Information) and used for further correlations as depicted in Figures 3 and 4.

In Figure 3a, the nucleophilicities N for the entire set of investigated thiophenolates **1a**-**1j** are shown to correlate linearly with Hammett σ constants,[27] which allows for a straightforward prediction of nucleophilicities of further substituted ArS^- ions. Though on a somewhat smaller data basis, the Brønsted-type correlation of N parameters for **1** with the corresponding basicities pK_{aH}[18a] (Figure 3b) spans almost 6 pK_{aH} units and is of similar quality as the Hammett-type correlation depicted in Figure 3a.

Figure 4a reflects that the relative reactivities of ArS^- determined toward the sp^2-hybridized carbon-centers of the *p*QMs **2** can also beneficially be used to predict the reactivity ordering of ArS^- toward sp^3-hybridized electrophiles, such as *n*-butyl chloride, in S_N2 reactions.[18a]

When a common reference electrophile is chosen, for example the *p*QM **2c**, the reactivities of *p*-substituted ArS^- and analogous phenolates (ArO^-)[20] in DMSO at 20 °C can be compared (Figure 4b). The slope >1 indicates, however, that phenolates are more sensitive toward substituent effects than their sulfur analogues.

To define the scope of the reactivity parameters for ArS^- determined in this work, we extended our kinetic studies to further classes of neutral electrophiles. Given that the Mayr reactivity scales for polar reactions currently span over 40 magnitudes of reactivity, a precision within 2 orders of magnitude is usually observed when eq 1 is used for predictions.[9b,c,24] We calculated the rate constants k_2^{eq1} for reactions of **1a**, **1c**, and **1g** with the structurally diverse carbon-centered electrophiles **E1**–**E3** (Table 3)[28] and studied the corresponding kinetics experimentally.

Experimentally determined k_2^{exptl} and the predicted k_2^{eq1} agreed within a factor <15 indicating that the N/s_N parameters for ArS^-, which were calibrated against the *p*QMs **2** as the reference electrophiles, also allow one to estimate the reactivity of ArS^- ions toward further classes of neutral electrophiles, including the Michael acceptor **E1**[29] as well as the

https://doi.org/10.1021/acs.joc.1c00025
J. Org. Chem. 2021, 86, 5965–5972

The Journal of Organic Chemistry pubs.acs.org/joc Note

Table 1. Second-Order Rate Constants k_2^{exptl} for the Reactions of Thiophenolates 1 with the Reference Electrophiles 2 (in DMSO, at 20 °C)[a]

		k_2^{exptl} (M^{-1} s^{-1})					
ArS^-	N/s_N	**2a**	**2b**	**2c**	**2d**	**2e**	**2f**
1a	24.97/0.68	6.60×10^4	1.36×10^5	7.59×10^5	1.86×10^6	n.d.	n.d.
1b	24.35/0.69	3.31×10^4	6.67×10^4	4.96×10^5	8.65×10^5	n.d.	n.d.
1c	23.36/0.74	1.33×10^4	2.75×10^4	2.25×10^5	4.61×10^5	n.d.	n.d.
1j	22.55/0.83	n.d.	2.61×10^4	1.97×10^5	3.48×10^5	2.05×10^6	n.d.
1d	22.80/0.78	8.06×10^3	1.84×10^4	1.49×10^5	2.83×10^5	1.39×10^6	n.d.
1e	22.50/0.78	4.38×10^3	1.00×10^4	9.19×10^4	1.14×10^5	7.94×10^5	n.d.
1f	21.75/0.86	2.33×10^3	5.65×10^3	5.63×10^4	n.d.	6.41×10^5	n.d.
1g	21.30/0.86	8.16×10^2	2.63×10^3	2.75×10^4 [b]	5.46×10^4	2.78×10^5	7.76×10^5
1h	19.71/0.86	n.d.	n.d.	1.18×10^3	2.34×10^3	1.27×10^4	3.80×10^4
1i	18.92/0.87	n.d.	n.d.	2.52×10^2	5.15×10^2	2.66×10^3	8.50×10^3

[a]Kinetics determined in the presence of 5.0 mM of the corresponding thiol **1**-H (≙100 equiv of **1**-H relative to [**2**]); the experimental error in k_2 is assumed to be ±10%. [b]With Na^+ as the counterion of **1g**, the analogous kinetics with K-**1g** gave $k_2^{exptl} = 2.85 \times 10^4$ M^{-1} s^{-1} (Figure 1).

Table 2. Counterion Dependence of the Kinetics for the Reactions of the *p*QM 2c with Na/K-1a in DMSO[a] (20 °C)

reaction	crown ether	k_{obs} (s^{-1})
Na-**1a** + **2c**	none	$(1.06 \pm 0.01) \times 10^3$
Na-**1a** + **2c**	15-crown-5 (1.0 mM)	$(9.46 \pm 0.06) \times 10^2$
K-**1a** + **2c**	none	$(1.00 \pm 0.01) \times 10^3$
K-**1a** + **2c**	18-crown-6 (1.0 mM)	$(9.83 \pm 0.02) \times 10^2$

[a]Solutions of Na-**1a** and K-**1a** in DMSO were generated by deprotonation of **1a**-H with NaH and KO*t*Bu, respectively. Initial reactant concentrations were $[\mathbf{1a}]_0 = 1.0$ mM, $[\mathbf{1a}\text{-H}]_0 = 5.0$ mM, and $[\mathbf{2c}]_0 = 0.050$ mM. The kinetics were followed at 393 nm.

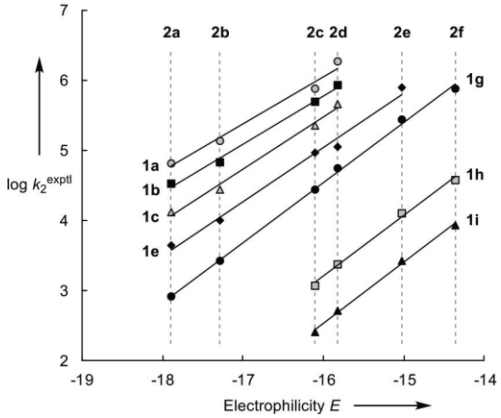

Figure 2. Determination of N/s_N for ArS^- (**1**) from the linear correlations of log k_2^{exptl} with the electrophilicities E of **2a**–**f**.

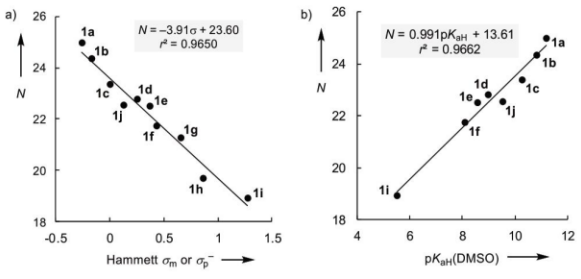

Figure 3. Linear relationships of $N(ArS^-)$ with (a) Hammett σ_m or σ_p^- substituent constants and (b) pK_{aH} (in DMSO).

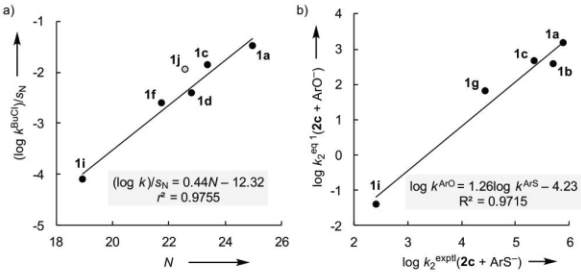

Figure 4. (a) Plot of (log k^{BuCl})/s_N for the reactions of **1** with *n*-butyl chloride (in DMSO, at 25 °C) vs the Mayr reactivities N; data for **1j** excluded when calculating the correlation line. (b) Linear correlation of the second-order rate constants for the reactions of phenolates (ArO^-) and thiophenolates (ArS^-) with the *p*QM **2c** in DMSO.

Table 3. Predicted and Experimentally Determined k_2 for Reactions of ArS^- (1) with E1–E3 (DMSO, 20 °C)

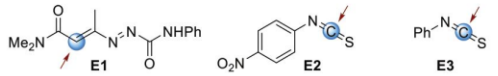

electrophile	ArS^-	k_2^{eq1} (M^{-1} s^{-1})	k_2^{exptl} (M^{-1} s^{-1})	k_2^{exptl}/k_2^{eq1}
E1	**1c**	8.0×10^5	7.19×10^5	1/1.1
E1	**1g**	1.2×10^5	8.78×10^4	1/1.4
E2	**1g**	4.5×10^4	5.69×10^5	13
E3	**1a**	4.3×10^4	4.75×10^4	1.1
E3	**1c**	7.2×10^3	4.90×10^3	1/1.5

heteroallenes **E2** and **E3** with C(sp)-hybridized electrophilic centers.[30]

In conclusion, we have used a set of *p*-quinone methides as reference electrophiles to characterize the Mayr nucleophilicity parameters N/s_N for meta- and para-substituted thiophenolates ArS^- in DMSO. Hammett- and Brønsted-type correlations of the nucleophilicities N make it possible to straightforwardly predict the reactivity of further thiophenolates. In addition, we have shown that applying the determined N/s_N values in eq 1 also holds for reactions of ArS^- with further types of neutral carbon-centered electrophiles.

In reactions of phenolate ions (ArO^-) with reference electrophiles, second-order rate constants in DMSO, acetonitrile, and DMF differed by less than 1 order of magnitude if the reference electrophile was kept constant.[20] We, therefore,

https://doi.org/10.1021/acs.joc.1c00025
J. Org. Chem. 2021, 86, 5965–5972

expect that the ArS^- reactivities in DMSO determined herein will be of value to predict reaction rates in other aprotic, polar solvents, such as MeCN. Thus, the comparison of thiophenolate reactivities with those of other S-nucleophiles, such as phenylsulfinate,[31] dithiocarbamates,[32] and dithiocarbonates[32] has now become possible within the framework of Mayr's reactivity scales (Figure 5).[24] The parent PhS^- (**1c**) is only slightly less reactive than the piperidine-1-carbodithioate (N = 23.8 in MeCN), the most reactive S-nucleophile characterized by N/s_N so far.[24] The donor-substituted thiophenolates **1b** and **1a** exceed the S-nucleophilicity of this dithiocarbamate.

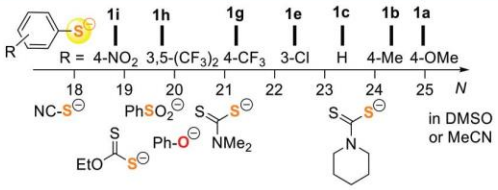

Figure 5. Nucleophilicity scale for sulfur-centered nucleophiles (and the parent phenolate ion) in aprotic polar solvents.

Given the UV−vis absorption of the thiophenolates,[25] we are currently investigating their capacity as reference nucleophiles in kinetic studies with colorless electrophiles.

EXPERIMENTAL SECTION

Chemicals. The thiophenols 4-methoxybenzenethiol (97%), 4-methylbenzenethiol (98%), benzenethiol (97%), and naphthalene-2-thiol (99%) were purchased from Sigma-Aldrich, 4-bromobenzenethiol (97%), 3-chlorobenzenethiol (>97%), and 3-(trifluoromethyl)-benzenethiol (>95%) from TCI, 4-(trifluoromethyl)benzenethiol (97%), 4-nitrobenzenethiol (96%), and 3,5-bis(trifluoromethyl)-benzenethiol (97%) from ABCR. The thiophenols were used without further purification. All thiophenols, KO*t*Bu (>98%, Acros Organics) and NaH (95%, Sigma-Aldrich) were stored in a glovebox under argon. Thiophenols were deprotonated with either KO*t*Bu or NaH prior to each use to give the potassium or sodium thiophenolates K-**1** and Na-**1**, respectively. The quinone methides **2** were prepared as described before.[21] **E1** was donated by the Attanasi group (Univ Urbino, Italy).[28a] 4-Nitrophenyl isothiocyanate (**E2**, >99.0%) was purchased from TCI. Phenyl isothiocyanate (**E3**) was purchased and purified by vacuum distillation prior to use. Silica gel plates with a F-254 fluorescence indicator were obtained from Merck and used for thin-layer chromatography. Flash column chromatography was performed with Merck silica gel 60 (0.040−0.063 mm) and distilled solvents.

Analytics. Nuclear magnetic resonance (NMR) spectra were recorded on 400 and 600 MHz spectrometers. Deuterated solvents were purchased from EurIsotop. The following abbreviations and their combinations are used in the analysis of NMR spectra: s = singlet, d = doublet, t = triplet, q = quartet, m = multiplet, br s = broad singlet. The ^{13}C NMR spectra were recorded under broad-band proton-decoupling. NMR signals were assigned based on information from additional 2D NMR experiments (COSY, gHSQC, gHMBC). Chemical shifts are given in ppm. Internal reference was set to the residual solvent signals (δ_H = 2.50 ppm, δ_C = 39.52 ppm for DMSO-d_6 and δ_H = 7.26 ppm, δ_C = 77.16 ppm for $CDCl_3$).[33]

Infrared (IR) spectra of neat samples were recorded on a PerkinElmer Spectrum BX-59343 instrument with a Smiths Detection DuraSamplIR II Diamond ATR sensor for detection in the range from 4500 to 600 cm^{-1}.

High-resolution mass spectra (HRMS) were acquired on a Thermo Finnigan LTQ FT Ultra Fourier transform ion cyclotron resonance, a Q-Exactive GC Orbitrap, a Finnigan MAT 95 or a Finnigan MAT 90 GC/MS. Samples were ionized either by electron impact (EI) or electron spray ionization (ESI).

UV−vis measurements were carried out using a J&M TIDAS diode array spectrophotometer, which was controlled by TIDASDAQ3 (v3) software and connected to a Hellma 661.502-QX quartz Suprasil immersion probe (light path d = 5 mm) via fiber optic cables and standard SMA connectors.

A DMSO solution of the thiophenol **1**-H was deprotonated (by NaH or KO*t*Bu) and added in multiple steps to a flask filled with DMSO. The increasing absorption of the solution was followed. The molar absorption coefficient ε was determined from the slope of the linear relationship of the absorbance (at λ_{max}) with [**1**], in accord with the Lambert−Beer law. All spectra were then normalized relative to the extinction coefficient at λ_{max} and are depicted in the Supporting Information.

Product Studies. *General Procedure.* A solution of the benzenethiol **1**-H (0.0408 mmol, in 0.1 mL DMSO-d_6) was partially (5%) deprotonated by adding an equal volume of a sodium dimsyl solution (19.5 mM in DMSO-d_6). The resulting **1**-H/Na-**1** mixture (0.2 mL) was mixed with a DMSO-d_6 solution of the *p*QM **2** (0.0389 mmol, in 1 mL). The color of the reaction mixture faded within seconds. Subsequently, the reaction mixture was analyzed by NMR spectroscopy and HRMS without further workup (see Supporting Information for atom labeling). NMR spectra of products **4** were usually found to be spectroscopically clean, indicating quantitative conversions (except for **4a** and **4i**, which show additional resonances caused by traces of starting materials).

*2,6-Di-tert-butyl-4-(((4-methoxyphenyl)thio)(p-tolyl)methyl)-phenol (**4a**).* According to the General Procedure, the thiophenol **1a**-H (5.7 mg, 0.041 mmol) and the *p*QM **2d** (12.0 mg, 0.0389 mmol) were mixed. The reaction mixture (in 1.2 mL DMSO-d_6) was analyzed by NMR spectroscopy and HRMS. ^1H NMR (600 MHz, DMSO-d_6) δ 7.32 (d, J = 8.1 Hz, 2 H, 9-H), 7.20 (d, J = 8.9 Hz, 2 H, 14-H), 7.10 (s, 2 H, 5-H), 7.09 (d, J = 7.9 Hz, 2 H, 10-H), 6.87 (s, 1 H, 1-OH), 6.77 (d, J = 8.9 Hz, 2 H, 15-H), 5.52 (s, 1 H, 7-H), 3.67 (s, 3 H, 17-H), 2.23 (s, 3 H, 12-H), 1.31 (s, 18 H, 4-H). $^{13}C\{^1H\}$ NMR (151 MHz, DMSO-d_6) δ 158.6 (C_q, C-16), 152.7 (C_q, C-1), 138.94 (C_q, C-8), 138.92 (C_q, C-2), 135.9 (C_q, C-11), 133.7 (CH, C-14), 132.1 (C_q, C-6), 128.9 (CH, C-10), 127.9 (CH, C-9), 125.7 (C_q, C-13), 124.2 (CH, C-5), 114.3 (CH, C-15), 57.1 (CH, C-7), 55.1 (CH, C-17), 34.5 (C_q, C-3), 30.3 (CH_3, C-4), 20.6 (CH_3, C-12) (additional resonances in the NMR spectra are caused by a slight excess of **1a**-H). HRMS (ESI) calcd m/z for $[C_{29}H_{35}O_2S^+]$ $[M - H^-]$ 447.2352, found 447.2360.

*2,6-Di-tert-butyl-4-(p-tolyl(p-tolylthio)methyl)phenol (**4b**).*[23a] According to the General Procedure, the thiophenol **1b**-H (5.1 mg, 0.041 mmol) and the *p*QM **2d** (12.0 mg, 0.0389 mmol) were mixed. The reaction mixture (in 1.2 mL DMSO-d_6) was analyzed by NMR spectroscopy and HRMS. ^1H NMR (600 MHz, DMSO-d_6) δ 7.35 (d, J = 8.1 Hz, 2 H, 9-H), 7.16 (d, J = 8.1 Hz, 2 H, 14-H), 7.14 (s, 2 H, 5-H), 7.08 (d, J = 7.9 Hz, 2 H, 10-H), 7.00 (d, J = 8.8 Hz, 2 H, 15-H), 6.89 (s, 1 H, 1-OH), 5.66 (s, 1 H, 7-H), 2.22 (s, 3 H, 12-H), 2.19 (s, 3 H, 17-H), 1.31 (s, 18 H, 4-H). $^{13}C\{^1H\}$ NMR (151 MHz, DMSO-d_6) δ 152.7 (C_q, C-1), 139.0 (C_q, C-2), 138.9 (C_q, C-8), 135.90 (C_q, C-11), 135.86 (C_q, C-16), 132.2 (C_q, C-13), 132.1 (C_q, C-6), 130.5 (CH, C-14), 129.4 (CH, C-15), 128.9 (CH, C-10), 127.8 (CH, C-9), 124.2 (CH, C-5), 55.6 (CH, C-7), 34.5 (C_q, C-3), 30.3 (CH_3, C-4), 20.6 (CH_3, C-12), 20.5 (CH_3, C-17). HRMS (ESI) calcd m/z for $[C_{29}H_{35}OS^+]$ $[M - H^-]$ 431.2403, found 431.2411.

*2,6-Di-tert-butyl-4-((phenylthio)(p-tolyl)methyl)phenol (**4c**).*[23b] According to the General Procedure, the thiophenol **1c**-H (4.5 mg, 0.041 mmol) and the *p*QM **2d** (12.0 mg, 0.0389 mmol) were mixed. The reaction mixture (in 1.2 mL DMSO-d_6) was analyzed by NMR spectroscopy and HRMS. ^1H NMR (600 MHz, DMSO-d_6) δ 7.38 (d, J = 8.1 Hz, 2 H, 9-H), 7.26 (dd, J = 8.4, 1.2 Hz, 2 H, 14-H), 7.19 (t, J = 7.6 Hz, 2 H, 15-H), 7.16 (s, 2 H, 5-H), 7.11 (dt, J = 8.0, 1.6 Hz, 1 H, 16-H), 7.09 (d, J = 7.9 Hz, 2 H, 10-H), 6.90 (s, 1 H, 1-OH), 5.75 (s, 1 H, 7-H), 2.23 (s, 3 H, 12-H), 1.32 (s, 18 H, 4-H). $^{13}C\{^1H\}$ NMR (151 MHz, DMSO-d_6) δ 152.8 (C_q, C-1), 139.1 (C_q, C-2), 138.8 (C_q, C-8), 136.03 (C_q, C-13), 135.99 (C_q, C-11), 131.9 (C_q, C-

https://doi.org/10.1021/acs.joc.1c00025
J. Org. Chem. 2021, 86, 5965−5972

6), 129.6 (CH, C-14), 129.0 (CH, C-10), 128.7 (CH, C-15), 127.8 (CH, C-9), 126.1 (CH, C-16), 124.2 (CH, C-5), 54.9 (CH, C-7), 34.5 (C_q, C-3), 30.3 (CH_3, C-4), 20.6 (CH_3, C-12). HRMS (ESI) calcd m/z for $[C_{28}H_{33}OS^+]$ $[M - H^-]$ 417.2247, found 417.2251.

*4-(((4-Bromophenyl)thio)(p-tolyl)methyl)-2,6-di-tert-butylphenol (**4d**).* According to the General Procedure, the thiophenol **1d**-H (7.7 mg, 0.041 mmol) and the *p*QM **2d** (12.0 mg, 0.0389 mmol) were mixed. The reaction mixture (in 1.2 mL DMSO-d_6) was analyzed by NMR spectroscopy and HRMS. ^{1}H NMR (600 MHz, DMSO-d_6) δ 7.37 (d, J = 8.6 Hz, 4 H, 9-H and 14/15-H), 7.21 (d, J = 8.6 Hz, 2 H, 14/15-H), 7.14 (s, 2 H, 5-H), 7.10 (d, J = 7.9 Hz, 2 H, 10-H), 6.92 (s, 1 H, 1-OH), 5.79 (s, 1 H, 7-H), 2.23 (s, 3 H, 12-H), 1.31 (s, 18 H, 4-H). $^{13}C\{^1H\}$ NMR (151 MHz, DMSO-d_6) δ 152.9 (C_q, C-1), 139.1 (C_q, C-2), 138.3 (C_q, C-8), 136.2 (C_q, C-11), 135.6 (C_q, C-13), 131.6 (CH, C-14 or C-15), 131.54 (C_q, C-6), 131.48 (CH, C-14 or C-15), 129.0 (CH, C-10), 127.8 (CH, C-9), 124.3 (CH, C-5), 119.2 (C_q, C-16), 54.9 (CH, C-7), 34.5 (C_q, C-3), 30.3 (CH_3, C-4), 20.6 (CH_3, C-12). HRMS (ESI) calcd m/z for $[C_{28}H_{32}{}^{79}BrOS^+]$ $[M - H^-]$ 495.1352, found 495.1357; calcd m/z for $[C_{28}H_{32}{}^{81}BrOS^+]$ $[M - H^-]$ 497.1331, found 497.1337.

*2,6-Di-tert-butyl-4-(((3-chlorophenyl)thio)(p-tolyl)methyl)phenol (**4e**).* According to the General Procedure, the thiophenol **1e**-H (5.9 mg, 0.041 mmol) and the *p*QM **2d** (12.0 mg, 0.0389 mmol) were mixed. The reaction mixture (in 1.2 mL DMSO-d_6) was analyzed by NMR spectroscopy and HRMS. ^{1}H NMR (600 MHz, DMSO-d_6) δ 7.40 (d, J = 8.1 Hz, 2 H, 9-H), 7.30 (s, 1 H, 18-H), 7.24–7.19 (m, 2 H, 14-H and 15-H), 7.18 (s, 2 H, 5-H), 7.16–7.14 (m, 1 H, 16-H), 7.12 (d, J = 8.0 Hz, 2 H, 10-H), 6.92 (s, 1 H, 1-OH), 5.88 (s, 1 H, 7-H), 2.24 (s, 3 H, 12-H), 1.32 (s, 18 H, 4-H). $^{13}C\{^1H\}$ NMR (151 MHz, DMSO-d_6) δ 152.9 (C_q, C-1), 139.1 (C_q, C-2), 138.6 (C_q, C-13), 138.3 (C_q, C-8), 136.2 (C_q, C-11), 133.2 (C_q, C-17), 131.5 (C_q, C-6), 130.2 (CH, C-15), 129.1 (CH, C-10), 128.5 (CH, C-18), 127.82 (CH, C-14), 127.78 (CH, C-9), 125.9 (CH, C-16), 124.4 (CH, C-5), 54.4 (CH, C-7), 34.6 (C_q, C-3), 30.3 (CH_3, C-4), 20.6 (CH_3, C-12). HRMS (ESI) calcd m/z for $[C_{28}H_{32}{}^{35}ClOS^+]$ $[M - H^-]$ 451.1857, found 451.1861; calcd m/z for $[C_{28}H_{32}{}^{37}ClOS^+]$ $[M - H^-]$ 453.1827, found 453.1831.

*2,6-Di-tert-butyl-4-(p-tolyl((3-(trifluoromethyl)phenyl)thio)-methyl)phenol (**4f**).* According to the General Procedure, the thiophenol **1f**-H (7.3 mg, 0.041 mmol) and the *p*QM **2d** (12.0 mg, 0.0389 mmol) were mixed. The reaction mixture (in 1.2 mL DMSO-d_6) was analyzed by NMR spectroscopy and HRMS. ^{1}H NMR (600 MHz, DMSO-d_6) δ 7.56 (d, J = 7.5 Hz, 1 H, 14-H), 7.51 (s, 1 H, 18-H), 7.44–7.41 (m, 2 H, 15-H, 16-H), 7.40 (d, J = 8.2 Hz, 2 H, 9-H), 7.20 (s, 2 H, 5-H), 7.12 (d, J = 7.9 Hz, 2 H, 10-H), 6.91 (s, 1 H, 1-OH), 5.94 (s, 1 H, 7-H), 2.23 (s, 3 H, 12-H), 1.31 (s, 18 H, 4-H). $^{13}C\{^1H\}$ NMR (151 MHz, DMSO-d_6) δ 152.9 (C_q, C-1), 139.1 (C_q, C-2), 138.1 (C_q, C-8), 137.9 (C_q, C-13), 136.3 (C_q, C-11), 133.3 (br, CH, C-14), 131.2 (C_q, C-6), 129.5 (CH, C-15), 129.4 (q, $J_{C,F}$ = 38 Hz, C_q, C-17), 129.1 (CH, C-10), 127.8 (CH, C-9), 125.6 (q, $J_{C,F}$ = 3.9 Hz, CH, C-18), 124.4 (CH, C-5), 123.8 (q, $J_{C,F}$ = 273 Hz, CF_3, C-19), 122.6 (q, $J_{C,F}$ = 3.7 Hz, CH, C-16), 54.5 (CH, C-7), 34.5 (C_q, C-3), 30.2 (CH_3, C-4), 20.6 (CH_3, C-12). HRMS (ESI) calcd m/z for $[C_{29}H_{32}F_3OS^+]$ $[M - H^-]$ 485.2120, found 485.2125.

*2,6-Di-tert-butyl-4-(p-tolyl((4-(trifluoromethyl)phenyl)thio)-methyl)phenol (**4g**).* According to the General Procedure, the thiophenol **1g**-H (7.3 mg, 0.041 mmol) and the *p*QM **2d** (12.0 mg, 0.0389 mmol) were mixed. The reaction mixture (in 1.2 mL DMSO-d_6) was analyzed by NMR spectroscopy and HRMS. ^{1}H NMR (600 MHz, DMSO-d_6) δ 7.53 (d, J = 8.3 Hz, 2 H, 15-H), 7.44–7.41 (m, 4 H, 9-H and 14-H), 7.17 (s, 2 H, 5-H), 7.12 (d, J = 7.9 Hz, 2 H, 10-H), 6.95 (s, 1 H, 1-OH), 5.97 (s, 1 H, 7-H), 2.23 (s, 3 H, 12-H), 1.31 (s, 18 H, 4-H). $^{13}C\{^1H\}$ NMR (151 MHz, DMSO-d_6) δ 153.0 (C_q, C-1), 142.4 (C_q, C-13), 139.2 (C_q, C-2), 138.1 (C_q, C-8), 136.3 (C_q, C-11), 131.3 (C_q, C-6), 129.1 (CH, C-10), 128.4 (CH, C-14), 127.7 (CH, C-9), 125.8 (q, $J_{C,F}$ = 32.0 Hz, C_q, C-16), 125.4 (q, $J_{C,F}$ = 3.7 Hz, CH, C-15), 124.3 (CH, C-5), 124.2 (q, $J_{C,F}$ = 272 Hz, C_q, C-17), 53.7 (CH, C-7), 34.6 (C_q, C-3), 30.3 (CH_3, C-4), 20.6 (CH_3, C-12). HRMS (ESI) calcd m/z for $[C_{29}H_{32}F_3OS^+]$ $[M - H^-]$ 485.2120, found 485.2124.

*4-(((3,5-Bis(trifluoromethyl)phenyl)thio)(p-tolyl)methyl)-2,6-di-tert-butylphenol (**4h**).* According to the General Procedure, the thiophenol **1h**-H (10.0 mg, 0.0408 mmol) and the *p*QM **2d** (12.0 mg, 0.0389 mmol) were mixed. The reaction mixture (in 1.2 mL DMSO-d_6) was analyzed by NMR spectroscopy and HRMS. ^{1}H NMR (400 MHz, DMSO-d_6) δ 7.86 (s, 2 H, 14-H), 7.76 (br s, 1 H, 16-H), 7.43–7.41 (m, 2 H, 9-H), 7.22 (s, 2 H, 5-H), 7.14 (d, J = 7.9 Hz, 2 H, 10-H), 6.91 (s, 1 H, 1-OH), 6.14 (s, 1 H, 7-H), 2.24 (s, 18 H, 4-H), 1.30 (s, 3 H, 12-H). $^{13}C\{^1H\}$ NMR (101 MHz, DMSO-d_6) δ 153.0 (C_q, C-1), 140.4 (C_q, C-13), 139.2 (C_q, C-2), 137.4 (C_q, C-8), 136.6 (C_q, C-11), 130.5 (C_q, C-6), 130.3 (q, $J_{C,F}$ = 32.9 Hz, C_q, C-15), 129.5 (br, CH, C-14), 129.2 (CH, C-10), 127.8 (CH, C-9), 124.5 (CH, C-5), 123.0 (q, $J_{C,F}$ = 273 Hz, C_q, C-17), 119.1 (br, CH, C-16), 54.2 (CH, C-7), 34.5 (C_q, C-3), 30.1 (CH_3, C-4), 20.6 (CH_3, C-12). HRMS (ESI) calcd m/z for $[C_{30}H_{31}F_6OS^+]$ $[M - H^-]$ 553.1994, found 553.2000.

*2,6-Di-tert-butyl-4-(((4-nitrophenyl)thio)(p-tolyl)methyl)phenol (**4i**).* According to the General Procedure, the thiophenol **1i**-H (6.3 mg, 0.041 mmol) and the *p*QM **2d** (12.0 mg, 0.0389 mmol) were mixed. The reaction mixture (in 1.2 mL DMSO-d_6) was analyzed by NMR spectroscopy and HRMS. ^{1}H NMR (400 MHz, DMSO-d_6) δ 8.03 (d, J = 9.0 Hz, 2 H, 15-H), 7.47–7.42 (m, 4 H, 9-H and 14-H), 7.20 (s, 2 H, 5-H), 7.13 (d, J = 7.9 Hz, 2 H, 10-H), 6.97 (s, 1 H, 1-OH), 6.09 (s, 1 H, 7-H), 2.24 (s, 3 H, 12-H), 1.32 (s, 18 H, 4-H). $^{13}C\{^1H\}$ NMR (101 MHz, DMSO-d_6) δ 153.1 (C_q, C-1), 147.0 (C_q, C-13), 144.6 (C_q, C-16), 139.3 (C_q, C-2), 137.7 (C_q, C-8), 136.4 (C_q, C-11), 130.9 (C_q, C-6), 129.2 (CH, C-10), 127.7 (CH, C-9), 127.4 (CH, C-14), 124.3 (CH, C-5), 123.6 (CH, C-15), 53.3 (CH, C-7), 34.5 (C_q, C-3), 30.2 (CH_3, C-4), 20.6 (CH_3, C-12) (additional resonances are caused by a slight excess of the *p*QM **2d**). HRMS (ESI) calcd m/z for $[C_{28}H_{32}NO_3S^+]$ $[M - H^-]$ 462.2097, found 462.2101.

*2,6-Di-tert-butyl-4-((naphthalen-2-ylthio)(p-tolyl)methyl)phenol (**4j**).* According to the General Procedure, the thiophenol **1j**-H (6.5 mg, 0.041 mmol) and the *p*QM **2d** (12.0 mg, 0.0389 mmol) were mixed. The reaction mixture (in 1.2 mL DMSO-d_6) was analyzed by NMR spectroscopy and HRMS. ^{1}H NMR (600 MHz, DMSO-d_6) δ 7.80 (d, J = 8.0 Hz, 1 H, 17-H), 7.79–7.78 (m, 1 H, 22-H), 7.74 (d, J = 8.7 Hz, 1 H, 15-H), 7.69 (d, J = 8.2, 1 H, 20-H), 7.47–7.40 (m, 5 H, 9-H, 14-H, 18-H, 19-H), 7.22 (s, 2 H, 5-H), 7.09 (d, J = 8.0 Hz, 2 H, 10-H), 6.90 (s, 1 H, 1-OH), 5.93 (s, 1 H, 7-H), 2.21 (s, 3 H, 12-H), 1.31 (s, 18 H, 4-H). $^{13}C\{^1H\}$ NMR (151 MHz, DMSO-d_6) δ 152.8 (C_q, C-1), 139.1 (C_q, C-2), 138.7 (C_q, C-8), 136.1 (C_q, C-11), 133.6 (C_q, C-13), 133.1 (C_q, C-21), 131.9 (C_q, C-6), 131.3 (C_q, C-16), 129.0 (CH, C-10), 128.0 (CH, C-15), 127.9 (CH, C-9), 127.8 (C_q, C-22), 127.7 (CH, C-18), 127.5 (CH, C-17), 126.9 (CH, C-20), 126.5 (CH, C-19), 125.8 (CH, C-14), 124.3 (CH, C-5), 54.8 (CH, C-7), 34.5 (C_q, C-3), 30.3 (CH_3, C-4), 20.6 (CH_3, C-12). HRMS (ESI) calcd m/z for $[C_{32}H_{35}OS^+]$ $[M - H^-]$ 467.2403, found 467.2409.

*2,6-Di-tert-butyl-4-((julolidin-9-yl)(p-tolylthio)methyl)phenol (**4k**).* According to the General Procedure, the thiophenol **1b**-H (6.3 mg, 0.041 mmol) and the *p*QM **2a** (15.2 mg, 0.0389 mmol) were mixed. The reaction mixture (in 1.2 mL DMSO-d_6) was analyzed by NMR spectroscopy and HRMS. ^{1}H NMR (400 MHz, DMSO-d_6) δ 7.14–7.11 (m, 4 H, 5-H and 16-H), 7.00 (d, J = 8.0 Hz, 2 H, 17-H), 6.82 (s, 1 H, 1-OH), 6.79 (s, 2 H, 9-H), 5.38 (s, 1 H, 7-H), 3.05–3.03 (m, 4 H, 14-H), 2.61 (t, J = 6.4 Hz, 4 H, 12-H), 2.20 (s, 3 H, 19-H), 1.82 (pent, J = 6.4 Hz, 4 H, 13-H), 1.31 (s, 18 H, 4-H). $^{13}C\{^1H\}$ NMR (101 MHz, DMSO-d_6) δ 152.4 (C_q, C-1), 141.6 (C_q, C-11), 138.8 (C_q, C-2), 135.6 (C_q, C-18), 132.8 (C_q, C-15), 132.7 (C_q, C-6), 130.5 (CH, C-16), 129.3 (CH, C-17), 128.2 (C_q, C-8), 126.2 (CH, C-9), 124.2 (CH, C-5), 120.6 (C_q, C-10), 56.0 (CH, C-7), 49.2 (CH_2, C-14), 34.5 (C_q, C-3), 30.3 (CH_3, C-4), 27.2 (CH_2, C-12), 21.6 (CH_2, C-13), 20.5 (CH_3, C-19). HRMS (ESI) calcd m/z for $[C_{34}H_{44}NOS^+]$ $[M + H^+]$ 514.3138, found 514.3139.

*2,6-Di-tert-butyl-4-((4-(dimethylamino)phenyl)(p-tolylthio)-methyl)phenol (**4l**).* According to the General Procedure, the thiophenol **1b**-H (6.3 mg, 0.041 mmol) and the *p*QM **2b** (13.1 mg, 0.0389 mmol) were mixed. The reaction mixture (in 1.2 mL DMSO-

https://doi.org/10.1021/acs.joc.1c00025
J. Org. Chem. 2021, 86, 5965–5972

d_6) was analyzed by NMR spectroscopy and HRMS. ^{1}H NMR (400 MHz, DMSO-d_6) δ 7.26 (d, J = 8.7 Hz, 2 H, 9-H), 7.16−7.14 (m, 4 H, 5-H, 14-H), 7.00 (d, J = 8.0 Hz, 2 H, 15-H), 6.87 (s, 1 H, 1-OH), 6.62 (d, J = 8.8 Hz, 2 H, 10-H), 5.57 (s, 1 H, 7-H), 2.83 (s, 6 H, 12-H), 2.19 (s, 3 H, 17-H), 1.32 (s, 18 H, 4-H). ^{13}C{^{1}H} NMR (101 MHz, DMSO-d_6) δ 152.5 (C_q, C-1), 149.2 (C_q, C-11), 138.9 (C_q, C-2), 135.6 (C_q, C-16), 132.7 (C_q, C-6), 132.6 (C_q, C-13), 130.4 (CH, C-14), 129.3 (CH, C-15), 129.1 (C_q, C-8), 128.5 (CH, C-9), 124.1 (CH, C-5), 112.1 (CH, C-10), 55.6 (CH, C-7), 40.1 (CH_3, C-12), 34.5 (C_q, C-3), 30.3 (CH_3, C-4), 20.5 (CH_3, C-17). HRMS (ESI) calcd m/z for $[C_{30}H_{40}NOS^+]$ $[M + H^+]$ 462.2825, found 462.2827.

*2,6-Di-tert-butyl-4-((4-methoxyphenyl)(p-tolylthio)methyl)-phenol (**4m**).*[23a] A solution of the thiol **1b**-H (128 mg, 1.03 mmol) in acetonitrile (1 mL) was mixed with a suspension of sodium hydride in DMSO (0.72 mg, 0.03 mmol in 1 mL). After gas formation had ceased, a DMSO solution of the *p*QM **2c** (324.5 mg, 1.00 mmol in 23 mL) was added to the reaction mixture. The color of the solution changed from yellow to green within a few seconds. After another 5 min of stirring, the solution was acidified by addition of two drops of aq HCl (2 M) to produce a solution of yellow color. Evaporation of the volatiles (in the vacuum) furnished a crude material, which was purified by column chromatography (silica gel, eluent: ethyl acetate/*n*-pentane = 5/95) to yield **4m** (393 mg, 88%) as a yellow solid. R_f 0.55 (ethyl acetate/*n*-pentane = 5/95). mp 112−114 °C. ^{1}H NMR (400 MHz, $CDCl_3$) δ 7.37 (d, J = 8.7 Hz, 2 H, 9-H), 7.13−7.11 (m, 4 H, 5-H and 14-H), 6.98 (d, J = 8.3 Hz, 2 H, 15-H), 6.84 (d, J = 8.6 Hz, 2 H, 10-H), 5.36 (s, 1 H, 7-H), 5.11 (s, 1 H, 1-OH), 3.79 (s, 3 H, 12-H), 2.27 (s, 3 H, 17-H), 1.39 (s, 18 H, 4-H). ^{13}C{^{1}H} NMR (101 MHz, $CDCl_3$) δ 158.6 (C_q, C-11), 152.9 (C_q, C-1), 136.8 (C_q, C-16), 135.7 (C_q, C-2), 134.0 (C_q, C-8), 132.8 (C_q, C-13), 132.1 (CH, C-14), 132.0 (C_q, C-6), 129.6 (CH, C-9), 129.5 (CH, C-15), 125.2 (CH, C-5), 113.8 (CH, C-10), 58.0 (CH, C-7), 55.4 (CH_3, C-12), 34.5 (C_q, C-3), 30.4 (CH_3, C-4), 21.2 (CH_3, C-17). IR (ATR probe, neat) $\tilde{\nu}$ 3592, 2952, 1721, 1609, 1512, 1485, 1431, 1234, 1207, 1175, 1132, 1118, 1111, 1026, 891, 841, 809, 792, 778, 739 cm^{-1}. HRMS (ESI) calcd m/z for $[C_{29}H_{35}O_2S^+]$ $[M - H^-]$ 447.2352, found 447.2357. Anal. Calcd for $C_{29}H_{36}O_2S$: C, 77.63; H, 8.09; S, 7.15. Found: C, 77.67; H, 8.15; S, 6.97.

*2,6-Di-tert-butyl-4-((3-fluorophenyl)(p-tolylthio)methyl)phenol (**4n**).* According to the General Procedure, the thiophenol **1b**-H (6.3 mg, 0.041 mmol) and the *p*QM **2e** (12.2 mg, 0.0389 mmol) were mixed. The reaction mixture (in 1.2 mL DMSO-d_6) was analyzed by NMR spectroscopy and HRMS. ^{1}H NMR (600 MHz, DMSO-d_6) δ 7.33−7.31 (m, 2 H, 12-H and 13-H), 7.28−7.27 (m, 1 H, 9-H), 7.19 (d, J = 8.1 Hz, 2 H, 15-H), 7.16 (s, 2 H, 5-H), 7.02 (d, J = 8.0 Hz, 2 H, 16-H), 7.01−6.99 (m, 1 H, 11-H), 6.96 (s, 1 H, 1-OH), 5.77 (s, 1 H, 7-H), 2.19 (s, 3 H, 18-H), 1.33 (s, 18 H, 4-H). ^{13}C{^{1}H} NMR (151 MHz, DMSO-d_6) δ 162.0 (d, $J_{C,F}$ = 244 Hz, C_q, C-10), 153.0 (C_q, C-1), 144.9 (d, $J_{C,F}$ = 6.9 Hz, C_q, C-8), 139.2 (C_q, C-2), 136.2 (C_q, C-17), 131.6 (C_q, C-14), 131.2 (C_q, C-6), 130.7 (CH, C-15), 130.3 (d, $J_{C,F}$ = 8.3 Hz, CH, C-12), 129.4 (CH, C-16), 124.3 (CH, C-5), 124.1 (CH, C-13), 114.6 (d, $J_{C,F}$ = 21.9 Hz, CH, C-9), 113.7 (d, $J_{C,F}$ = 20.9 Hz, CH, C-11), 55.2 (CH, C-7), 34.6 (C_q, C-3), 30.3 (CH_3, C-4), 20.5 (CH_3, C-18). HRMS (ESI) calcd m/z for $[C_{28}H_{32}FOS^+]$ $[M - H^-]$ 435.2152, found 435.2154; calcd m/z for $[C_{28}H_{32}FOS^-]$ $[M - H^+]$ 435.2163, found 435.2163.

*2,6-Di-tert-butyl-4-((4-nitrophenyl)(p-tolylthio)methyl)phenol (**4o**).*[23a] According to the General Procedure, the thiophenol **1b**-H (6.3 mg, 0.041 mmol) and the *p*QM **2f** (13.2 mg, 0.0389 mmol) were mixed. The reaction mixture (in 1.2 mL DMSO-d_6) was analyzed by NMR spectroscopy and HRMS. ^{1}H NMR (400 MHz, DMSO-d_6) δ 8.14 (d, J = 8.6 Hz, 2 H, 10-H), 7.75 (d, J = 8.6 Hz, 2 H, 9-H), 7.22 (d, J = 7.9 Hz, 2 H, 13-H), 7.19 (s, 2 H, 5-H), 7.02 (d, J = 8.2 Hz, 2 H, 14-H), 5.95 (s, 1 H, 7-H), 2.19 (s, 3 H, 16-H), 1.33 (s, 18 H, 4-H). ^{13}C{^{1}H} NMR (151 MHz, DMSO-d_6) δ 153.2 (C_q, C-1), 149.9 (C_q, C-8), 146.2 (C_q, C-11), 139.4 (C_q, C-2), 136.5 (C_q, C-15), 131.1 (C_q, C-12), 130.9 (CH, C-13), 130.6 (C_q, C-6), 129.6 (CH, C-14), 129.2 (CH, C-9), 124.3 (CH, C-5), 123.6 (CH, C-10), 55.0 (CH, C-7), 34.6 (C_q, C-3), 30.2 (CH_3, C-4), 20.5 (CH_3, C-16). HRMS (ESI) calcd m/z for $[C_{28}H_{32}NO_3S^-]$ $[M - H^+]$ 462.2108, found 462.2110.

*(E)-2-(4-(Dimethylamino)-4-oxo-3-(phenylthio)butan-2-ylidene)-N-phenylhydrazine-1-carboxamide (**5**).* In analogy to the General Procedure, the thiophenol **1c**-H (7.6 mg, 0.069 mmol) and the electrophile **E1** (17.0 mg, 0.0653 mmol) were mixed. The reaction mixture (in 0.6 mL DMSO-d_6) was analyzed by NMR spectroscopy and HRMS. ^{1}H NMR (400 MHz, DMSO-d_6, + 20 °C) δ 9.73 (br s, 1 H, 8-H), 8.55 (s, 1 H, 10-H), 7.50−7.48 (m, 4 H, 12-H and 16-H), 7.31−7.27 (m, 4 H, 13-H and 17-H), 7.19 (t, J = 7.4 Hz, 1 H, 14-H), 7.01 (t, J = 7.3 Hz, 1 H, 18-H), 5.35 (s, 1 H, 4-H), 3.11 and 2.87 (2 s, 2 × 3 H, 1-H and 2-H), 1.92 (s, 3 H, 6-H). ^{13}C{^{1}H} NMR (101 MHz, DMSO-d_6, at +80 °C) δ 166.3 (C_q, C-3), 152.6 (C_q, C-9), 144.9 (C_q, C-5), 138.5 (C_q, C-15), 133.3 (C_q, C-11), 131.3 (CH, C-12), 128.4 (CH, C-13), 128.2 (CH, C-17), 126.9 (CH, C-14), 122.1 (CH, C-18), 118.9 (CH, C-16), 57.2 (CH, C-4), 36.9 and 35.3 (2 × CH_3, C-1 or C-2), 12.5 (CH_3, C-6). HRMS (EI) calcd m/z for $[C_{19}H_{22}N_4O_2S^{\bullet+}]$ $[M^{\bullet+}]$ 370.1458, found 370.1452.

Kinetics. Kinetic measurements were performed on Applied Photophysics SX.20 stopped-flow UV−vis photometric systems. The temperature (20.0 ± 0.2 °C) was maintained constant by using circulating bath cryostats. All solutions were freshly prepared under an atmosphere of dry argon by using dry DMSO (over molecular sieves, Acros Organics).

To achieve pseudo-first-order kinetics, the ArS^- concentrations were kept constant through thiophenolate regeneration from thiophenols or chosen at least ten times higher than the electrophile concentrations. The rates of the consumption of the *p*QMs (λ_{max} = 354−520 nm)[25] were followed photometrically at or close to their absorption maxima. Due to an overlap of the absorption bands with the thiophenolates,[25] the absorbances did not reach zero in all reactions investigated. Rate constants were obtained from the kinetics by least-squares fitting of the absorbance A with the equation $A_t = A_0 e^{-k_{obs}t} + C$.

The kinetics of the reactions of K-**1g** with **E2** gave rise to formation of a colored product whose increasing absorption was followed at 440 nm. The rates of product formation were also detected in the kinetics of reactions of K-**1a** and K-**1c** with **E3** (at λ = 320−326 nm), respectively, which were performed with excess concentrations of **E3** (>10 equiv). Least-squares fitting of the function $A_t = A_0 \cdot (1 - e^{-k_{obs}t}) + C$ to the increasing absorptions of the solutions furnished k_{obs}.

Plots of k_{obs} versus [ArS^-] (or [**E3**]) gave k_2 as the slopes of the linear correlations.

■ ASSOCIATED CONTENT

Supporting Information

The Supporting Information is available free of charge at https://pubs.acs.org/doi/10.1021/acs.joc.1c00025.

Additional data used for correlations, details on kinetic measurements, and copies of NMR spectra (PDF)

■ AUTHOR INFORMATION

Corresponding Author

Armin R. Ofial − *Department Chemie, Ludwig-Maximilians-Universität München, 81377 München, Germany;* orcid.org/0000-0002-9600-2793; Email: ofial@lmu.de

Authors

Patrick M. Jüstel − *Department Chemie, Ludwig-Maximilians-Universität München, 81377 München, Germany*

Cedric D. Pignot − *Department Chemie, Ludwig-Maximilians-Universität München, 81377 München, Germany*

Complete contact information is available at: https://pubs.acs.org/10.1021/acs.joc.1c00025

https://doi.org/10.1021/acs.joc.1c00025
J. Org. Chem. 2021, 86, 5965−5972

Notes

The authors declare no competing financial interest.

■ ACKNOWLEDGMENTS

We thank the Department Chemie (LMU München) for financial support, Nathalie Hampel for preparing the *p*QMs, and Professor Herbert Mayr for helpful discussions.

■ REFERENCES

(1) (a) Weerapana, E.; Wang, C.; Simon, G.; Richter, F.; Khare, S.; Dillon, M. B. D.; Bachovchin, D. A.; Mowen, K.; Baker, D.; Cravatt, B. F. Quantitative reactivity profiling predicts functional cysteines in proteomes. *Nature* **2010**, *468*, 790−795. (b) Wang, C.; Weerapana, E.; Blewett, M.; Cravatt, B. F. A chemoproteomic platform to quantitatively map targets of lipid-derived electrophiles. *Nat. Methods* **2014**, *11*, 79−85.

(2) *Glutathione: Biosynthesis, Functions and Biological Implications*; Perjési, P., Ed.; Nova Science Publishers, 2019.

(3) Wright, M. H.; Sieber, S. A. Chemical proteomics approaches for identifying the cellular targets of natural products. *Nat. Prod. Rep.* **2016**, *33*, 681−708.

(4) Jackson, P. A.; Widen, J. C.; Harki, D. A.; Brummond, K. M. Covalent Modifiers: A Chemical Perspective on the Reactivity of α,β-Unsaturated Carbonyls with Thiols via Hetero-Michael Addition Reactions. *J. Med. Chem.* **2017**, *60*, 839−885.

(5) Lonsdale, R.; Burgess, J.; Colclough, N.; Davies, N. L.; Lenz, E. M.; Orton, A. L.; Ward, R. A. Expanding the Armory: Predicting and Tuning Covalent Warhead Reactivity. *J. Chem. Inf. Model.* **2017**, *57*, 3124−3137.

(6) Minegishi, S.; Mayr, H. How Constant Are Ritchie's "Constant Selectivity Relationships"? A General Reactivity Scale for n-, π-, and σ-Nucleophiles. *J. Am. Chem. Soc.* **2003**, *125*, 286−295.

(7) Brotzel, F.; Mayr, H. Nucleophilicities of amino acids and peptides. *Org. Biomol. Chem.* **2007**, *5*, 3814−3820.

(8) Mayer, R. J.; Ofial, A. R. Nucleophilicity of Glutathione: A Link to Michael Acceptor Reactivities. *Angew. Chem., Int. Ed.* **2019**, *58*, 17704−17708.

(9) (a) Mayr, H.; Patz, M. Scales of Nucleophilicity and Electrophilicity: A System for Ordering Polar Organic and Organometallic Reactions. *Angew. Chem., Int. Ed. Engl.* **1994**, *33*, 938−957. (b) Mayr, H.; Ofial, A. R. A Quantitative Approach to Polar Organic Reactivity. *SAR QSAR Environ. Res.* **2015**, *26*, 619−646. (c) Mayr, H. Reactivity Scales for Quantifying Polar Organic Reactivity: The Benzhydrylium Methodology. *Tetrahedron* **2015**, *71*, 5095−5111.

(10) Kuwajima, I.; Murofushi, T.; Nakamura, E. Quaternary Ammonium Fluoride-Catalyzed Conjugate Addition of Thiols to C = C Double Bonds. *Synthesis* **1976**, 602−604.

(11) Campbell, M. M.; Jigajinni, V. B.; Wightman, R.H. Michael Additions to Steroidal 1-Ene-3-ones. *Tetrahedron Lett.* **1979**, *20*, 2455−2456.

(12) Bakuzis, P.; Bakuzis, M. L. F. Oxidative Functionalization of the β-Carbon in α,β-Unsaturated Systems. Preparation of 3-Phenylthio Enones, Acrylates, and Other Vinyl Derivatives. *J. Org. Chem.* **1981**, *46*, 235−239.

(13) Mudryk, B.; Cohen, T. Generation, Some Synthetic Uses, and 1,2-Vinyl Rearrangements of Secondary and Tertiary Homoallyllithiums, Including Ring Contractions and A Ring Expansion. Remarkable Acceleration of the Rearrangement by an Oxyanionic Group. *J. Am. Chem. Soc.* **1993**, *115*, 3855−3865.

(14) (a) Chipinda, I.; Ajibola, R. O.; Morakinyo, M. K.; Ruwona, T. B.; Simoyi, R. H.; Siegel, P. D. Rapid and Simple Kinetics Screening Assay for Electrophilic Dermal Sensitizers Using Nitrobenzenethiol. *Chem. Res. Toxicol.* **2010**, *23*, 918−925. (b) Mbiya, W.; Chipinda, I.; Siegel, P. D.; Mhike, M.; Simoyi, R. H. Substituent Effects on the Reactivity of Benzoquinone Derivatives with Thiols. *Chem. Res. Toxicol.* **2013**, *26*, 112−123.

(15) Hine, J.; Brader, W. H., Jr. The Effect of Halogen Atoms on the Reactivity of Other Halogen Atoms in the Same Molecule. III. The S_N2 Reactivity of Ethylene Halides. *J. Am. Chem. Soc.* **1953**, *75*, 3964−3966.

(16) Hudson, R. F.; Klopman, G. Nucleophilic reactivity. Part II. The reaction between substituted thiophenols and benzyl bromides. *J. Chem. Soc.* **1962**, 1062−1067.

(17) Westaway, C.; Ali, S. F. Isotope effects in nucleophilic substitution reactions. III. The effect of changing the leaving group on transition state structure in S_N2 reactions. *Can. J. Chem.* **1979**, *57*, 1354−1367.

(18) (a) Bordwell, F. G.; Hughes, D. L. Thiol Acidities and Thiolate Ion Reactivities toward Butyl Chloride in Dimethyl Sulfoxide Solution. The Question of Curvature in Brønsted Plots. *J. Org. Chem.* **1982**, *47*, 3224−3232. (b) For a discussion on the advantageous solvent properties of DMSO for studying reactions that involve neutral organic molecules, anions, and cations, see: Bordwell, F. G.; Branca, J. C.; Hughes, D. L.; Olmstead, W. N. Equilibriums involving organic anions in dimethyl sulfoxide and N-methylpyrrolidin-2-one: acidities, ion pairing, and hydrogen bonding. *J. Org. Chem.* **1980**, *45*, 3305−3313.

(19) Fang, Y.-R.; Westaway, K. C. Isotope effects in nucleophilic substitution reactions. VIII. The effect of the form of the reacting nucleophile on the transition state structure of an S_N2 reaction. *Can. J. Chem.* **1991**, *69*, 1017−1021.

(20) Mayer, R. J.; Breugst, M.; Hampel, N.; Ofial, A. R.; Mayr, H. Ambident Reactivity of Phenolate Anions Revisited: A Quantitative Approach to Phenolate Reactivities. *J. Org. Chem.* **2019**, *84*, 8837−8858.

(21) (a) Lucius, R.; Loos, R.; Mayr, H. Kinetic Studies of Carbocation−Carbanion Combinations: Key to a General Concept of Polar Organic Reactivity. *Angew. Chem., Int. Ed.* **2002**, *41*, 91−95. (b) Richter, D.; Hampel, N.; Singer, T.; Ofial, A. R.; Mayr, H. Synthesis and Characterization of Novel Quinone Methides: Reference Electrophiles for the Construction of Nucleophilicity Scales. *Eur. J. Org. Chem.* **2009**, 3203−3211.

(22) Jadhav, A. S.; Anand, R. V. Triflic Acid Catalyzed 1,6-Conjugate Addition of Thiols to *p*-Quinone Methides under Continuous-Flow Conditions. *Eur. J. Org. Chem.* **2017**, 3716−3721.

(23) (a) Liang, X.; Xu, H.; Li, H.; Chen, L.; Lu, H. Recyclable Bismuth Complex Catalyzed 1,6-Conjugate Addition of Various Nucleophiles to *para*-Quinone Methides: Expedient Access to Unsymmetrical Diaryl- and Triarylmethanes. *Eur. J. Org. Chem.* **2020**, 217−226. (b) Xiong, B.; Xu, S.; Liu, Y.; Tang, K.-W.; Wong, W.-Y. Metal-Free, Acid/Phosphine-Induced Regioselective Thiolation of *p*-Quinone Methides with Sodium Aryl/Alkyl Sulfinates. *J. Org. Chem.* **2021**, *86*, 1516−1527.

(24) A database of Mayr's reactivity parameters *E*, *N*, and s_N is freely accessible at www.cup.lmu.de/oc/mayr/DBintro.html.

(25) See the Supporting Information for UV−vis spectra of the thiophenolates **1** and *p*QMs **2**.

(26) Bordwell, F. G.; Cheng, J.-P. Substituent Effects on the Stabilities of Phenoxyl Radicals and the Acidities of Phenoxyl Radical Cations. *J. Am. Chem. Soc.* **1991**, *113*, 1736−1743.

(27) Hansch, C.; Leo, A.; Hoekman, D. *Exploring QSAR—Hydrophobic, Electronic, and Steric Constants*; ACS Professional Reference Book; American Chemical Society: Washington, D.C., 1995.

(28) (a) Kanzian, T.; Nicolini, S.; De Crescentini, L.; Attanasi, O. A.; Ofial, A. R.; Mayr, H. Electrophilic Reactivities of 1,2-Diaza-1,3-dienes. *Chem. - Eur. J.* **2010**, *16*, 12008−12016. (b) Li, Z.; Mayer, R. J.; Ofial, A. R.; Mayr, H. From Carbodiimides to Carbon Dioxide: Quantification of the Electrophilic Reactivities of Heteroallenes. *J. Am. Chem. Soc.* **2020**, *142*, 8383−8402.

(29) (a) Attanasi, O. A.; De Crescentini, L.; Favi, G.; Filippone, P.; Mantellini, F.; Perrulli, F. R.; Santeusanio, S. Cultivating the Passion to Build Heterocycles from 1,2-Diaza-1,3-dienes: the Force of Imagination. *Eur. J. Org. Chem.* **2009**, 3109−3127. (b) NMR spectroscopic investigation of the reaction of **1c** with **E1** in DMSO-d_6 confirmed the formation of the adduct **5** (Experimental Section and Supporting Information).

https://doi.org/10.1021/acs.joc.1c00025
J. Org. Chem. 2021, 86, 5965−5972

(30) (a) Chen, N.; Zhong, X.; Li, P.; Xu, J. A Mild Radical Method for the Dimerzation of Dithiocarbamates. *Eur. J. Org. Chem.* **2015**, 802−809. (b) Hagooly, Y.; Gatenyo, J.; Hagooly, A.; Rozen, S. Toward the Synthesis of the Rare *N*-(Trifluoromethyl)amides and the *N*-(Difluoromethylene)-*N*-(trifluoromethyl)amines [$RN(CF_3)CF_2R'$] Using BrF_3. *J. Org. Chem.* **2009**, *74*, 8578−8582.
(31) Baidya, M.; Kobayashi, S.; Mayr, H. Nucleophilicity and Nucleofugality of Phenylsulfinate ($PhSO_2^-$): A Key to Understanding its Ambident Reactivity. *J. Am. Chem. Soc.* **2010**, *132*, 4796−4805.
(32) Duan, X.-H.; Maji, B.; Mayr, H. Characterization of the nucleophilic reactivities of thiocarboxylate, dithiocarbonate and dithiocarbamate anions. *Org. Biomol. Chem.* **2011**, *9*, 8046−8050.
(33) Fulmer, G. R.; Miller, A. J. M.; Sherden, N. H.; Gottlieb, H. E.; Nudelman, A.; Stoltz, B. M.; Bercaw, J. E.; Goldberg, K. I. NMR Chemical Shifts of Trace Impurities: Common Laboratory Solvents, Organics, and Gases in Deuterated Solvents Relevant to the Organometallic Chemist. *Organometallics* **2010**, *29*, 2176−2179.

https://doi.org/10.1021/acs.joc.1c00025
J. Org. Chem. 2021, 86, 5965−5972

2.2 Supporting Information

2.2.1 Additional Table

Table S1. Kinetic and Thermodynamic Data for the Reactions of Thiophenolates **1**

ArS^-	N/s_N	log k_2^{exptl} (**1** + **2c**)[a]	Hammett σ_p^- or σ_m[b]	pK_{aH} (DMSO)[c]	(log k_2)/s_N (**1** + *n*BuCl)[d]	Phenolate Ions ArO^-	log k_2 (ArO^- + **2c**)[e]
1a	24.97/0.68	5.88	–0.26	11.19	–1.00	*p*-MeO-$C_6H_4O^-$	3.18
1b	24.35/0.69	5.70	–0.17	10.82		*p*-Me-$C_6H_4O^-$	2.58
1c	23.36/0.74	5.35	0	10.28	–1.37	$C_6H_5O^-$	2.66
1j	22.55/0.83	5.29	0.12	9.53	–1.60		
1d	22.80/0.78	5.17	0.25	8.98	–1.88		
1e	22.50/0.78	4.96	0.37	8.57			
1f	21.75/0.86	4.75	0.43	8.09	–2.24		
1g	21.30/0.86	4.44	0.65			*p*-F_3C-$C_6H_4O^-$	1.81
1h	19.71/0.86	3.07	0.86				
1i	18.92/0.87	2.40	1.27	5.5	–3.55	*p*-O_2N-$C_6H_4O^-$	–1.38

[a] Data from Table 1 (this work). [b] Hammett substituent constants σ_p^- or σ_m from ref S1. [c] Acidity constants for thiophenols in DMSO; from ref S2. [d] Calculated with second-order rate constants k_2 for the reactions of ArS^- (**1**) with *n*-butyl chloride in DMSO at 25 °C from ref S2. [e] Calculated from second-order rate constants k_2 in DMSO at 20 °C; ref S3.

2.2.2 UV-Vis Spectra of Thiophenolates 1 and Quinone Methides 2 in DMSO

UV-Vis Spectra of Thiophenolates 1

A DMSO solution of the thiophenol **1**-H was deprotonated (by NaH or KO*t*Bu) and added in multiple steps to a flask filled with DMSO. The increasing absorptions of the DMSO solutions were followed by utilizing a diode array photometer (J&M TIDAS). In accord with the Lambert-Beer law, molar absorption coefficients ε_{max} (at λ_{max}) were determined from the slope of the linear relationship of the absorbance (at λ_{max}) with [**1**]. The depicted UV-vis spectra were then normalized relative to the extinction coefficient at λ_{max}.

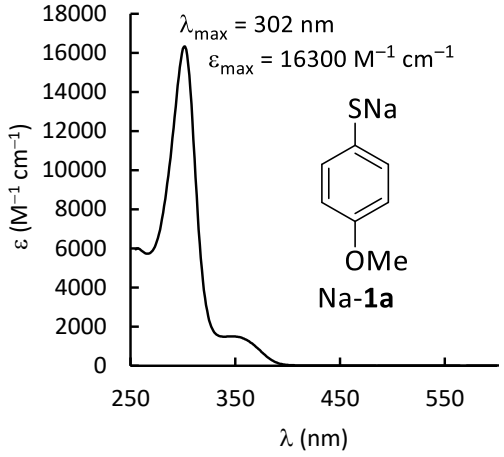

Figure S1. UV-vis spectrum of Na-**1a** in DMSO.

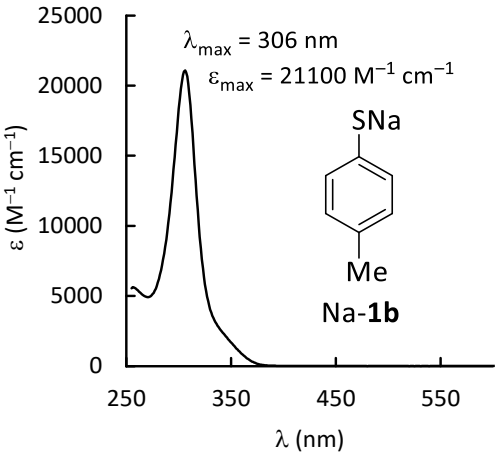

Figure S2. UV-vis spectrum of Na-**1b** in DMSO.

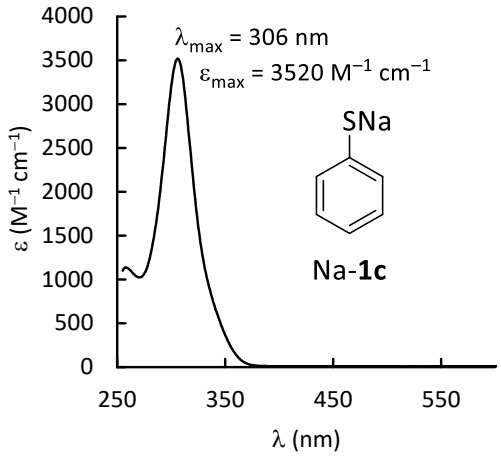

Figure S3. UV-vis spectrum of Na-**1c** in DMSO.

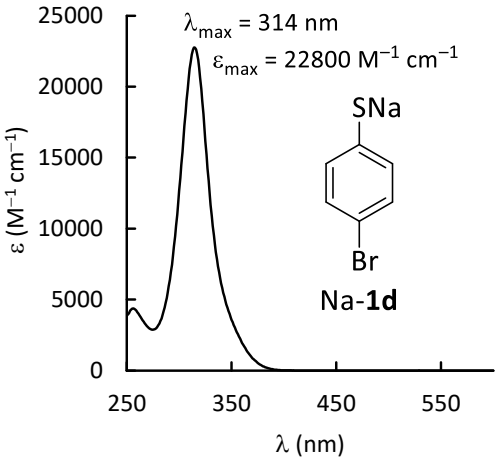

Figure S4. UV-vis spectrum of Na-**1d** in DMSO.

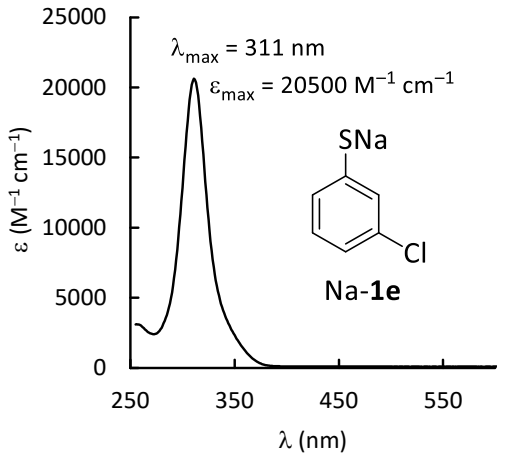

Figure S5. UV-vis spectrum of Na-**1e** in DMSO.

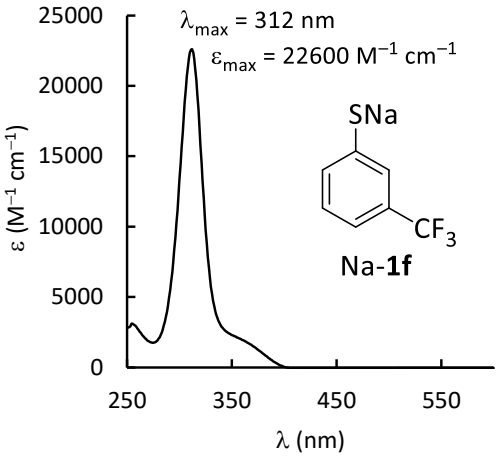

Figure S6. UV-vis spectrum of Na-**1f** in DMSO.

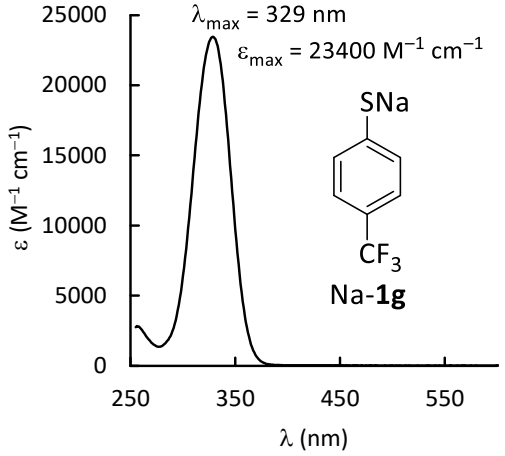

Figure S7. UV-vis spectrum of Na-**1g** in DMSO.

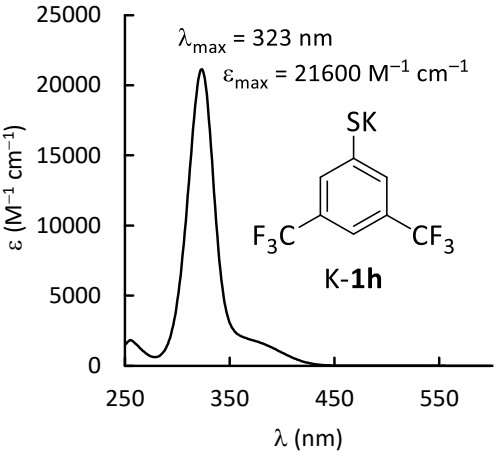

Figure S8. UV-vis spectrum of K-**1h** in DMSO.

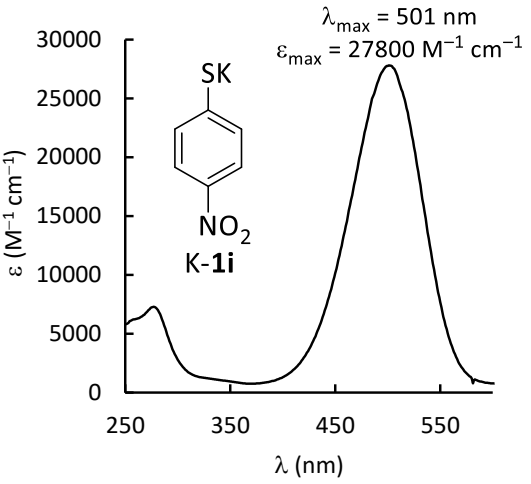

Figure S9. UV-vis spectrum of K-**1i** in DMSO.

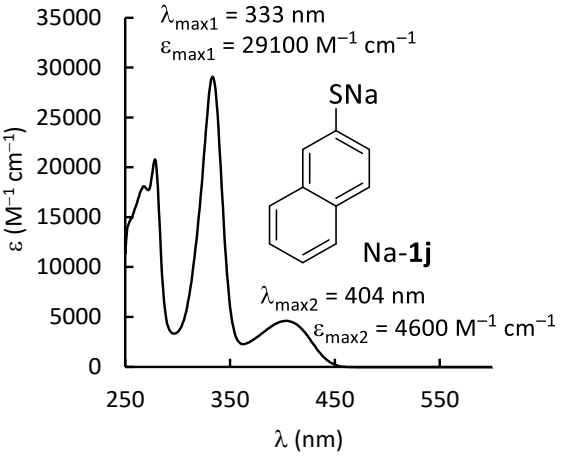

Figure S10. UV-vis spectrum of Na-**1j** in DMSO.

UV-Vis Spectra of Quinone Methides 2

A DMSO solution of the quinone methide **2** was added in multiple steps to a flask filled with DMSO. The increasing absorptions of the DMSO solutions were followed by utilizing a diode array photometer (J&M TIDAS). In accord with the Lambert-Beer law, extinction coefficients at λ_{max} were determined from the slope of the linear relationship of the absorbance (at λ_{max}) with [**2**]. The depicted UV-vis spectra were then normalized relative to the extinction coefficient at λ_{max}.

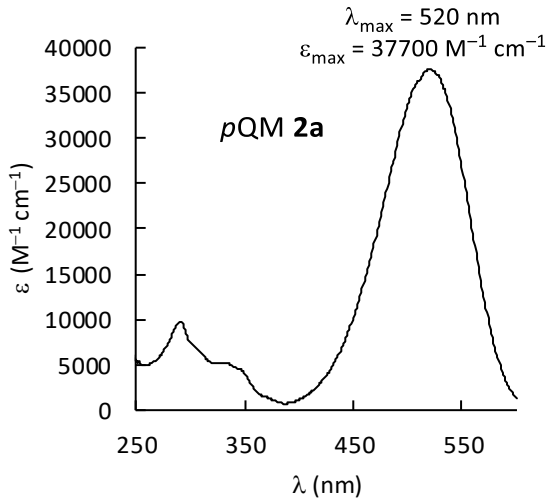

Figure S11. UV-vis spectrum of **2a** in DMSO.

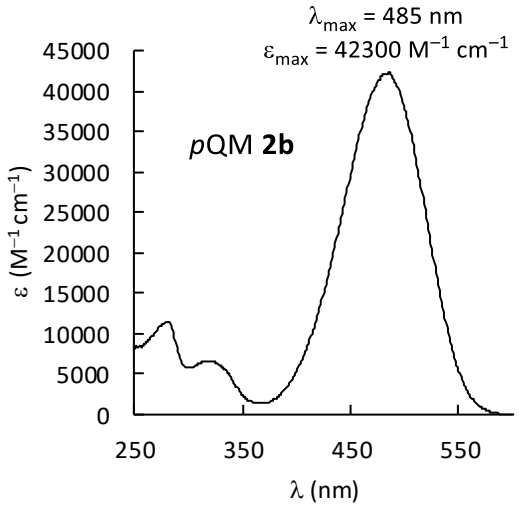

Figure S12. UV-vis spectrum of **2b** in DMSO.

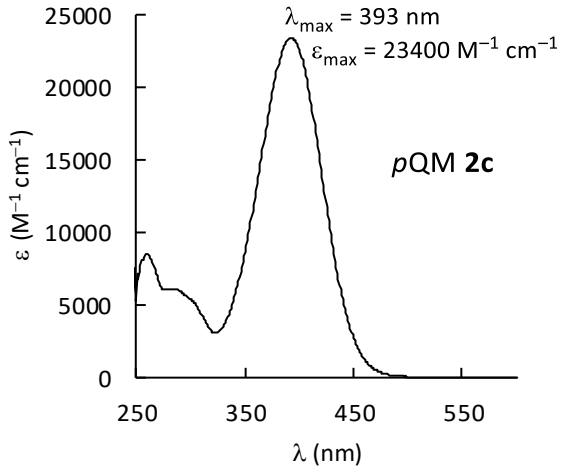

Figure S13. UV-vis spectrum of **2c** in DMSO.

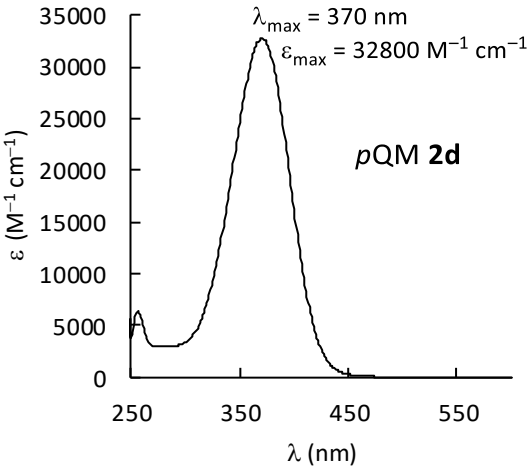

Figure S14. UV-vis spectrum of **2d** in DMSO.

UV-vis spectral data for *p*QMs **2e** and **2f** (in DMSO) were reported in ref S4:

For **2e**: λ_{max} = 354 nm, ε_{max} = 31600 M^{-1} cm^{-1}

For **2f**: λ_{max} = 374 nm, ε_{max} = 30100 M^{-1} cm^{-1}

2.2.3 Kinetics

Kinetics at variable thiophenol concentrations

Table S2. Quinone methide **2c** and potassium 4-methoxythiophenolate (K-**1a**) in DMSO (detection at 393 nm) with variable **1a**-H concentration

#	[**2c**]$_0$ (M)	[**1a**]$_0$ (M)	[**1a**-H]$_0$ (M)	k_{obs} (s^{-1})
1	5.00×10^{-5}	1.00×10^{-3}	2.50×10^{-3}	858 ± 7
2	5.00×10^{-5}	1.00×10^{-3}	5.00×10^{-3}	911 ± 5
3	5.00×10^{-5}	1.00×10^{-3}	1.00×10^{-2}	909 ± 6
4	5.00×10^{-5}	1.00×10^{-3}	2.00×10^{-2}	876 ± 6

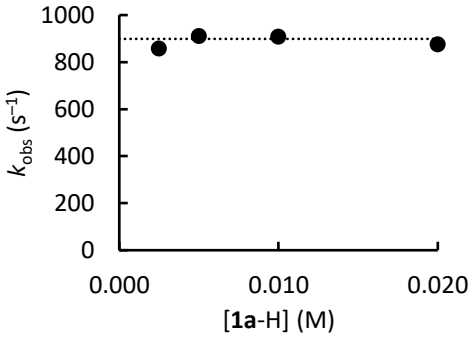

The dashed line shows the average k_{obs} of entries #2, #3, and #4, that is, k_{obs} = (899 ± 16) s^{-1}.

Table S3. Quinone methide **2c** and sodium thiophenolate (Na-**1c**) in DMSO (detection at 393 nm) with variable **1c**-H concentration

#	[**2c**]$_0$ (M)	[**1c**]$_0$ (M)	[**1c**-H]$_0$ (M)	k_{obs} (s^{-1})
1	5.00×10^{-5}	1.00×10^{-3}	2.50×10^{-4}	128 ± 1
2	5.00×10^{-5}	1.00×10^{-3}	5.00×10^{-4}	194 ± 1
3	5.00×10^{-5}	1.00×10^{-3}	1.00×10^{-3}	225 ± 1
4	5.00×10^{-5}	1.00×10^{-3}	1.50×10^{-3}	224 ± 1
5	5.00×10^{-5}	1.00×10^{-3}	2.00×10^{-3}	236 ± 1
6	5.00×10^{-5}	1.00×10^{-3}	5.00×10^{-3}	243 ± 1

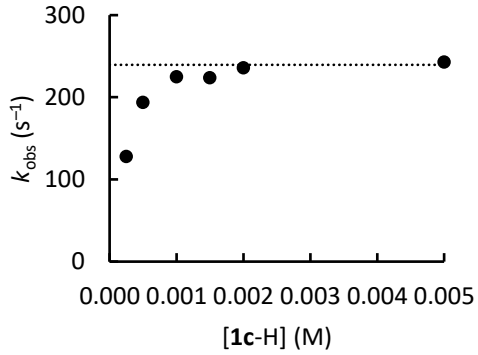

The dashed line shows the average k_{obs} of entries #5 and #6, that is, k_{obs} = (240 ± 4) s^{-1}.

Kinetics of reactions of 4-methoxythiophenolate (1a) with quinone methides 2

Table S4. Quinone methide **2a** and sodium 4-methoxythiophenolate (Na-**1a**) in DMSO (detection at 521 nm)

[**2a**]$_0$ (M)	[**1a**]$_0$ (M)	[**1a**-H]$_0$ (M)	k_{obs} (s^{-1})
5.00×10^{-5}	5.00×10^{-4}	5.00×10^{-3}	30.9
5.00×10^{-5}	7.50×10^{-4}	5.00×10^{-3}	47.4
5.00×10^{-5}	1.00×10^{-3}	5.00×10^{-3}	63.4
5.00×10^{-5}	1.25×10^{-3}	5.00×10^{-3}	82.1
5.00×10^{-5}	1.50×10^{-3}	5.00×10^{-3}	96.0

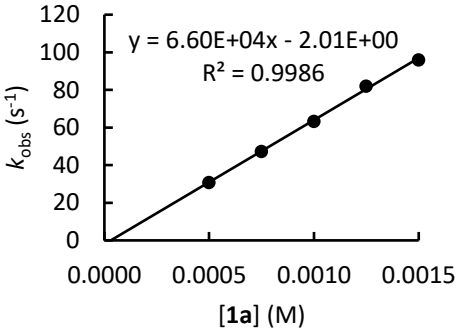

$k_2 = 6.60 \times 10^4\ M^{-1}\ s^{-1}$

Table S5. Quinone methide **2b** and sodium 4-methoxythiophenolate (Na-**1a**) in DMSO (detection at 486 nm)

[**2b**]$_0$ (M)	[**1a**]$_0$ (M)	[**1a**-H]$_0$ (M)	k_{obs} (s^{-1})
5.00×10^{-5}	5.00×10^{-4}	5.00×10^{-3}	64.2
5.00×10^{-5}	7.50×10^{-4}	5.00×10^{-3}	97.5
5.00×10^{-5}	1.00×10^{-3}	5.00×10^{-3}	130
5.00×10^{-5}	1.25×10^{-3}	5.00×10^{-3}	169
5.00×10^{-5}	1.50×10^{-3}	5.00×10^{-3}	199

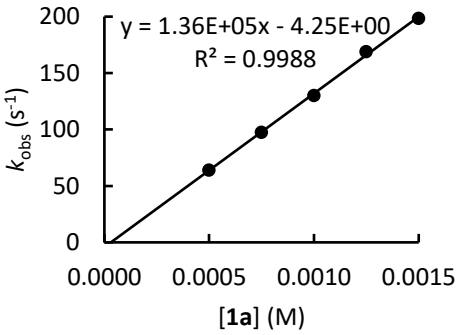

$k_2 = 1.36 \times 10^5\ M^{-1}\ s^{-1}$

Table S6. Quinone methide **2c** and sodium 4-methoxythiophenolate (Na-**1a**) in DMSO (detection at 393 nm)

[**2c**]$_0$ (M)	[**1a**]$_0$ (M)	[**1a**-H]$_0$ (M)	k_{obs} (s^{-1})
5.00×10^{-5}	5.00×10^{-4}	5.00×10^{-3}	480
5.00×10^{-5}	7.50×10^{-4}	5.00×10^{-3}	693
5.00×10^{-5}	1.00×10^{-3}	5.00×10^{-3}	895
5.00×10^{-5}	1.25×10^{-3}	5.00×10^{-3}	1.07×10^3
5.00×10^{-5}	1.50×10^{-3}	5.00×10^{-3}	1.24×10^3

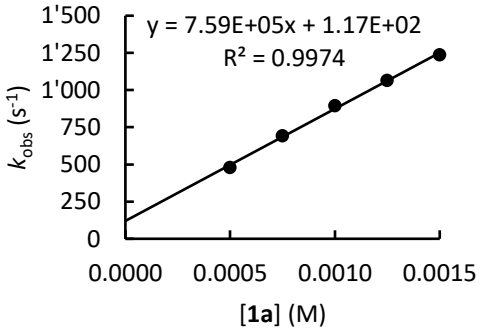

$k_2 = 7.59 \times 10^5\ M^{-1}\ s^{-1}$

Table S7. Quinone methide **2d** and potassium 4-methoxythiophenolate (K-**1a**) in DMSO (detection at 371 nm)

[**2d**]$_0$ (M)	[**1a**]$_0$ (M)	[**1a**-H]$_0$ (M)	k_{obs} (s^{-1})
5.00×10^{-5}	1.16×10^{-4}	5.00×10^{-3}	164
5.00×10^{-5}	2.32×10^{-4}	5.00×10^{-3}	371
5.00×10^{-5}	3.48×10^{-4}	5.00×10^{-3}	603
5.00×10^{-5}	4.64×10^{-4}	5.00×10^{-3}	807

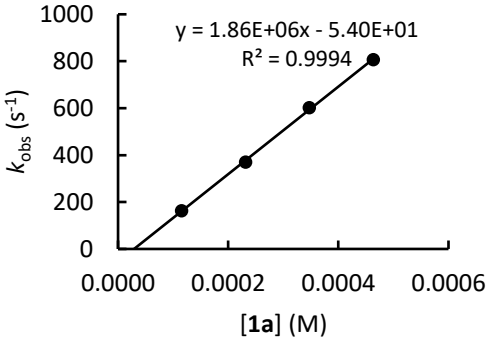

$k_2 = 1.86 \times 10^6$ M^{-1} s^{-1}

Table S8. Determination of N and s_N parameters for 4-methoxythiophenolate (**1a**) in DMSO.

Quinone methide	E	k_2 (M^{-1} s^{-1})	log k_2
2a	–17.90	6.60×10^4	4.82
2b	–17.29	1.36×10^5	5.13
2c	–16.11	7.59×10^5	5.88
2d	–15.83	1.86×10^6	6.27

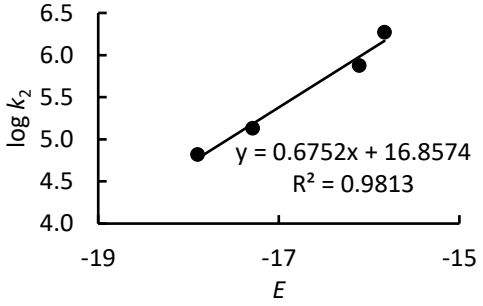

$N = 24.97$
$s_N = 0.68$

Kinetics of reactions of 4-methylthiophenolate (1b) with quinone methides 2

Table S9. Quinone methide **2a** and sodium 4-methylthiophenolate (Na-**1b**) in DMSO (detection at 521 nm)

[**2a**]$_0$ (M)	[**1b**]$_0$ (M)	[**1b**-H]$_0$ (M)	k_{obs} (s^{-1})
5.00×10^{-5}	5.00×10^{-4}	5.00×10^{-3}	17.1
5.00×10^{-5}	1.00×10^{-3}	5.00×10^{-3}	31.5
5.00×10^{-5}	1.50×10^{-3}	5.00×10^{-3}	50.5
5.00×10^{-5}	2.00×10^{-3}	5.00×10^{-3}	65.9

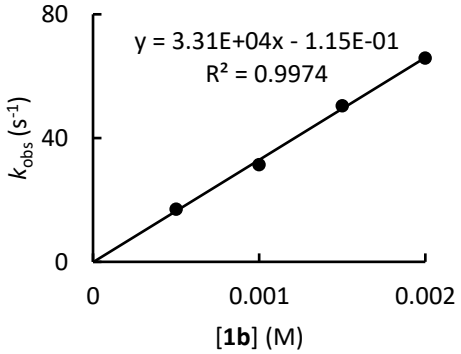

$k_2 = 3.31 \times 10^4$ M^{-1} s^{-1}

Table S10. Quinone methide **2b** and sodium 4-methylthiophenolate (Na-**1b**) in DMSO (detection at 486 nm)

[**2b**]$_0$ (M)	[**1b**]$_0$ (M)	[**1b**-H]$_0$ (M)	k_{obs} (s^{-1})
5.00×10^{-5}	5.00×10^{-4}	5.00×10^{-3}	34.2
5.00×10^{-5}	1.00×10^{-3}	5.00×10^{-3}	64.9
5.00×10^{-5}	1.50×10^{-3}	5.00×10^{-3}	102
5.00×10^{-5}	2.00×10^{-3}	5.00×10^{-3}	133

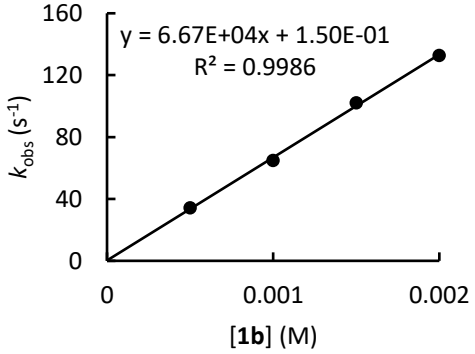

$k_2 = 6.67 \times 10^4$ M^{-1} s^{-1}

Table S11. Quinone methide **2c** and sodium 4-methylthiophenolate (Na-**1b**) in DMSO (detection at 393 nm)

[**2c**]$_0$ (M)	[**1b**]$_0$ (M)	[**1b**-H]$_0$ (M)	k_{obs} (s^{-1})
5.00×10^{-5}	5.00×10^{-4}	5.00×10^{-3}	262
5.00×10^{-5}	1.00×10^{-3}	5.00×10^{-3}	519
5.00×10^{-5}	1.50×10^{-3}	5.00×10^{-3}	801
5.00×10^{-5}	2.00×10^{-3}	5.00×10^{-3}	994

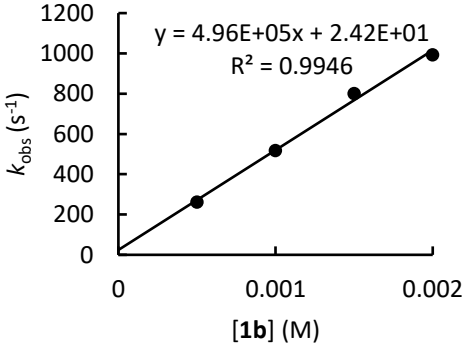

$k_2 = 4.96 \times 10^5$ M^{-1} s^{-1}

Table S12. Quinone methide **2d** and potassium 4-methylthiophenolate (K-**1b**) in DMSO (detection at 371 nm)

[**2d**]$_0$ (M)	[**1b**]$_0$ (M)	[**1b**-H]$_0$ (M)	k_{obs} (s^{-1})
5.00×10^{-5}	1.34×10^{-4}	5.00×10^{-3}	110
5.00×10^{-5}	2.67×10^{-4}	5.00×10^{-3}	230
5.00×10^{-5}	4.01×10^{-4}	5.00×10^{-3}	345
5.00×10^{-5}	5.35×10^{-4}	5.00×10^{-3}	457

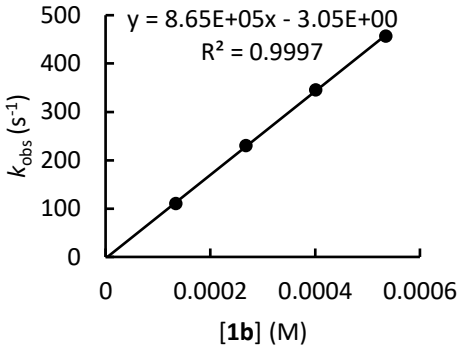

$k_2 = 8.65 \times 10^5$ M^{-1} s^{-1}

Table S13. Determination of N and s_N parameters for 4-methylthiophenolate (**1b**) in DMSO.

Quinone methide	E	k_2 (M^{-1} s^{-1})	log k_2
2a	–17.90	3.31×10^4	4.52
2b	–17.29	6.67×10^4	4.82
2c	–16.11	4.96×10^5	5.70
2d	–15.83	8.65×10^5	5.94

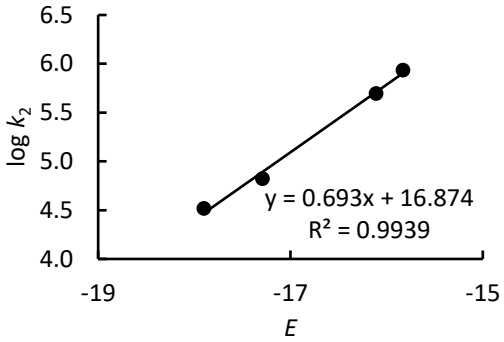

$N = 24.35$
$s_N = 0.69$

Kinetics of reactions of thiophenolate (1c) with quinone methides 2

Table S14. Quinone methide **2a** and sodium thiophenolate (Na-**1c**) in DMSO (detection at 521 nm)

[**2a**]$_0$ (M)	[**1c**]$_0$ (M)	[**1c**-H]$_0$ (M)	k_{obs} (s^{-1})
5.00×10^{-5}	5.00×10^{-4}	5.00×10^{-3}	9.83
5.00×10^{-5}	1.00×10^{-3}	5.00×10^{-3}	16.2
5.00×10^{-5}	1.50×10^{-3}	5.00×10^{-3}	22.6
5.00×10^{-5}	2.00×10^{-3}	5.00×10^{-3}	29.8

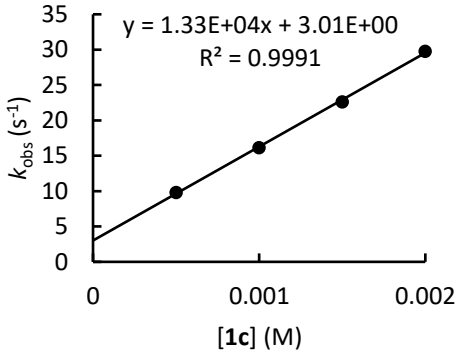

$k_2 = 1.33 \times 10^4\ M^{-1}\ s^{-1}$

Table S15. Quinone methide **2b** and sodium thiophenolate (Na-**1c**) in DMSO (detection at 486 nm)

[**2b**]$_0$ (M)	[**1c**]$_0$ (M)	[**1c**-H]$_0$ (M)	k_{obs} (s^{-1})
5.00×10^{-5}	5.00×10^{-4}	5.00×10^{-3}	17.0
5.00×10^{-5}	1.00×10^{-3}	5.00×10^{-3}	30.3
5.00×10^{-5}	1.50×10^{-3}	5.00×10^{-3}	44.1
5.00×10^{-5}	2.00×10^{-3}	5.00×10^{-3}	58.3

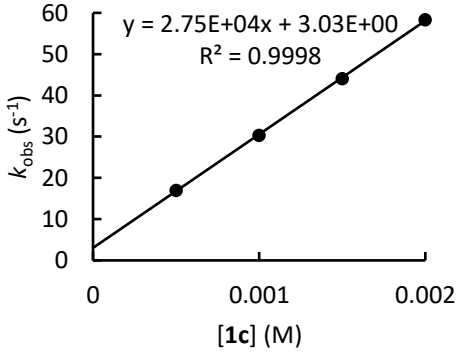

$k_2 = 2.75 \times 10^4\ M^{-1}\ s^{-1}$

Table S16. Quinone methide **2c** and sodium thiophenolate (Na-**1c**) in DMSO (detection at 393 nm)

[**2c**]$_0$ (M)	[**1c**]$_0$ (M)	[**1c**-H]$_0$ (M)	k_{obs} (s^{-1})
5.00×10^{-5}	5.00×10^{-4}	5.00×10^{-3}	147
5.00×10^{-5}	1.00×10^{-3}	5.00×10^{-3}	256
5.00×10^{-5}	1.50×10^{-3}	5.00×10^{-3}	375
5.00×10^{-5}	2.00×10^{-3}	5.00×10^{-3}	483

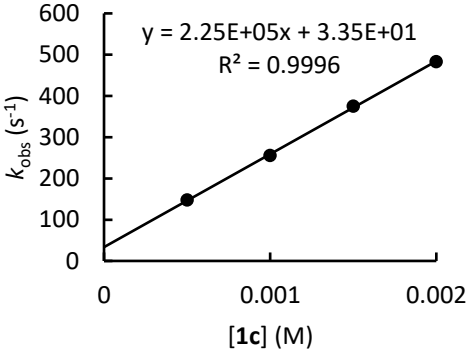

$k_2 = 2.25 \times 10^5\ M^{-1}\ s^{-1}$

Table S17. Quinone methide **2d** and potassium thiophenolate (K-**1c**) in DMSO (detection at 371 nm)

[**2d**]$_0$ (M)	[**1c**]$_0$ (M)	[**1c**-H]$_0$ (M)	k_{obs} (s^{-1})
5.00×10^{-5}	1.58×10^{-4}	5.00×10^{-3}	78.7
5.00×10^{-5}	3.16×10^{-4}	5.00×10^{-3}	152
5.00×10^{-5}	4.75×10^{-4}	5.00×10^{-3}	221
5.00×10^{-5}	6.33×10^{-4}	5.00×10^{-3}	299

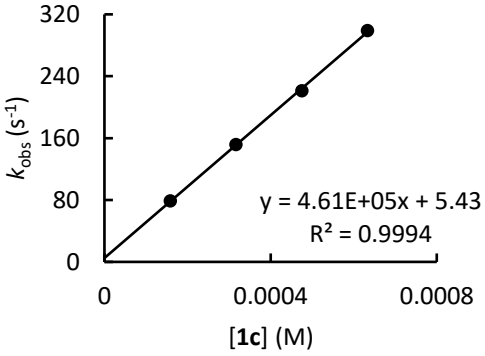

$k_2 = 4.61 \times 10^5$ M^{-1} s^{-1}

Table S18. Determination of N and s_N parameters for thiophenolate (**1c**) in DMSO.

Quinone methide	E	k_2 (M^{-1} s^{-1})	log k_2
2a	–17.90	1.33×10^4	4.12
2b	–17.29	2.75×10^4	4.44
2c	–16.11	2.25×10^5	5.35
2d	–15.83	4.61×10^5	5.66

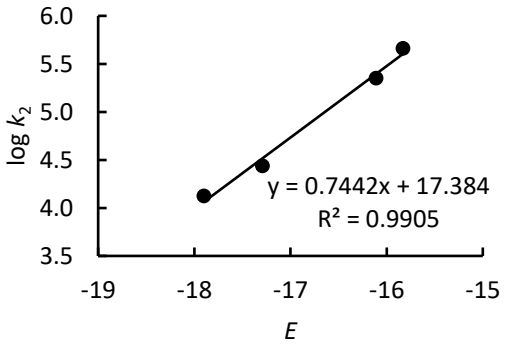

$N = 23.36$
$s_N = 0.74$

Kinetics of reactions of 4-bromo-thiophenolate (1d) with quinone methides 2

Table S19. Quinone methide **2a** and potassium 4-bromo-thiophenolate (K-**1d**) in DMSO (detection at 521 nm)

[**2a**]$_0$ (M)	[**1d**]$_0$ (M)	[**1d**-H]$_0$ (M)	k_{obs} (s^{-1})
5.00×10^{-5}	3.70×10^{-4}	5.00×10^{-3}	2.91
5.00×10^{-5}	7.40×10^{-4}	5.00×10^{-3}	5.70
5.00×10^{-5}	1.11×10^{-3}	5.00×10^{-3}	8.87
5.00×10^{-5}	1.48×10^{-3}	5.00×10^{-3}	11.8

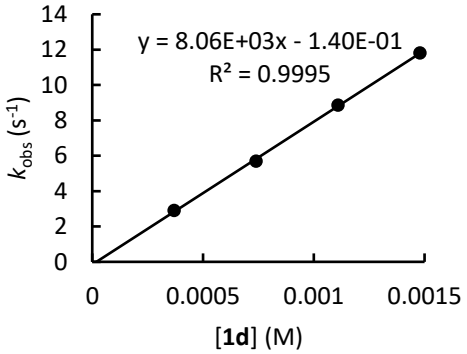

$k_2 = 8.06 \times 10^3\ M^{-1}\ s^{-1}$

Table S20. Quinone methide **2b** and potassium 4-bromo-thiophenolate (K-**1d**) in DMSO (detection at 490 nm)

[**2b**]$_0$ (M)	[**1d**]$_0$ (M)	[**1d**-H]$_0$ (M)	k_{obs} (s^{-1})
5.00×10^{-5}	3.70×10^{-4}	5.00×10^{-3}	6.46
5.00×10^{-5}	7.40×10^{-4}	5.00×10^{-3}	13.0
5.00×10^{-5}	1.11×10^{-3}	5.00×10^{-3}	20.7
5.00×10^{-5}	1.48×10^{-3}	5.00×10^{-3}	26.6

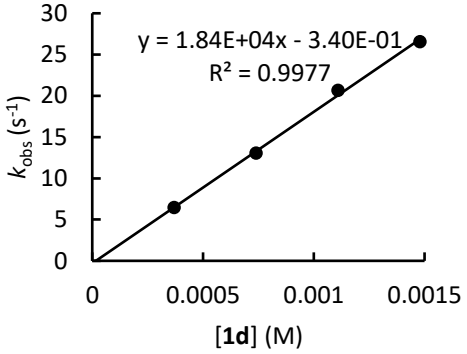

$k_2 = 1.84 \times 10^4\ M^{-1}\ s^{-1}$

Table S21. Quinone methide **2c** and potassium 4-bromo-thiophenolate (K-**1d**) in DMSO (detection at 390 nm)

[**2c**]$_0$ (M)	[**1d**]$_0$ (M)	[**1d**-H]$_0$ (M)	k_{obs} (s^{-1})
5.00×10^{-5}	3.70×10^{-4}	5.00×10^{-3}	55.3
5.00×10^{-5}	7.40×10^{-4}	5.00×10^{-3}	113
5.00×10^{-5}	1.11×10^{-3}	5.00×10^{-3}	170
5.00×10^{-5}	1.48×10^{-3}	5.00×10^{-3}	220

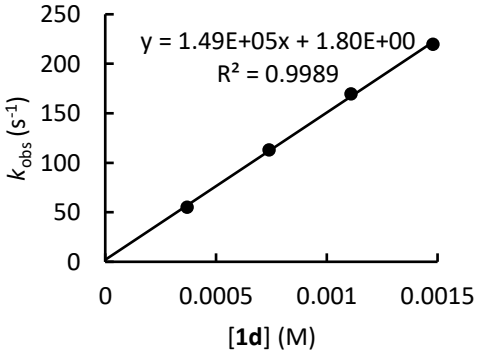

$k_2 = 1.49 \times 10^5\ M^{-1}\ s^{-1}$

Table S22. Quinone methide **2d** and potassium 4-bromo-thiophenolate (K-**1d**) in DMSO (detection at 371 nm)

$[\mathbf{2d}]_0$ (M)	$[\mathbf{1d}]_0$ (M)	$[\mathbf{1d}\text{-H}]_0$ (M)	k_{obs} (s^{-1})
5.00×10^{-5}	3.70×10^{-4}	5.00×10^{-3}	92.6
5.00×10^{-5}	7.40×10^{-4}	5.00×10^{-3}	191
5.00×10^{-5}	1.11×10^{-3}	5.00×10^{-3}	304
5.00×10^{-5}	1.48×10^{-3}	5.00×10^{-3}	404

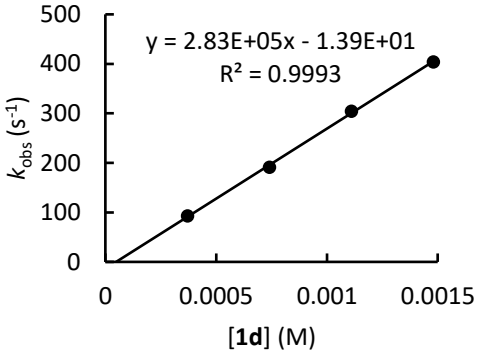

$k_2 = 2.83 \times 10^5\ M^{-1}\ s^{-1}$

Table S23. Quinone methide **2e** and potassium 4-bromo-thiophenolate (K-**1d**) in DMSO (detection at 350 nm)

$[\mathbf{2e}]_0$ (M)	$[\mathbf{1d}]_0$ (M)	$[\mathbf{1d}\text{-H}]_0$ (M)	k_{obs} (s^{-1})
5.00×10^{-5}	1.85×10^{-4}	5.00×10^{-3}	225
5.00×10^{-5}	2.78×10^{-4}	5.00×10^{-3}	323
5.00×10^{-5}	3.70×10^{-4}	5.00×10^{-3}	505
5.00×10^{-5}	7.40×10^{-4}	5.00×10^{-3}	1.01×10^3
5.00×10^{-5}	1.11×10^{-3}	5.00×10^{-3}	1.50×10^3

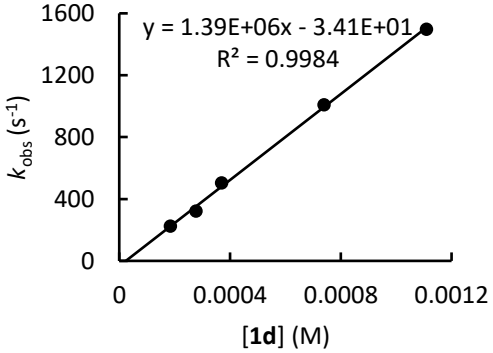

$k_2 = 1.39 \times 10^6\ M^{-1}\ s^{-1}$

Table S24. Determination of N and s_N parameters for 4-bromo-thiophenolate (K-**1d**) in DMSO.

Quinone methide	E	k_2 ($M^{-1}\ s^{-1}$)	log k_2
2a	–17.90	8.06×10^3	3.91
2b	–17.29	1.84×10^4	4.26
2c	–16.11	1.49×10^5	5.17
2d	–15.83	2.83×10^5	5.45
2e	–15.03	1.39×10^6	6.14

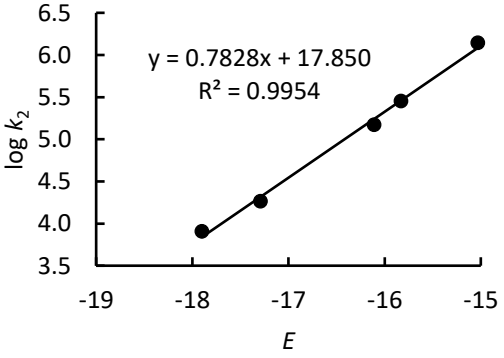

$N = 22.80$
$s_N = 0.78$

Kinetics of reactions of 3-chloro-thiophenolate (1e) with quinone methides 2

Table S25. Quinone methide **2a** and potassium 3-chloro-thiophenolate (K-**1e**) in DMSO (detection at 520 nm)

[**2a**]$_0$ (M)	[**1e**]$_0$ (M)	[**1e**-H]$_0$ (M)	k_{obs} (s^{-1})
5.00×10^{-5}	2.04×10^{-4}	5.00×10^{-3}	1.03
5.00×10^{-5}	4.08×10^{-4}	5.00×10^{-3}	1.83
5.00×10^{-5}	6.12×10^{-4}	5.00×10^{-3}	2.69
5.00×10^{-5}	8.16×10^{-4}	5.00×10^{-3}	3.72

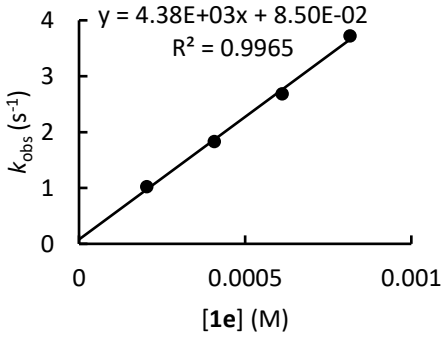

$k_2 = 4.38 \times 10^3\ M^{-1}\ s^{-1}$

Table S26. Quinone methide **2b** and potassium 3-chloro-thiophenolate (K-**1e**) in DMSO (detection at 490 nm)

[**2b**]$_0$ (M)	[**1e**]$_0$ (M)	[**1e**-H]$_0$ (M)	k_{obs} (s^{-1})
5.00×10^{-5}	2.04×10^{-4}	5.00×10^{-3}	2.06
5.00×10^{-5}	4.08×10^{-4}	5.00×10^{-3}	3.82
5.00×10^{-5}	6.12×10^{-4}	5.00×10^{-3}	5.84
5.00×10^{-5}	8.16×10^{-4}	5.00×10^{-3}	8.21

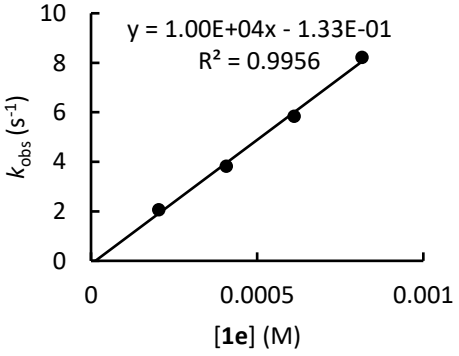

$k_2 = 1.00 \times 10^4\ M^{-1}\ s^{-1}$

Table S27. Quinone methide **2c** and potassium 3-chloro-thiophenolate (K-**1e**) in DMSO (detection at 393 nm)

[**2c**]$_0$ (M)	[**1e**]$_0$ (M)	[**1e**-H]$_0$ (M)	k_{obs} (s^{-1})
5.00×10^{-5}	2.04×10^{-4}	5.00×10^{-3}	18.9
5.00×10^{-5}	4.08×10^{-4}	5.00×10^{-3}	35.4
5.00×10^{-5}	6.12×10^{-4}	5.00×10^{-3}	52.1
5.00×10^{-5}	8.16×10^{-4}	5.00×10^{-3}	75.8

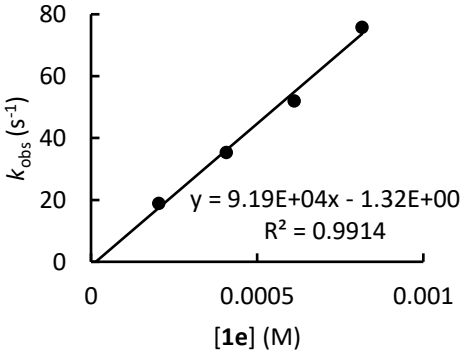

$k_2 = 9.19 \times 10^4\ M^{-1}\ s^{-1}$

Table S28. Quinone methide **2d** and sodium 3-chloro-thiophenolate (Na-**1e**) in DMSO (detection at 371 nm)

[**2d**]$_0$ (M)	[**1e**]$_0$ (M)	[**1e**-H]$_0$ (M)	k_{obs} (s^{-1})
5.00×10^{-5}	5.00×10^{-4}	5.00×10^{-3}	68.1
5.00×10^{-5}	1.00×10^{-3}	5.00×10^{-3}	124
5.00×10^{-5}	1.50×10^{-3}	5.00×10^{-3}	187
5.00×10^{-5}	2.00×10^{-3}	5.00×10^{-3}	237

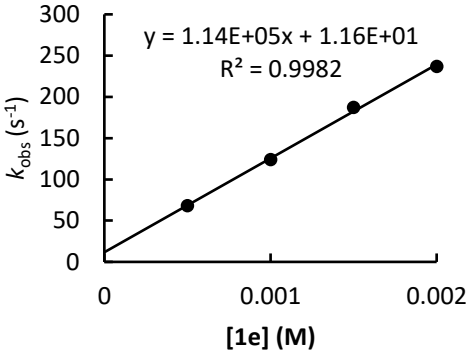

$k_2 = 1.14 \times 10^5$ M^{-1} s^{-1}

Table S29. Quinone methide **2e** and potassium 3-chloro-thiophenolate (K-**1e**) in DMSO (detection at 350 nm)

[**2e**]$_0$ (M)	[**1e**]$_0$ (M)	[**1e**-H]$_0$ (M)	k_{obs} (s^{-1})
5.00×10^{-5}	2.04×10^{-4}	5.00×10^{-3}	156
5.00×10^{-5}	4.08×10^{-4}	5.00×10^{-3}	298
5.00×10^{-5}	6.12×10^{-4}	5.00×10^{-3}	466
5.00×10^{-5}	8.16×10^{-4}	5.00×10^{-3}	640

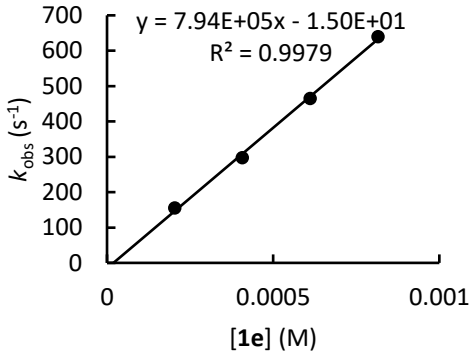

$k_2 = 7.94 \times 10^5$ M^{-1} s^{-1}

Table S30. Determination of N and s_N parameters for 3-chloro-thiophenolate (**1e**) in DMSO.

Quinone methide	E	k_2 (M^{-1} s^{-1})	log k_2
2a	–17.90	4.38×10^3	3.64
2b	–17.29	1.00×10^4	4.00
2c	–16.11	9.19×10^4	4.96
2d	–15.83	1.14×10^5	5.06
2e	–15.03	7.94×10^6	5.90

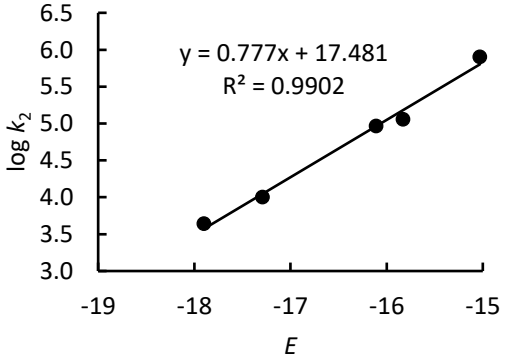

$N = 22.50$
$s_N = 0.78$

Kinetics of reactions of 3-(trifluoromethyl)thiophenolate (1f) with quinone methides 2

Table S31. Quinone methide **2a** and potassium 3-(trifluoromethyl)thiophenolate (K-**1f**) in DMSO (detection at 520 nm)

[**2a**]$_0$ (M)	[**1f**]$_0$ (M)	[**1f**-H]$_0$ (M)	k_{obs} (s^{-1})
5.00×10^{-5}	4.01×10^{-4}	5.00×10^{-3}	1.23
5.00×10^{-5}	8.02×10^{-4}	5.00×10^{-3}	2.09
5.00×10^{-5}	1.20×10^{-3}	5.00×10^{-3}	3.04
5.00×10^{-5}	1.60×10^{-3}	5.00×10^{-3}	4.02

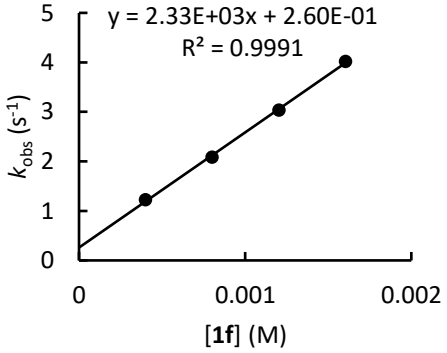

$k_2 = 2.33 \times 10^3\ M^{-1}\ s^{-1}$

Table S32. Quinone methide **2b** and potassium 3-(trifluoromethyl)thiophenolate (K-**1f**) in DMSO (detection at 490 nm)

[**2b**]$_0$ (M)	[**1f**]$_0$ (M)	[**1f**-H]$_0$ (M)	k_{obs} (s^{-1})
5.00×10^{-5}	4.01×10^{-4}	5.00×10^{-3}	2.36
5.00×10^{-5}	8.02×10^{-4}	5.00×10^{-3}	4.45
5.00×10^{-5}	1.20×10^{-3}	5.00×10^{-3}	6.81
5.00×10^{-5}	1.60×10^{-3}	5.00×10^{-3}	9.10

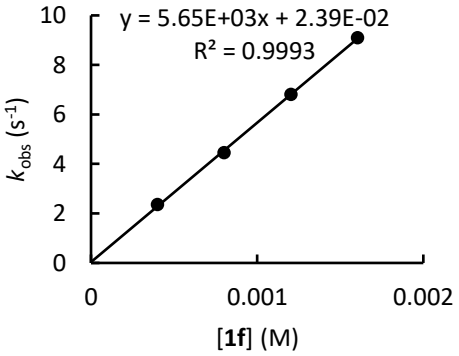

$k_2 = 5.65 \times 10^3\ M^{-1}\ s^{-1}$

Table S33. Quinone methide **2c** and potassium 3-(trifluoromethyl)thiophenolate (K-**1f**) in DMSO (detection at 393 nm)

[**2c**]$_0$ (M)	[**1f**]$_0$ (M)	[**1f**-H]$_0$ (M)	k_{obs} (s^{-1})
5.00×10^{-5}	4.01×10^{-4}	5.00×10^{-3}	22.7
5.00×10^{-5}	8.02×10^{-4}	5.00×10^{-3}	43.8
5.00×10^{-5}	1.20×10^{-3}	5.00×10^{-3}	68.0
5.00×10^{-5}	1.60×10^{-3}	5.00×10^{-3}	89.6

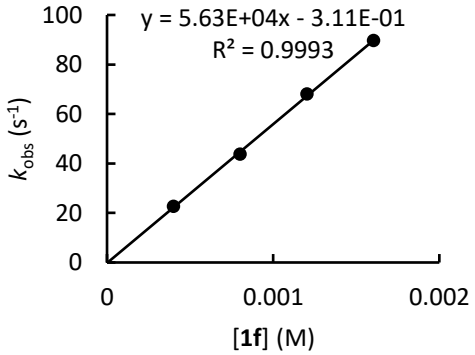

$k_2 = 5.63 \times 10^4\ M^{-1}\ s^{-1}$

Table S34. Quinone methide **2e** and potassium 3-(trifluoromethyl)thiophenolate (K-**1f**) in DMSO (detection at 350 nm)

[**2e**]$_0$ (M)	[**1f**]$_0$ (M)	[**1f**-H]$_0$ (M)	k_{obs} (s^{-1})
5.00×10^{-5}	2.01×10^{-4}	5.00×10^{-3}	104
5.00×10^{-5}	4.01×10^{-4}	5.00×10^{-3}	198
5.00×10^{-5}	8.02×10^{-3}	5.00×10^{-3}	447
5.00×10^{-5}	1.20×10^{-3}	5.00×10^{-3}	740

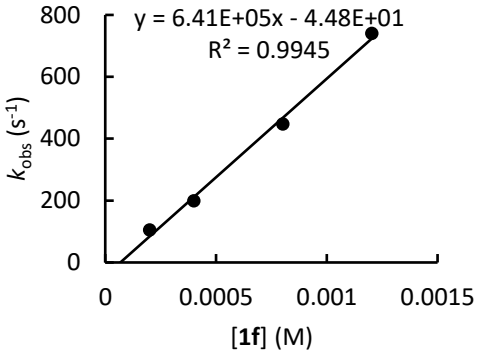

$k_2 = 6.41 \times 10^5$ M^{-1} s^{-1}

Table S35. Determination of N and s_N parameters for 3-(trifluoromethyl)thiophenolate (**1f**) in DMSO.

Quinone methide	E	k_2 (M^{-1} s^{-1})	log k_2
2a	–17.90	2.33×10^3	3.37
2b	–17.29	5.65×10^3	3.75
2c	–16.11	5.63×10^4	4.75
2e	–15.03	6.41×10^5	5.80

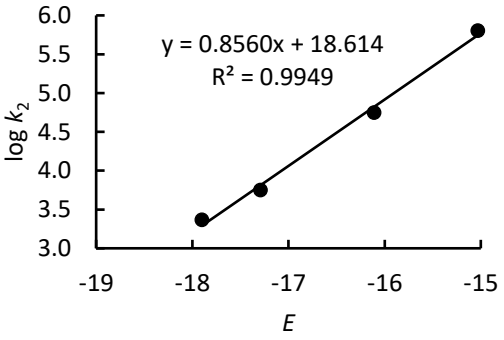

$N = 21.75$
$s_N = 0.86$

Kinetics of reactions of 4-(trifluoromethyl)thiophenolate (1g) with quinone methides 2

Table S36. Quinone methide **2a** and potassium or sodium 4-(trifluoromethyl)thiophenolate (K/Na-**1g**) in DMSO (detection at 520 nm)

[**2a**]$_0$ (M)	[**1g**]$_0$ (M)	[**1g**-H]$_0$ (M)	k_{obs} (s^{-1})
5.00×10^{-5}	4.91×10^{-4}	5.00×10^{-3}	0.912
5.00×10^{-5}	9.82×10^{-4}	5.00×10^{-3}	1.42
5.00×10^{-5}	1.03×10^{-3} [a]	5.00×10^{-3}	1.41
5.00×10^{-5}	1.47×10^{-3}	5.00×10^{-3}	1.79
5.00×10^{-5}	1.96×10^{-3}	5.00×10^{-3}	2.15
5.00×10^{-5}	2.05×10^{-3} [a]	5.00×10^{-3}	2.21

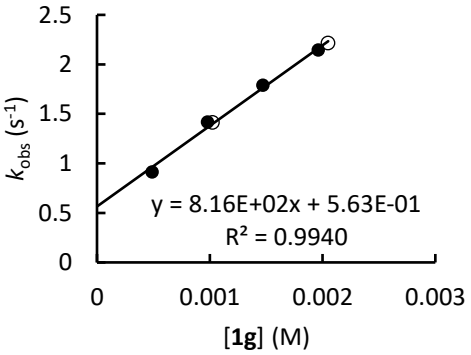

[a] The counterion Na^+ was used instead of K^+.

$k_2 = 8.16 \times 10^2\ M^{-1}\ s^{-1}$

Table S37. Quinone methide **2b** and potassium or sodium 4-(trifluoromethyl)thiophenolate (K/Na-**1g**) in DMSO (detection at 490 nm)

[**2b**]$_0$ (M)	[**1g**-K]$_0$ (M)	[**1g**-H]$_0$ (M)	k_{obs} (s^{-1})
5.00×10^{-5}	4.91×10^{-4}	5.00×10^{-3}	1.51
5.00×10^{-5}	9.82×10^{-4}	5.00×10^{-3}	3.01
5.00×10^{-5}	1.03×10^{-3} [a]	5.00×10^{-3}	3.01
5.00×10^{-5}	1.47×10^{-3}	5.00×10^{-3}	4.22
5.00×10^{-5}	1.96×10^{-3}	5.00×10^{-3}	5.39

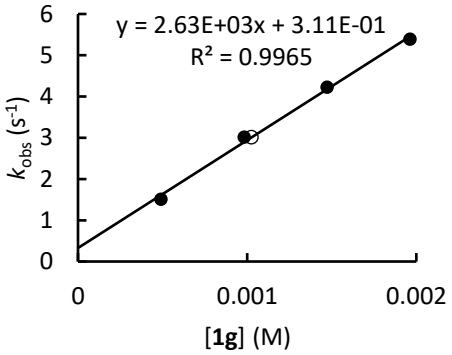

[a] The counterion Na^+ was used instead of K^+.

$k_2 = 2.63 \times 10^3\ M^{-1}\ s^{-1}$

Table S38. Quinone methide **2c** and potassium 4-(trifluoromethyl)thiophenolate (K-**1g**) in DMSO (detection at 393 nm)

[**2c**]$_0$ (M)	[**1g**]$_0$ (M)	[**1g**-H]$_0$ (M)	k_{obs} (s^{-1})
5.00×10^{-5}	4.91×10^{-4}	5.00×10^{-3}	15.2
5.00×10^{-5}	9.82×10^{-4}	5.00×10^{-3}	30.8
5.00×10^{-5}	1.47×10^{-3}	5.00×10^{-3}	43.6
5.00×10^{-5}	1.96×10^{-3}	5.00×10^{-3}	57.5

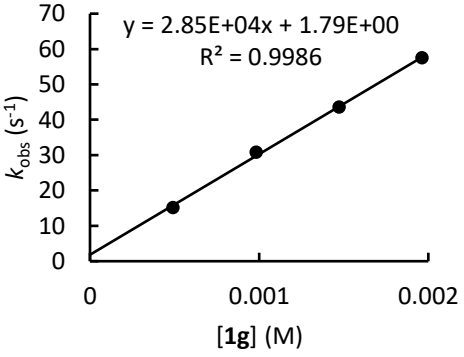

$k_2 = 2.85 \times 10^4\ M^{-1}\ s^{-1}$

Table S39. Quinone methide **2c** and sodium 4-(trifluoromethyl)thiophenolate (Na-**1g**) in DMSO (detection at 393 nm)

[**2c**]$_0$ (M)	[**1g**]$_0$ (M)	[**1g**-H]$_0$ (M)	k_{obs} (s^{-1})
5.00×10^{-5}	5.00×10^{-4}	5.00×10^{-3}	15.8
5.00×10^{-5}	1.00×10^{-3}	5.00×10^{-3}	28.8
5.00×10^{-5}	1.50×10^{-3}	5.00×10^{-3}	40.8
5.00×10^{-5}	2.00×10^{-3}	5.00×10^{-3}	57.7

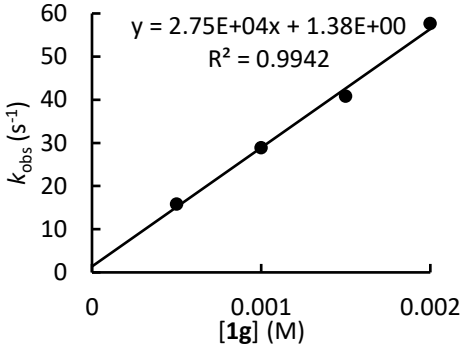

$k_2 = 2.75 \times 10^4\ M^{-1}\ s^{-1}$

Table S40. Quinone methide **2d** and sodium 4-(trifluoromethyl)thiophenolate (Na-**1g**) in DMSO (detection at 371 nm)

[**2d**]$_0$ (M)	[**1g**]$_0$ (M)	[**1g**-H]$_0$ (M)	k_{obs} (s^{-1})
5.00×10^{-5}	5.00×10^{-4}	5.00×10^{-3}	26.6
5.00×10^{-5}	1.00×10^{-3}	5.00×10^{-3}	52.9
5.00×10^{-5}	1.50×10^{-3}	5.00×10^{-3}	78.7
5.00×10^{-5}	2.00×10^{-3}	5.00×10^{-3}	109

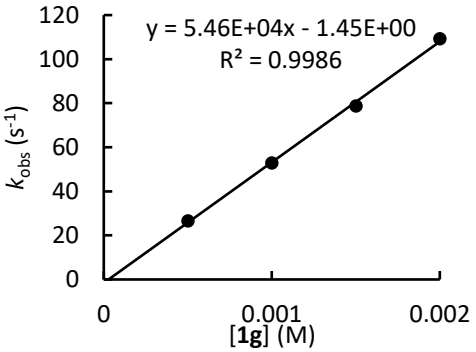

$k_2 = 5.46 \times 10^4\ M^{-1}\ s^{-1}$

Table S41. Quinone methide **2e** and sodium 4-(trifluoromethyl)thiophenolate (Na-**1g**) in DMSO (detection at 350 nm)

[**2e**]$_0$ (M)	[**1g**]$_0$ (M)	[**1g**-H]$_0$ (M)	k_{obs} (s^{-1})
5.00×10^{-5}	5.00×10^{-4}	5.00×10^{-3}	134
5.00×10^{-5}	1.00×10^{-3}	5.00×10^{-3}	270
5.00×10^{-5}	1.50×10^{-3}	5.00×10^{-3}	408
5.00×10^{-5}	2.00×10^{-3}	5.00×10^{-3}	551

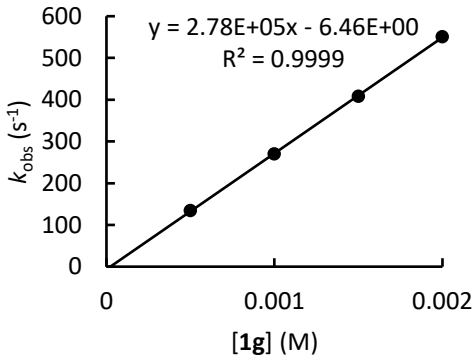

$k_2 = 2.78 \times 10^5\ M^{-1}\ s^{-1}$

Table S42. Quinone methide **2f** and sodium 4-(trifluoromethyl)thiophenolate (Na-**1g**) in DMSO (detection at 374 nm)

$[\mathbf{2f}]_0$ (M)	$[\mathbf{1g}]_0$ (M)	$[\mathbf{1g}\text{-H}]_0$ (M)	k_{obs} (s^{-1})
5.00×10^{-5}	5.00×10^{-4}	5.00×10^{-3}	627
5.00×10^{-5}	1.00×10^{-3}	5.00×10^{-3}	1.07×10^{3}
5.00×10^{-5}	1.50×10^{-3}	5.00×10^{-3}	1.40×10^{3}
5.00×10^{-5}	2.00×10^{-3}	5.00×10^{-3}	1.81×10^{3}

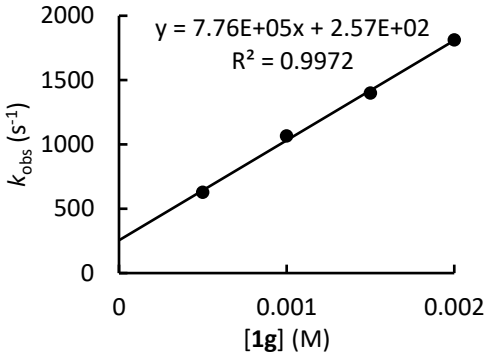

$k_2 = 7.76 \times 10^5$ M^{-1} s^{-1}

Table S43. Determination of N and s_N parameters for 4-(trifluoromethyl)thiophenolate (**1g**) in DMSO.

Quinone methide	E	k_2 (M^{-1} s^{-1})	log k_2
2a	–17.90	8.16×10^{2}	2.91
2b	–17.29	2.63×10^{3}	3.42
2c	–16.11	2.75×10^{4}	4.45
2d	–15.83	5.46×10^{4}	4.74
2e	–15.03	2.78×10^{5}	5.44
2f	–14.36	7.76×10^{5}	5.89

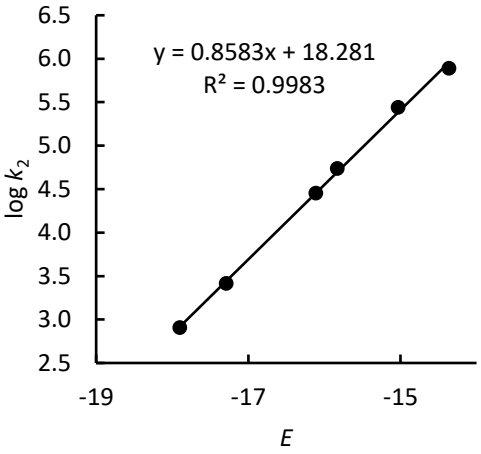

$N = 21.30$
$s_N = 0.86$

Kinetics of reactions of 3,5-bis(trifluoromethyl)thiophenolate (1h) with quinone methides 2

Table S44. Quinone methide **2c** and potassium 3,5-bis(trifluoromethyl)thiophenolate (K-**1h**) in DMSO (detection at 394 nm)

[**2c**]$_0$ (M)	[**1h**]$_0$ (M)	[**1h**-H]$_0$ (M)	k_{obs} (s^{-1})
5.00×10^{-5}	1.27×10^{-4}	5.00×10^{-3}	0.208
5.00×10^{-5}	2.53×10^{-4}	5.00×10^{-3}	0.358
5.00×10^{-5}	5.06×10^{-4}	5.00×10^{-3}	0.661
5.00×10^{-5}	1.01×10^{-3}	5.00×10^{-3}	1.25

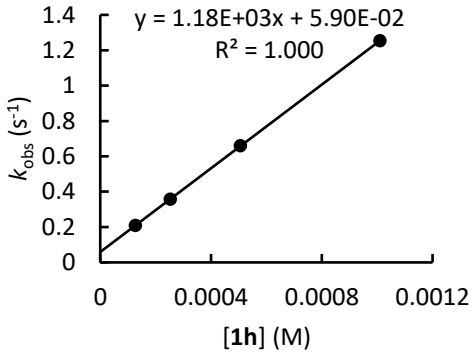

$k_2 = 1.18 \times 10^3$ M^{-1} s^{-1}

Table S45. Quinone methide **2d** and potassium 3,5-bis(trifluoromethyl)thiophenolate (K-**1h**) in DMSO (detection at 372 nm)

[**2d**]$_0$ (M)	[**1h**]$_0$ (M)	[**1h**-H]$_0$ (M)	k_{obs} (s^{-1})
5.00×10^{-5}	1.27×10^{-4}	5.00×10^{-3}	0.432
5.00×10^{-5}	2.53×10^{-4}	5.00×10^{-3}	0.724
5.00×10^{-5}	5.06×10^{-4}	5.00×10^{-3}	1.32
5.00×10^{-5}	1.01×10^{-3}	5.00×10^{-3}	2.50

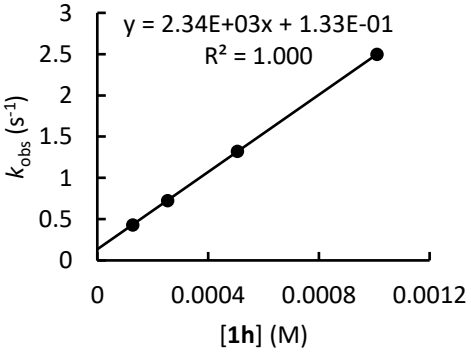

$k_2 = 2.34 \times 10^3$ M^{-1} s^{-1}

Table S46. Quinone methide **2e** and potassium 3,5-bis(trifluoromethyl)thiophenolate (K-**1h**) in DMSO (detection at 386 nm)

[**2e**]$_0$ (M)	[**1h**]$_0$ (M)	[**1h**-H]$_0$ (M)	k_{obs} (s^{-1})
3.50×10^{-4}	1.27×10^{-4}	5.00×10^{-3}	2.12
3.50×10^{-4}	2.53×10^{-4}	5.00×10^{-3}	3.82
3.50×10^{-4}	5.06×10^{-4}	5.00×10^{-3}	6.82
3.50×10^{-4}	1.01×10^{-3}	5.00×10^{-3}	13.4

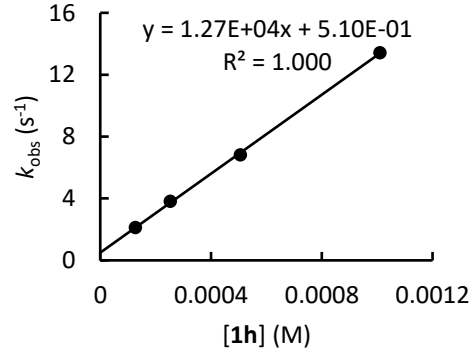

$k_2 = 1.27 \times 10^4$ M^{-1} s^{-1}

Table S47. Quinone methide **2f** and potassium 3,5-bis(trifluoromethyl)thiophenolate (K-**1h**) in DMSO (detection at 374 nm)

[**2f**]$_0$ (M)	[**1h**]$_0$ (M)	[**1h**-H]$_0$ (M)	k_{obs} (s^{-1})
5.00×10^{-5}	1.27×10^{-4}	5.00×10^{-3}	6.43
5.00×10^{-5}	2.53×10^{-4}	5.00×10^{-3}	11.2
5.00×10^{-5}	5.06×10^{-4}	5.00×10^{-3}	21.0
5.00×10^{-5}	1.01×10^{-3}	5.00×10^{-3}	40.0

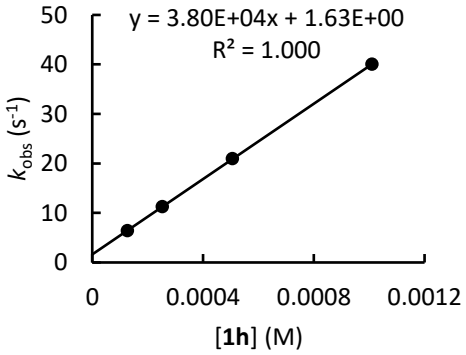

$k_2 = 3.80 \times 10^4$ M^{-1} s^{-1}

Table S48. Determination of N and s_N parameters for 3,5-bis(trifluoromethyl)thiophenolate (**1h**) in DMSO.

Quinone methide	E	k_2 (M^{-1} s^{-1})	log k_2
2c	–16.11	1.18×10^3	3.07
2d	–15.83	2.34×10^3	3.37
2e	–15.03	1.27×10^4	4.11
2f	–14.36	3.80×10^4	4.58

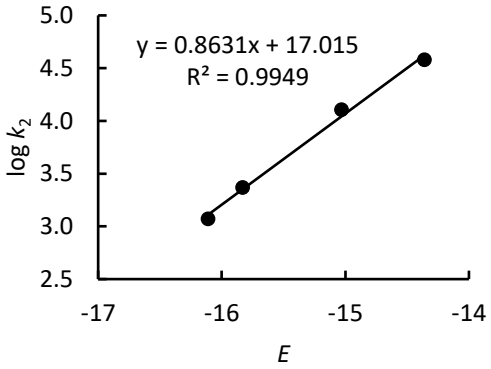

$N = 19.71$
$s_N = 0.86$

Kinetics of reactions of 4-nitro-thiophenolate (1i) with quinone methides

Table S49. Quinone methide **2c** and sodium 4-nitro-thiophenolate (Na-**1i**) in DMSO (detection at 392 nm)

[**2c**]$_0$ (M)	[**1i**]$_0$ (M)	[**1h**-H]$_0$ (M)	k_{obs} (s^{-1})
6.20×10^{-5}	1.59×10^{-4}	5.00×10^{-3}	9.54×10^{-2}
6.20×10^{-5}	3.13×10^{-4}	5.00×10^{-3}	1.39×10^{-1}
6.20×10^{-5}	4.61×10^{-4}	5.00×10^{-3}	1.74×10^{-1}
6.20×10^{-5}	6.45×10^{-4}	5.00×10^{-3}	2.19×10^{-1}

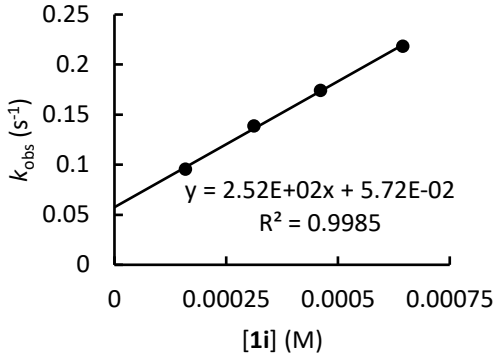

$k_2 = 2.52 \times 10^2\ M^{-1}\ s^{-1}$

Table S50. Quinone methide **2d** and sodium 4-nitro-thiophenolate (Na-**1i**) in DMSO (detection at 390 nm)

[**2d**]$_0$ (M)	[**1i**]$_0$ (M)	[**1h**-H]$_0$ (M)	k_{obs} (s^{-1})
1.12×10^{-4}	1.59×10^{-4}	5.00×10^{-3}	1.91×10^{-1}
1.12×10^{-4}	3.13×10^{-4}	5.00×10^{-3}	2.76×10^{-1}
1.12×10^{-4}	4.61×10^{-4}	5.00×10^{-3}	3.50×10^{-1}
1.12×10^{-4}	6.45×10^{-4}	5.00×10^{-3}	4.42×10^{-1}

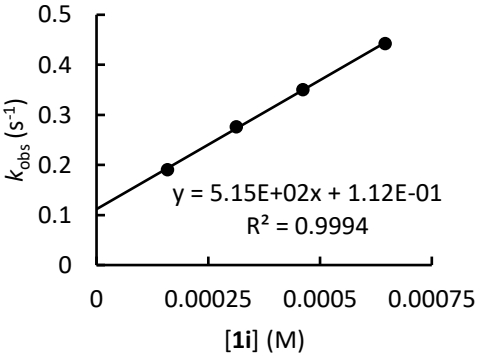

$k_2 = 5.15 \times 10^2\ M^{-1}\ s^{-1}$

Table S51. Quinone methide **2e** and sodium 4-nitro-thiophenolate (Na-**1i**) in DMSO (detection at 390 nm)

[**2e**]$_0$ (M)	[**1i**]$_0$ (M)	[**1h**-H]$_0$ (M)	k_{obs} (s^{-1})
3.75×10^{-4}	1.59×10^{-4}	5.00×10^{-3}	0.930
3.75×10^{-4}	3.13×10^{-4}	5.00×10^{-3}	1.44
3.75×10^{-4}	4.61×10^{-4}	5.00×10^{-3}	1.83
3.75×10^{-4}	6.45×10^{-4}	5.00×10^{-3}	2.23

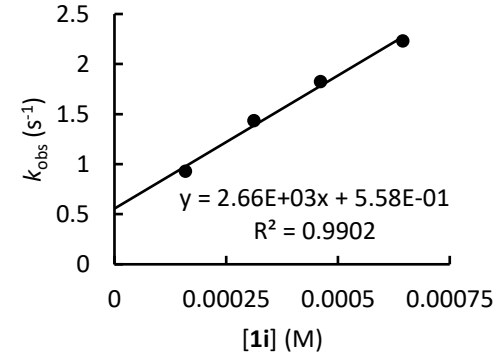

$k_2 = 2.66 \times 10^3\ M^{-1}\ s^{-1}$

Table S52. Quinone methide **2f** and sodium 4-nitro-thiophenolate (Na-**1i**) in DMSO (detection at 390 nm)

[**2f**]$_0$ (M)	[**1i**]$_0$ (M)	[**1h**-H]$_0$ (M)	k_{obs} (s^{-1})
1.12×10^{-4}	1.59×10^{-4}	5.00×10^{-3}	3.22
1.12×10^{-4}	3.13×10^{-4}	5.00×10^{-3}	4.95
1.12×10^{-4}	4.61×10^{-4}	5.00×10^{-3}	6.23
1.12×10^{-4}	6.45×10^{-4}	5.00×10^{-3}	7.37

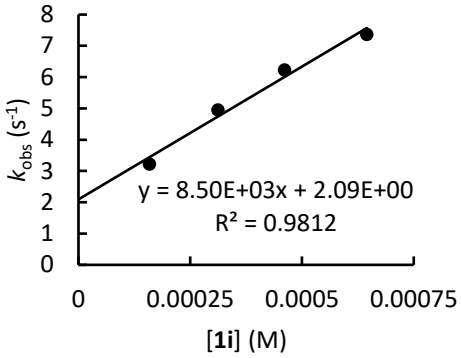

$k_2 = 8.50 \times 10^3$ M^{-1} s^{-1}

Table S53. Determination of N and s_N parameters for 4-nitro-thiophenolate (**1i**) in DMSO.

Quinone methide	E	k_2 (M^{-1} s^{-1})	log k_2
2c	–16.11	2.51×10^2	2.40
2d	–15.83	5.15×10^2	2.71
2e	–15.03	2.66×10^3	3.42
2f	–14.36	8.49×10^3	3.93

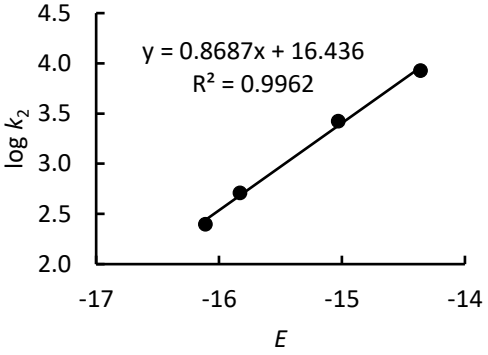

$N = 18.91$
$s_N = 0.87$

Kinetics of the reactions of napthalene-2-thiolate (1j) with quinone methides

Table S54. Quinone methide **2b** and potassium napthalene-2-thiolate (K-**1j**) in DMSO (at 490 nm)

[**2b**]$_0$ (M)	[**1j**]$_0$ (M)	[**1j**-H]$_0$ (M)	k_{obs} (s^{-1})
5.00×10^{-5}	9.92×10^{-5}	5.00×10^{-3}	2.70
5.00×10^{-5}	1.98×10^{-4}	5.00×10^{-3}	5.23
5.00×10^{-5}	2.97×10^{-4}	5.00×10^{-3}	8.30
5.00×10^{-5}	3.97×10^{-4}	5.00×10^{-3}	10.3

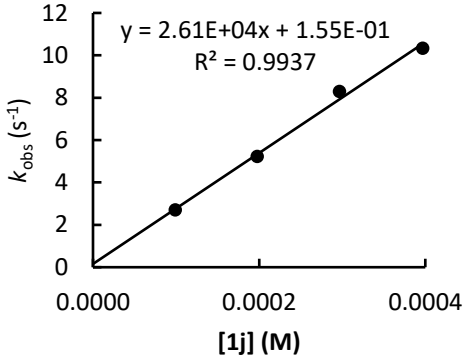

$k_2 = 2.61 \times 10^4\ M^{-1}\ s^{-1}$

Table S55. Quinone methide **2c** and potassium napthalene-2-thiolate (K-**1j**) in DMSO (detection at 393 nm)

[**2c**]$_0$ (M)	[**1j**]$_0$ (M)	[**1j**-H]$_0$ (M)	k_{obs} (s^{-1})
5.00×10^{-5}	9.92×10^{-5}	5.00×10^{-3}	21.9
5.00×10^{-5}	1.98×10^{-4}	5.00×10^{-3}	44.0
5.00×10^{-5}	2.97×10^{-4}	5.00×10^{-3}	62.9
5.00×10^{-5}	3.97×10^{-4}	5.00×10^{-3}	80.8

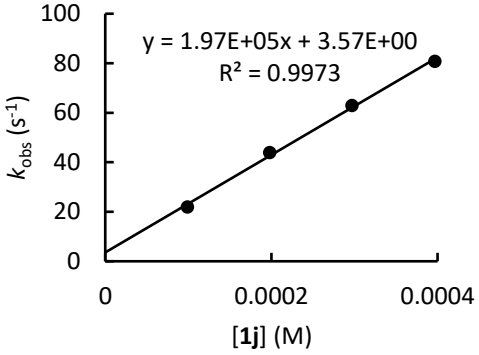

$k_2 = 1.97 \times 10^5\ M^{-1}\ s^{-1}$

Table S56. Quinone methide **2d** and potassium napthalene-2-thiolate (K-**1j**) in DMSO (detection at 371 nm)

[**2d**]$_0$ (M)	[**1j**]$_0$ (M)	[**1j**-H]$_0$ (M)	k_{obs} (s^{-1})
5.00×10^{-5}	9.92×10^{-5}	5.00×10^{-3}	35.3
5.00×10^{-5}	1.98×10^{-4}	5.00×10^{-3}	76.5
5.00×10^{-5}	2.97×10^{-4}	5.00×10^{-3}	111
5.00×10^{-5}	3.97×10^{-4}	5.00×10^{-3}	139

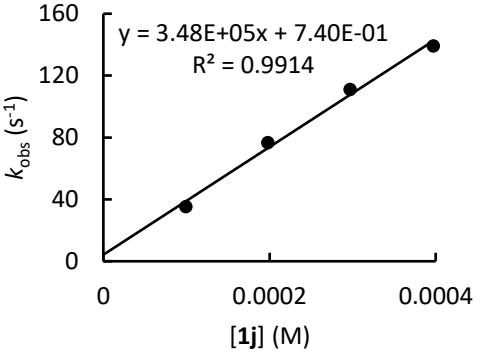

$k_2 = 3.48 \times 10^5\ M^{-1}\ s^{-1}$

Table S57. Quinone methide **2e** and potassium napthalene-2-thiolate (K-**1j**) in DMSO (detection at 350 nm)

[**2e**]$_0$ (M)	[**1j**]$_0$ (M)	[**1j**-H]$_0$ (M)	k_{obs} (s^{-1})
5.00×10^{-5}	9.92×10^{-5}	5.00×10^{-3}	182
5.00×10^{-5}	1.98×10^{-4}	5.00×10^{-3}	431
5.00×10^{-5}	2.97×10^{-4}	5.00×10^{-3}	628
5.00×10^{-5}	3.97×10^{-4}	5.00×10^{-3}	795

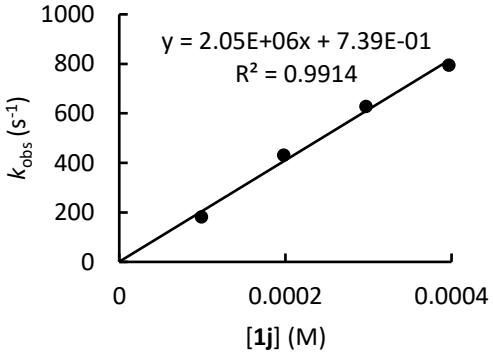

$k_2 = 2.05 \times 10^6\ M^{-1}\ s^{-1}$

Table S58. Determination of N and s_N parameters for napthalene-2-thiolate (**1j**) in DMSO.

Quinone methide	E	k_2 ($M^{-1}\ s^{-1}$)	log k_2
2b	–17.29	2.61×10^4	4.42
2c	–16.11	1.97×10^5	5.29
2d	–15.83	3.48×10^5	5.54
2e	–15.03	2.05×10^6	6.31

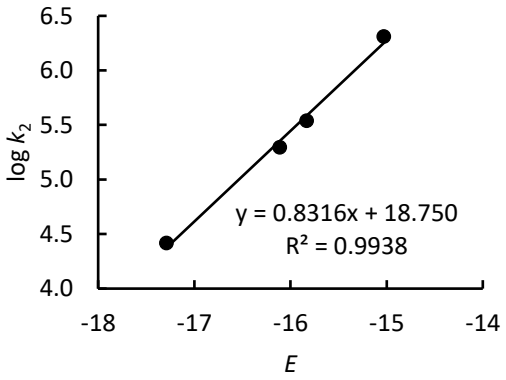

$N = 22.55$
$s_N = 0.83$

Kinetics of reactions of thiophenolates with further electrophiles E1-E3

- Kinetics of thiophenolate reactions with the 1,2-diaza-1,3-diene **E1**

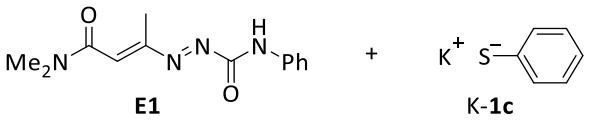

E1 + K-**1c**

Table S59. 1,2-Diaza-1,3-diene **E1** and potassium thiophenolate (K-**1c**) in DMSO (detection at 380 nm)

[**E1**]$_0$ (M)	[**1c**]$_0$ (M)	[**1c**-H]$_0$ (M)	k_{obs} (s^{-1})
1.79×10^{-3}	6.25×10^{-5}	5.00×10^{-3}	37.6
1.79×10^{-3}	1.25×10^{-4}	5.00×10^{-3}	79.6
1.79×10^{-3}	1.88×10^{-4}	5.00×10^{-3}	123
1.79×10^{-3}	2.50×10^{-4}	5.00×10^{-3}	173

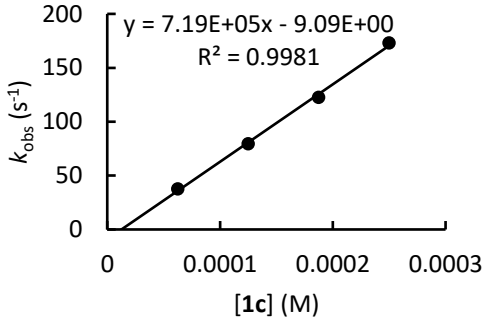

$k_2 = 7.19 \times 10^5\ M^{-1}\ s^{-1}$

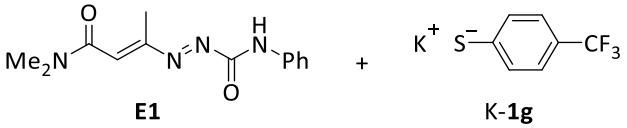

E1 + K-**1g**

Table S60. 1,2-Diaza-1,3-diene **E1** and potassium 4-(trifluoromethyl)thiophenolate (K-**1g**) in DMSO (detection at 380 nm)

[**E1**]$_0$ (M)	[**1g**]$_0$ (M)	[**1g**-H]$_0$ (M)	k_{obs} (s^{-1})
1.79×10^{-3}	4.86×10^{-4}	5.00×10^{-3}	43.1
1.79×10^{-3}	9.71×10^{-4}	5.00×10^{-3}	85.9
1.79×10^{-3}	1.46×10^{-3}	5.00×10^{-3}	131
1.79×10^{-3}	1.94×10^{-3}	5.00×10^{-3}	170

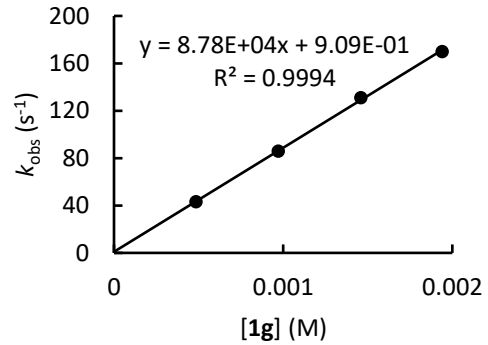

$k_2 = 8.78 \times 10^4\ M^{-1}\ s^{-1}$

- Kinetics of thiophenolate reactions with the isothiocyanate **E2**

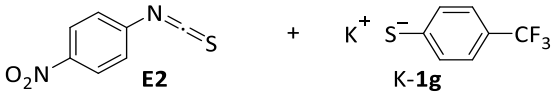

Table S61 Isothiocyanate **E2** and potassium 4-(trifluoromethyl)thiophenolate (K-**1g**) in DMSO (detection of increase at 440 nm)

[**E2**]$_0$ (M)	[**1g**]$_0$ (M)	[**1g**-H]$_0$ (M)	k_{obs} (s^{-1})
5.39×10^{-4}	4.86×10^{-4}	5.00×10^{-3}	314
5.39×10^{-4}	9.71×10^{-4}	5.00×10^{-3}	602
5.39×10^{-4}	1.46×10^{-3}	5.00×10^{-3}	886
5.39×10^{-4}	1.94×10^{-3}	5.00×10^{-3}	1.14×10^{3}

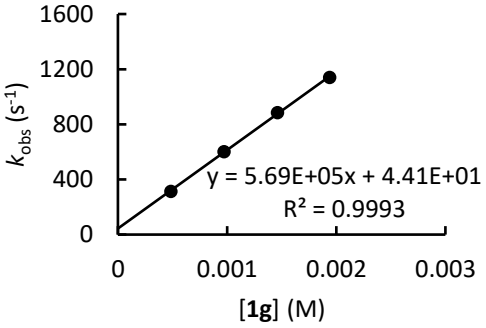

$k_2 = 5.69 \times 10^5$ M^{-1} s^{-1}

- Kinetics of thiophenolate reactions with the isothiocyanate **E3**

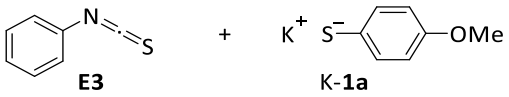

Table S62. Ph-NCS (**E3**) and potassium 4-methoxy-thiophenolate (K-**1a**) in DMSO (detection of increase at 320 nm)

[**E3**]$_0$ (M)	[**1a**]$_0$ (M)	[**1a**-H]$_0$ (M)	k_{obs} (s^{-1})
5.93×10^{-3}	6.00×10^{-4}	0	316
1.19×10^{-2}	6.00×10^{-4}	0	603
1.78×10^{-2}	6.00×10^{-4}	0	886
2.37×10^{-2}	6.00×10^{-4}	0	1.16×10^{3}

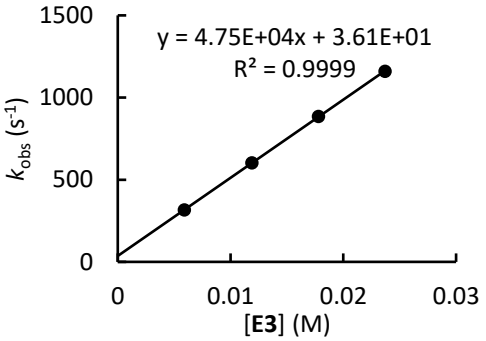

$k_2 = 4.75 \times 10^4$ M^{-1} s^{-1}

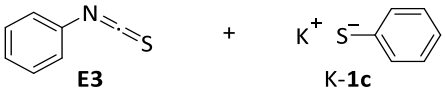

Table S63. Ph-NCS (**E3**) and potassium thiophenolate (K-**1c**) in DMSO (detection of increase at 326 nm)

[**E3**]$_0$ (M)	[**1c**]$_0$ (M)	[**1c**-H]$_0$ (M)	k_{obs} (s^{-1})
5.93×10^{-3}	6.00×10^{-4}	0	55.3
1.19×10^{-2}	6.00×10^{-4}	0	83.2
1.78×10^{-2}	6.00×10^{-4}	0	113
2.37×10^{-2}	6.00×10^{-4}	0	142

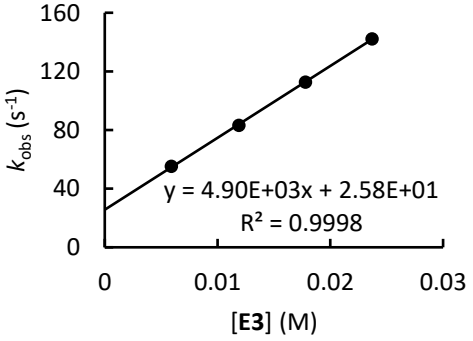

$k_2 = 4.90 \times 10^3$ M^{-1} s^{-1}

2.2.4 Copies of NMR Spectra

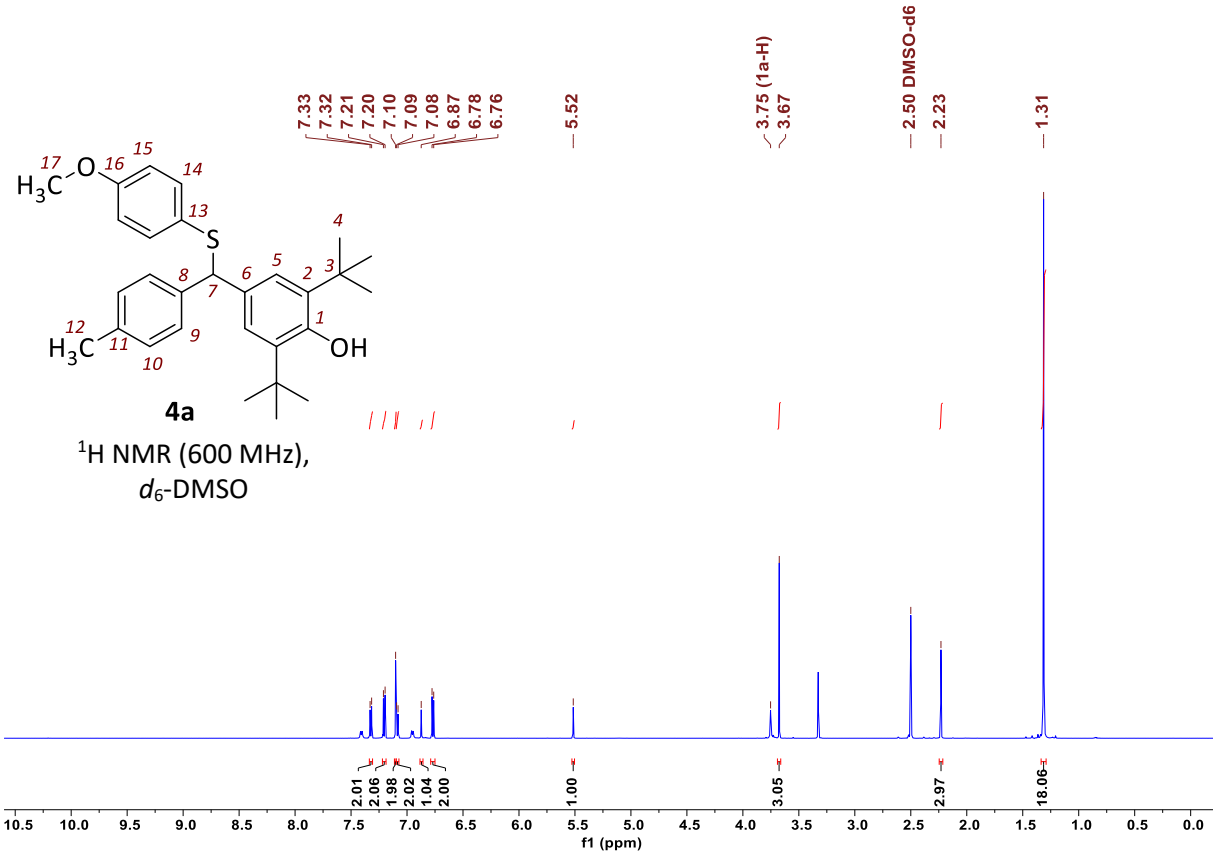

4a

^{1}H NMR (600 MHz), d_6-DMSO

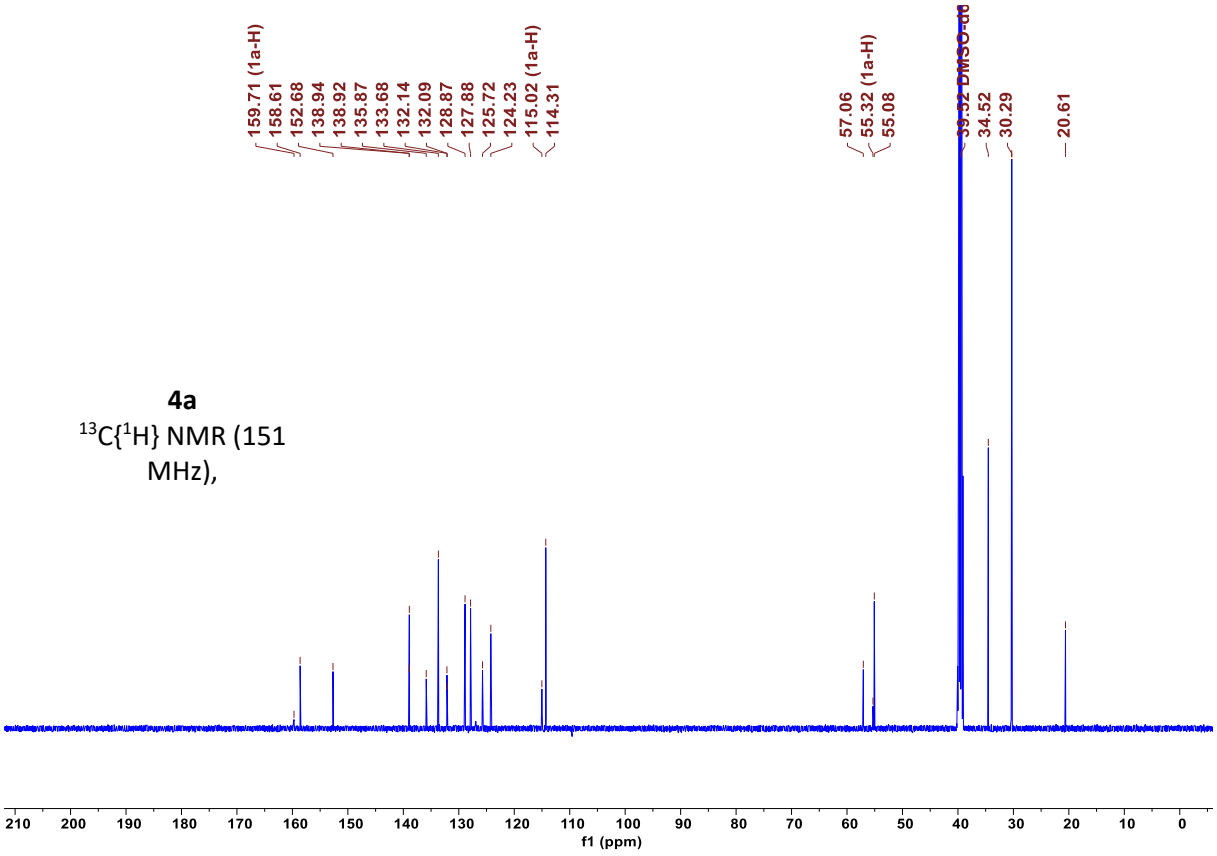

4a

^{13}C{^{1}H} NMR (151 MHz),

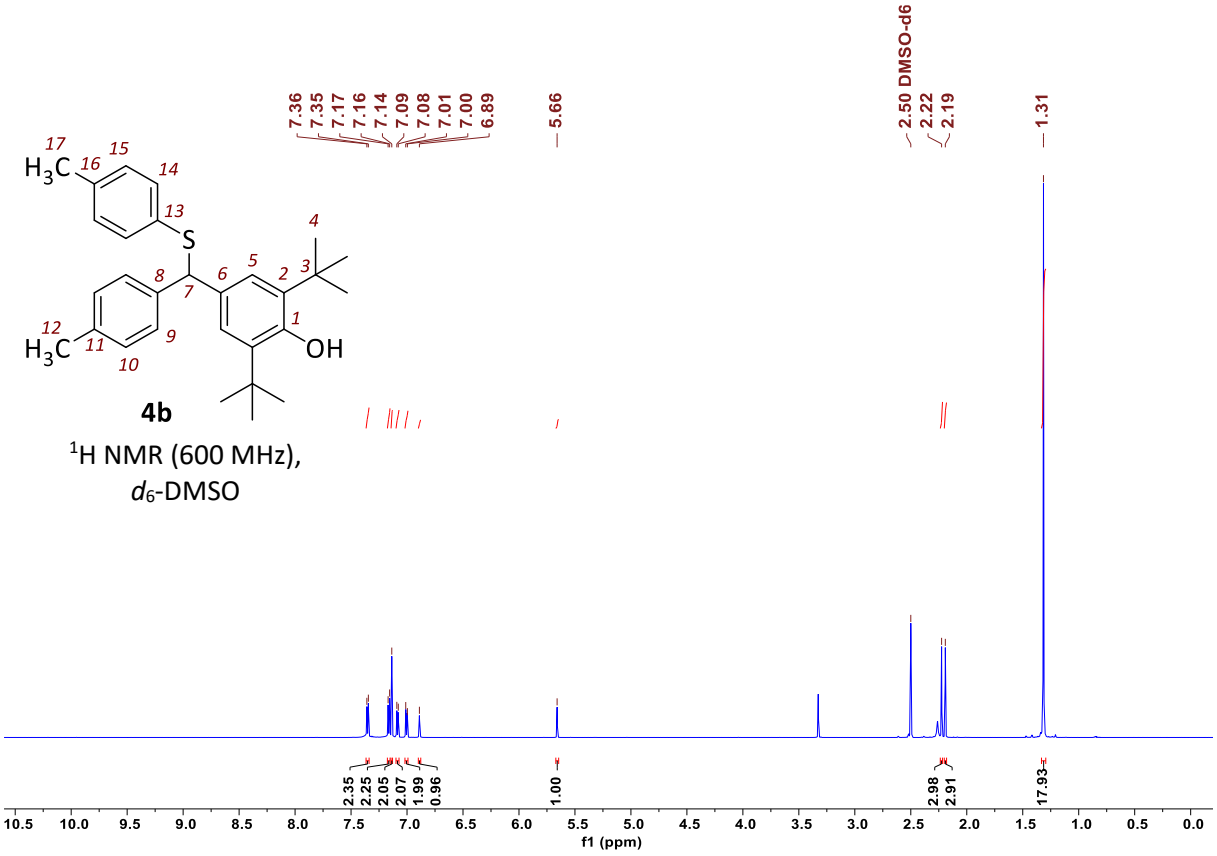

4b

^{1}H NMR (600 MHz),
d_6-DMSO

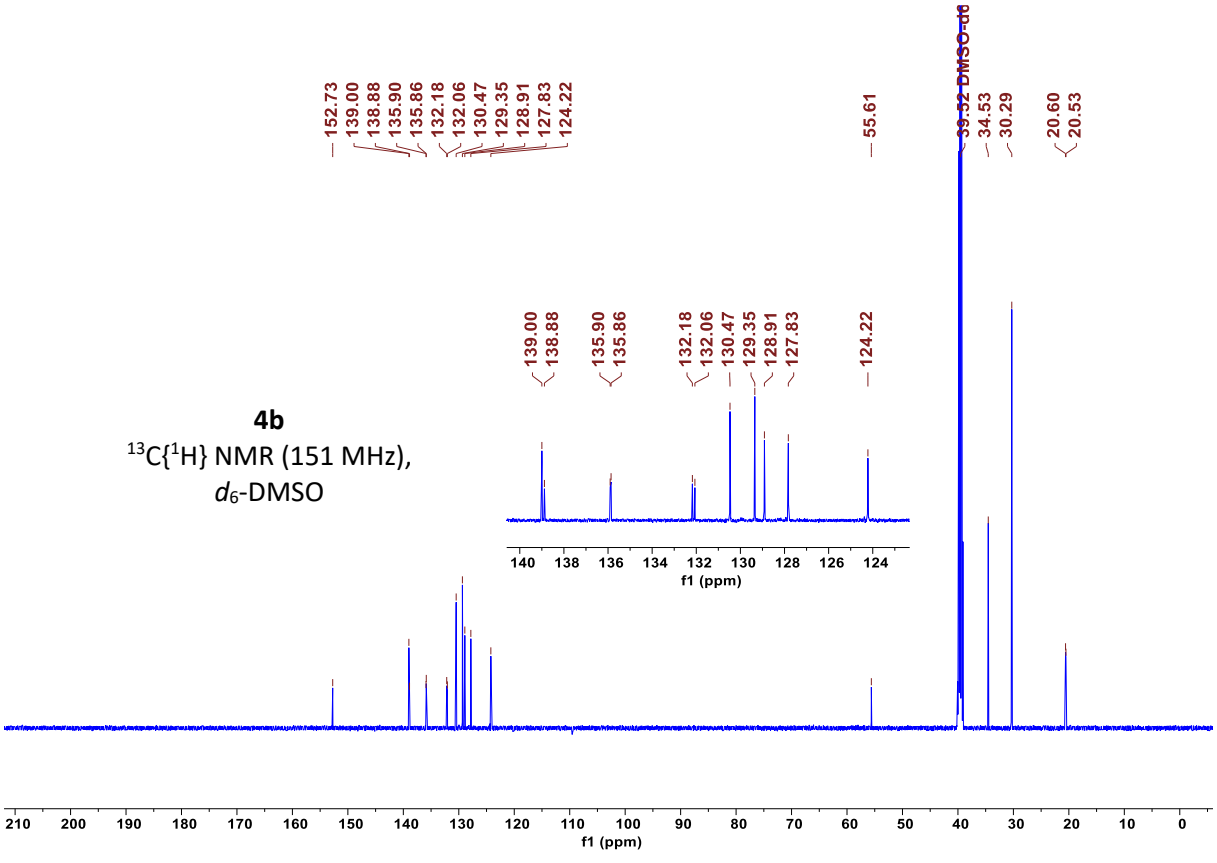

4b

^{13}C{^{1}H} NMR (151 MHz),
d_6-DMSO

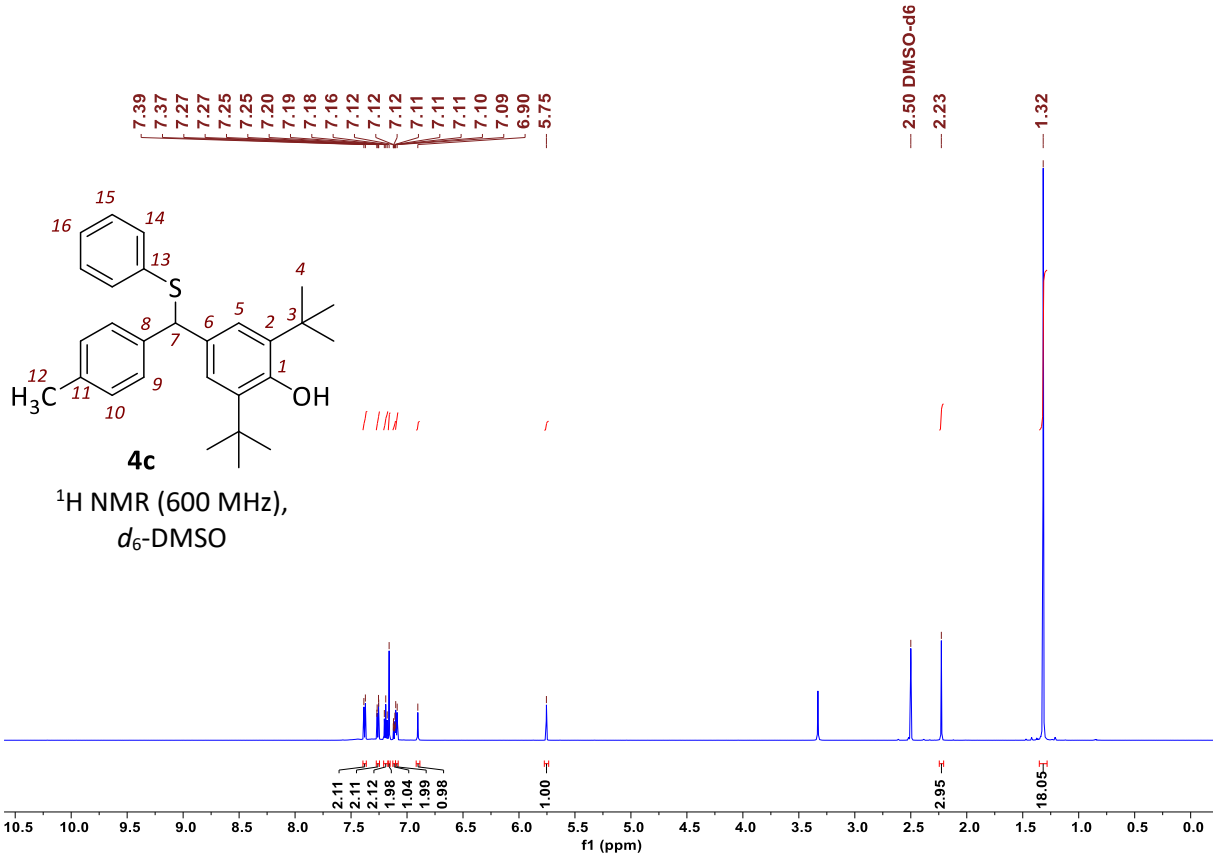

4c

^{1}H NMR (600 MHz),
d_6-DMSO

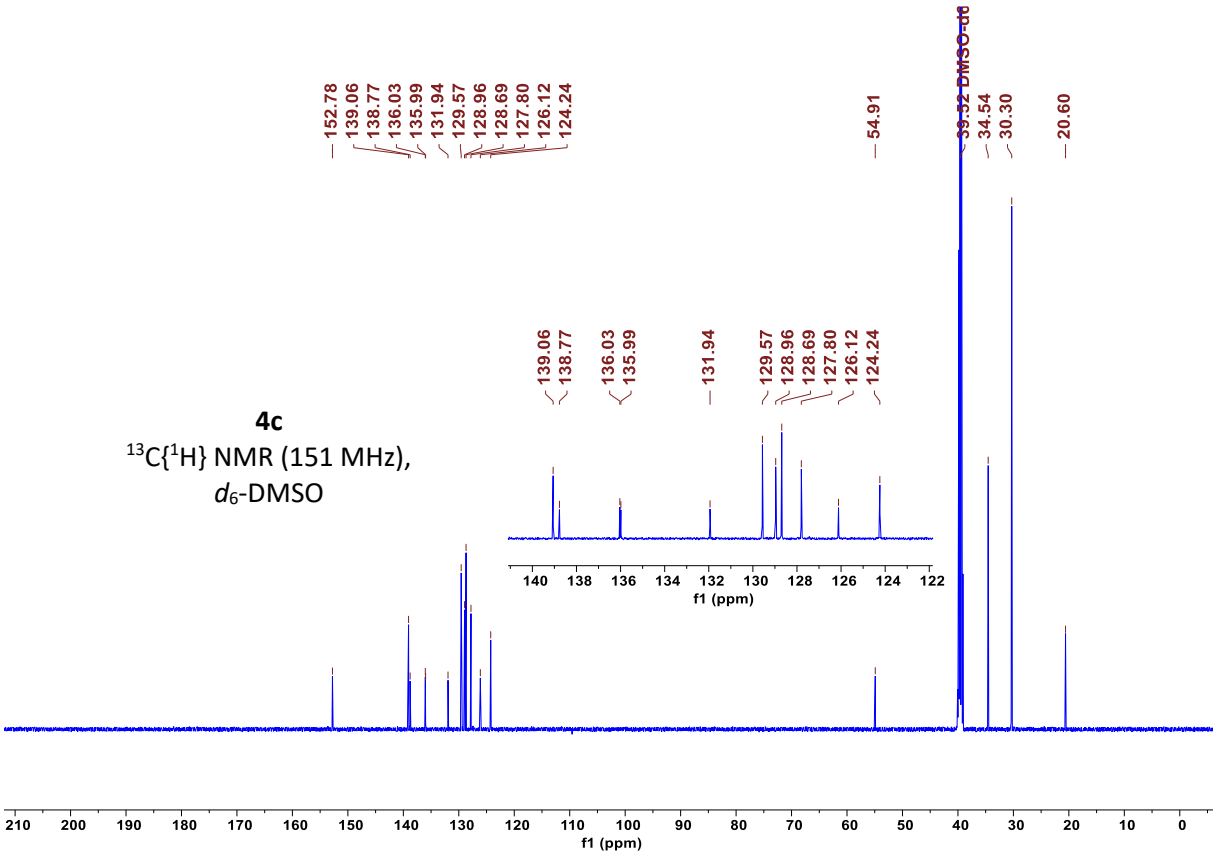

4c

^{13}C{^{1}H} NMR (151 MHz),
d_6-DMSO

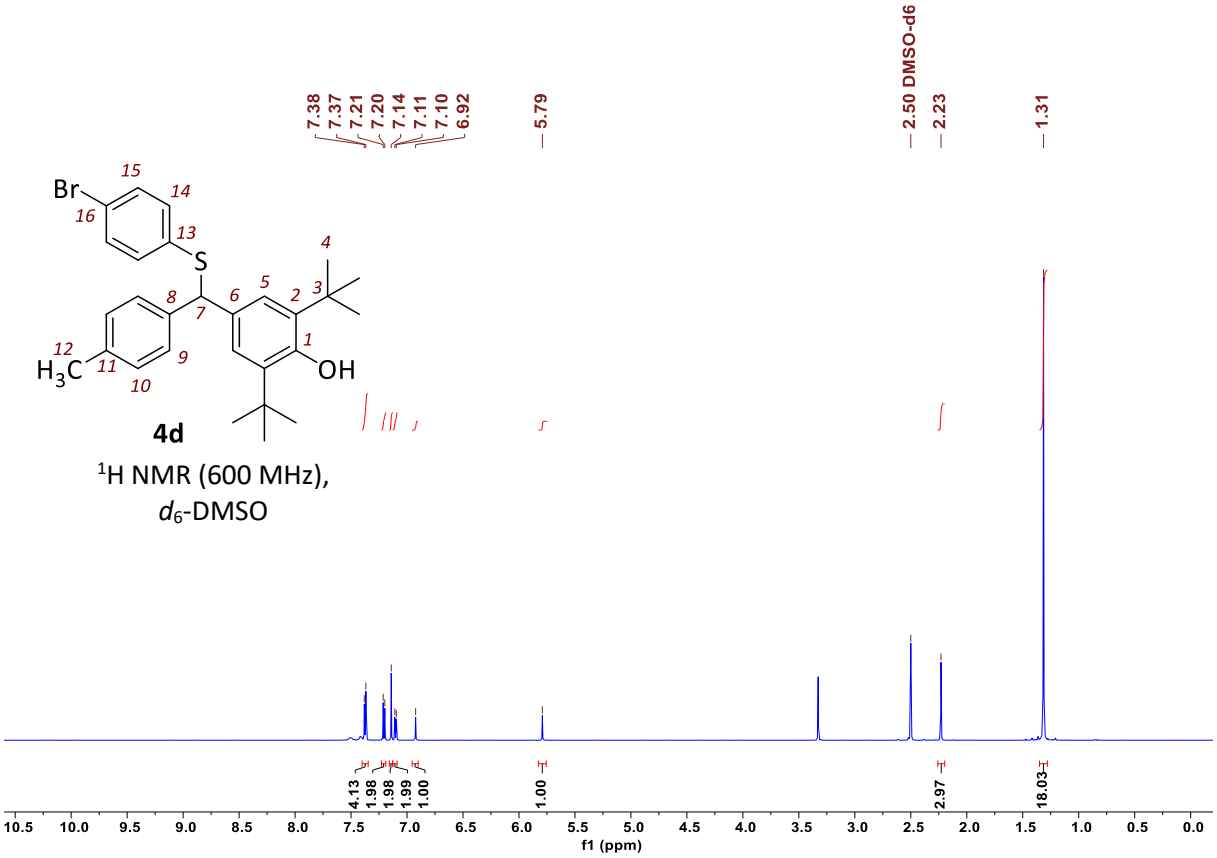
7.38
7.37
7.21
7.20
7.14
7.11
7.10
6.92
5.79
2.50 DMSO-d6
2.23
1.31
Br
S
OH
H3C
4d
1H NMR (600 MHz),
d6-DMSO
4.13
1.98
1.98
1.99
1.00
1.00
2.97
18.03
f1 (ppm)

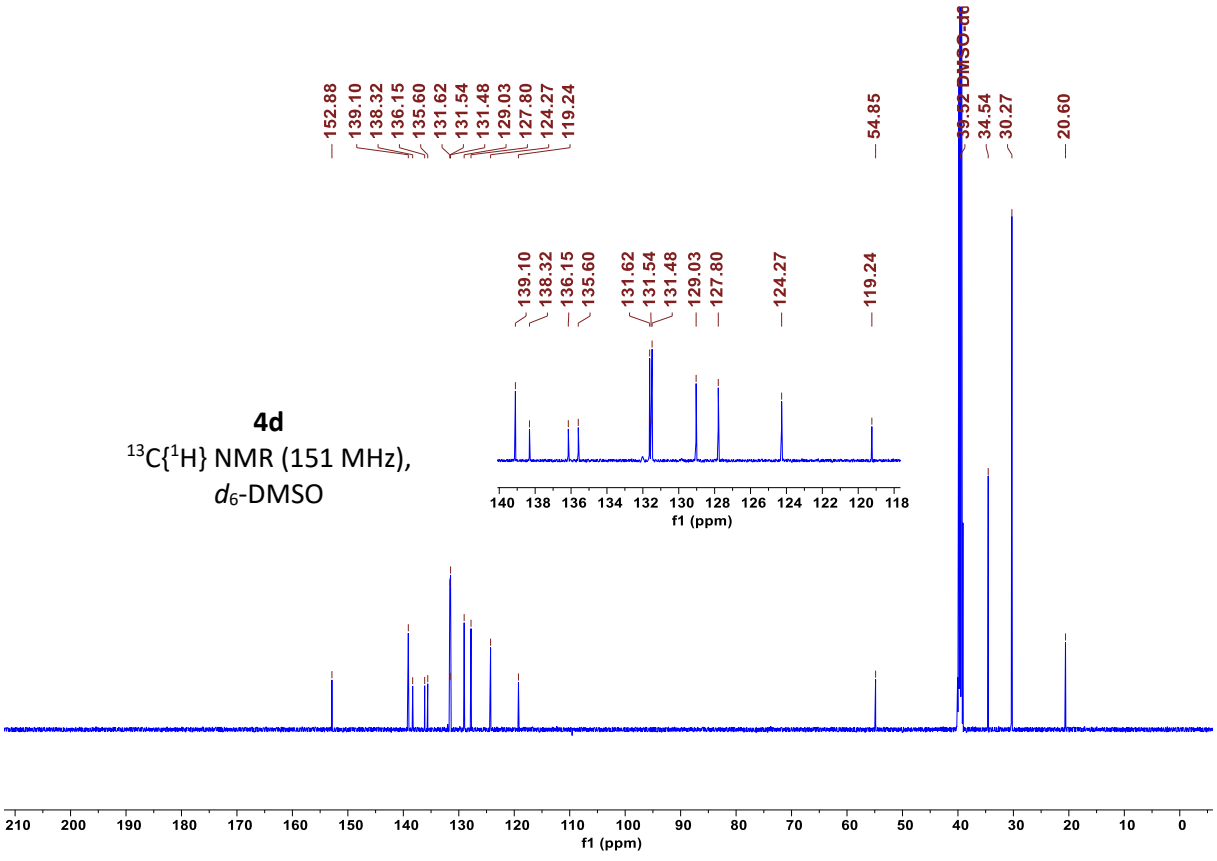
152.88
139.10
138.32
136.15
135.60
131.62
131.54
131.48
129.03
127.80
124.27
119.24
54.85
39.52 DMSO-d6
34.54
30.27
20.60
4d
13C{1H} NMR (151 MHz),
d6-DMSO
f1 (ppm)

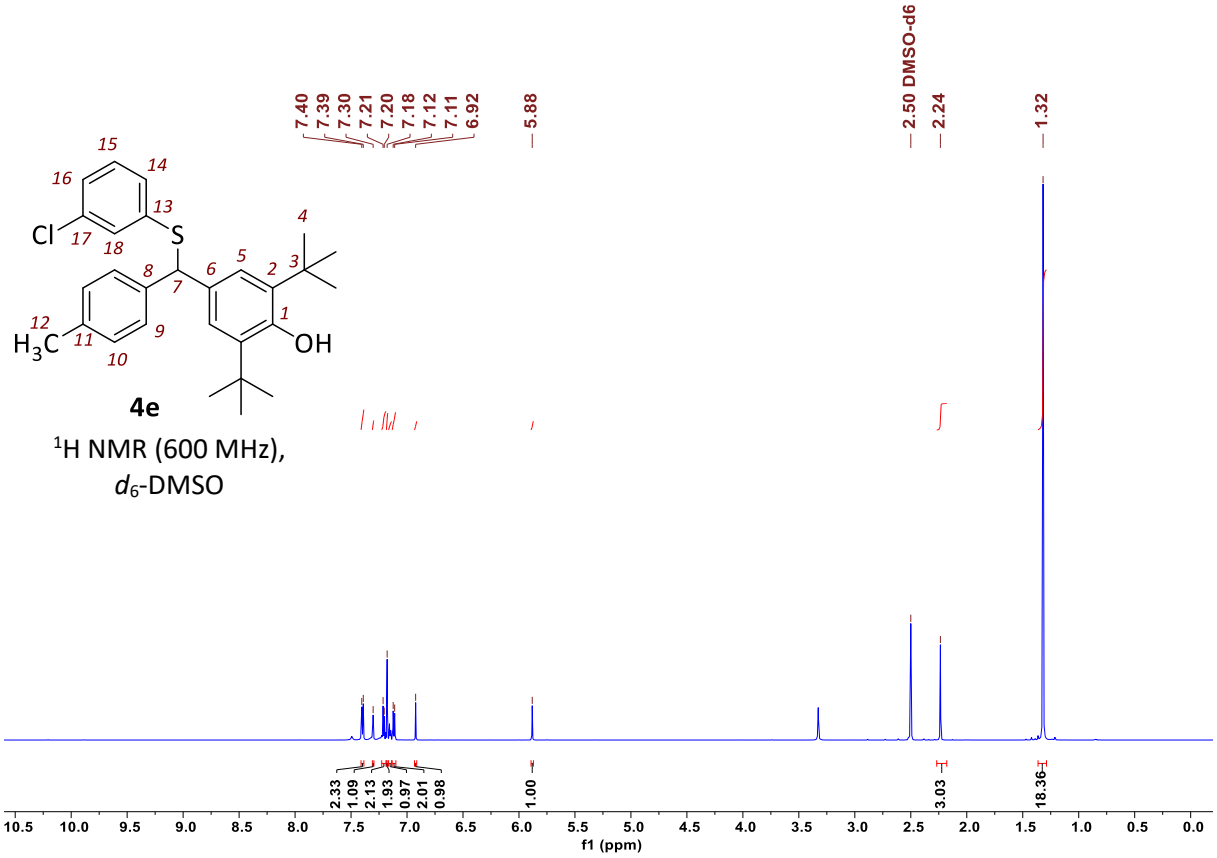

4e

^{1}H NMR (600 MHz),
d_6-DMSO

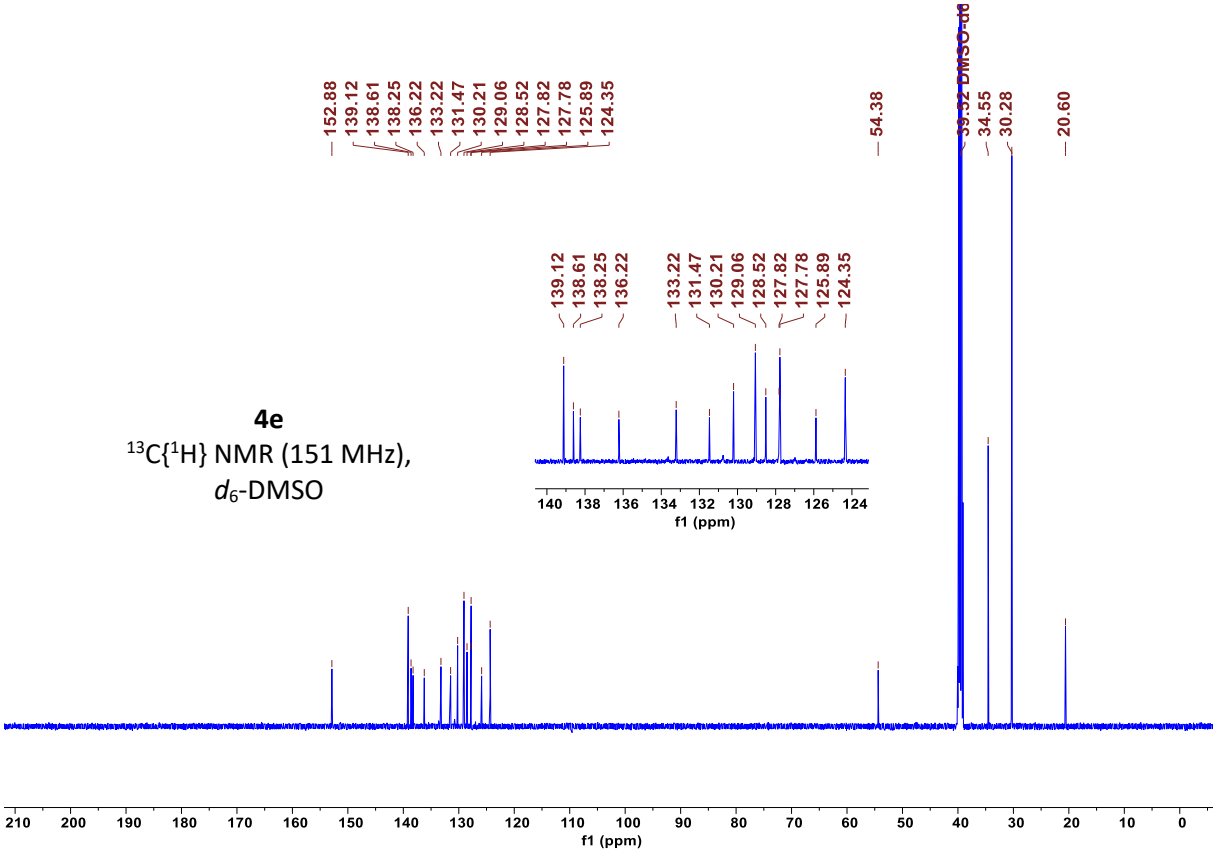

4e

^{13}C{^{1}H} NMR (151 MHz),
d_6-DMSO

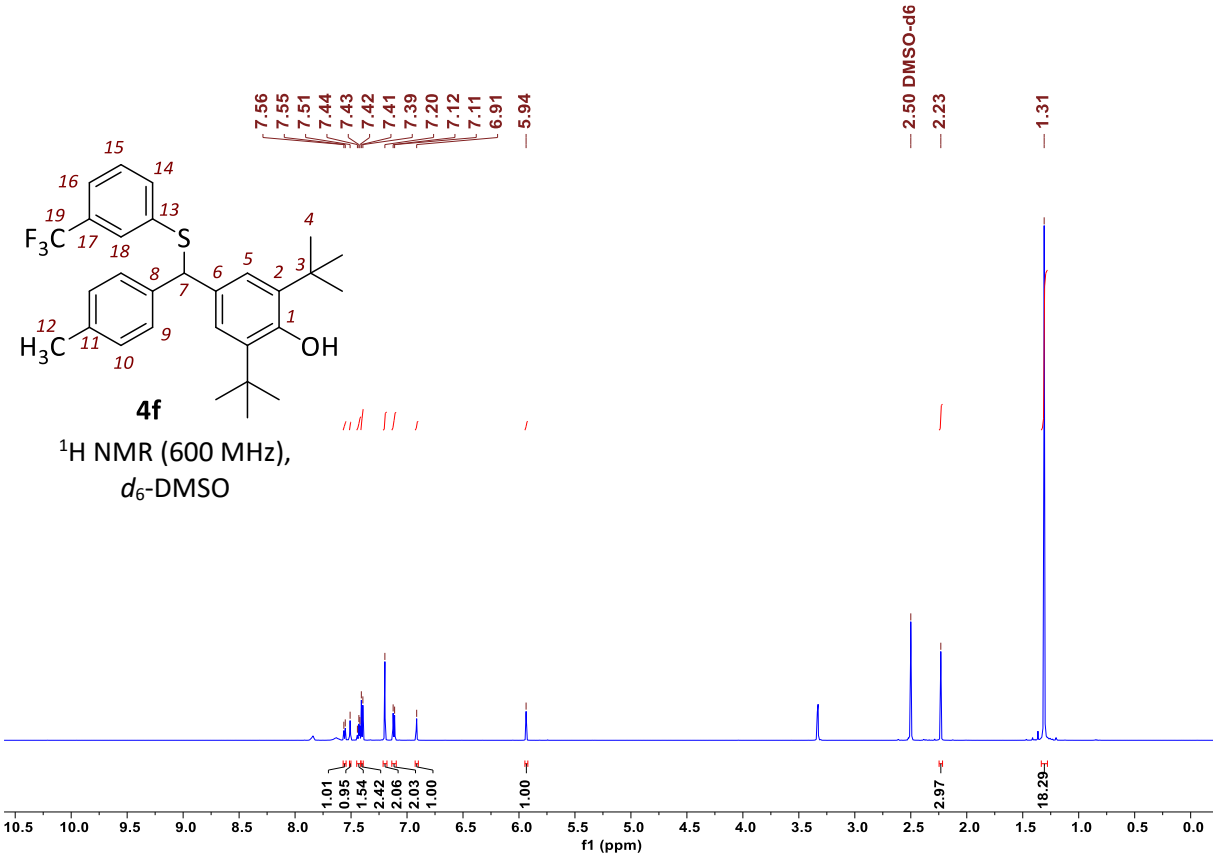

4f

^{1}H NMR (600 MHz), d_6-DMSO

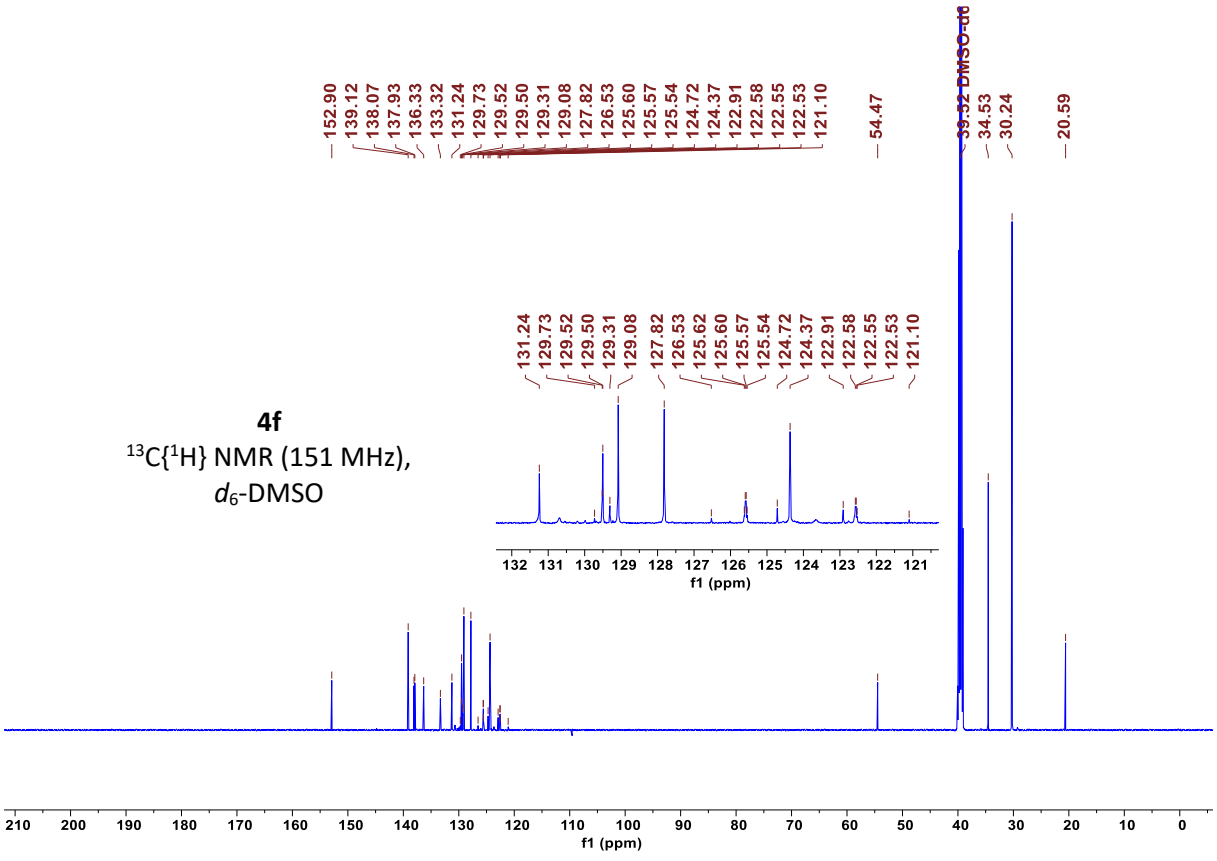

4f

^{13}C{^{1}H} NMR (151 MHz), d_6-DMSO

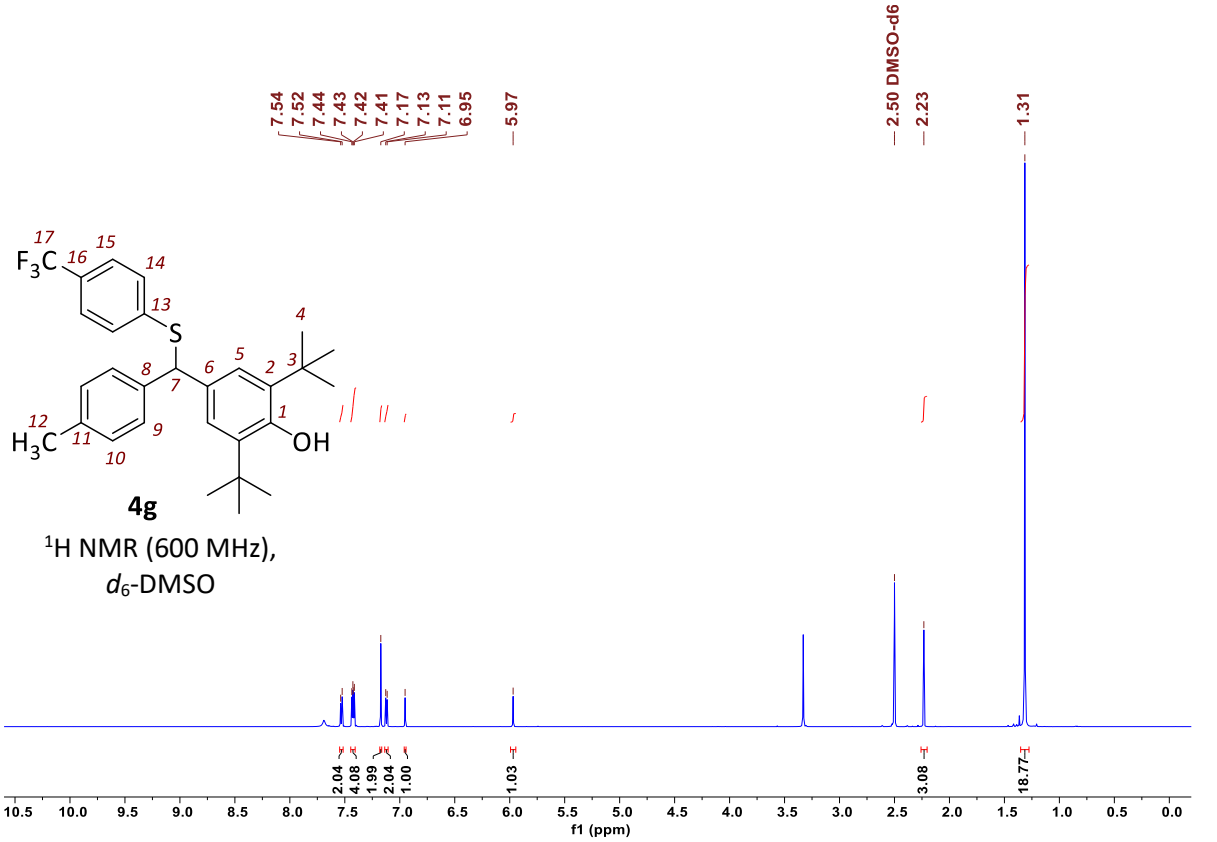

4g

^{1}H NMR (600 MHz), d_6-DMSO

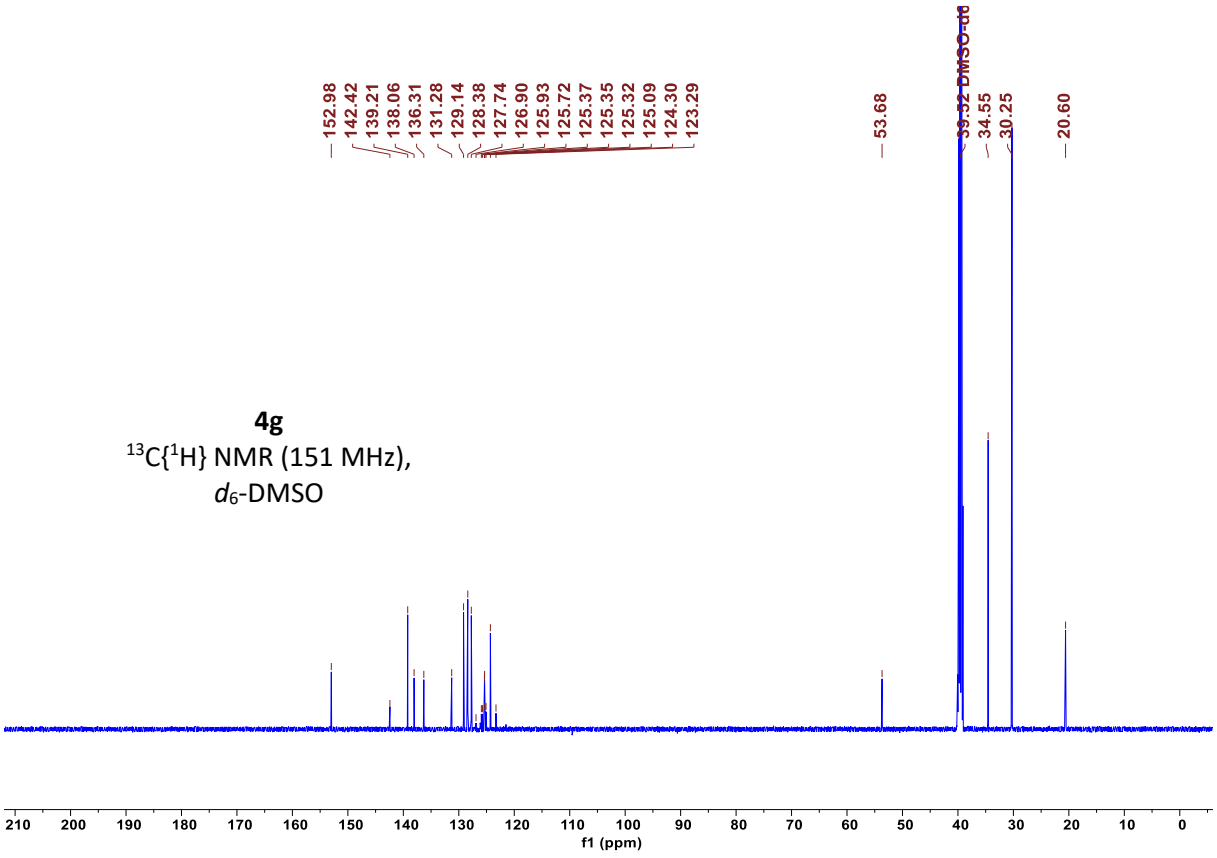

4g

^{13}C{^{1}H} NMR (151 MHz), d_6-DMSO

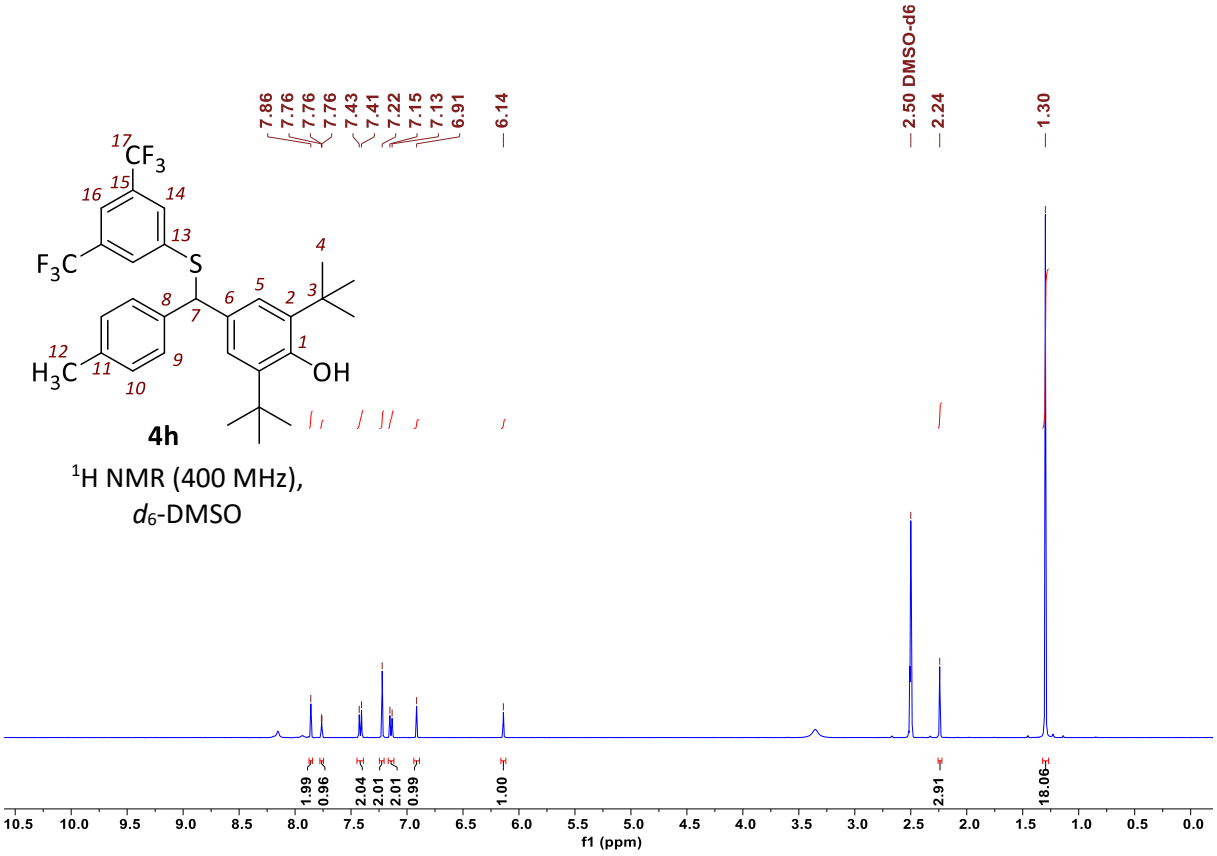

4h

^{1}H NMR (400 MHz), d_6-DMSO

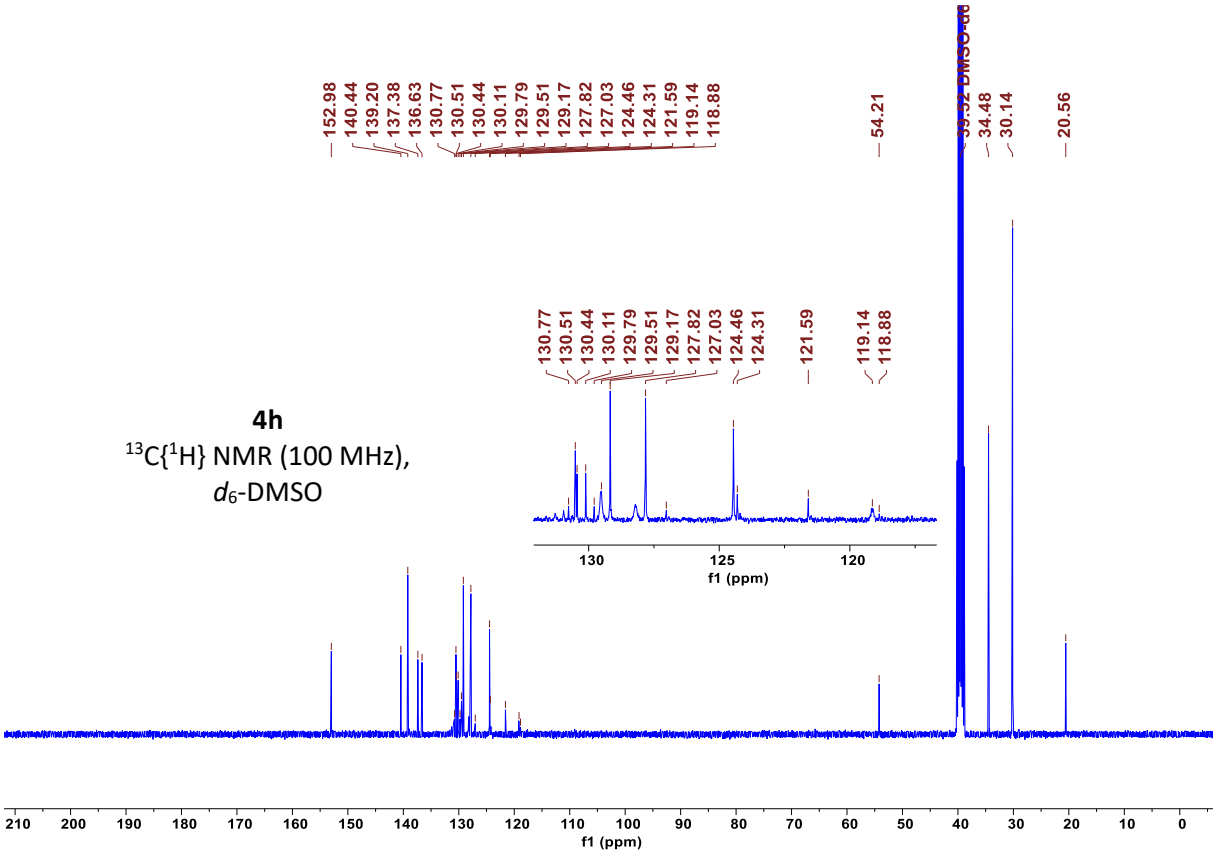

4h

^{13}C{^{1}H} NMR (100 MHz), d_6-DMSO

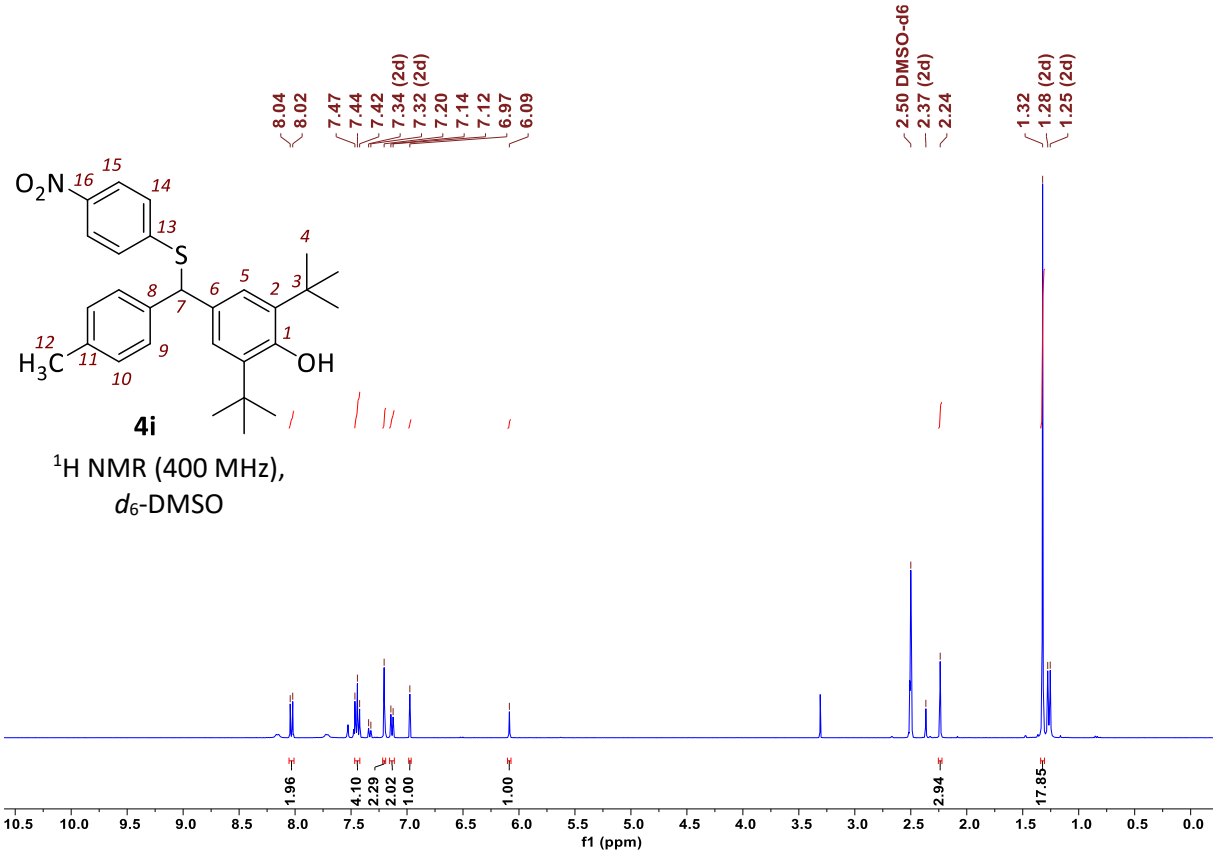

4i

^{1}H NMR (400 MHz),
d_6-DMSO

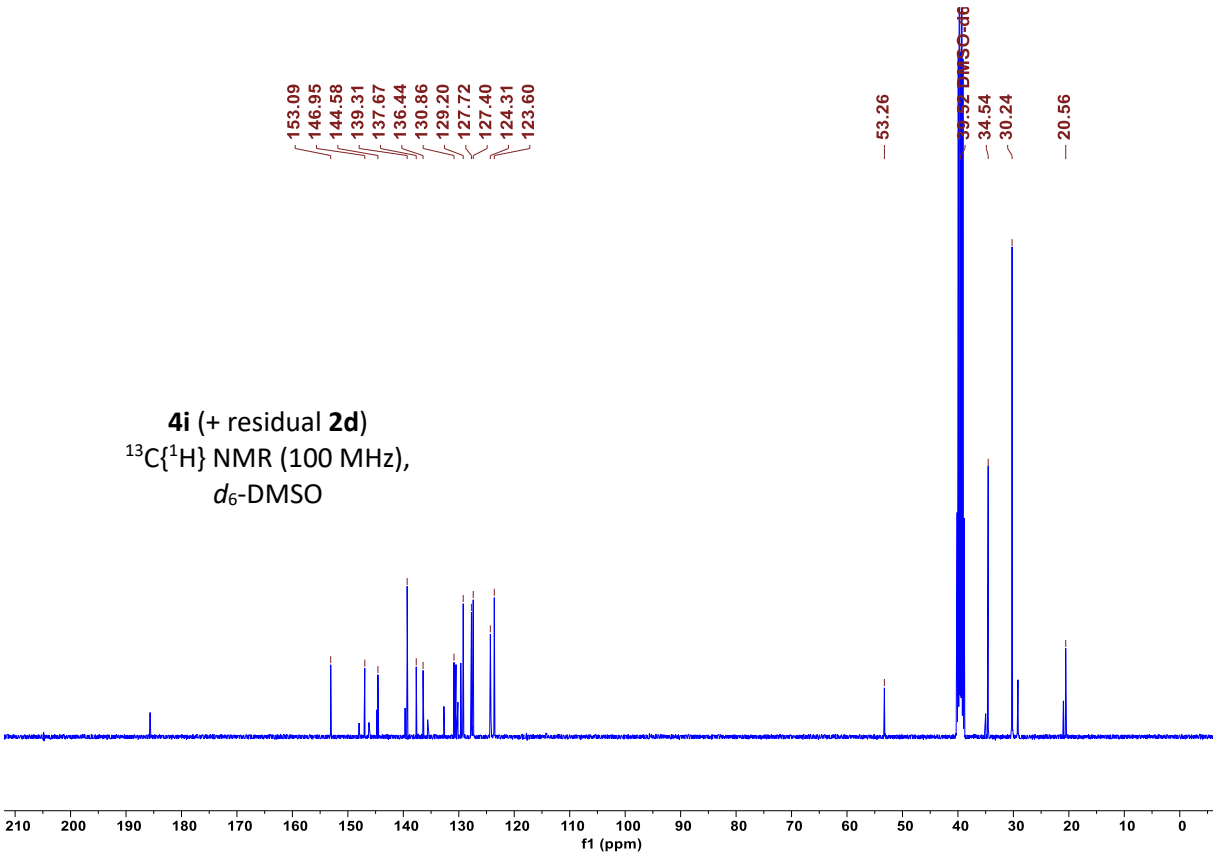

4i (+ residual **2d**)
^{13}C{^{1}H} NMR (100 MHz),
d_6-DMSO

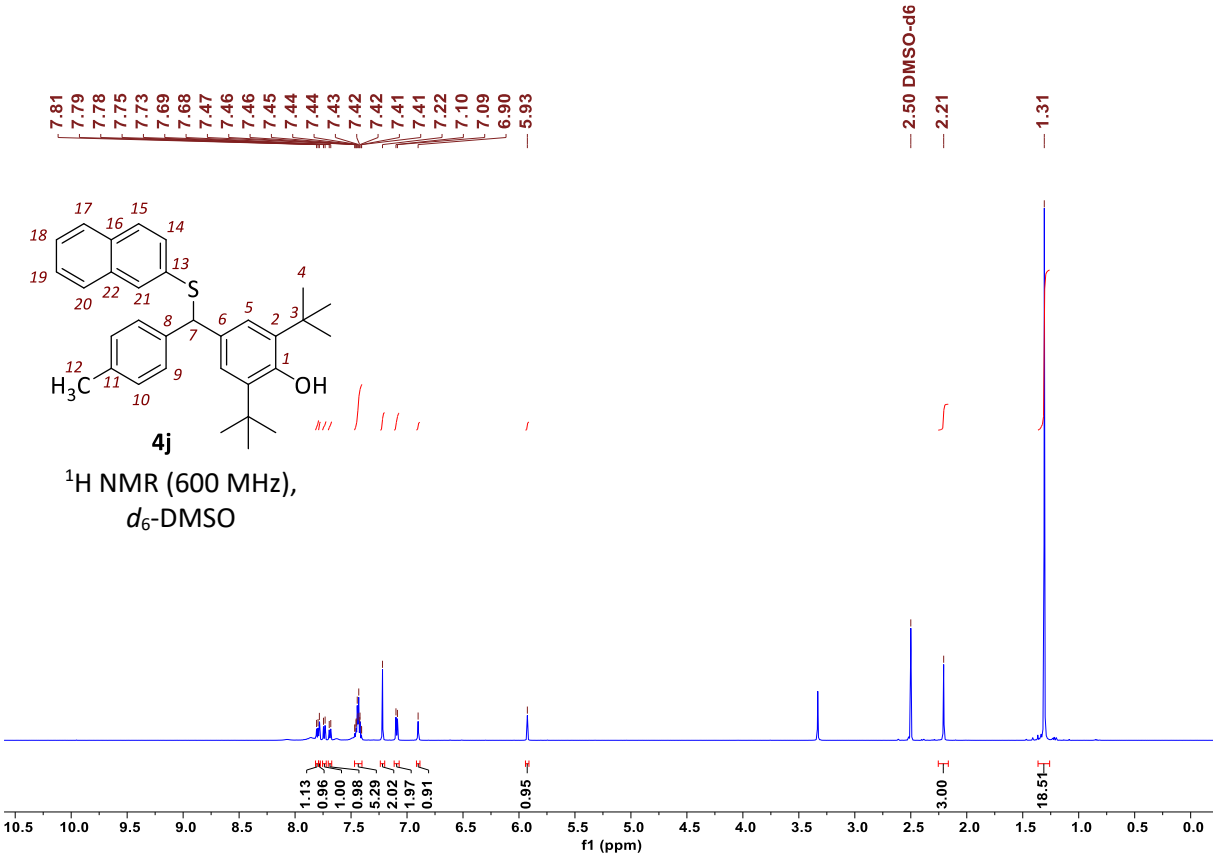
7.81
7.79
7.78
7.75
7.73
7.69
7.68
7.47
7.46
7.46
7.45
7.44
7.44
7.43
7.42
7.42
7.41
7.41
7.22
7.10
7.09
6.90
5.93
2.50 DMSO-d6
2.21
1.31
17 15 16 14 18 19 20 22 21 13 S 8 7 6 5 2 3 4 1 OH 12 H3C 11 9 10
4j
1H NMR (600 MHz),
d6-DMSO
1.13
0.96
1.00
0.98
5.29
2.02
1.97
0.91
0.95
3.00
18.51
10.5 10.0 9.5 9.0 8.5 8.0 7.5 7.0 6.5 6.0 5.5 5.0 4.5 4.0 3.5 3.0 2.5 2.0 1.5 1.0 0.5 0.0
f1 (ppm)

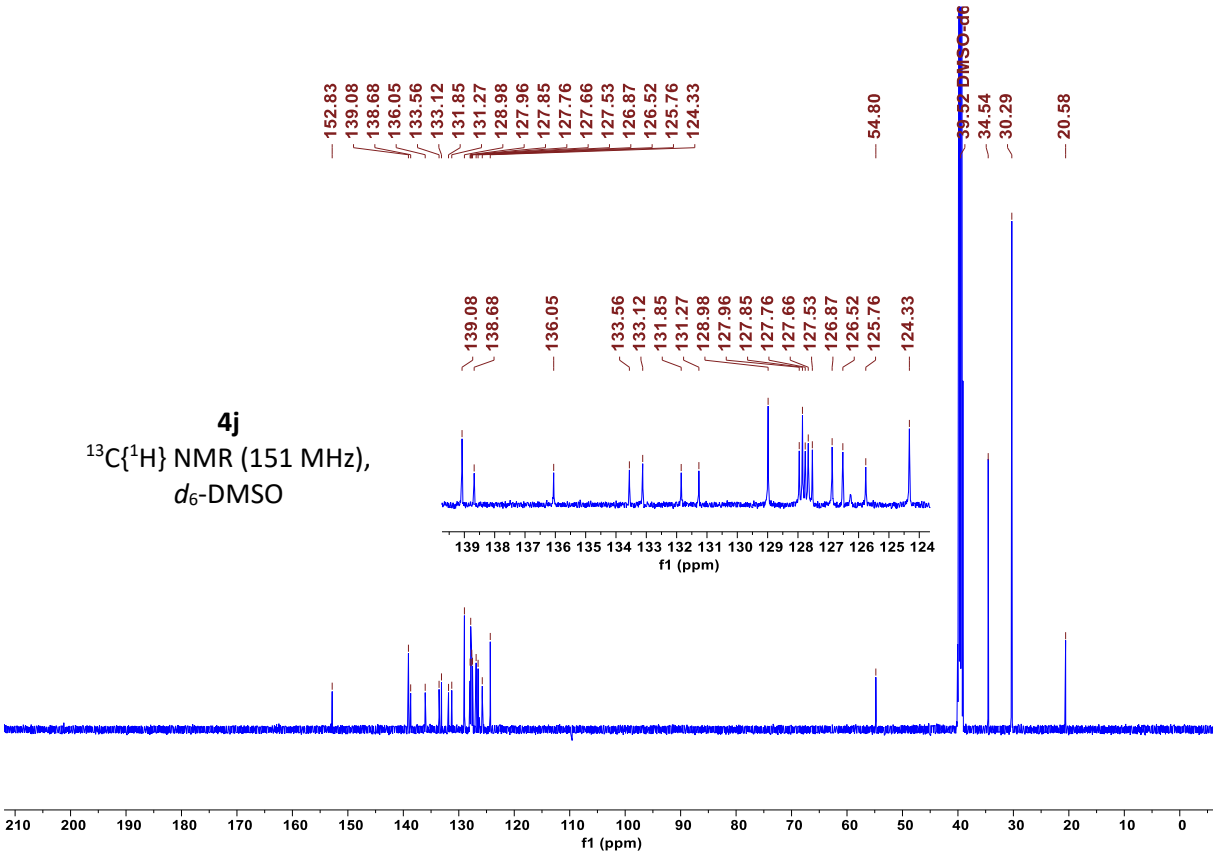
152.83
139.08
138.68
136.05
133.56
133.12
131.85
131.27
128.98
127.96
127.85
127.76
127.66
127.53
126.87
126.52
125.76
124.33
54.80
39.32 DMSO-d6
34.54
30.29
20.58
4j
13C{1H} NMR (151 MHz),
d6-DMSO
139 138 137 136 135 134 133 132 131 130 129 128 127 126 125 124
f1 (ppm)
210 200 190 180 170 160 150 140 130 120 110 100 90 80 70 60 50 40 30 20 10 0
f1 (ppm)

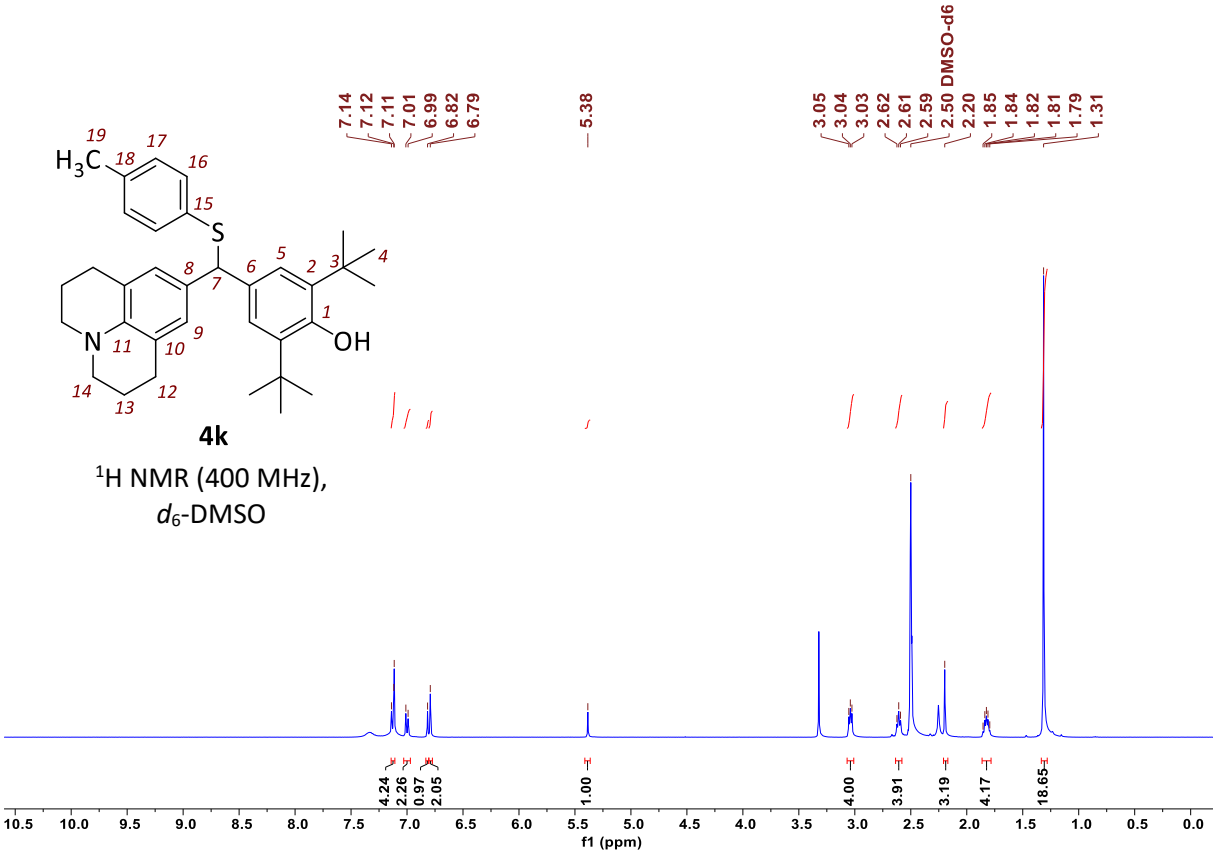

4k

^{1}H NMR (400 MHz), d_6-DMSO

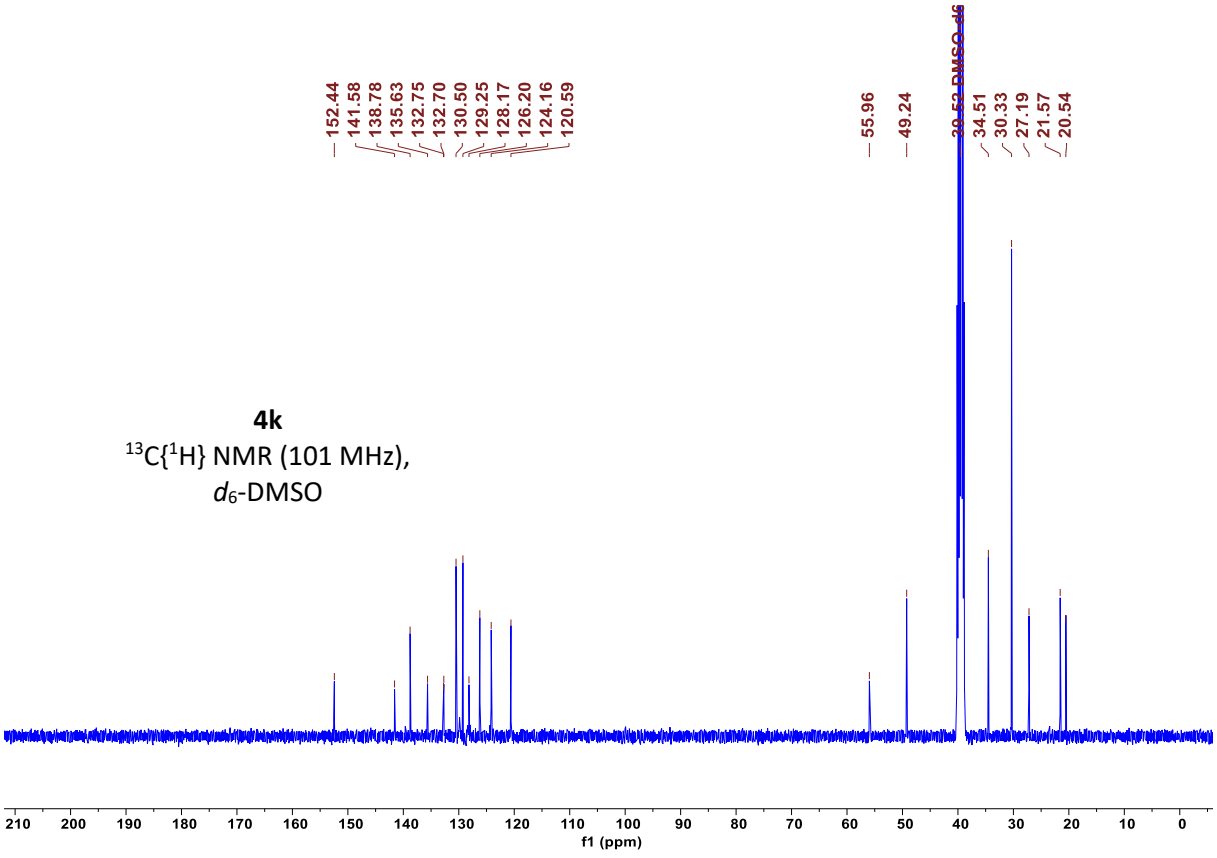

4k

^{13}C{^{1}H} NMR (101 MHz), d_6-DMSO

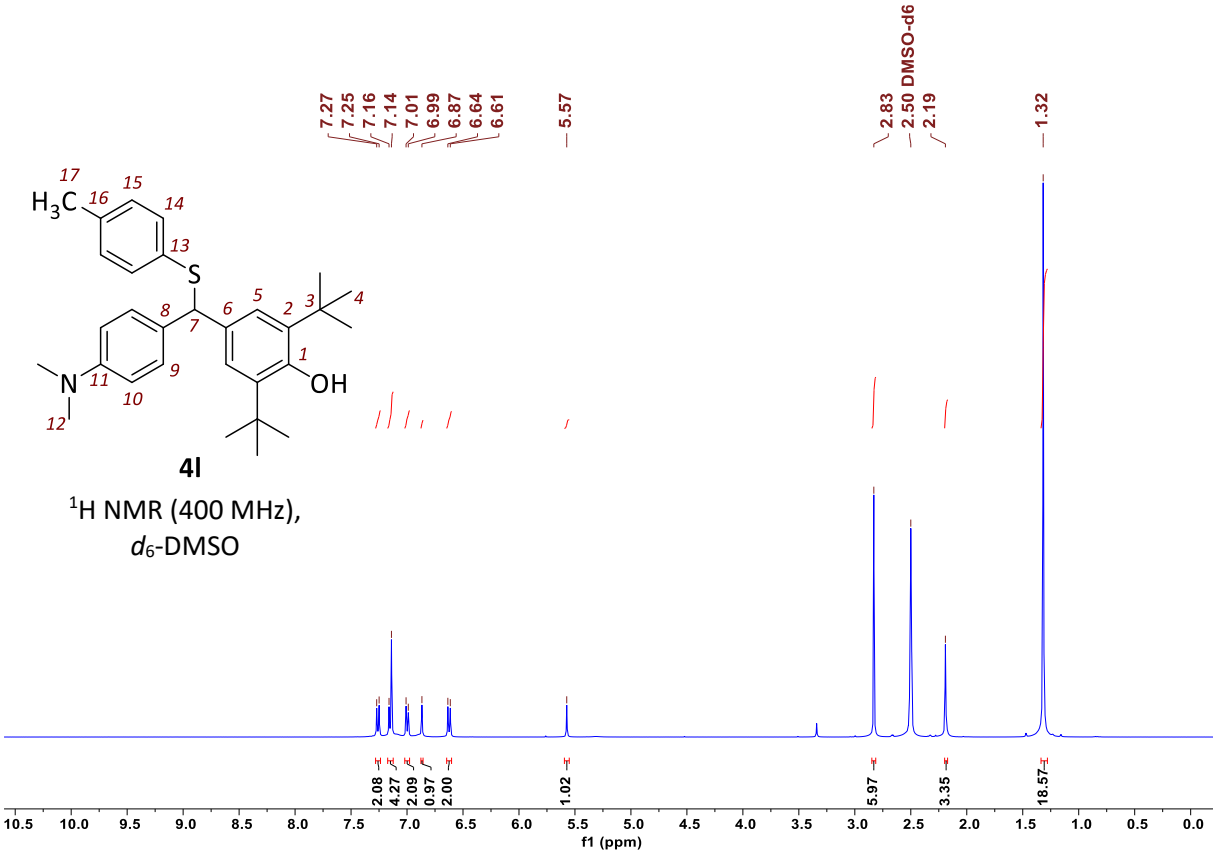

4l

^{1}H NMR (400 MHz), d_6-DMSO

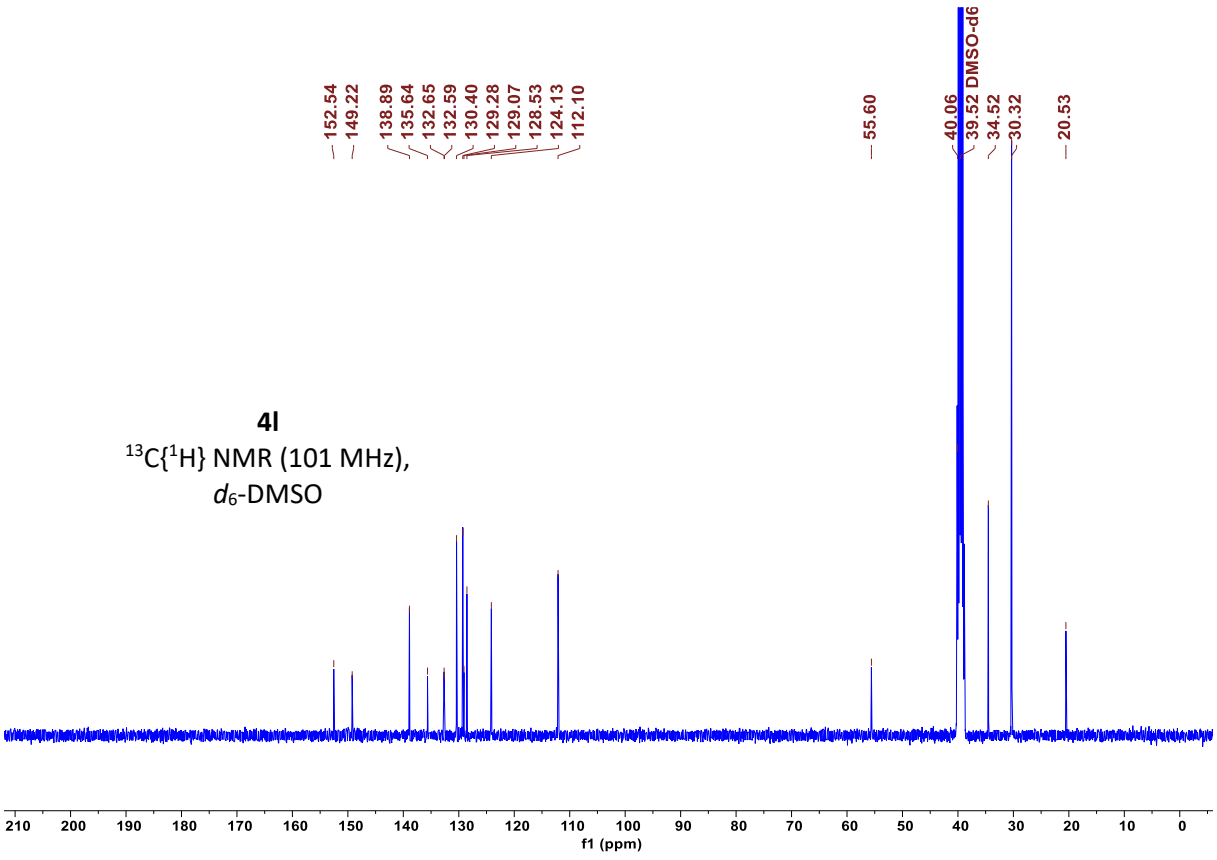

4l

^{13}C{^{1}H} NMR (101 MHz), d_6-DMSO

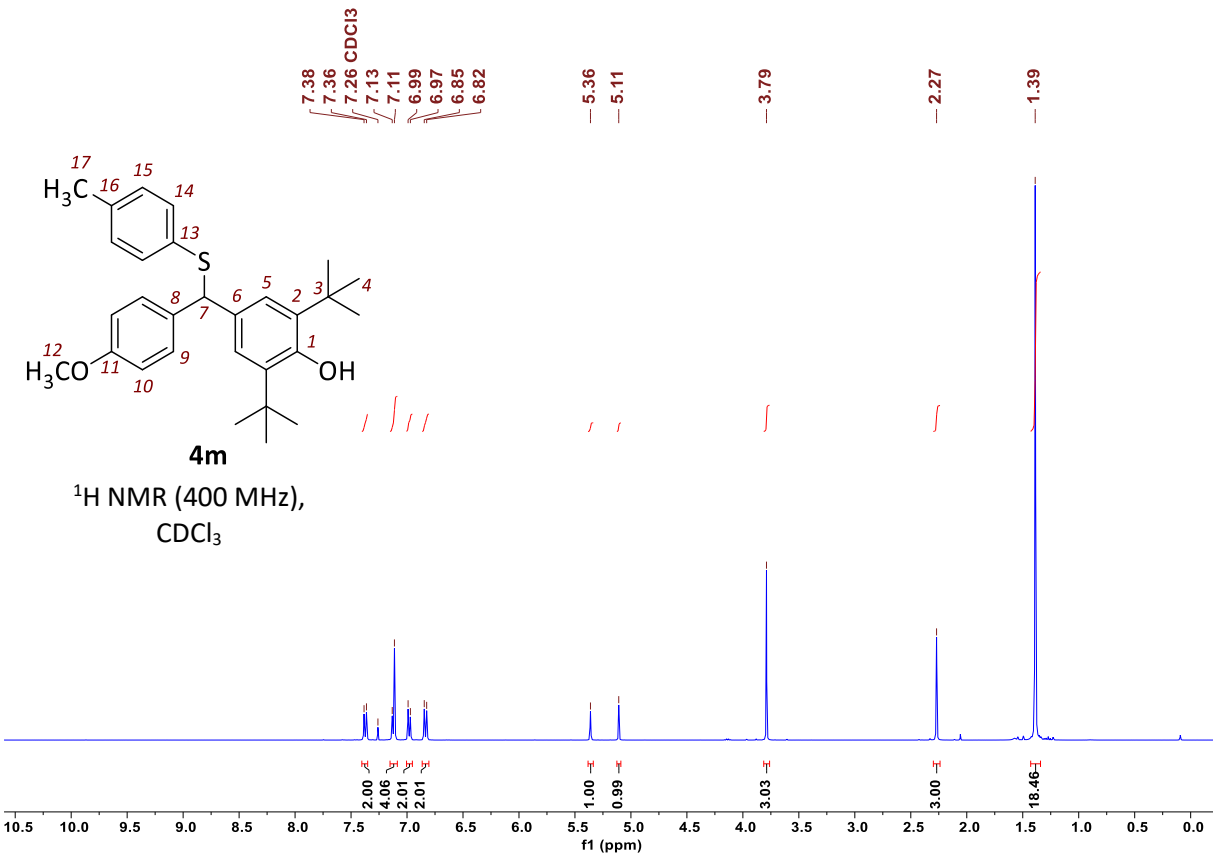

4m

^{1}H NMR (400 MHz), $CDCl_3$

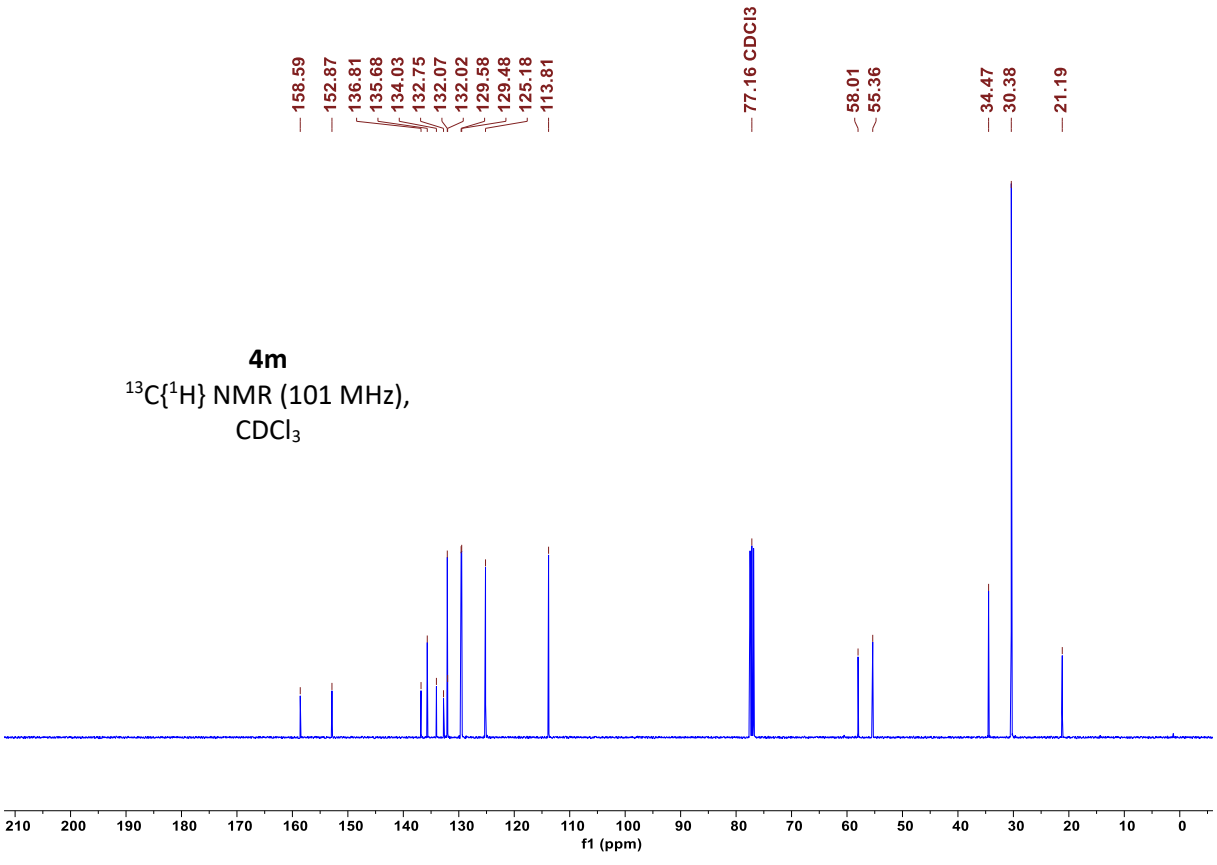

4m

^{13}C{^{1}H} NMR (101 MHz), $CDCl_3$

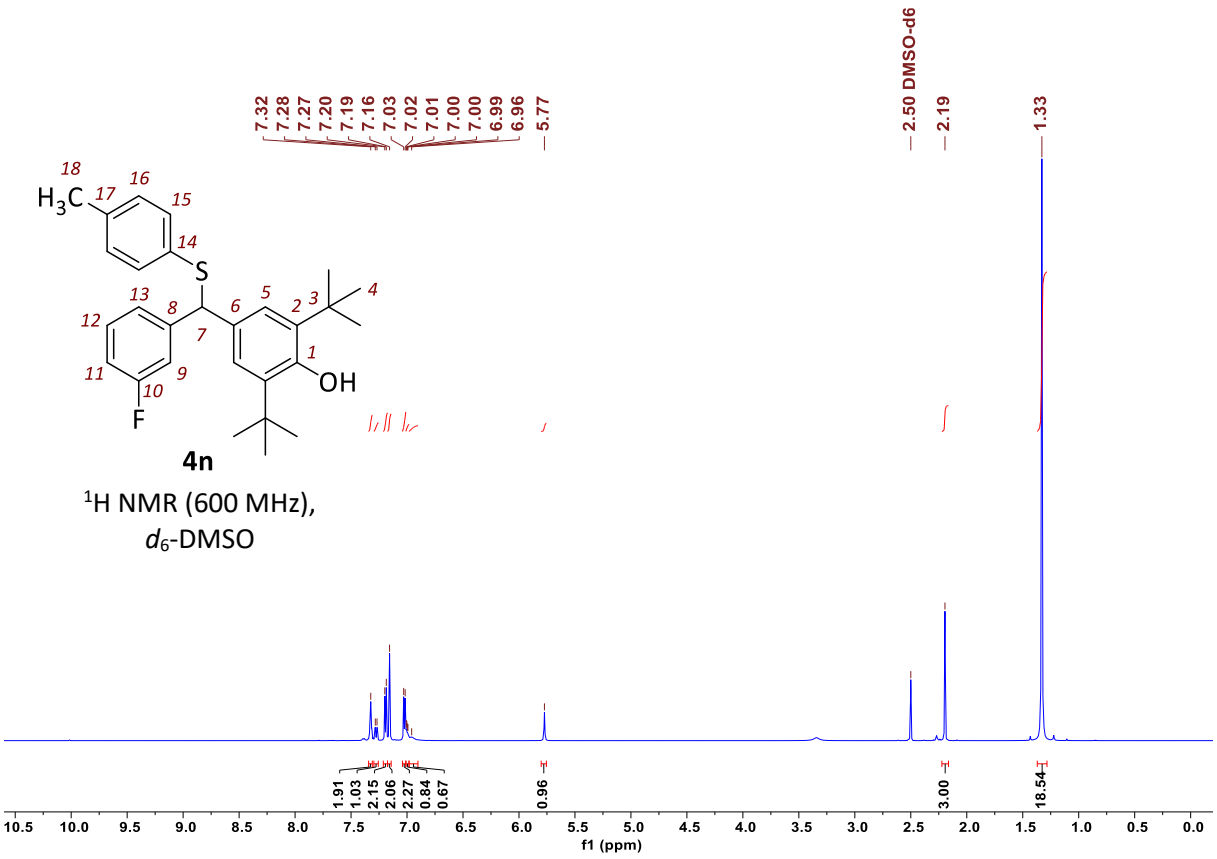
7.32
7.28
7.27
7.20
7.19
7.16
7.03
7.02
7.01
7.00
7.00
6.99
6.96
5.77
2.50 DMSO-d6
2.19
1.33
18
16
17
15
14
S
13
8
6
5
2
3
4
12
7
1
11
9
10
OH
F
4n
1H NMR (600 MHz),
d6-DMSO
1.91
1.03
2.15
2.06
2.27
0.84
0.67
0.96
3.00
18.54
f1 (ppm)

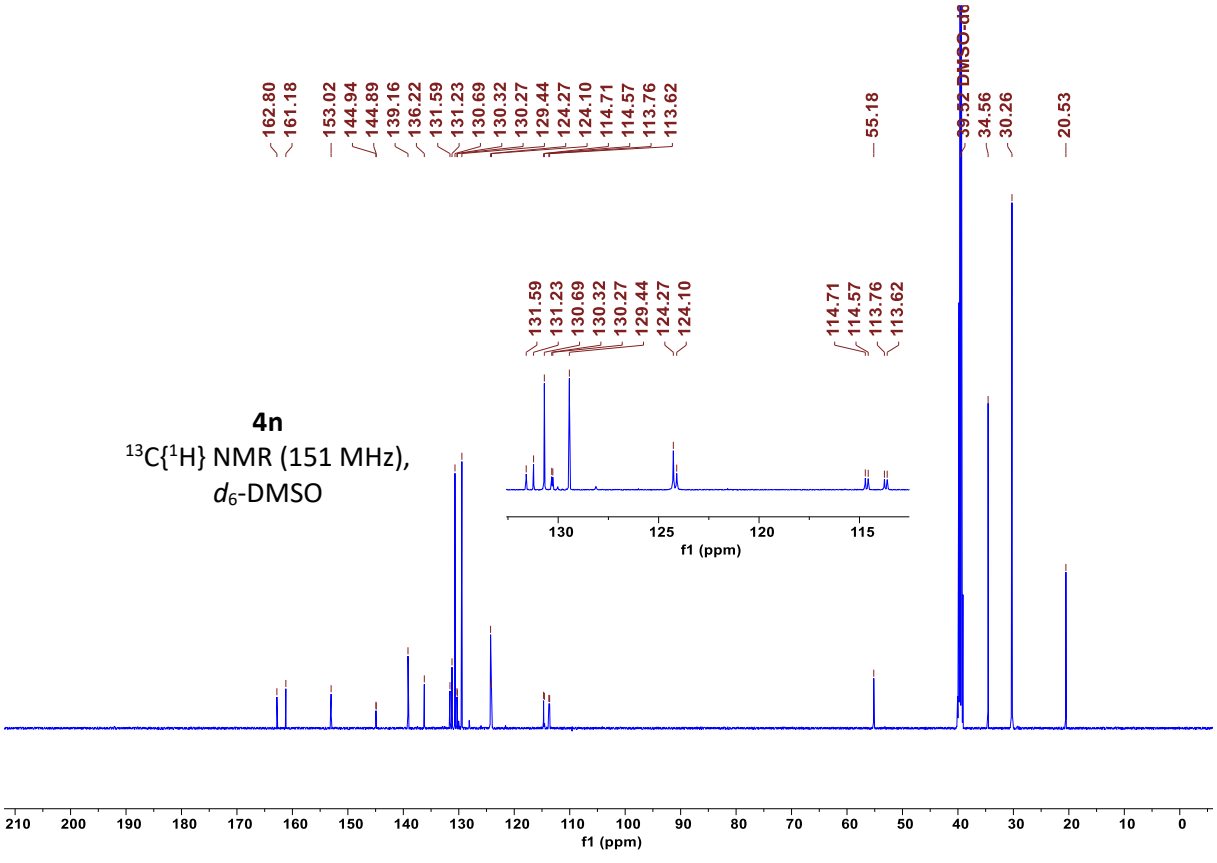
162.80
161.18
153.02
144.94
144.89
139.16
136.22
131.59
131.23
130.69
130.32
130.27
129.44
124.27
124.10
114.71
114.57
113.76
113.62
55.18
39.32 DMSO-d6
34.56
30.26
20.53
4n
13C{1H} NMR (151 MHz),
d6-DMSO
f1 (ppm)

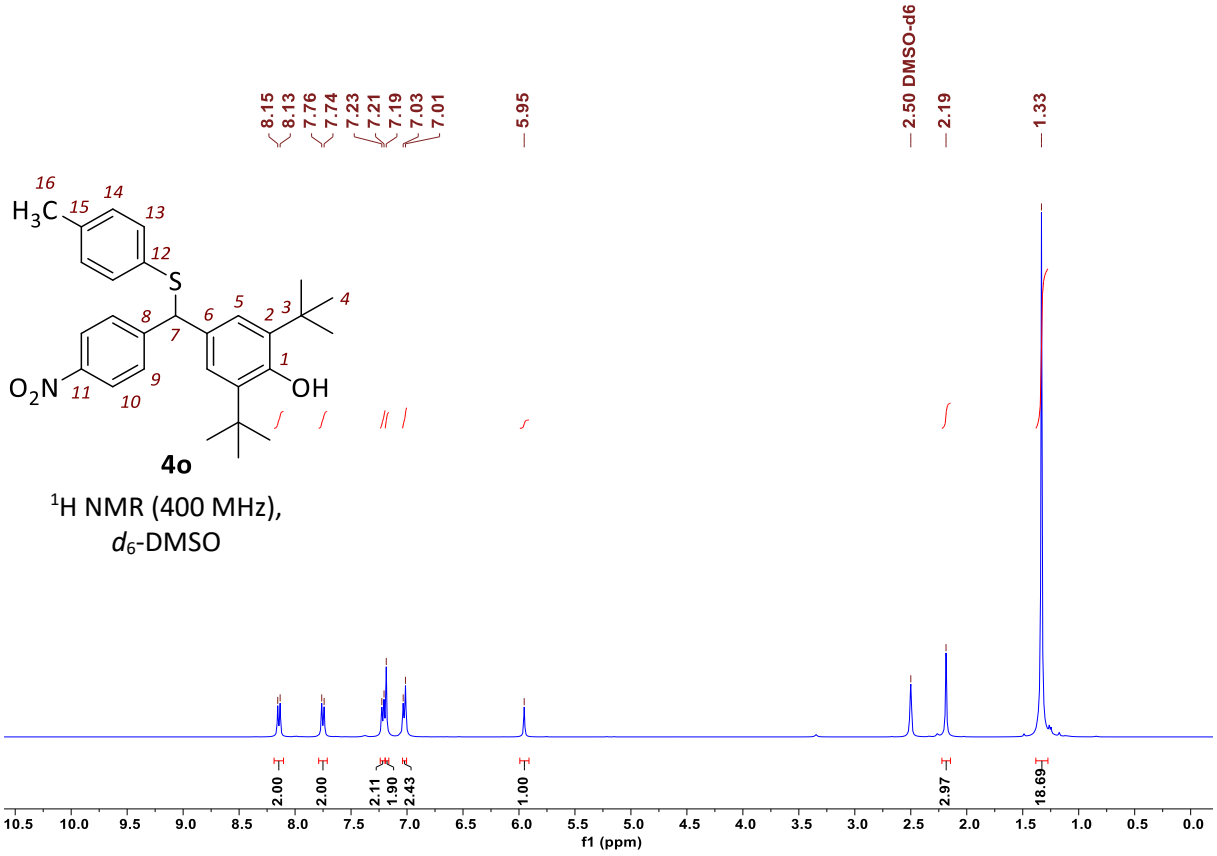

4o

^{1}H NMR (400 MHz),
d_6-DMSO

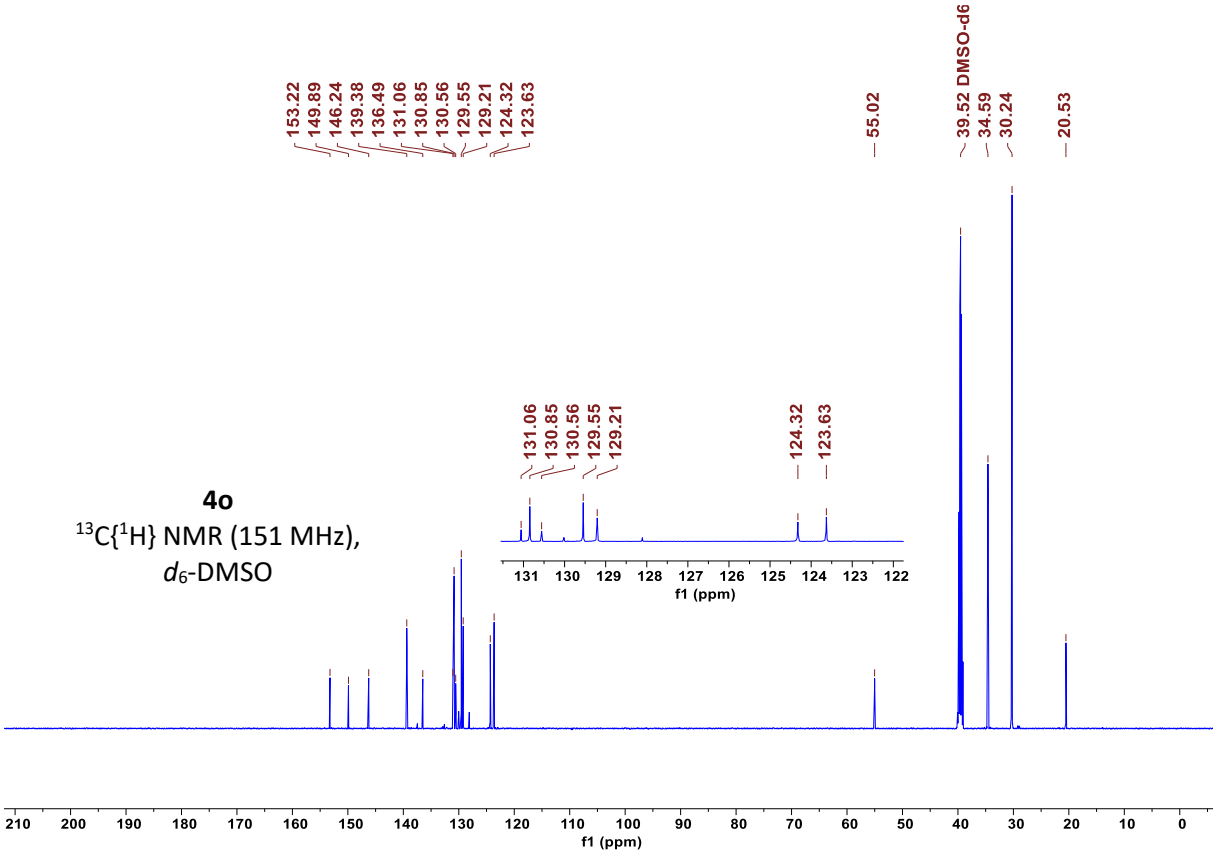

4o

^{13}C{^{1}H} NMR (151 MHz),
d_6-DMSO

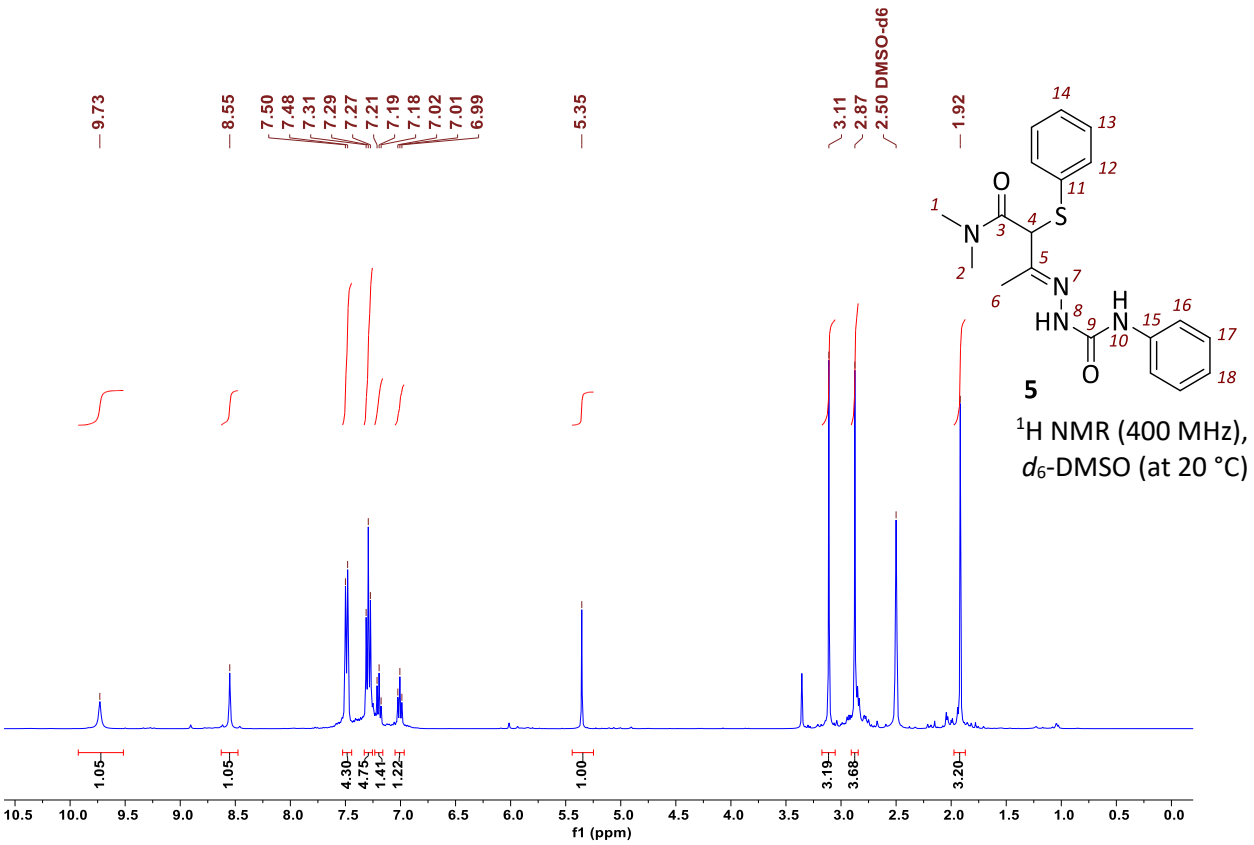

5

^{1}H NMR (400 MHz), d_6-DMSO (at 20 °C)

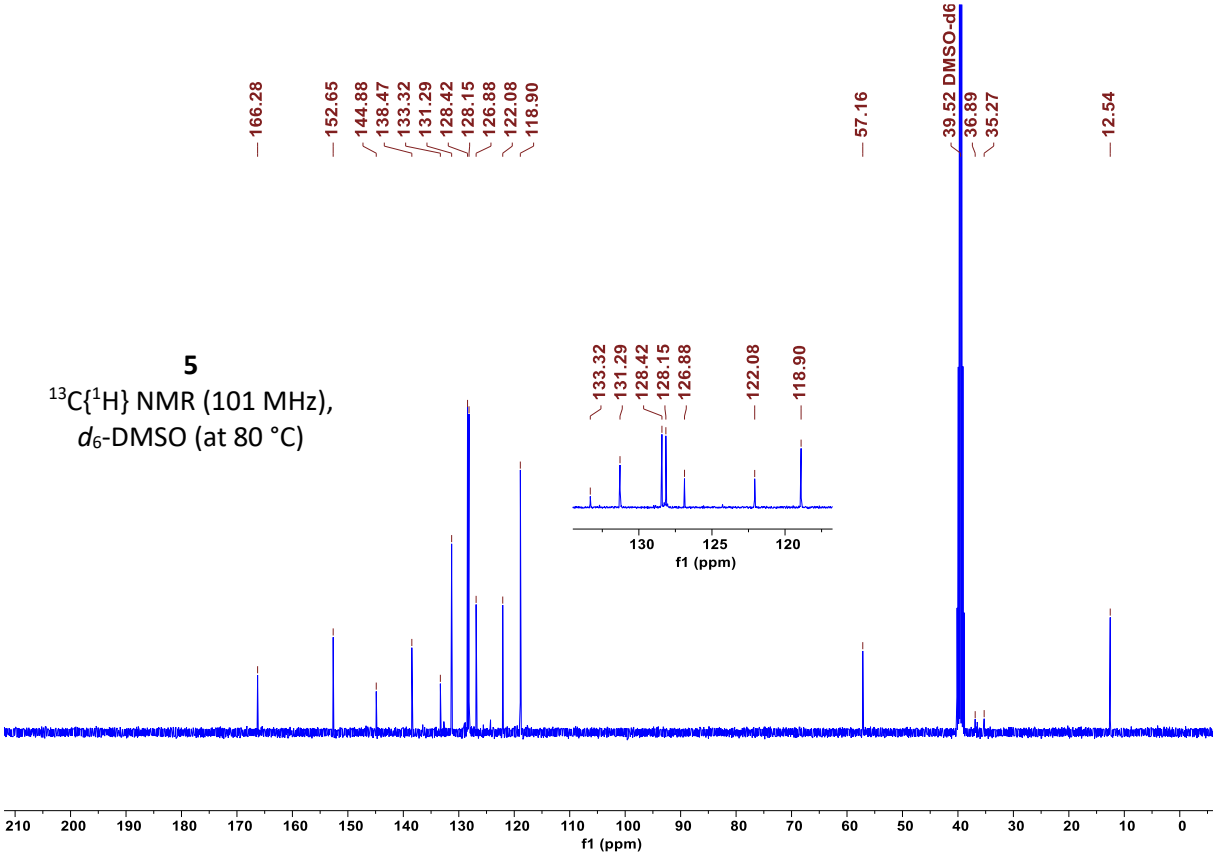

5

^{13}C{^{1}H} NMR (101 MHz), d_6-DMSO (at 80 °C)

2.2.5 References

(S1) Hansch, C.; Leo, A.; Hoekman, D. *Exploring QSAR – Hydrophobic, Electronic, and Steric Constants.* ACS Professional Reference Book; American Chemical Society; Washington, DC, 1995.

(S2) Bordwell, F. G.; Hughes, D. L. Thiol Acidities and Thiolate Ion Reactivities toward Butyl Chloride in Dimethyl Sulfoxide Solution. The Question of Curvature in Brønsted Plots. *J. Org. Chem*. **1982**, *47*, 3224-3232.

(S3) Mayer, R. J.; Breugst, M.; Hampel, N.; Ofial, A. R.; Mayr, H. Ambident Reactivity of Phenolate Anions Revisited: A Quantitative Approach to Phenolate Reactivities. *J. Org. Chem*. **2019**, *84*, 8837-8858.

(S4) Richter, D.; Hampel, N.; Singer, T.; Ofial, A. R.; Mayr, H. Synthesis and Characterization of Novel Quinone Methides: Reference Electrophiles for the Construction of Nucleophilicity Scales. *Eur. J. Org. Chem.* **2009**, 3203-3211.

Chapter 3. Electrophilicities of Acceptor and Donor-Acceptor Cyclopropanes

Contributions

All experiments were performed by Patrick M. Jüstel or by Alexandra Stan and Cedric D. Pignot under the supervision of Patrick M. Jüstel. The manuscript was written jointly by Patrick M. Jüstel and Armin R. Ofial.

3.1 Introduction

Owing to the relative weak carbon-carbon bonds in cyclopropanes, which can be further polarized by electron-donating or -accepting groups, numerous examples exist for utilizing the attack of nucleophiles at the carbocycle of suitably substituted cyclopropanes to generate a multitude of ring-opened products.[1]

The reactivities of Lewis acid-activated 1,1-diester-substituted cyclopropanes in formal (3+2)-cycloadditions with *p*-fluorobenzaldehyde have recently been investigated by ^{19}F NMR spectroscopy in the group of Werz.[2] Only few efforts have been undertaken to study the immanent reactivity of acceptor-substituted cyclopropanes. Hanafusa investigated pyridine-attack at a two-fold dimedone substituted cyclopropane, which does not allow general conclusions because of the unique structure of the electrophilic substrates.[3] The kinetic studies by McKinney, on the other hand, are limited to the reactions of pyridines with only two Meldrum's acid substituted cyclopropanes in acetonitrile.[4]

In this chapter it will be described how nucleophiles with known Mayr reactivity parameters *N* and s_N can be employed to characterize the electrophilicity of bis-acceptor-activated cyclopropanes in DMSO (Scheme 1).

Scheme 1. Ring-opening reaction of anionic nucleophiles with bis-acceptor-activated cyclopropanes in DMSO.

Given that the nucleophilic substitution can be expected to follow an S_N2 mechanism, the applicability of the Mayr-Patz equation (1), which was constructed for S_N1-type reactions,[5] will be discussed in comparison with the extended version of the Mayr-Patz equation (2), which was previously suggested for S_N2-type reactions.[6] Equation (2) comprises an additional electrophile-dependent parameter s_E, which reflects the enhanced influence of the electrophile in S_N2 reactions.

$$\log k_2 = s_N(N + E) \quad (1)$$

$$\log k_2 = s_N s_E(N + E) \quad (2)$$

For reactions at sp^2-centered electrophiles, typically $s_E = 1$ is found, which simplifies equation (2) into equation (1). In the few previously investigated S_N2 reactions, $s_E < 1$ was observed.[6] It remains to be tested whether this pattern will also be seen for ring-opening nucleophilic substitution reactions of cyclopropanes.

Given that thiophenolates in DMSO were found to be potent nucleophiles that have been characterized with their Mayr reactivity parameters in Chapter 2 of this thesis, they were used to initiate the reactivity investigations of cyclopropanes. Thiophenolates absorb light in the UV-vis region

of the electromagnetic spectrum and allowed monitoring the kinetics by photometric methods. Substituents in the thiophenolates and cyclopropanes were varied systematically to gain understanding of the electronic factors that control the immanent cyclopropane reactivities.

The investigations were then extended towards carbon-centered anionic nucleophiles in DMSO. Finally, a series of cyclopropane reactions with pyridines in acetonitrile was used to link the kinetic data in this work to previously determined rate constants by the McKinney group.

3.2 Results and Discussion

Preparation of Cyclopropanes.

The Meldrum's acid derived spirocyclopropane **1a** was purchased. Corey-Chaykovsky cyclopropanations of active methylene compounds furnished **1c**-**e**, **1g**, and **1j** in yields of 36-84% according to procedures described in ref.[7] Further information and analytic data can be found in the Experimental Section.

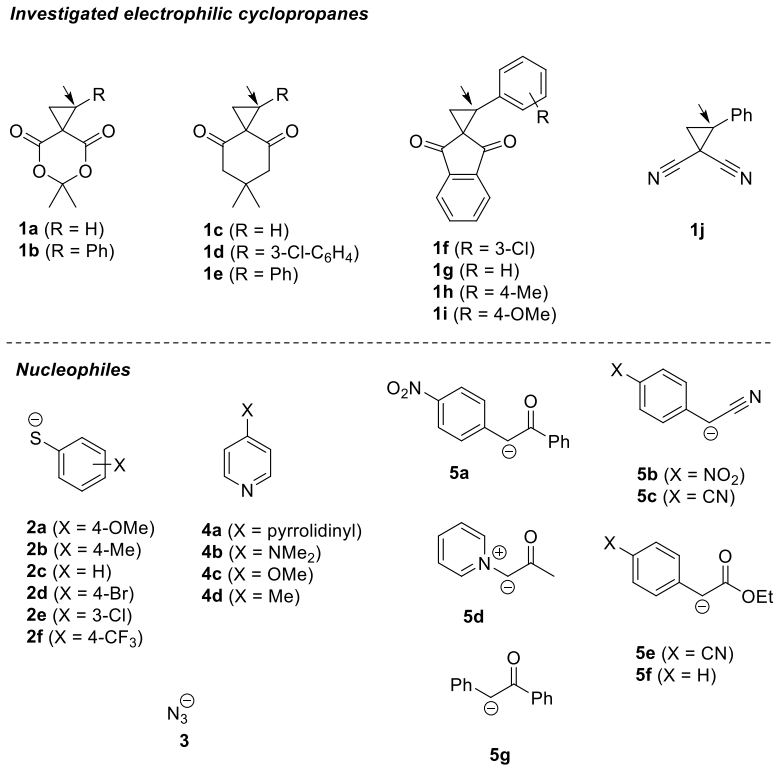

Chart 1. Investigated electrophilic cyclopropanes in this work (top) and reference nucleophiles (bottom).

Product Studies.

Products of 15 reactions of cyclopropanes **1** with thiophenolates **2** were investigated with or without aqueous workup and characterized by NMR-spectroscopy or isolated with yields of 39-99% (Scheme 2) respectively. The electrophilic reaction center was observed exclusively to be at the more substituted cyclopropane carbon. Regardless whether the phenyl, the group that this carbon was substituted with, was carrying an electron withdrawing chloro substituent in the meta position or an electron donating methoxy group in the para position. We noted the anions **7** of the ring-opening reaction to be reasonably stable in DMSO.

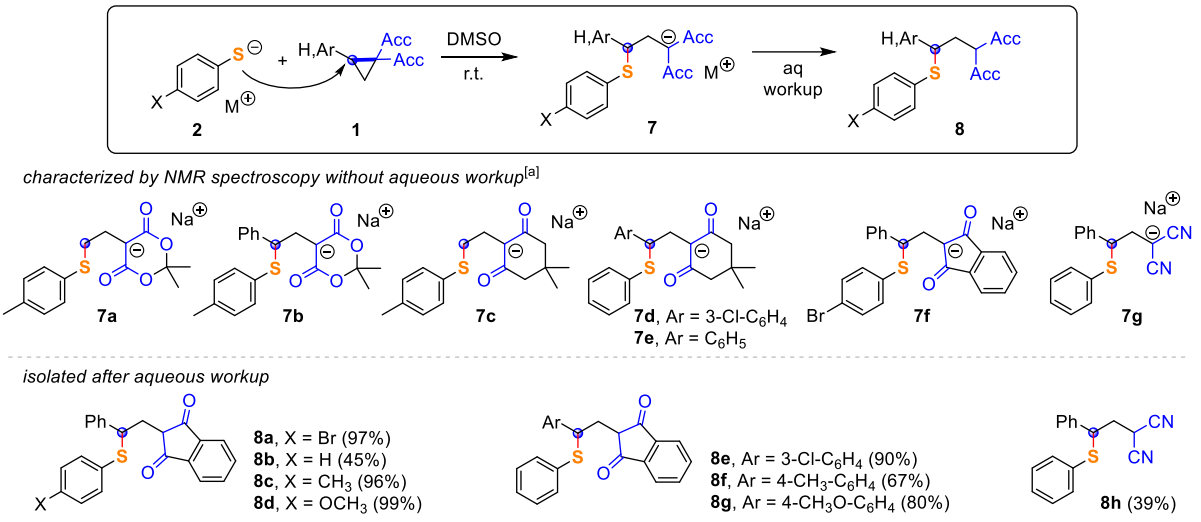

Scheme 2. Reactions of cyclopropanes **1** with sodium or potassium thiophenolates Na/K-**2** furnished ring-opened products **8** via the initial adducts **7** (yields are given for isolated products). [a] Reactions in d_6-DMSO.

Kinetics of Ring-Opening Reactions of Nucleophiles with Cyclopropanes

Thiophenolates can be monitored easily via UV-Vis photometry due to their absorption in the near UV region. We exploited this fact to follow the decay of the absorption of the thiophenolates near their λ_{max} in their reaction with cyclopropanes **1** at 20 °C in DMSO. Reactions with nitrogen- or carbon-centered nucleophiles (**3-5**) other than thiophenolates were also monitored photospectrometrically, either by observing the nucleophiles or the emerging products. For fast reactions stopped-flow photometry was used, while conventional photometry was employed for slower reactions. Electrophilic cyclopropanes were used in an at least 10 times higher concentration relative to the nucleophile to achieve pseudo first-order kinetics. In select cases, the nucleophiles were used in excess instead. The mono-exponential decay or increase was fitted with the function $A = A_0 \exp(-k_{obs}t) + C$ or $A = A_0 \exp(k_{obs}t) + C$, respectively, to give rate constants k_{obs} (Figure 1a, 1b). The corresponding rate constants k_{obs} were measured for each nucleophile/electrophile pair at a minimum of four different

concentrations of the excess reactants. Plotting k_{obs} versus the concentration of the excess compound resulted in linear correlations whose slopes correspond to the second-order rate constants k_2 (Figure 1c). All k_2 values obtained in this work are compiled in Tables 1, 2, and 3.

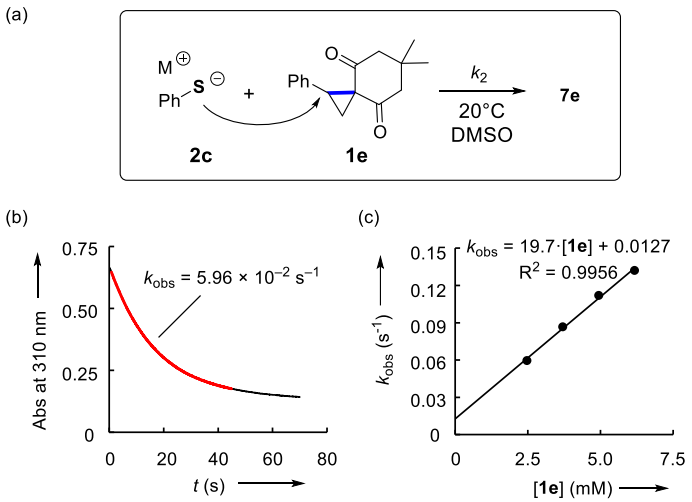

Figure 1. (a) Kinetics of the reaction of cyclopropane **1e** with thiophenolate (**2c**). (b) Monoexponential decay of the absorbance *A* at 310 nm in the reaction of **2c** (0.247 mM, $M^+ = K^+$) with **1e** (2.47 mM). (c) Linear correlation of observed rate constant k_{obs} versus the concentration of cyclopropane **1e**.

Correlation Analysis.

Figure 2b demonstrates the determination of the electrophilicity parameters *E* and s_E of the extended Mayr-Patz equation (1)[6] at the example of the electrophilic cyclopropanes **1e** and **1g**.

$$\log k_2(20\ °C) = s_E s_N(N + E) \qquad \text{(equation 1)}$$

The logarithm of the rate constants k_2 divided by s_N correlate linearly with the known nucleophilicity parameters *N* of the employed thiophenolates **2**. The intercept of the resulting linear correlation represents $E \times s_E$ and the slope s_E. It should be noted, that $s_E < 1$ is typical for the S_N2 reactions. The resulting *E* and s_E parameters are compiled in Table 1 for reactions of cyclopropanes **1** with thiophenolates **2** in DMSO. Plots like the one in Figure 1c have been depicted in the Experimental Section for all employed electrophiles. The Mayr-Patz equation ($s_E = 1$ in equation 1) usually only holds for addition reactions, in which only one new σ-bond is formed. For S_N2 reactions, an additional electrophile-dependent parameter s_E is necessary to semi quantitatively predict rate constants. A value around 0.5 for s_E has been reported before for S_N2 reactions.[6] The investigated cyclopropanes displayed a s_E between 0.33 – 0.50 (Table 1).

Reported pK_{aH} values in DMSO show that the Brønsted basicity of thiophenolates **2** increases when going from acceptor- to donor-substituted derivatives. Accordingly, the logarithmic second-order rate

constants (log k_2) of the ring-opening reactions with the cyclopropanes **1** increase linearly with the increase of pK_{aH} of **2** (Figure 2c) because substituents in **2** are varied in meta- and para-positions and, thus, remote from the reacting sulfur atom. Brønsted β values, that is, the slope of the correlations in Figure 2c, do not show significant differences between the β values of 0.22 and 0.24 for the spiro-activated cyclopropanes **1d** and **1g**, respectively, and the β value of 0.26 for the (1,1-dicyano)-activated **1j**, which lacks the spiro motif.

The logarithm of the second-order rate constants k_2 also correlates linearly with Hammett σ constants (Figure 2d) of the employed thiophenolates and thus allows to predict rate constants for thiophenolates that have not been investigated. Substitution of the D-A cyclopropane however did not result in a linear correlation of log k_2 versus Hammett σ constants (Figure 2e). Instead log k_2 goes through a minimum for the unsubstituted cyclopropane **1g** and electron donating as well as electron withdrawing substituents in the cyclopropanes **1i**, **1h** and**1f** enhance the reaction rates.

Table 1. Second order rate constants k_2 (20 °C) for the reactions of electrophilic cyclopropanes with thiophenolates in DMSO.

Electrophile	E/s_E	k_2 (M^{-1} s^{-1})					
		2a N=24.97 s_N=0.68	**2b** N=24.35 s_N=0.69	**2c** N=23.36 s_N=0.74	**2d** N=22.80 s_N=0.78	**2e** N=22.50 s_N=0.78	**2f** N=21.30 s_N=0.86
1a	−20.5/0.49	30.7[a]	18.0[a]	11.3[a]	n.d.	n.d.	n.d.
1b	−16.9/0.46	332 [a]	242 [a]	170 [a]	n.d.	n.d.	n.d.
1c	−20.5/0.35	11.2[a]	8.89[a]	5.52[a]	n.d.	n.d.	n.d.
1d	−18.9/0.48	84.7	59.2	40.3	25.7	n.d.	n.d.
1e	−18.1/0.33	30.9	28.2	19.7	16.6	14.3	7.74
1f	−19.9/0.50	47.7	32.9	20.5	12.3	n.d.	n.d.
1g	−19.9/0.44	31.5	21.9	15.0	8.38	6.90	3.68
1h	−18.8/0.37	33.7	26.1	20.3	13.4	n.d.	n.d.
1i	−18.4/0.45	93.9	65.3	44.9	33.6	n.d.	n.d.
1j	−20.8/0.44	17.4	11.3	8.54	4.30	n.d.	n.d.

[a] Sodium instead of potassium used as counterion for thiophenolate

The curved Hammett plot is the result of changes in the transition state. This particular effect has already been reported for the reaction of thiophenolates with benzyl bromides[8] and investigated with theoretical methods[9]. Aggarwal *et al.*[9] explained the rate enhancing effect of electron withdrawing groups (EWG) with a change in the partial charge on the reaction center in the transition state. If the carbon, where the nucleophilic substitution is occurring, is bearing a partial positive charge in the transition state, then electron donating substituents (EDG) are rate enhancing.

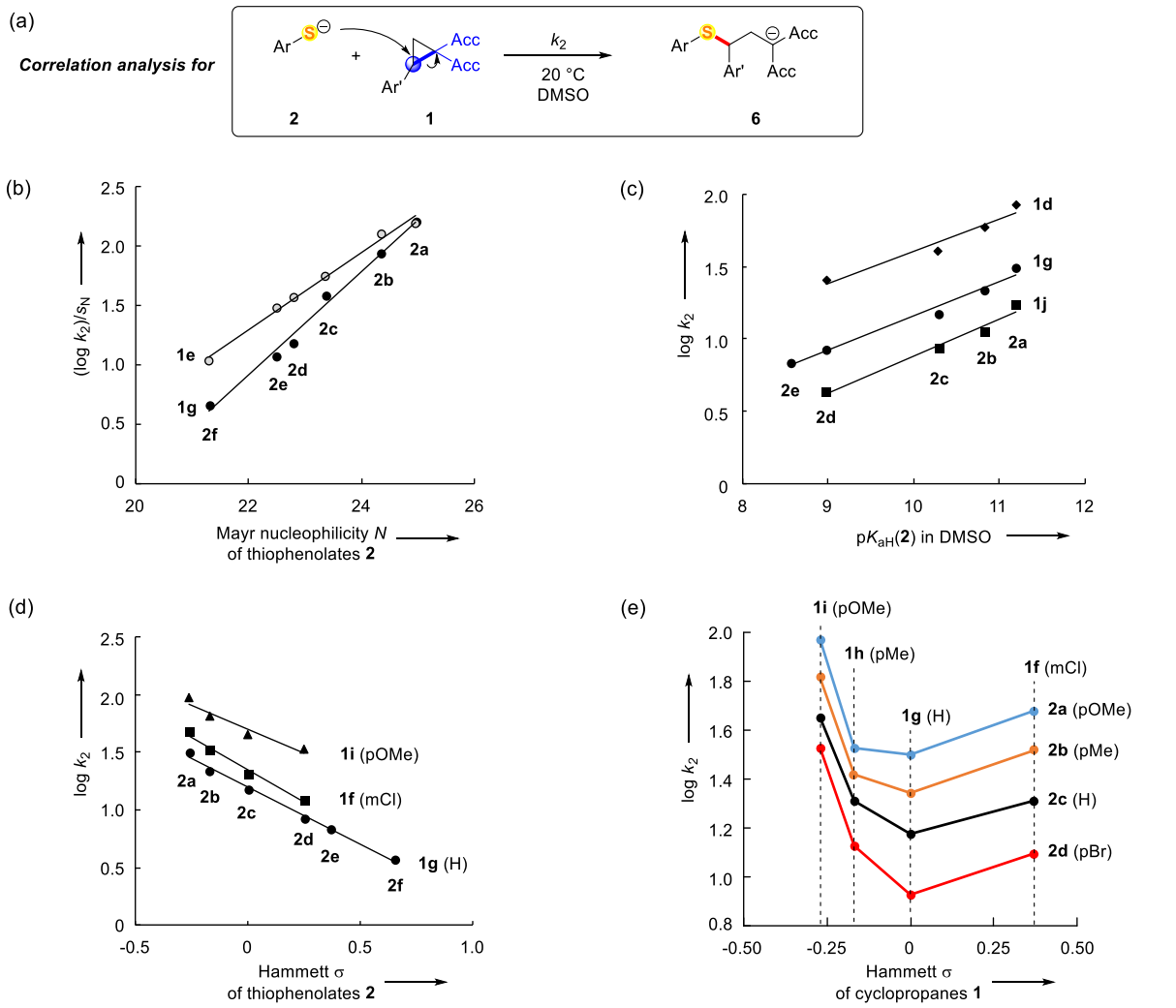

Figure 2 (a) Nucleophilic attack of thiophenolates **2** at spirocyclopropanes **1** (in DMSO at 20 °C). (b) Applying the Mayr-Patz equation (eq 1) to reactions of **1** with **2** results in a linear increase of (log k_2)/s_N with the nucleophilicity descriptors N of the thiophenolates 2 (with N, s_N from ref[10]). (c) Brønsted plots for the cyclopropanes **1d**, **1g**, and **1j** show linear correlations of the second-order rate constants (log k_2) for the ring-opening reactions **1** + **2** with the basicities of the thiophenolates **2a**-**e** (pK_{aH} in DMSO, from ref[11]). (d) Linear correlation of the second-order rate constants (log k_2) for reactions of **1f-i** + **2** with the Hammett substituent constants σ_p^- or σ_m of the nucleophiles **2a-f**. For clarity, data for reactions of **2** with **1h** are not shown. (e) Curved relationship of the second-order rate constant (log k_2) for the reactions **1f-i** + **2** with the Hammett substituent constants σ of the electrophiles **1f-i**.

Electron withdrawing substituents on the other hand do not slow the reaction down in this special case, but instead they compensate the partial negative charge at the reaction center. The result are enhanced rates with both electron donating and withdrawing substituents. This phenomenon is only observed with strong, anionic nucleophiles, such as thiophenolates. Other nucleophiles apparently cannot induce a partial negative charge on the reaction center in the transition state and consequently such reactions are only slowed down by EWG on the electrophile.[9,12]

A limit in the possible strength of electron donating substituents was encountered when *para* methyl or methoxy substituents were added to to **1e**, since the resulting compounds spontaneously underwent a S_N1 type heterolytic cleavage, a Cloke-Wilson type rearrangement to dihydrofurans (Scheme 3).[13]

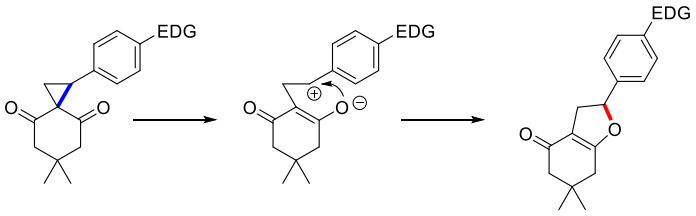

Scheme 3. Spontaneous Cloke-Wilson rearrangement of donor substituted cyclopropanes. EDG = Me or OMe.

A comparison of the different acceptor groups on the employed D-A cyclopropanes is only rudimentary possible due to the paucity of data. Figure 3 shows a Brønsted plot of log k_2 of the reaction of thiophenolate (**2c**) with the cyclopropanes **1b**, **1d**, **1g**, and **1j** against the pK_a values of the parent acceptor moieties in H_2O in lieu of pK_a values in DMSO.[14] The behavior is not linear. Nonetheless it can still be demonstrated, that a more acidic acceptor/leaving group accelerates the reaction of the corresponding cyclopropane with the thiophenolates (**2c**).

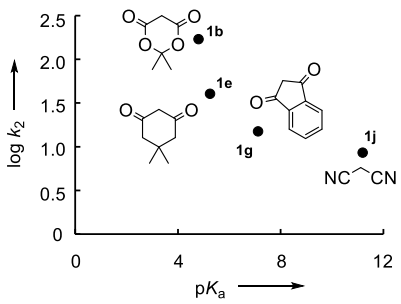

Figure 3. Brønsted plot of log k_2 of the reaction of **1b**, **1d**, **1g**, and **1j** with thiophenolate (**2c**) versus pK_a (H_2O) of the corresponding C-H acids.

Comparing the Reactivities of Cyclopropanes and Michael Acceptors.

How does the reactivity of electrophilic cyclopropanes compare to other electrophiles? One class of electrophiles that lends itself particularly well for comparison are Michael acceptors. A nucleophilic cyclopropane ring-opening reaction can be seen as a homologous Michael addition (Scheme 4).

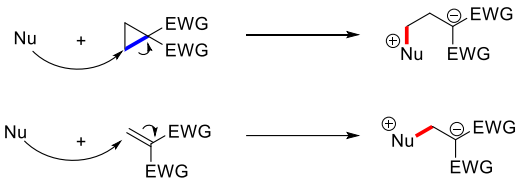

Scheme 4. Cyclopropane ring-opening reaction (top) and Michael addition (bottom).

However, while these two reactions look very similar on paper, they are very different in terms of thermodynamics and kinetics. In reactions of cyclopropanes a ring strain of 115 kJ mol^{-1} is released, which provides a strong thermodynamic driving force. Interestingly, this thermodynamic advantage does not translate into more favorable kinetics for cyclopropanes. The opposite is the case, Michael acceptors are much more reactive than cyclopropanes that carry identical acceptor groups (Figure 4 and 5).

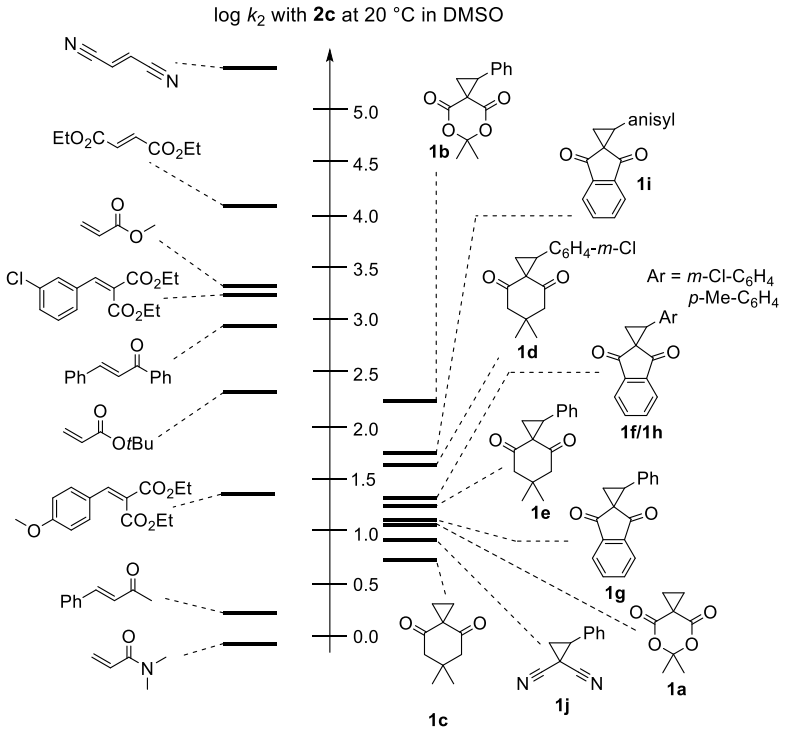

Figure 4. Comparison of log k_2 for the reaction of Michael acceptors with thiophenolate (**2c**) (left side, calculated with the Mayr-Patz equation (equation 1 with s_E = 1)) with the ring-opening reaction of cyclopropanes **1** with thiophenolate (**2c**) (Table 1).

Comparison of only *E* parameters would be misleading here, as the significant effect of s_E would be overlooked in this case. Therefore, Figure 4 shows a direct comparison of the rate constants log k_2 for reactions of **2c** with Michael acceptors[15] (Figure 4, left side) and cyclopropanes **1** (Figure 4, right side). Direct comparison of log k_2 is a better metric in this case, at the cost of only being valid for a single nucleophile. Thiophenolate (**2c**) is as reactive towards the most electrophilic cyclopropane **1b** investigated in this work as towards the weak Michael acceptor *tert*-butyl acrylate (Figure 4). This fact shows impressively how much Michael acceptors are more reactive when compared to cyclopropanes. Also notable is the small range of reactivity of the cyclopropanes when compared to the Michael acceptors (Figure 4). The quite diverse set of electrophilic cyclopropanes covers a reactivity range slightly larger than the two very similar Michael acceptors *tert*-butyl acrylate and methyl acrylate. This demonstrates the small influence of cyclopropane substitution in relation to its reactivity. The same insight can be gained from the Brønsted plot in Figure 3: a big change in pK_a leads to only a minute change in reactivity.

In Figure 5, cyclopropanes and Michael acceptor reactions with **2c** with identical substitution are directly compared, demonstrating a difference in k_2 of 6 to 9 orders of magnitude. The rate constants for the Michael acceptors are purely hypothetical though, as they would actually be lower due to the diffusion limit. The comparison is not perfect though, since a tertiary cyclopropane is compared to a secondary Michael acceptor. Steric hindrance plays a huge role in these reactions and it was reported before that the reactivities of Michael acceptors decrease by more than 7 orders of magnitude when the secondary reaction center is substituted with a methyl to become tertiary.[16] In cyclopropanes phenyl substitution is leading to a roughly 15 fold rate enhancement (**1a** to **1b**, table 1) in one case and still 3 times rate enhancement (**1c** to **1e**, Table 1) in the other. This is due to sterics being pitted against electronics in this case, with electronics' positive effect on rates barely outweighing the negative effect of sterics. This effect is big enough, however, to only observe nucleophilic attack at the more substituted cyclopropane **1** in our study. Here we also note one more profound difference in cyclopropane and Michael acceptor reactivity: adding a phenyl moiety to the reaction center leads to a small rate increase for cyclopropanes, but to a huge decrease in rates for Michael acceptors.[17] Furthermore, the need to break a carbon-carbon σ bond instead of a weaker π bond causes higher activation barriers. The degree of reorganization is also bigger for cyclopropanes, which causes an increase in activation barriers relative to Michael acceptors according to the principle of least nuclear motion.[18]

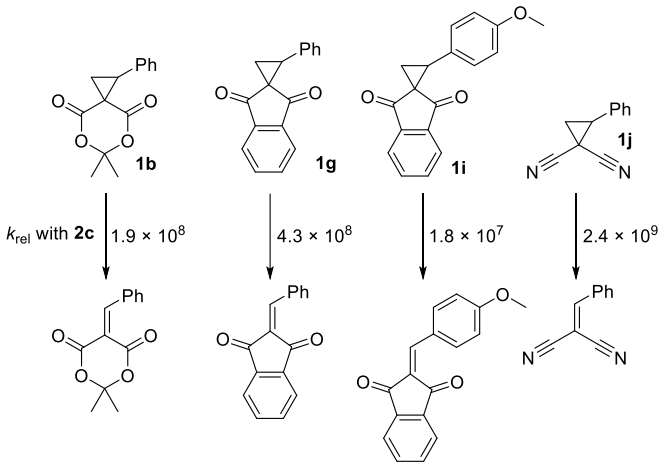

Figure 5. Comparison of relative rate constants k_{rel} for the ring-opening reaction of cyclopropanes **1** with thiophenolate (**2c**) (top, Table 1) with the reaction of Michael acceptors with thiophenolate (**2c**) (bottom, calculated with the Mayr-Patz equation).[19]

While reactions with D-A cyclopropanes have much higher intrinsic barriers than comparable reactions with Michael acceptors, in terms of the Gibbs reaction energy, the cyclopropanes have a clear advantage. Thiophenolates **2** form stable products with cyclopropanes **1**, but not with quinone methides (Scheme 5).[10] This still holds true, when the quinone methide is more reactive by 5 orders of magnitude than a cyclopropane towards thiophenolates. We also investigated further D-A cyclopropanes without spiro ring systems like **1j**. The structurally related diketone and diester analogues of dinitrile **1j** failed to deliver well-behaved kinetics as well as the desired products in acceptable yields. Apparently the electrophilicity of the carbonyl groups is exceeding the cyclopropane electrophilicity at that point. Consequently, Lewis acid catalysis is a requirement for a clean ring-opening reaction in this case. Therefore, the relative reactivity of these compounds cannot be compared without Lewis acid catalysis and is thus beyond the scope of this work.

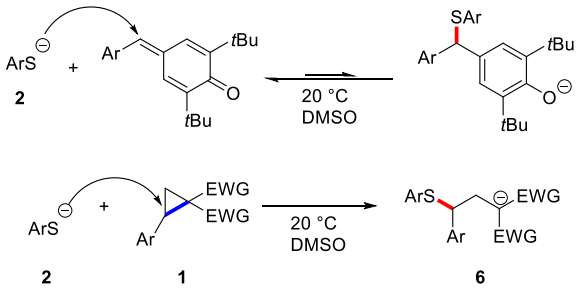

Scheme 5. Reaction of quinone methides with thiophenolates (top) and reaction of cyclopropanes **1** with thiophenolates **2** (bottom).

It should also be mentioned that the cyclopropanes derived from Meldrum's acid (**1a** and **1b**) are not only more reactive than other cyclopropanes, but also offer more synthetic options, as the acceptor ester groups can be easily saponificated, decarboxylated or otherwise transformed into functional groups that are much weaker electron withdrawing groups and thus would not allow for a nucleophilic cyclopropane ring-opening reaction.

C-Nucleophiles.

The reactions and the rate constants (Table 2) of D-A cyclopropane **1g** with seven C-nucleophiles (**5a-g**) (Figure 6a, 6b) and sodium azide (**3**) were investigated. All seven C-nucleophiles absorb light in the UV-Vis spectrum and conventional photometry was used to follow their decay in reactions with cyclopropanes **1** (Figure 6c). The carbanionic products **9** also absorb light in the visible spectrum (Figure 7), this was used to monitor the reaction with azide (**3**). Three products were isolated and characterized (Figue 6d).

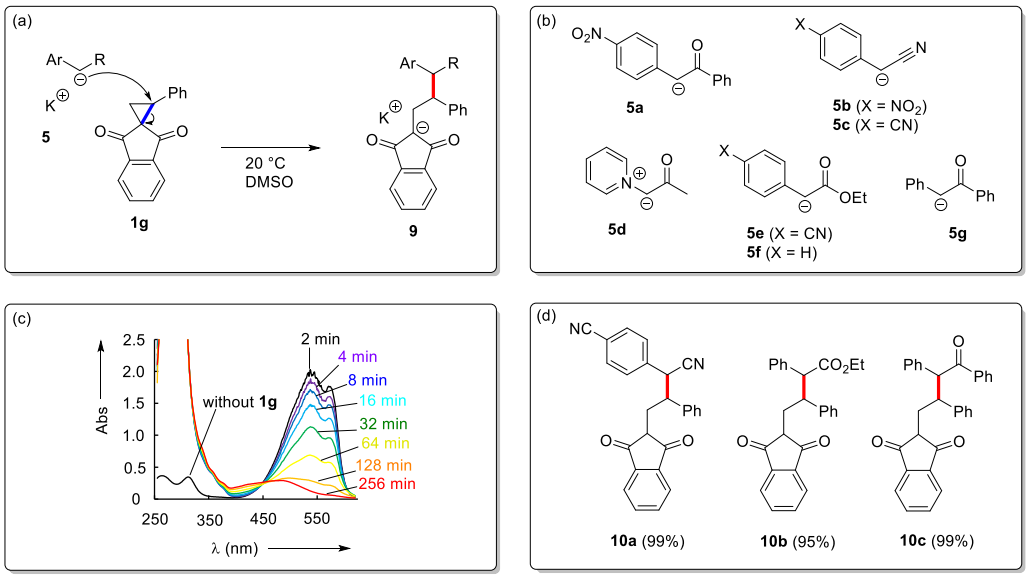

Figure 6. (a) Ring-opening reaction of D-A cyclopropane **1g** with carbanions **5a-g** to carbanions **9**. (b) Employed C-nucleophiles. (c) UV-Vis spectra over the course of the reaction of **5b** (0.125 mM) with **1g** (7.5 mM) in DMSO at 20 °C. The black spectrum was acquired without the subsequently added electrophile **1g**. (d) Isolated products after aqueous workup with respective yield.

The reaction of cyclopropanes with sodium azide (**3**) proceeded analogously to the ring-opening reactions with carbanions. The procedure to gain rate constants k_{obs} and k_2 was as described for the analogous kinetic measurements with thiophenolates **2** (Figure 1). Again, the reaction was highly

chemoselective, and nucleophilic attack was observed only at the higher substituted carbon. The rate constants k_2 are gathered in Table 2.

Table 2. Second-order rate constants k_2 (20 °C) for the reactions of electrophilic cyclopropane (**1g**) with carbanions (**5a-g**) and sodium azide (**3**) and their Mayr nucleophilicity parameters N/s_N in DMSO.

Nucleophile	N/s_N[a]	k_2 [M^{-1} s^{-1}]	k_2/k_{2calc}[b]
5f-K	27.54/0.57	47.3	1/1.7
5e-K	23.64/0.65	4.60	1/2.6
5g-K	23.15/0.60	3.73	1/1.9
5c-K	25.11/0.64	3.11	1/9.4
6-Na	20.50/0.59	8.24×10^{-2}	1/17
5a-K	19.46/0.58	2.62×10^{-2}	1/29
5b-K	19.67/0.68	2.04×10^{-2}	1/42
5d-K	20.24/0.60	1.76×10^{-2}	1/70

[a] Parameters from www.cup.lmu.de/oc/mayr/DBintro.html.

[b] k_{2calc} was calculated with equation 1 (E=–19.9 ,s_E=0.44) for **1g**.

Carbanions were employed as reference nucleophiles to check whether the electrophilicity parameters E and s_E depend on the class of nucleophile used. Usually the electrophilicity parameters E and s_E are independent of the nucleophile class used, but here steric influence is becoming a significant factor for the application of equation 1.[20] Even though the difference in steric demand of the reactive centers of the potassium thiophenolates **2** and the secondary potassium carbanions **5** are considerable, the differences in reactivity are small (Table 2, Figure 7).

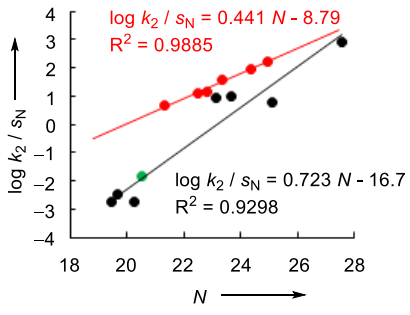

Figure 7. Linear correlation of log k_2/s_N versus N for the reactions of the carbon nucleophiles **5a-g** with cyclopropane **1g** (black dots and black correlation line). The red dots and red correlation line represent the reaction of **1g** with the potassium thiophenolates **2a-e**. The green dot represents the reaction of **1g** with sodium azide (**3**). Data taken from Tables 1 and 2. All reactions were performed in DMSO at 20 °C.

Steric hindrance is expected to cause the bulkier carbanions **5** to be less reactive than thiophenolates towards tertiary D-A cyclopropane **1g**. The increased scattering in the linear correlation of the C-nucleophiles **5** compared to the thiophenolates **2** is also credited to steric effects. Sodium azide (**3**) was excluded from the carbanion correlation line, while being accidentally a perfect fit. For the investigated, practical reactivity range, the deviation of carbanion reactivity compared to thiophenolate reactivity was less than a factor of 100, which is considered the expected accuracy of the (extended) Mayr-Patz equation. So even with the steric differences, the electrophilicity parameters E and s_E gained from reactions with thiophenolates can be used to estimate rate constants with other nucleophiles like carbanions **5** and azide (**3**). We expect a smaller error for the electrophilic cyclopropanes **1a** and **1c**, as they are much less bulky and thus less susceptible to steric effects.

Pyridines as N-Nucleophiles in Acetonitrile.

Furthermore, we investigated the reaction of the D-A cyclopropane **1b** with substituted pyridines **4** in acetonitrile at 20 °C (Figure 8, Table 3). Zwitterions **10** absorb light in the visible spectrum, unlike cyclopropanes **1** or substituted pyridines **4** and their appearance was followed with conventional photometry to obtain rate constants k_{obs} (Figure 8b) and subsequently k_2 as mentioned before.

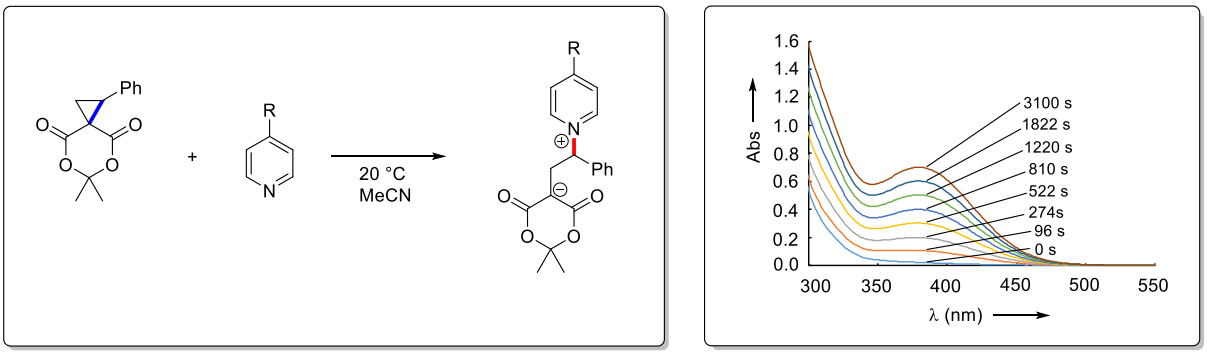

Figure 8. (a) Ring-opening reaction of D-A cyclopropane **1b** with substituted pyridines **4a-d** to yield zwitterions **10**. (b) UV-Vis spectra over the course of the reaction of **4d** (0.8 M) with **1b** (2 mM) in acetonitrile at 20 °C.

McKinney *et al*. had reported rate constants and activation parameters for the reaction of the cyclopropanes **1a** and **1b** with pyridine in acetonitrile.[4] In this thesis this work was expanded upon to not only gain insight into the ring-opening reaction of cyclopropanes in DMSO, but also in acetonitrile. While both solvents are polar and aprotic, it is unknown whether s_E is solvent-dependent like s_N or solvent-independent like E.

Table 3. Second order rate constants k_2 (20 °C) for the reactions of D-A cyclopropane (**1b**) with substituted pyridines (**4a-d**) and their Mayr nucleophilicity parameters N/s_N in acetonitrile.

Nucleophile	N/s_N[a]	k_2 [M^{-1} s^{-1}]	k_2/k_{2calc}[b]
4a	15.9/0.67	1.72×10^{-2}	1/29
4b	15.8/0.66	1.37×10^{-2}	1/34
4c	13.7/0.67	1.07×10^{-3}	1/96
4d	13.7/0.67	1.06×10^{-3}	1/97

[a] Parameters from www.cup.lmu.de/oc/mayr/DBintro.html. Nucleophilicity parameters determined in CH_2Cl_2 have been used.

[b] k_{2calc} was calculated with equation 1 (E=−16.9 ,s_E=0.46).

The linear correlation of log k_2/s_N for the reaction of **1b** with the substituted pyridines **4a-d** versus N is displayed in Figure 9 (see also Table 3). This plot was used to determine E and s_E for cyclopropane **1b** in acetonitrile, the most electrophilic cyclopropane employed in this work. Nucleophilicity parameters N and s_N for the substituted pyridines **4** in dichloromethane have been used in lieu of such parameters in acetonitrile. However, the error should be systematic and small, as can be seen by the comparison of nucleophilicity parameters for **4b**, which were determined in both solvents (N/s_N =15.51/0.62 (MeCN) and 15.80/0.66 (CH_2Cl_2)).[15]

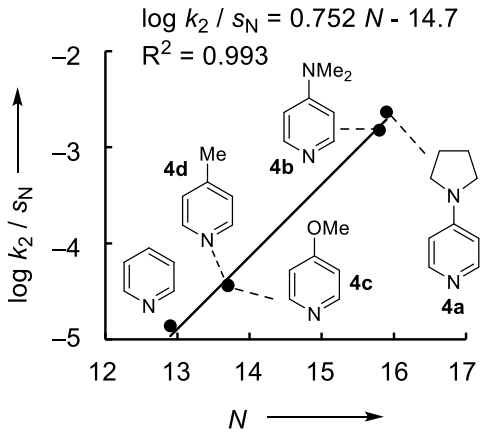

Figure 9. Linear correlation of log k_2/s_N versus N for the reactions of the substituted pyridines **4a-d** with cyclopropane **1b** in acetonitrile at 20 °C. Data taken from Table 3. Rate constant for the reaction with pyridine at 20 °C has been calculated from activation parameters published by McKinney *et al*.[4] It should be noted, that there are 5 data points in this graph. E = -19.5, s_E = 0.75.

Does the electrophilicity of cyclopropane **1b** depend on the nucleophile type and solvent used? Yes, but only to a small degree, as can be seen by the comparison of parameters E and s_E for **1b** in DMSO (E=−16.9 s_E=0.46, Table 1) and acetonitrile (E=−19.5 s_E=0.75 Figure 6). The differences in E and s_E compensate each other partially. In Table 3 the deviation of the experimentally determined k_2 values

and k_{2calc} is shown in the last column. Rate constants k_{2calc} were calculated with equation 1 and the E and s_E parameters for cyclopropane **1b** determined in DMSO with thiophenolates **2** (Table 1). This small change in reactivity, as expressed by the different E/s_E parameters for **1b**, can be attributed to the sterically more demanding substituted pyridines and solvent effects. Pyridines **4** are expected to be less reactive towards cyclopropanes **1** than thiophenolates **2**, resulting in slightly different E and s_E parameters. The same effect can be seen in Figure 7 for thiophenolates **2** and C-nucleophiles **5**, without a change in solvent at the same time. Given that the relations between thiophenolates **2** versus C-nucleophiles **5** reactivities (Table 2) and thiophenolates **2** versus substituted pyridine **4** reactivities (Table 3) towards cyclopropanes **1** look quite similar, we would assume the solvent effect on E and s_E to be small when changing the solvent from DMSO to acetonitrile. Instead we attribute the changes in reactivity mostly to sterics. As a consequence, rate constants can also semi-quantitatively be estimated for neutral nucleophiles in different (aprotic polar) solvents. The calculated rate constants in Table 3 would barely suffice the requirements of prediction accuracy within a factor of 100. But it has to be mentioned, that this is almost a worst case scenario: Sterics play a huge role here, the solvent was switched from DMSO to acetonitrile, the nucleophile switched from anionic sulfur to neutral nitrogen, a S_N2 mechanism is at play and the error would only become smaller if stronger nucleophiles were employed. The nucleophilicity (N) range of the employed substituted pyridines **4** has the error k_2/k_{2calc} (Table 3) at its maximum, substantially weaker nucleophiles cannot be employed due to thermodynamic and kinetic reasons. Furthermore, nucleophilicity parameters N and s_N for substituted pyridines **4** were determined in CH_2Cl_2 instead of MeCN and contribute to an increase of the deviation. This demonstrates the applicability of the extended Mayr-Patz equation even under adverse conditions and how the electrophilicity parameters E and s_E for cyclopropanes **1** presented in this work can be used to predict rate constants on a semi-quantitative level.

3.3 Conclusion

The electrophilic reactivity of acceptor and donor-acceptor cyclopropanes **1** was systematically surveyed for the first time and the acquired second-order rate constants for the reactions with thiophenolates **2**, C-nucleophiles **5** and sodium azide (**3**) were used to determine the electrophile specific parameters E and s_E of the extended Mayr-Patz equation (equation 1). It has now become possible to semi-quantitatively predict rate constants for these cyclopropanes with over 1200 previously characterized nucleophiles.[15] It was demonstrated that steric effects lead to a decrease in prediction accuracy. Now the stage is set for systematic investigations on the effect of different Lewis acids on the reactivity of (donor-)acceptor substituted cyclopropanes. Furthermore, electrophilic

cyclopropanes were compared to Michael acceptors and the enormous differences in reactivity were quantified. The small influence of cyclopropane substitution upon rate constants was reported. Uncommon, U-shaped Hammett plots were observed for the reactions of cyclopropanes **1** with differently substituted aryls with thiophenolates **2**.

3.4 References

(1) (a) Pirenne, V.; Muriel, B.; Waser, J., *Chem. Rev.* **2020**. (b) Liu, J.; Liu, R.; Wei, Y.; Shi, M., *Trends Chem.* **2019,** *1*, 779−793. (c) Liu, Y.; Wang, Q.-L.; Chen, Z.; Zhou, C.-S.; Xiong, B.-Q.; Zhang, P.-L.; Yang, C.-A.; Zhou, Q., *Beilstein J. Org. Chem.* **2019,** *15*, 256−278. (d) Talukdar, R.; Saha, A.; Ghorai, M. K., *Isr. J. Chem.* **2016,** *56*, 445−453. (e) Budynina, E. M.; Ivanov, K. L.; Sorokin, I. D.; Melnikov, M. Y., *Synthesis* **2017,** *49*, 3035−3068. (f) Cavitt, M. A.; Phun, L. H.; France, S., *Chem. Soc. Rev.* **2014,** *43*, 804−818. (g) Craig, A. J.; Hawkins, B. C., *Synthesis* **2020,** *52*, 27−39. (h) Augustin, A. U.; Werz, D. B., *Acc. Chem. Res.* **2021,** *54*, 1528−1541. (i) Ghosh, K.; Das, S., *Org. Biomol. Chem.* **2021,** *19*, 965−982.

(2) Kreft, A.; Lücht, A.; Grunenberg, J.; Jones, P. G.; Werz, D. B., *Angew. Chem., Int. Ed.* **2019,** *58*, 1955−1959.

(3) Ohkata, K.; Nagai, T.; Tamaru, A.; Nandate, M.-a.; Hanafusa, T., *J. Chem. Soc., Perkin Trans. 2* **1982**, 1255−1259.

(4) McKinney, M. A.; Kremer, K. G.; Aicher, T., *Tetrahedron Lett.* **1984,** *25*, 5477−5480.

(5) (a) Mayr, H.; Patz, M., *Angew. Chem., Int. Ed.* **1994,** *33*, 938−957. (b) Mayr, H.; Bug, T.; Gotta, M. F.; Hering, N.; Irrgang, B.; Janker, B.; Kempf, B.; Loos, R.; Ofial, A. R.; Remennikov, G.; Schimmel, H., *J. Am. Chem. Soc.* **2001,** *123*, 9500−9512. (c) Mayr, H.; Kempf, B.; Ofial, A. R., *Acc. Chem. Res.* **2003,** *36*, 66−77. (d) Mayr, H., *Tetrahedron* **2015,** *32*, 5095−5111.

(6) Phan, T. B.; Breugst, M.; Mayr, H., *Angew. Chem., Int. Ed.* **2006,** *45*, 3869−3874.

(7) (a) Nambu, H.; Ono, N.; Hirota, W.; Fukumoto, M.; Yakura, T., *Chem. Pharm. Bull.* **2016,** *64*, 1763−1768. (b) Tukhtaev, H. B.; Ivanov, K. L.; Bezzubov, S. I.; Cheshkov, D. A.; Melnikov, M. Y.; Budynina, E. M., *Org. Lett.* **2019,** *21*, 1087−1092.

(8) Hudson, R.; Klopman, G., *J. Chem. Soc.* **1962**, 1062−1067.

(9) Robiette, R.; Trieu-Van, T.; Aggarwal, V. K.; Harvey, J. N., *J. Am. Chem. Soc.* **2016,** *138*, 734−737.

(10) Jüstel, P. M.; Pignot, C. D.; Ofial, A. R., *J. Org. Chem.* **2021,** *86*, 5965−5972.

(11) Bordwell, F. G.; Hughes, D. L., *J. Org. Chem.* **1982,** *47*, 3224−3232.

(12) Ballistreri, F. P.; Maccarone, E.; Mamo, A., *J. Org. Chem.* **1976,** *41*, 3364−3367.

(13) Ortega, A.; Manzano, R.; Uria, U.; Carrillo, L.; Reyes, E.; Tejero, T.; Merino, P.; Vicario, J. L., *Angew. Chem., Int. Ed.* **2018,** *57*, 8225−8229.

(14) (a) Bordwell, F. G., *Acc. Chem. Res.* **1988,** *21*, 456−463. (b) Tschesche, R.; Blumbach, J.; Welzel, P., *Liebigs Ann. Chem.* **1973**, 407−418. (c) Yoji, H.; Morio, K.; Kohji, M., *Bull. Chem. Soc. Jpn.* **1971,** *44*, 2506−2510. (d) Pearson, R. G.; Dillon, R. L., *J. Am. Chem. Soc.* **1953,** *75*, 2439−2443.

(15) A database for reactivity parameters *E*, *N*,and s_N is freely accessible via http://www.cup.lmu.de/oc/mayr/DBintro.html.

(16) Mayer, R. J.; Allihn, P. W. A.; Hampel, N.; Mayer, P.; Sieber, S. A.; Ofial, A. R., *Chem. Sci.* **2021,** *12*, 4850−4865.

(17) Allgäuer, D. S.; Jangra, H.; Asahara, H.; Li, Z.; Chen, Q.; Zipse, H.; Ofial, A. R.; Mayr, H., *J. Am. Chem. Soc.* **2017,** *139*, 13318−13329.

(18) Hine, J., *Adv. Phys. Org. Chem.* **1977,** *15*, 1−61.

(19) (a) Lemek, T.; Mayr, H., *J. Org. Chem.* **2003,** *68*, 6880−6886. (b) Berger, S. T. A.; Seeliger, F. H.; Hofbauer, F.; Mayr, H., *Org. Biomol. Chem.* **2007,** *5*, 3020−3026. (c) Kaumanns, O.; Mayr, H., *J. Org. Chem.* **2008,** *73*, 2738−2745.

(20) Ofial, A. R., *Pure Appl. Chem.* **2015,** *87*, 341−351.

3.5 Experimental Section

3.5.1 General

All compounds used for the synthesis of the cyclopropanes and of the thiophenolates excepting the differently substituted styrenes were purchased from commercial suppliers and used without further purification. Bromine (99.8%), acetylacetone (>99%), malonodinitrile (99%) and potassium *tert*-butanolate (>98%) were purchased from Acros Organics. Dimethyl sulfide (>99%), sodium hydride (95%), 1,3-indandione (97%), 1,5,7-triazobicyclo[4.4.0]dec-5-ene (98%), 4-methoxythiophenol (97%), 4-methylthiophenol (98%) and thiophenol (97%) were obtained from Sigma-Aldrich. Dimedone (98%) and *N*-iodosuccinimide (97%) were purchased from abcr GmbH and diethyl malonate was obtained from Jansen Chimica at 99% purity. Potassium carbonate was purchased from AppliChem at analytical grade. Styrene (99.5%) was obtained from Acros Organics, 4-trifluoromethylthiophenolate (>95%), 4-methoxystyrene (>98%) and 4-methylstyrene (>96%) from TCI and 3-chlorostyrene (98%) from Alfa Aesar. All styrenes were distilled *in vacuo* prior to use to remove the stabilizer. NaH, KO*t*Bu and the differently substituted thiophenols were stored in a glovebox under argon atmosphere. Cyclopropane **1a** was acquired from TCI (>98%).

n-Pentane was distilled prior to use. DMSO and dichloromethane (DCM) over molecular sieves were purchased from Acros Organics with a purity of 99.8%.

The used deuterated solvents were obtained from EurIsotop. For thin layer chromatography silica gel plates with F-254 fluorescence indicator from Merck were used. Flash column chromatography was performed on silica gel 60 (0.040-0.063 mm) from Merck with mixtures of ethyl acetate (EtOAc) and *n*-pentane.

^{1}H and ^{13}C spectra were acquired using a 400 MHz or a 600 MHz nuclear magnetic resonance (NMR) spectrometer. For the ^{13}C-spectra proton decoupling was applied. The following abbreviations and combinations of them were used when characterising the NMR spectra: s = singlet, d = doublet, t = triplet, q = quartet, m = multiplet. Chemical shifts are given in parts per million (ppm) and the internal reference was set to either *d*-chloroform (δ_H = 7.26 ppm, δ_C = 77.0 ppm) or DMSO-d_6 (δ_H = 2.50 ppm, δ_C = 39.5 ppm).

High-resolution mass spectrometry (HRMS) was performed with either a Thermo Finnigan LTQ FT Ultra Fourier transform ion cyclotron resonance spectrometer, a Q-Exactive GC Orbitrap, a Finnigan MAT 95 or a Finnigan MAT 90 GC/MS. Samples were ionized either by electron spray ionisation (ESI) or electron impact ionisation (EI).

Infrared (IR) spectra were acquired on PerkinElmer SpectrumBX-59343 instrument with a Smiths Detection DuraSamplIR II Diamond ATR sensor for detection in the range of 4500−600 cm^{-1}. Melting points were measured using a Büchi melting-point M-560 device and are not corrected.

3.5.2 Synthesis

General Procedure A (GP A): Synthesis of Cyclopropanes *via* Bromosulfonium Bromides

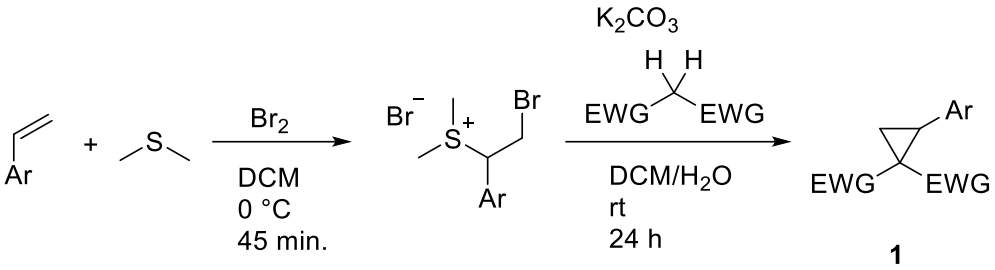

1

The synthesis route *via* bromosulfonium bromides was done according to a procedure by Tukhtaev *et al*.[1]

In a dry round-bottom flask under argon atmosphere a solution of dimethyl sulfide in DCM (5 M, 5 equiv.) was prepared under stirring prior to adding either unsubstituted or substituted styrene (1 M, 1 equiv.). The reaction mixture was cooled to 0 °C and a solution of bromine in DCM (5 M, 1 equiv.) was added dropwise under stirring. Colorless precipitates formed within 2 minutes after bromine was added. The reaction mixture was stirred at 0 °C for 45 min. After complete decoloration, the resulting precipitate was filtrated *in vacuo* and washed with diethyl ether (2x).

The collected bromosulfonium bromide was directly used in the synthesis of the cyclopropanes **1**. Potassium carbonate (1.5 M, 3 equiv.) was first added to a stirred solution of bromosulfonium bromide in a 50 v% DCM:H_2O mixture (0.5 M, 1 equiv.) under argon atmosphere. The methylene compound was then quickly added (0.5 M, 1 equiv.) and the reaction mixture was stirred for 24 h at room temperature. The reaction was followed by GC-MS. After reaction completion the organic layer was separated, and the aqueous layer was washed with DCM (3x). The combined organic layers were dried ($MgSO_4$) and DCM was removed *in vacuo*. The obtained crude product was purified by flash column chromatography on silica gel with mixtures of *n*-pentane/ethyl acetate.

General Procedure B (GP B): Synthesis of Cyclopropanes *via* a Radical Pathway

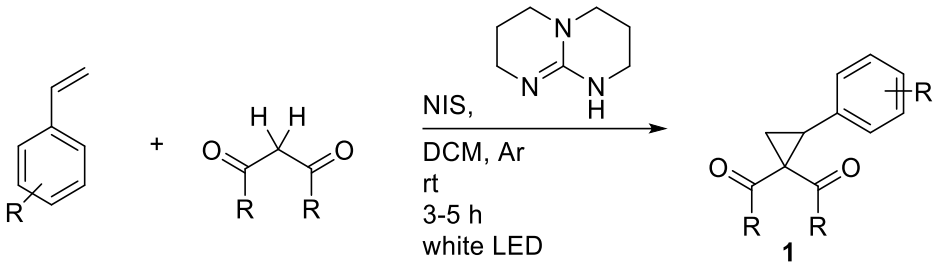

Into a dry, argon-flushed round-bottom flask the 1,3-dicarbonyl compound (0.1 M, 1 equiv.) was added together with *N*-iodosuccinimide (NIS) (0.2 M, 2 equiv.) and 1,5,7-triazobicyclo[4.4.0]dec-5-ene (TBD) (0.1 M, 1 equiv.) to dry DCM according to a modified procedure by Qian *et al.*[2] Unsubstituted or substituted styrene (0.3 M, 3 equiv.) was then added while stirring. The white LED was turned on and the reaction was stirred for 3 to 5 h. The reaction progress was followed by TLC.

After reaction completion, the brown mixture was extracted first with an equal amount of sodium thiosulphate solution until decoloration to orange/yellow was observed. The organic phase was separated from the aqueous phase and the aqueous phase was extracted three times with an equal volume of DCM. The organic phase was washed three times with aq. NaOH (1 M) and subsequently with brine. The combined organic layers were dried over $MgSO_4$ and DCM was removed *in vacuo*. The obtained crude product was purified by flash column chromatography with *n*-pentane/EtOAc mixtures.

(2-bromo-1-phenylethyl)dimethylsulfonium bromide

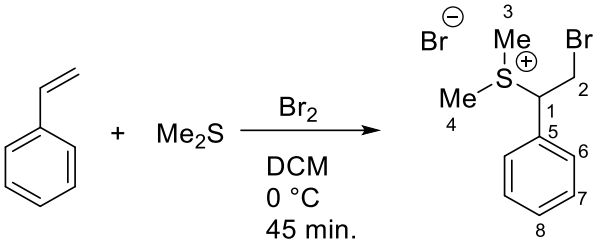

According to GP A: A solution of dimethyl sulfide (17.6 mL, 14.9 g, 0.24 mol) and styrene (5.50 mL, 5.00 g, 48.0 mmol) in DCM (48 mL) was cooled to 0 °C. Under stirring a solution of bromine (2.46 mL, 7.70 g, 48.0 mmol) in DCM (9.6 mL) was added and stirred at 0 °C for 45 minutes. Decoloration of the reaction mixture was observed. The reaction mixture was worked up according to GP A. (2-bromo-1-phenylethyl)dimethylsulfonium bromide precipitated as a colorless solid (11.5 g, 35.0 mmol, 73%).

^{1}H NMR (400 MHz, DMSO-*d*$_6$): δ = 7.57– 7.53 (m, 5 H, 6-H, 7-H, 8-H), 5.37 – 5.33 (m, 1 H, 1-H), 4.44 – 4.34 (m, 2 H, 2-H), 2.94 (s, 3 H, 3-H), 2.67 (s, 3 H, 4-H).

^{13}C{^{1}H} NMR (101 MHz, DMSO-*d*$_6$): δ = 130.5 (C_q, C-5), 130.0 (CH, C-8), 129.6 (CH, C-6), 129.4 (CH, C-7), 58.5 (CHS, C-1), 29.2 (CH_2Br, C-2), 23.9 (CH_3S, C-3), 22.7 (CH_3S, C-4).

HRMS (ESI-positive): 244.9996 found for $C_{10}H_{14}BrS^+$ (calculated: 244.9994).

NMR spectroscopic data agree with spectroscopic data in D_2O.[3]

6,6-dimethyl-1-phenyl-5,7-dioxaspiro[2.5]octane-4,8-dione (1b)

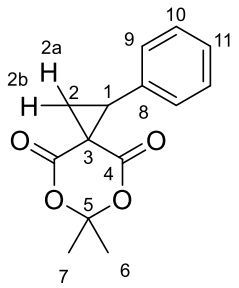

1b

According to GP B: Meldrum's acid (1.00 g, 6.94 mmol) was stirred with styrene (2.17 g, 20.8 mmol), NIS (3.14 g, 13.9 mmol) and TBD (974 mg, 7.00 mmol) in 60 mL dry DCM for 2 h in the presence of a white LED. Reaction progress was assessed by TLC. The organic phase was separated from the aqueous phase and the aqueous phase was extracted three times with DCM. The organic phase was separated from the aqueous phase and the aqueous phase was extracted three times with DCM. The organic phase was washed with 3 × NaOH solution (1 M) and brine. The combined organic layers were dried over $MgSO_4$ and DCM was removed *in vacuo*. Flash column chromatography (*n*-pentane:EtOAc 90:10 → 70:30) yielded **1b** (1011 mg, 4.11 mmol, 59%) as a colorless solid.

^{1}H NMR (400 MHz, $CDCl_3$): δ = 7.35 – 7.32 (m, 5 H, 9-H, 10-H, 11-H), 3.45 (t, *J* = 9.4 Hz, 1 H, 1-H), 2.70 (dd, *J* = 9.3, 4.8 Hz, 1 H, 2a-H), 2.55 (dd, *J* = 9.5, 4.8 Hz, 1 H, 2b-H), 1.73 (s, 3 H, 6-H), 1.73 (s, 3 H, 7-H).

HRMS (EI): 246.0892 found for $C_{14}H_{14}O_4^{\bullet+}$ (calculated: 246.0887).

Melting point: 128 °C. Literature: 130 – 131 °C.[2]

Analytical data match the existing literature.[2]

6,6-Dimethylspiro[2.5]octane-4,8-dione (1c)

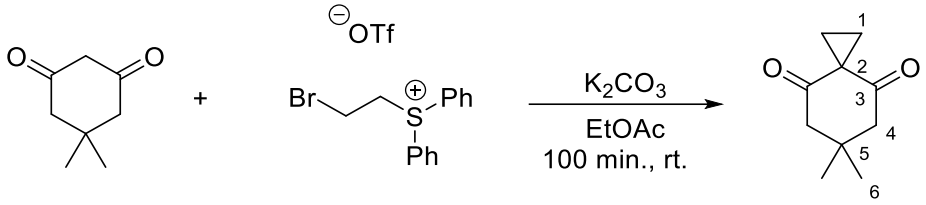

1c

To a stirred suspension of dimedone (414 mg, 2.95 mmol) in ethyl acetate (30 mL) was added K_2CO_3 (1.27 g, 9.19 mmol) and (2-bromoethyl)diphenylsulfonium triflate (1.31 g, 2.96 mmol) simultaneously. (2-bromoethyl)diphenylsulfonium triflate was obtained in a procedure described by Yakura *et al*.[4] After 100 minutes TLC and GCMS control indicated that the reaction was completed.

The reaction mixture was quenched with water (60 mL) and extracted with ethyl acetate (2 × 60 mL). The organic layers were combined and washed with brine (60 mL), dried ($MgSO_4$) and concentrated *in vacuo*.

The residue was purified by column chromatography (*SiO_2, n-pentane/EtOAc* 95/5→80/20%).

6,6-Dimethylspiro[2.5]octane-4,8-dione **1c** (412 mg, 2.48 mmol, 84 %) was obtained as a colorless liquid.

^{1}H NMR (400 MHz, $CDCl_3$): δ = 2.55 (s, 4 H, 4-H), 1.76 (s, 4 H, 1-H), 1.12 (s, 6 H, 6-H).

^{13}C{^{1}H} NMR (101 MHz, $CDCl_3$): δ = 207.1 (CO, C-3), 53.4 (CH_2, C-4), 39.8 (C_q, C-2), 30.5 (C_q, C-5), 28.7 (C-1), 27.6 (C-6).

Analytical data match the existing literature[4]

1-(3-chlorophenyl)-6,6-dimethylspiro[2.5]octane-4,8-dione (1d)

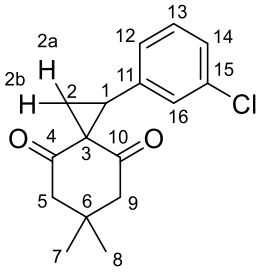

1d

According to GP A: 3-chlorostyrene (0.90 mL, 1.00 g, 7.22 mmol) was mixed with dimethyl sulfide (2.64 mL, 2.24 g, 36.1 mmol) in 7.2 mL DCM. Bromine (0.37 mL, 1.15 g, 7.22 mmol) in 1.5 mL DCM was added at 0 °C while stirring. After reaction completion, the resulting light-yellow solid was directly employed in the synthesis of the cyclopropane by reacting it with dimedone (513 mg, 3.66 mmol) and K_2CO_3 (1.52 g, 11.0 mmol) in 7.30 mL 50 v% DCM:H_2O. The crude product was isolated as a brown oil and purified by flash column chromatography (*n*-pentane:EtOAc 95:5 → 85:15). **1d** (360 mg, 1.30 mmol, 36%) was isolated as a colorless solid.

^{1}H NMR (400 MHz, $CDCl_3$): δ = 7.23 – 7.18 (m, 3 H, 12-H, 13-H, 14-H), 7.10 – 7.08 (m, 1 H, 16-H), 3.20 (t, *J* = 8.9 Hz, 1 H, 1-H), 2.66 – 2.55 (m, 2 H, 5-H), 2.46 (dd, *J* = 8.9, 3.8 Hz, 1 H, 2a-H), 2.40 – 2.24 (m, 3 H, 2b-H and 9-H), 1.14 (s, 3 H, 7-H), 1.05 (s, 3 H, 8-H).
^{13}C{^{1}H} NMR (101 MHz, $CDCl_3$): δ = 205.7 (CO, C-4), 201.8 (CO, C-10), 135.6 (C_q, C-11), 134.1 (CCl, C-15), 129.9 (CH, C-14), 129.4 (CH, C-13), 128.3 (CH, C-12), 127.4 (CH, C-16), 54.2 (CH_2, C-5), 53.4 (CH_2, C-9), 48.2 (C_q, C-3), 47.0 (CH, C-1), 30.6 (C_q, C-6), 29.5 (CH_3, C-7), 28.0 (CH_3, C-8), 22.7 (CH_2, C-2).

HRMS (EI): 276.0913 found for $C_{16}H_{17}ClO_2^{\bullet+}$ (calculated: 276.0912).

IR (neat): 2955, 2869, 2837, 1625, 1514, 1463, 1417, 1400, 1367, 1351, 1305, 1247, 1217, 1176, 1167, 1141, 1101, 1031, 959, 914, 884, 830, 811, 769, 726 cm^{-1}.

Melting point: 89 °C.

6,6-dimethyl-1-phenylspiro[2.5]octane-4,8-dione (1e)

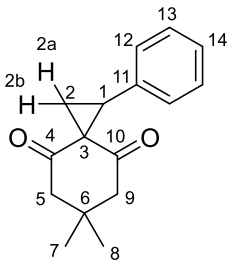

1e

According to GP A: (2-bromo-1-phenylethyl)dimethylsulfonium bromide (3.00 g, 9.20 mmol) was reacted with dimedone (1.30 g, 9.27 mmol) and K_2CO_3 (3.81 g, 27.6 mmol) in 18.4 mL 50 v% DCM:H_2O. The reaction progress was followed by GC-MS. The crude product was obtained as a yellow oil and purified by flash column chromatography (*n*-pentane:EtOAc 95:5 → 90:10). **1e** (1.01 g, 4.20 mmol, 46%) was isolated as a colorless solid.

^{1}H NMR (400 MHz, $CDCl_3$): δ = 7.28 – 7.18 (m, 5 H, 12-H, 13-H, 14-H), 3.24 (t, *J* = 9.0 Hz, 1 H, 1-H), 2.63 – 2.49 (m, 3 H, 2a-H and 5-H), 2.35 – 2.17 (m, 3 H, 2b-H and 9-H), 1.11 (s, 3 H, 7-H), 1.02 (s, 3 H, 8-H).

^{13}C{^{1}H} NMR (101 MHz, $CDCl_3$): δ = 205.9 (CO, C-4), 201.8 (CO, C-10), 133.3 (C_q, C-11), 129.7 (CH, C-13), 128.2 (CH, C-12), 128.1 (CH, C-14), 54.2 (CH_2, C-5), 53.4 (CH_2, C-9), 48.8 (C_q, C-3), 48.6 (CH, C-1), 30.6 (C_q, C-6), 29.5 (CH_3, C-7), 28.0 (CH_3, C-8), 22.3 (CH_2, C-2).

HRMS (EI): 242.1301 found for $C_{16}H_{18}O_2^{\bullet+}$ (calculated: 242.1301).

IR (neat): 3063, 2951, 2891, 2871, 1699, 1672, 1645, 1601, 1501, 1456, 1425, 1415, 1380, 1369, 1335, 1318, 1295, 1274, 1218, 1179, 1156, 1146, 1122, 1111, 1078, 1031, 1008, 962, 945, 924, 861, 785, 775, 769, 722, 700, 679, 693 cm^{-1}.

Melting point: 132 – 134 °C. Previously reported were 126 – 128 °C.[5]

Analytical data match the existing literature.[6]

2-(3-chlorophenyl)spiro[cyclopropane-1,2'-indene]-1',3'-dione (1f)

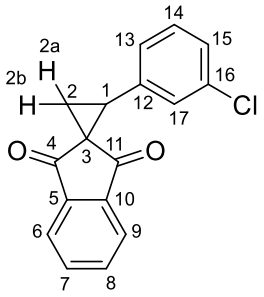

1f

According to GP B: 1,3-Indandione (439 mg, 3.00 mmol) was stirred with 3-chlorostyrene (1.12 mL, 1.25 g, 9.00 mmol), NIS (1.35 g, 6.00 mmol) and TBD (418 mg, 3.00 mmol) in 30 mL dry DCM for 5 h in the presence of a white LED. Reaction progress was assessed by TLC. After reaction completion, the brown mixture was extracted first with sodium thiosulphate solution until decoloration to orange/yellow was observed. The organic phase was separated from the aqueous phase and the aqueous phase was extracted three times with DCM. The organic phase was washed with 3 × NaOH solution (1 M) and brine. The combined organic layers were dried over $MgSO_4$ and DCM was removed *in vacuo*. Flash column chromatography (*n*-pentane:EtOAc 95:5 → 85:15) yielded **1f** (776 mg, 2.74 mmol, 91%) as a light yellow solid.

^{1}H NMR (400 MHz, $CDCl_3$): δ = 7.96 – 7.94 (m, 1 H, 6-H), 7.81 – 7.72 (m, 3 H, 7-H, 8-H, 9-H), 7.26 – 7.14 (m, 4 H, 13-H, 14-H, 15-H, 17-H), 3.36 (t, *J* = 8.9 Hz, 1 H, 1-H), 2.40 (dd, *J* = 8.7, 4.3 Hz, 1 H, 2a-H), 2.25 (dd, *J* = 9.0, 4.4 Hz, 1 H, 2b-H).

^{13}C{^{1}H} NMR (101 MHz, $CDCl_3$): δ = 197.9 (CO, C-4), 195.7 (CO, C-11), 142.7 (C_q, C-5), 141.7 (C_q, C-10), 135.8 (C_q, C-12), 135.1 (CH, C-7), 134.9 (CH, C-8), 134.1 (C_q, C-16), 129.5 (CH, C-17), 129.4 (CH, C-14), 128.0 (CH, C-15), 127.4 (CH, C-13), 122.68 (CH, C-6), 122.67 (CH, C-9), 42.4 (C_q, C-3), 39.9 (CH, C-1), 22.2 (CH_2, C-2).

HRMS (EI): 282.0448 found for $C_{17}H_{11}ClO_2^{\bullet+}$ (calculated: 282.0442).

IR (neat): 3073, 1738, 1701, 1597, 1571, 1478, 1466, 1443, 1375, 1350, 1332, 1313, 1289, 1222, 1193, 1171, 1156, 1114, 1093, 1079, 1041, 1010, 999, 947, 899, 820, 786, 759, 716, 701, 687, 674 cm^{-1}.

Melting point: 108 – 109 °C.

2-phenylspiro[cyclopropane-1,2'-indene]-1',3'-dione (1g)

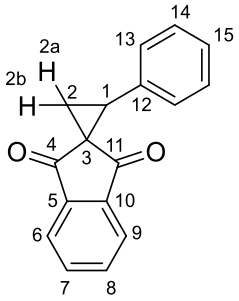

1g

According to GP A: (2-bromo-1-phenylethyl)dimethylsulfonium bromide (5.22 g, 16.0 mmol) was reacted with 1,3-indandione (2.34 g, 16.0 mmol) and K_2CO_3 (6.63 g, 48.0 mmol) in 32 mL 50 v% DCM:H_2O. The reaction progress was followed by GC-MS. The crude product was obtained as a yellow oil and purified by flash column chromatography (*n*-pentane:EtOAc 95:5 → 90:10). **1g** (2.70 g, 10.9 mmol, 68%) was isolated as a light orange solid, which crystallizes easily.

^{1}H NMR (400 MHz, $CDCl_3$): δ = 7.95 – 7.93 (m, 1 H, 6-H), 7.78 – 7.69 (m, 3 H, 7-H, 8-H, 9-H), 7.27 – 7.22 (m, 5 H, 13-H, 14-H, 15-H), 3.42 (t, *J* = 8.9 Hz, 1 H, 1-H), 2.45 (dd, *J* = 8.5, 4.5 Hz, 1 H, 2a-H), 2.27 (dd, *J* = 9.4, 3.9 Hz, 1 H, 2b-H).

^{13}C{^{1}H} NMR (101 MHz, $CDCl_3$): δ = 198.4 (CO, C-4), 196.0 (CO, C-11), 142.8 (C_q, C-5), 141.7 (C_q, C-10), 135.0 (CH, C-7), 134.8 (CH, C-8), 133.7 (C_q, C-12), 129.4 (CH, C-14), 128.3 (CH, C-13), 127.9 (CH, C-15), 122.6 (CH, C-6), 122.6 (CH, C-9), 42.8 (C_q, C-3), 41.3 (CH, C-1), 22.4 (CH_2, C-2).

HRMS (EI): 248.0826 found for $C_{17}H_{12}O_2^{\bullet+}$ (calculated: 248.0832).

IR (neat): 3058, 1702, 1600, 1498, 1456, 1429, 1384, 1333, 1311, 1289, 1223, 1195, 1156, 1117, 1080, 1060, 1043, 1009, 1000, 947, 833, 771, 745, 703 cm^{-1}.

Melting point: 136 °C. Previously reported were 126 – 128 °C.[2]

Analytical data match the existing literature.[2]

2-(*p*-tolyl)spiro[cyclopropane-1,2'-indene]-1',3'-dione (1h)

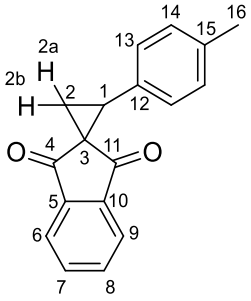

1h

According to GP B: 1,3-Indandione (439 mg, 3.00 mmol.) was stirred with 4-methylstyrene (1.20 mL, 1.06 g, 9.00 mmol), NIS (1.35 g, 6.00 mmol) and TBD (418 mg, 3.00 mmol) in 30 mL dry DCM for 5 h in the presence of a white LED. Reaction progress was assessed by TLC. After reaction completion, the brown mixture was extracted first with sodium thiosulphate solution until decoloration to orange/yellow was observed. The organic phase was separated from the aqueous phase and the aqueous phase was extracted three times with DCM. The organic phase was washed with 3 × NaOH solution (1 M) and brine. The combined organic layers were dried over $MgSO_4$ and DCM was removed *in vacuo*. Flash column chromatography (*n*-pentane:EtOAc 95:5 → 92:8) yielded **1h** (589 mg, 2.25 mmol, 75%) as a yellow solid.

^{1}H NMR (400 MHz, $CDCl_3$): δ = 7.98 – 7.96 (m, 1 H, 6-H), 7.82 – 7.72 (m, 3 H, 7-H, 8-H, 9-H), 7.20 – 7.10 (m, 4 H, 13-H, 14-H), 3.43 (t, *J* = 9.0 Hz, 1 H, 1-H), 2.47 (dd, *J* = 8.8, 4.2 Hz, 1 H, 2a-H), 2.32 (s, 3 H, 16-H), 2.30 (dd, *J* = 9.1, 4.2 Hz, 1 H, 2b-H).

^{13}C{^{1}H} NMR (101 MHz, $CDCl_3$): δ = 198.4 (CO, C-4), 196.1 (CO, C-11), 142.8 (C_q, C-5), 141.7 (C_q, C-10), 137.7 (C_q, C-15), 134.9 (CH, C-7), 134.7 (CH, C-8), 130.6 (C_q, C-12), 129.2 (CH, C-13), 129.0 (CH, C-14), 122.6 (CH, C-6), 122.5 (CH, C-9), 43.0 (C_q, C-3), 41.5 (CH, C-1), 22.4 (CH_2, C-2), 21.3 (CH_3, C-16).

HRMS (EI): 262.0990 found for $C_{18}H_{14}O_2^{\bullet+}$ (calculated: 262.0988).

IR (neat): 3018, 2921, 1737, 1699, 1599, 1519, 1449, 1376, 1349, 1332, 1309, 1288, 1222, 1193, 1171, 1156, 1102, 1065, 1040, 1009, 947, 840, 815, 759, 723, 685 cm^{-1}.

Melting point: 123 – 126 °C. Literature: 126 – 128 °C.[7]

Analytical data match the existing literature.[2]

2-(4-methoxyphenyl)spiro[cyclopropane-1,2'-indene]-1',3'-dione (1i)

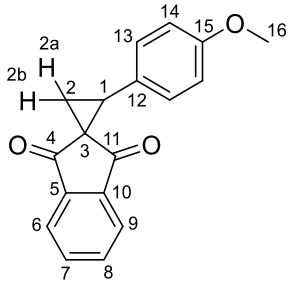

1i

According to GP B: 1,3-Indandione (439 mg, 3.00 mmol) was stirred with 4-methoxystyrene (1.21 mL, 1.21 g, 9.00 mmol), NIS (1.35 g, 6.00 mmol) and TBD (418 mg, 3.00 mmol) in 30 mL dry DCM for 5 h in the presence of a white LED. Reaction progress was assessed by TLC. After reaction completion, the brown mixture was extracted first with sodium thiosulphate solution until decoloration to orange/yellow was observed. The organic phase was separated from the aqueous phase and the aqueous phase was extracted three times with DCM. The organic phase was washed with 3 × NaOH solution (1 M) and brine. The combined organic layers were dried over $MgSO_4$ and DCM was removed *in vacuo*. Flash column chromatography (*n*-pentane:EtOAc 95:5 → 85:15) yielded **1i** (508 mg, 1.83 mmol, 61%) as a light pink solid.

^{1}H NMR (400 MHz, $CDCl_3$): δ = 7.97 – 7.95 (m, 1 H, 6-H), 7.81 – 7.72 (m, 3 H, 7-H, 8-H, 9-H), 7.22 (d, *J* = 8.2 Hz, 2 H, 13-H), 6.83 (d, *J* = 8.8 Hz, 2 H, 14-H), 3.78 (s, 3 H, 16-H), 3.42 (t, *J* = 8.9 Hz, 1 H, 1-H), 2.45 (dd, *J* = 8.9, 4.3 Hz, 1 H, 2-Ha), 2.30 (dd, *J* = 9.1, 4.3 Hz, 1 H, 2-Hb).
^{13}C{^{1}H} NMR (101 MHz, $CDCl_3$): δ = 198.4 (CO, C-4), 196.1 (CO, C-11), 159.3 (C_q, C-15), 142.8 (C_q, C-5), 141.8 (C_q, C-10), 134.9 (CH, C-7), 134.7 (CH, C-8), 130.4 (CH, C-13), 125.6 (C_q, C-12), 122.5 (CH, C-6), 122.5 (CH, C-9), 113.7 (CH, C-114), 55.3 (CH_3, C-16), 43.2 (C_q, C-3), 41.5 (CH, C-1), 22.5 (CH_2, C-2).

HRMS (EI): 278.0938 found for $C_{18}H_{14}O_3^{\bullet+}$ (calculated: 278.0937).

IR (neat): 2934, 2835, 1701, 1610, 1558, 1517, 1456, 1376, 1333, 1308, 1290, 1250, 1224, 1179, 1157, 1066, 1043, 1009, 841, 825, 813, 759, 729, 685, 668 cm^{-1}.

Melting point: 143 – 145 °C. Literature: 148 – 150 °C.[2]

Analytical data match the existing literature.[2]

2-Phenylcyclopropane-1,1-dicarbonitrile (1j)

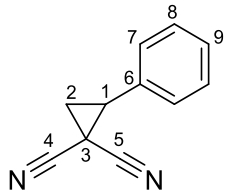

1j

According to GP A: (2-bromo-1-phenylethyl)dimethylsulfonium bromide (465 mg, 1.43 mmol) was reacted with malonodinitrile (97.8 mg, 1.48 mmol) and K_2CO_3 (593 mg, 4.30 mmol) in 3.00 mL 50 v% DCM:H_2O. The reaction progress was followed by GC-MS. The crude product was obtained as a brown oil and purified by flash column chromatography (*n*-pentane:EtOAc 95:5 → 85:15). **1j** (141.1 mg, 0.84 mmol, 59%) was obtained as a yellow oil.

^{1}H NMR (400 MHz, $CDCl_3$): δ = 7.46 – 7.41 (m, 3 H, Ar-H), 7.31 – 7.29 (m, 2 H, Ar-H), 3.31 (t, *J* = 9.0 Hz, 1 H, 1-H), 2.29-2.23 (m, 2 H, 2-H).

^{13}C{^{1}H} NMR (101 MHz, $CDCl_3$): δ = 130.7 (C_q, C-6), 129.7 (CH, C-9), 129.3 (CH, C-7), 128.5 (CH, C-8), 115.4 (CN, C-4), 113.1 (CN, C-5), 35.3 (CH, C-1), 22.5 (CH_2, C-2), 7.4 (C_q, C-3).

HRMS (EI): 168.0687 found for $C_{11}H_8N_2^{\bullet+}$ (calculated: 168.0682).

IR (film): 3105, 3032, 2248, 1605, 1501, 1458, 1438, 1375, 1278, 1198, 1087, 1032, 982, 956, 777, 736, 696 cm^{-1}.

Analytical data match the existing literature.[1]

Product Studies

For selected successfully measured kinetics, product studies were performed by mixing equimolar quantities of the cyclopropane and the nucleophile in 1 mL dry DMSO under argon atmosphere. After the reaction was completed, the resulting product was poured in 10 mL 0.01 M HCl solution and extracted 3 times with DCM. The combined organic phases were washed 3 times with 0.01 M hydrochloric brine. DCM was evaporated *in vacuo*.

Sodium 2,2-dimethyl-4-oxo-5-(2-(*p*-tolylthio)ethyl)-4H-1,3-dioxin-6-olate (7a)

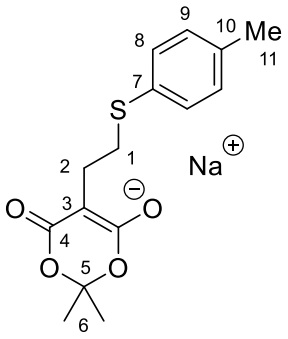

7a

4-Methylthiophenol (144.1 mg, 1.16 mmol, 1.0 equiv.) and NaH (27.8 mg, 1.16 mmol, 1.0 equiv.) were dissolved in dry DMSO-d_6 (10 mL) to generate the nucleophile stock solution (0.116 M). 1.0 mL of this solution were added to **1a** (20.0 mg, 0.116 mmol, 1.0 equiv.) in an NMR-tube and mixed well.

^{1}H NMR (400 MHz, DMSO-d_6): δ = 7.23 (d, *J* = 8.7 Hz, 2 H, 9-H), 7.08 (d, *J* = 8.1 Hz, 2 H, 8-H), 2.83 – 2.79 (m, 2 H, 1-H), 2.32 – 2.28 (m, 2 H, 2-H), 2.25 (s, 3 H, 11-H), 1.43 (s, 6 H, 6-H).

^{13}C{^{1}H} NMR (101 MHz, DMSO-d_6): δ = 165.1 (CO, C-4), 134.2 (C_q, C-10), 134.0 (C_q, C-7), 129.5 (CH, C-8), 127.4 (CH, C-9), 99.0 (C_q, C-5), 71.0 (C_q, C-3), 31.9 (CH_2, C-1), 26.0 (CH_3, C-6), 25.2 (CH_2, C-2), 20.5 (CH_3, C-11).

Sodium 2,2-dimethyl-4-oxo-5-(2-phenyl-2-(*p*-tolylthio)ethyl)-4H-1,3-dioxin-6-olate (7b)

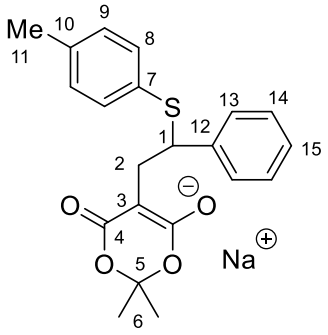

7b

4-Methylthiophenol (144.1 mg, 1.16 mmol, 1.0 equiv.) and NaH (27.8 mg, 1.16 mmol, 1.0 equiv.) were dissolved in dry DMSO-d_6 (10 mL) to generate the nucleophile stock solution (0.116 M). 0.7 mL of this solution were added to **1b** (20.0 mg, 0.081 mmol, 1.0 equiv.) in an NMR-tube and mixed well.

^{1}H NMR (400 MHz, DMSO-d_6): δ = 7.22 – 7.00 (m, 9 H, Ar-H), 4.72 (dd, *J* = 9.2, 6.9 Hz, 1 H, 1-H), 2.71 (dd, *J* = 13.8, 6.9 Hz 1 H, 2-Ha), 2.61 (dd, *J* = 13.8, 6.9 Hz 1 H, 2-Hb), 2.21 (s, 3 H, 11-H), 1.21 (s, 6 H, 6-H).
^{13}C{^{1}H} NMR (101 MHz, DMSO-d_6): δ = 165.2 (C_q, C-4), 143.0 (C_q, C-12), 135.2 (C_q, C-10), 132.9 (C_q, C-7), 130.4 (CH, C-8), 129.3 (CH, C-9), 128.1 (CH, C-14), 127.6.0 (CH, C-13), 126.2 (CH, C-15), 98.9 (C_q, C-5), 70.2 (C_q, C-3), 51.1 (CH, C-1), 31.2 (CH_2, C-2), 25.7 (CH_3, C-6), 20.6 (CH_3, C-11).

Sodium 5,5-dimethyl-3-oxo-2-(2-(*p*-tolylthio)ethyl)cyclohex-1-en-1-olate (7c)

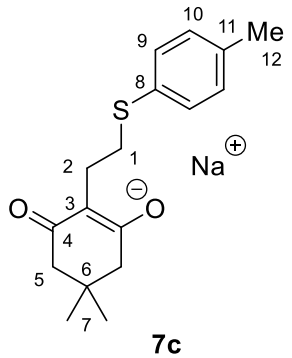

7c

4-Methylthiophenol (144.1 mg, 1.20 mmol, 1.0 equiv.) and NaH (27.8 mg, 1.16 mmol, 1.0 equiv.) were dissolved in dry DMSO-d_6 (10 mL) to generate the nucleophile stock solution (0.116 M). 1.0 mL of this solution were added to **1b** (20.0 mg, 0.116 mmol, 1.0 equiv.) in an NMR-tube and mixed well.

^{1}H NMR (400 MHz, DMSO-d_6): δ = 7.27 (d, *J* = 8.2 Hz, 2 H, 10-H), 7.07 (d, *J* = 8.1 Hz, 2 H, 9-H), 2.73 – 2.69 (m, 2 H, 1-H), 2.42 – 2.38 (m, 2 H, 2-H), 2.24 (s, 3 H, 12-H), 1.88 (s, 4 H, 5-H), 0.91 (s, 6 H, 7-H).
^{13}C{^{1}H} NMR (101 MHz, DMSO-d_6): δ = 187.6 (CO, C-4), 134.9 (C_q, C-11), 133.4 (C_q, C-8), 129.4 (CH, C-9), 126.9 (CH, C-10), 106.7 (C_q, C-3), 50.7 (CH_2, C-8), 31.4 (C_q, C-6), 31.2 (C_q, C-1), 29.1 (CH_3, C-7), 23.6 (CH_2, C-2), 20.5 (CH_3, C-12).

Sodium 1-(2-(3-chlorophenyl)-2-(phenylthio)ethyl)-4,4-dimethyl-2,6-dioxocyclohexan-1-ide (7d)

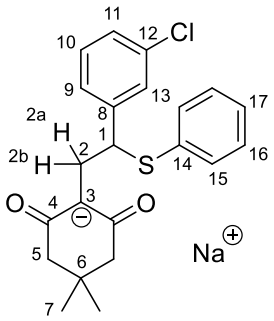

7d

Thiophenol (14.7 mg, 0.13 mmol, 1.0 eq.) and NaH (3.1 mg, 0.13 mmol) were dissolved in dry d_6-DMSO (1 mL) to generate a solution of potassium thiophenolate. After addition of the cyclopropane **1d** (37.8 mg, 0.13 mmol), the mixture was shaken and transferred into an NMR tube. The ring-opened product **7d**, quantitatively generated in this way, was characterized by NMR spectroscopy and HRMS.

^{1}H NMR (400 MHz, DMSO-d_6): δ = 7.29 – 7.08 (m, 9 H, H_{ar}), 5.00 (dd, *J* = 9.5, 6.5 Hz, 1 H, 1-H), 2.88 (dd, *J* = 12.9, 9.5 Hz, 1 H, 2-Ha), 2.64 (dd, *J* = 13.0, 6.5 Hz, 1 H, 2-Hb), 1.84 – 1.75 (m, 4 H, 5-H), 0.74 (s, 6 H, 7-H).

^{13}C{^{1}H} NMR (101 MHz, DMSO-d_6): δ = 187.8 (CO, C-4), 145.8 (C_q, C-8), 137.0 (C_q, C-14), 132.0 (C_q, C-12), 129.1 (CH, C_{ar}), 128.6 (CH, C_{ar}), 127.9 (CH, C_{ar}), 126.8 (CH, C_{ar}), 125.9 (CH, C_{ar}), 125.3 (CH, C_{ar}), 104.9 (C^-, C-3), 50.5 (CH_2, C-5), 49.4 (CH, C-1), 31.0 (C_q, C-6), 29.6 (CH_2, C-2), 28.8 (CH_3, C-7).

HRMS (ESI positive): 387.1182 found for $C_{22}H_{24}ClO_2S^+$ (calculated: 387.1180).

HRMS (ESI negative): 385.1037 found for $C_{22}H_{22}ClO_2S^-$ (calculated: 385.1035).

Potassium 4,4-dimethyl-2,6-dioxo-1-(2-phenyl-2-(phenylthio)ethyl)cyclohexan-1-ide (7e)

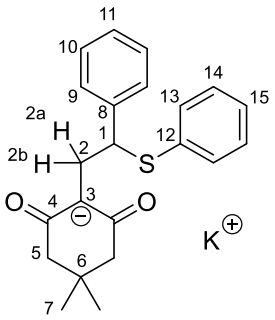

7e

Thiophenol (9.8 mg, 0.089 mmol, 1.0 eq.) and KO*t*Bu (10.0 mg, 0.089 mmol) were dissolved in dry d_6-DMSO (1 mL) to generate a solution of potassium thiophenolate. After addition of the cyclopropane **1e** (21.6 mg, 0.089 mmol), the mixture was shaken and transferred into an NMR tube. The ring-opened product **7e**, quantitatively generated in this way, was characterized by NMR spectroscopy and HRMS.

^{1}H NMR (400 MHz, DMSO-d_6): δ = 7.32 – 7.27 (m, 4 H, 13-H and 14-H), 7.19 – 7.02 (m, 6 H, 9-H, 10-H, 11-H, 15-H), 5.05 (dd, *J* = 9.1, 6.7 Hz, 1 H, 1-H), 2.88 (dd, *J* = 12.9, 9.1 Hz, 1 H, 2a-H), 2.66 (dd, *J* = 13.0, 6.7 Hz, 1 H, 2b-H), 1.80 – 1.72 (m, 4 H, 5-H), 0.74 (s, 6 H, 7-H).

^{13}C{^{1}H} NMR (101 MHz, DMSO-d_6): δ = 187.5 (CO, C-4), 143.4 (C_q, C-8), 138.2 (C_q, C-12), 128.5 (CH, C-13), 128.4 (CH, C-14), 128.1 (CH, C-9), 127.3 (CH, C-10), 125.8 (CH, C-11), 124.7 (CH, C-15), 104.7 (C^-, C-3), 50.8 (CH_2, C-5), 49.7 (CH, C-1), 31.0 (C_q, C-6), 29.8 (CH_2, C-2), 29.0 (CH_3, C-7).

HRMS (ESI positive): 353.1572 found for $C_{22}H_{25}O_2S^+$ (calculated: 353.1570).

HRMS (ESI negative): 351.1426 found for $C_{22}H_{23}O_2S^-$ (calculated: 351.1424).

Sodium 2-(2-((4-bromophenyl)thio)-2-phenylethyl)-1-oxo-1*H*-inden-3-olate (7f)

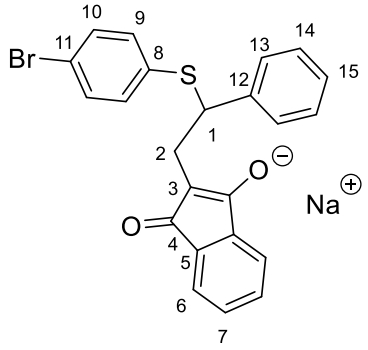

7f

4-Bromothiophenol (98.5 mg, 0.52 mmol, 1.0 equiv.) and NaH (12.5 mg, 0.52 mmol, 1.0 equiv.) were dissolved in dry DMSO-d_6 (5 mL) to generate the nucleophile stock solution (0.104 M). 0.35 mL of this solution were added to 0.35 mL of a solution of **1g** (0.104 M, 1.0 equiv.) in dry DMSO-d_6 in an NMR-tube and mixed well. The solution turned dark brown instantaneously.

^{1}H NMR (400 MHz, DMSO-d_6): δ = 7.41 – 7.38 (m, 2 H, 10-H), 7.30 (d, *J* = 7.3 Hz, 2 H, 13-H), 7.28 (d, *J* = 8.6 Hz, 2 H, 9-H), 7.18 (t, *J* = 7.4 Hz, 2 H, 14-H), 7.12 – 7.09 (m, 1 H, 15-H), 7.08 (dd, *J* = 5.0, 3.0 Hz, 2 H, 7-H), 6.91 – 6.87 (m, 2 H, 6-H), 4.98 (dd, *J* = 8.6, 6.8 Hz, 1 H, 1-H), 2.71 (dd, *J* = 13.9, 8.8 Hz, 1 H, 2-Ha), 2.64 (dd, *J* = 14.0, 6.6 Hz, 1 H, 2-Hb).

^{13}C{^{1}H} NMR (101 MHz, DMSO-d_6): δ = 188.7 (CO, C-4), 142.1 (C_q, C-3), 141.1 (C_q, C-5), 136.4 (C_q, C-8), 131.40 (CH, C-10), 131.36 (CH, C-9), 128.3 (CH, C-7), 127.9 (CH, C-13), 127.8 (CH, C-14), 126.5 (CH, C-15), 118.5 (C-Br, C-11), 115.9 (CH, C-6), 101.3 (C_q, C-12), 49.7 (CH, C-1), 28.8 (CH_2, C-2).

HRMS (ESI): 435.0060 found for $C_{23}H_{16}O_2{}^{79}BrS^-$ (calculated: 435.0060).
437.0040 found for $C_{23}H_{16}O_2{}^{81}BrS^-$ (calculated: 437.0039).

2-(2-((4-bromophenyl)thio)-2-phenylethyl)-1*H*-indene-1,3(2*H*)-dione (8a)

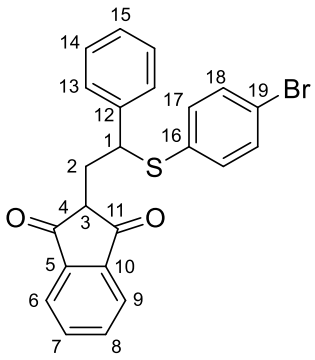

8a

To 25.3 mg (0.13 mmol, 1.0 equiv.) 4-bromothiophenol 0.5 mL KO*t*Bu stock solution in dry DMSO (0.27 M, 15.0 mg, 0.13 mmol, 1.0 equiv.) were added. 0.5 mL **1g** stock solution in dry DMSO (0.27 M, 33.2 mg, 0.13 mmol, 1.0 equiv.) were then added. The reaction mixture was mixed well and the work-up was done according to the procedure above.

8a (57.1 mg, 0.13 mmol, 97%) was obtained as a yellow oil.

^{1}H NMR (400 MHz, $CDCl_3$): δ = 7.95 – 7.89 (m, 2 H, 6-H and 9-H), 7.82 – 7.80 (m, 2 H, 7-H and 8-H), 7.33 – 7.28 (m, 4 H, 14-H, 17-H), 7.29 – 7.17 (m, 3 H, 13-H, 15-H), 7.13 – 7.09 (m, 2 H, 18-H), 4.82 (dd, J = 9.1, 7.2 Hz, 1 H, 1-H), 3.11 (dd, J = 8.0, 5.7 Hz, 1 H, 3-H), 2.54-2.38 (m, 2 H, 2-H).

^{13}C{^{1}H} NMR (101 MHz, $CDCl_3$): δ = 200.2 (CO, C-4), 200.0 (CO, C-11), 142.2 (C_q, C-5), 142.1 (C_q, C-10), 140.3 (C_q, C-12), 135.82 (CH, C-7), 135.78 (CH, C-8), 134.2 (CH, C-18), 133.4 (C_q, C-16), 132.0 (CH, C-17), 128.8 (CH, C-14), 128.3 (CH, C-13), 127.9 (CH, C-15), 123.31 (CH, C-6), 123.29 (CH, C-9), 121.7 (C_q, C-19), 51.3 (CH, C-3), 50.4 (CH, C-1), 33.1 (CH_2, C-2).

HRMS (EI): 436.0126 found for $C_{23}H_{17}BrO_2{}^{32}S^{\bullet+}$ (calculated: 436.0127).

IR (film): 3060, 3028, 2922, 2854, 1742, 1704, 1599, 1492, 1472, 1453, 1385, 1345, 1266, 1244, 1224, 1158, 1090, 1067, 1009, 922, 812, 767, 749, 719, 699 cm^{-1}.

2-(2-phenyl-2-(phenylthio)ethyl)-1*H*-indene-1,3(2*H*)-dione (8b)

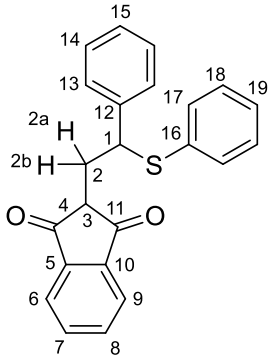

8b

9.80 mg (0.089 mmol, 1.0 equiv.) thiophenol was mixed with 1 mL DMSO and added to 10.0 mg (0.089 mmol, 1.0 equiv.) KO*t*Bu. The mixture was transferred to a vial containing 22.1 mg (0.089 mmol, 1.0 equiv.) **1g** and mixed well. The work-up was done according to the procedure above.

8b (14.4 mg, 0.04 mmol, 45%) was obtained as a yellow oil.

^{1}H NMR (400 MHz, $CDCl_3$): δ = 7.94 – 7.92 (m, 1 H, 6-H), 7.90 – 7.88 (m, 1 H, 9-H), 7.81 – 7.79 (m, 2 H, 7-H and 8-H), 7.33 – 7.17 (m, 10 H, 13-H, 14-H, 15-H, 17-H, 18-H, 19-H), 4.84 (dd, *J* = 9.2, 7.1 Hz, 1 H, 1-H), 3.13 (dd, *J* = 8.0, 5.7 Hz, 1 H, 3-H), 2.55 – 2.50 (m, 1 H, 2-Ha), 2.47 – 2.43 (m, 1 H, 2-Hb).

^{13}C{^{1}H} NMR (101 MHz, $CDCl_3$): δ = 200.3 (CO, C-4), 200.1 (CO, C-11), 142.2 (C_q, C-5), 142.1 (C_q, C-10), 140.7 (C_q, C-12), 135.74 (CH, C-7), 135.70 (CH, C-8), 134.3 (C_q, C-16), 132.6 (CH, C-18), 128.9 (CH, C-17), 128.7 (CH, C-14), 128.4 (CH, C-13), 127.7 (CH, C-15), 127.4 (CH, C-19), 123.28 (CH, C-6), 123.25 (CH, C-9), 51.4 (CH, C-3), 50.2 (CH, C-1), 33.3 (CH_2, C-2).

HRMS (EI): 358.1024 found for $C_{23}H_{18}O_2{}^{32}S^{\bullet+}$ (calculated: 358.1022).

IR (film): 2923, 2167, 2161, 2122, 2008, 1917, 1742, 1707, 1600, 2438, 1346, 1246, 750, 695 cm^{-1}.

2-(2-phenyl-2-(*p*-tolylthio)ethyl)-1*H*-indene-1,3(2*H*)-dione (8c)

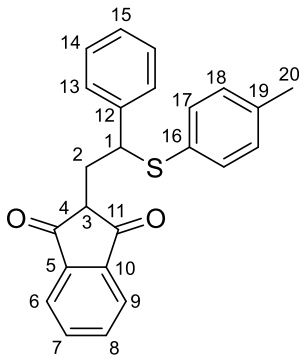

8c

To 16.6 mg (0.13 mmol, 1.0 equiv.) 4-methylthiophenol 0.5 mL KO*t*Bu stock solution in dry DMSO (0.27 M, 15.0 mg, 0.13 mmol, 1.0 equiv.) were added. 0.5 mL **1g** stock solution in dry DMSO (0.27 M, 33.2 mg, 0.13 mmol, 1.0 equiv.) were then added and the reaction mixture was mixed well. The work-up was done according to the procedure above.

8c (47.7 mg, 0.13 mmol, 96%) was obtained as a yellow oil.

^{1}H NMR (400 MHz, $CDCl_3$): δ = 7.93 – 7.88 (m, 2 H, 6-H and 9-H), 7.81 – 7.78 (m, 2 H, 7-H and 8-H), 7.30 – 7.17 (m, 5 H, 13-H, 14-H, 15-H), 7.17 – 7.14 (m, 2 H, 17-H), 7.02 – 7.00 (m, 2 H, 18-H), 4.76 (dd, *J* = 9.1, 7.2 Hz, 1 H, 1-H), 3.13 (dd, *J* = 7.9, 5.7 Hz, 1 H, 3-H), 2.54 – 2.39 (m, 2 H, 2-H), 2.27 (s, 3 H, 20-H).

^{13}C{^{1}H} NMR (101 MHz, $CDCl_3$): δ = 200.3 (CO, C-4), 200.1 (CO, C-11), 142.2 (C_q, C-5), 142.1 (C_q, C-10), 140.8 (C_q, C-12), 137.7 (C_q, C-19), 135.71 (CH, C-7), 135.67 (CH, C-8), 133.3 (CH, C-17), 130.4 (C_q, C-16), 129.7 (CH, C-18), 128.6 (CH, C-14), 128.4 (CH, C-13), 127.6 (CH, C-15), 123.3 (CH, C-6), 123.2 (CH, C-9), 51.4 (CH, C-3), 50.6 (CH, C-1), 33.1 (CH_2, C-2), 21.3 (CH_3, C-20).

HRMS (EI): 372.1174 found for $C_{24}H_{20}O_2{}^{32}S^{\bullet+}$(calculated: 372.1179).

IR (film): 3027, 2120, 2861, 1742, 1705, 1599, 1491, 1453, 1345, 1323, 1301, 1265, 1244, 1179, 1159, 1089, 1077, 1017, 1001, 921, 808, 767, 749, 719, 699 cm^{-1}.

2-(2-((4-methoxyphenyl)thio)-2-phenylethyl)-1*H*-indene-1,3(2*H*)-dione (8d)

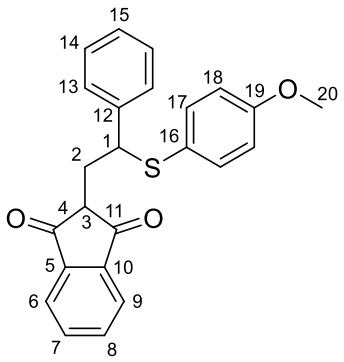

8d

To 18.7 mg (0.13 mmol, 1.0 equiv.) 4-methoxythiophenol 0.5 mL KO*t*Bu stock solution in dry DMSO (0.27 M, 15.0 mg, 0.13 mmol, 1.0 equiv.) were added. 0.5 mL **1g** stock solution in dry DMSO (0.27 M, 33.2 mg, 0.13 mmol, 1.0 equiv.) were then added. The reaction mixture was mixed well and the work-up was done according to the procedure above.

8d (51.4 mg, 0.13 mmol, 99%) was obtained as a yellow oil.

^{1}H NMR (400 MHz, $CDCl_3$): δ = 7.94 – 7.88 (m, 2 H, 6-H and 9-H), 7.81 – 7.79 (m, 2 H, 7-H and 8-H), 7.23 – 7.18 (m, 5 H, 13-H, 14-H, 15-H), 7.16 (d, *J* = 7.9 Hz, 2 H, 17-H), 6.74 (d, *J* = 7.9 Hz, 2 H, 18-H), 4.66 (dd, *J* = 8.8, 7.5 Hz, 1 H, 1-H), 3.76 (s, 3 H, 20-H), 3.17 (dd, *J* = 7.7, 6.0 Hz, 1 H, 3-H), 2.52 – 2.38 (m, 2 H, 2-H).

^{13}C{^{1}H} NMR (101 MHz, $CDCl_3$): δ = 200.4 (CO, C-4), 200.2 (CO, C-11), 159.8 (C_q, C-19), 142.21 (C_q, C-5), 142.15 (C_q, C-10), 140.9 (C_q, C-12), 136.2 (CH, C-17), 135.72 (CH, C-7), 135.68 (CH, C-8), 128.5 (CH, C-14), 128.4 (CH, C-13), 127.5 (CH, C-15), 124.1 (C_q, C-16), 123.3 (CH, C-6), 123.2 (CH, C-9), 114.4 (CH, C-18), 55.4 (CH_3, C-20), 51.4 (CH, C-3), 51.4 (CH, C-1), 32.8 (CH_2, C-2).

HRMS (EI): 388.1128 found for $C_{24}H_{20}O_3{}^{32}S^{\bullet+}$ (calculated: 388.1128).

IR (film): 3027, 2938, 2835, 1742, 1705, 1590, 1569, 1492, 1463, 1453, 1440, 1345, 1323, 1298, 1285, 1265, 1244, 1172, 1104, 1029, 1003, 921, 829, 798, 767, 749, 720, 699 cm^{-1}.

2-(2-(3-chlorophenyl)-2-(phenylthio)ethyl)-1*H*-indene-1,3(2*H*)-dione (8e)

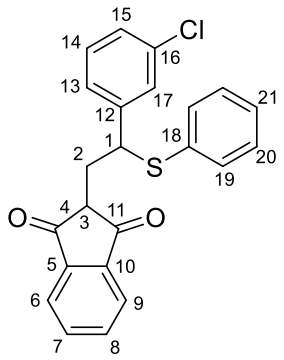

8e

0.5 mL thiophenol stock solution in dry DMSO (0.27 M, 14.7 mg, 0.13 mmol, 1.0 equiv.) and 0.5 mL KO*t*Bu stock solution in dry DMSO (0.27 M, 15.0 mg, 1.0 equiv.) were mixed to generate the nucleophile. To the resulting mixture 37.8 mg (0.13 mmol, 1.0 equiv.) **1f** were added and mixed well. The work-up was done according to the procedure above.

8e (47.3 mg, 0.12 mmol, 90%) was obtained as a yellow oil.

^{1}H NMR (400 MHz, $CDCl_3$): δ = 7.95 – 7.90 (m, 2 H, 6-H and 9-H), 7.83 – 7.81 (m, 2 H, 7-H and 8-H), 7.26 – 7.15 (m, 9 H, 13-H, 14-H, 15-H, 17-H, 19-H, 20-H, 21-H), 4.78 (t, *J* = 8.1 Hz, 1 H, 1-H), 3.16 (t, *J* = 6.9 Hz, 1 H, 3-H), 2.45 (dd, *J* = 8.2, 6.8 Hz, 2 H, 2-H).

^{13}C{^{1}H} NMR (101 MHz, $CDCl_3$): δ = 200.1 (CO, C-4), 199.9 (CO, C-11), 143.1 (C_q, C-12), 142.2 (C_q, C-5), 142.08 (C_q, C-10), 135.9 (CH, C-7), 135.8 (CH, C-8), 134.4 (C_q, C-16), 133.6 (C_q, C-18), 132.9 (CH, C_{ar}), 129.9 (CH, C_{ar}), 129.0 (CH, C_{ar}), 128.5 (CH, C_{ar}), 127.9 (CH, C_{ar}), 127.8 (CH, C_{ar}), 126.4 (CH, C_{ar}), 123.4 (CH, C-6), 123.3 (CH, C-9), 51.2 (CH, C-3), 50.0 (CH, C-1), 33.1 (CH_2, C-2).

HRMS (EI): 392.0628 found for $C_{23}H_{17}ClO_2{}^{32}S^{\bullet+}$ (calculated: 392.0632).

IR (film): 3057, 2920, 1743, 1730, 1706, 1595, 1573, 1475, 1437, 1345, 1319, 1265, 1243, 1160, 1080, 1025, 998, 924, 884, 787, 747, 715, 692 cm^{-1}.

2-(2-(phenylthio)-2-(*p*-tolyl)ethyl)-1*H*-indene-1,3(2*H*)-dione (8f)

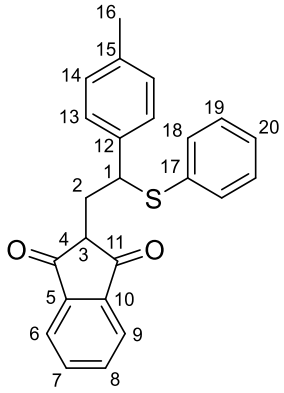

8f

0.5 mL thiophenol stock solution in dry DMSO (0.27 M, 14.7 mg, 0.13 mmol, 1.0 equiv.) and 0.5 mL KO*t*Bu stock solution in dry DMSO (0.27 M, 15.0 mg, 1.0 equiv.) were mixed to generate the nucleophile. To the resulting mixture 35.1 mg (0.13 mmol, 1.0 equiv.) **1h** were added and mixed well. The work-up was done according to the procedure above.

8f (33.4 mg, 0.09 mmol, 67%) was obtained as a yellow oil.

^{1}H NMR (400 MHz, $CDCl_3$): δ = 7.93 – 7.88 (m, 2 H, 6-H and 9-H), 7.80 – 7.78 (m, 2 H, 7-H and 8-H), 7.29 – 7.27 (m, 2 H, 13-H), 7.23 – 7.16 (m, 5 H, 18-H, 19-H, 20-H), 7.04 (d, *J* = 7.7 Hz, 2 H, 14-H), 4.82 (dd, *J* = 9.4, 7.0 Hz, 1 H, 1-H), 3.10 (dd, *J* = 8.2, 5.4 Hz, 1 H, 3-H), 2.55 – 2.38 (m, 2 H, 2-H), 2.27 (s, 3 H, 16-H).

^{13}C{^{1}H} NMR (101 MHz, $CDCl_3$): δ = 200.4 (CO, C-4), 200.1 (CO, C-11), 142.2 (C_q, C-5), 142.1 (C_q, C-10), 137.44 (C_q, C-12), 137.41 (C_q, C-15), 135.7 (CH, C-7), 135.6 (CH, C-8), 134.6 (C_q, C-17), 132.3 (CH, C-14), 129.4 (CH, C-13), 128.9 (CH, C-19), 128.3 (CH, C-18), 127.2 (CH, C-20), 123.24 (CH, C-6), 123.22 (CH, C-9), 51.4 (CH, C-3), 49.8 (CH, C-1), 33.4 (CH_2, C-2), 21.2 (CH_3, C-16).

HRMS (EI): 372.1178 found for $C_{24}H_{20}O_2{}^{32}S^{\bullet+}$ (calculated: 372.1179).

IR (film): 3054, 3020, 2919, 2858, 1742, 1705, 1599, 1583, 1512, 1480, 1438, 1345, 1321, 1296, 1266, 1243, 1183, 1159, 1112, 1088, 1067, 1024, 999, 920, 818, 793, 747, 721, 691 cm^{-1}.

2-(2-(4-methoxyphenyl)-2-(phenylthio)ethyl)-1*H*-indene-1,3(2*H*)-dione (8g)

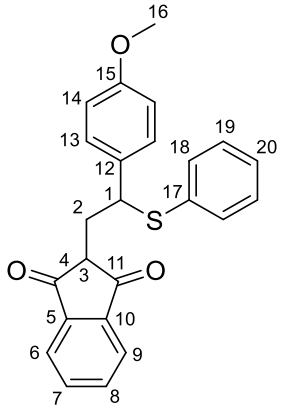

8g

0.5 mL thiophenol stock solution in dry DMSO (0.27 M, 14.7 mg, 0.13 mmol, 1.0 equiv.) and 0.5 mL KO*t*Bu stock solution in dry DMSO (0.27 M, 15.0 mg, 1.0 equiv.) were mixed to generate the nucleophile. To the resulting mixture 37.2 mg (0.13 mmol, 1.0 equiv.) **1i** were added and mixed well. The work-up was done according to the procedure above. The crude reaction mixture was subsequently purified with preparative TLC (60% Et_2O in pentane, R_f=0.75).

8g (39.0 mg, 0.10 mmol, 75%) was obtained as a colorless oil.

^{1}H NMR (600 MHz, $CDCl_3$): δ = 7.92 (dd, *J* = 5.6, 2.9 Hz, 1 H, 9-H), 7.88 (dd, *J* = 5.1, 3.0 Hz, 1 H, 6-H), 7.81 – 7.77 (m, 2 H, 7-H and 8-H), 7.28 (d, *J* = 6.9 Hz, 2 H, 13-H), 7.23 – 7.15 (m, 5 H, 18-H, 19-H, 20-H), 6.76 (d, *J* = 8.7 Hz, 2 H, 14-H), 4.81 (dd, *J* = 9.5, 6.8 Hz, 1 H, 1-H), 3.75 (s, 3 H, 16-H), 3.09 (dd, *J* = 8.3, 5.2 Hz, 1 H, 3-H), 2.53 – 2.40 (m, 2 H, 2-H).

^{13}C{^{1}H} NMR (151 MHz, $CDCl_3$): δ = 200.3 (CO, C-4), 200.1 (CO, C-11), 159.1 (C_q, C-15), 142.2 (C_q, C-5), 142.1 (C_q, C-10), 135.7 (CH, C-7), 135.6 (CH, C-8), 134.5 (C_q, C-12), 132.5 (CH, C-13), 132.4 (C_q, C-17), 129.5 (CH, C-19), 128.9 (CH, C-18), 127.3 (CH, C-20), 123.22 (CH, C-6), 123.20 (CH, C-9), 114.0 (CH, C-14), 55.4 (CH_3, C-16), 51.4 (CH, C-3), 49.5 (CH, C-1), 33.4 (CH_2, C-2).

HRMS (EI): 388.1127 found for $C_{24}H_{20}O_3{}^{32}S^{\bullet+}$ (calculated: 388.1128).

IR (film): 3058, 2933, 2835, 1742, 1705, 1609, 1583, 1511, 1480, 1438, 1345, 1322, 1303, 1249, 1176, 1109, 1089, 1032, 1000, 920, 832, 794, 747, 691 cm^{-1}.

Sodium 1,1-dicyano-3-phenyl-3-(phenylthio)propan-1-ide (7g) + 2-(2-phenyl-2-(phenylthio)ethyl)malononitrile (8h)

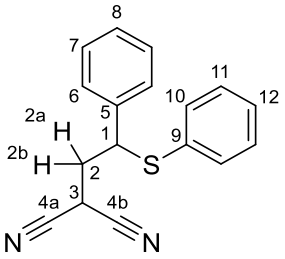

8h

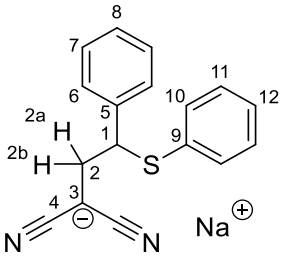

7g

6.2 mg (0.056 mmol, 1.0 equiv.) thiophenol was mixed with 1 mL dry DMSO-d_6 and added to 1.4 mg (0.058 mmol, 1.0 equiv.) sodium hydride. After gas development ceased, the nucleophile was transferred to a vial containing 9.7 mg (0.058 mmol, 1.0 equiv.) **1j** and mixed vigorously. NMR and mass spectra of **7g** were acquired. The work-up was done according to the procedure above. The crude reaction mixture was subsequently purified with preparative TLC (R_f=0.6 in 30% Et_2O in pentane).
8h (6.5 mg, 0.0234 mmol, 42%) was obtained as a colorless oil.

Sodium 1,1-dicyano-3-phenyl-3-(phenylthio)propan-1-ide (7g)

^{1}H NMR (600 MHz, DMSO-d$_6$): δ = 7.27 – 7.20 (m, 8 H, 6-H, 7-H, 10-H, 11-H), 7.17 – 7.12 (m, 2 H, 8-H and 12-H), 4.16 (dd, *J* = 8.8, 6.1 Hz, 1 H, 1-H), 2.35 (dd, *J* = 14.6, 6.1 Hz, 1 H, 2a-H), 2.25 (dd, *J* = 14.6, 8.9 Hz, 1 H, 2b-H).

^{13}C{^{1}H} NMR (151 MHz, DMSO-d$_6$): δ = 141.9 (C_q, C-5), 135.9 (C_q, C-9), 132.0 (CN, C-4), 130.2 (CH, C-7), 128.8 (CH, C-6), 128.04 (CH, C-11), 127.97 (CH, C-10), 126.7 (CH, C-12), 126.1 (CH, C-8), 53.7 (CH, C-1), 35.9 (CH_2, C-2), 9.6 (C^-, C-3).

HRMS (ESI negative): 277.0805 found for $C_{17}H_{13}N_2{}^{32}S^-$ (calculated: 277.0805).

2-(2-phenyl-2-(phenylthio)ethyl)malononitrile (8h)

^{1}H NMR (400 MHz, CDCl$_3$): δ = 7.38 – 7.23 (m, 10 H, Ar-H), 4.29 (dd, *J* = 8.7, 7.2 Hz, 1 H, 1-H), 3.77 (dd, *J* = 8.6, 7.1 Hz, 1 H, 3-H), 2.66 – 2.52 (m, 2 H, 2-Ha, 2-Ha).

^{13}C{^{1}H} NMR (101 MHz, CDCl$_3$): δ = 138.1 (C_q, C-5), 133.7 (CH, C-Ar), 132.2 (C_q, C-9), 129.44 (CH, C-Ar), 129.43 (CH, C-Ar), 128.9 (CH, C-Ar), 128.8 (CH, C-Ar), 127.8 (CH, C-Ar), 112.2 (CN, C-4a), 112.0 (CN, C-4b), 50.5 (CH, C-1), 36.9 (CH_2, C-2), 21.2 (CH, C-3).

HRMS (EI): 278.0875 found for $C_{17}H_{14}N_2{}^{32}S^{\bullet+}$ (calculated: 278.0872).

4-(1-cyano-3-(1,3-dioxo-2,3-dihydro-1*H*-inden-2-yl)-2-phenylpropyl)benzonitrile (10a)

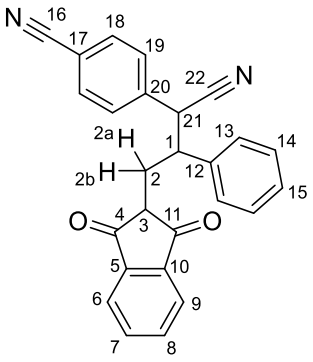

10a

To 19.0 mg (0.13 mmol, 1.0 equiv.) 4-(cyanomethyl)benzonitrile 0.5 mL KO*t*Bu stock solution in dry DMSO (0.27 M, 15.0 mg, 0.13 mmol, 1.0 equiv.) were added. 0.5 mL **1g** stock solution in dry DMSO (0.27 M, 33.2 mg, 0.13 mmol, 1.0 equiv.) were then added. The reaction mixture was mixed well and the work-up was done according to the procedure above.

10a (51.7 mg, 0.13 mmol, 99%) was obtained as a yellow solid. NMR analysis showed the presence of two diastereomers (1st diastereomer:2nd diastereomer = 1:1.4).

1st diastereomer

^{1}H NMR (400 MHz, $CDCl_3$): δ = 7.92 – 7.78 (m, 4 H, 6-H, 7-H, 8-H, 9-H), 7.60 – 7.13 (m, 9 H, 13-H to 19-H), 4.04 (d, *J* = 8.4 Hz, 1 H, 21-H), 3.91 – 3.81 (m, 1 H, 1-H), 2.74 (dd, *J* = 11.2, 3.1 Hz, 1 H, 3-H), 2.67 – 2.63 (m, 1 H, 2a-H), 2.33 (ddd, *J* = 13.8, 11.2, 3.8 Hz, 1 H, 2b-H).

^{13}C{^{1}H} NMR (101 MHz, $CDCl_3$): δ = 200.2 (CO, C-4), 200.1 (CO, C-11), 141.94 (C_q, C-5), 141.93 (C_q, C-10), 139.5 (C_q, C-20), 137.1 (C_q, C-12), 135.91 (CH, C-7), 135.89 (CH, C-8), 132.6 (CH, C_{ar}), 129.2 (CH, C_{ar}), 129.0 (CH, C_{ar}), 128.9 (CH, C_{ar}), 128.5 (CH, C_{ar}), 123.31 (CH, C-6), 123.29 (CH, C-9), 118.8 (CN, C-22), 118.2 (CN, C-16), 112.5 (C_q, C-17), 50.3 (CH, C-3), 47.6 (CH, C-1), 44.8 (CH, C-21), 29.8 (CH_2, C-2).

2nd diastereomer

^{1}H NMR (400 MHz, $CDCl_3$): δ = 7.92 – 7.78 (m, 4 H, 6-H, 7-H, 8-H, 9-H), 7.60 – 7.13 (m, 9 H, 13-H to 19-H), 4.22 (d, *J* = 6.8 Hz, 1 H, 21-H), 3.91 – 3.81 (m, 1 H, 1-H), 2.82 (dd, *J* = 10.5, 3.9 Hz, 1 H, 3-H), 2.67 – 2.63 (m, 1 H, 2a-H), 2.09 (ddd, *J* = 14.0, 10.5, 4.7 Hz, 1 H, 2b-H).

^{13}C{^{1}H} NMR (101 MHz, $CDCl_3$): δ = 199.5 (CO, C-4 and C-11), 141.9 (C_q, C-5), 141.9 (C_q, C-10), 139.4 (C_q, C-20), 136.5 (C_q, C-12), 136.0 (CH, C-7), 135.9 (CH, C-8), 132.7 (CH, C_{ar}), 129.1 (CH, C_{ar}), 129.0 (CH, C_{ar}), 128.7 (CH, C_{ar}), 128.6 (CH, C_{ar}), 123.3 (CH, C-6), 123.3 (CH, C-9), 118.4 (CN; C-22), 118.2 (CN, C-16), 112.6 (C_q, C-17), 50.5 (CH, C-3), 47.3 (CH, C-1), 44.4 (CH, C-21), 30.5 (CH_2, C-2).

HRMS (EI): 390.1359 found for $C_{26}H_{18}N_2O_2^{\bullet+}$ (calculated: 390.1363).

IR (neat): 3064, 2925, 2229, 1743, 1705, 1600, 1506, 1455, 1417, 1346, 1279, 1248, 1223, 1021, 925, 840, 760, 704 cm^{-1}.

Melting point: 84.0 °C.

Ethyl 4-(1,3-dioxo-2,3-dihydro-1*H*-inden-2-yl)-2,3-diphenylbutanoate (10b)

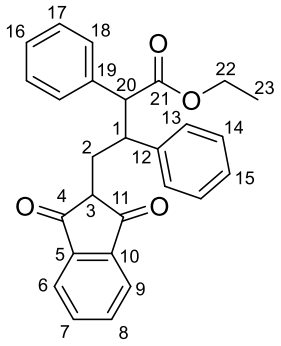

10b

To 21.9 mg (0.13 mmol, 1.0 equiv.) ethyl 2-phenylacetate 0.5 mL KO*t*Bu stock solution in dry DMSO (0.27 M, 15.0 mg, 0.13 mmol, 1.0 equiv.) were added. 0.5 mL **1g** stock solution in dry DMSO (0.27 M, 33.2 mg, 0.13 mmol, 1.0 equiv.) were then added and the reaction mixture was mixed well. The work-up was done according to the procedure above.

10b (50.9 mg, 0.12 mmol, 95%) was obtained as a yellow oil. NMR analysis showed the presence of two diastereomers (1st diastereomer:2nd diastereomer = 1:1.6).

1st diastereomer

^{1}H NMR (400 MHz, $CDCl_3$): δ = 7.89 – 7.71 (m, 4 H, 6-H, 7-H, 8-H, 9-H), 7.53 – 6.96 (m, 10 H, 13-H to 18-H), 4.17 – 4.02 (m, 1 H, 1-H), 3.87 – 3.70 (m, 3 H, 3-H and 22-H), 2.62 (d, *J* = 3.0 Hz, 1 H, 20-H), 2.22 – 2.09 (m, 1 H, 2a-H), 1.71 (ddd, *J* = 13.9, 11.1, 3.8 Hz, 1 H, 2b-H), 0.86 (t, *J* = 7.1 Hz, 3 H, 23-H).

^{13}C{^{1}H} NMR (101 MHz, $CDCl_3$): δ = 200.5 (CO, C-4), 200.2 (CO, C-11), 172.4 (CO; C-21), 142.1 (C_q, C-5), 142.0 (C_q, C-10), 139.7 (C_{ar}), 137.2 (C_{ar}), 135.5 (CH, C-7), 135.4 (CH, C-8), 129.1 (C_{ar}), 128.8 (C_{ar}), 128.6 (C_{ar}), 128.2 (C_{ar}), 127.4 (C_{ar}), 126.9 (C_{ar}), 123.1 (CH, C-6), 123.0 (CH, C-9), 59.4 (CH_2, C-22), 58.8 (CH, C-3), 50.7 (CH, C-20), 45.6 (CH, C-1), 31.0 (CH_2, C-2), 13.9 (CH_3, C-23).

2nd diastereomer

^{1}H NMR (400 MHz, $CDCl_3$): δ = 7.89 – 7.71 (m, 4 H, 6-H, 7-H, 8-H, 9-H), 7.53 – 6.96 (m, 10 H, 13-H to 18-H), 4.17 – 4.02 (m, 3 H, 1-H and 22-H), 3.87 – 3.70 (m, 1 H, 3-H), 2.72 (dd, *J* = 11.0, 3.2 Hz, 1 H, 20-H), 2.51 – 2.44 (m, 1 H, 2a-H), 2.22 – 2.09 (m, 1 H, 2b-H), 1.20 (t, *J* = 7.1 Hz, 3 H, 23-H).

$^{13}C\{^{1}H\}$ NMR (101 MHz, $CDCl_3$): δ = 200.6 (CO, C-4), 200.5 (CO, C-11), 173.2 (CO, C-21), 142.2 (C_q, C-5), 142.0 (C_q, C-10), 140.6 (C_{ar}), 137.3 (C_{ar}), 135.6 (CH, C-7), 135.4 (CH, C-8), 129.1 (C_{ar}), 128.9 (C_{ar}), 128.7 (C_{ar}), 128.3 (C_{ar}), 127.8 (C_{ar}), 127.1 (C_{ar}), 123.2 (CH, C-6), 123.1 (CH, C-9), 61.0 (CH, C-3), 60.6 (CH_2, C-22), 51.0 (CH, C-20), 46.3 (CH, C-1), 32.0 (CH_2, C-2), 14.2 (CH_3, C-23).

HRMS (EI): 412.1677 found for $C_{27}H_{24}O_4^{\bullet+}$ (calculated: 412.1669).

IR (film): 3061, 3029, 2981, 1727, 1707, 1600, 1495, 1454, 1369, 1343, 1326, 1270, 1246, 1154, 1024, 952, 925, 762, 743, 699 cm^{-1}.

2-(4-oxo-2,3,4-triphenylbutyl)-1*H*-indene-1,3(2*H*)-dione (10c)

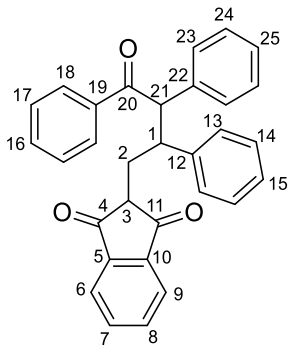

10c

To 26.2 mg (0.13 mmol, 1.0 equiv.) 1,2-diphenylethan-1-one 0.5 mL KO*t*Bu stock solution in dry DMSO (0.27 M, 15.0 mg, 1.0 equiv.) were added. 0.5 mL **1g** stock solution in dry DMSO (0.27 M, 33.2 mg, 0.13 mmol, 1.0 equiv.) were then added and the reaction mixture was mixed well. The work-up was done according to the procedure above.

10c (58.9 mg, 0.13 mmol, 99%) was obtained as a colorless solid. NMR analysis showed the presence of two diastereomers (1st diastereomer:2nd diastereomer = 1:1.5).

1st diastereomer

^{1}H NMR (400 MHz, $CDCl_3$): δ = 8.02 – 6.87 (m, 13 H, H_{ar}), 4.81 (d, *J* = 10.8 Hz, 1 H, 21-H), 4.37 – 4.25 (m, 1 H, 1-H), 2.75 – 2.66 (m, 1 H, 3-H), 2.40 (td, *J* = 12.7, 11.6, 5.4 Hz, 1 H, 2a-H), 2.28 – 2.17 (m, 1 H, 2b-H).

$^{13}C\{^{1}H\}$ NMR (101 MHz, $CDCl_3$): δ = 200.8 (CO, C-4), 200.7 (CO, C-11), 199.3 (CO, C-20), 142.3 (C_{ar}), 142.2 (C_{ar}), 142.03 (C_{ar}), 141.96 (C_{ar}), 141.6 (C_{ar}), 140.3 (C_{ar}), 137.4 (C_{ar}), 137.34 (C_{ar}), 137.30 (C_{ar}), 137.2 (C_{ar}), 135.5 (C_{ar}), 135.3 (C_{ar}), 133.2 (C_{ar}), 132.7 (C_{ar}), 129.3 (C_{ar}), 129.23 (C_{ar}), 129.20 (C_{ar}), 129.15 (C_{ar}), 129.0 (C_{ar}), 128.74 (C_{ar}), 128.71 (C_{ar}), 128.6 (C_{ar}), 128.5 (C_{ar}), 128.4 (C_{ar}), 128.3 (C_{ar}), 128.0 (C_{ar}), 127.8 (C_{ar}), 127.6 (C_{ar}), 127.0 (C_{ar}), 126.7 (C_{ar}), 123.3 (C_{ar}), 123.2 (C_{ar}), 123.1 (C_{ar}), 123.0 (C_{ar}), 122.9 (C_{ar}), 122.8 (C_{ar}), 60.3 (CH, C-21), 51.1 (CH, C-3), 46.5 (CH, C-1), 32.1 (CH_2, C-2).

2nd diastereomer

^{1}H NMR (400 MHz, $CDCl_3$): δ = 8.02 – 6.87 (m, 13 H, H_{ar}), 4.95 (d, *J* = 10.9 Hz, 1H), 4.37 – 4.25 (m, 1 H, 1-H), 2.75 – 2.66 (m, 1 H, 3-H), 2.28 – 2.17 (m, 1 H, 2a-H), 1.75 (ddd, *J* = 14.3, 10.8, 3.9 Hz, 1 H, 2b-H).

^{13}C{^{1}H3 NMR (101 MHz, $CDCl_3$): δ = 200.4 (CO, C-4), 200.2 (CO, C-11), 198.8 (CO, C-20), 142.3 (C_{ar}), 142.2 (C_{ar}), 142.03 (C_{ar}), 141.96 (C_{ar}), 141.6 (C_{ar}), 140.3 (C_{ar}), 137.4 (C_{ar}), 137.34 (C_{ar}), 137.30 (C_{ar}), 137.2 (C_{ar}), 135.5 (C_{ar}), 135.3 (C_{ar}), 133.2 (C_{ar}), 132.7 (C_{ar}), 129.3 (C_{ar}), 129.23 (C_{ar}), 129.20 (C_{ar}), 129.15 (C_{ar}), 129.0 (C_{ar}), 128.74 (C_{ar}), 128.71 (C_{ar}), 128.6 (C_{ar}), 128.5 (C_{ar}), 128.4 (C_{ar}), 128.3 (C_{ar}), 128.0 (C_{ar}), 127.8 (C_{ar}), 127.6 (C_{ar}), 127.0 (C_{ar}), 126.7 (C_{ar}), 123.3 (C_{ar}), 123.2 (C_{ar}), 123.1 (C_{ar}), 123.0 (C_{ar}), 122.9 (C_{ar}), 122.8 (C_{ar}), 60.3 (CH, C-21), 50.8 (CH, C-3), 45.1 (CH, C-1), 31.2 (CH_2, C-2).

HRMS (EI): 444.1717 found for $C_{31}H_{24}O_3^{\bullet+}$ (calculated: 444.1720).

IR (neat): 3060, 3028, 1742, 1707, 1680, 1597, 1493, 1447, 1343, 1267, 1246, 1221, 1178, 1075, 1031, 1001, 972, 927, 751, 698 cm^{-1}.

Melting point: 213.0 °C.

3.5.3 Kinetics

The reactions in DMSO were followed spectrophotometrically with a stopped-flow spectrophotometer (Applied Photophysics SX20). Slower reactions in acetonitrile were followed with a Hellma 661.502-QX quartz Suprasil immersion probe (light path d = 5 mm). Conventional photometric measurements were obtained on a J&M TIDAS diode array. Spectrophotometer and probe were connected by fiber-optic cables and standard SMA-connectors. The temperature was kept constant at 20 °C (±0.1 °C) with a circulating bath thermostat. Nucleophile concentrations were at least ten times higher than electrophile concentrations to achieve pseudo-first order kinetics. Rate constants were obtained from these kinetics by least squares fitting of the absorbance A with the equation $A_t = A_0\, e^{-kt} + C$. Plots of k_{obs} versus thiophenolate concentration gave k_2 as the slope of the linear correlation.

For stopped-flow kinetics two syringes were prepared for each experiment, one containing the nucleophile in DMSO and the other one the cyclopropane in DMSO. For conventional spectrophotometry the compounds were added as DMSO solutions *via* syringe into the reaction flask. The flask was sealed by a septum and kept under a dry argon atmosphere.

Kinetics of reactions of 6,6-dimethyl-5,7-dioxaspiro[2.5]octane-4,8-dione (1a)

1a + sodium thiophenolate (**2c**) in DMSO (stopped flow, detection at 310 nm)

[**2c**]$_0$ (M)	[**1a**]$_0$ (M)	k_{obs} (s^{-1})
3.21×10^{-4}	3.28×10^{-3}	4.70×10^{-2}
3.21×10^{-4}	4.18×10^{-3}	5.29×10^{-2}
3.21×10^{-4}	5.18×10^{-3}	6.55×10^{-2}
3.21×10^{-4}	6.56×10^{-3}	8.82×10^{-2}
3.21×10^{-4}	9.84×10^{-3}	1.18×10^{-1}

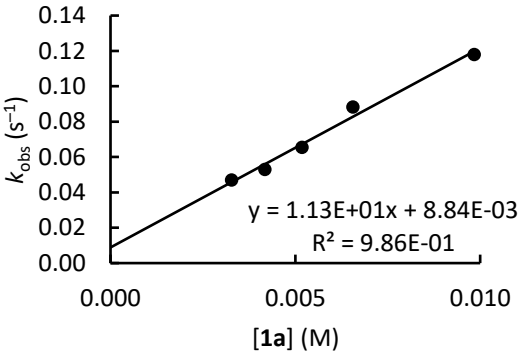

$k_2 = 1.13 \times 10^1\ M^{-1}\ s^{-1}$

1a + sodium 4-methylthiophenolate (**2b**) in DMSO (stopped flow, detection at 306 nm)

$[\mathbf{2b}]_0$ (M)	$[\mathbf{1a}]_0$ (M)	k_{obs} (s^{-1})
3.21×10^{-4}	3.28×10^{-3}	7.64×10^{-2}
3.21×10^{-4}	4.18×10^{-3}	8.67×10^{-2}
3.21×10^{-4}	5.18×10^{-3}	1.07×10^{-1}
3.21×10^{-4}	6.56×10^{-3}	1.45×10^{-1}
3.21×10^{-4}	9.84×10^{-3}	1.90×10^{-1}

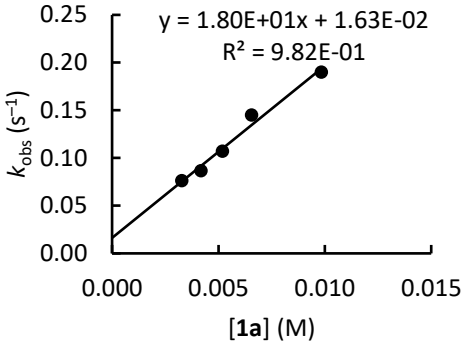

$k_2 = 1.80 \times 10^1$ M^{-1} s^{-1}

1a + sodium 4-methoxythiophenolate (**2a**) in DMSO (stopped flow, detection at 302 nm)

$[\mathbf{2a}]_0$ (M)	$[\mathbf{1a}]_0$ (M)	k_{obs} (s^{-1})
3.21×10^{-4}	3.28×10^{-3}	9.39×10^{-2}
3.21×10^{-4}	4.18×10^{-3}	1.20×10^{-1}
3.21×10^{-4}	5.18×10^{-3}	1.50×10^{-1}
3.21×10^{-4}	6.56×10^{-3}	2.06×10^{-1}
3.21×10^{-4}	9.84×10^{-3}	2.92×10^{-1}

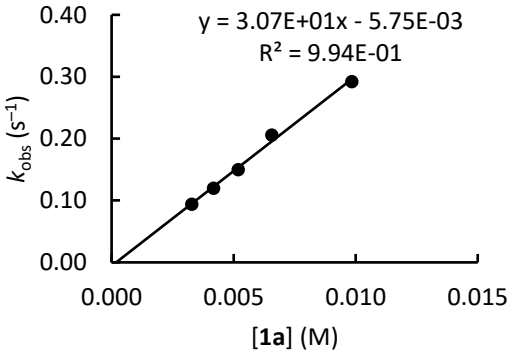

$k_2 = 3.07 \times 10^1$ M^{-1} s^{-1}

Determination of E and s_E parameters for **1a** in DMSO.

Reference Nucleophile	Nucleophilicity N (s_N)	k_2 (M^{-1} s^{-1})	log k_2/s_N
4-H (**2c**)	23.36 (0.74)	1.13×10^1	1.42
4-Me (**2b**)	24.35 (0.69)	1.80×10^1	1.82
4-MeO (**2a**)	24.97 (0.67)	3.07×10^1	2.22

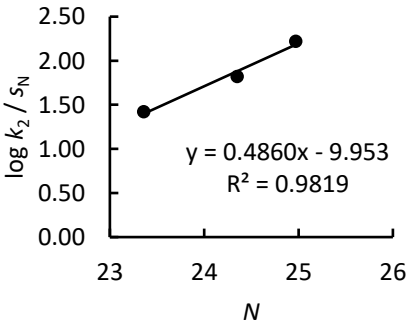

***E* = –20.5**

s_E = 0.49

Kinetics of reactions of 6,6-dimethyl-1-phenyl-5,7-dioxaspiro[2.5]octane-4,8-dione (1b)

1b + sodium thiophenolate (**2c**) in DMSO (stopped flow, detection at 310 nm)

$[\mathbf{2c}]_0$ (M)	$[\mathbf{1b}]_0$ (M)	k_{obs} (s^{-1})
1.29×10^{-4}	1.29×10^{-3}	2.00×10^{-1}
1.29×10^{-4}	2.58×10^{-3}	4.13×10^{-1}
1.29×10^{-4}	3.87×10^{-3}	6.30×10^{-1}
1.29×10^{-4}	5.16×10^{-3}	8.57×10^{-1}

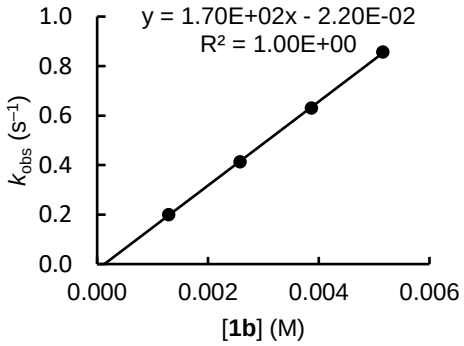

$k_2 = 1.70 \times 10^2$ M^{-1} s^{-1}

1b + sodium 4-methylthiophenolate (**2b**) in DMSO (stopped flow, detection at 306 nm)

$[\mathbf{2b}]_0$ (M)	$[\mathbf{1b}]_0$ (M)	k_{obs} (s^{-1})
1.29×10^{-4}	1.29×10^{-3}	2.95×10^{-1}
1.29×10^{-4}	2.58×10^{-3}	5.88×10^{-1}
1.29×10^{-4}	3.87×10^{-3}	9.05×10^{-1}
1.29×10^{-4}	5.16×10^{-3}	1.23×10^{0}

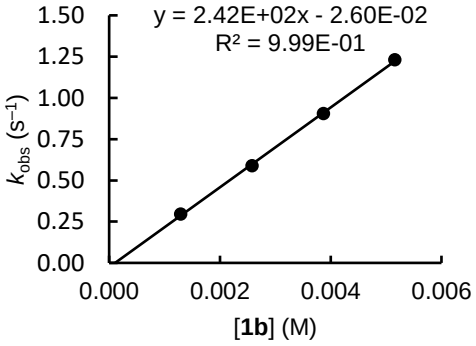

$k_2 = 2.42 \times 10^2$ M^{-1} s^{-1}

1b + sodium 4-methoxythiophenolate (**2a**) in DMSO (stopped flow, detection at 302 nm)

$[\mathbf{2a}]_0$ (M)	$[\mathbf{1b}]_0$ (M)	k_{obs} (s^{-1})
1.29×10^{-4}	1.29×10^{-3}	3.97×10^{-1}
1.29×10^{-4}	2.58×10^{-3}	8.11×10^{-1}
1.29×10^{-4}	3.87×10^{-3}	1.25×10^{0}
1.29×10^{-4}	5.16×10^{-3}	1.68×10^{0}

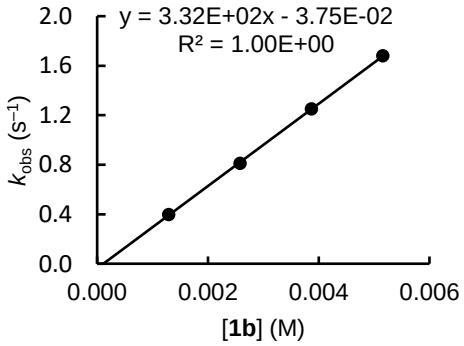

$k_2 = 3.32 \times 10^2$ M^{-1} s^{-1}

Determination of E and s_E parameters for **1b** in DMSO.

Reference Nucleophile	Nucleophilicity N (s_N)	k_2 (M^{-1} s^{-1})	log k_2/s_N
4-H (**2c**)	23.36 (0.74)	5.52×10^0	1.00
4-Me (**2b**)	24.35 (0.69)	8.89×10^0	1.38
4-MeO (**2a**)	24.97 (0.67)	1.12×10^1	1.57

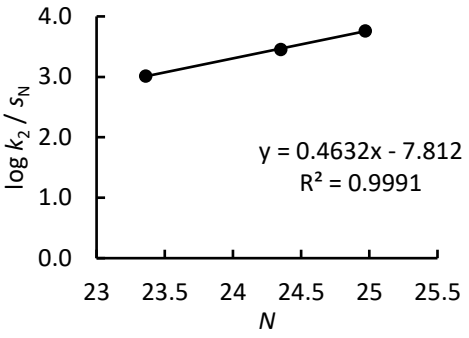

***E* = –16.9**

s_E = 0.46

Kinetics of reactions of 6,6-dimethylspiro[2.5]octane-4,8-dione (1c)

1c + sodium thiophenolate (**2c**) in DMSO (stopped flow, detection at 310 nm)

[2c]$_0$ (M)	**[1c]$_0$** (M)	k_{obs} (s^{-1})
1.61×10^{-4}	1.61×10^{-3}	1.11×10^{-2}
1.61×10^{-4}	3.22×10^{-3}	1.96×10^{-2}
1.61×10^{-4}	4.83×10^{-3}	2.87×10^{-2}
1.61×10^{-4}	6.44×10^{-3}	3.77×10^{-2}

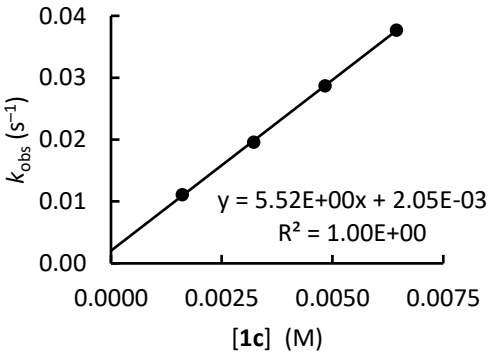

$k_2 = 5.52 \times 10^0$ M^{-1} s^{-1}

1c + sodium 4-methylthiophenolate (**2b**) in DMSO (stopped flow, detection at 306 nm)

[2b]$_0$ (M)	**[1c]$_0$** (M)	k_{obs} (s^{-1})
1.61×10^{-4}	1.61×10^{-3}	1.69×10^{-2}
1.61×10^{-4}	3.22×10^{-3}	3.07×10^{-2}
1.61×10^{-4}	4.83×10^{-3}	4.52×10^{-2}
1.61×10^{-4}	6.44×10^{-3}	5.98×10^{-2}

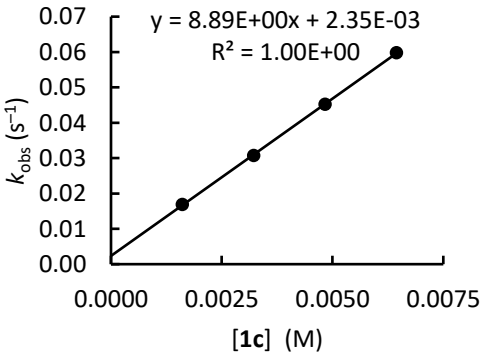

$k_2 = 8.89 \times 10^0$ M^{-1} s^{-1}

1c + sodium 4-methoxythiophenolate (**2a**) in DMSO (stopped flow, detection at 302 nm)

$[\mathbf{2a}]_0$ (M)	$[\mathbf{1c}]_0$ (M)	k_{obs}, s^{-1}
1.61×10^{-4}	1.61×10^{-3}	2.20×10^{-2}
1.61×10^{-4}	3.22×10^{-3}	3.92×10^{-2}
1.61×10^{-4}	4.83×10^{-3}	5.80×10^{-2}
1.61×10^{-4}	6.44×10^{-3}	7.60×10^{-2}

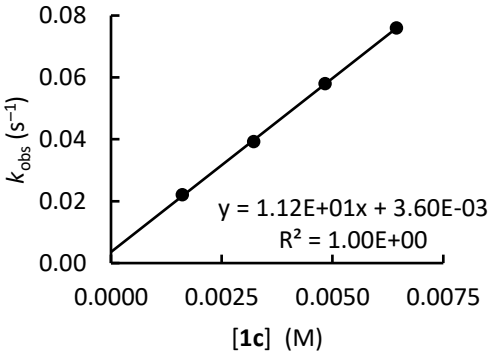

$k_2 = 1.12 \times 10^1\ M^{-1}\ s^{-1}$

Determination of E and s_E parameters for **1c** in DMSO.

Reference Nucleophile	Nucleophilicity N (s_N)	k_2 ($M^{-1}\ s^{-1}$)	log k_2/s_N
4-H (**2c**)	23.36 (0.74)	5.52×10^0	1.00
4-Me (**2b**)	24.35 (0.69)	8.89×10^0	1.38
4-MeO (**2a**)	24.97 (0.67)	1.12×10^1	1.57

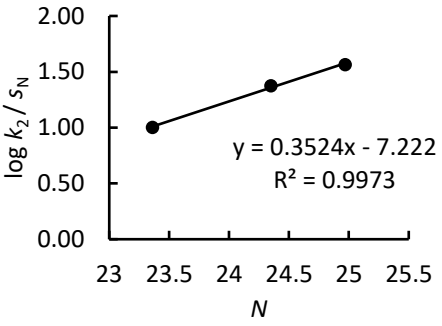

***E* = –20.5**

s_E = 0.35

Kinetics of reactions of 1-(3-chlorophenyl)-6,6-dimethylspiro[2.5]octane-4,8-dione (1d)

1d + potassium 4-bromothiophenolate (**2d**) in DMSO (stopped flow, detection at 310 nm)

$[\mathbf{2d}]_0$ (M)	$[\mathbf{1d}]_0$ (M)	k_{obs} (s^{-1})
2.50×10^{-4}	2.50×10^{-3}	6.55×10^{-2}
2.50×10^{-4}	3.75×10^{-3}	1.02×10^{-1}
2.50×10^{-4}	5.00×10^{-3}	1.31×10^{-1}
2.50×10^{-4}	6.25×10^{-3}	1.63×10^{-1}

$k_2 = 2.57 \times 10^{1}\ M^{-1}\ s^{-1}$

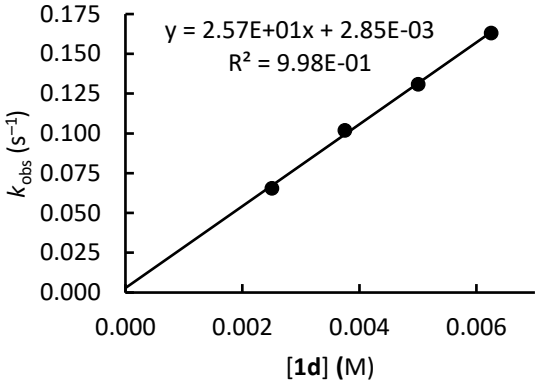

1d + potassium thiophenolate (**2c**) in DMSO (stopped flow, detection at 310 nm)

$[\mathbf{2c}]_0$ (M)	$[\mathbf{1d}]_0$ (M)	k_{obs} (s^{-1})
2.50×10^{-4}	2.50×10^{-3}	1.02×10^{-1}
2.50×10^{-4}	3.75×10^{-3}	1.56×10^{-1}
2.50×10^{-4}	5.00×10^{-3}	2.04×10^{-1}
2.50×10^{-4}	6.25×10^{-3}	2.54×10^{-1}

$k_2 = 4.03 \times 10^{1}\ M^{-1}\ s^{-1}$

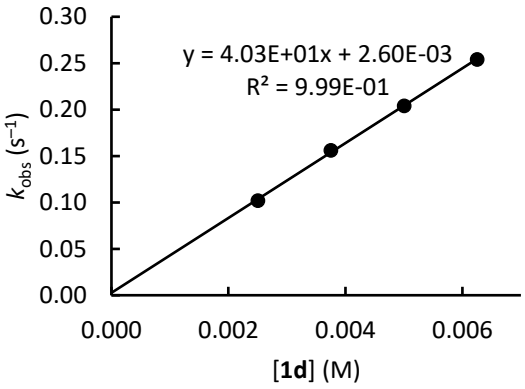

1d + potassium 4-methylthiophenolate (**2b**) in DMSO (stopped flow, detection at 300 nm)

$[\mathbf{2b}]_0$ (M)	$[\mathbf{1d}]_0$ (M)	k_{obs} (s^{-1})
2.50×10^{-4}	2.50×10^{-3}	1.58×10^{-1}
2.50×10^{-4}	3.75×10^{-3}	2.41×10^{-1}
2.50×10^{-4}	5.00×10^{-3}	3.15×10^{-1}
2.50×10^{-4}	6.25×10^{-3}	3.80×10^{-1}

$k_2 = 5.92 \times 10^{1}\ M^{-1}\ s^{-1}$

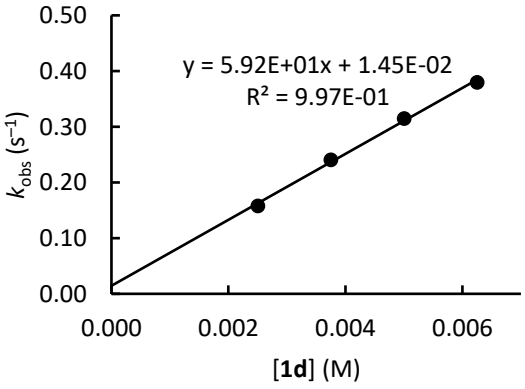

1d + potassium 4-methoxythiophenolate (**2a**) in DMSO (stopped flow, detection at 300 nm)

$[\mathbf{2a}]_0$ (M)	$[\mathbf{1d}]_0$ (M)	k_{obs} (s^{-1})
2.50×10^{-4}	2.50×10^{-3}	2.47×10^{-1}
2.50×10^{-4}	3.75×10^{-3}	3.39×10^{-1}
2.50×10^{-4}	5.00×10^{-3}	4.62×10^{-1}
2.50×10^{-4}	6.25×10^{-3}	5.59×10^{-1}

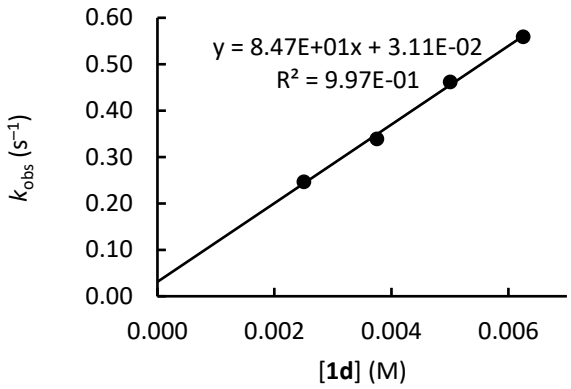

$k_2 = 8.47 \times 10^1\ M^{-1}\ s^{-1}$

Determination of E and s_E parameters for **1d** in DMSO.

Reference Nucleophile	Nucleophilicity N (s_N)	k_2 ($M^{-1}\ s^{-1}$)	log k_2/s_N
4-Br (**2d**)	22.81 (0.78)	2.57×10^1	1.81
4-H (**2c**)	23.36 (0.74)	4.03×10^1	2.17
4-Me (**2b**)	24.35 (0.69)	5.92×10^1	2.57
4-MeO (**2a**)	24.97 (0.67)	8.47×10^1	2.88

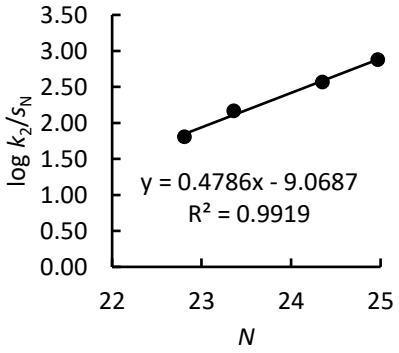

***E* = –18.95**

s_E = 0.48

Kinetics of reactions of 6,6-dimethyl-1-phenylspiro[2.5]octane-4,8-dione (1e)

1e + potassium 4-(trifluoromethyl)thiophenolate (**2f**) in DMSO (stopped flow, detection at 330 nm)

$[\mathbf{2f}]_0$ (M)	$[\mathbf{1e}]_0$ (M)	k_{obs} (s^{-1})
2.45×10^{-4}	2.47×10^{-3}	2.14×10^{-2}
2.45×10^{-4}	3.70×10^{-3}	3.14×10^{-2}
2.45×10^{-4}	4.94×10^{-3}	4.14×10^{-2}
2.45×10^{-4}	6.17×10^{-3}	4.99×10^{-2}

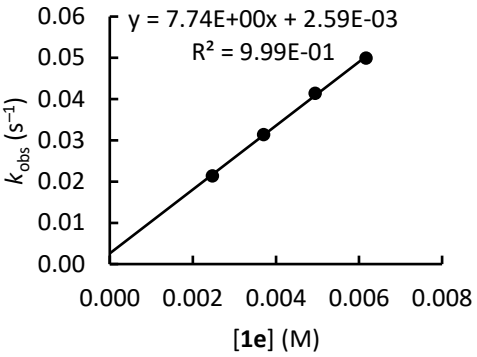

$k_2 = 7.74 \times 10^0$ M^{-1} s^{-1}

1e + potassium 3-chlorothiophenolate (**2e**) in DMSO (stopped flow, detection at 330 nm)

$[\mathbf{2e}]_0$ (M)	$[\mathbf{1e}]_0$ (M)	k_{obs} (s^{-1})
2.45×10^{-4}	2.46×10^{-3}	3.34×10^{-2}
2.45×10^{-4}	3.70×10^{-3}	5.08×10^{-2}
2.45×10^{-4}	4.93×10^{-3}	6.81×10^{-2}
2.45×10^{-4}	6.16×10^{-3}	8.64×10^{-2}

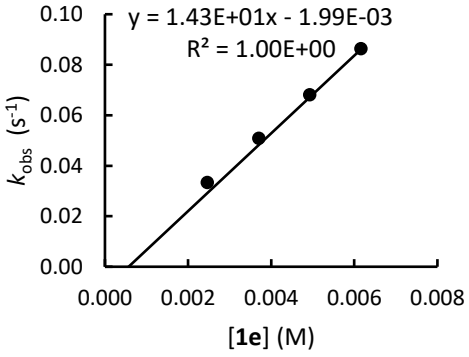

$k_2 = 1.43 \times 10^1$ M^{-1} s^{-1}

1e + potassium 4-bromothiophenolate (**2d**) in DMSO (stopped flow, detection at 318 nm)

$[\mathbf{2d}]_0$ (M)	$[\mathbf{1e}]_0$ (M)	k_{obs} (s^{-1})
2.45×10^{-4}	2.47×10^{-3}	4.25×10^{-2}
2.45×10^{-4}	3.70×10^{-3}	6.39×10^{-2}
2.45×10^{-4}	4.94×10^{-3}	8.57×10^{-2}
2.45×10^{-4}	6.17×10^{-3}	1.04×10^{-1}

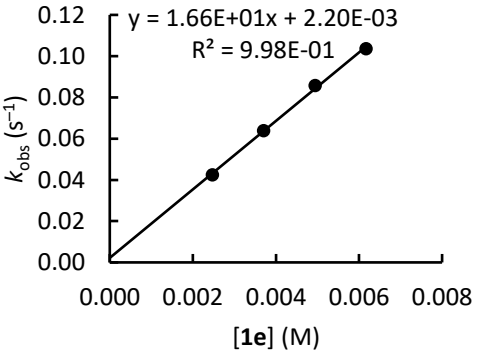

$k_2 = 1.66 \times 10^1$ M^{-1} s^{-1}

1e + potassium thiophenolate (**2c**) in DMSO (stopped flow, detection at 310 nm)

$[\mathbf{2c}]_0$ (M)	$[\mathbf{1e}]_0$ (M)	k_{obs} (s^{-1})
2.45×10^{-4}	2.47×10^{-3}	5.96×10^{-2}
2.45×10^{-4}	3.70×10^{-3}	8.67×10^{-2}
2.45×10^{-4}	4.94×10^{-3}	1.12×10^{-1}
2.45×10^{-4}	6.17×10^{-3}	1.32×10^{-1}

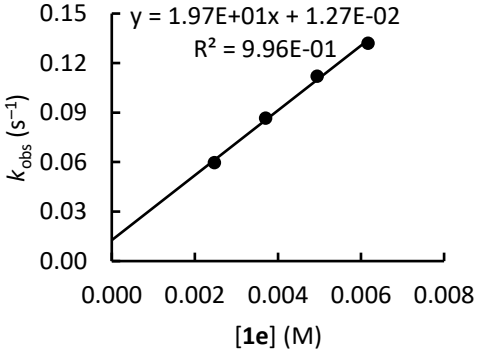

$k_2 = 1.97 \times 10^1\ M^{-1}\ s^{-1}$

1e + potassium 4-methylthiophenolate (**2b**) in DMSO (stopped flow, detection at 310 nm)

$[\mathbf{2b}]_0$ (M)	$[\mathbf{1e}]_0$ (M)	k_{obs} (s^{-1})
2.45×10^{-4}	2.47×10^{-3}	8.54×10^{-2}
2.45×10^{-4}	3.70×10^{-3}	1.24×10^{-1}
2.45×10^{-4}	4.94×10^{-3}	1.58×10^{-1}
2.45×10^{-4}	6.17×10^{-3}	1.90×10^{-1}

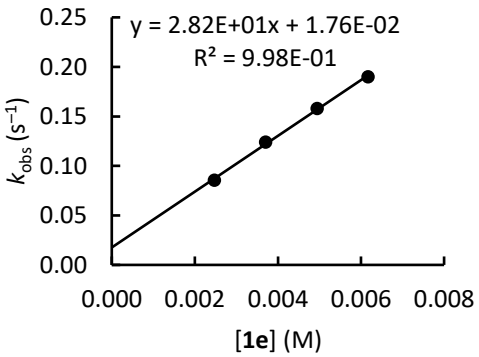

$k_2 = 2.82 \times 10^1\ M^{-1}\ s^{-1}$

1e + potassium 4-methoxythiophenolate (**2a**) in DMSO (stopped flow, detection at 310 nm)

$[\mathbf{2a}]_0$ (M)	$[\mathbf{1e}]_0$ (M)	k_{obs} (s^{-1})
2.45×10^{-4}	2.47×10^{-3}	1.10×10^{-1}
2.45×10^{-4}	3.70×10^{-3}	1.45×10^{-1}
2.45×10^{-4}	4.94×10^{-3}	1.90×10^{-1}
2.45×10^{-4}	6.17×10^{-3}	2.22×10^{-1}

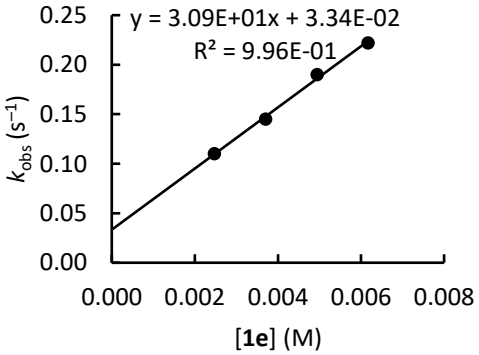

$k_2 = 3.09 \times 10^1\ M^{-1}\ s^{-1}$

Determination of E and s_E parameters for **1e** in DMSO.

Reference Nucleophile	Nucleophilicity N (s_N)	k_2 (M^{-1} s^{-1})	log k_2/s_N
4-CF_3 (**2f**)	21.30 (0.86)	7.74	1.03
3-Cl (**2e**)	22.50 (0.78)	1.43×10^1	1.48
4-Br (**2d**)	22.81 (0.78)	1.66×10^1	1.56
4-H (**2c**)	23.36 (0.74)	1.97×10^1	1.75
4-Me (**2b**)	24.35 (0.69)	2.82×10^1	2.10
4-MeO (**2a**)	24.97 (0.67)	3.09×10^1	2.22

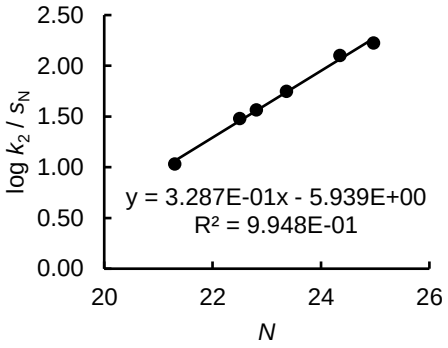

***E* = –18.07**

s_E = 0.33

Kinetics of reactions of 2-(3-chlorophenyl)spiro[cyclopropane-1,2'-indene]-1',3'-dione (1f)

1f + potassium 4-bromothiophenolate (**2d**) in DMSO (stopped flow, detection at 390 nm)

[2d]$_0$ (M)	**[1f]$_0$** (M)	k_{obs} (s^{-1})
2.50×10^{-4}	2.50×10^{-3}	3.16×10^{-2}
2.50×10^{-4}	3.75×10^{-3}	4.67×10^{-2}
2.50×10^{-4}	5.00×10^{-3}	6.37×10^{-2}
2.50×10^{-4}	6.25×10^{-3}	7.72×10^{-2}

$k_2 = 1.23 \times 10^1$ M^{-1} s^{-1}

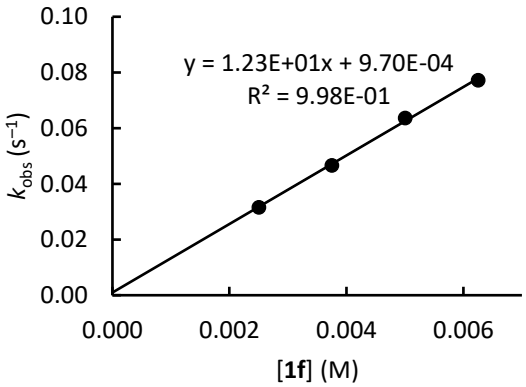

1f + potassium thiophenolate (**2c**) in DMSO (stopped flow, detection at 390 nm)

$[\mathbf{2c}]_0$ (M)	$[\mathbf{1f}]_0$ (M)	k_{obs} (s^{-1})
2.50×10^{-4}	2.50×10^{-3}	5.19×10^{-2}
2.50×10^{-4}	3.75×10^{-3}	7.45×10^{-2}
2.50×10^{-4}	5.00×10^{-3}	1.03×10^{-1}
2.50×10^{-4}	6.25×10^{-3}	1.28×10^{-1}

$k_2 = 2.05 \times 10^{1}\ M^{-1}\ s^{-1}$

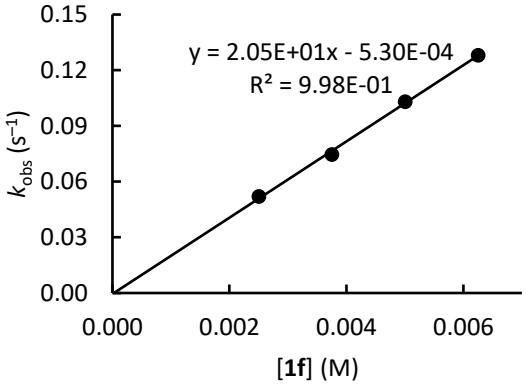

1f + potassium 4-methylthiophenolate (**2b**) in DMSO (stopped flow, detection at 390 nm)

$[\mathbf{2b}]_0$ (M)	$[\mathbf{1f}]_0$ (M)	k_{obs} (s^{-1})
2.50×10^{-4}	2.50×10^{-3}	8.27×10^{-2}
2.50×10^{-4}	3.75×10^{-3}	1.23×10^{-1}
2.50×10^{-4}	5.00×10^{-3}	1.67×10^{-1}
2.50×10^{-4}	6.25×10^{-3}	2.05×10^{-1}

$k_2 = 3.29 \times 10^{1}\ M^{-1}\ s^{-1}$

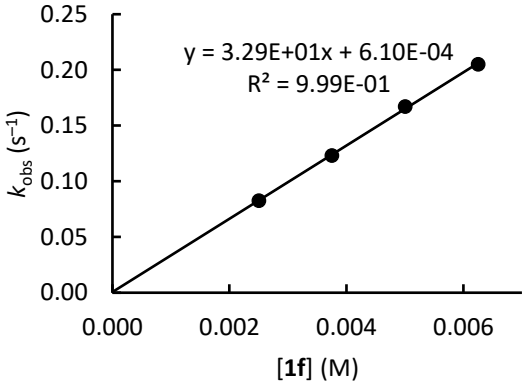

1f + potassium 4-methoxythiophenolate (**2a**) in DMSO (stopped flow, detection at 390 nm)

$[\mathbf{2a}]_0$(M)	$[\mathbf{1f}]_0$ (M)	k_{obs} (s^{-1})
2.50×10^{-4}	2.50×10^{-3}	1.17×10^{-1}
2.50×10^{-4}	3.75×10^{-3}	1.79×10^{-1}
2.50×10^{-4}	5.00×10^{-3}	2.41×10^{-1}
2.50×10^{-4}	6.25×10^{-3}	2.95×10^{-1}

$k_2 = 4.77 \times 10^{1}\ M^{-1}\ s^{-1}$

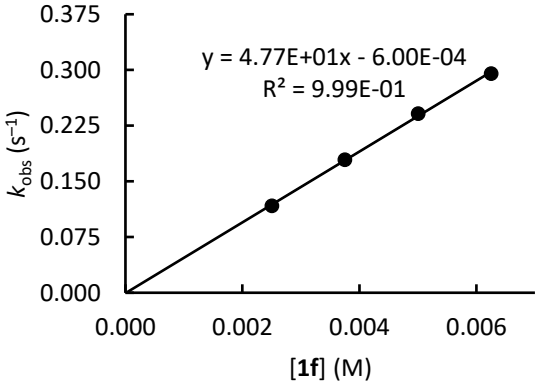

Determination of *E* and s_E parameters for **1f** in DMSO.

Reference Nucleophile	Nucleophilicity *N* (s_N)	k_2 (M^{-1} s^{-1})	log k_2/s_N
4-Br (**2d**)	22.81 (0.78)	1.23×10^1	1.40
4-H (**2c**)	23.36 (0.74)	2.05×10^1	1.77
4-Me (**2b**)	24.35 (0.69)	3.29×10^1	2.20
4-MeO (**2a**)	24.97 (0.67)	4.77×10^1	2.50

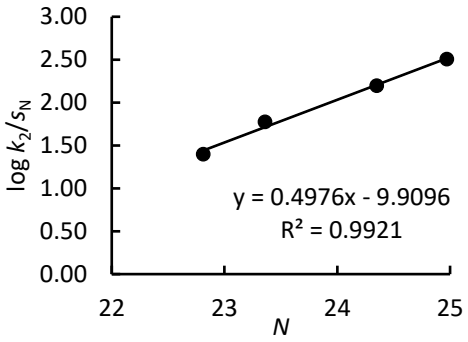

***E* = –19.91**

s_E = 0.50

Kinetics of reactions of 2-phenylspiro[cyclopropane-1,2'-indene]-1',3'-dione (1g)

Thiophenolates

1g + potassium 4-(trifluoromethyl)thiophenolate (**2f**) in DMSO (stopped flow, detection at 396 nm)

[2f]$_0$ (M)	**[1g]**$_0$ (M)	k_{obs} (s^{-1})
2.50×10^{-4}	2.50×10^{-3}	9.68×10^{-3}
2.50×10^{-4}	3.75×10^{-3}	1.42×10^{-2}
2.50×10^{-4}	5.00×10^{-3}	1.87×10^{-2}
2.50×10^{-4}	6.25×10^{-3}	2.45×10^{-2}
2.50×10^{-4}	1.25×10^{-2}	4.64×10^{-2}

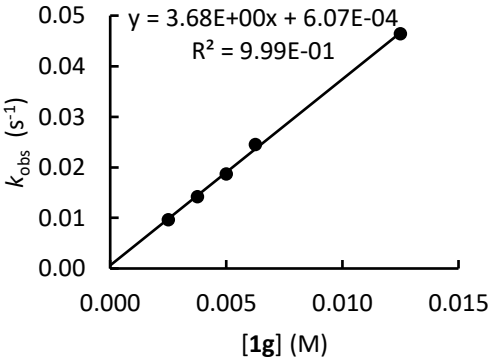

$k_2 = 3.68 \times 10^0$ M^{-1} s^{-1}

1g + potassium 3-chlorothiophenolate (**2e**) in DMSO (stopped flow, detection at 396 nm)

$[\mathbf{2e}]_0$ (M)	$[\mathbf{1g}]_0$ (M)	k_{obs} (s^{-1})
2.50×10^{-4}	2.50×10^{-3}	1.63×10^{-2}
2.50×10^{-4}	3.75×10^{-3}	2.49×10^{-2}
2.50×10^{-4}	5.00×10^{-3}	3.29×10^{-2}
2.50×10^{-4}	6.25×10^{-3}	4.24×10^{-2}

$k_2 = 6.90 \times 10^{0}\ M^{-1}\ s^{-1}$

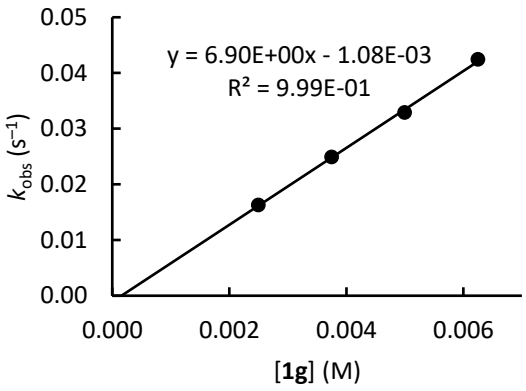

1g + potassium 4-bromothiophenolate (**2d**) in DMSO (stopped flow, detection at 396 nm)

$[\mathbf{2d}]_0$ (M)	$[\mathbf{1g}]_0$ (M)	k_{obs} (s^{-1})
2.50×10^{-4}	2.50×10^{-3}	2.13×10^{-2}
2.50×10^{-4}	3.75×10^{-3}	3.03×10^{-2}
2.50×10^{-4}	5.00×10^{-3}	4.23×10^{-2}
2.50×10^{-4}	6.25×10^{-3}	5.22×10^{-2}

$k_2 = 8.38 \times 10^{0}\ M^{-1}\ s^{-1}$

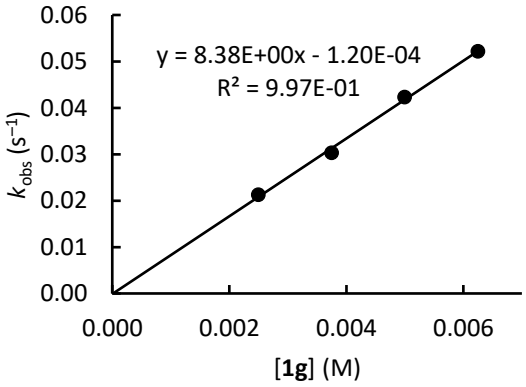

1g + potassium thiophenolate (**2c**) in DMSO (stopped flow, detection at 310 nm)

$[\mathbf{2c}]_0$ (M)	$[\mathbf{1g}]_0$ (M)	k_{obs} (s^{-1})
2.50×10^{-4}	2.50×10^{-3}	3.55×10^{-2}
2.50×10^{-4}	3.75×10^{-3}	5.63×10^{-2}
2.50×10^{-4}	5.00×10^{-3}	7.20×10^{-2}
2.50×10^{-4}	6.25×10^{-3}	9.28×10^{-2}

$k_2 = 1.50 \times 10^{1}\ M^{-1}\ s^{-1}$

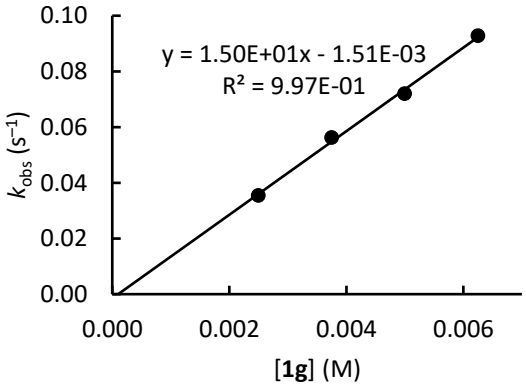

1g + potassium 4-methylthiophenolate (**2b**) in DMSO (stopped flow, detection at 310 nm)

$[\mathbf{2b}]_0$ (M)	$[\mathbf{1g}]_0$ (M)	k_{obs} (s^{-1})
2.50×10^{-4}	2.50×10^{-3}	5.19×10^{-2}
2.50×10^{-4}	3.75×10^{-3}	8.17×10^{-2}
2.50×10^{-4}	5.00×10^{-3}	1.06×10^{-1}
2.50×10^{-4}	6.25×10^{-3}	1.35×10^{-1}

$k_2 = 2.19 \times 10^1$ M^{-1} s^{-1}

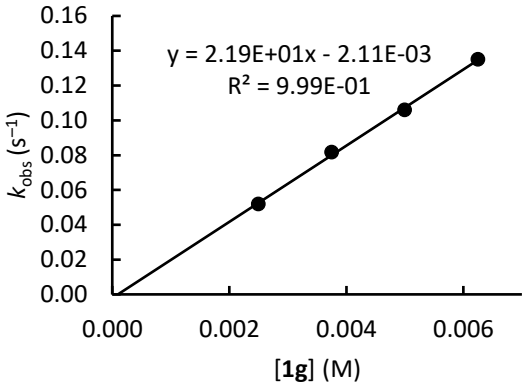

1g + potassium 4-methoxythiophenolate (**2a**) in DMSO (stopped flow, detection at 310 nm)

$[\mathbf{2a}]_0$ (M)	$[\mathbf{1g}]_0$ (M)	k_{obs} (s^{-1})
2.50×10^{-4}	2.50×10^{-3}	7.40×10^{-2}
2.50×10^{-4}	3.75×10^{-3}	1.13×10^{-1}
2.50×10^{-4}	5.00×10^{-3}	1.44×10^{-1}
2.50×10^{-4}	6.25×10^{-3}	1.95×10^{-1}

$k_2 = 3.15 \times 10^1$ M^{-1} s^{-1}

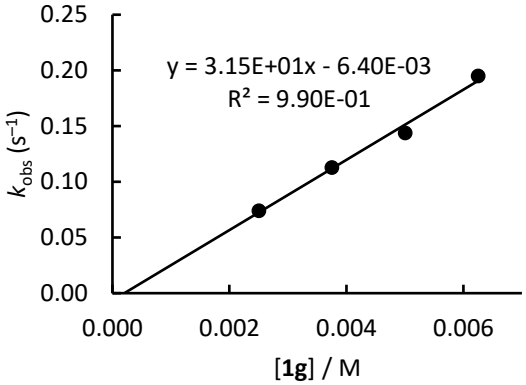

Determination of E and s_E parameters for **1g** in DMSO in reactions with thiophenolates.

Reference Nucleophile	Nucleophilicity N (s_N)	k_2 (M^{-1} s^{-1})	log k_2/s_N
4-CF_3 (**2f**)	21.30 (0.86)	3.68×10^0	0.66
3-Cl (**2e**)	22.50 (0.78)	6.90×10^0	1.08
4-Br (**2d**)	22.81 (0.78)	8.38×10^0	1.18
4-H (**2c**)	23.36 (0.74)	1.50×10^1	1.59
4-Me (**2b**)	24.35 (0.69)	2.19×10^1	1.94
4-MeO (**2a**)	24.97 (0.67)	3.15×10^1	2.46

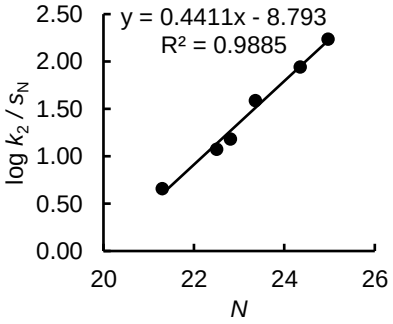

***E* = –20.54**

s_E = 0.54

C-Nucleophiles

1g + potassium 1-(4-nitrophenyl)-2-oxo-2-phenylethan-1-ide (**7a**) in DMSO (J&M, detection at 580 nm)

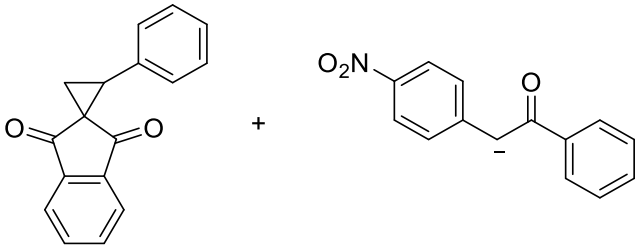

1g **5a**

[5a]$_0$ (M)	**[1g]$_0$** (M)	k_{obs} (s^{-1})
1.25×10^{-4}	2.50×10^{-3}	6.66×10^{-5}
1.25×10^{-4}	5.00×10^{-3}	1.02×10^{-4}
1.25×10^{-4}	7.50×10^{-3}	1.91×10^{-4}
1.25×10^{-4}	1.00×10^{-2}	2.55×10^{-4}

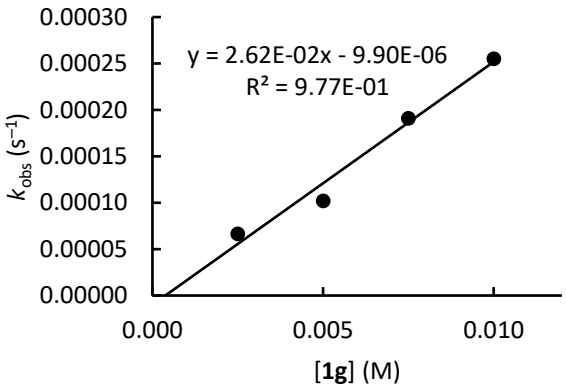

$k_2 = 2.62 \times 10^{-2}$ M^{-1} s^{-1}

1g + potassium cyano(4-nitrophenyl)methanide (**5b**) in DMSO (J&M, detection at 580 nm)

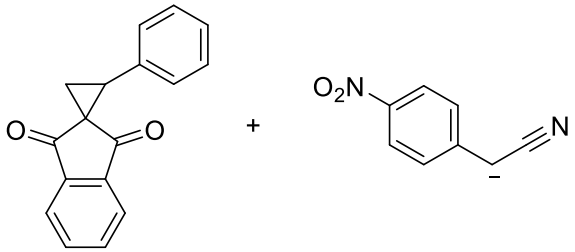

1g **5b**

[5b]$_0$ (M)	**[1g]$_0$** (M)	k_{obs} (s^{-1})
1.25×10^{-4}	2.50×10^{-3}	1.87×10^{-4}
1.25×10^{-4}	5.00×10^{-3}	2.28×10^{-4}
1.25×10^{-4}	7.50×10^{-3}	2.84×10^{-4}
1.25×10^{-4}	1.00×10^{-2}	3.17×10^{-4}
1.25×10^{-4}	1.25×10^{-2}	3.97×10^{-4}

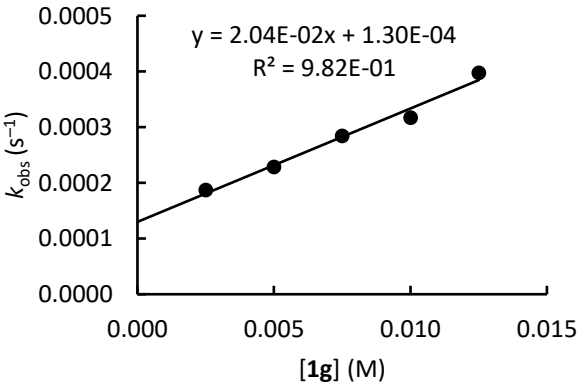

$k_2 = 2.04 \times 10^{-2}$ M^{-1} s^{-1}

1g + potassium cyano(4-cyanophenyl)methanide (**5c**) in DMSO (stopped flow, detection at 340 nm)

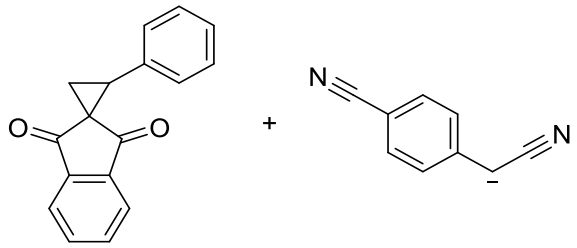

1g **5c**

[5c]$_0$ (M)	**[1g]**$_0$ (M)	k_{obs} (s^{-1})
2.50×10^{-4}	2.50×10^{-3}	9.34×10^{-3}
2.50×10^{-4}	3.75×10^{-3}	1.11×10^{-2}
2.50×10^{-4}	5.00×10^{-3}	1.34×10^{-2}
2.50×10^{-4}	6.25×10^{-2}	1.57×10^{-2}

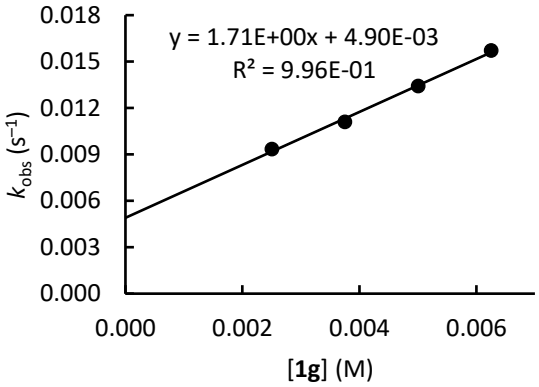

$k_2 = 1.71 \times 10^0$ M^{-1} s^{-1}

1g + potassium 2-oxo-1-(pyridin-1-ium-1-yl)propan-1-ide (**5d**) in DMSO (J&M, detection at 420 nm)

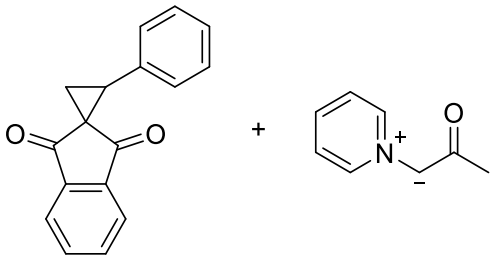

1g **5d**

[5d]$_0$ (M)	**[1g]**$_0$ (M)	k_{obs} (s^{-1})
2.50×10^{-4}	2.50×10^{-3}	8.28×10^{-5}
2.50×10^{-4}	3.75×10^{-3}	1.12×10^{-4}
2.50×10^{-4}	5.00×10^{-3}	1.41×10^{-4}
2.50×10^{-4}	6.25×10^{-2}	1.69×10^{-4}

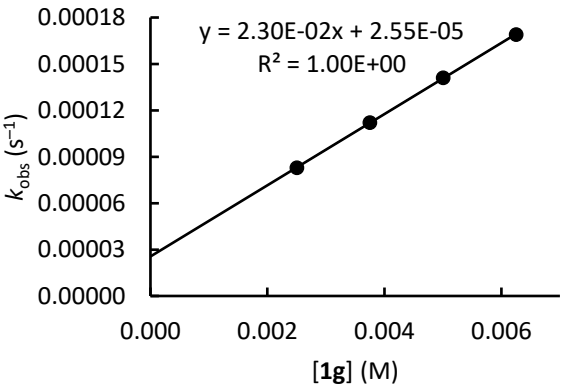

$k_2 = 2.30 \times 10^{-2}$ M^{-1} s^{-1}

1g + potassium 1-(4-cyanophenyl)-2-ethoxy-2-oxoethan-1-ide (**5e**) in DMSO (stopped flow, detection at 340 nm)

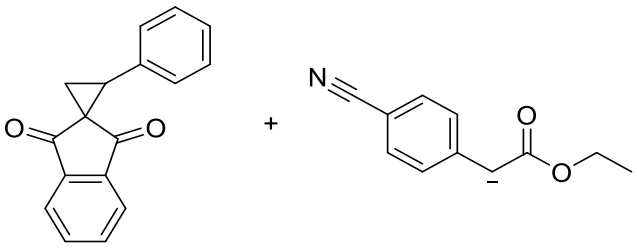

1g **5e**

$[\mathbf{5e}]_0$ (M)	$[\mathbf{1g}]_0$ (M)	k_{obs} (s^{-1})
2.50×10^{-4}	2.50×10^{-3}	9.05×10^{-3}
2.50×10^{-4}	3.75×10^{-3}	1.40×10^{-2}
2.50×10^{-4}	5.00×10^{-3}	1.94×10^{-2}
2.50×10^{-4}	6.25×10^{-2}	2.64×10^{-2}

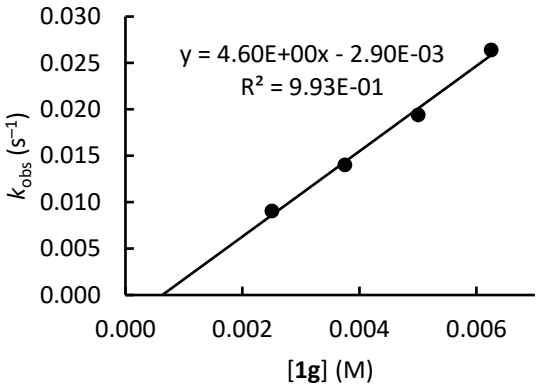

$k_2 = 4.60 \times 10^0\ M^{-1}\ s^{-1}$

1g + potassium 2-ethoxy-2-oxo-1-phenylethan-1-ide (**5f**) in DMSO (stopped flow, detection at 340 nm)

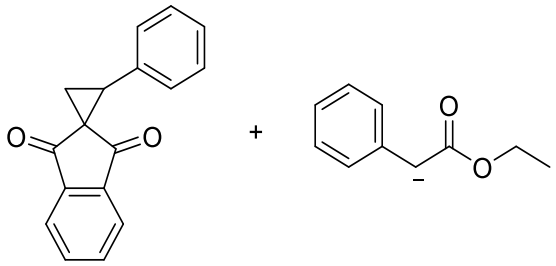

1g **5f**

$[\mathbf{5f}]_0$ (M)	$[\mathbf{1g}]_0$ (M)	k_{obs} (s^{-1})
2.50×10^{-4}	2.50×10^{-3}	1.19×10^{-1}
2.50×10^{-4}	3.75×10^{-3}	1.77×10^{-1}
2.50×10^{-4}	5.00×10^{-3}	2.34×10^{-1}
2.50×10^{-4}	6.25×10^{-3}	2.97×10^{-1}

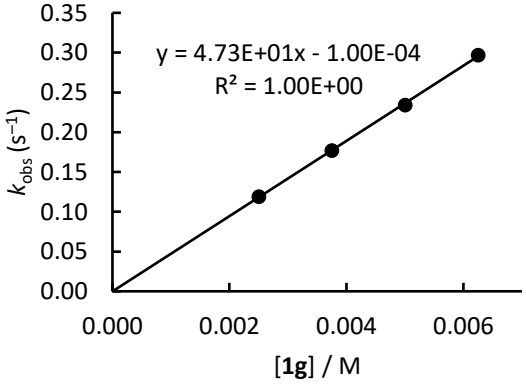

$k_2 = 4.73 \times 10^1\ M^{-1}\ s^{-1}$

1g + potassium 2-oxo-1,2-diphenylethan-1-ide (**5g**) in DMSO (stopped flow, detection at 412 nm)

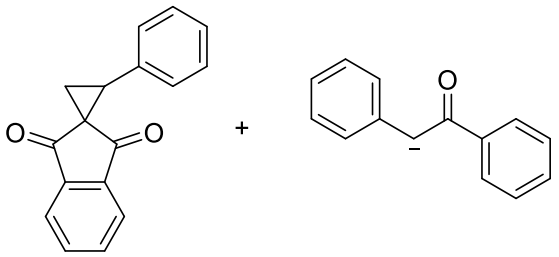

1g **5g**

$[\mathbf{5g}]_0$ (M)	$[\mathbf{1g}]_0$ (M)	k_{obs} (s^{-1})
2.50×10^{-4}	2.50×10^{-3}	8.27×10^{-3}
2.50×10^{-4}	3.75×10^{-3}	1.29×10^{-2}
2.50×10^{-4}	5.00×10^{-3}	1.83×10^{-2}
2.50×10^{-4}	6.25×10^{-2}	2.20×10^{-2}

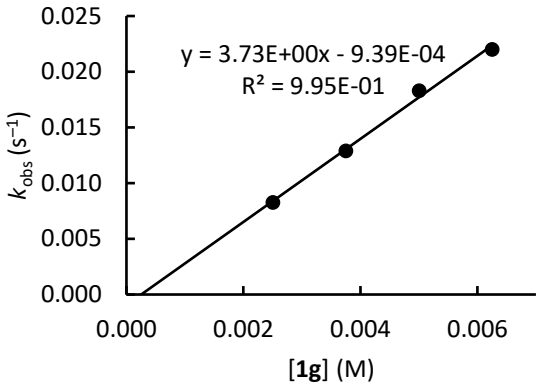

$k_2 = 3.73 \times 10^0$ M^{-1} s^{-1}

Determination of E and s_E parameters for **1g** in DMSO in reactions with carbanions.

Reference Nucleophile	Nucleophilicity N (s_N)	k_2 (M^{-1} s^{-1})	log k_2/s_N
5a	19.46 (0.58)	2.62×10^{-2}	-2.73
5b	19.67 (0.68)	2.04×10^{-2}	-2.49
5d	20.24 (0.60)	2.30×10^{-2}	-2.73
5g	23.15 (0.60)	3.73×10^{0}	0.95
5e	23.64 (0.65)	4.60×10^{0}	1.02
5c	25.11 (0.64)	1.71×10^{0}	0.36
5f	27.54 (0.57)	4.73×10^{1}	2.94

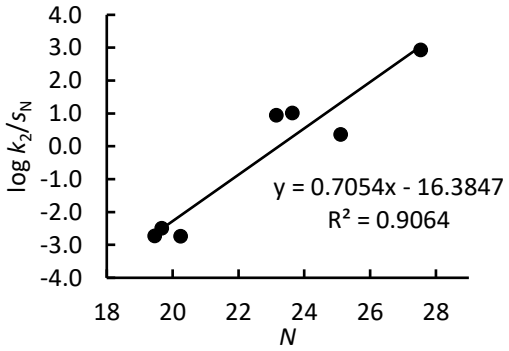

***E* = –23.23**

s_E = 0.71

1g + sodium azide (**3**) in DMSO (stopped flow, detection at 396 nm)

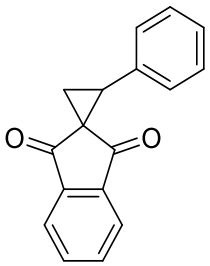

1g + NaN_3

$[\mathbf{1g}]_0$ (M)	$[\mathbf{3}]_0$ (M)	k_{obs} (s^{-1})
4.98×10^{-4}	5.80×10^{-3}	5.16×10^{-4} *a*
5.96×10^{-4}	6.24×10^{-3}	5.41×10^{-4}
5.96×10^{-4}	1.28×10^{-2}	1.09×10^{-3}
5.96×10^{-4}	2.56×10^{-2}	2.13×10^{-3}
5.96×10^{-4}	3.90×10^{-2}	3.30×10^{-3}
5.96×10^{-4}	5.20×10^{-2}	4.29×10^{-3}

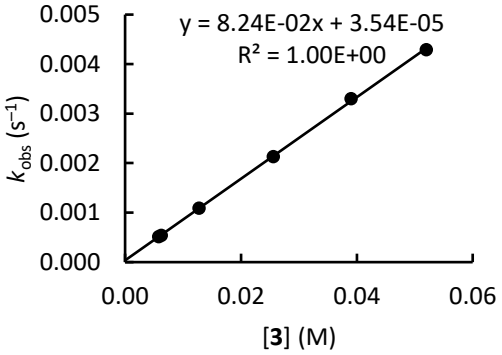

a measured with conventional UV-Vis photometry

$k_2 = 8.24 \times 10^{-2}\ M^{-1}\ s^{-1}$

Kinetics of reactions of 2-(*p*-tolyl)spiro[cyclopropane-1,2'-indene]-1',3'-dione (1h)

1h + potassium 4-bromothiophenolate (**2d**) in DMSO (stopped flow, detection at 396 nm)

$[\mathbf{2d}]_0$ (M)	$[\mathbf{1h}]_0$ (M)	k_{obs} (s^{-1})
2.50×10^{-4}	2.50×10^{-3}	3.72×10^{-2}
2.50×10^{-4}	3.75×10^{-3}	5.24×10^{-2}
2.50×10^{-4}	5.00×10^{-3}	7.33×10^{-2}
2.50×10^{-4}	6.25×10^{-3}	8.59×10^{-2}

$k_2 = 1.34 \times 10^{1}$ M^{-1} s^{-1}

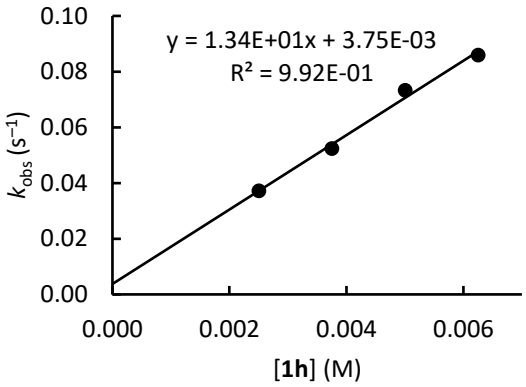

1h + potassium thiophenolate (**2c**) in DMSO (stopped flow, detection at 396 nm)

$[\mathbf{2c}]_0$ (M)	$[\mathbf{1h}]_0$ (M)	k_{obs} (s^{-1})
2.50×10^{-4}	2.50×10^{-3}	4.95×10^{-2}
2.50×10^{-4}	3.75×10^{-3}	7.37×10^{-2}
2.50×10^{-4}	5.00×10^{-3}	9.75×10^{-2}
2.50×10^{-4}	6.25×10^{-3}	1.26×10^{-1}

$k_2 = 2.03 \times 10^{1}$ M^{-1} s^{-1}

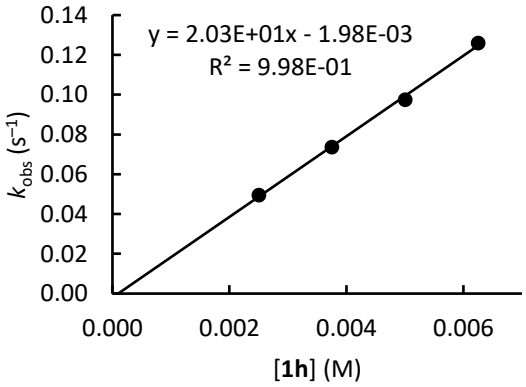

1h + potassium 4-methylthiophenolate (**2b**) in DMSO (stopped flow, detection at 396 nm)

$[\mathbf{2b}]_0$ (M)	$[\mathbf{1h}]_0$ (M)	k_{obs} (s^{-1})
2.50×10^{-4}	2.50×10^{-3}	7.35×10^{-2}
2.50×10^{-4}	3.75×10^{-3}	1.09×10^{-1}
2.50×10^{-4}	5.00×10^{-3}	1.40×10^{-1}
2.50×10^{-4}	6.25×10^{-3}	1.72×10^{-1}

$k_2 = 2.61 \times 10^{1}$ M^{-1} s^{-1}

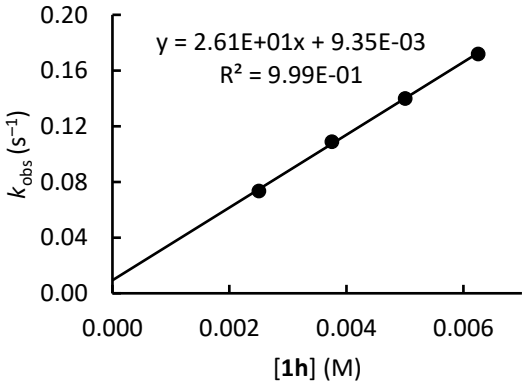

1h + potassium 4-methoxythiophenolate (**2a**) in DMSO (stopped flow, detection at 396 nm)

$[\mathbf{2a}]_0$ (M)	$[\mathbf{1h}]_0$ (M)	k_{obs} (s^{-1})
2.50×10^{-4}	2.50×10^{-3}	9.63×10^{-2}
2.50×10^{-4}	3.75×10^{-3}	1.35×10^{-1}
2.50×10^{-4}	5.00×10^{-3}	1.85×10^{-1}
2.50×10^{-4}	6.25×10^{-3}	2.20×10^{-1}

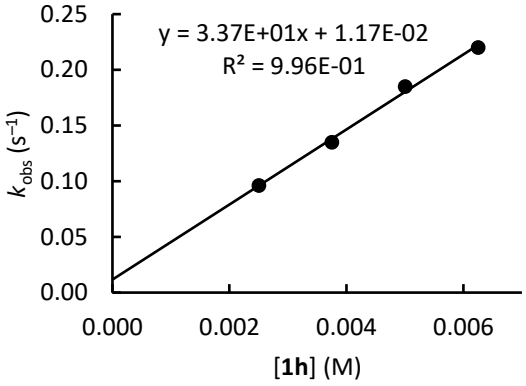

$k_2 = 3.37 \times 10^1$ M^{-1} s^{-1}

Determination of E and s_E parameters for **1h** in DMSO.

Reference Nucleophile	Nucleophilicity N (s_N)	k_2 (M^{-1} s^{-1})	log k_2/s_N
4-Br (**2d**)	22.81 (0.78)	1.34×10^1	1.44
4-H (**2c**)	23.36 (0.74)	2.03×10^1	1.77
4-Me (**2b**)	24.35 (0.69)	2.61×10^1	2.05
4-MeO (**2a**)	24.97 (0.67)	3.37×10^1	2.28

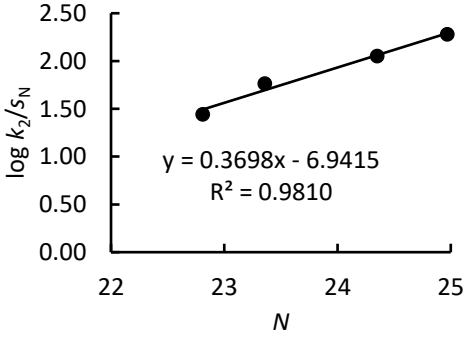

E = –18.77

s_E = 0.37

Kinetics of reactions of 2-(4-methoxyphenyl)spiro[cyclopropane-1,2'-indene]-1',3'-dione (1i)

1i + potassium 4-bromothiophenolate (**2d**) in DMSO (stopped flow, detection at 396 nm)

$[\mathbf{2d}]_0$ (M)	$[\mathbf{1i}]_0$ (M)	k_{obs} (s^{-1})
2.50×10^{-4}	2.50×10^{-3}	8.11×10^{-2}
2.50×10^{-4}	3.75×10^{-3}	1.23×10^{-1}
2.50×10^{-4}	5.00×10^{-3}	1.65×10^{-1}
2.50×10^{-4}	6.25×10^{-3}	2.07×10^{-1}

$k_2 = 3.36 \times 10^{1}\ M^{-1}\ s^{-1}$

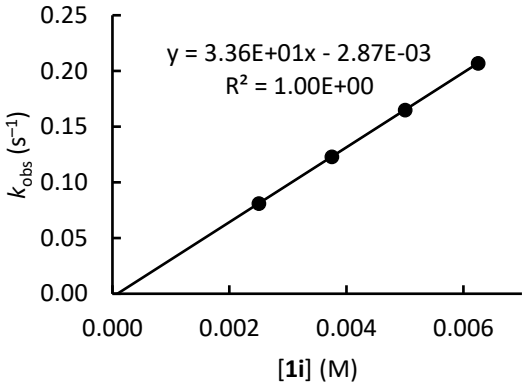

1i + potassium thiophenolate (**2c**) in DMSO (stopped flow, detection at 396 nm)

$[\mathbf{2c}]_0$ (M)	$[\mathbf{1i}]_0$ (M)	k_{obs} (s^{-1})
2.50×10^{-4}	2.50×10^{-3}	1.07×10^{-1}
2.50×10^{-4}	3.75×10^{-3}	1.60×10^{-1}
2.50×10^{-4}	5.00×10^{-3}	2.17×10^{-1}
2.50×10^{-4}	6.25×10^{-3}	2.75×10^{-1}

$k_2 = 4.49 \times 10^{1}\ M^{-1}\ s^{-1}$

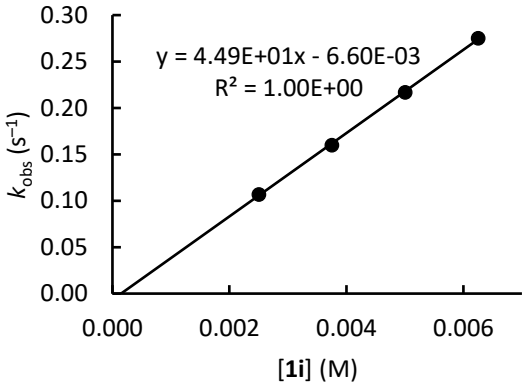

1i + potassium 4-methylthiophenolate (**2b**) in DMSO (stopped flow, detection at 396 nm)

$[\mathbf{2b}]_0$ (M)	$[\mathbf{1i}]_0$ (M)	k_{obs} (s^{-1})
2.50×10^{-4}	2.50×10^{-3}	1.51×10^{-1}
2.50×10^{-4}	3.75×10^{-3}	2.33×10^{-1}
2.50×10^{-4}	5.00×10^{-3}	3.23×10^{-1}
2.50×10^{-4}	6.25×10^{-3}	3.93×10^{-1}

$k_2 = 6.53 \times 10^{1}\ M^{-1}\ s^{-1}$

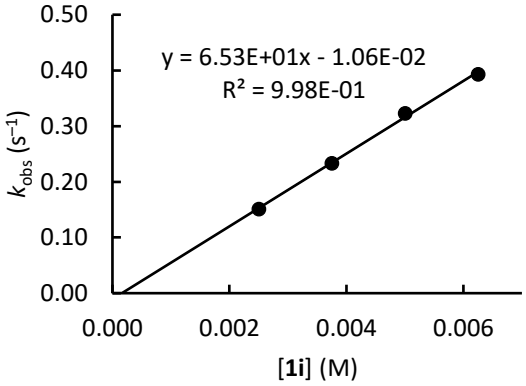

1i + potassium 4-methoxythiophenolate (**2a**) in DMSO (stopped flow, detection at 396 nm)

$[\mathbf{2a}]_0$ (M)	$[\mathbf{1i}]_0$ (M)	k_{obs} (s^{-1})
2.50×10^{-4}	2.50×10^{-3}	2.05×10^{-1}
2.50×10^{-4}	3.75×10^{-3}	3.11×10^{-1}
2.50×10^{-4}	5.00×10^{-3}	4.44×10^{-1}
2.50×10^{-4}	6.25×10^{-3}	5.52×10^{-1}

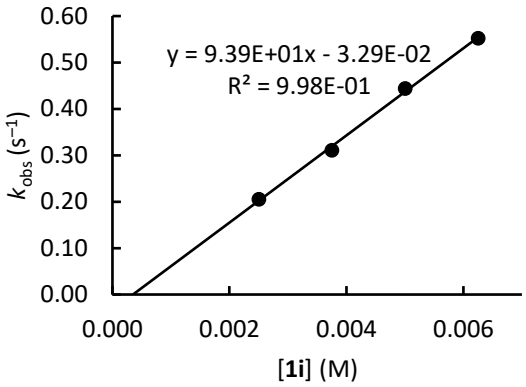

$k_2 = 9.39 \times 10^1\ M^{-1}\ s^{-1}$

Determination of E and s_E parameters for **1i** in DMSO.

Reference Nucleophile	Nucleophilicity N (s_N)	k_2 ($M^{-1}\ s^{-1}$)	log k_2/s_N
4-Br (**2d**)	22.81 (0.78)	3.36×10^1	1.96
4-H (**2c**)	23.36 (0.74)	4.49×10^1	2.23
4-Me (**2b**)	24.35 (0.69)	6.53×10^1	2.63
4-MeO (**2a**)	24.97 (0.67)	9.39×10^1	2.94

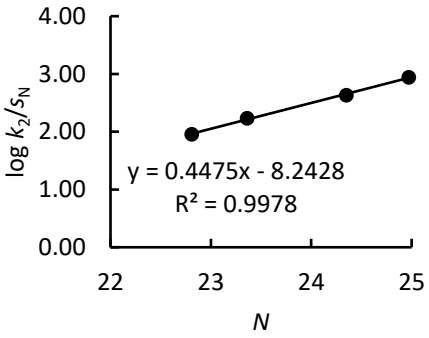

***E* = –18.42**

s_E = 0.45

Kinetics of reactions of 2-phenylcyclopropane-1,1-dicarbonitrile (1j)

1j + potassium 4-bromothiophenolate (**2d**) in DMSO (stopped flow, detection at 320 nm)

$[\mathbf{2d}]_0$ (M)	$[\mathbf{1j}]_0$ (M)	k_{obs} (s^{-1})
2.50×10^{-4}	2.50×10^{-3}	1.28×10^{-2}
2.50×10^{-4}	3.75×10^{-3}	1.94×10^{-2}
2.50×10^{-4}	5.00×10^{-3}	2.46×10^{-2}
2.50×10^{-4}	6.25×10^{-3}	2.90×10^{-2}

$k_2 = 4.30 \times 10^{0}$ M^{-1} s^{-1}

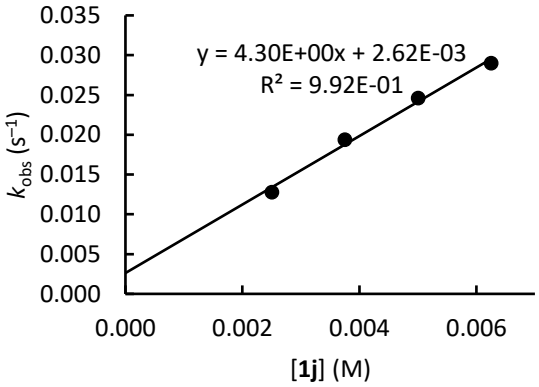

1j + potassium thiophenolate (**2c**) in DMSO (stopped flow, detection at 310 nm)

$[\mathbf{2c}]_0$ (M)	$[\mathbf{1j}]_0$ (M)	k_{obs} (s^{-1})
2.50×10^{-4}	2.50×10^{-3}	2.56×10^{-2}
2.50×10^{-4}	3.75×10^{-3}	3.72×10^{-2}
2.50×10^{-4}	5.00×10^{-3}	4.77×10^{-2}
2.50×10^{-4}	6.25×10^{-3}	5.77×10^{-2}

$k_2 = 8.54 \times 10^{0}$ M^{-1} s^{-1}

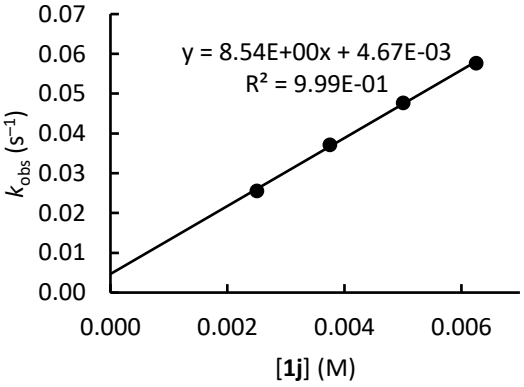

1j + potassium 4-methylthiophenolate (**2b**) in DMSO (stopped flow, detection at 300 nm)

$[\mathbf{2b}]_0$ (M)	$[\mathbf{1j}]_0$ (M)	k_{obs} (s^{-1})
2.50×10^{-4}	2.50×10^{-3}	3.45×10^{-2}
2.50×10^{-4}	3.75×10^{-3}	4.92×10^{-2}
2.50×10^{-4}	5.00×10^{-3}	6.25×10^{-2}
2.50×10^{-4}	6.25×10^{-3}	7.72×10^{-2}

$k_2 = 1.13 \times 10^{1}$ M^{-1} s^{-1}

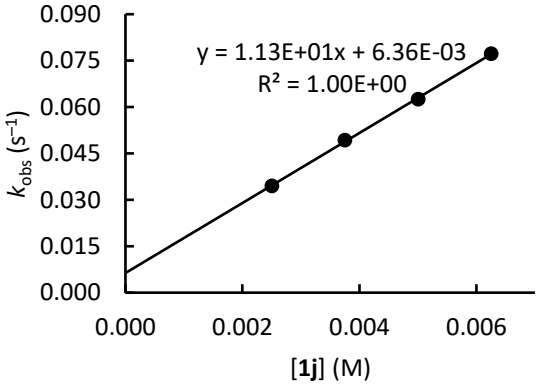

1j + potassium 4-methoxythiophenolate (**2a**) in DMSO (stopped flow, detection at 300 nm)

$[\mathbf{2a}]_0$ (M)	$[\mathbf{1j}]_0$ (M)	k_{obs} (s^{-1})
2.50×10^{-4}	2.50×10^{-3}	4.99×10^{-2}
2.50×10^{-4}	3.75×10^{-3}	7.33×10^{-2}
2.50×10^{-4}	5.00×10^{-3}	9.54×10^{-2}
2.50×10^{-4}	6.25×10^{-3}	1.15×10^{-1}

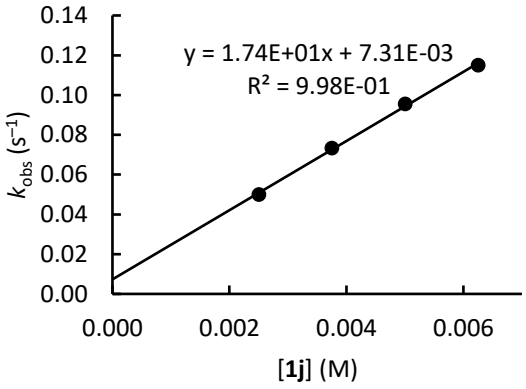

$k_2 = 1.74 \times 10^1\ M^{-1}\ s^{-1}$

Determination of E and s_E parameters for **1j** in DMSO.

Reference Nucleophile	Nucleophilicity N (s_N)	k_2 ($M^{-1}\ s^{-1}$)	log k_2/s_N
4-Br (**2d**)	22.81 (0.78)	4.30×10^0	0.81
4-H (**2c**)	23.36 (0.74)	8.54×10^0	1.26
4-Me (**2b**)	24.35 (0.69)	1.13×10^1	1.53
4-MeO (**2a**)	24.97 (0.67)	1.74×10^1	1.85

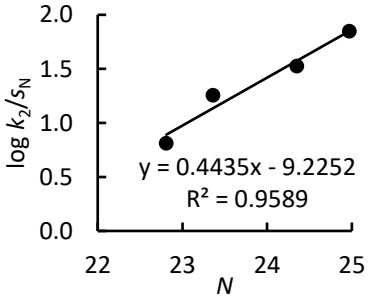

***E* = –20.80**

s_E = 0.44

Kinetics of reactions of 6,6-dimethyl-5,7-dioxaspiro[2.5]octane-4,8-dione (1a) in acetonitrile

For the reactions with pyridines, the appearing absorption of the zwitterionic product was followed with conventional UV-Vis spectrometry.

1a + 4-methylpyridine (**4d**) in acetonitrile (J&M, detection at 380 nm)

$[\mathbf{1a}]_0$ (M)	$[\mathbf{4d}]_0$ (M)	k_{obs} (s^{-1})
2.00×10^{-3}	2.00×10^{-1}	2.14×10^{-4}
2.00×10^{-3}	4.00×10^{-1}	4.27×10^{-4}
2.00×10^{-3}	6.00×10^{-1}	6.41×10^{-4}
2.00×10^{-3}	8.00×10^{-1}	8.50×10^{-4}

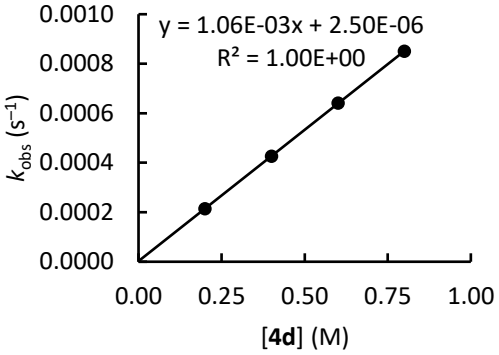

$k_2 = 1.06 \times 10^{-3}\ M^{-1}\ s^{-1}$

1a + 4-methoxypyridine (**4c**) in acetonitrile (J&M, detection at 350 nm)

$[\mathbf{1a}]_0$ (M)	$[\mathbf{4c}]_0$ (M)	k_{obs} (s^{-1})
2.00×10^{-3}	1.00×10^{-1}	1.16×10^{-4}
2.00×10^{-3}	2.00×10^{-1}	2.37×10^{-4}
2.00×10^{-3}	3.00×10^{-1}	3.55×10^{-4}
2.00×10^{-3}	4.00×10^{-1}	4.33×10^{-4}

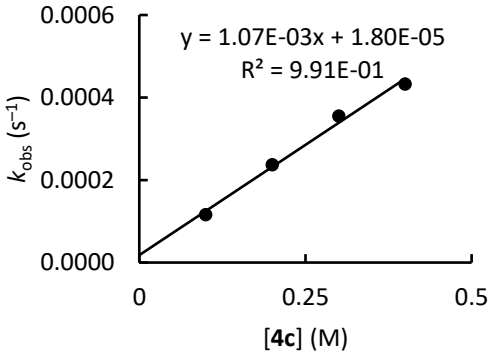

$k_2 = 1.07 \times 10^{-3}\ M^{-1}\ s^{-1}$

1a + 4-(dimethylamino)pyridine (**4b**) in acetonitrile (J&M, detection at 325 nm)

$[\mathbf{1a}]_0$ (M)	$[\mathbf{4b}]_0$ (M)	k_{obs} (s^{-1})
2.00×10^{-3}	2.00×10^{-2}	2.36×10^{-4}
2.00×10^{-3}	4.00×10^{-2}	4.81×10^{-4}
2.00×10^{-3}	6.00×10^{-2}	7.70×10^{-4}
2.00×10^{-3}	8.00×10^{-2}	1.05×10^{-3}

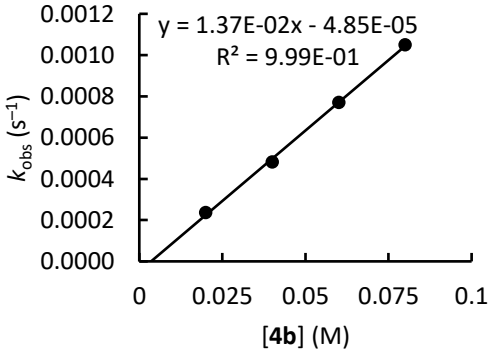

$k_2 = 1.37 \times 10^{-2}$ M^{-1} s^{-1}

1a + 4-(pyrrolidin-1-yl)pyridine (**4a**) in acetonitrile (J&M, detection at 325 nm)

[1a]$_0$, (M)	**[4a]**$_0$ (M)	k_{obs} (s^{-1})
2.00×10^{-3}	2.00×10^{-2}	3.30×10^{-4}
2.00×10^{-3}	4.00×10^{-2}	6.79×10^{-4}
2.00×10^{-3}	6.00×10^{-2}	1.03×10^{-3}
2.00×10^{-3}	8.00×10^{-2}	1.36×10^{-3}

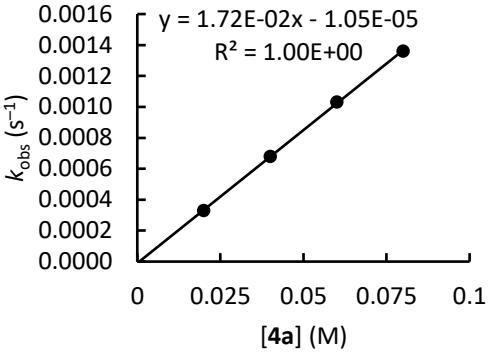

$k_2 = 1.72 \times 10^{-2}$ M^{-1} s^{-1}

Determination of E and s_E parameters for **1a** in acetonitrile.

Reference Nucleophile	Nucleophilicity N (s_N) [a]	k_2 (M^{-1} s^{-1})	log k_2/s_N
4-H [b]	12.9 (0.67)	5.57×10^{-4} [b]	-4.86
4-Me (**4d**)	13.7 (0.67)	1.06×10^{-3}	-4.44
4-OMe (**4c**)	13.7 (0.67)	1.07×10^{-3}	-4.43
4-NMe_2 (**4b**)	15.8 (0.66)	1.37×10^{-2}	-2.82
4-pyrrolidinyl (**4a**)	15.9 (0.67)	1.72×10^{-2}	-2.63

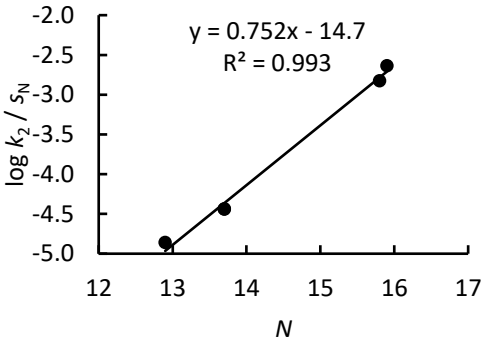

a N and s_N parameters acquired in dichloromethane have been used, in lieu of parameters in acetonitrile.

b derived from the activation parameters published by McKinney *et al*.[8]

***E* = –19.5**

s_E = 0.75

3.5.4 Copies of NMR Spectra

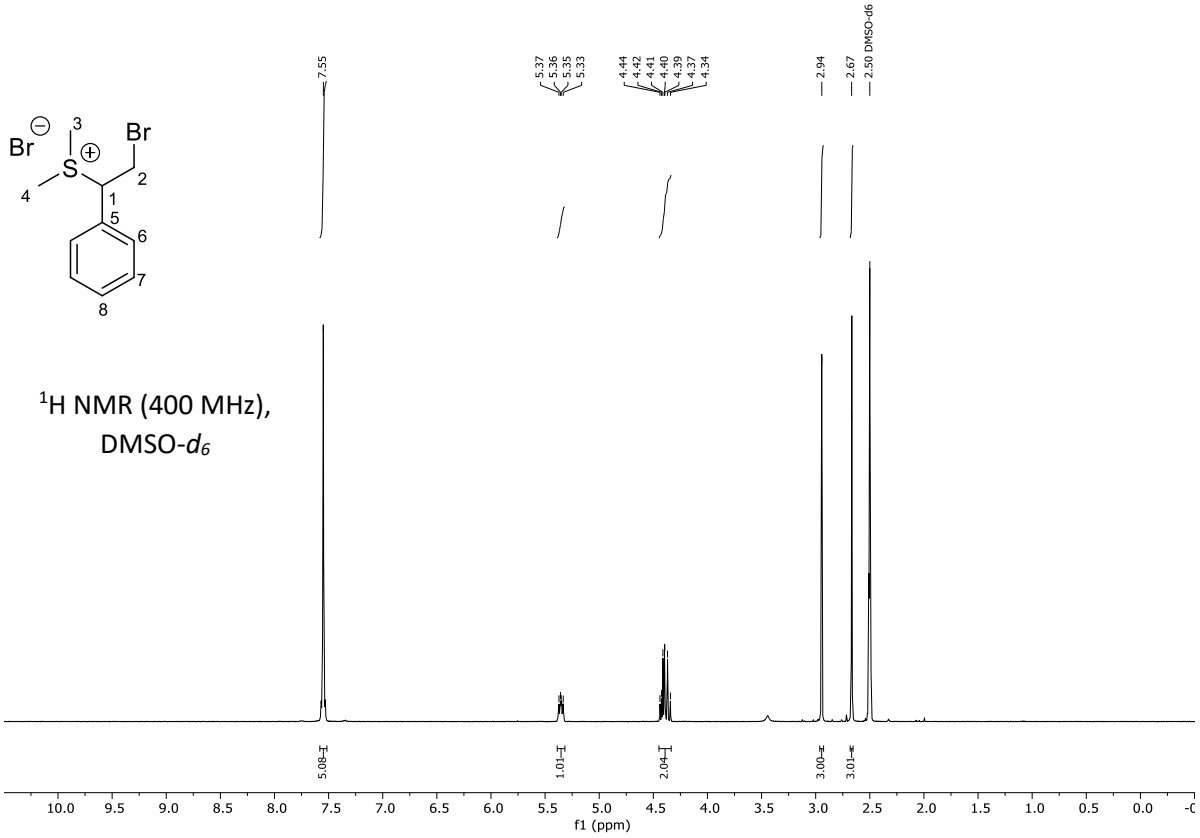

^{1}H NMR (400 MHz), DMSO-d_6

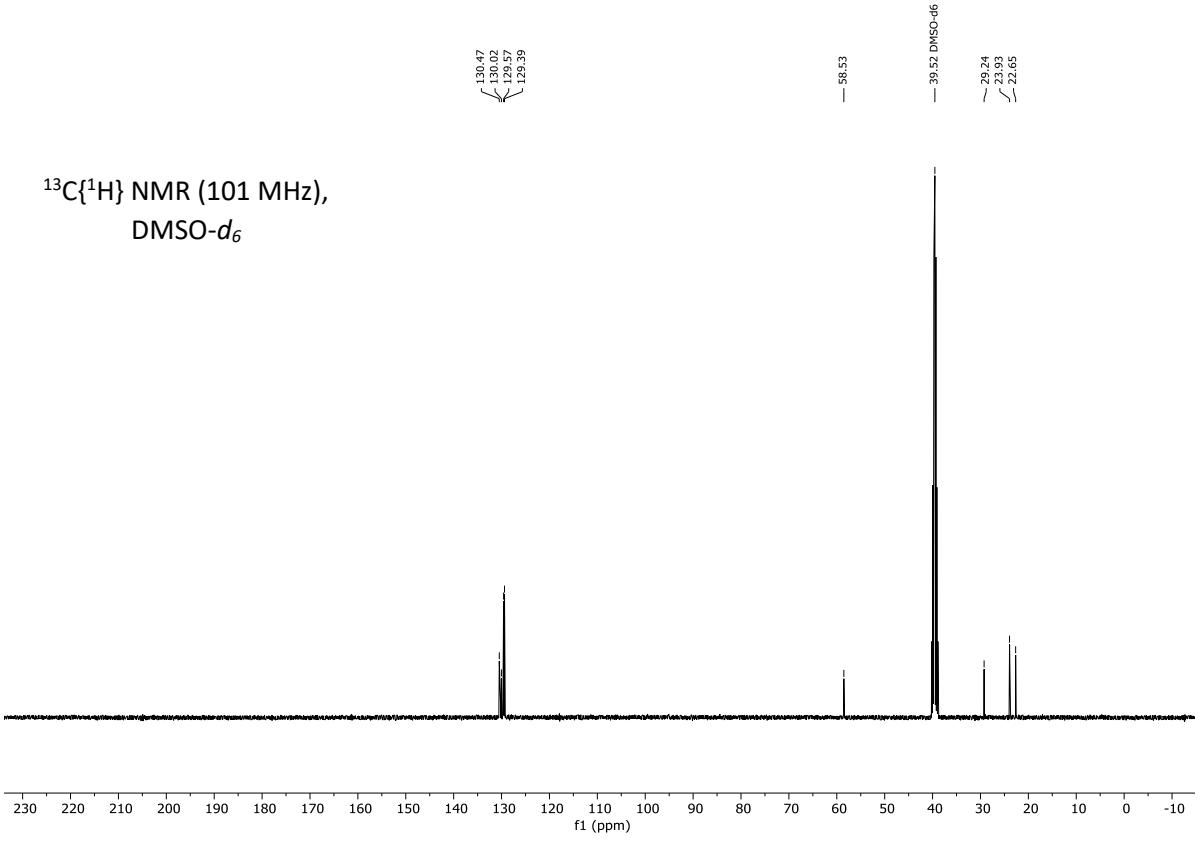

^{13}C{^{1}H} NMR (101 MHz), DMSO-d_6

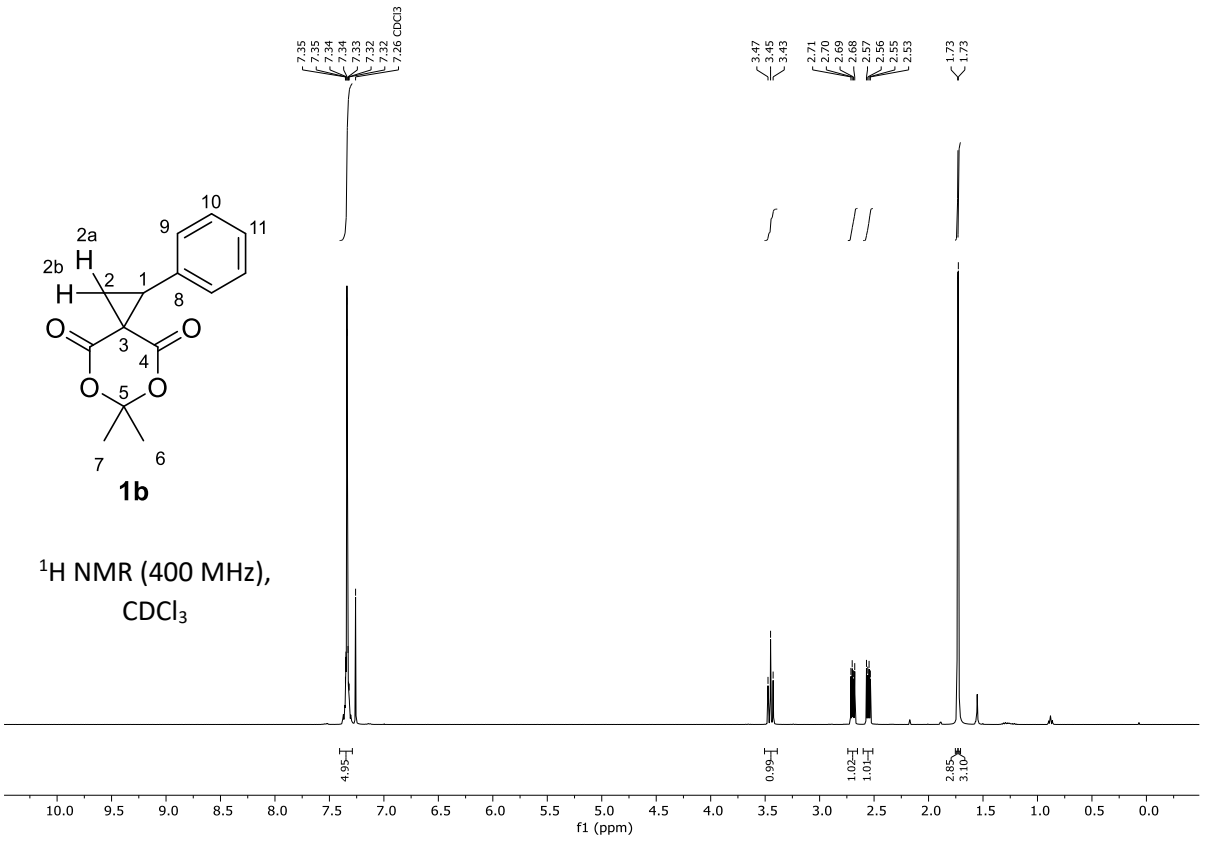
7.35
7.35
7.34
7.34
7.33
7.32
7.32
7.26 CDCl3
3.47
3.45
3.43
2.71
2.70
2.69
2.68
2.57
2.56
2.55
2.53
1.73
1.73
2a
2b
H
H
1
2
3
4
5
6
7
8
9
10
11
O
O
O
O
1b
1H NMR (400 MHz),
CDCl3
4.95
0.99
1.02
1.01
2.85
3.10
10.0
9.5
9.0
8.5
8.0
7.5
7.0
6.5
6.0
5.5
5.0
4.5
4.0
3.5
3.0
2.5
2.0
1.5
1.0
0.5
0.0
f1 (ppm)

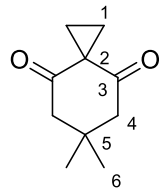

1c

^{1}H NMR (400 MHz), $CDCl_3$

^{13}C{^{1}H} NMR (101 MHz), $CDCl_3$

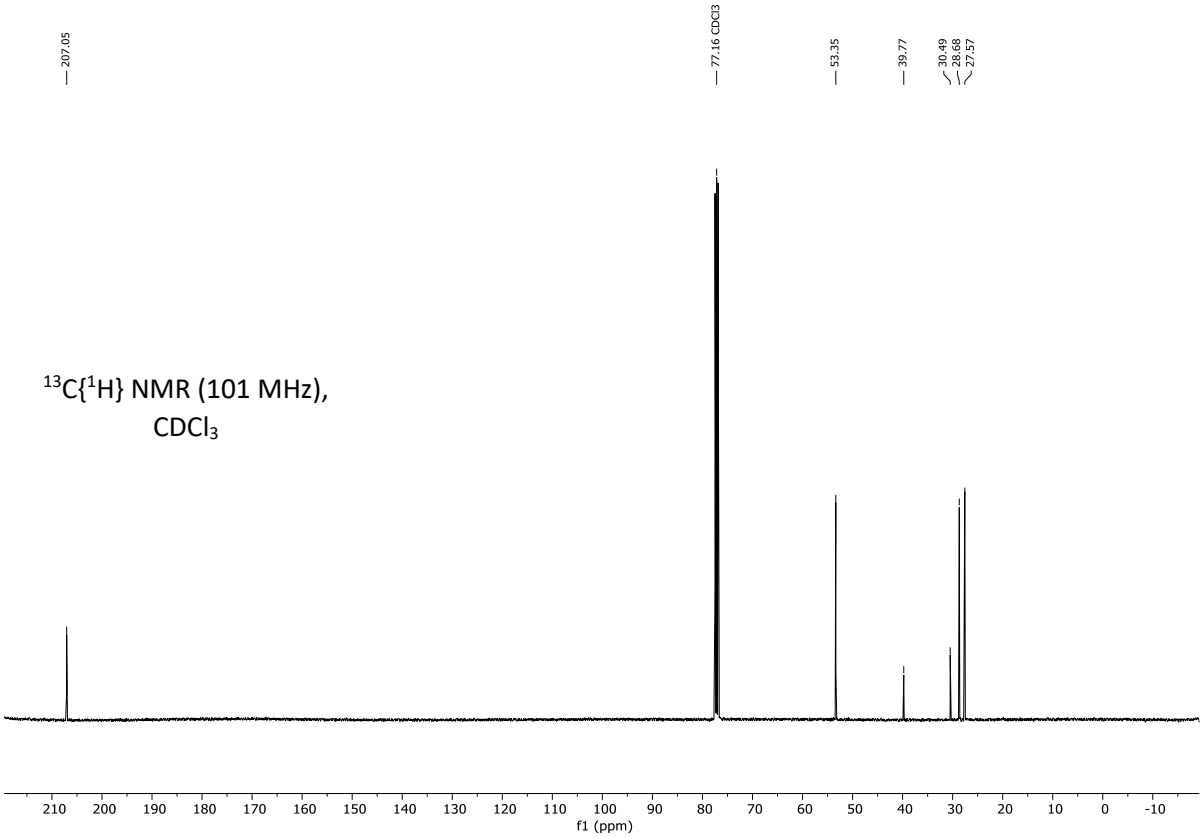

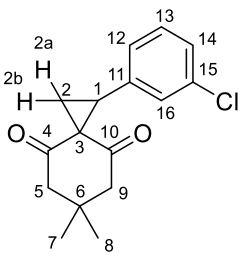

1d

^{1}H NMR (400 MHz), $CDCl_3$

^{13}C{^{1}H} NMR (101 MHz), $CDCl_3$

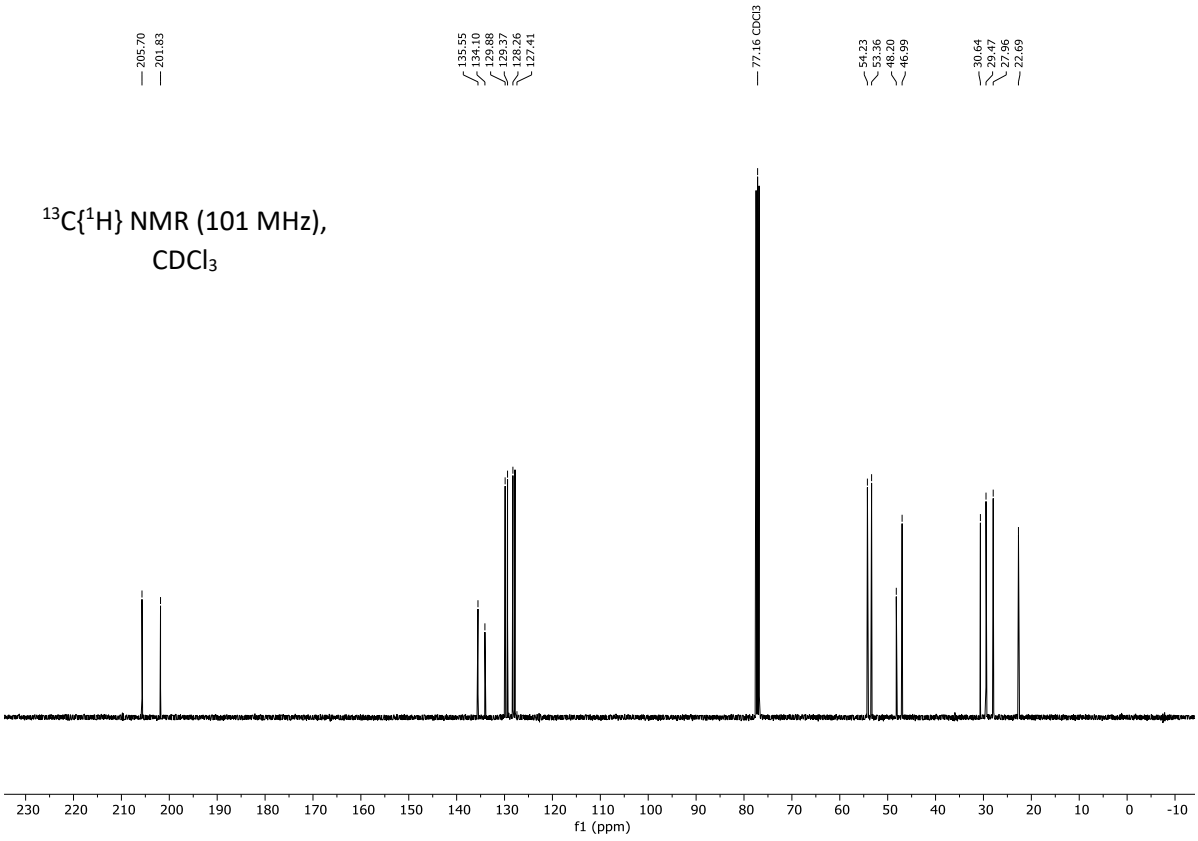

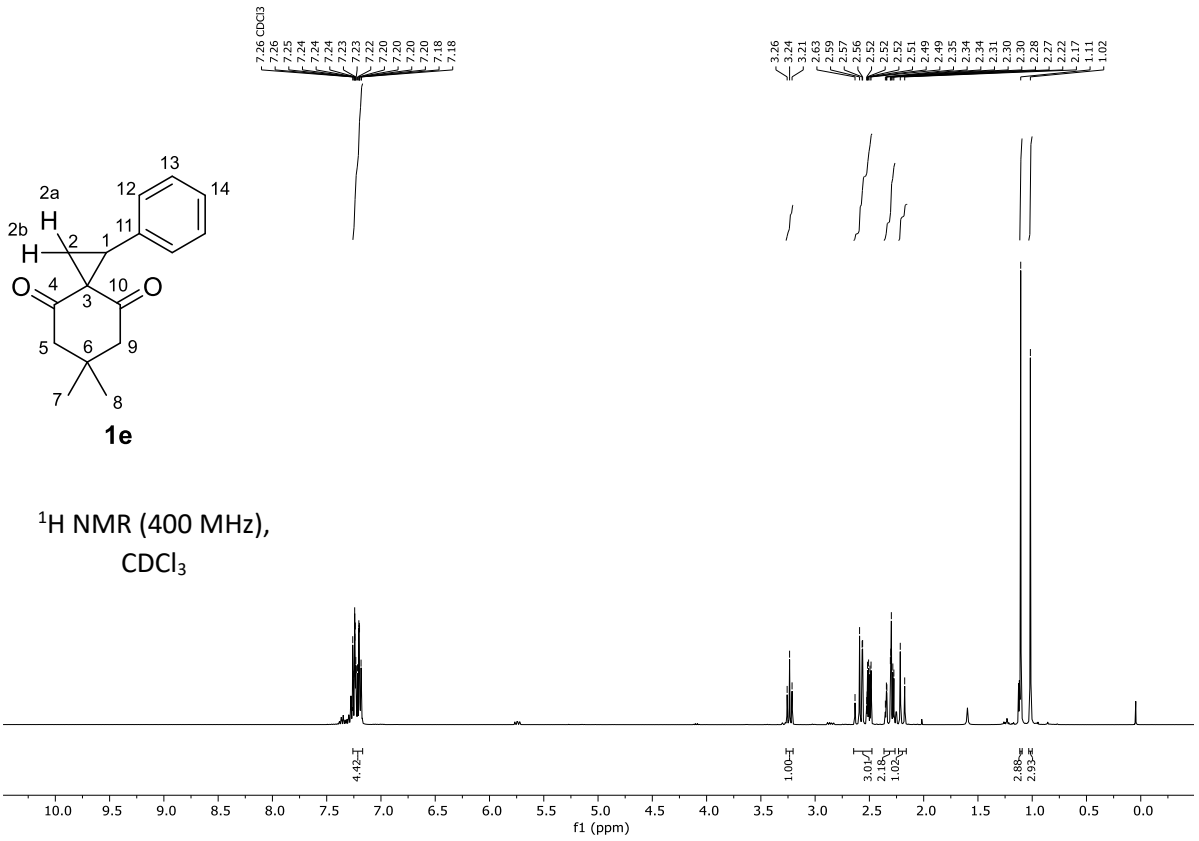

^{1}H NMR (400 MHz), $CDCl_3$

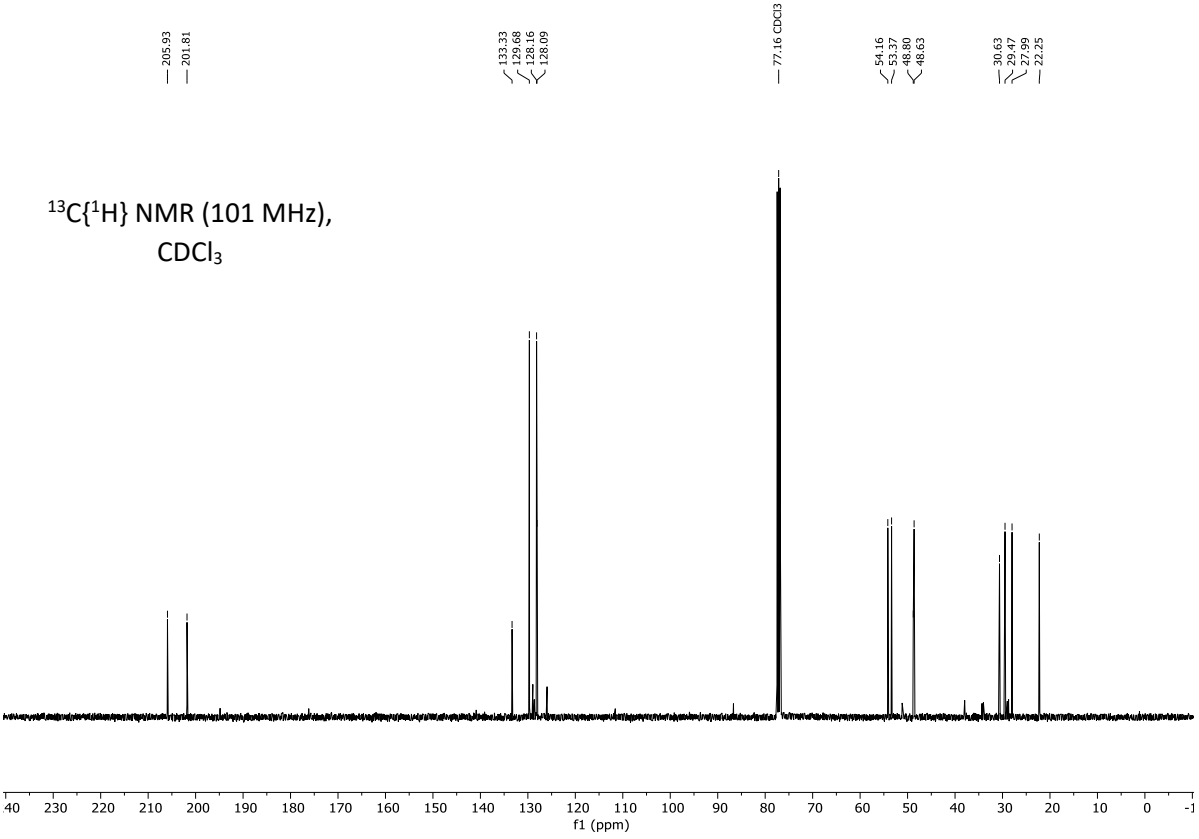

$^{13}C\{^{1}H\}$ NMR (101 MHz), $CDCl_3$

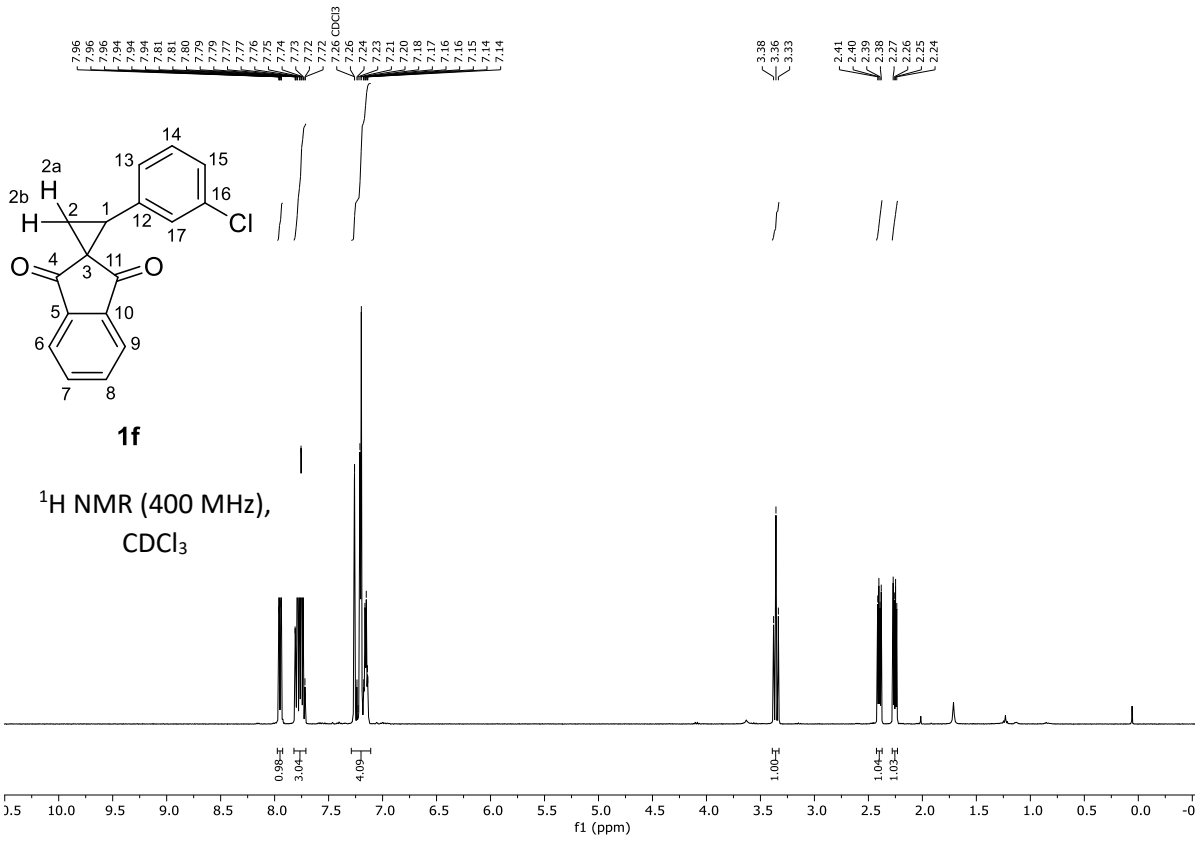
7.96
7.96
7.96
7.94
7.94
7.94
7.81
7.81
7.80
7.79
7.79
7.77
7.77
7.76
7.75
7.74
7.73
7.72
7.72
7.26 CDCl3
7.26
7.24
7.23
7.21
7.20
7.18
7.17
7.16
7.16
7.15
7.14
7.14
3.38
3.36
3.33
2.41
2.40
2.39
2.38
2.27
2.26
2.25
2.24
14
13
15
2a
2b
H
16
H
2
1
12
Cl
17
O
4
3
11
O
5
10
6
9
7
8
1f
1H NMR (400 MHz),
CDCl3
0.98
3.04
4.09
1.00
1.04
1.03
f1 (ppm)

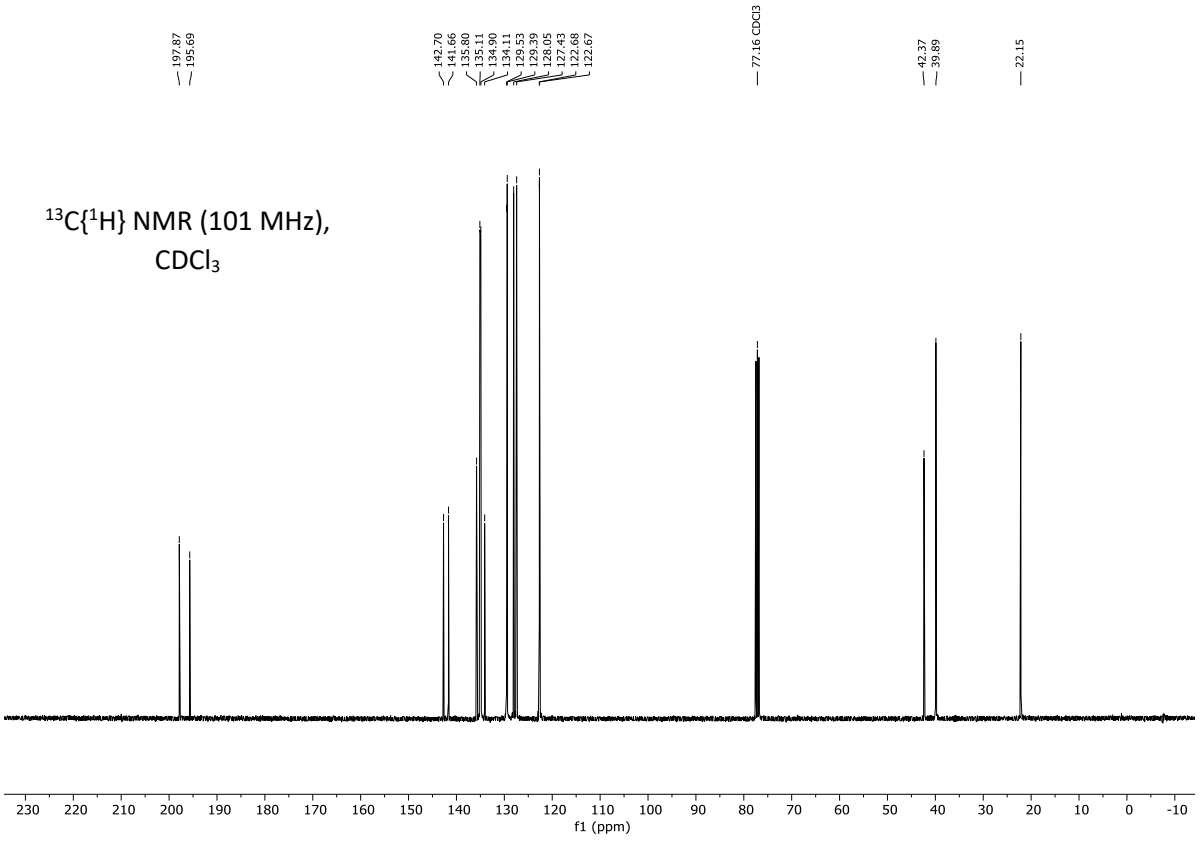
197.87
195.69
142.70
141.66
135.80
135.11
134.90
134.11
129.53
129.39
128.05
127.43
122.68
122.67
77.16 CDCl3
42.37
39.89
22.15
13C{1H} NMR (101 MHz),
CDCl3
f1 (ppm)

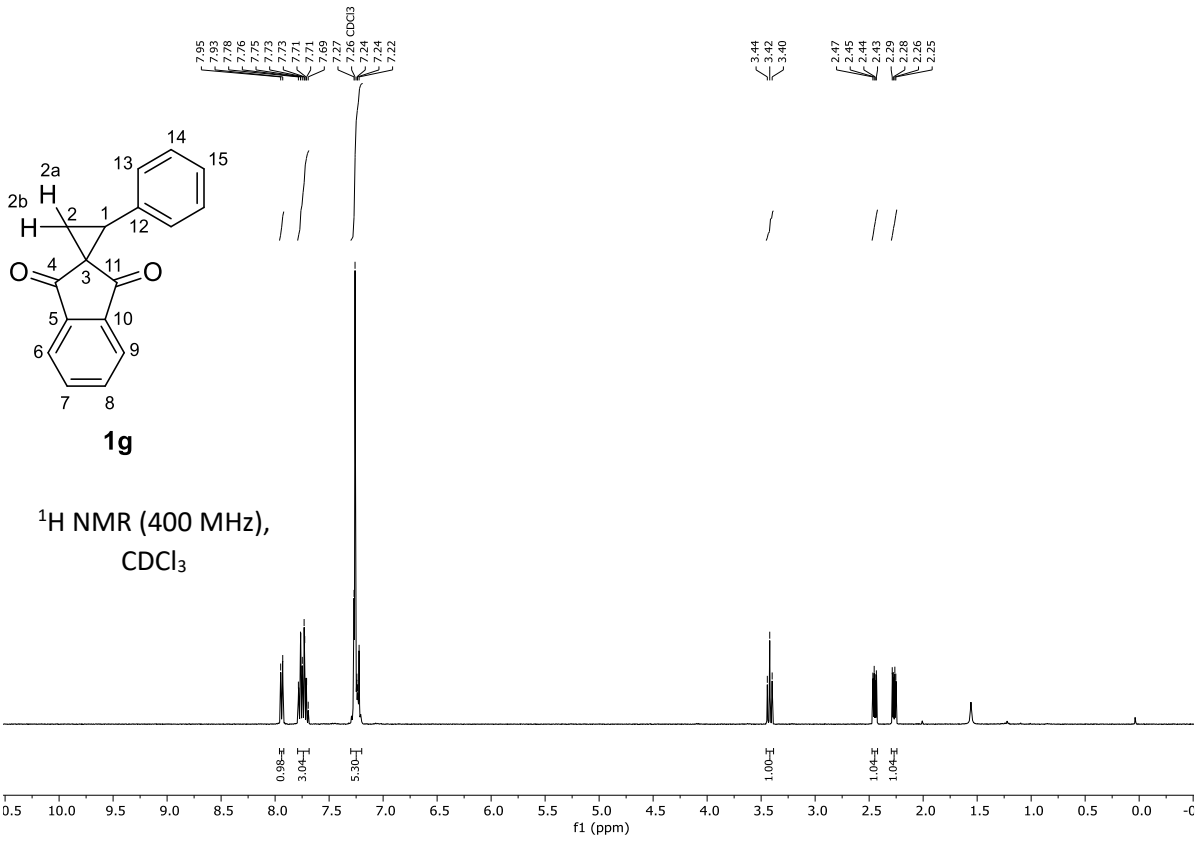

1g

^{1}H NMR (400 MHz), $CDCl_3$

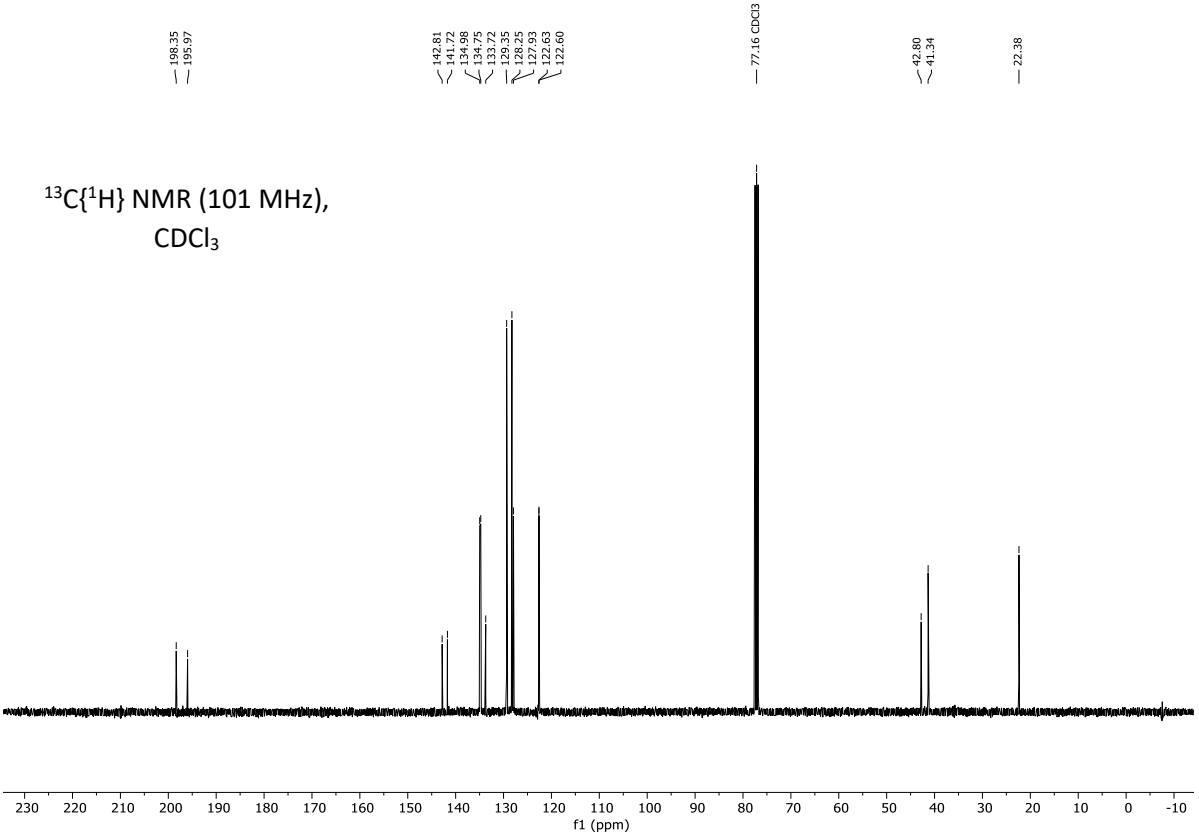

$^{13}C\{^{1}H\}$ NMR (101 MHz), $CDCl_3$

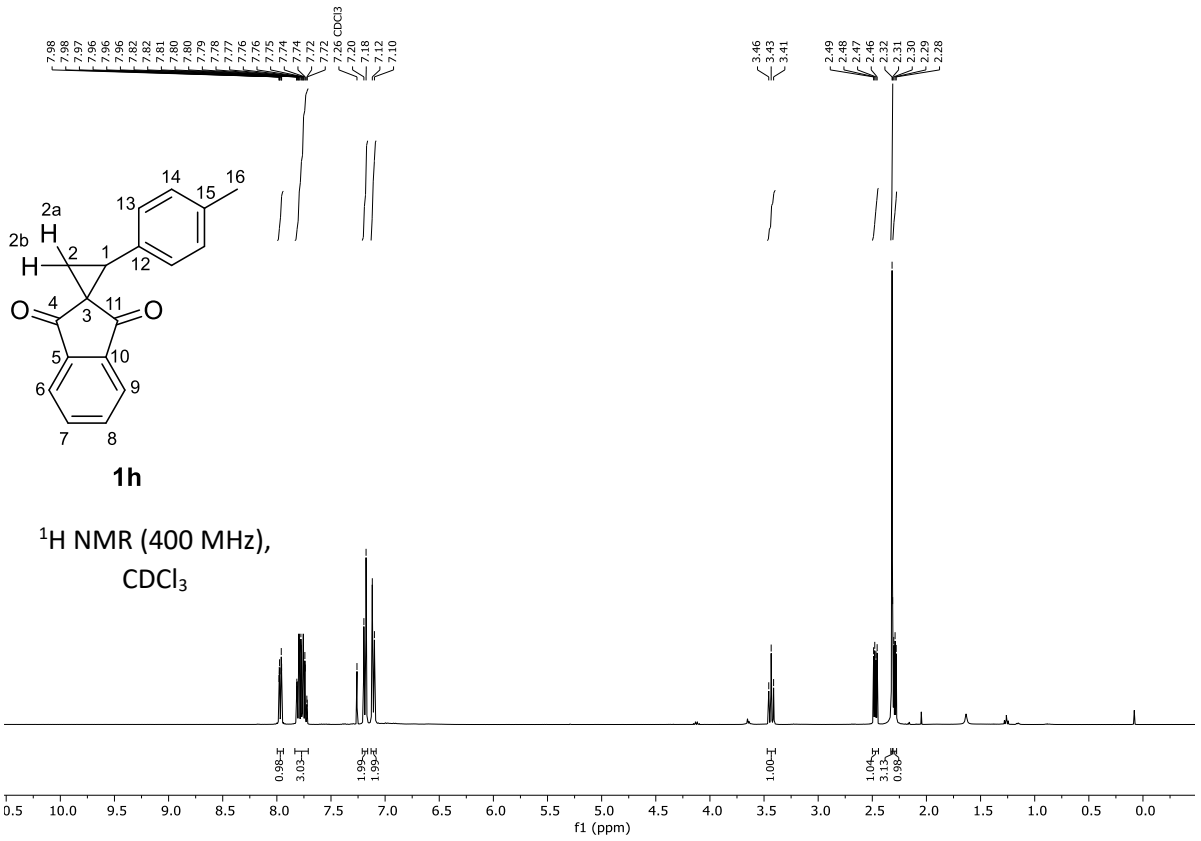
7.98
7.98
7.97
7.96
7.96
7.96
7.82
7.81
7.80
7.80
7.79
7.78
7.77
7.76
7.76
7.75
7.74
7.74
7.72
7.72
7.26 CDCl3
7.20
7.18
7.12
7.10
3.46
3.43
3.41
2.49
2.48
2.47
2.46
2.32
2.31
2.30
2.29
2.28
14
15
16
13
2a
2b
H
H
2
1
12
O
4
3
11
O
5
10
6
9
7
8
1h
1H NMR (400 MHz),
CDCl3
0.98
3.03
1.99
1.99
1.00
1.04
3.13
0.98
f1 (ppm)

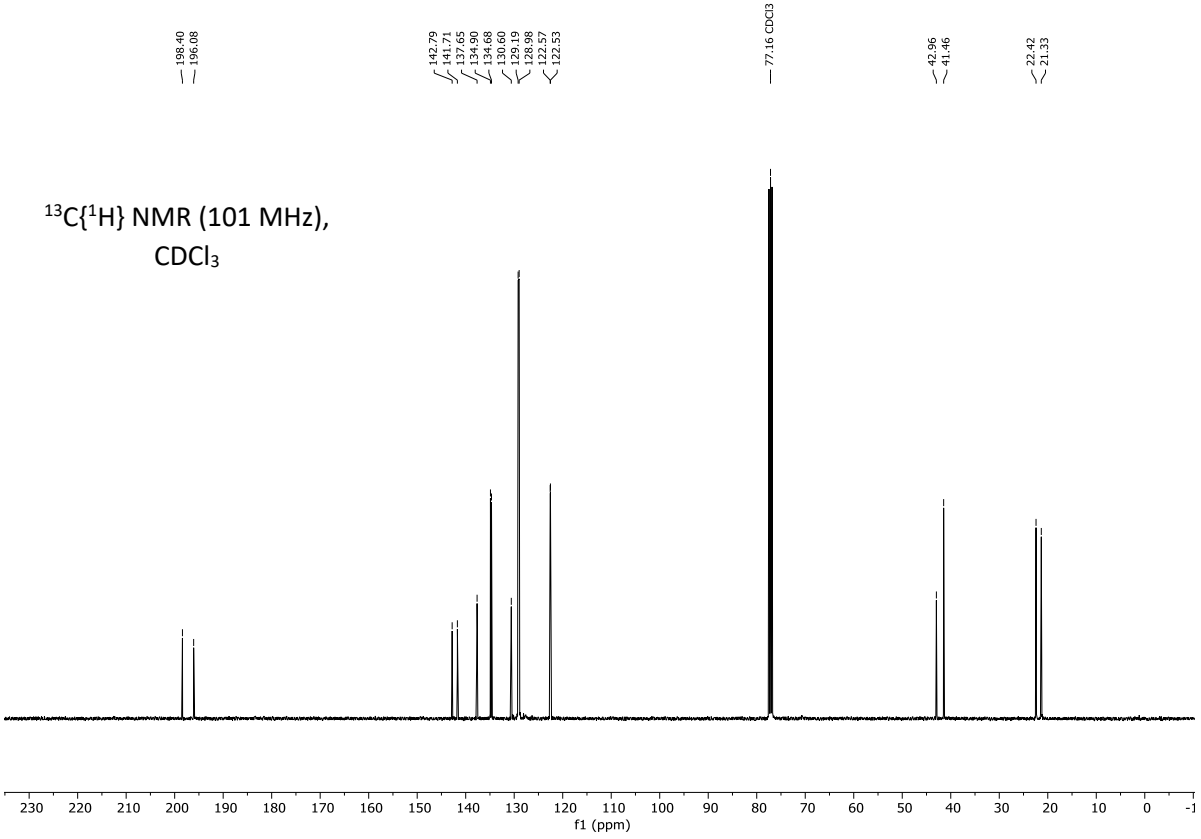
198.40
196.08
142.79
141.71
137.65
134.90
134.68
130.60
130.19
128.98
122.57
122.53
77.16 CDCl3
42.96
41.46
22.42
21.33
13C{1H} NMR (101 MHz),
CDCl3
f1 (ppm)

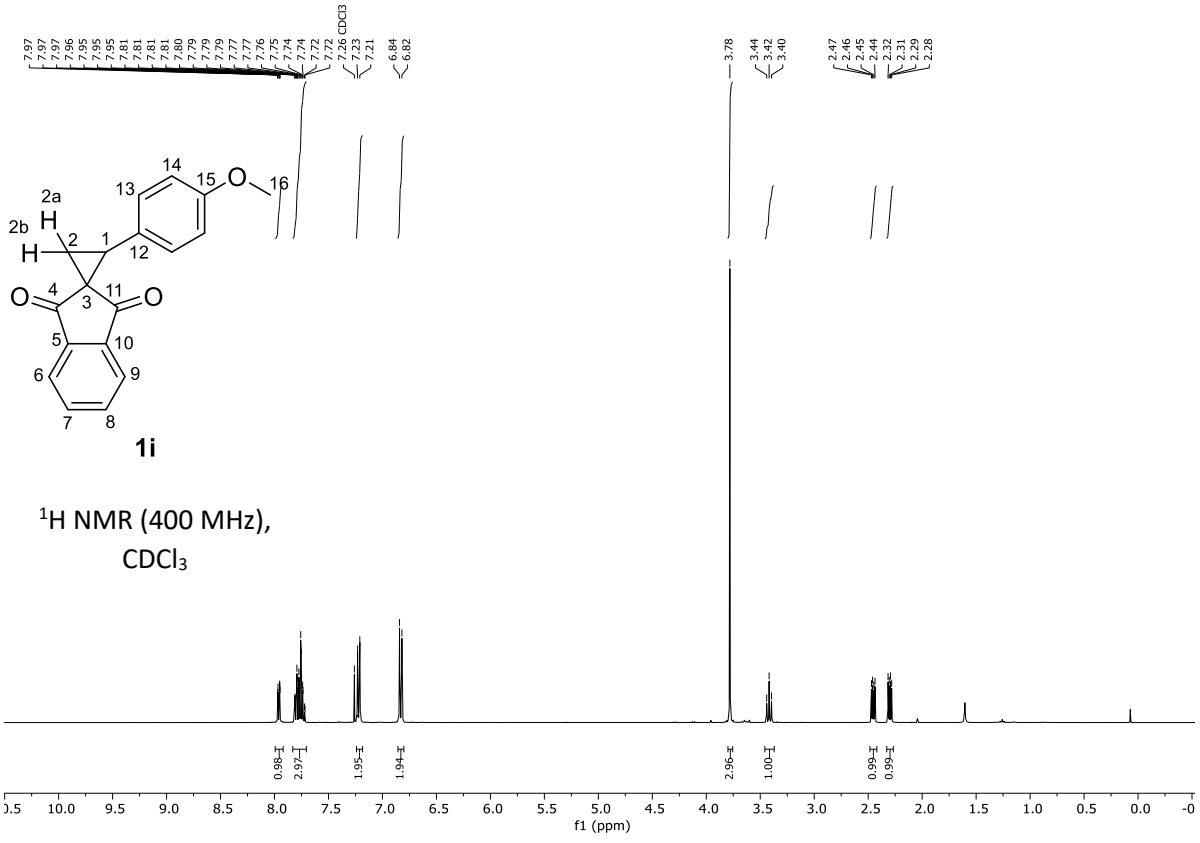

^{1}H NMR (400 MHz),
$CDCl_3$

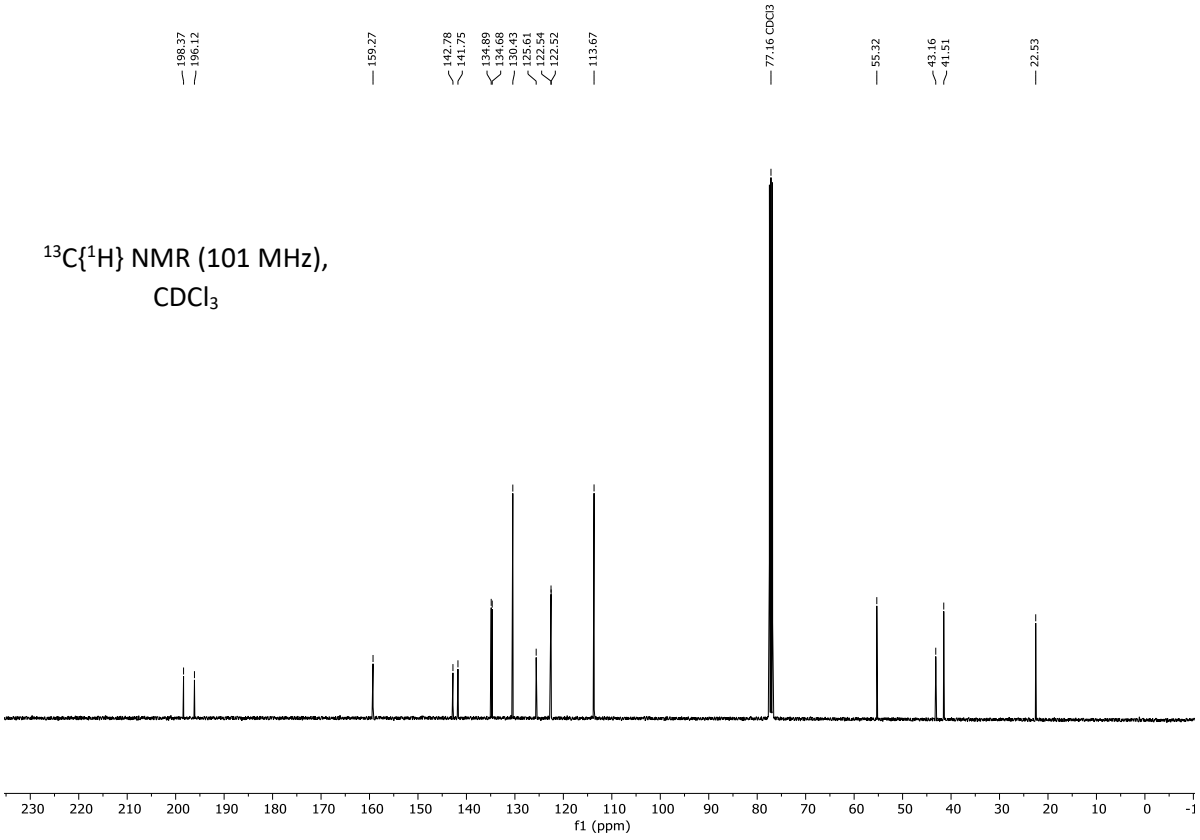

^{13}C{^{1}H} NMR (101 MHz),
$CDCl_3$

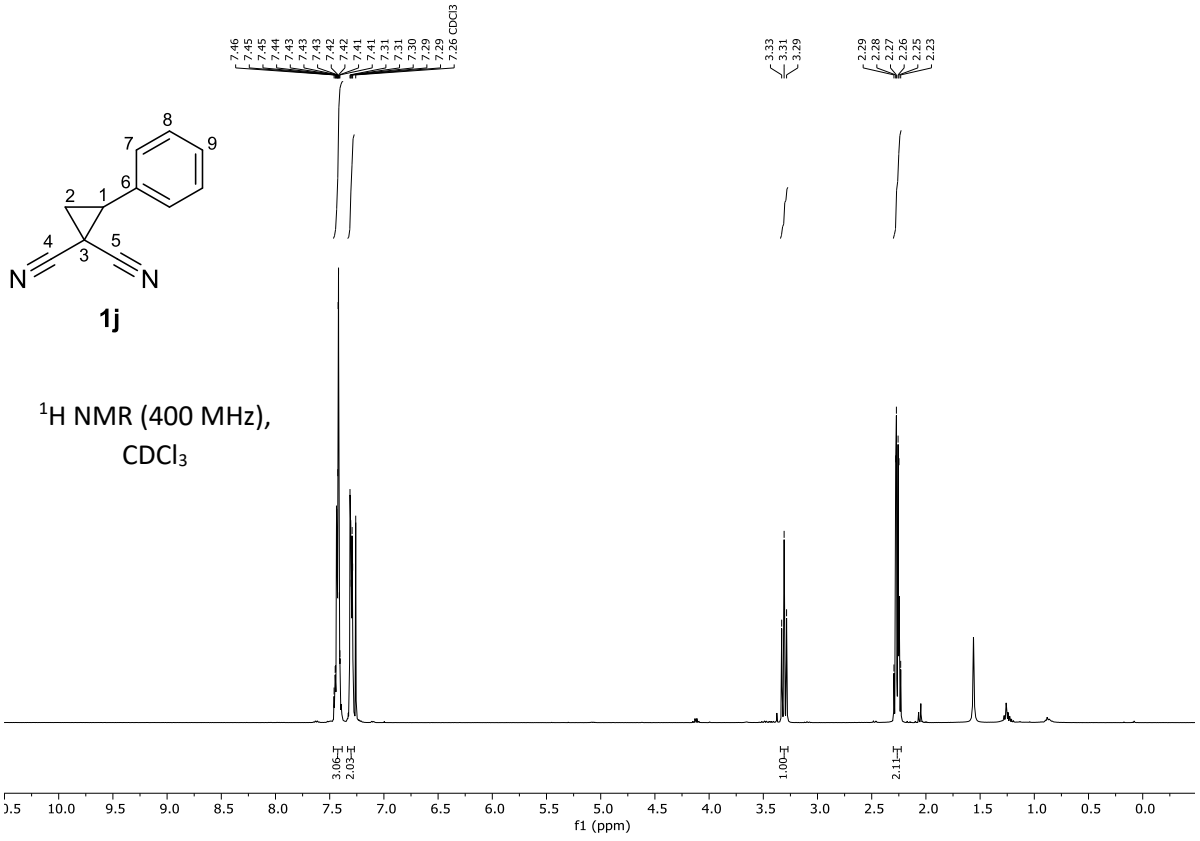

1j

^{1}H NMR (400 MHz), $CDCl_3$

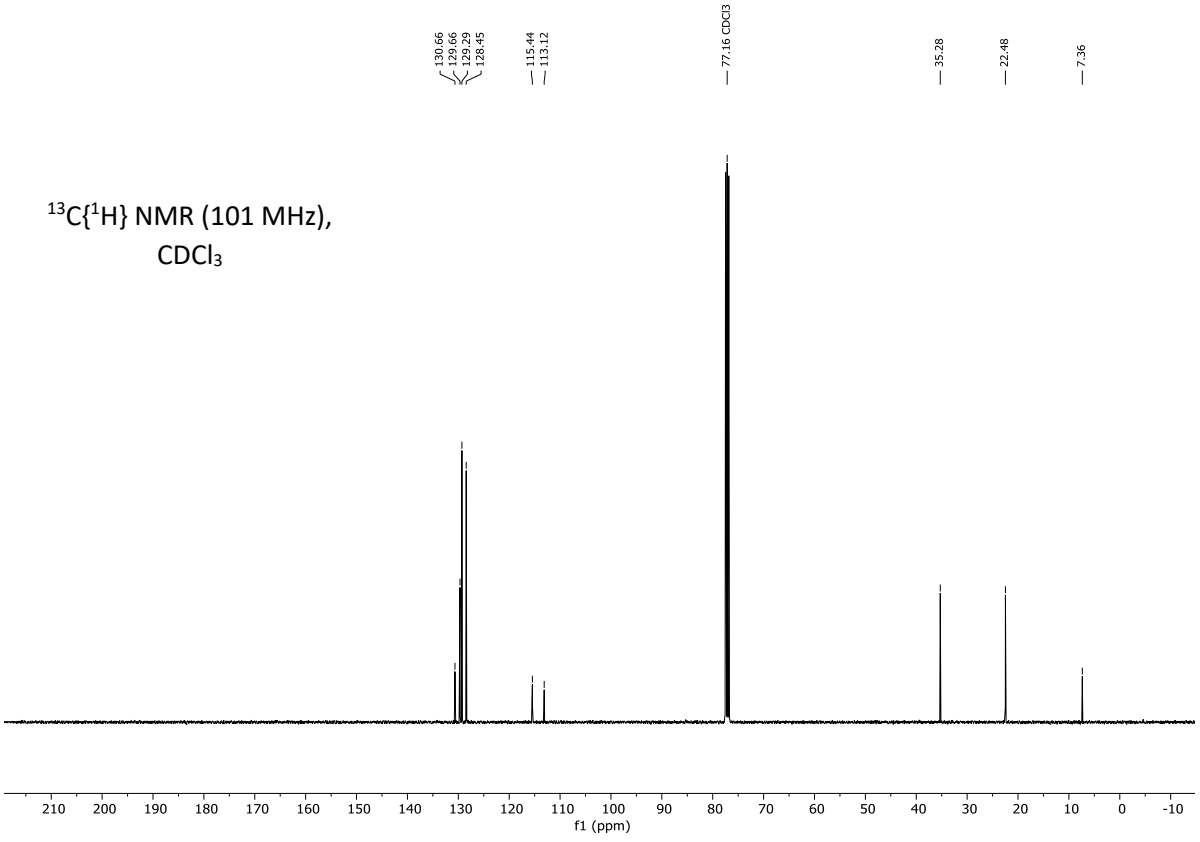

$^{13}C\{^{1}H\}$ NMR (101 MHz), $CDCl_3$

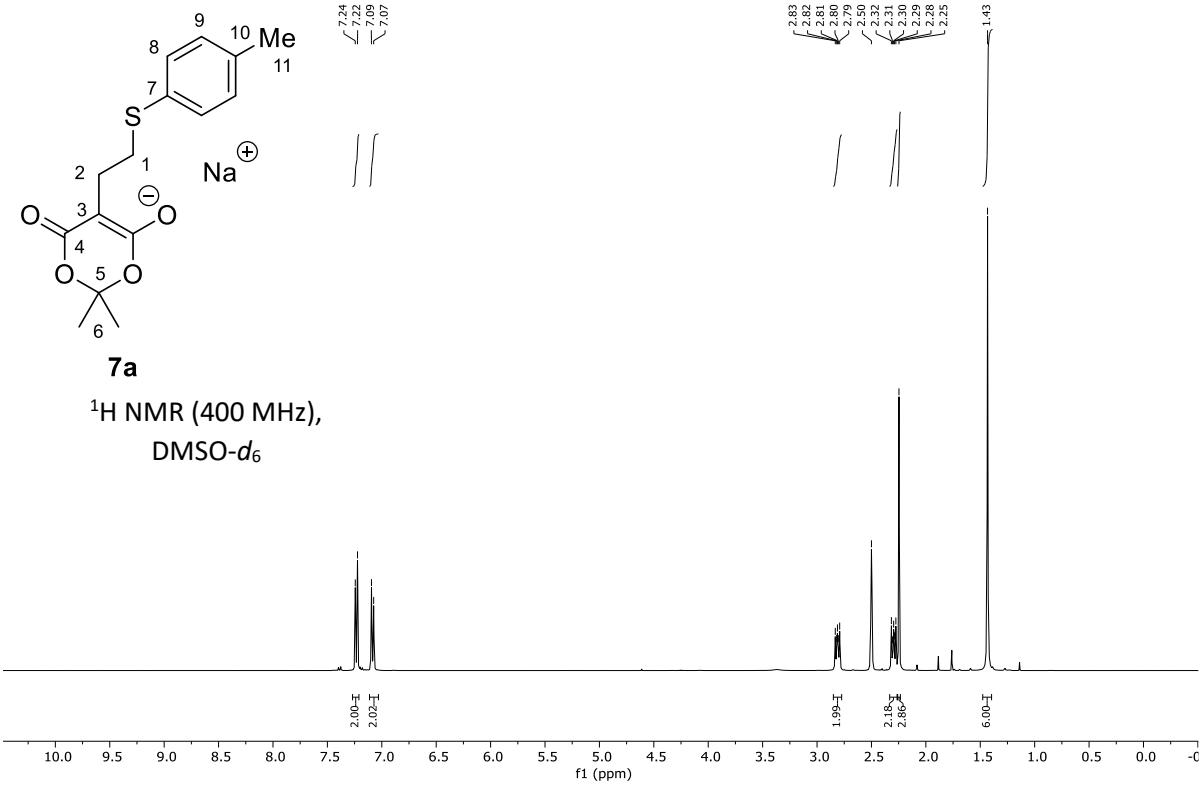

7a

^{1}H NMR (400 MHz),
DMSO-d_6

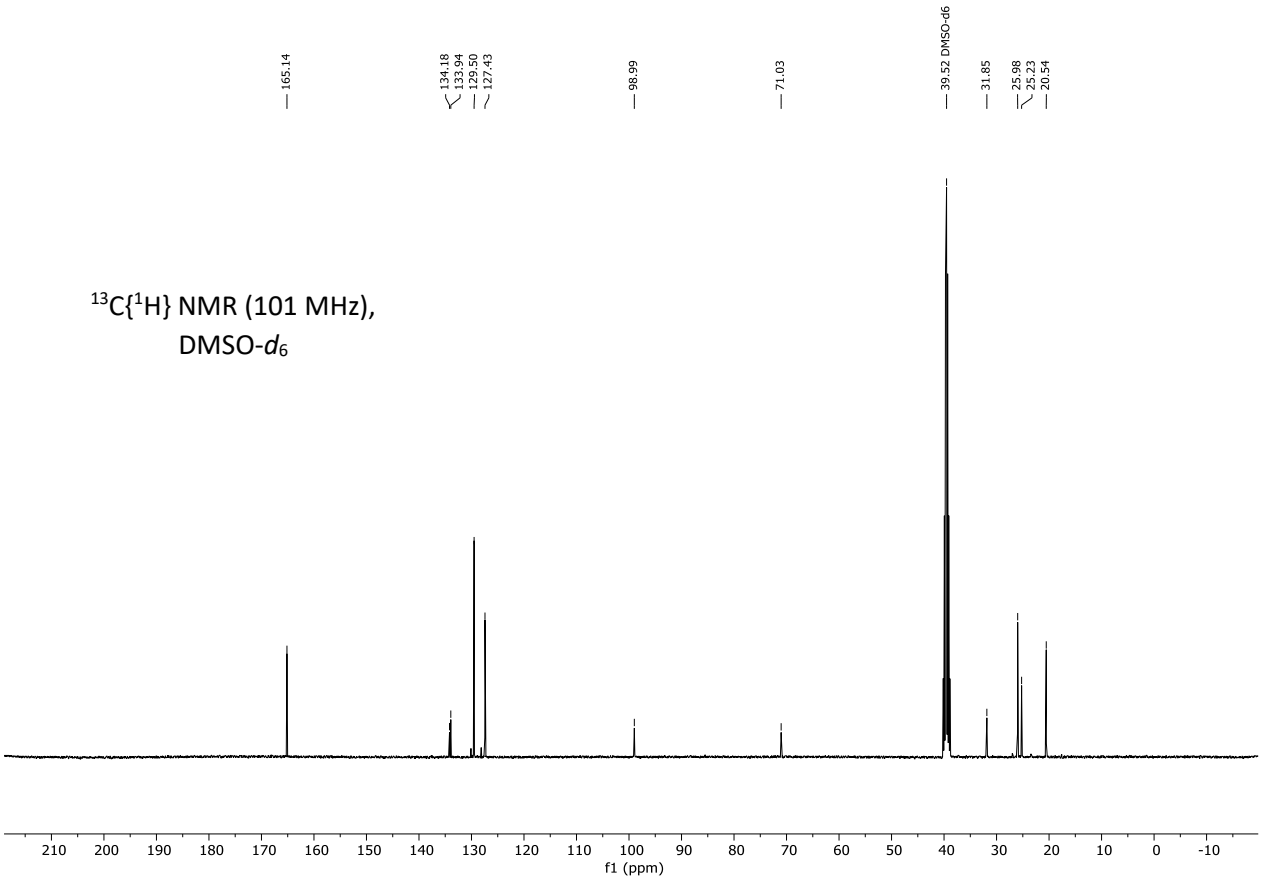

^{13}C{^{1}H} NMR (101 MHz),
DMSO-d_6

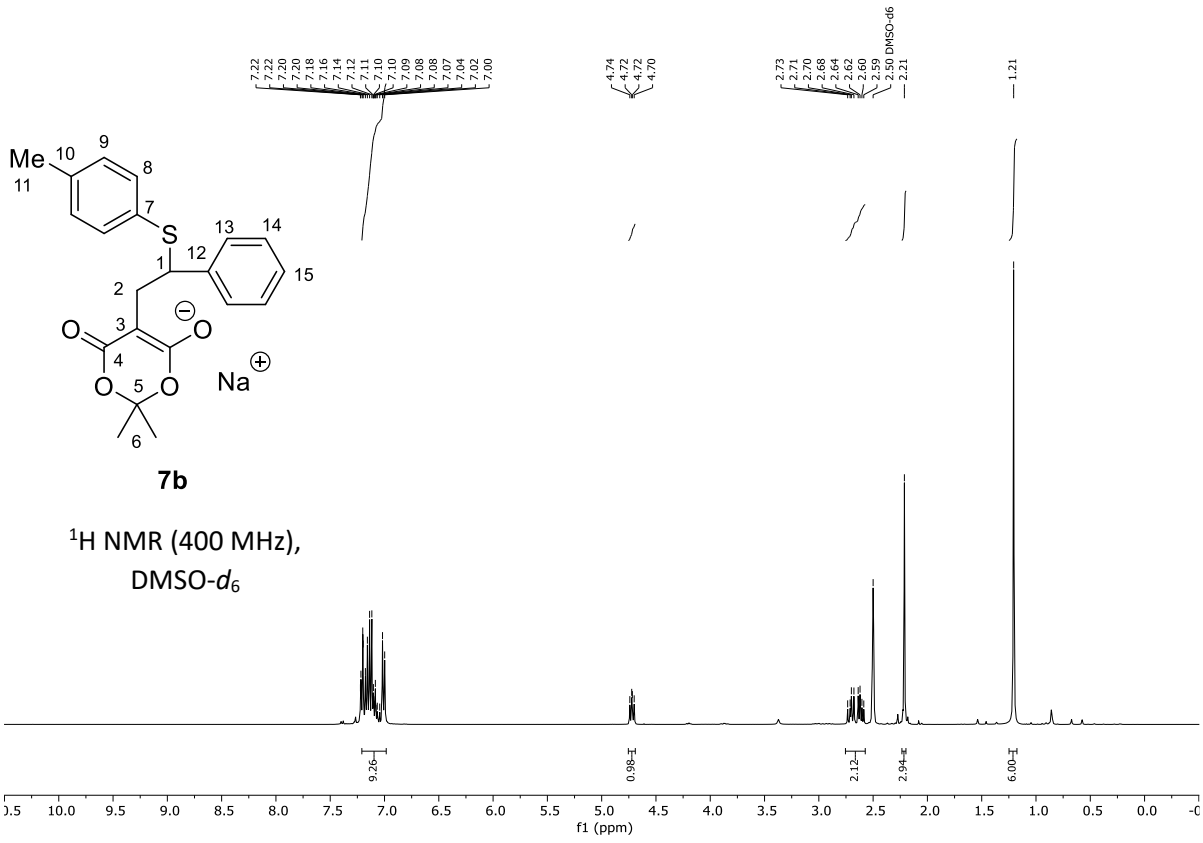

7b

^{1}H NMR (400 MHz),
DMSO-d_6

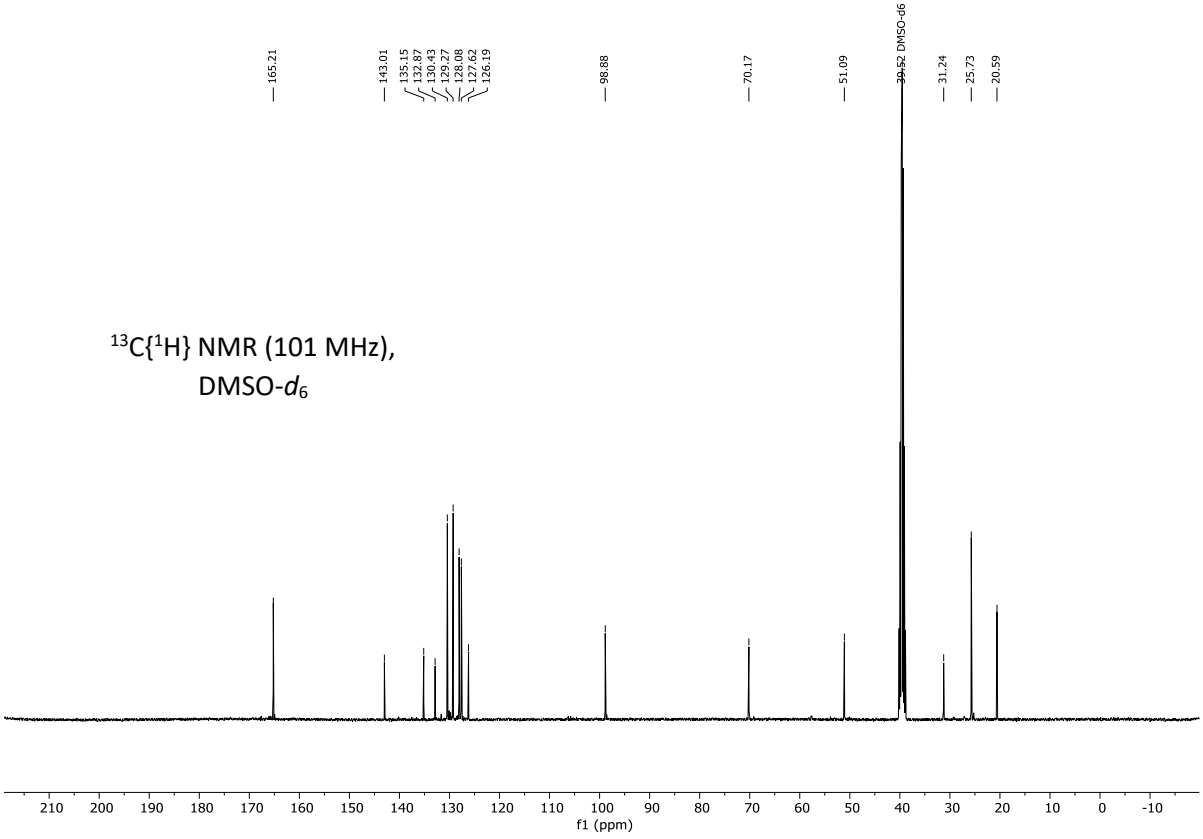

^{13}C{^{1}H} NMR (101 MHz),
DMSO-d_6

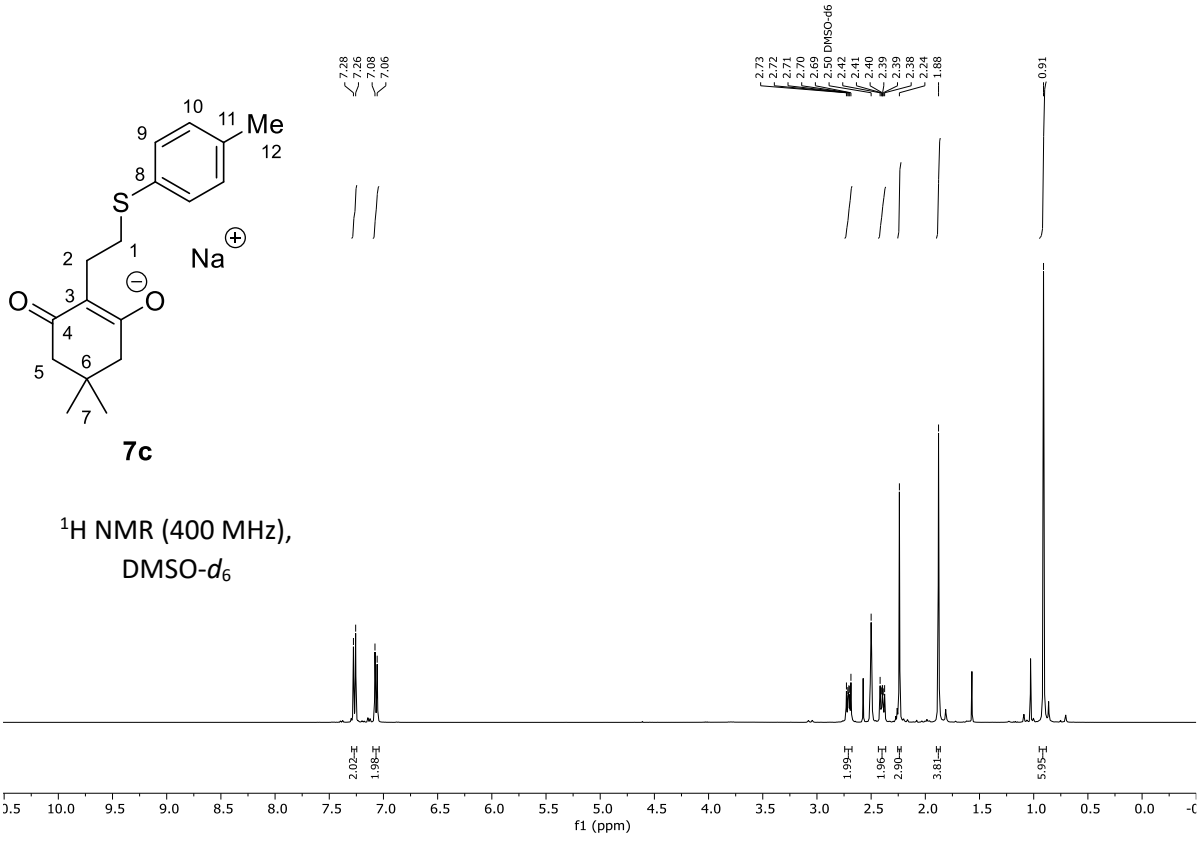

7c

^{1}H NMR (400 MHz), DMSO-d_6

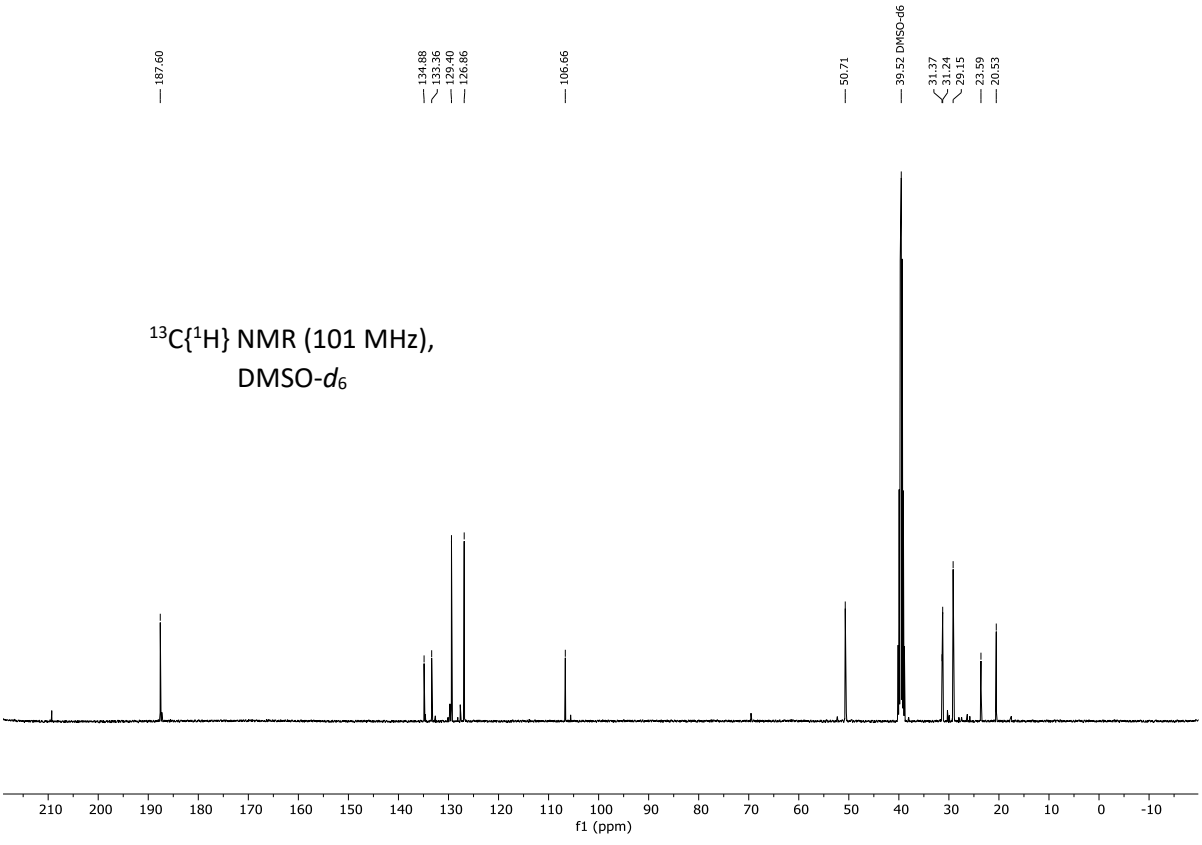

^{13}C{^{1}H} NMR (101 MHz), DMSO-d_6

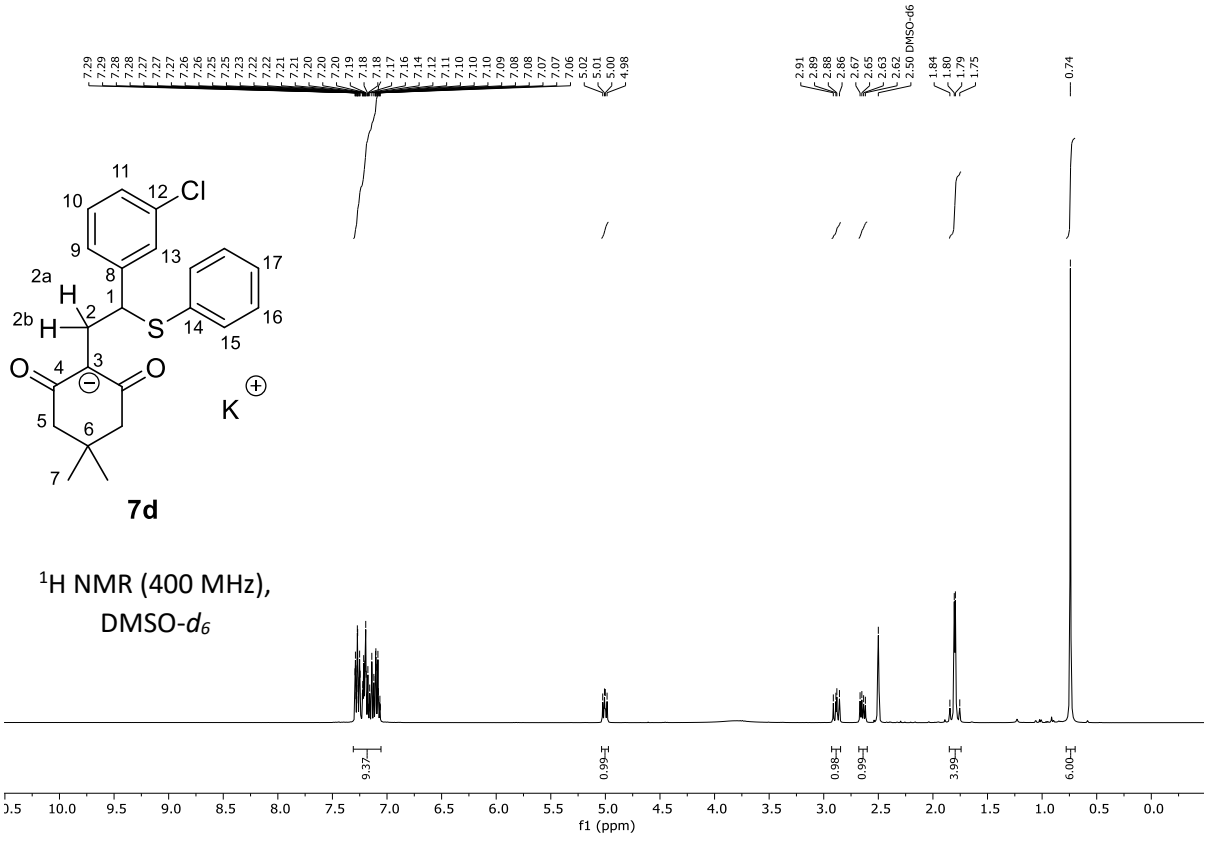

7d

^{1}H NMR (400 MHz),
DMSO-d_6

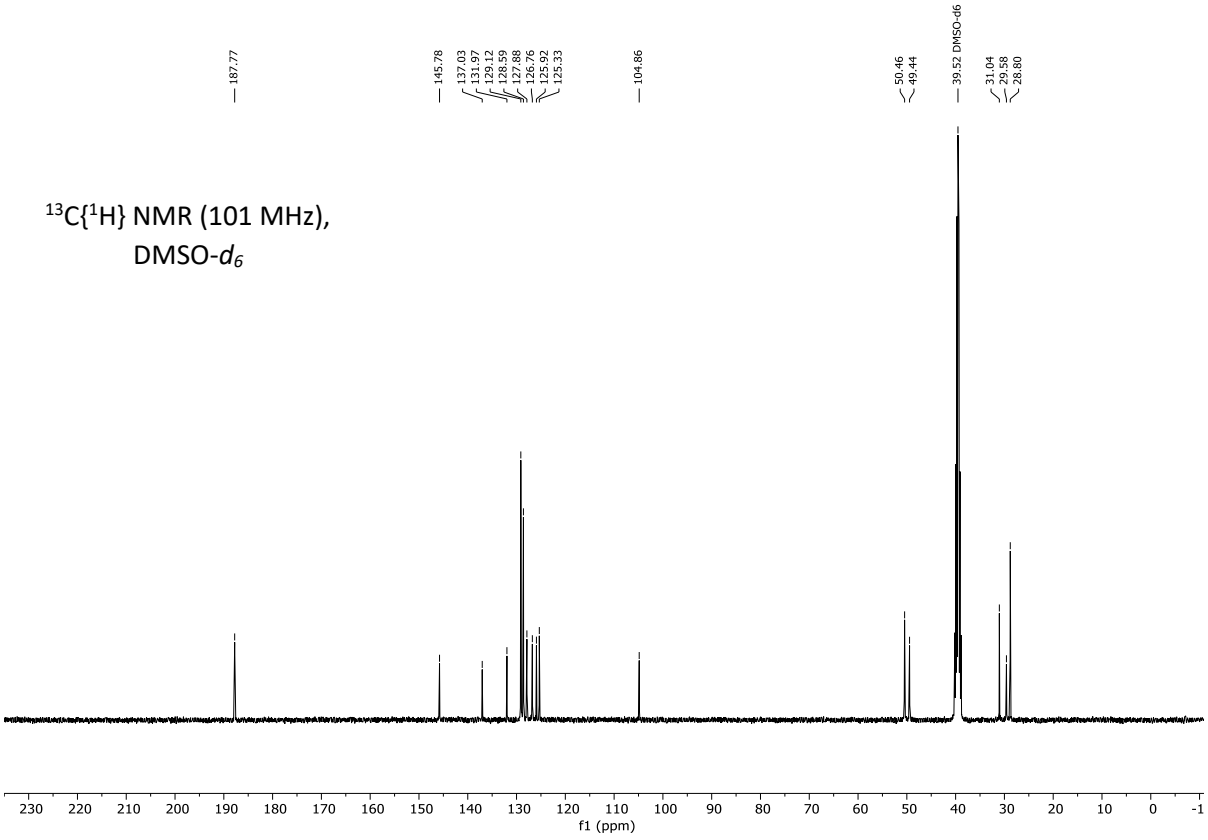

^{13}C{^{1}H} NMR (101 MHz),
DMSO-d_6

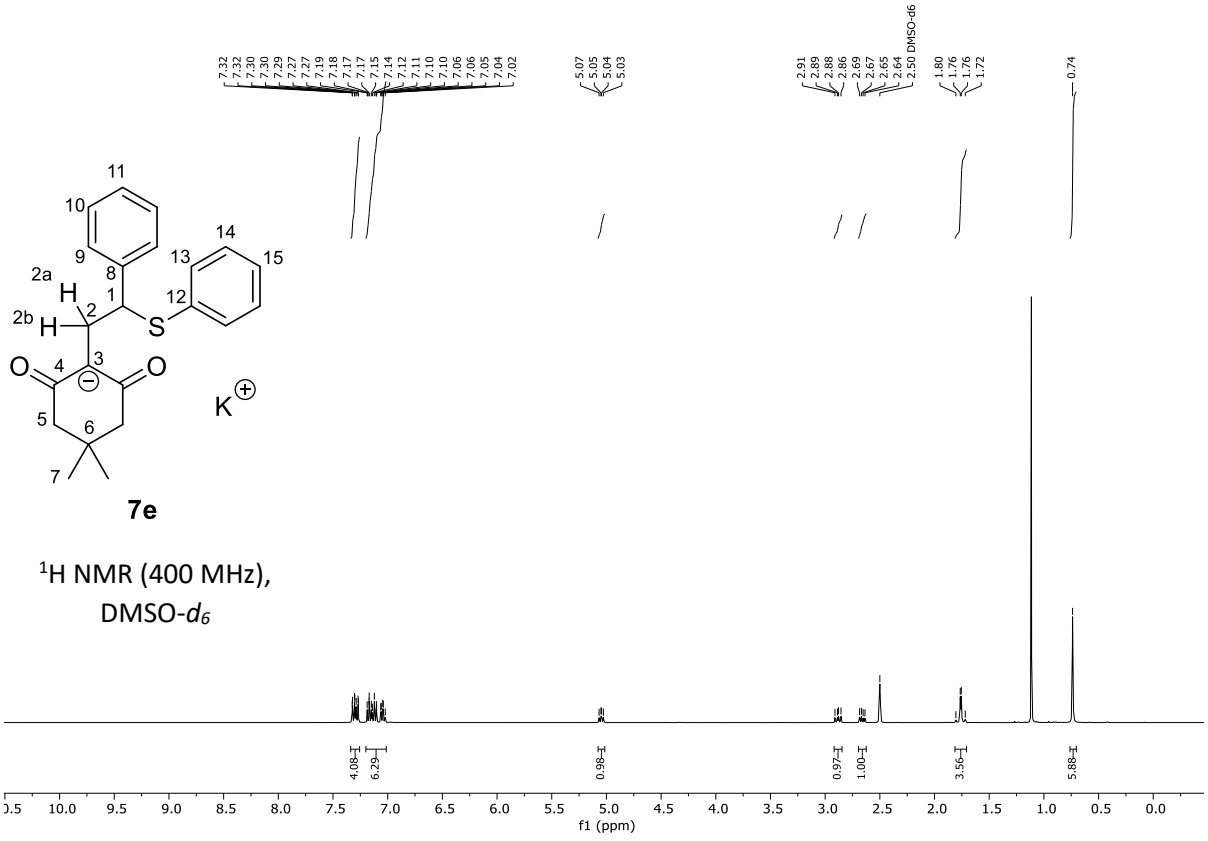

7e

^{1}H NMR (400 MHz),
DMSO-d_6

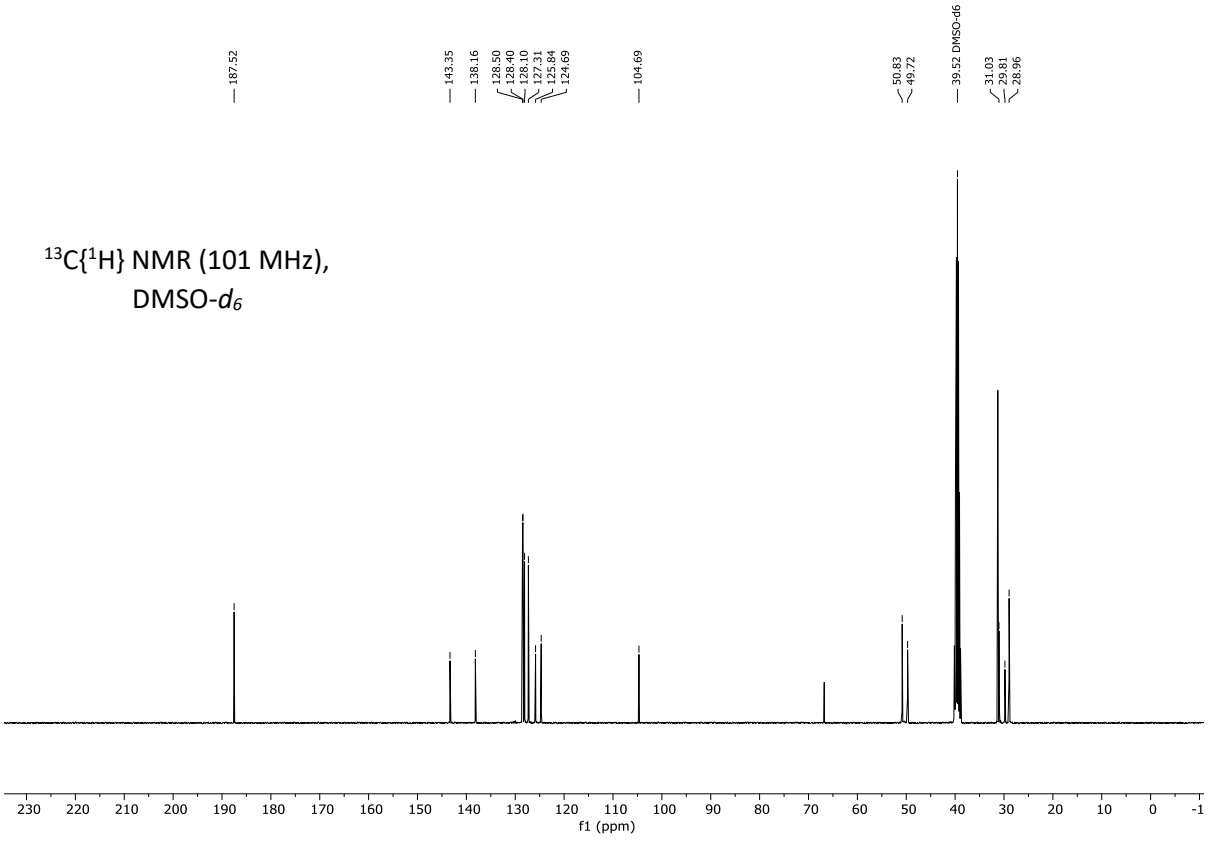

^{13}C{^{1}H} NMR (101 MHz),
DMSO-d_6

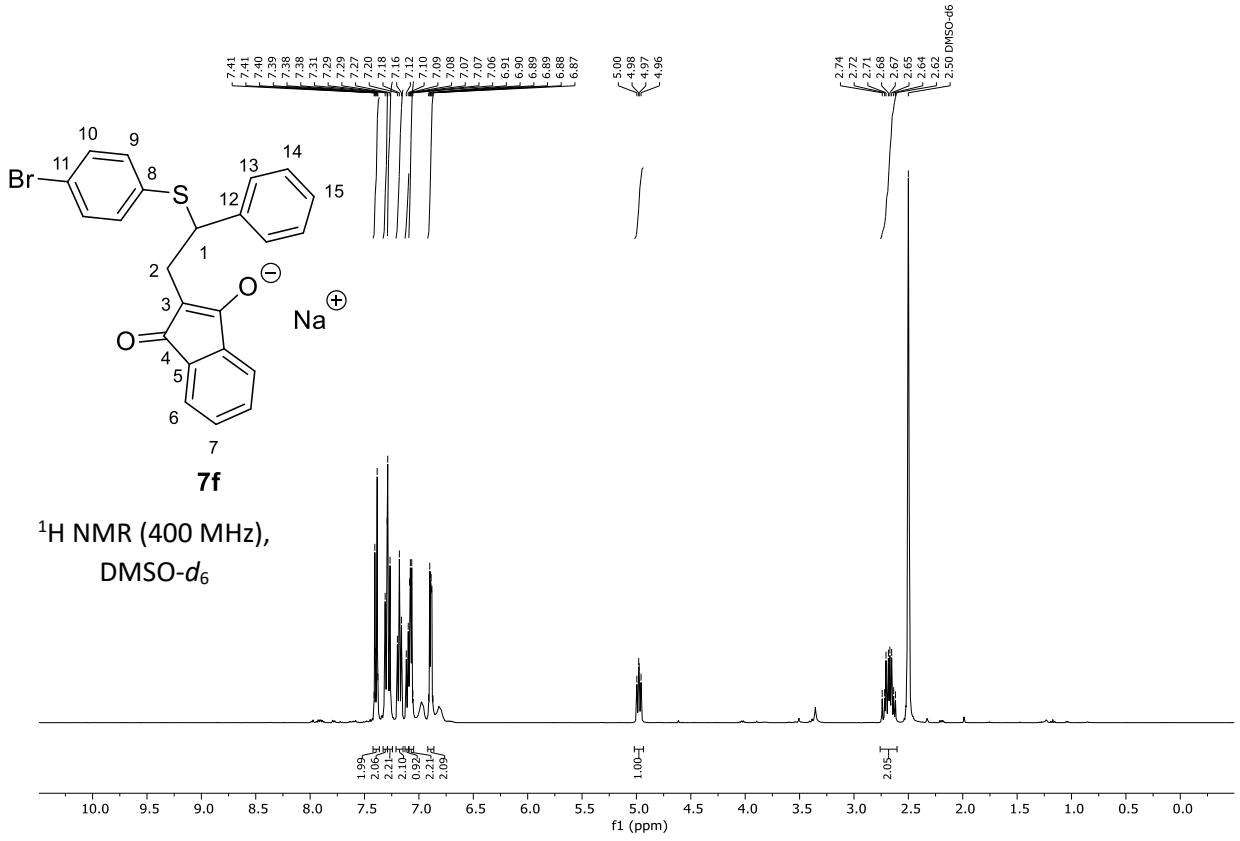
Br
S
O
Na
7f
1H NMR (400 MHz),
DMSO-d6
f1 (ppm)

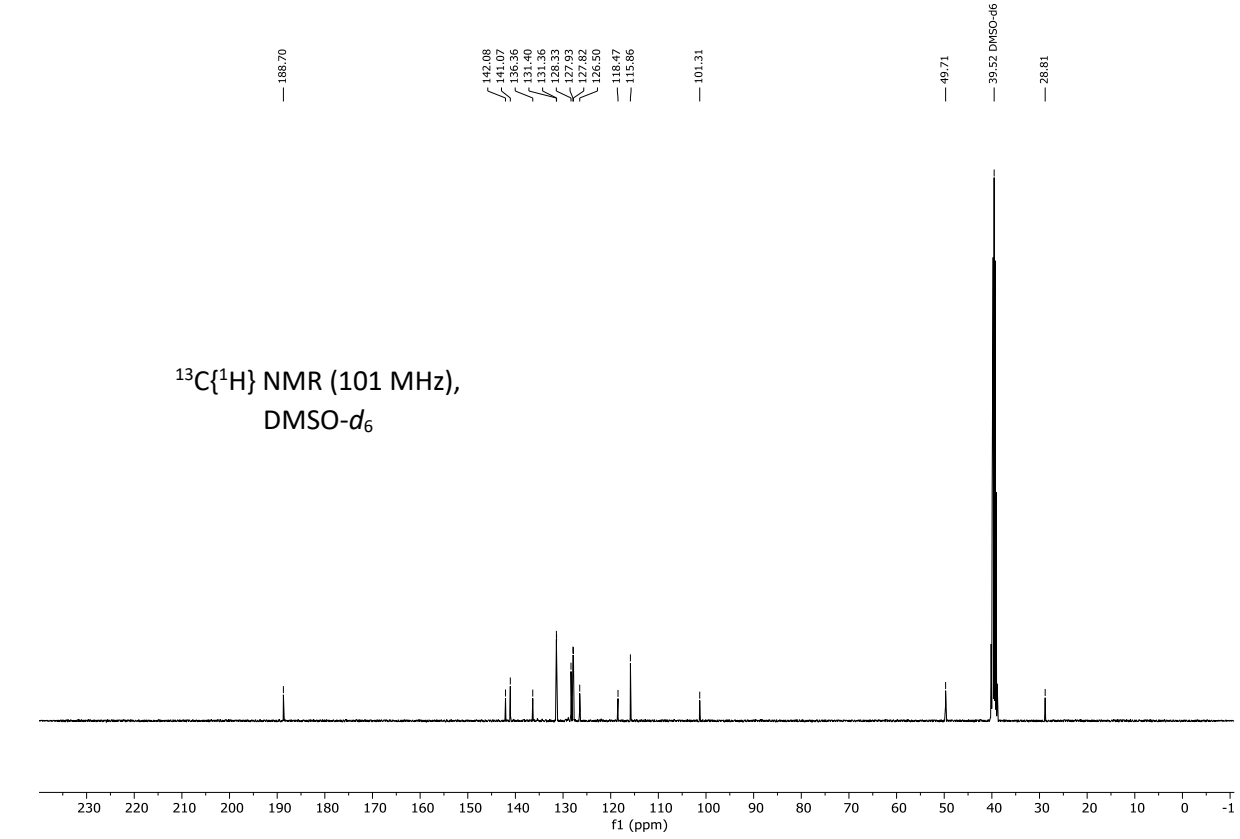
13C{1H} NMR (101 MHz),
DMSO-d6
f1 (ppm)

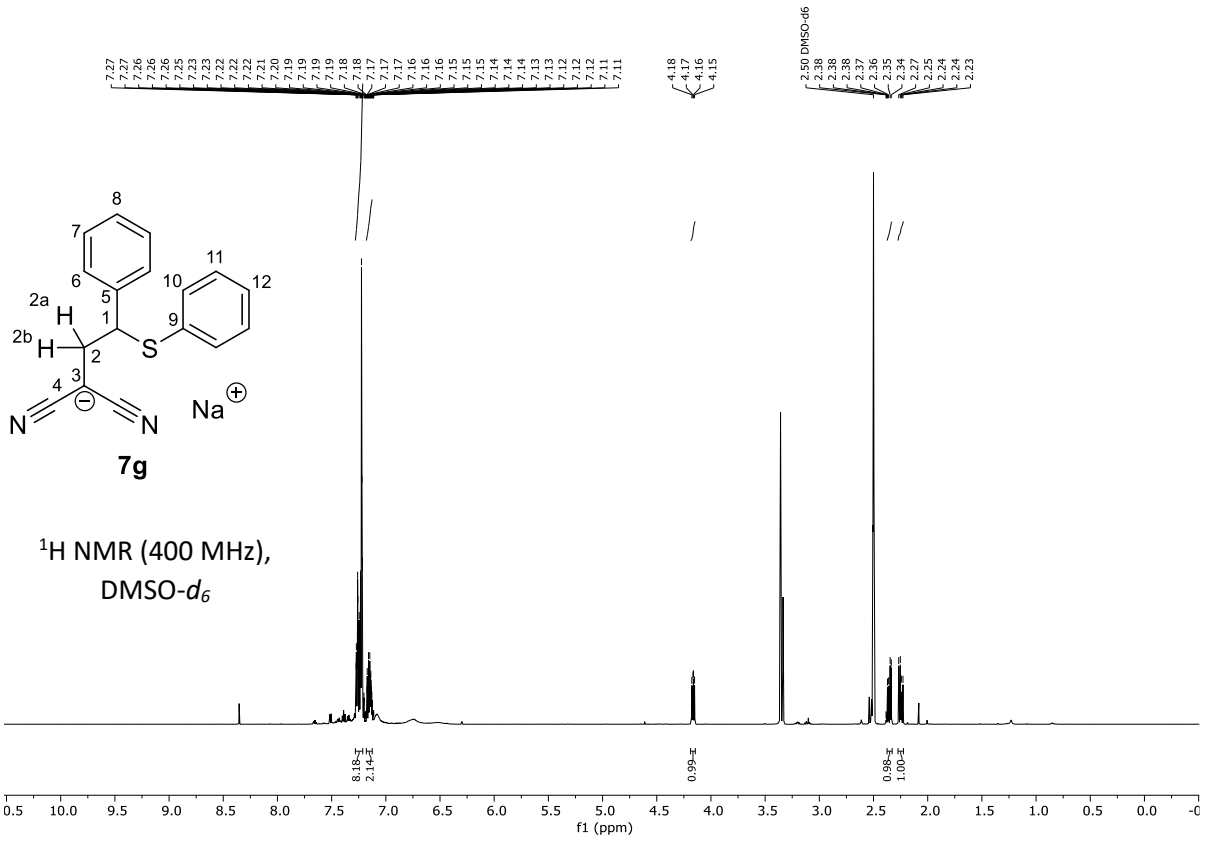
7g
Na
1H NMR (400 MHz),
DMSO-d6
f1 (ppm)

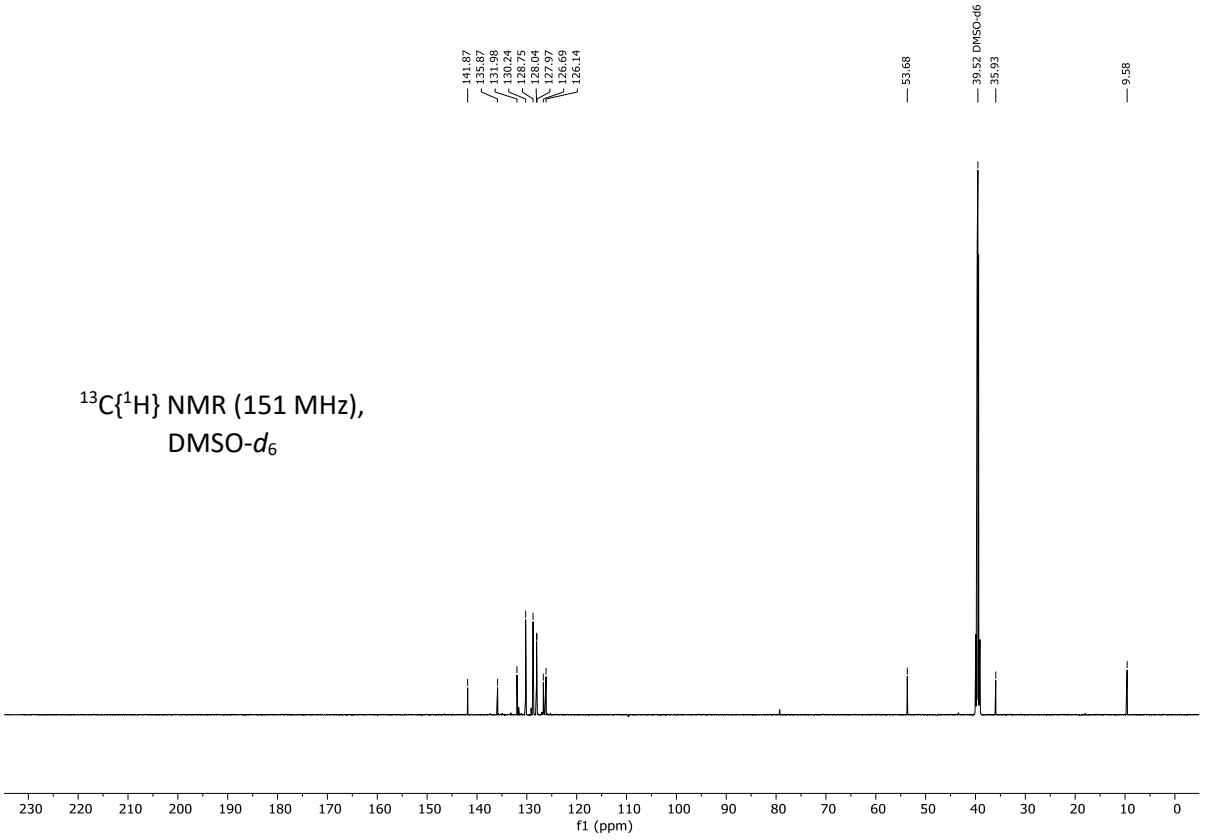
13C{1H} NMR (151 MHz),
DMSO-d6
f1 (ppm)

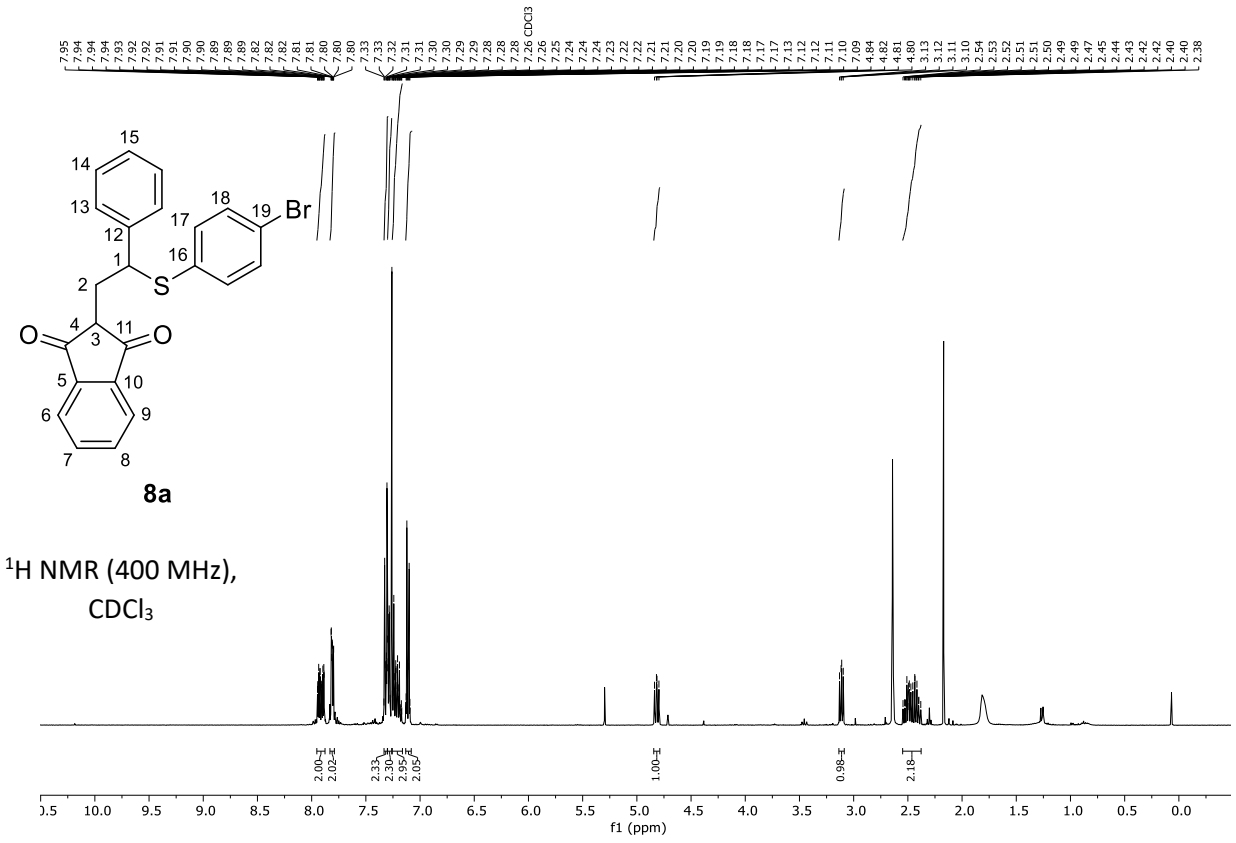

8a

^{1}H NMR (400 MHz), $CDCl_3$

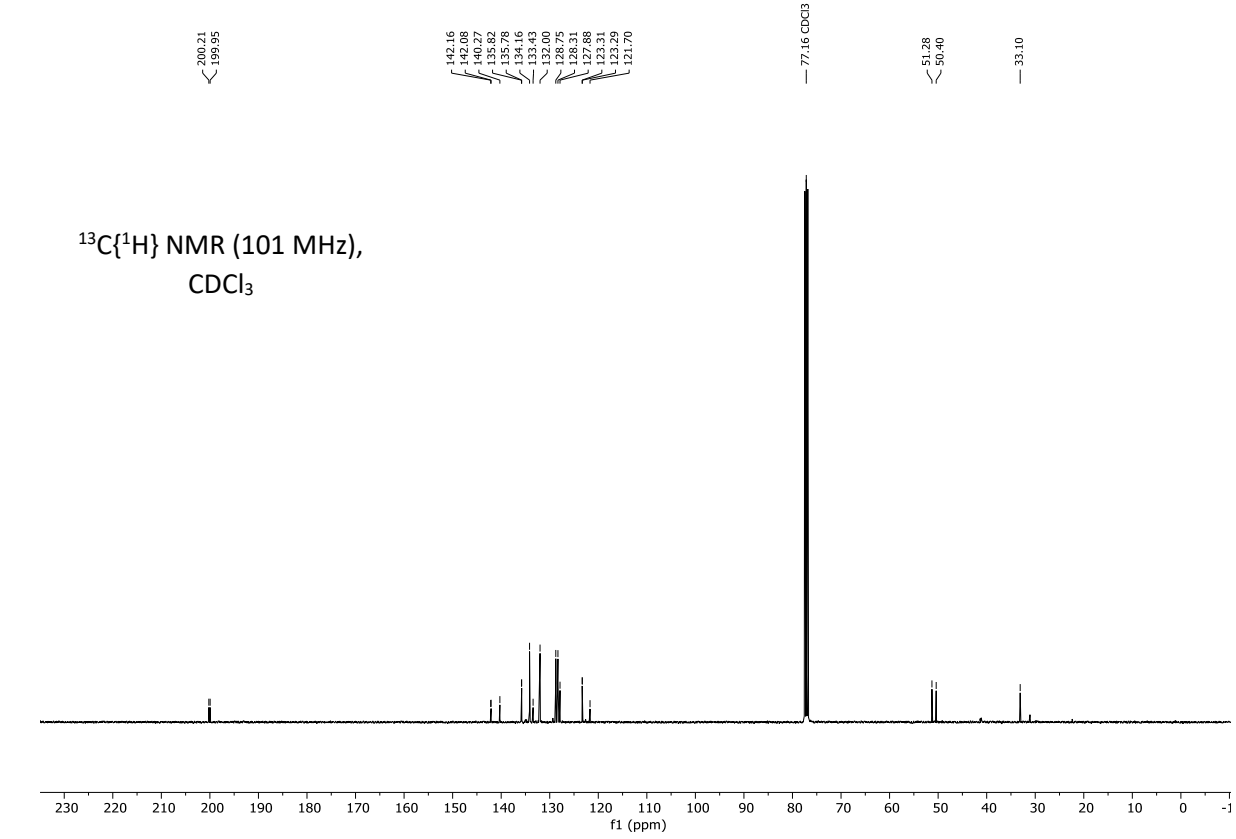

$^{13}C\{^{1}H\}$ NMR (101 MHz), $CDCl_3$

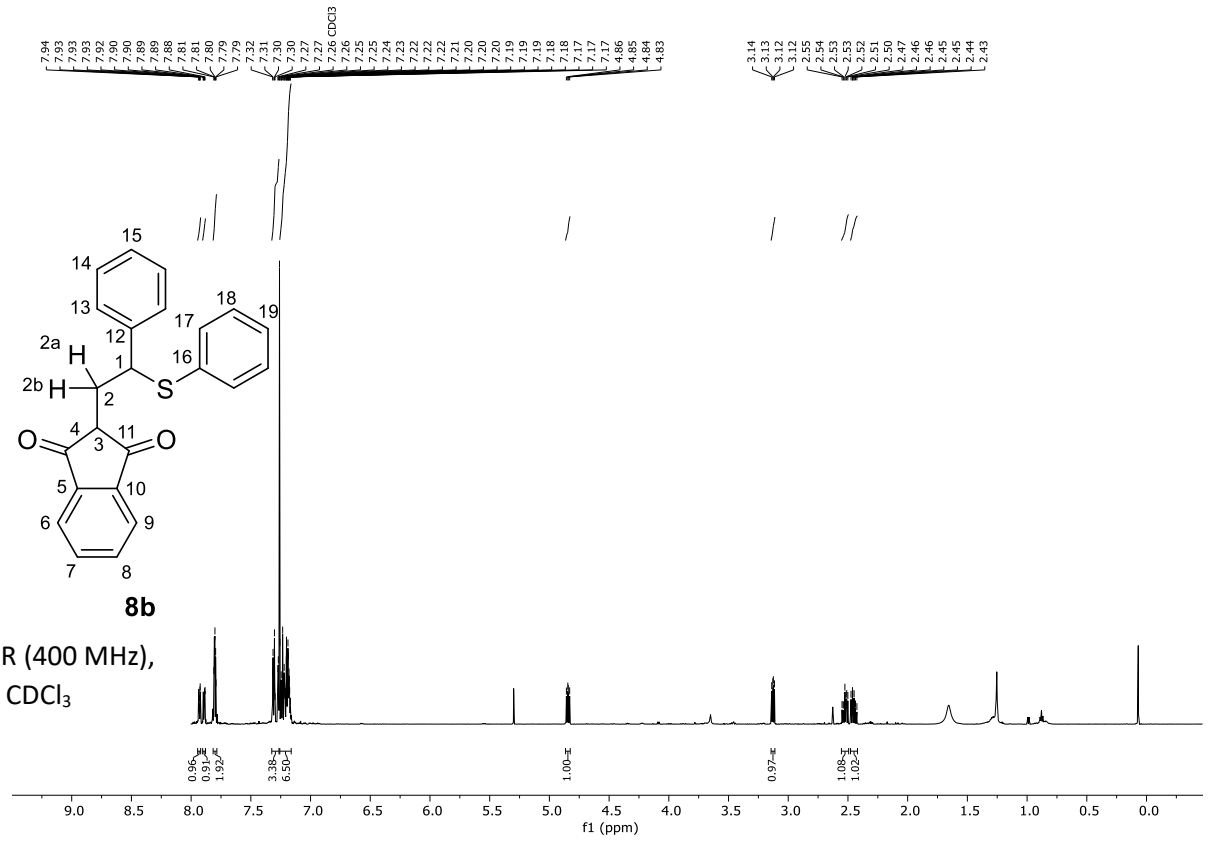

^{1}H NMR (400 MHz), $CDCl_3$

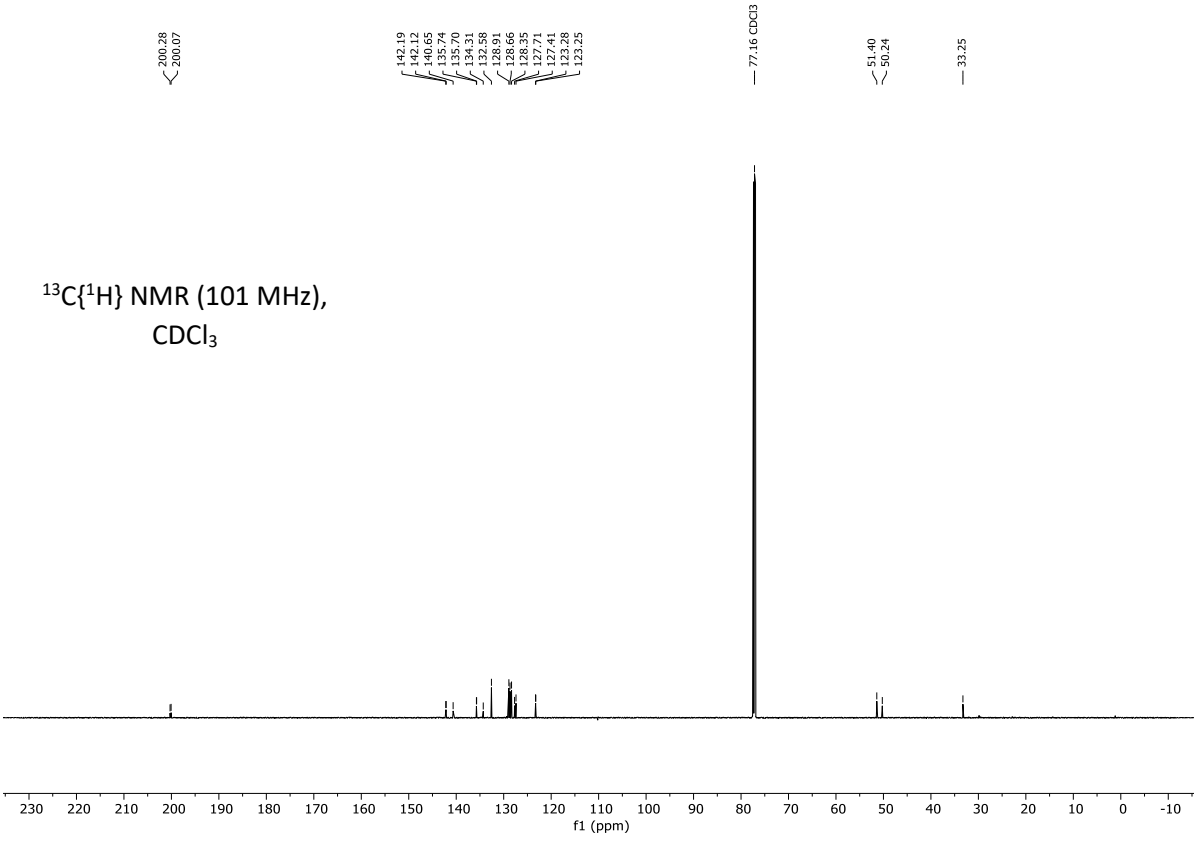

^{13}C{^{1}H} NMR (101 MHz), $CDCl_3$

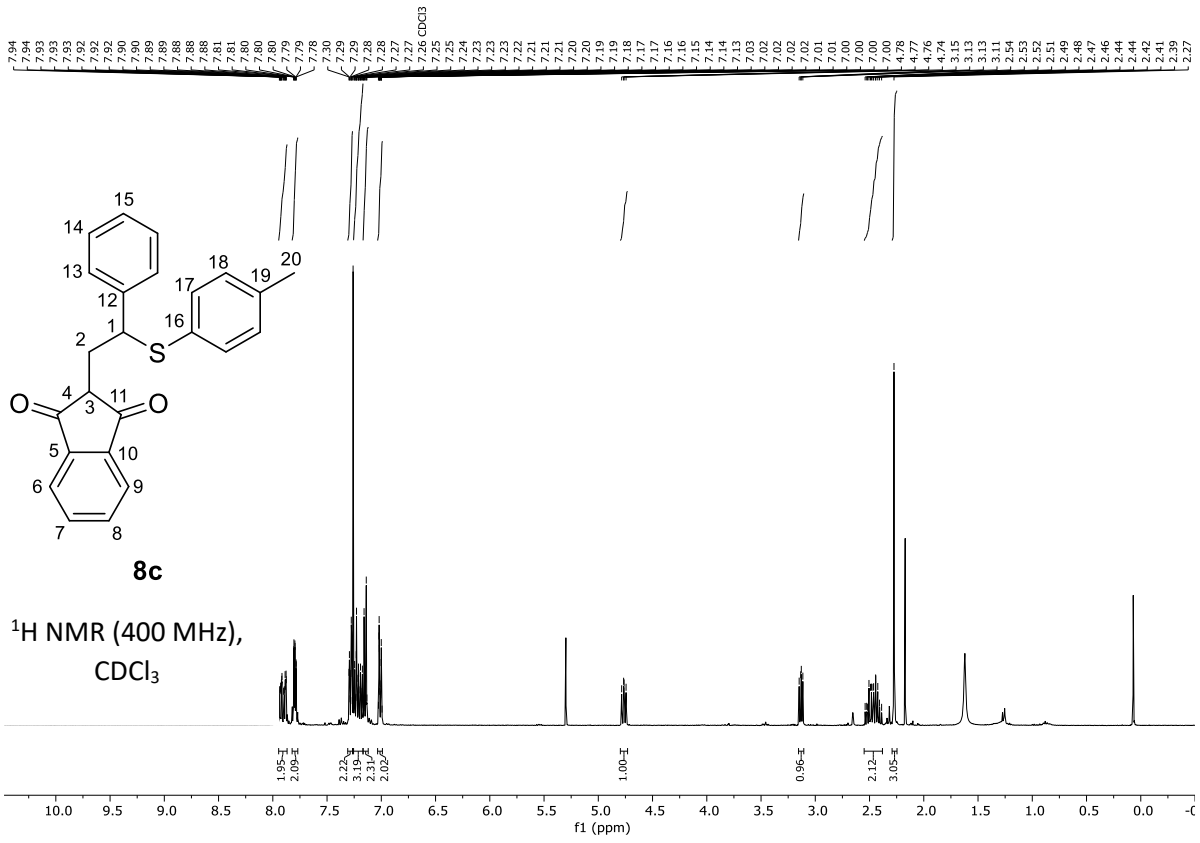

^{1}H NMR (400 MHz), $CDCl_3$

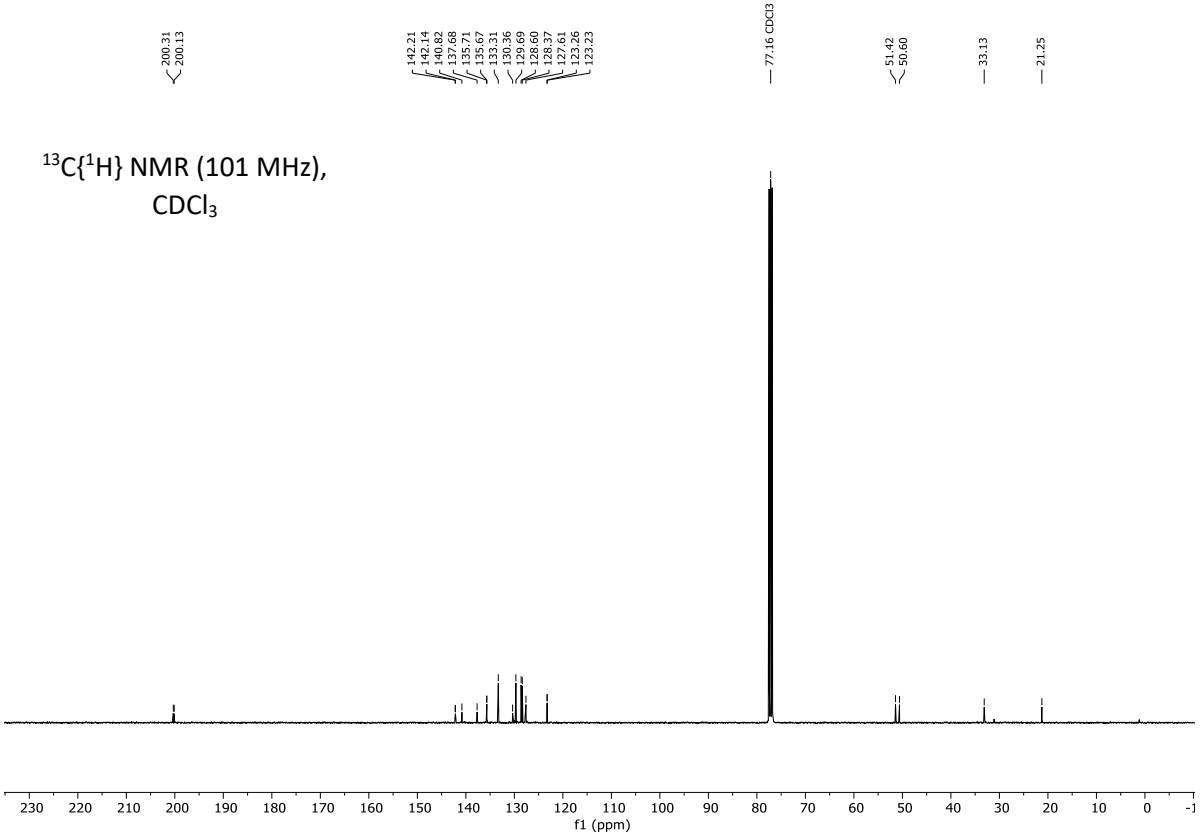

^{13}C{^{1}H} NMR (101 MHz), $CDCl_3$

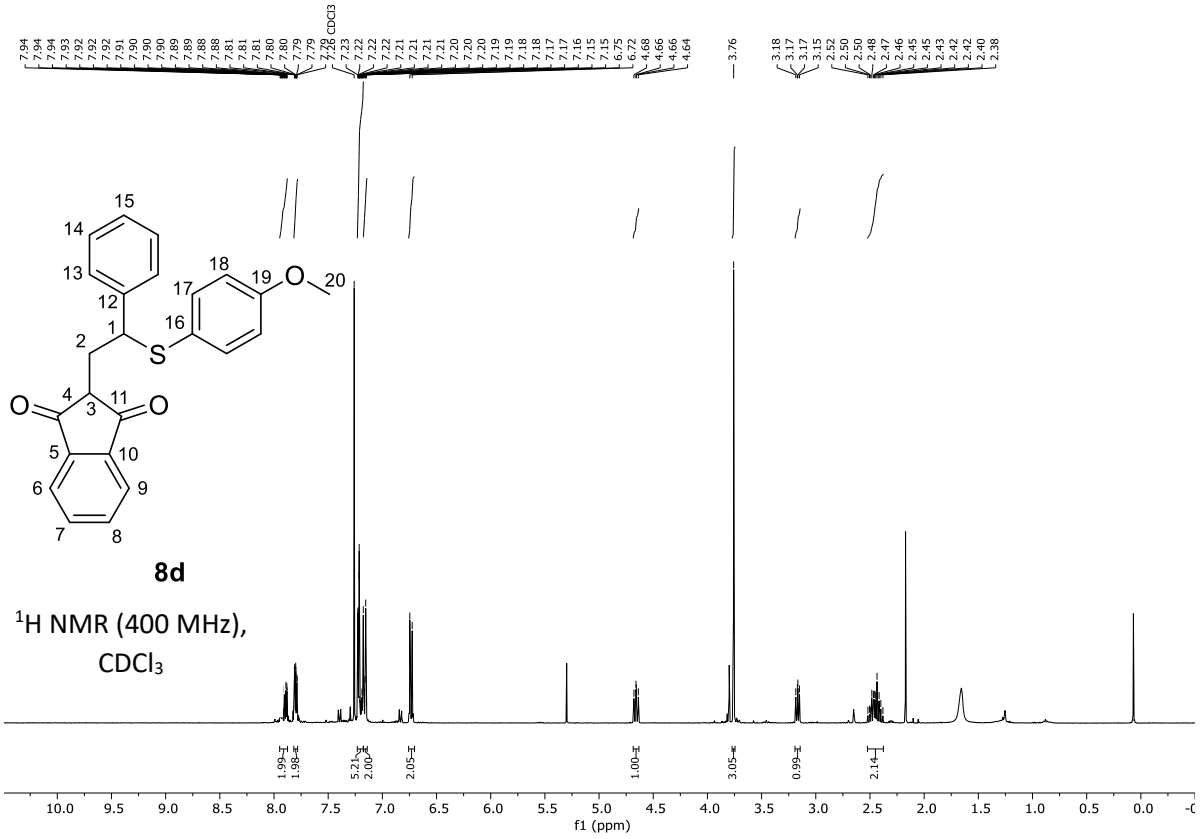
7.94 7.94 7.94 7.93 7.92 7.92 7.92 7.91 7.90 7.90 7.90 7.89 7.89 7.88 7.88 7.81 7.81 7.81 7.80 7.80 7.79 7.79 7.78 CDCl3 7.23 7.22 7.22 7.22 7.21 7.21 7.21 7.21 7.20 7.20 7.20 7.19 7.19 7.18 7.18 7.17 7.17 7.16 7.15 7.15 6.75 6.72 4.68 4.66 4.66 4.64 3.76 3.18 3.17 3.17 3.15 2.52 2.50 2.50 2.48 2.47 2.46 2.45 2.45 2.43 2.42 2.42 2.40 2.38
15 14 13 12 1 2 S 16 17 18 19 O 20 4 3 11 O O 5 10 6 9 7 8
8d
1H NMR (400 MHz), CDCl3
1.99 1.98 5.21 2.00 2.05 1.00 3.05 0.99 2.14
10.0 9.5 9.0 8.5 8.0 7.5 7.0 6.5 6.0 5.5 5.0 4.5 4.0 3.5 3.0 2.5 2.0 1.5 1.0 0.5 0.0
f1 (ppm)

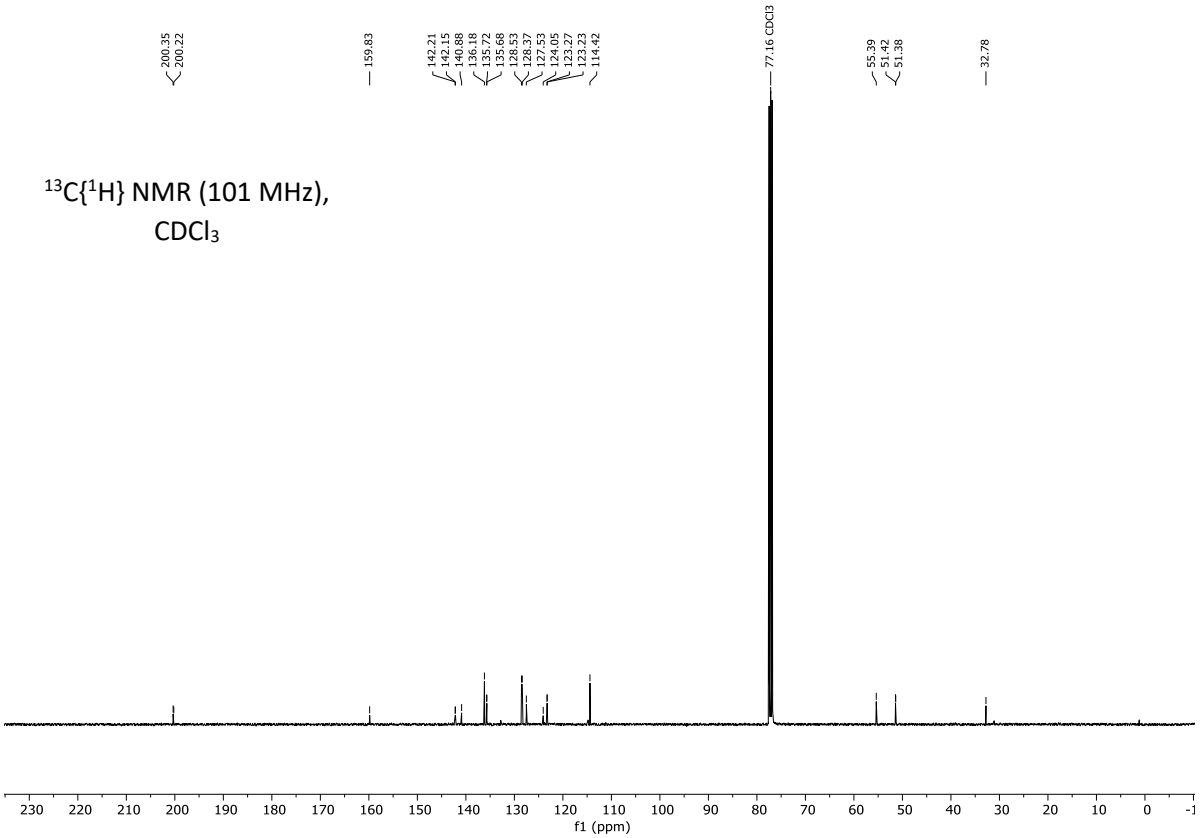
200.35 200.22 159.83 142.21 142.15 140.88 136.18 135.72 135.68 128.53 128.37 127.53 124.05 123.27 123.23 114.42 77.16 CDCl3 55.39 51.42 51.38 32.78
13C{1H} NMR (101 MHz), CDCl3
230 220 210 200 190 180 170 160 150 140 130 120 110 100 90 80 70 60 50 40 30 20 10 0
f1 (ppm)

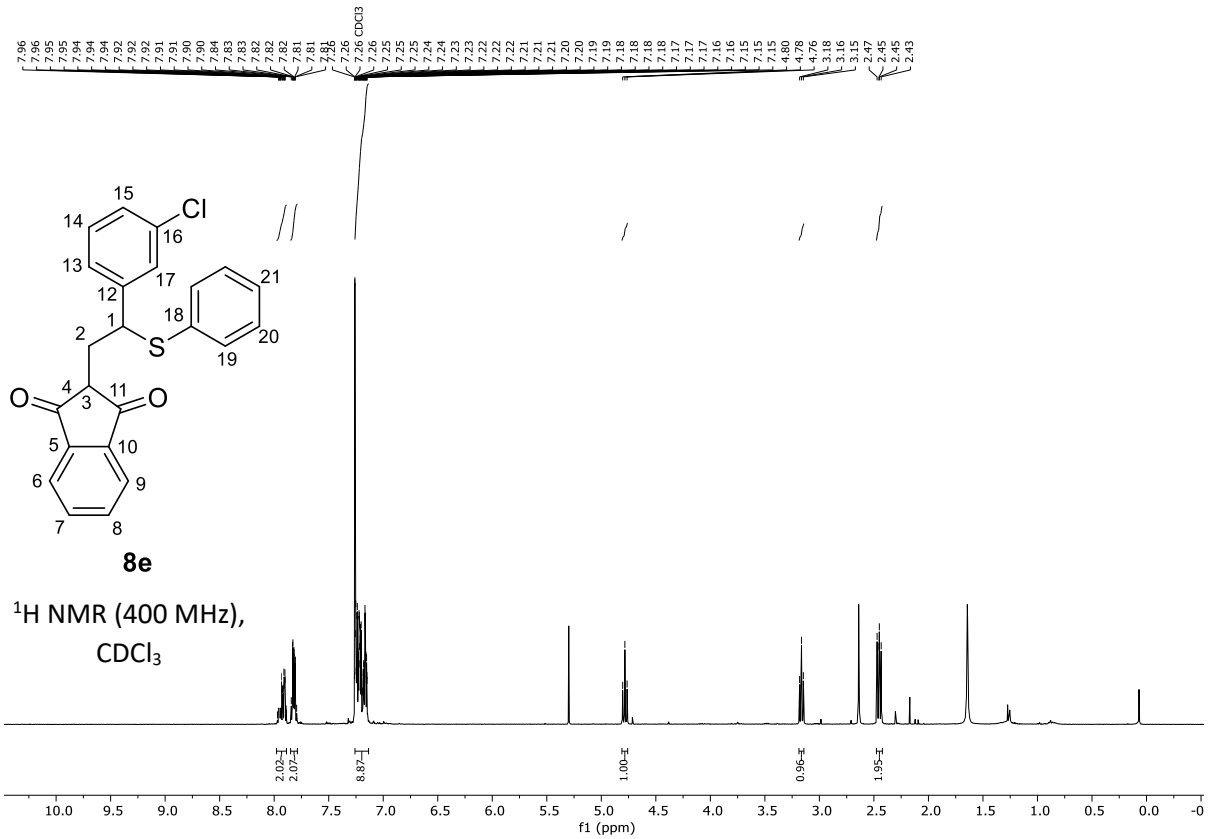
Cl
S
O
O
8e
^{1}H NMR (400 MHz),
$CDCl_3$
f1 (ppm)

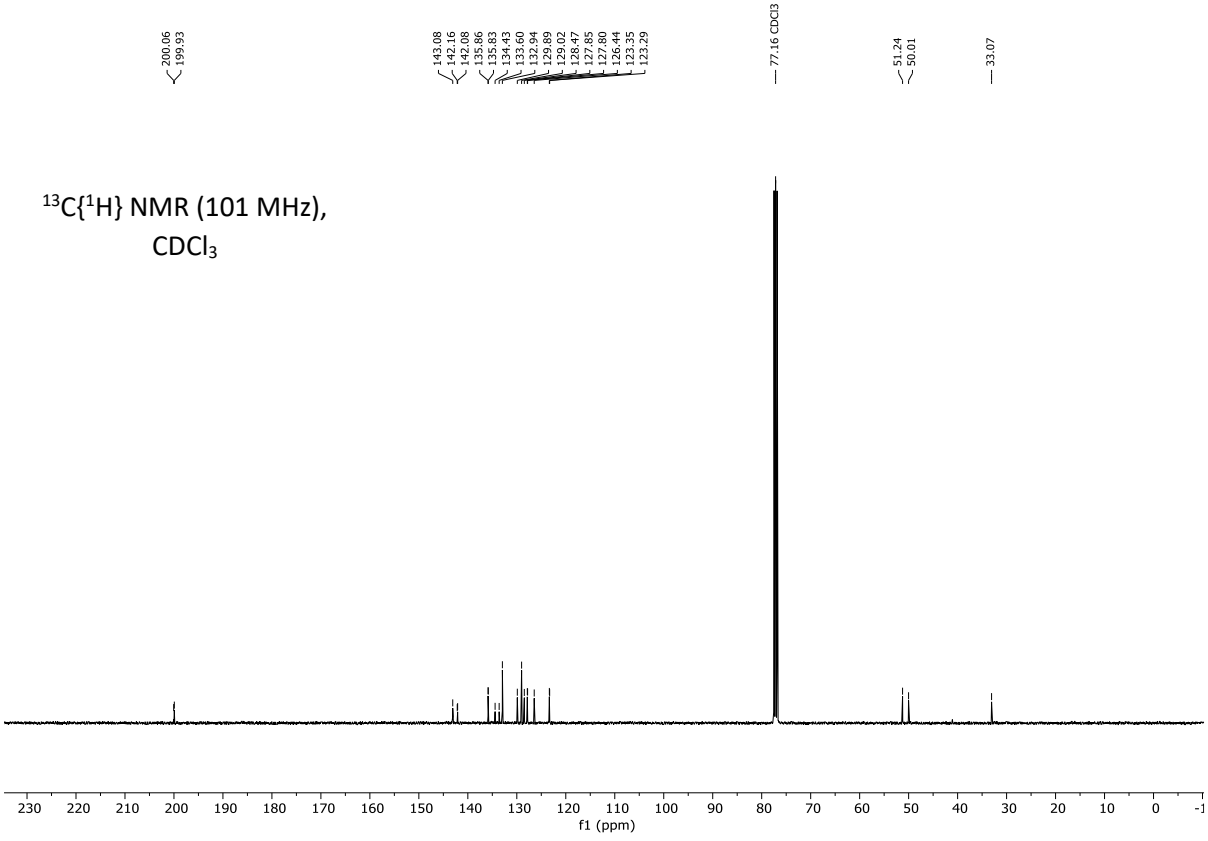
$^{13}C\{^1H\}$ NMR (101 MHz),
$CDCl_3$
f1 (ppm)

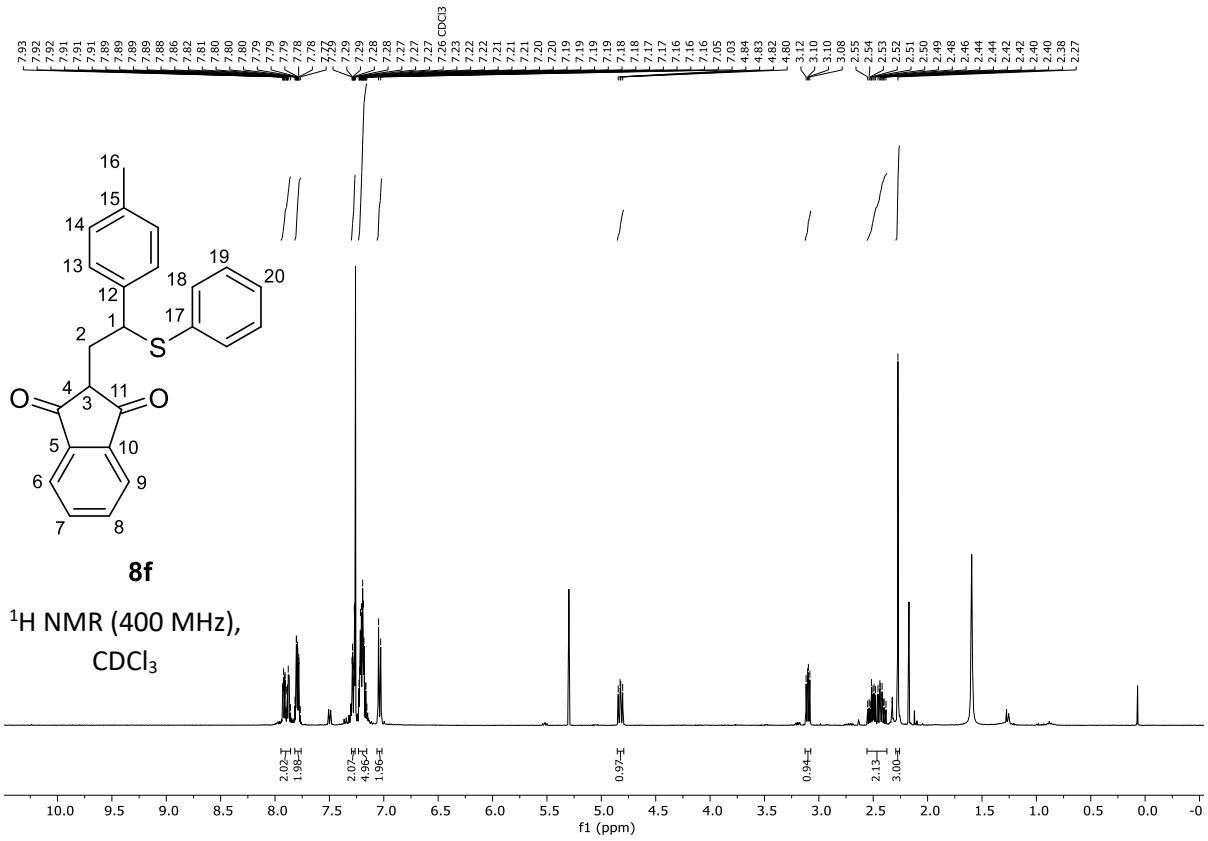
7.93 7.92 7.92 7.91 7.91 7.91 7.89 7.89 7.89 7.89 7.88 7.86 7.82 7.81 7.80 7.80 7.80 7.79 7.79 7.79 7.78 7.78 7.77 7.75 7.29 7.29 7.28 7.28 7.27 7.27 7.27 7.26 CDCl3 7.23 7.22 7.22 7.21 7.21 7.21 7.20 7.20 7.19 7.19 7.19 7.19 7.18 7.18 7.17 7.17 7.16 7.16 7.16 7.05 7.03 4.84 4.83 4.82 4.80 3.12 3.10 3.10 3.08 2.55 2.54 2.53 2.52 2.51 2.50 2.49 2.48 2.46 2.44 2.42 2.42 2.40 2.40 2.38 2.27
16 15 14 13 12 1 2 S 17 18 19 20 O 4 3 11 O 5 10 6 9 7 8
8f
1H NMR (400 MHz), CDCl3
2.02 1.98 2.07 4.96 1.96 0.97 0.94 2.13 3.00
10.0 9.5 9.0 8.5 8.0 7.5 7.0 6.5 6.0 5.5 5.0 4.5 4.0 3.5 3.0 2.5 2.0 1.5 1.0 0.5 0.0
f1 (ppm)

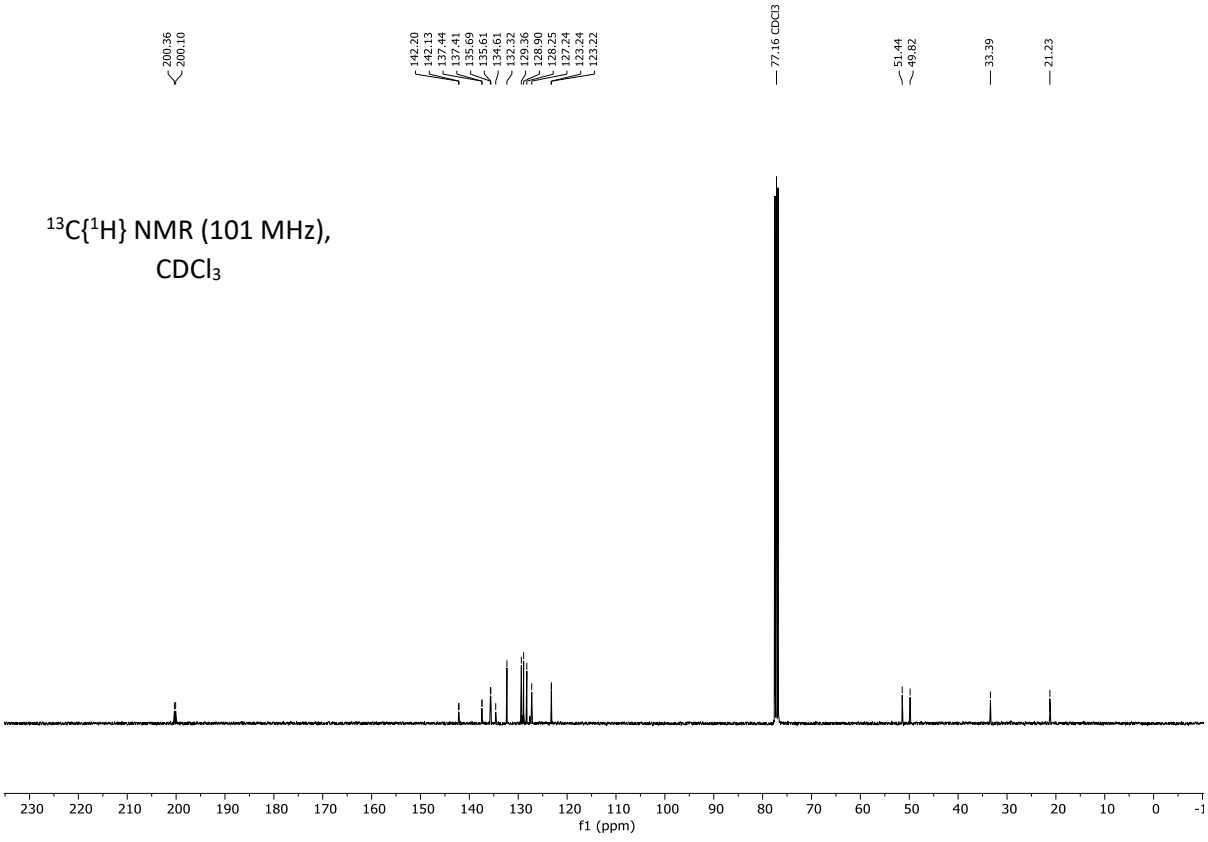
200.36 200.10 142.20 142.13 137.44 137.41 135.69 135.61 134.61 132.32 129.36 128.90 128.25 127.24 123.24 123.22 77.16 CDCl3 51.44 49.82 33.39 21.23
13C{1H} NMR (101 MHz), CDCl3
230 220 210 200 190 180 170 160 150 140 130 120 110 100 90 80 70 60 50 40 30 20 10 0
f1 (ppm)

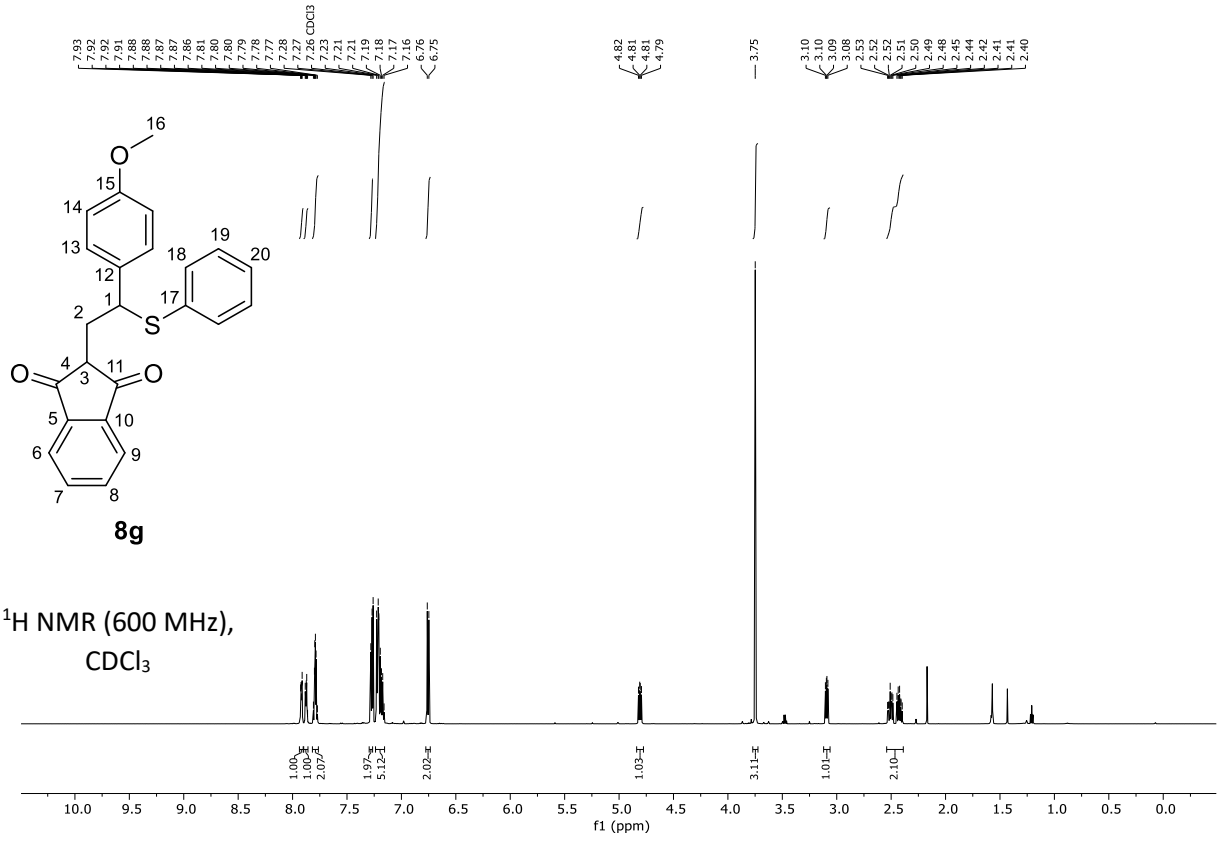

8g

^{1}H NMR (600 MHz), $CDCl_3$

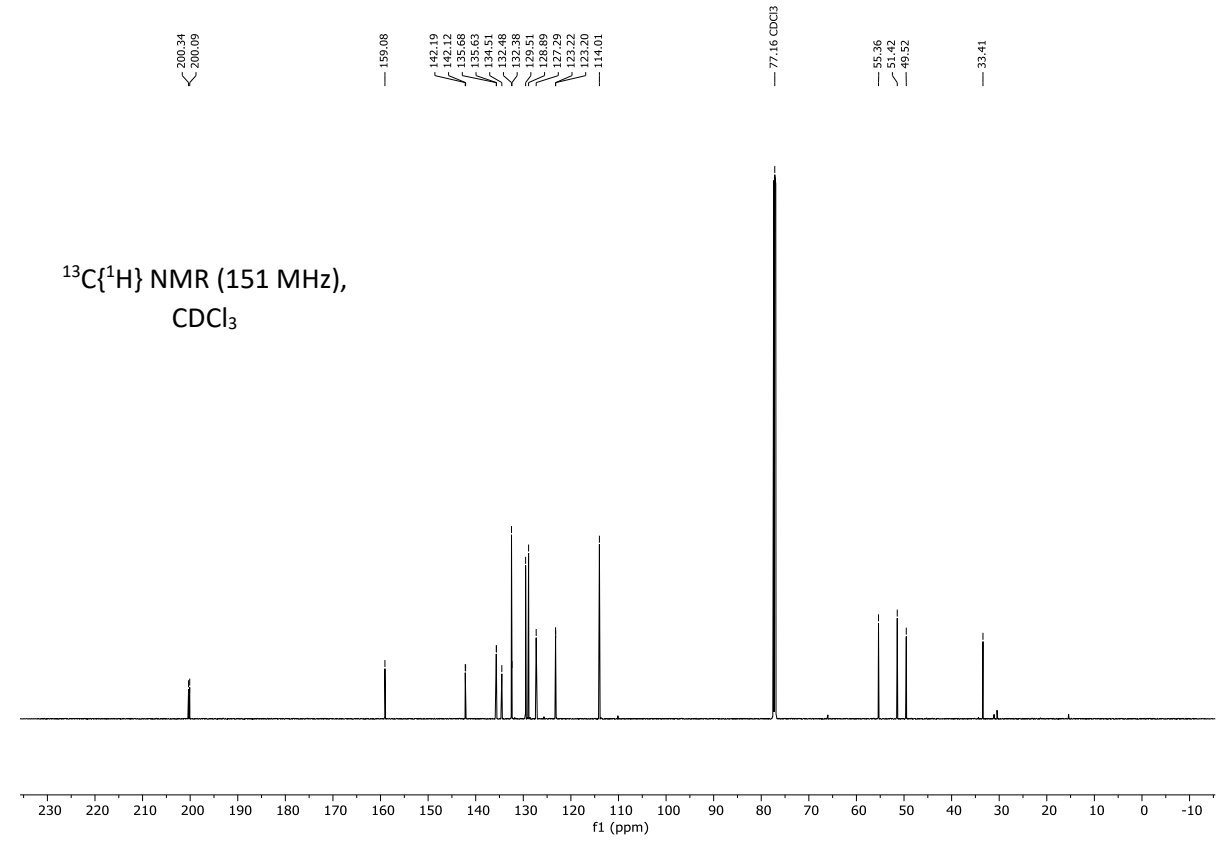

^{13}C{^{1}H} NMR (151 MHz), $CDCl_3$

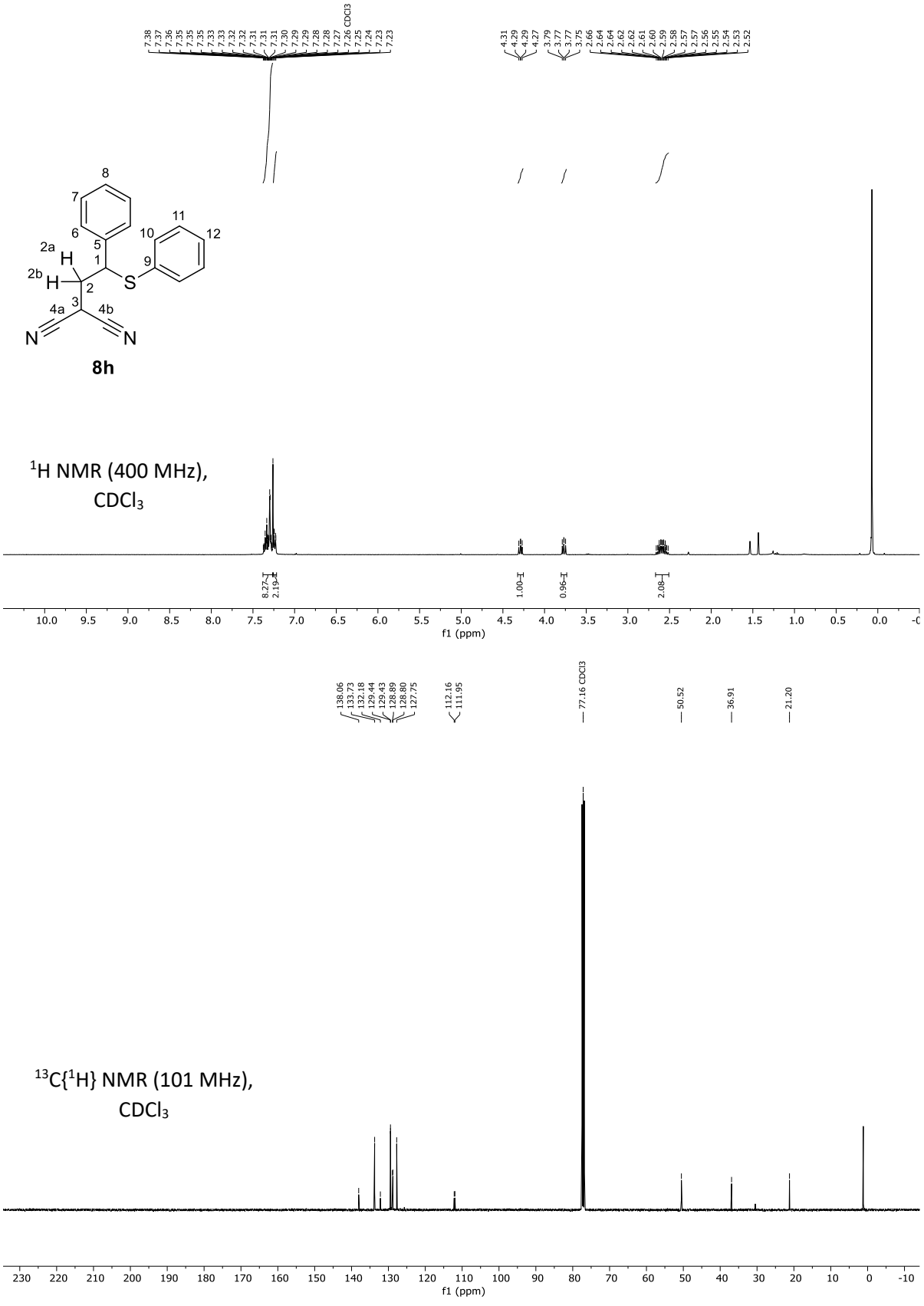
8h
^{1}H NMR (400 MHz), CDCl$_3$
^{13}C{^{1}H} NMR (101 MHz), CDCl$_3$
f1 (ppm)

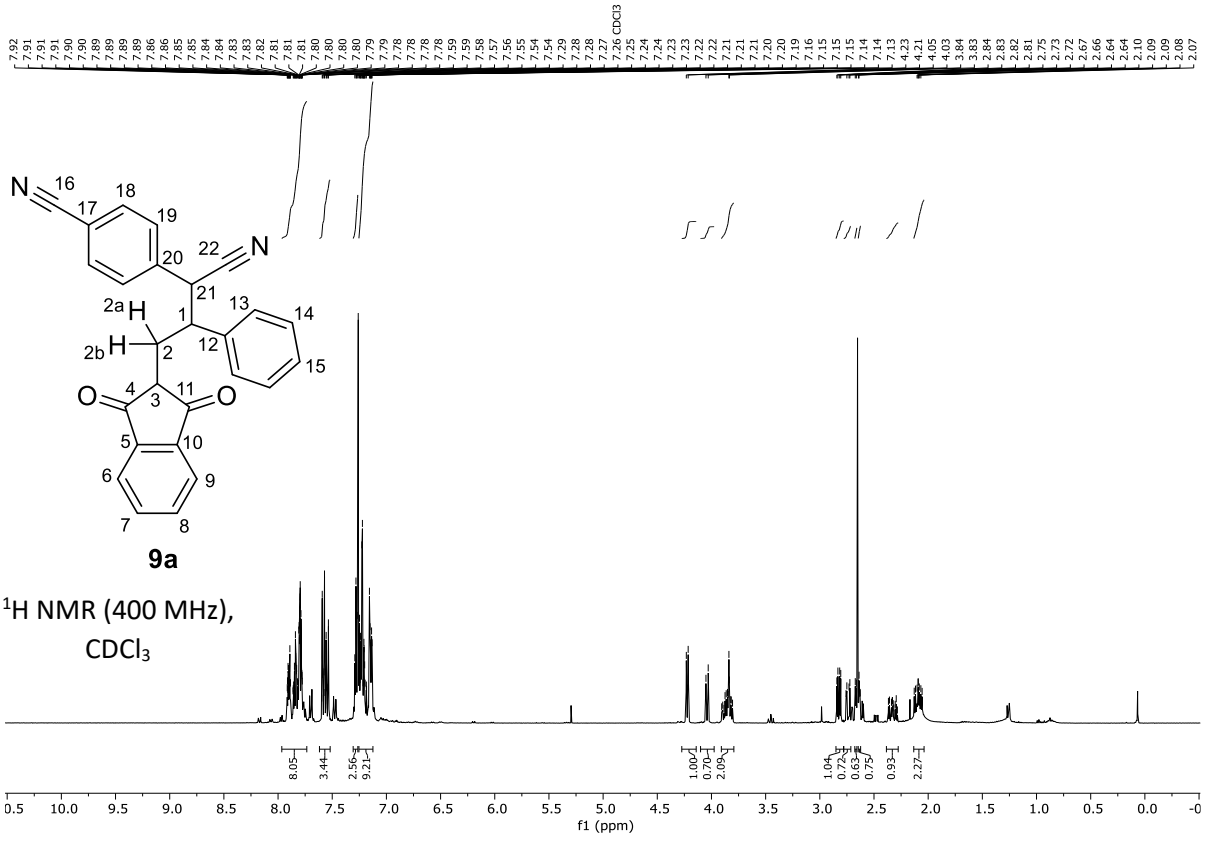
9a
1H NMR (400 MHz),
CDCl3
f1 (ppm)

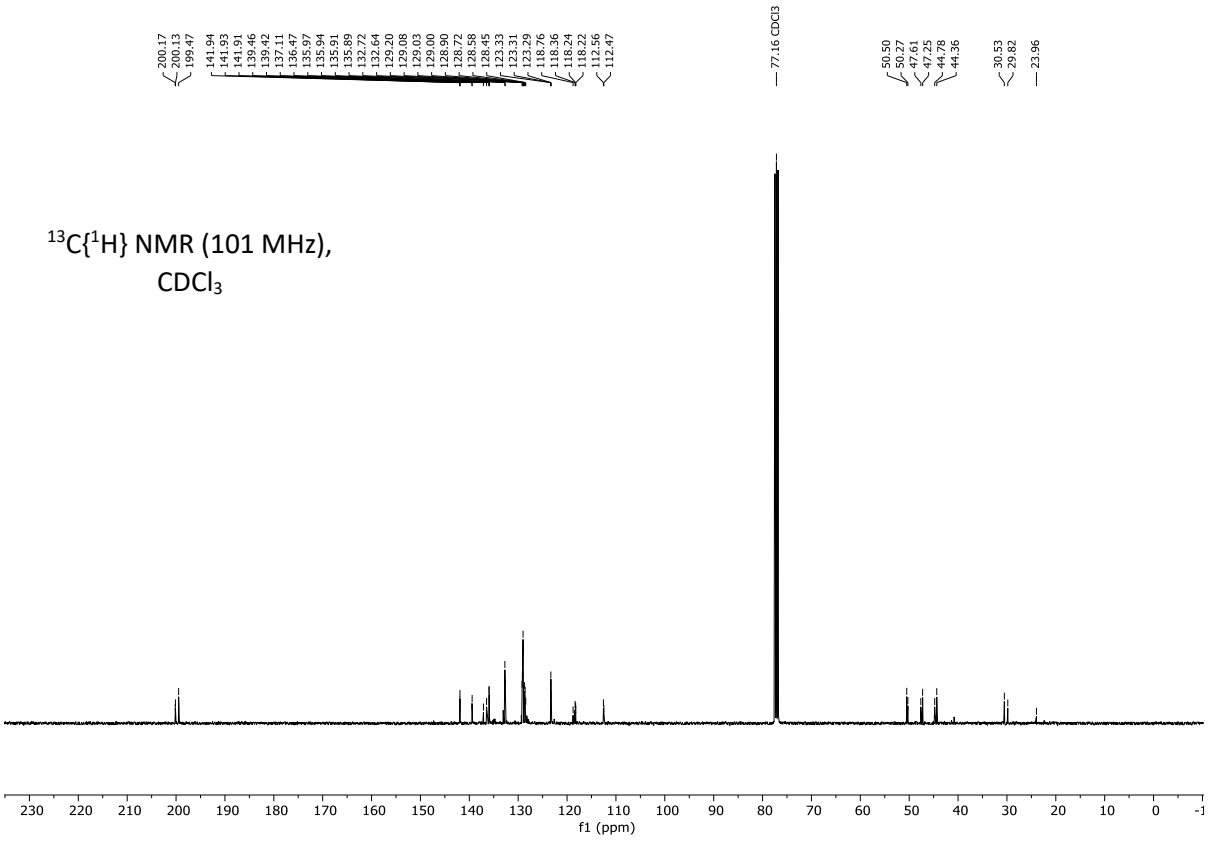
13C{1H} NMR (101 MHz),
CDCl3
f1 (ppm)

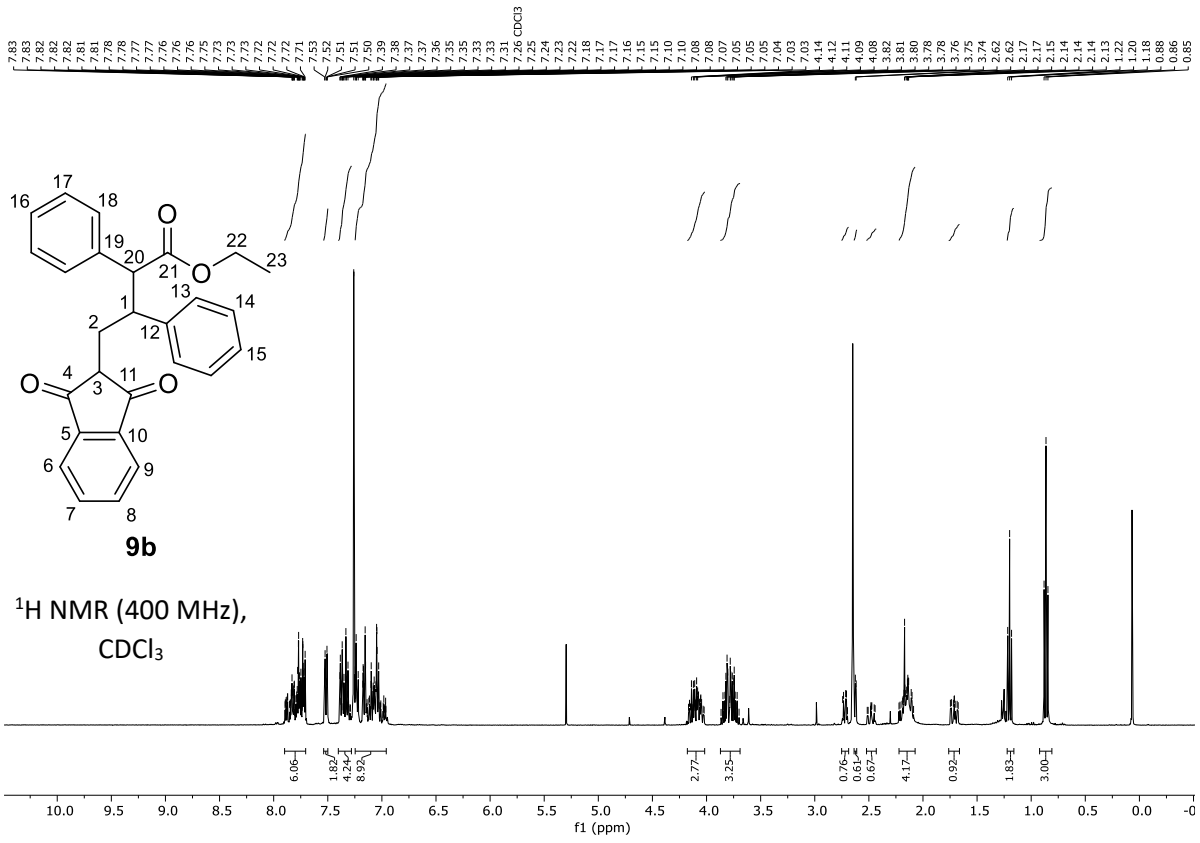
9b
^{1}H NMR (400 MHz),
CDCl$_3$
f1 (ppm)

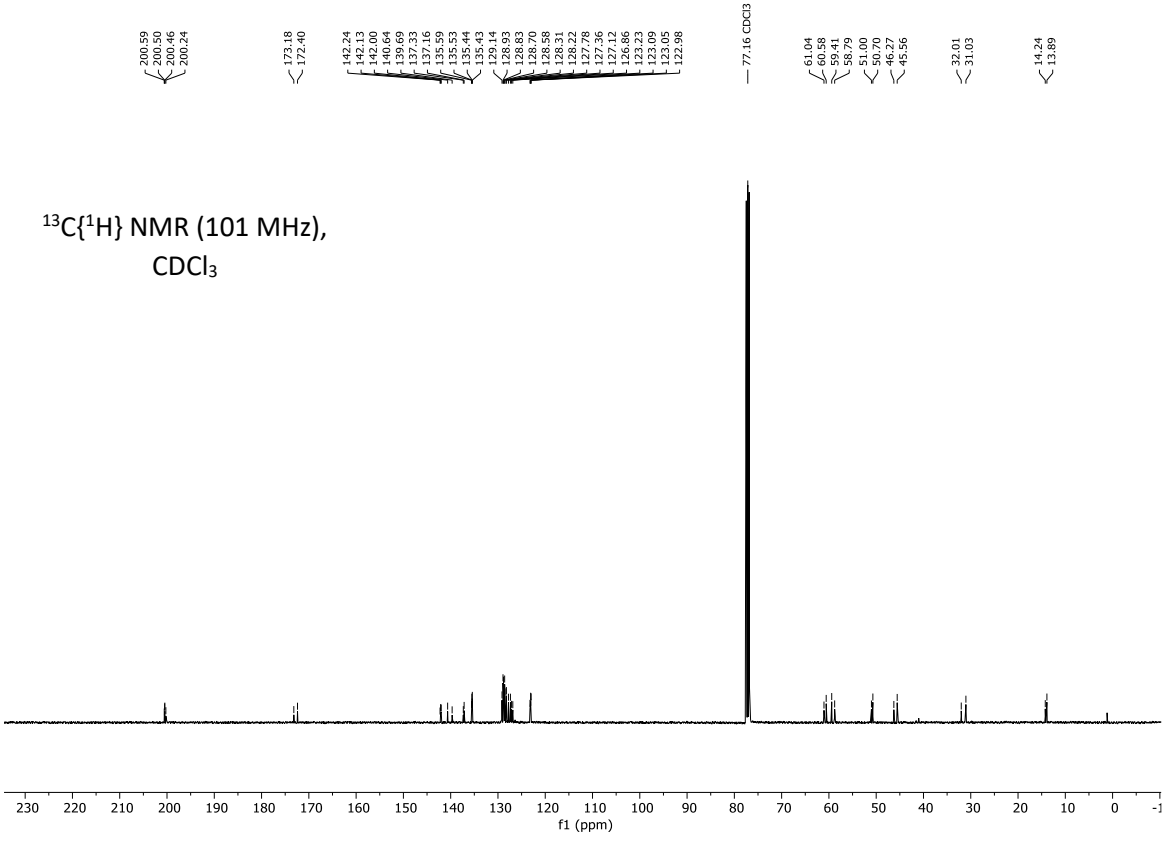
^{13}C{^{1}H} NMR (101 MHz),
CDCl$_3$
f1 (ppm)

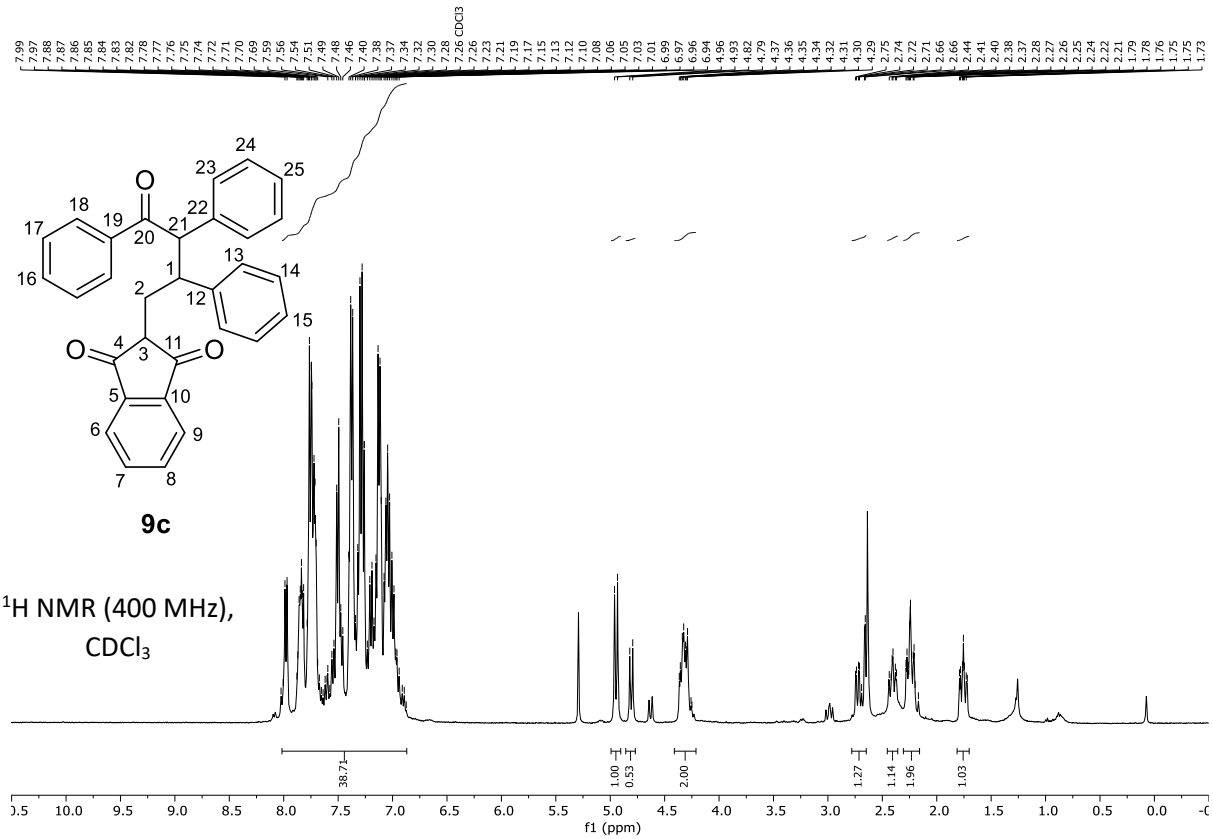
9c
1H NMR (400 MHz),
CDCl3
f1 (ppm)

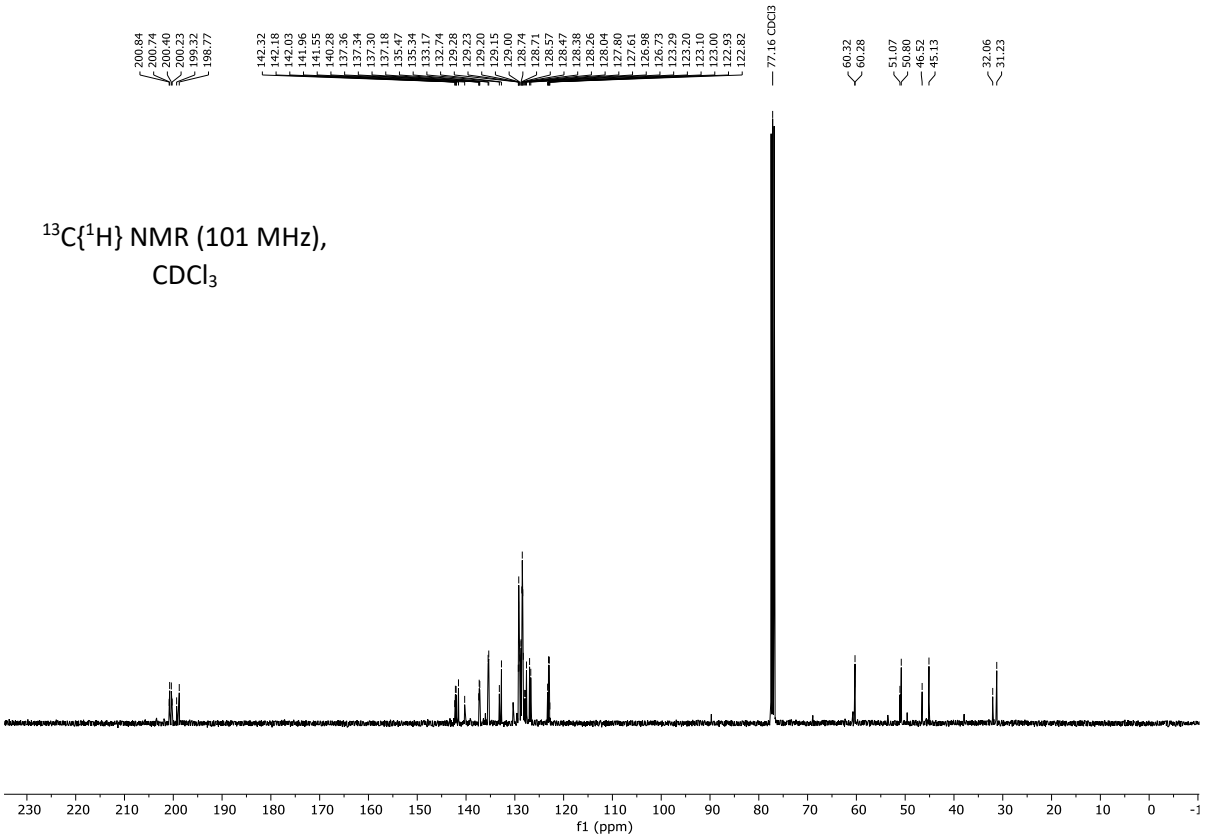
13C{1H} NMR (101 MHz),
CDCl3
f1 (ppm)

3.5.5 References

(1) Tukhtaev, H. B.; Ivanov, K. L.; Bezzubov, S. I.; Cheshkov, D. A.; Melnikov, M. Y.; Budynina, E. M., *Org. Lett.* **2019,** *21*, 1087−1092.

(2) Qian, P.; Du, B.; Song, R.; Wu, X.; Mei, H.; Han, J.; Pan, Y., *J. Org. Chem.* **2016,** *81*, 6546−6553.

(3) (a) Chow, Y. L.; Bakker, B. H.; Iwai, K., *J. Chem. Soc., Chem. Commun.* **1980**, 521−522. (b) Chow, Y. L.; Bakker, B. H., *Synthesis* **1982,** *1982*, 648−650.

(4) Nambu, H.; Ono, N.; Hirota, W.; Fukumoto, M.; Yakura, T., *Chem. Pharm. Bull.* **2016,** *64*, 1763−1768.

(5) Nambu, H.; Fukumoto, M.; Hirota, W.; Yakura, T., *Org. Lett.* **2014,** *16*, 4012−4015.

(6) Chidley, T.; Jameel, I.; Rizwan, S.; Peixoto, P. A.; Pouységu, L.; Quideau, S.; Hopkins, W. S.; Murphy, G. K., *Angew. Chem., Int. Ed.* **2019,** *58*, 16959−16965.

(7) Rosenfeld, M. J.; Shankar, B. K. R.; Shechter, H., *J. Org. Chem.* **1988,** *53*, 2699−2705.

(8) McKinney, M. A.; Kremer, K. G.; Aicher, T., *Tetrahedron Lett.* **1984,** *25*, 5477−5480.

Chapter 4. Kinetic Investigations of Concomitant S_N1 and S_N2 Mechanisms in Menschutkin Reactions

Contributions

Patrick M. Jüstel performed all experiments. Robert J. Mayer performed the computational experiments and wrote the accompanying text. The manuscript was written jointly by Patrick M. Jüstel and Armin R. Ofial.

4.1 Introduction

Nucleophilic substitutions at sp^3-hybridized electrophilic carbon centers belong to the most often studied reactions in physical organic chemistry.[1] Owing to their importance for teaching organic chemistry, each organic chemistry textbook contains a discussion on the various effects that influence the rates of nucleophilic substitutions, consequences for the stereochemistry of the products, and, thus, the mechanism of the reactions.[2]

In general, nucleophilic substitutions proceed via two mechanisms, the S_N1 mechanism and the S_N2 mechanism.[2] In the S_N1 mechanism, the electrophilic substrate first ionizes by the heterolytic bond cleavage between a leaving groups and a carbon (Figure 1a). This heterolysis reaction generates in a rate-determining step a carbocation along with a neutral or negatively charged leaving group. In contrast, the S_N2 mechanism requires concerted bond formation and bond cleavage (Figure 1b). Because the incoming nucleophile and the electrophilic substrate have to interact in the transition state of the S_N2 reaction, concentrations of both reaction partners contribute to the rate law.

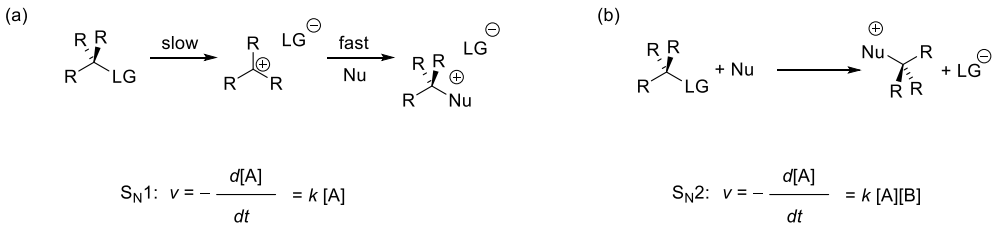

Figure 1. (a) S_N1 reaction and first-order rate law. (b) S_N2 reaction and second-order rate law.

How temperature,[1a,1g,1h,3] solvent,[1b,4] leaving group,[4e,5] or structural variations in the electrofuge[4e,6] impact either the S_N1 or the S_N2 reactions has been studied to huge extent in previous work and led to a good understanding of the individual reaction mechanisms. However, there is still no straightforward answer to the question whether a good leaving group in S_N1 reactions is also a good leaving group in S_N2 reactions. For example, whether bromide and tosylate are equally good leaving groups or tosylate is the by a factor of 1000 better leaving group than bromide depends on the acting mechanism.[5]

In order to avoid a significant influence of steric environment at the electrophilic center, it was therefore intended in this study to use electrophilic substrates that reacted concomitantly via S_N1 and S_N2 mechanisms. In this way, it was possible to derive tendencies in the leaving groups abilities for S_N1 and S_N2 reactions without changing the electrofuge structure, which comprised secondary carbons as the reaction centers.

Conductivity was used to monitor the kinetics of the reactions, in which ionic species are formed from neutral reactants. Non-linearities of solution conductivity with increasing ion concentrations needed

to be considered and were handled by separate calibration experiments, which finally allowed to connect experimentally measured conductivity values to a certain salt concentration in solution.

Rate constants for S_N1 reactions were determined in acetonitrile or mixtures of acetonitrile with protic solvents. The same solvents were utilized to determine rate constants for the S_N2 reactions, in which variable concentrations of added amines acted as the nucleophiles. By using this experimental setup, it was possible to investigate various effects on both types of nucleophilic substitutions, which allowed us to identify the susceptibility of the individual reaction channels toward changes in temperature, solvent, leaving group, electrofuge structure, or type of added nucleophile.

It will be shown, that the results in this thesis along with rate constants reported previously by others make it possible to develop guidelines to predict which external changes can be made to direct the reaction mechanism either toward an S_N1 or an S_N2 path. Analyzing the energy profiles of related reactions, in which the electrofuge was kept constant and the leaving group was varied, revealed intrinsic barriers as important factors to explain the variability of relative Br/OTs leaving group abilities in nucleophilic substitutions.

4.2 Results and Discussion

Kinetics.

Uncharged nucleophiles **9-13** reacted with 1-phenethyl halides (**1-X** - **5-X**), tosylates (**1-OTs**), benzhydryl halides (**6-Br**, **7-Br**), 1,3-diarylallyl halides (**8-Br**, **8-Cl**) or 1-butyl halides and tosylates (**BuX**) in acetonitrile or acetonitrile/methanol mixtures at 20 °C (Chart 1).

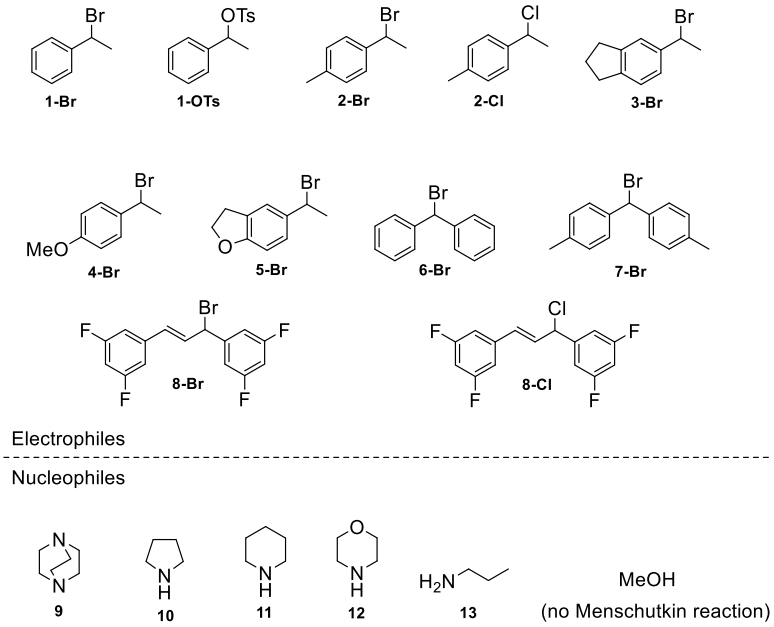

Chart 1. Employed electrophiles **1**-**8** and nucleophiles **9**-**13**. MeOH reacts as nucleophile with carbocations but not with alkyl halides or tosylates.

In Figure 2a, the reaction of **7-Br** with DABCO (**9**) is depicted as example. Due to the ionic nature of the products, time-resolved conductometry was used to follow the kinetics of the aforementioned reactions (Figure 2b). Products of some typical reactions have been analyzed in more detail (see below). The linear correlation between conductance and ammonium ion concentration was shown for piperidinium chloride in acetonitrile/methanol mixtures (Figure 3). In pure acetonitrile without methanol this correlation was no longer linear for secondary or primary amines. Solutions of protonated primary, secondary and tertiary amines in acetonitrile with chloride, bromide or tosylate counterions deviate from the ideal behavior (the molar conductivity $\Lambda_m = \kappa/c$ becomes concentration dependent)[7] and show a curvature in plots of conductance versus concentration. This is due to ion pairing, which has to be considered when deriving k_{obs} and k_2 from measurements of conductance.

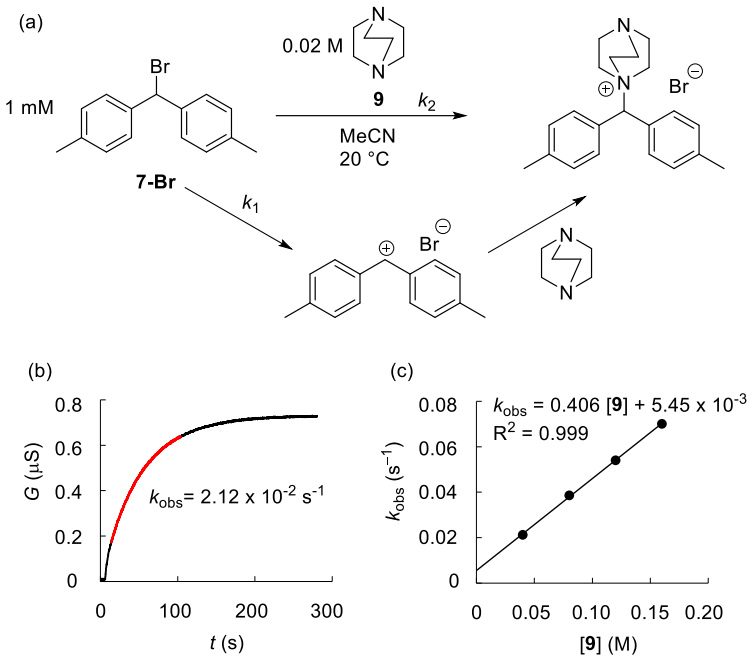

Figure 2. (a) Concurrent S_N1 and S_N2 reaction of **7-Br** with DABCO (**9**) at 20 °C in acetonitrile. (b) Plot of conductance *G* versus time *t* for the above reaction. (c) Linear correlation of k_{obs} versus nucleophile concentration. The intercept represents the nucleophile independent rate constant k_1 and the slope represents the nucleophile dependent rate constant k_2.

To consider this non-linear behavior, the ammonium chlorides, bromides and tosylates were added in portions to solutions of the corresponding amines in acetonitrile while the resulting conductance was recorded. Figure 4 depicts a plot of salt concentration versus conductance resulting from the stepwise addition of morpholinium hydrobromide as acetonitrile solution to a solution of 0.05 M morpholine (**12**) in acetonitrile. The plot of concentration versus conductance was fitted with a second-order polynomial which accurately describes the behavior in the relevant concentration range (Figure 4). The second-order polynomial was then used to convert the measured conductance of the kinetic experiments into the actual concentrations of the formed product. All kinetics that have been evaluated in this way are marked in Table 1 (footnote *g*). The conducting species is the protonated, primary or secondary amine due to amine excess in the kinetic experiments. Tertiary amines form quaternary ammonium ions which cannot transfer a proton and undergo ion pairing to a much lower extent with the employed halides and tosylate. Consequently, the conductance does not depend on the electrophile when secondary or primary amines are employed as nucleophiles, due to proton transfer to the excess amine. This protonated amine is the charged species that is detected by conductometry. This was also shown by the comparison of the concentration-dependent conductance of the products of **4-Br** and **7-Br** with piperidine (**11**) and that of the corresponding hydrobromide **11·HBr**, which show matching plots of salt concentration versus conductance (Figure 5). While the plots do not agree perfectly, the deviation was considered acceptable for our purposes. We observed, that higher amine and/or methanol concentrations reduce the degree of curvature. Consequently, ion pairing does depend on the quantity of the H-bond donor/acceptor, which solvates the cation and anion. Also, certain ammonium salts, like morpholinium hydrobromide (**12·HBr**) show more curvature than other ammonium salts, e.g. propylammonium hydrobromide (**13·HBr**) at equal amine concentration in acetonitrile.

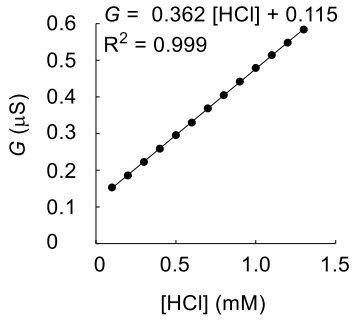

Figure 3. Conductance versus HCl concentration in 0.2 M piperidine in 20% (v/v) methanol in acetonitrile.

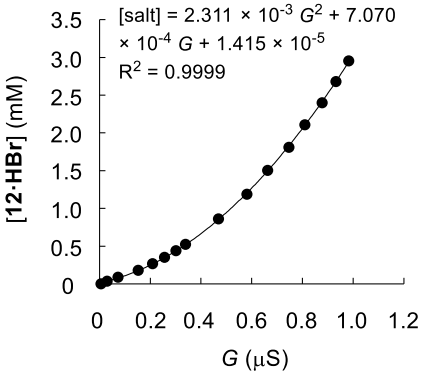

Figure 4. Plot of morpholinium hydrobromide (**12·HBr**) concentration versus conductance. Solvent is acetonitrile with 0.05 M morpholine at 20 °C. This example shows the strongest curvature.

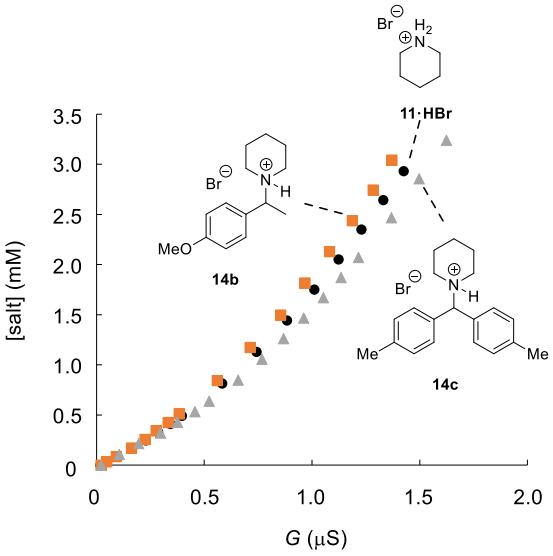

Figure 5. Plot of salt (**11·HBr**, **14b** or **14c**) concentration versus conductance. Solvent is acetonitrile with 0.1 M piperidine (**11**) at 20 °C. Orange squares represent **14b**, black dots represent piperidinium hydrobromide (**11·HBr**) and grey triangles represent **14c**.

In Figure 2b, the change in conductance over the course of the reaction in Figure 2a is depicted. For fast reactions that are complete in less than 10 minutes the stopped-flow technique was employed. Pseudo first-order kinetics were observed when the electrophiles were treated with an at least 10-fold excess of nucleophile. First-order rate constants were calculated by least-squares fitting of the function $A_t = A_0\ (1 - \exp(-k_{obs}t)) + C$ to the increasing conductance (red part in Figure 2b). Different concentrations of the nucleophiles **9**-**13** give different k_{obs} values, which can be interpreted by plotting k_{obs} versus nucleophile concentration which results in a linear correlation (Figure 2c). Equation 1 shows the connection between k_{obs}, k_1 and k_2.

$$k_{obs} = k_1 + k_2\,[Nu] \qquad \text{(equation 1)}$$

The nucleophile-independent rate constant k_1 represents the heterolytic cleavage as rate-determining step followed by a fast nucleophilic addition. The intercept of the plot in Figure 2c equals k_1.

The rate of the bimolecular S_N2 reaction is represented by the nucleophile concentration multiplied with k_2, which equals the slope of the linear correlation in Figure 2c. Four different concentrations of nucleophile were measured for each electrophile-nucleophile pair to determine k_1 and k_2 from a linear correlation of k_{obs} versus nucleophile concentration (see Table 1). Since the nucleophile is used in excess, the final conductances at the end of the reactions depend only on the amount and type of substrate and type of amine.

Conditions could be found, under which S_N1 and S_N2 reactions occurred concomitantly, by fine-tuning the amount of methanol in acetonitrile. When this was not possible because the S_N2 reaction was much faster than the S_N1 reaction, the weakly nucleophilic triethylamine was used instead of the nucleophile to monitor only the progress of the S_N1 reaction (Figure 6). The observed rate constants (k_{obs}) were independent of the triethylamine concentration. The rates of the reactions **1-X**-**8-X** with triethylamine (<1 M) in acetonitrile or acetonitrile/methanol at 20 °C did not depend on the concentration of triethylamine, thus giving rise to the first-order rate constants k_1. Further plots of k_{obs} versus triethylamine concentration are reported in the Experimental Section. Apparently, triethylamine is too sterically hindered to undergo a reaction *via* an S_N2 mechanism with the electrophiles **1-8** and cannot compete with the faster S_N1 mechanism. If methanol is present, triethylamine acts as Brønsted base and ethers are formed as products. Without methanol triethylamine acts as nucleophile in an S_N1 mechanism and ammonium salts are formed as products. If one reaction path is significantly faster than the other, then the method of Figure 2c becomes inaccurate for the slower rate constant. We resolved this limitation for S_N2 reactions that were much faster than the concomitant S_N1 reactions by measuring the kinetics separately with triethylamine instead of the actual nucleophile. However, no such workaround is possible, if the S_N1 reaction is substantially faster than the S_N2 reaction.

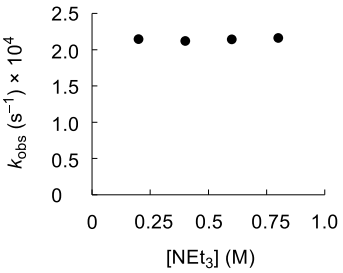

Figure 6. Observed rate of the ionization of **2-Br** in 20% (v/v) methanol in acetonitrile versus triethylamine concentration.

Rate constants k_2 and k_1 of the reactions of the employed electrophiles with the nucleophiles **9**-**13** and methanol are summarized in Table 1 and depicted as plots of k_{obs} versus amine concentration in Figure 6. Further rate constants, for example at different temperatures, will be presented in the appropriate sections, where they are discussed.

Table 1. First and second-order rate constants (20 °C) for the reactions of amines with alkyl halides in acetonitrile or acetonitrile/methanol mixtures.

Electrophile	solvent	k_1 (s^{-1}) [d]	DABCO (**9**) k_2 (M^{-1} s^{-1})	Pyrrolidine (**10**) k_2 (M^{-1} s^{-1})	Piperidine (**11**) k_2 (M^{-1} s^{-1})	Morpholine (**12**) k_2 (M^{-1} s^{-1})	Propylamine (**13**) k_2 (M^{-1} s^{-1})
1-Br	AN	n.d.	3.19×10^{-2}	8.36×10^{-3} [g]	5.18×10^{-3} [g]	1.18×10^{-3} [g]	3.29×10^{-4} [g]
1-OTs	AN [a]	1.65×10^{-5}	2.45×10^{-2}	5.48×10^{-3} [g]	3.41×10^{-3} [g]	1.19×10^{-3} [g]	4.74×10^{-4} [g]
2-Br	80AN20M	2.16×10^{-4}	1.81×10^{-2}	3.52×10^{-3}	2.70×10^{-3}	1.71×10^{-3}	5.76×10^{-4}
2-Cl	80AN20M	4.28×10^{-6}	1.39×10^{-4}	2.37×10^{-5}	1.51×10^{-5}	1.14×10^{-5}	n.d.
3-Br	AN	2.11×10^{-5}	1.09×10^{-1}	2.06×10^{-2} [g]	1.30×10^{-2} [g]	3.94×10^{-3} [g]	9.09×10^{-4} [g]
4-Br	AN	3.95×10^{-3}	4.40×10^{-1}	5.75×10^{-2} [g]	5.11×10^{-2} [g]	1.93×10^{-2} [g]	6.76×10^{-3} [g]
5-Br	AN	2.71×10^{-1} [c]	2.14	7.45×10^{-1}	4.66×10^{-1}	[b]	[b]
6-Br	AN	6.92×10^{-6}	2.53×10^{-2}	7.53×10^{-3} [g]	5.15×10^{-3} [g]	1.49×10^{-3} [g]	3.53×10^{-4} [g]
7-Br	AN	4.31×10^{-3} [e]	4.06×10^{-1}	9.58×10^{-2} [g]	6.05×10^{-2} [g]	3.50×10^{-2} [g]	1.25×10^{-2}
8-Br	90AN10M	3.29×10^{-3}	n.d.	1.39×10^{-1}	1.54×10^{-1}	5.21×10^{-2}	6.96×10^{-3}
8-Cl	90AN10M	1.33×10^{-4} [f]	n.d.	2.62×10^{-4}	3.09×10^{-4}	[b]	[b]
BuCl	AN	n.d.	1.06×10^{-5}	n.d.	n.d.	n.d.	n.d.
BuBr	AN	n.d.	1.77×10^{-3}	n.d.	5.58×10^{-4} [g]	8.61×10^{-5} [g]	n.d.
BuI	AN	n.d.	9.48×10^{-3}	n.d.	2.80×10^{-3}	4.78×10^{-4}	n.d.
BuOTs	AN	n.d.	7.35×10^{-4}	n.d.	1.91×10^{-4} [g]	3.32×10^{-5} [g]	n.d.

a Compounds that were not sufficiently stable in MeCN were added to the reaction as toluene solutions. The addition of up to 5% toluene to acetonitrile showed no effect on k_1 or k_2 when compared to pure MeCN.

b Reaction could not be accurately measured due to the fast S_N1 reaction.

c Rate constant was determined with piperidine.

d Triethylamine instead of the nucleophile was used to measure k_1 if k_2 was deemed to large to allow an accurate determination of k_1 by the intercept.

e Rate constant was determined with propylamine.

f Rate constant was determined with benzylamine.

g For kinetics affected by significant ion pairing, conductivity data were converted to concentrations by using the polynomial fit method described in Figure 4.

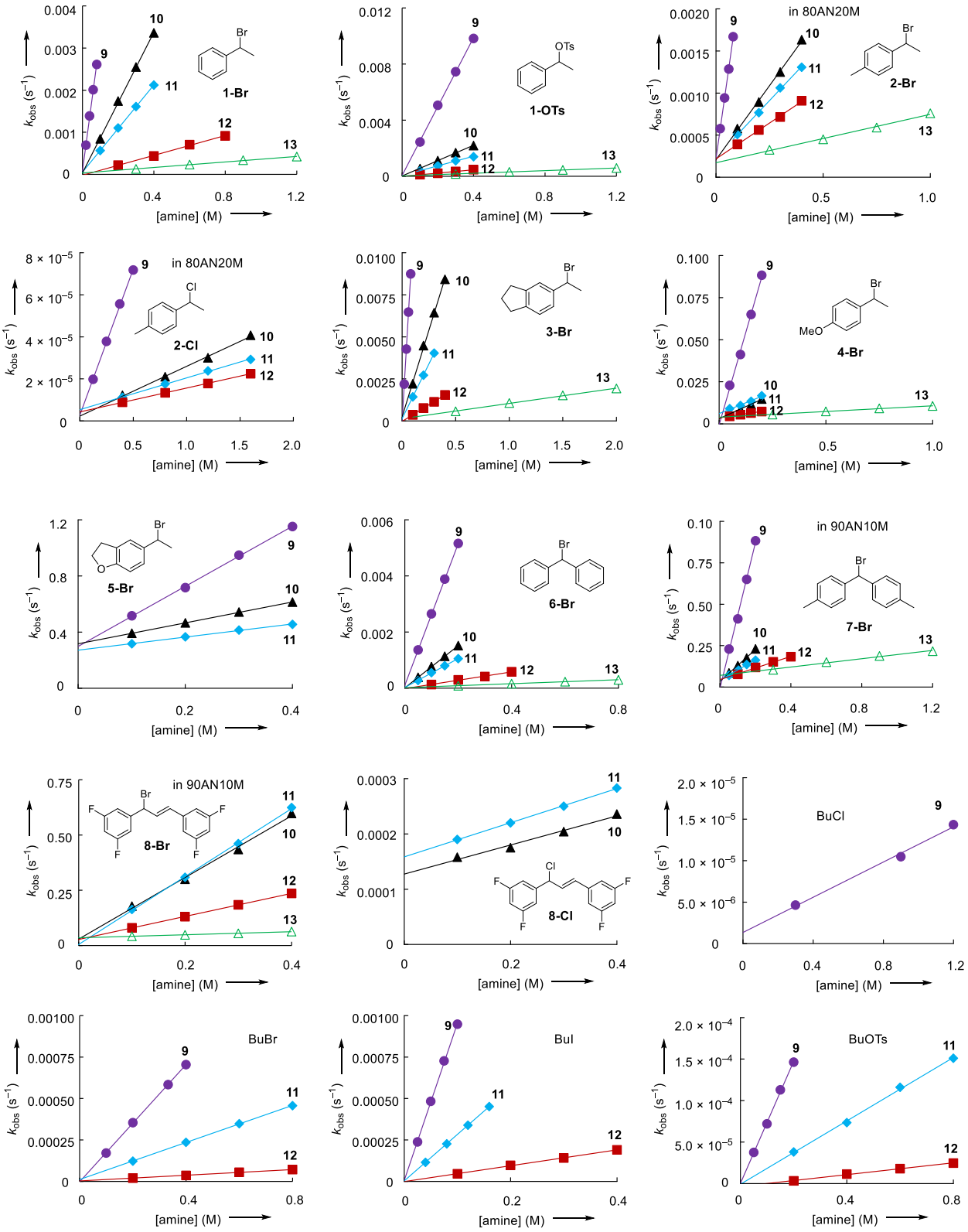

Figure 7. Plots of k_{obs} versus amine concentration for each electrophile entry in Table 1. The amines DABCO (**9**, purple circles), pyrrolidine (**10**, black triangles), piperidine (**11,** blue diamonds), morpholine (**12**, red squares) and propylamine (**13**, unfilled green triangles) are color coded. All reactions that have not been recorded in acetonitrile have their solvent mixture of acetonitrile (AN) and MeOH (M) denoted as v/v%. E.g. 80AN20M is 80% (v/v) acetonitrile, 20% MeOH.

Product studies.

The products of the reactions of secondary, benzylic halides or tosylates with primary, secondary or tertiary amines were studied by ^{1}H NMR spectroscopy for one nucleophile/electrophile combination in 80% acetonitrile and 20% methanol. The solvolysis of benzhydryl chlorides in acetone/water mixtures in the presence of amines had been studied earlier and gave analogous products.[8]

Ideally, the only product of the S_N2 pathway should be ammonium bromide **14a** (Scheme 1). Both, the ammonium bromide **14a** and methyl ether **15a** are possible products of the competing S_N1 pathway.

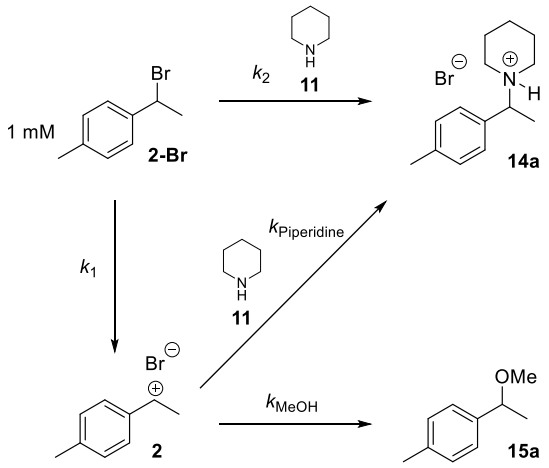

Scheme 1. Reaction of **2-Br** with piperidine (**11**) in 80AN20M at 20 °C.

Table 2. Reaction of **2-Br** with different piperidine (**11**) concentrations in 80AN20M (80% MeCN, 20% D_3COD (v/v)) at 20 °C. [D_3COD] = 4.92 M.

[**11**]	0.052 M	0.104 M	0.155 M	0.207 M
Found product ratio [**14a**]/[**15a**]	0.73	1.6	2.7	3.9
Calculated[a] product ratio [**14a**]/[**15a**]	0.67	1.4	2.0	2.8

a Calculated with equation (V).

The product ratio is equal to the ratio of the rates at which these products are formed. The actual product ratio was determined by ^{1}H-NMR spectroscopy (Table 2). The alkylated amine **14a** is produced in the S_N2 pathway at a rate of:

$$\frac{d[\mathbf{14a}]}{dt} = k_2\,[\mathbf{2\text{-}Br}]\,[\mathbf{11}] \qquad (I)$$

In the S_N1 pathway **14a** and **15a** are both formed. We assume methanol (N=7.54, s_N=0.92 in MeOH)[9] and piperidine (**11**) (N=17.35, s_N=0.68 in AN)[10] both react under diffusion control (log k_{calc} > 10) with carbocation **2** (E>6.0 of the similar, but more stable (2,4,6-trimethylphenyl)ethylium ion),[11] due to an estimation with the Mayr-Patz equation (equation 2) ($k_{piperidine} = k_{MeOH} = k_{diff}$).

$\log k_{20\,°C} = s_N (N + E)$ (equation 2)

We also assume that k_1 is the slowest and thus rate determining step of the S_N1 pathway. As a result, the amount of **14a** or **15a** formed through the S_N1 pathway can be described with the following equations:

$$\frac{d[\mathbf{14a}]}{dt} = k_1\,[\mathbf{2\text{-}Br}]\;\frac{[\mathbf{11}]}{[D_3COD] + [\mathbf{11}]} \qquad \text{(II)}$$

$$\frac{d[\mathbf{15a}]}{dt} = k_1\,[\mathbf{2\text{-}Br}]\;\frac{[D_3COD]}{[D_3COD] + [\mathbf{11}]} \qquad \text{(III)}$$

Equation (II) and (III) equal the rate of formation of carbenium ion **2** multiplied with the relative amount of piperidine (**11**) or deuterated methanol, respectively. Adding both rates for the formation of **14a** ((I) and (II)) and dividing by the rate of formation of **15a** (III) gives the full term required to calculate the product ratio (Scheme 1, Table 2) of the concurrent S_N1 and S_N2 reactions:

$$\frac{[\mathbf{14a}]}{[\mathbf{15a}]} = \frac{k_2\,[\mathbf{11}]\,[\mathbf{2\text{-}Br}] + k_1\,[\mathbf{2\text{-}Br}]\;\dfrac{[\mathbf{11}]}{[D_3COD] + [\mathbf{11}]}}{k_1\,[\mathbf{2\text{-}Br}]\;\dfrac{[D_3COD]}{[D_3COD] + [\mathbf{11}]}} \qquad \text{(IV)}$$

Which can be simplified to:

$$\frac{[\mathbf{14a}]}{[\mathbf{15a}]} = \frac{k_2\,[\mathbf{11}] + k_1\;\dfrac{[\mathbf{11}]}{[D_3COD] + [\mathbf{11}]}}{k_1\;\dfrac{[D_3COD]}{[D_3COD] + [\mathbf{11}]}} \qquad \text{(V)}$$

The calculated product ratio differs slightly from the experimentally found product ratio (Table 2). In fact, piperidine appears to be more reactive than methanol ($k_{piperidine} > k_{MeOH}$) towards the free carbocation **2**, as more **14a** is found than expected. Consequently, methanol is not reacting as rapidly as piperidine with the carbocation **2** and less of **15a** is formed than expected. Piperidine and methanol have to react at rates close to or at the diffusion limit with the free carbocation, however, as otherwise no ether product **15a** would be detected due to the much higher nucleophilicity of piperidine.[12]

Another explanation for the deviation between in found and calculated product ratios (Table 2) would be an error in the determination of the rate constants k_1 and k_2. An error in k_1 of the required magnitude is unlikely, because the intercepts, which represent k_1, of the plots of k_{obs} versus amine concentration agree well with each other (Figure 7). An error in k_2 this big is also unlikely, as the rate constants k_2 were determined as linear correlations of plots of k_{obs} versus amine concentration with

good R^2. However, the deviations of the found and the calculated product ratios in Table 2 are small enough to not be of concern.

In pure acetonitrile the product formed through the S_N1 and S_N2 pathway is the same (Scheme 2), and multiple alkylations of the same amine are not observed.

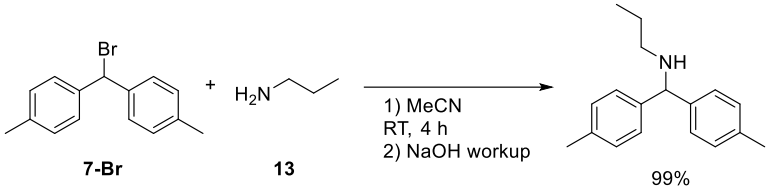

Scheme 2. Reaction of **7-Br** with propylamine in acetonitrile at room temperature.

Effect of substituents.

The effect of para substituents on 1-arylethyl bromides in reactions with pyridine was studied by Tsuno et. al.[13] In their study they investigated concurrent S_N1 and S_N2 reactions and analyzed their data with Yukawa-Tsuno plots. While the S_N1 reaction showed a linear correlation with σ, the S_N2 reaction showed significant curvature in the Hammett plot, indicating a change in the transition state. The S_N2 transition state is quite susceptible to changes in substituent constant σ once the substituents are sufficiently strong electron donors (σ < -0.3 in this instance). Before that point, that is for substituents with σ < -0.3, substituent effects are miniscule.

Table 3. Reaction of phenethyl and benzhydryl bromides with piperidine (**11**) in AN at 20 °C. Selected data points from table 1.

Electrophile		k_1 (s^{-1})	k_2 (M^{-1} s^{-1})	k_2/k_1
1-Br		1.85×10^{-8} *a*	5.18×10^{-3} *b*	2.80×10^{5}
2-Br		4.83×10^{-6}	1.10×10^{-2}	2280
3-Br		2.11×10^{-5} *b*	1.30×10^{-2}	616
4-Br		3.95×10^{-3} *b*	5.11×10^{-2}	12.9
5-Br		2.71×10^{-1} *b*	4.66×10^{-1}	1.72
6-Br		6.92×10^{-6} *b*	5.15×10^{-3}	744
7-Br	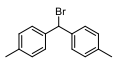	4.31×10^{-3} *b*	6.05×10^{-2}	14.0

a calculated using reactivity parameters reported in ref[14]

b data taken from Table 1

The S_N1 reaction, which is generally more susceptible to changes in the electronic structure, shows a constant strong influence of the aryl substituents on reactivity.[13] The changing magnitude of the influence of aryl substituents on reaction rates of the S_N2 reactions (the curvature in the Yukawa-Tsuno plot[13] found by Tsuno) can be rationalized by the change in transition state structure: Strong electron donors in para position make charge separation more favorable and consequently the reactive carbon center in the S_N2 mechanism develops more carbocationic character as the nucleophile and leaving group are more distant in the transition state.[15] In the literature this is described as a "loose" transition state.[6b,13,16] So with strong electron donors the S_N2 mechanism is similar to the S_N1 mechanism in terms of susceptibility to electronic effects. In reactions of phenethyl bromides with neutral or electron-withdrawing substituents, however, the S_N2 transition state is tightly bound and charge separation does not occur to a significant magnitude.[13] This in turn explains why the change in σ has barely any effect on the S_N2 reaction rates for electron withdrawing groups in the study by Tsuno.[13] Without charge separation, there is no charge which can be stabilized or destabilized by electronic effects.

Our observations with aliphatic amines at 20 °C (Table 3) are in line with those of Tsuno *et al*. who observed the reaction of substituted phenethyl bromides with pyridine at 35 °C and got similar results and reactivity trends. Addition of a methyl substituent to 1-bromo phenethyl (**1-Br**) in *para* position (**2-Br**) leads only to a twofold increase in k_2 while replacement of the methoxy group by a tetrahydrofuran ring **4-Br** yields an almost 10-fold increase in k_2 (**4-Br** versus **5-Br**, Table 3). On the other hand, k_2 increases only by a factor of 1.18 when comparing the rate constants k_2 of **2-Br** and **3-Br**. Consequently the change of the transition state structure and thus susceptibility to electron donating groups for S_N2 when going from neutral to electron donating substituents on arylethyl systems is analogous to the effects observed by Tsuno.[13]

Effect of solvent.

It is common knowledge, that solvent is the easiest, highly effective way to control the reaction pathway. Highly polar, aprotic solvents favor S_N2 (Figure 8, black dots, reaction in 10M90AN), while protic, polar solvents favor S_N1 (Figure 8, red squares, reaction in 91M9AN). In 91% methanol no dependency of k_{obs} on nucleophile concentration could be observed. By changing from 91% methanol in acetonitrile to 10% methanol in acetonitrile the dominant reaction mechanism could be switched from S_N1 to S_N2. According to the Hughes-Ingold rules,[17] neutral reactants, which are converted into ionic species, should react faster in methanol [$E_T(30)$ = 55.4 kcal mol^{-1}] than in acetonitrile [$E_T(30)$ = 45.6 kcal mol^{-1}].[18] As depicted in Figure 9, this is true for the S_N1 reaction, however the rate constants k_2 for the S_N2 reactions decreases with increasing methanol content.

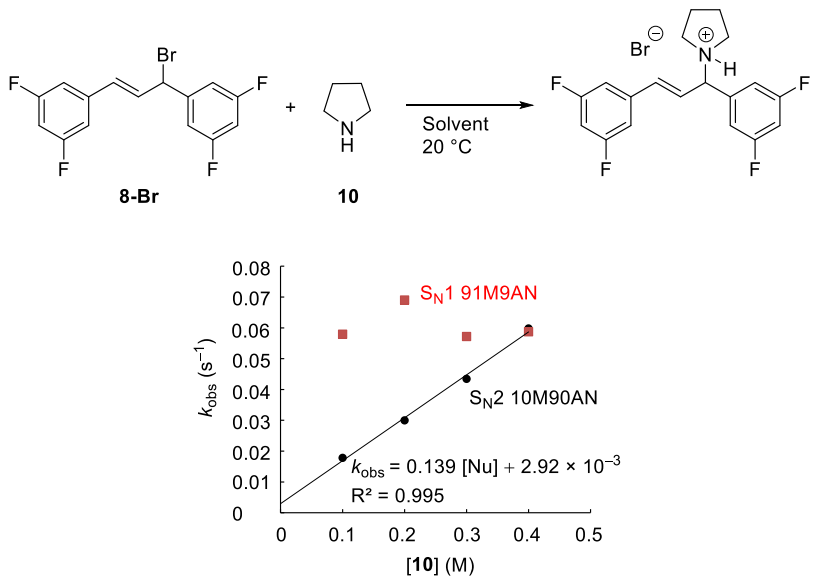

Figure 8. Depiction of k_{obs} of the reaction of **8-Br** with pyrrolidine at 20 °C in 91% methanol/9% acetonitrile (red squares) or in 10% methanol/90% acetonitrile (black dots) versus pyrrolidine concentration.

To study the solvent effect, we changed the solvent composition of a system that showed concomitant S_N1 and S_N2 mechanisms while keeping the temperature and concentrations of the educts constant (Table 4). With increasing amounts of methanol in the AN/M mixtures we observed a decrease in the rate of the S_N2 reaction and an increase in the rate of the S_N1 reaction (Table 4, Figure 9). The ratio k_2/k_1 changes by more than 3 orders of magnitude. In solutions containing more than 50% (v/v) methanol in acetonitrile the rate of the S_N2 reaction cannot any longer be precisely determined, as the S_N1 mechanism becomes highly dominating.

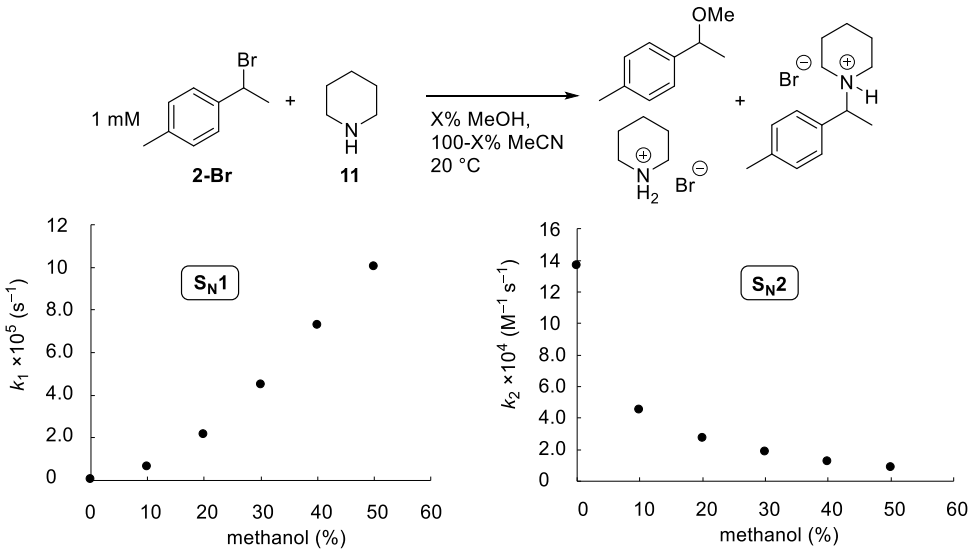

Figure 9. Dependence of k_1 (left, S_N1) and k_2 (right, S_N2) on the methanol content (v/v) of acetonitrile solutions for the reaction of **2-Br** with piperidine (**11**) in AN/MeOH mixtures (Table 4).

Table 4. Reaction of **2-Br** with piperidine (**11**) (k_2) or NEt_3 (k_1) in acetonitrile/methanol mixtures at 20 °C.

Solvent [a]	k_1 (s^{-1})	k_2 (M^{-1} s^{-1})	k_2/k_1
AN [a]	4.83×10^{-6}	1.10×10^{-2}	2280
90AN10M [a]	6.53×10^{-5}	4.50×10^{-3}	68.9
80AN20M [a]	2.16×10^{-4}	2.70×10^{-3}	12.5
70AN30M [a]	4.50×10^{-4}	1.82×10^{-3}	4.04
60AN40M [a]	7.29×10^{-4}	1.22×10^{-3}	1.67
50AN50M [a]	1.03×10^{-3}	8.64×10^{-4}	0.838

a AN is acetonitrile, M is methanol. 90AN10M means 90% acetonitrile (v/v) and 10% methanol.

The observations for the reactivity trends of separate S_N1 and S_N2 reactions and concurrent S_N1 and S_N2 reactions are in line with each other. The decrease in nucleophilicity of amines and other nucleophiles for the transfer from aprotic to protic solvents is a well-known phenomenon. For example, benzylamine is more nucleophilic in DMSO (N=15.28, s_N=0.62)[1a] by around 2 orders of magnitude and by around 1 order of magnitude in acetonitrile (N=14.29, s_N=0.67)[10] than in the protic solvent water (N=13.44, s_N=0.55).[19] Also benzylamine is more nucleophilic towards benzhydrylium ions in pure acetonitrile than in a acetonitrile/methanol (9AN91M) mixture by almost an order of magnitude.[10,20] Similar trends have also been reported for ethanolamine and morpholine.[12] S_N2 reactions generally tend to be faster in aprotic than in protic media of comparable polarity.[21] Higher polarity of the solvent results in greater overall rates in Menschutkin reactions.[22] However, a study by Haberfield *et al*. demonstrated that the negative enthalpy for the transfer of pyridine from aprotic dimethylformamide (DMF) to protic methanol is compensated by the decreased solvation of benzyl halides, their reaction partners. The nucleophile is better solvated and thus stabilized in protic media like methanol due to hydrogen bonding. The actual rate decreasing effect is due to the positive enthalpy of transfer of the transition states when changing the solvent from aprotic DMF to protic methanol as shown by Haberfield *et al*.. While the Hughes-Ingold rules for reactions with charge separation and the similarity of mechanisms would indicate that S_N1 and S_N2 follow the same trends in terms of the effect of the solvent on the rate, this is obviously not the case as demonstrated in Figure 9.

Comparison of the reaction of allyl bromide **8**-**Br** in 10M90AN and 10W90AN shows that the S_N1 reaction is 15 times faster in aqueous acetonitrile (intercepts) while the S_N2 reactivity is almost equally fast (slopes) (Figure 10). Water is known to be better at facilitating the S_N1 reaction than methanol.[23] Water [E_T(30) = 63.1 kcal mol^{-1}] is also more polar than methanol [E_T(30) = 55.4 kcal mol^{-1}],[18] which might account for the slight increase of the rate of the S_N2 reaction. Furthermore, it has to be

mentioned, that one mL of water contains 56 mmol water while one mL of methanol contains only 25 mmol of methanol.

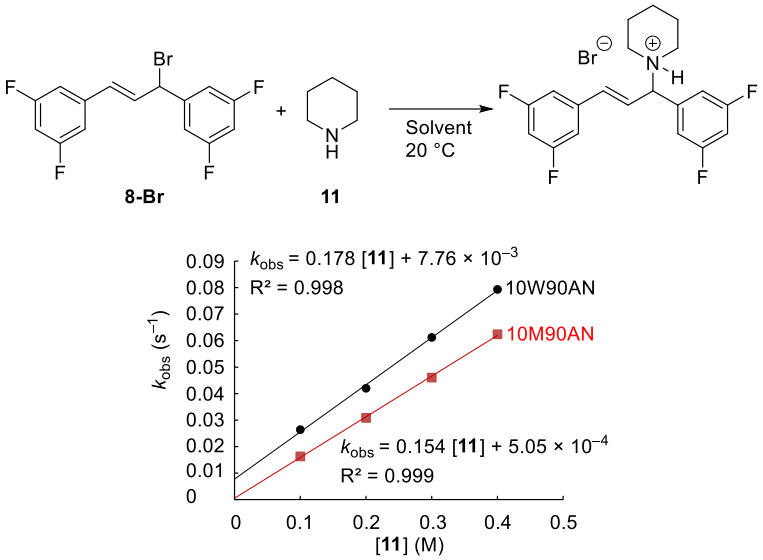

Figure 10. Dependence of k_{obs} of the reaction of **8-Br** with piperidine at 20 °C in 10% methanol/90% acetonitrile (red squares) or in 10% water/90% acetonitrile (black dots) on the piperidine (**11**) concentration.

Effect of nucleophile.

Independent of arylethyl substitution, all employed nucleophiles displayed an almost constant relative reactivity, as the ratios of k_2^{DABCO}, $k_2^{pyrrolidine}$, $k_2^{piperidine}$, $k_2^{morpholine}$ and $k_2^{propylamine}$ towards each other did not change substantially when the electrophile was varied (Figure 7). The tertiary amine DABCO (**9**) was always the most reactive, followed by the secondary amines pyrrolidine (**10**), piperidine (**11**) and morpholine (**12**) and the least reactive, primary amine propylamine (**13**) (**9**>**10**>**11**>**12**>**13**). In contrast, in reactions with the 1,3-diarylallyls **8-Br** and **8-Cl** piperidine (**11**) was slightly more reactive than pyrrolidine (**10**) (Table 5, Figures 11 and 12). Only triethylamine was less reactive than propylamine. In all reactions investigated, an S_N2 reaction of triethylamine could not be observed because of the much faster S_N1 reaction. When looking at the tertiary amines DABCO and triethylamine and their difference in reactivity, the importance of conformation and sterics becomes obvious. DABCO is the most reactive amine in our studies and triethylamine the least reactive.

Leaving group, electrofuge and solvent had little influence on relative reactivity of the investigated amines.

Table 5. First and second-order rate constants (20 °C) for the reactions of amines with allyl halides in 90AN10M mixtures

nucleophile	**8-Br** k_2 (M^{-1} s^{-1})	**8-Cl** k_2 (M^{-1} s^{-1})
pyrrolidine (**10**)	1.39×10^{-1} *a*	2.62×10^{-4} *a*
piperidine (**11**)	1.54×10^{-1} *a*	3.09×10^{-4} *a*
morpholine (**12**)	5.21×10^{-2} *a*	2.35×10^{-4}
propylamine (**13**)	6.96×10^{-3} *a*	n. d.
diethanolamine (**16**)	1.03×10^{-2}	2.73×10^{-4}
ethanolamine (**17**)	4.95×10^{-3}	8.40×10^{-5}
benzylamine (**18**)	3.88×10^{-3}	2.01×10^{-5}
imidazole (**19**)	2.72×10^{-3}	1.25×10^{-4}
k_1 (s^{-1}) *a*	3.29×10^{-3} *a*	1.33×10^{-4} *a*

a data taken from Table 1

In our earlier work, however, we observed reactivity crossover of different nucleophiles.[1a] Thus, diethanolamine (**16**) is as reactive as benzylamine (**18**) towards benzhydryl bromide, while it is 5 times less reactive than benzylamine towards 4,4'-bis(trifluromethyl)benzhydryl bromide. We assume this was due to solvent effects. In particular, diethanolamine was more reactive than expected.

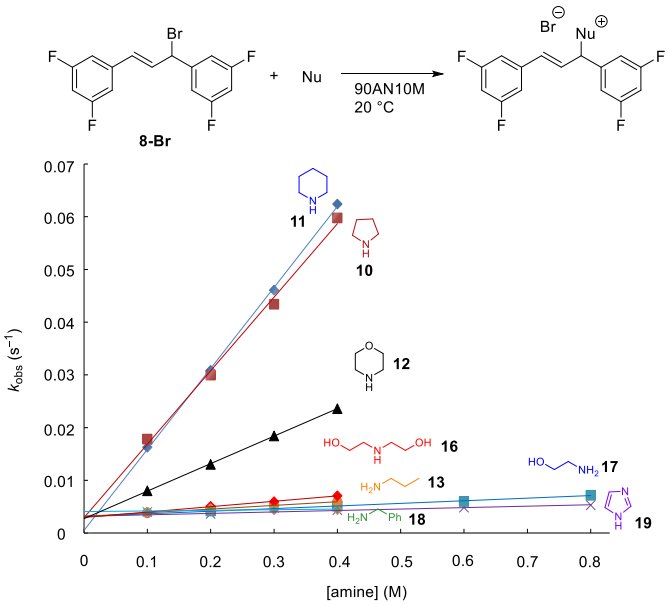

Figure 11. Observed rate constants k_{obs} for the reactions of **8-Br** with various amines in 90AN10M at 20 °C at different amine concentrations. The behaviour of the nucleophiles towards each other in this plot is considered "normal" and is similarly observed with all bromides (**1-8-Br**), the tosylate **1-OTs**, and the chloride **2-Cl**.

The k_2 for the reactions of **8-Cl** with diethanolamine cannot be determined from the slopes of the linear correlations of the nucleophile concentration against k_{obs}, because the slopes also reflect the linear

increase of k_1 with the nucleophile concentration in analogy to the increase of k_1 with increasing methanol concentration in AN/M mixtures (see Figure 9).

Depicted in Figure 11 is the plot of k_{obs} against nucleophile concentration for **8-Br,** where S_N2 is the dominant reaction mechanism ($k_2>k_1$). All linear correlations in Figure 11 have almost the same intercept, which is the observed rate constant in the absence of nucleophilic amines, due to the S_N1 reaction. In this case the slope of the linear correlation can be solely attributed to the S_N2 reaction and equation 1 can be applied. As long as the S_N2 mechanism is the prevalent mechanism, the relative reactivity of all employed amines stayed almost constant.

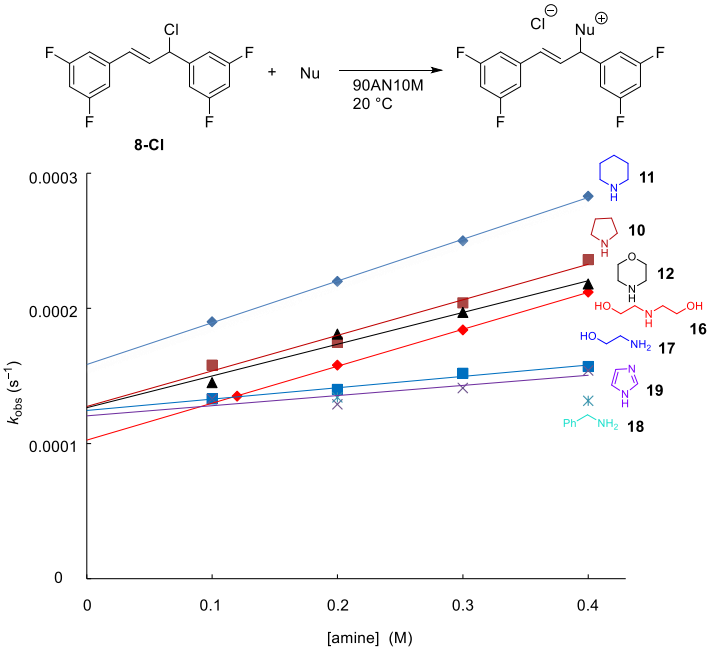

Figure 12. Observed rate constants k_{obs} for the reactions of **8-Cl** with various amines in 90AN10M at 20 °C at different amine concentrations.

In Figure 12 the plot of k_{obs} versus the amine concentration is depicted for the reactions with **8-Cl**. In S_N1 reactions k_{obs} should be independent of the nucleophile concentration. However, Figure 12 demonstrates that k_{obs} increases linearly with increasing amine concentrations. This is, however, not only due to the operation of S_N2 processes, but also due to the effect of high amine concentrations on the bulk solvent properties, which may cause a rate enhancement for the respective S_N1 reactions.

We have also reported a linear increase of the observed rate constant with increased methanol content in acetonitrile for the reactions of **2-Br** (Figure 9). The slope of diethanolamine is due to the solvent effect of its two hydroxy groups. Its inherent low nucleophilicity relative to the other amines is a minor reason of the concentration dependency of k_{obs}. Diethanolamine is the least nucleophilic secondary amine investigated by us and only slightly more nucleophilic than the primary propylamine in S_N2 reactions (Figure 11). In an S_N1 dominated system like **8-Cl** in 90AN10M (Figure 12), however,

diethanolamine has a higher slope than morpholine in k_{obs} versus [amine] plots, which we attribute to solvent effects and not S_N2 reactivity.

Morpholine is also more reactive towards **8-Cl** than expected when compared to piperidine and pyrrolidine (Figure 12). Morpholine should be considerably less reactive than piperidine and pyrrolidine, like in Figure 11, which is obviously not the case. Equation 1 could no longer be applied, because k_{obs} displays a nucleophile concentration dependency for S_N1 and S_N2 and thus neither k_1 nor k_2 can be determined for morpholine (**12**), diethanolamine (**16**), ethanolamine (**17**), benzylamine (**18**) and imidazole (**19**). Consequently, we disregarded all data from Figure 12 except for piperidine (**11**) and pyrrolidine (**10**), which have k_2 values large enough to be sufficiently reliable. Piperidine and pyrrolidine also should experience only a small solvent effect, since they have no other polar groups besides their necessary amine functionalities.

The Brønsted plot in Figure 13 (Table 6) shows a good correlation of log k_2 versus pK_{aH} only for secondary, cyclic amines. The tertiary amine DABCO and the primary, acylic propylamine deviate considerably from the correlation.

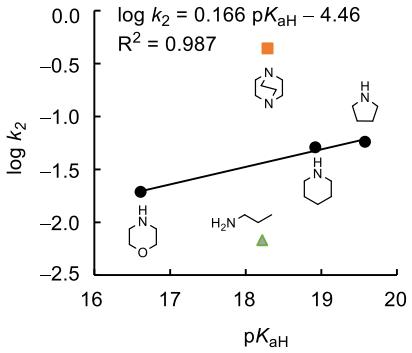

Figure 13. Brønsted plot for the reaction of **4-Br** with the secondary amines (black dots) at 20 °C in acetonitrile. DABCO and propylamine were omitted when calculating the correlation line.

Table 6. Reaction of **4-Br** at 20 °C with different nucleophiles in acetonitrile

nucleophile	pK_{aH} (in AN)[a]	log k_2	k_2/k_1
DABCO (**9**)	18.29	–0.357	111
pyrrolidine (**10**)	19.58	–1.24	14.6
piperidine (**11**)	18.92	–1.29	12.9
morpholine (**12**)	16.61	–1.21	4.89
propylamine (**13**)	18.22	–2.17	1.71

a taken from reference[24].

The second-order rate constants of the reactions of amines with electrophiles **1-X**-**8-X** in all investigated solvents did not correlate well with the nucleophilicity parameters *N* and s_N of the Mayr scale. The observed reactivity trends however were predicted correctly with Mayr *N* and s_N parameters: DABCO (*N*=18.80, s_N=0.70)[25] >.piperidine (*N*=17.35, s_N=0.68)[10] > morpholine (*N*=15.65, s_N=0.74)[10] > propylamine (*N*=15.11, s_N=0.63).[10] Obviously, these parameters hold for some S_N2 reactions substrates,[20,26] but not for others.[1a]

Effect of temperature.

We also determined activation parameters for one nucleophile/electrophile combination by measuring rate constants at 5 different temperatures (Figure 14, Table 7, Table 8).

In Figure 14 an Eyring[27] plot of ln (*k*/*T*) versus 1/*T* for the reaction of **2-Br** with piperidine (**11**) in 80AN20M is depicted. The black dots represent k_1 and the red squares k_2. $\Delta H^{\ddagger}$ and $\Delta S^{\ddagger}$ were calculated from these linear correlations according to Eyring theory for the S_N1 and the S_N2 reaction respectively. Once again differences between the S_N1 and S_N2 mechanism become clear. While the S_N1 mechanism is entropically more favorable than the S_N2 mechanism, it still displays a considerably negative activation entropy. This can be explained by the amount of solvent ordering around the cation and the anion that has to occur, which results from the charge separation. As the S_N2 transition state is highly ordered and involves the participation of an additional molecule, the entropic contribution to the activation barrier becomes even higher. However, the additional molecule, the nucleophile, reduces the activation enthalpy by assisting the cleavage of the carbon bromide bond.

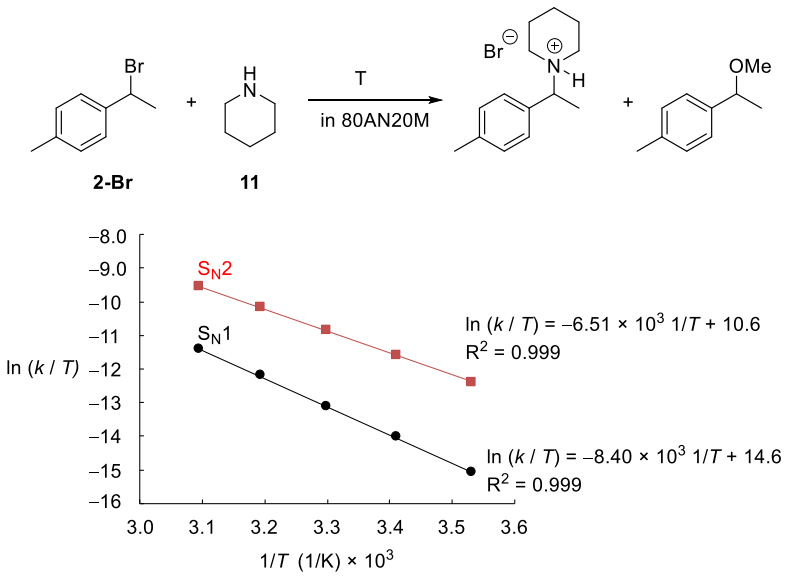

Figure 14. Eyring plot of the reaction of **2-Br** with piperidine (**11**). Red squares represent the rate constant k_2 of the S_N2 reaction at 10 to 50 °C. Black dots represent the rate constant k_1 of the S_N1 reaction at 10 to 50 °C.

Table 7. Reaction of **2-Br** at different temperatures with piperidine (**11**) in 80AN20M

temperature	k_1 (s^{-1})	k_2 (M^{-1} s^{-1})	k_2/k_1
10.0 °C	7.90×10^{-5}	1.16×10^{-3}	14.7
20.0 °C	2.37×10^{-4}	2.70×10^{-3}	11.4
30.0 °C	5.98×10^{-4}	5.91×10^{-3}	9.88
40.0 °C	1.58×10^{-3}	1.19×10^{-2}	7.53
50.0 °C	3.53×10^{-3}	2.27×10^{-2}	6.43

Table 8. Activation parameters of **2-Br** with piperidine (**11**) in 80AN20M according to the Eyring equation.

mechanism	$\Delta G^{\ddagger}_{20°C}$ (kJ mol^{-1})	$\Delta H^{\ddagger}$ (kJ mol^{-1})	$\Delta S^{\ddagger}$ (J mol^{-1} K^{-1})
S_N1	92.2	69.8	−76.3
S_N2	86.1	54.1	−109

The resulting piperidinium ion is also enthalpically more favorable than a carbocation, which is the short-lived intermediate product of the S_N1 mechanism. A factor of 2 in terms of mechanism selectivity (k_2/k_1) can be achieved by varying the temperature over a range of 40 K in this instance (Table 7). S_N1 and S_N2 display differences in their behavior when temperature is concerned, the effects are small compared to the effects of solvent variation.

Effect of leaving group.

It has been known for more than 80 years, that the reactivity of leaving groups depend on the acting mechanism.[5,28] However, to this day there is no specific study on the relative reactivity of bromide and tosylate as leaving groups attached to the same electrofuge in concomitant S_N1 and S_N2 reaction. While bromide is always a better leaving group than chloride independent of mechanism (Table 9, Table 10), the same cannot be said for the tosylate/bromide relationship (Table 11). Hoffmann *et al.* reported, that the ratios of bromide and tosylate rate constants of otherwise identical reactions vary by multiple orders of magnitude.[5] In S_N1 reactions tosylates usually react faster than bromides by three orders of magnitude (Table 12), sometimes even more.[5a,29] In S_N2 reactions tosylates and bromides show very similar reactivity, often bromide is the slightly better leaving group.[5]

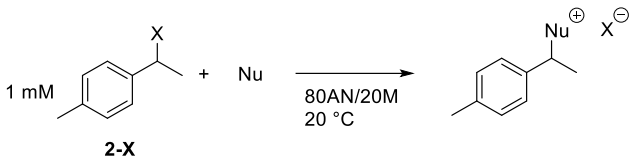

Table 9. Reaction of **2-Cl** and **2-Br** with amines in 80AN20M at 20 °C.

nucleophile	k_2^{Br} (M^{-1} s^{-1})	k_2^{Cl} (M^{-1} s^{-1})	k_{Cl} /k_{Br}
DABCO (**9**)	1.81×10^{-2}	1.39×10^{-4}	1/130
pyrrolidine (**10**)	3.52×10^{-3}	2.37×10^{-5}	1/149
piperidine (**11**)	2.70×10^{-3}	1.51×10^{-5}	1/179
morpholine (**12**)	1.71×10^{-3}	1.14×10^{-5}	1/150
k_1 (s^{-1}) [a]	2.15×10^{-4}	4.28×10^{-6}	1/50

a k_1 was determined with NEt_3 as proton trap

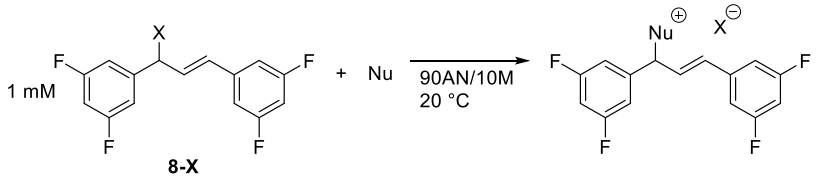

Table 10. Reaction of **8-Cl** and **8-Br** with amines in 90AN10M at 20 °C.

nucleophile	k_2^{Br} (M^{-1} s^{-1})	k_2^{Cl} (M^{-1} s^{-1})	k_{Cl} /k_{Br}
pyrrolidine (**10**)	1.39×10^{-1}	2.62×10^{-4}	1/531
piperidine (**11**)	1.54×10^{-1}	3.09×10^{-4}	1/499
k_1 (s^{-1})	3.29×10^{-3} [a]	1.33×10^{-4} [b]	1/25

a k_1 was determined with NEt_3 as proton trap

b k_1 was determined with benzylamine

Similarly, the halogenides differ in their relative reactivity depending on the acting mechanism (Table 9, Table 10). Bromide as leaving group reacts about 150 times faster *via* S_N2 than chloride in 80/20 acetonitrile/methanol (Table 9). The nucleophile type has a negligible effect on k_{Cl}/k_{Br} in our study. In line with related studies, the increase in the S_N1 reactivity is only a factor of 50 when changing from chloride to bromide (Table 9). In 90/10 acetonitrile/methanol the ratio k_{Cl}/k_{Br} is around 1/500 for **8-X** instead of around 1/150 for **2-X** for the S_N2 mechanism (Tables 9, 10). For the S_N1 mechanism k_{Cl}/k_{Br} is 1/25 for **8-X** and 1/50 for **2-X** (Tables 9, 10). The opposite trends for the changes of k_{Cl}/k_{Br} depending on the acting mechanism imply a different sensitivity of each reaction mechanism towards leaving groups and their respective attributes.

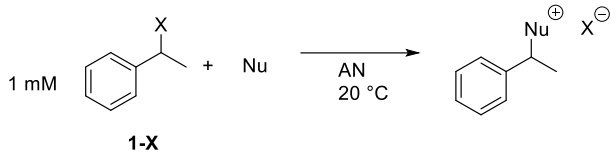

Table 11. Reaction of **1-OTs** and **1-Br** with amines in AN at 20 °C.

nucleophile	k_2^{Br} (M^{-1} s^{-1})	k_2^{OTs} (M^{-1} s^{-1})	k_{OTs}/k_{Br}
DABCO (**9**)	3.19×10^{-2}	2.45×10^{-2}	0.77
pyrrolidine (**10**)	8.36×10^{-3}	5.48×10^{-3}	0.66
piperidine (**11**)	5.18×10^{-3}	3.41×10^{-3}	0.66
morpholine (**12**)	1.18×10^{-3}	1.19×10^{-3}	1.01
propylamine (**13**)	3.29×10^{-4}	4.74×10^{-4}	1.44
k_1 (s^{-1})	1.85×10^{-8} *b*	1.65×10^{-5} *a*	892

a k_1 was determined with NEt_3 as proton trap

b is experimentally not accessible and was calculated using $\log k = s_f (N_f + E_f)$[14]

While bromide and tosylate proved to be about equally good leaving groups in the S_N2 pathway, tosylate was the significantly better leaving group in the S_N1 pathway (Table 11). There seems to be a trend for k_{OTs}/k_{Br} dependent on nucleophilicity: stronger nucleophiles react faster with bromide as nucleofuge, weaker nucleophiles react faster with tosylate as nucleofuge. The rate of the S_N1 reaction of **1-Br** (Table 11) was experimentally not accessible and, therefore, estimated with the Mayr-Kronja (equation 3).[14,30]

$$\log k_{25\,°C} = s_f (N_f + E_f). \qquad \text{(equation 3)}$$

Existing fugality parameters s_f and N_f for nucleofuges in various protic solvents and solvent mixtures[4e,14,30] provide a clear picture of the relative reactivity of bromide, chloride and tosylate under S_N1 conditions (Table 12). Tosylates ionize most rapidly, roughly 3 orders of magnitude faster than bromides (ΔN_f is around 3), which in turn are about 1 order of magnitude more reactive than the corresponding chlorides. The relative reactivities increase or decrease slightly depending on the solvent and the electrofuge. The ratio of bromide/tosylate reactivity seems to be mainly determined by the reaction mechanism. As a consequence, attributes that make a good S_N1 leaving group do not necessarily make a good S_N2 leaving group, and *vice versa*. This further illustrates the fundamental differences in S_N1 and S_N2 mechanisms. Whether bromide or tosylate is the better leaving group cannot be answered generally.

Table 12. Nucleofugality parameters of chloride, bromide and tosylate in miscellaneous solvents at 25 °C.[a]

Nucleofuge	Cl^-	Br^-	OTs^-
N_f /s_f in TFE	5.54/0.85	6.19/0.95	9.73/0.94
N_f /s_f in MeOH	2.91/0.99	4.23/0.99	7.33/0.82
N_f /s_f in 60AN40W	3.84/0.96	5.23/0.99	7.97/0.82
N_f /s_f in 90A10W	1.14/1.11	2.29/1.01	5.38/0.89

a data taken from reference[4e]

The answer will depend on the mechanism and while tosylate is always the better leaving group than bromide when S_N1 mechanisms are considered, the same cannot be said for S_N2. Apparently the S_N2 mechanism is more complex, and bromide tends to be as good as leaving group as tosylate in S_N2 reactions. The complexity of the S_N2 reaction has thus far only allowed for a few S_N2 type electrophiles to be included in the Mayr scales.[26] In this work a connection to the Mayr scales could not be made, not even with the inclusion of an electrophile-dependent s_E parameter. Addition reactions can be described semiquantitatively with the Mayr-Patz equation (equation 2) and heterolysis reactions with the aforementioned Mayr-Kronja equation (equation 3). In the transition states of these reactions only one bond is formed or broken, respectively. In S_N2 reactions one bond is formed while another bond is broken at the same time, which makes the accurate prediction of rate constants more difficult.
By choosing the appropriate leaving group, one can achieve control over the reaction pathway. With bromide being the better choice if one desires an S_N2 mechanism and tosylate being better for an S_N1 mechanism.[31]

Relative Electrophilic Reactivities of Halides and Tosylates.

Table 13 compiles several second-order rate constants for the reactions of anionic nucleophiles with 1-propyl or methyl halides and tosylates. The k_{OTs}/k_{Br} ratio is changing more than the ratios of the rate constants of halides, even when only reactions following the S_N2 mechanism are taken into account (Table 13). In S_N1 reactions the reported ratios of k_{OTs}/k_{Br} are high (around 1000 and up to 10000) and low for E2 and S_N2 reactions (around 1 to 0.1).[29]
The ratios k_{Cl}/k_{Br} and k_I/k_{Br} also show variation (Table 13). But while the ratios of k_I/k_{Br} and k_{Cl}/k_{Br} vary only by less than a factor of 5, the ratio k_{OTs}/k_{Br} varies by around a factor of 160 under analogous conditions (Table 13). The logarithm of the rate constants of an S_N2 reaction with different leaving groups correlates linearly with the logarithm of rate constants of other S_N2 reactions where the same leaving groups are employed (Figure 15). This holds true whether the nucleophiles are charged or

uncharged, the reactive carbon center is modified, or if the solvent is changed from polar aprotic to polar protic.

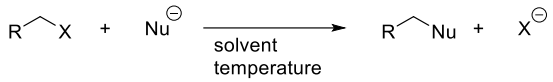

Table 13. Reaction conditions and rates of primary alkyl halides or tosylates with miscellaneous nucleophiles at 25 °C.

Electrophile	Nucleophile	Solvent	k_2 (M^{-1} s^{-1})	k_{OTs}/k_{Br}	k_I/k_{Br}	k_{Cl}/k_{Br}
PrCl	*p*-Methylthiophenolate	EtOH	1.00 [a]			1/136
PrOTs	*p*-Methylthiophenolate	EtOH	6.00×10^{1} [a]	1/2.3		
PrBr	*p*-Methylthiophenolate	EtOH	1.36×10^{2} [a]			
PrI	*p*-Methylthiophenolate	EtOH	4.73×10^{2} [a]		3.5	
MeCl	N_3^-	DMF	1.6×10^{-3} [b]			1/250
MeOTs	N_3^-	DMF	5.0×10^{-2} [b]	1/8.0		
MeBr	N_3^-	DMF	4.0×10^{-1} [b]			
MeI	N_3^-	DMF	3.2×10^{0} [b]		8.0	
MeCl	N_3^-	MeOH	8.0×10^{-7} [b]			1/63
MeOTs	N_3^-	MeOH	5.0×10^{-4} [b]	10		
MeBr	N_3^-	MeOH	5.0×10^{-5} [b]			
MeI	N_3^-	MeOH	8.0×10^{-5} [b]		1.6	
MeCl	NCS^-	DMF	4.4×10^{-5} [b]			1/300
MeOTs	NCS^-	DMF	8.0×10^{-4} [b]	1/16		
MeBr	NCS^-	DMF	1.3×10^{-2} [b]			
MeI	NCS^-	DMF	8.0×10^{-2} [b]		6.2	
MeCl	NCS^-	MeOH	1.6×10^{-6} [b]			1/160
MeOTs	NCS^-	MeOH	1.3×10^{-4} [b]			
MeBr	NCS^-	MeOH	2.5×10^{-4} [b]			
MeI	NCS^-	MeOH	5.0×10^{-4} [b]		2.0	

a relative rate constants from reference[5a]

b second-order rate constants calculated with Arrhenius activation parameters from reference[4a]

Only tosylate is markedly deviating, while the more closely related halides follow a constant linear behavior. Other groups have also found this constant relationship for the relative reactivity of halide leaving groups.[4a,5a,32] Only one point (the reaction of MeOTs with the azide ion in methanol) deviates substantially from this correlation. A k_{OTs}/k_{Br} ratio of 10 in an S_N2 reaction is unusual, but not unheard of,[29] but values close to one or smaller than one are found more regularly.[5a] Without that exception, bromide always reacts faster than tosylate.

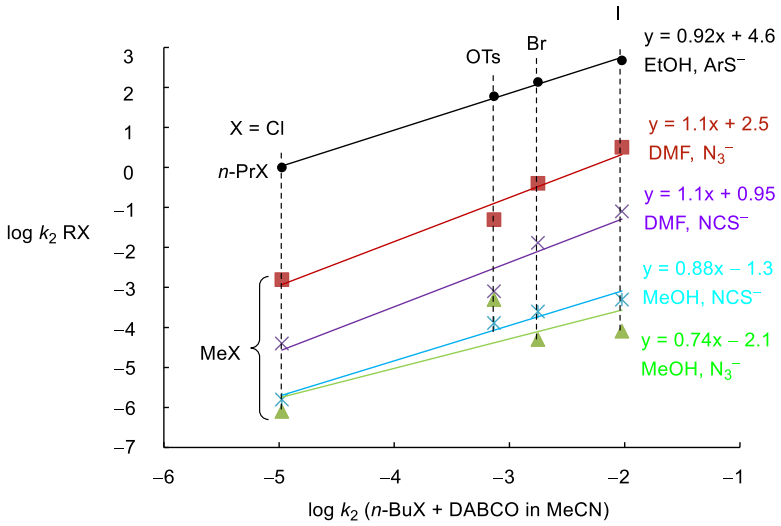

Figure 15: Correlation of the logarithm of the rate constants of the reactions of alkyl halides/tosylates with identical leaving groups (Table 13) versus the rate constants of the reactions of 1-butyl halides/tosylates with DABCO in acetonitrile at 20 °C (Table 1). Each colored line represents a specific reaction series (electrofuge, nucleophile, solvent, temperature of entries in Table, same color code used as in Table 13) and each point represents one specific leaving group within that reaction. The black line consists of relative instead of absolute rate constants, which results in a correct slope and an arbitrary intercept.

The slope appears to be related to the solvent, as reactions in the same solvent show similar or identical slopes. However, further data are required to give a clear and reliable picture. A semi-quantitative prediction of S_N2 rate constants should be possible in light of these results, at least for halides and other well defined classes of nucleofuges. Swain and Scott[33] had already established a linear free energy relationship for S_N2 reactions, however Pearson[34] reported discrepancies of the Swain-Scott equation and doubted whether it is actually possible to quantitatively predict rate constants for a diverse range of reaction partners.

Energy Profiles.

According to the Hammond postulate, the transient carbocations which result from the endothermic phenethyl halide ionization should closely resemble the transition state (Figure 16). The exothermic S_N2 reaction of phenethyl halides with amines however should have a transition state which is more closely resembling the starting material and should, thus, have a stronger carbon-leaving group bond. Tosylate is a thermodynamically more favorable anion than bromide, which is evident from their respective S_N1 reactivity. That tosylate or the closely related benzenesulphonate are energetically more favorable than bromide is also supported by their free energies of hydration (Table 14).[35] It has also to be mentioned that the hydrophobic phenyl moiety is unfavorably affecting the hydration

energies, but the trend should be the same nonetheless. Bromide and other halides receive more stabilization than benzenesulphonate for their transfer from the gas phase into water.[35]

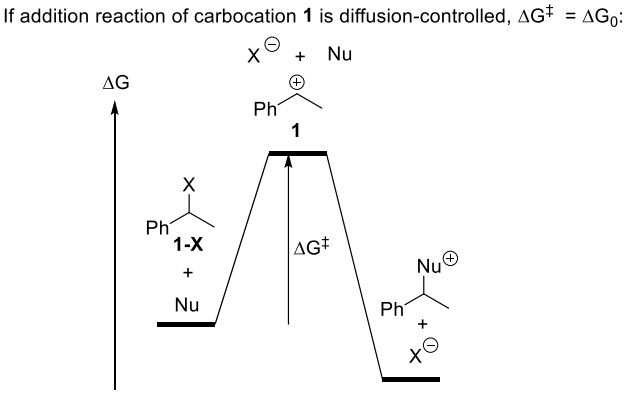

Figure 16: S_N1 reaction with diffusion-controlled reverse recombination for the reaction of **1** with X^- (X=OMs, Cl or Br).

This stabilization is mainly due to the formation of hydrogen bonds, which stabilizes the halides with localized negative charge more than benzenesulphonate/tosylate with less localized negative charge. Without (protic) solvent, benzenesulphonate/tosylate are the thermodynamically more favorable anions relative to bromide. This is also confirmed by computational methods (Figure 17 below).

What makes bromide an equally strong leaving group in S_N2 reactions as tosylate though it is less favored by thermodynamics? To answer this question, we need to take a look at Marcus intrinsic barriers.[36]

$$\Delta G^{\ddagger} = \Delta G_0^{\ddagger} + 0.5\ \Delta G^0 + (\Delta G^0)^2/16\Delta G_0^{\ddagger} \quad \text{(equation 4)}$$

In equation 4, $\Delta G^{\ddagger}$ is the free energy of activation, $\Delta G_0^{\ddagger}$ is the intrinsic barrier and ΔG^0 is the reaction Gibbs energy. According to the Marcus equation (equation 4), the lower intrinsic barrier ($\Delta G_0^{\ddagger}$) has to be the reason why bromide is as good as a leaving group as tosylate in S_N2 reactions.

Table 14. Free energies and heats of hydration at 25 °C of halides[a] and benzenesulphonate[b].

	F^-	Cl^-	Br^-	I^-	$PhSO_3^-$
ΔH^o (kJ / mol)	−513	−371	−341	−302	−236
ΔG^o (kJ / mol)	−477	−352	−326	−293	−236 [c]

a from reference[35a].

b from reference[35b]

c assuming $\Delta S^o = 0$.

This would also be in line with the aforementioned argument: In a reaction with large positive ΔG^o, ΔG^o almost equals $\Delta G^{\ddagger}$, and the influence of ΔG^o on $\Delta G^{\ddagger}$ is more important than the influence of $\Delta G_0^{\ddagger}$ on $\Delta G^{\ddagger}$ (Figure 16). This situation is qualitatively expressed by Hammond's postulate. The opposite is the case in reactions in which ΔG^o is small or even zero, like in identity reactions. In these reactions the effects of $\Delta G_0^{\ddagger}$ on $\Delta G^{\ddagger}$ become significant. The rate determing step of the S_N1 reaction of phenethyl halides can be seen as a reaction with $\Delta G^{\ddagger} = \Delta G^o$, since the backward reaction, the addition of halide anion and carbocation would proceed without activation barrier (diffusion control). S_N2 reactions, however, are different and the intrinsic barrier will play a more significant role. The oxygen centered anion tosylate has a substantially higher intrinsic barrier than bromide as was shown by Hoz *et al*..[37] Tosylate is outperforming bromide in S_N1 reactions since it is the thermodynamically more favorable anion and intrinsic barriers are less important. In S_N2 reactions the intrinsic barriers are more important and bromide can catch up to or even slightly surpass tosylate as a leaving group due to its inherently lower intrinsic barrier.

Other groups reported similar trends in the k_2/k_1 ratio for the leaving groups bromide and tosylate.[5] Table 15 is a compilation of rate constants k_1 and k_2 of concurrent S_N1 and S_N2 reactions of alkyl bromides and tosylates in acetonitrile or acetonitrile/water mixtures. Bromides have a roughly 50 times higher k_2/k_1 ratio than analogous reactions of tosylates in acetonitrile if all other parameters are unchanged (Compare entries 8 versus 9 and 3 versus 4 in Table 15). This difference in k_2/k_1 ratio drops from around factor 50 to around 6 for the solvent 25AN75W (Compare entry 19 and 20 in Table 15). Here the rate of the S_N1 reaction of tosylate is only 18 times faster than the rate of the analogous bromide reaction at 70 °C. This appears to be in contrast to Table 12 and we do not have an explanation for this issue.

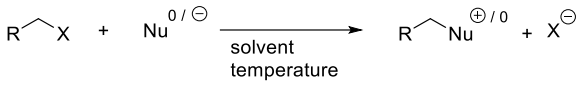

Table 15. Reaction conditions and rates of benzylic bromides or tosylates with miscellaneous nucleophiles.

Entry	Electrophile	Nucleophile	Solvent	*T* (°C)	k_2 (M^{-1} s^{-1})	k_1 (s^{-1})	k_2/k_1
1	*p*-Methoxybenzyl bromide [a]	Pyridine	AN	50	1.50×10^{-2}	5.6×10^{-5}	268
2	*p*-Methoxybenzyl bromide [a]	Pyridine	AN	35	6.88×10^{-3}	$<2 \times 10^{-5}$	>350
3	*p*-Methoxybenzyl bromide [e]	*N,N*-dimethylaniline	AN	50	2.26×10^{-2}	2.07×10^{-4}	109
4	*p*-Methoxybenzyl tosylate [a]	*N,N*-dimethylaniline	AN	35	3.3×10^{-2} [b]	1.7×10^{-2} [b]	1.94
5	*p*-Thiomethylbenzyl tosylate [a]	*N,N*-dimethylaniline	AN	35	1.37×10^{-2}	2.03×10^{-3}	6.75
6	*p*-Thiomethylbenzyl tosylate [a]	4-methoxy-*N,N*-dimethylaniline	AN	35	3.5×10^{-2}	1.9×10^{-3}	18.4
7	*p*-Methoxyphenethyl bromide (**4-Br**) [c]	Pyridine	AN	35	2.82×10^{-2}	1.66×10^{-2}	1.70
8	Phenethyl bromide (**1-Br**) [c]	Pyridine	AN	35	5.54×10^{-5}	3×10^{-7}	185
9	Phenethyl tosylate (**1-OTs**) [a]	Pyridine	AN	35	4.53×10^{-4}	1.08×10^{-4}	4.19
10	Phenethyl tosylate (**1-OTs**) [a]	*N,N*-dimethylaniline	AN	35	7.98×10^{-4}	1.07×10^{-4}	7.46
11	*p*-Phenoxybenzyl tosylate [b]	*N,N*-dimethylaniline	AN	35	9.81×10^{-3}	2.25×10^{-4}	43.6
12	*p*-Phenoxybenzyl tosylate [b]	4-methoxy-*N,N*-dimethylaniline	AN	35	3.36×10^{-2}	2.24×10^{-4}	150
13	*p*-Methoxy-*m*-chlorobenzyl tosylate [b]	*N,N*-dimethylaniline	AN	35	8.68×10^{-3}	2.05×10^{-4}	42.3
14	*p*-Methoxy-*m*-chlorobenzyl tosylate [b]	4-methoxy-*N,N*-dimethylaniline	AN	35	3.36×10^{-2}	2.28×10^{-4}	147
15	3,4,5-Trimethylbenzyl tosylate [b]	*N,N*-dimethylaniline	AN	35	9.07×10^{-3}	3.76×10^{-5}	241
16	3,4,5-Trimethylbenzyl tosylate [b]	4-methoxy-*N,N*-dimethylaniline	AN	35	3.47×10^{-2}	3.48×10^{-5}	997
17	3,4-Dimethylbenzyl tosylate [b]	*N,N*-dimethylaniline	AN	35	5.29×10^{-3}	1.55×10^{-5}	341
18	3,4-Dimethylbenzyl tosylate [b]	4-methoxy-*N,N*-dimethylaniline	AN	35	2.28×10^{-2}	1.18×10^{-5}	1930
19	9-(1-bromido-ethyl)fluorene [d]	NCS^-	25AN75W	70	1.64×10^{-5}	1.00×10^{-5}	1.64
20	9-(1-tosyloxy-ethyl)fluorene [d]	NCS^-	25AN75W	55	4.68×10^{-5}	1.79×10^{-4}	0.26
21	9-(1-tosyloxy-ethyl)fluorene [d]	N_3^-	25AN75W	55	8.58×10^{-5}	1.50×10^{-4}	0.57
22	9-(1-tosyloxy-ethyl)fluorene [d]	Br^-	25AN75W	55	1.53×10^{-5}	1.49×10^{-4}	0.10

a Data taken from reference[38]

b Estimated with the Yukawa-Tsuno correlations[15]

c Data taken from reference[13]

d Data taken from reference[1e]

e Data taken from reference[39]

Computational Analysis of the S_N1 and the S_N2 Mechanism.

To get a deeper insight into the effects of different leaving groups on the rates of S_N1 and S_N2 reactions, we performed quantum chemical calculations at the IEFPCM(UA0, MeCN)/DLPNO-CCSD(T)/ma-def2-TZVP//IEFPCM(UA0, MeCN)/MN15/ma-def2-TZVP level of theory considering acetonitrile solvation by the IEFPCM model with UA0 radii.[40] As model systems we studied the nucleophilic substitution reactions of phenethyl bromide, chloride and mesylate with the nucleophiles NH_3 and DABCO (**9**) with mesylate being a model for the experimentally characterized tosylate (Figure 17).

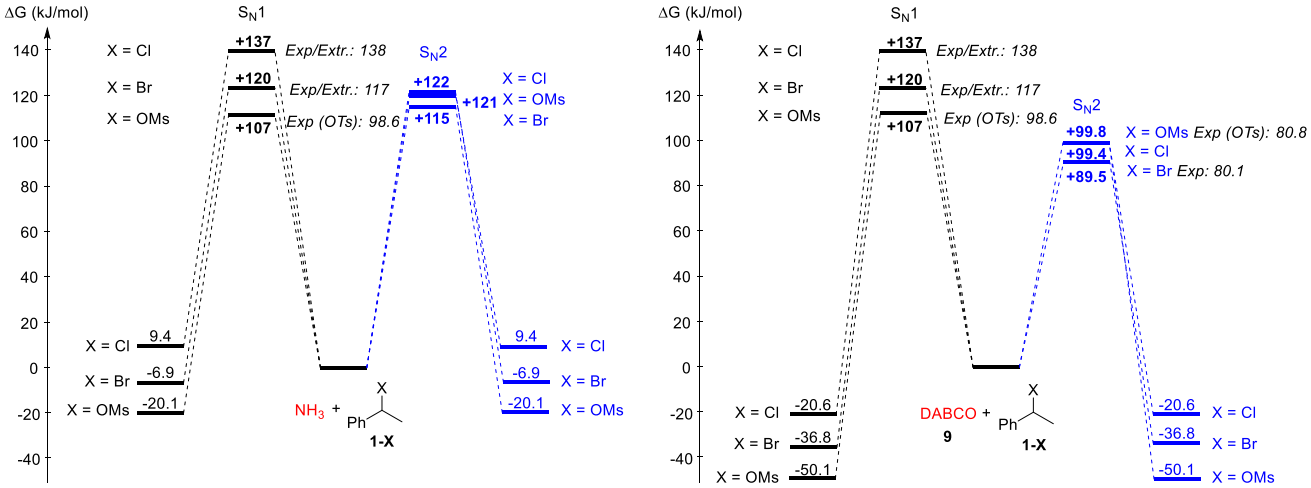

Figure 17: Comparison of S_N1 and S_N2 reactions of **1-X** with either NH_3 (left) or DABCO (right) at the IEFPCM(UA0, MeCN)/DLPNO-CCSD(T)/ma-def2-TZVP//IEFPCM(UA0, MeCN)/MN15/ma-def2-TZVP level, corrected to a 1 M solution. Experimental $\Delta G^{\ddagger}$ value for mesylate (tosylate) S_N1 has been taken from this work, the value for bromide and chloride were estimated with the Kronja-Mayr equation (equation 3).

While the experimental S_N1 barriers of phenethyl bromide and chloride as well as the barrier for the S_N2 reaction of DABCO with phenethyl bromide are well reproduced by our computational method, higher deviations are observed when the computed barriers for the reactions of phenethyl mesylates are compared with the experimental ones for tosylate: This indicates a deficiency of the computational method or that mesylate is not a perfect mimic for tosylate. Nevertheless, the relative reactivity trends are still well represented and will be discussed in the following.

Analysis of the reaction energetics with Marcus' equation (equation 4) allowed to derive the intrinsic barriers $\Delta G_0^{\ddagger}$ for the leaving group abilities of bromide, chloride and mesylate in the reactions with both ammonia and DABCO (**9**) (Table 16).

While the intrinsic barriers in reactions with chloride and bromide are similar, mesylates reacts via significantly higher intrinsic barriers (+12 kJ/mol for NH_3 and +17 kJ/mol for DABCO).

Table 16. Intrinsic barriers derived from the Marcus equation (equation 4)[36] for the reactions of the nucleophiles NH_3 and DABCO (**9**) with phenethyl bromide (**1-Br**), chloride (**1-Cl**) and mesylate (**1-OMs**) at the IEFPCM(UA0, MeCN)/DLPNO-CCSD(T)/ma-def2-TZVP//IEFPCM(UA0, MeCN)/MN15/ma-def2-TZVP level of theory.

$\Delta G_0^{\ddagger}$ (kJ mol^{-1})	X = Cl	X = Br	X = OMs
Nu = NH_3	118	118	130
Nu = DABCO	109	107	124

This observation is in line with the studies of Hoz[37b], who determined the intrinsic barriers for the identity S_N2 reactions of monosubstituted methanes: He found that chalcogen nucleophiles react via higher barriers than halogens while within one group of elements in the periodic table of elements the intrinsic barriers are of similar magnitude. While the mesylate has the most exergonic reaction, this only translates to the lowest value for $\Delta G^{\ddagger}$ for the S_N1 reaction, where thermodynamic effects are more important than the intrinsic barrier as already discussed (Figure 16). In the S_N2 reaction the intrinsic barrier gains more influence on the activation barrier and so bromide has the lowest value for $\Delta G^{\ddagger}$ for the S_N2 reaction, as confirmed by experimental results.

If one now compares the relative reactivity of phenethyl mesylates or halides in a reaction with a specific nucleophile, the operative mechanism is mostly decided by the strength of the nucleophile: With weak nucleophiles, the S_N1 pathway dominates and the relative reactivity of phenethyl mesylate and bromide is shifted mostly to mesylate as the reaction is controlled by more favored thermodynamics for mesylate heterolysis. With strong nucleophiles, however, the high intrinsic barrier for mesylate (or tosylate) as a leaving group counteracts the thermodynamics. As a consequence, bromides are the more electrophilic substrates towards strong nucleophiles in S_N2 reactions. While the computations indicate that in reactions with both NH_3 and DABCO (**9**) phenethyl mesylate becomes a weaker electrophile than phenethyl bromide by 7-10 kJ/mol, the trend is less pronounced for tosylate: For phenethyl tosylate the experimental data show that the electrophilicities are comparable to phenethyl bromide.

Nucleofugality of Bromide in Acetonitrile.

Our accumulated S_N1 data (Table 17) enabled us to determine the nucleofugality parameters N_f and s_f (see equation 3) of bromide in acetonitrile (Figure 18). The required electrofugality parameters were published by Mayr and Kronja.[30] It has to be mentioned, that equation 3 is only valid at 25 °C. The rate constants in Table 17 were determined at 20 °C, however. The resulting error is not of concern and the nucleofugality parameters N_f = 1.20 and s_f = 1.08 determined for bromide in acetonitrile should prove useful for semi-quantitatively predicting heterolysis rate constants of alkyl bromides with known E_f parameter.

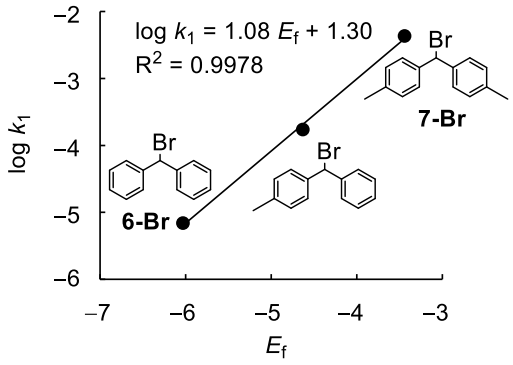

Figure 18. Correlation of log k_1 in acetonitrile at 20 °C versus electrofugality parameters E_f. The slope represents the susceptibility parameter s_f and the intercept the nucleofugality parameter N_f of Br^- in acetonitrile (N_f = 1.20, s_f = 1.08).

Table 17. Ionization rate constants k_1 of benzhydryl bromides and electrofugality parameters E_f of benzhydrylium ions in acetonitrile at 20 °C.

Electrophile	k_1 (s^{-1})	log k_1	E_f[a]
6-Br	6.92×10^{-6}	−5.16	−6.03
7-Br	4.31×10^{-3}	−2.37	−3.44
4-Methylbenzhydryl bromide	1.73×10^{-4}	−3.76	−4.63

a taken from reference[14]

Conflicting Results in the Literature.

Our results are in conflict with results from Lee *et al.*[41] who reported the investigations of reactions of **1-OTs** with substituted anilines in comparable acetonitrile/methanol mixtures. Their report of a second-order rate constant k_2 of 3.32×10^{-2} M^{-1} s^{-1} for the reaction of **1-OTs** with aniline (N = 12.64, s_N = 0.68 in acetonitrile)[19] in 50% acetonitrile/methanol at 25 °C appears to be highly unlikely, since the most nucleophilic amine we used, DABCO (N = 18.80, s_N = 0.70 in acetonitrile),[25] only had a k_2 of 2.45×10^{-2} M^{-1} s^{-1} for the reaction with **1-OTs** in acetonitrile at 20 °C. For the reaction of **1-OTs** with propylamine (N = 15.11, s_N = 0.70 in acetonitrile)[10] we determined a k_2 of 4.90×10^{-4} M^{-1} s^{-1} (Figure 19). The fact that our measurements with DABCO and propylamine were carried out in acetonitrile should even enhance this discrepancy, as Menschutkin reactions of amines with alkyl derivatives are generally faster in acetonitrile than in protic solvents of similar polarity.[21]

The origin of the discrepancy can easily be found by inspection of Table II in Lee's 1988 paper. Lee and coworkers performed the kinetic measurements of the reactions of phenethyl tosylates in methanol and methanol/acetonitrile mixture. However, these substrates would not have sufficient life-times in these solutions to "wait" for the reaction with aniline.

The *p*-methoxyphenethyl chloride (**4-Cl**) has previously been reported to solvolyze with a first-order rate constant of 0.394 s^{-1}.[42] This value is in agreement with solvolysis studies of **4-Cl** in different solvents by another group.[43] Since S_N1 reactivities of alkyl tosylates are generally 3-5 orders of magnitude higher than those of the corresponding alkyl chlorides, it is impossible to handle **4-OTs** in methanol or methanol/acetonitrile mixtures. Nevertheless, Lee *et al*. also explicitly mention that methanolysis rates were always at least 20 times lower than the S_N2 substitution rates, which is impossible.

The problem is even deeper. Attempts to synthesize **1-OTs** in the common way by treatment of 1-phenethyl alcohol or alcoholate with *p*-toluenesulfonic chloride failed. Only through a two-step synthesis involving a mild method[44] could **1-OTs** be synthesized without decomposition (Scheme 3).

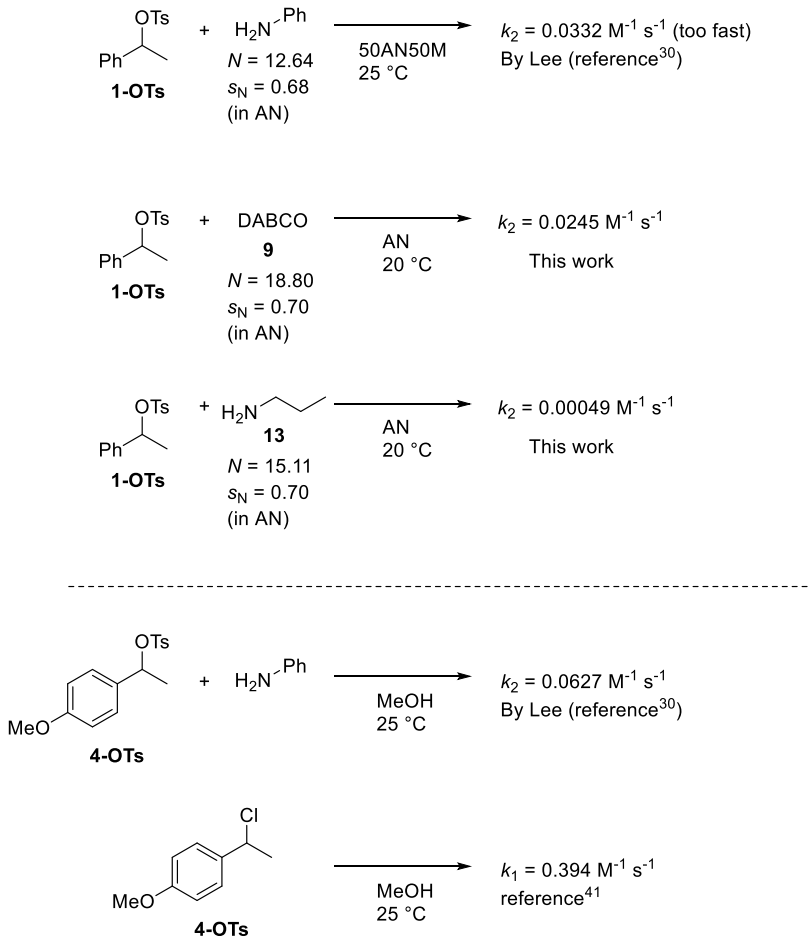

Figure 19. Comparison of rate constants for the reaction of **1-OTs** with different amines in acetonitrile or acetonitrile/methanol mixtures (top). Comparison of the rate constants of the reaction of aniline with **4-OTs** with the solvolysis of **4-Cl** in methanol at 25 °C.

Most reaction conditions resulted only in decomposition of **1-OTs**, as it proved to be very sensitive, especially to protic solvents and nucleophiles. The synthesis described by Lee *et al*. did not yield any product in our attempts and decomposition was observed.

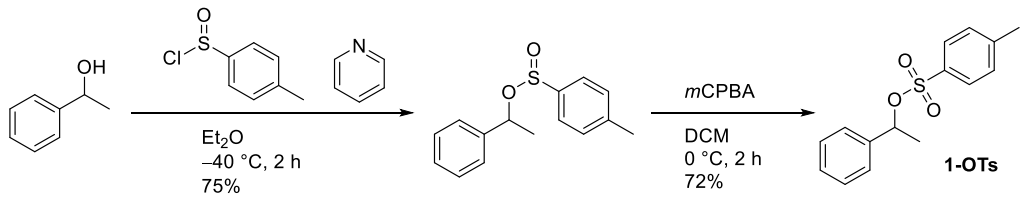

Scheme 3. Synthesis of the sensitive **1-OTs**.

At room temperature decomposition of the neat **1-OTs** occurred within hours. To avoid decomposition, **1-OTs** was frozen at −20 °C under dry argon in toluene solution for storage. The instability of 1-arylethyl tosylates was also reported by Park *et al*.[45] They failed to keep **2-OTs** from decomposing after synthesis at room temperature. Synthesis of **2-OTs** appears to be only possible with a procedure that is devoid of strong nucleophiles and ionizing solvents at low temperatures. Synthesizing **4-OTs** would presumably require huge effort. Park *et al*.[45] report the benzylic hydrogen at 5.54-5.60 ppm in the ^{1}H-NMR spectrum for **1-OTs**. We find 5.50 ppm for our sample, in good agreement with Park's report. Lee *et al*. however reported 4.66 ppm for the same hydrogen. They did not mention the solvent, which was $CDCl_3$ for Park *et al*. and our measurements. 4-Methylbenzyl tosylate (**2-OTs**) has also been reported as unstable compound.[6b]

Presently, we do not know the nature of the compounds systematically studied by Lee. Since this paper has been quoted 33 times so far, several discussions on structure reactivity correlations have to be revised.

4.3 Conclusions

Multiple options exist to control the mechanism of nucleophilic substitutions on a secondary, benzylic carbon (Figure 20). Electron donating groups greatly enhance the rate of both S_N1 and S_N2. However, only the lack of such groups leads to a dominant S_N2 mechanism. Changing the starting material is often not feasible when specific products are desired. The same can be said for the reacting nucleophile. For an S_N2 reaction the nucleophile needs to be sufficiently strong, while also weaker nucleophiles can participate in S_N1 reactions. Nucleophiles in S_N1 reactions only need to outcompete other nucleophiles, eliminations or other side reactions. Control can normally be achieved with the correct concentrations of the nucleophiles. Fortunately, leaving group, solvent and temperature can often be adjusted freely. Leaving groups are a powerful tool to influence the reaction mechanism. The

S_N1/S_N2 ratio changes by 3 orders of magnitude when exchanging tosylate with bromide. Bromide is favoring the S_N2 mechanism and tosylate the S_N1 mechanism. This change alone can be enough to flip a reaction system from only S_N1 to only S_N2 in borderline cases.

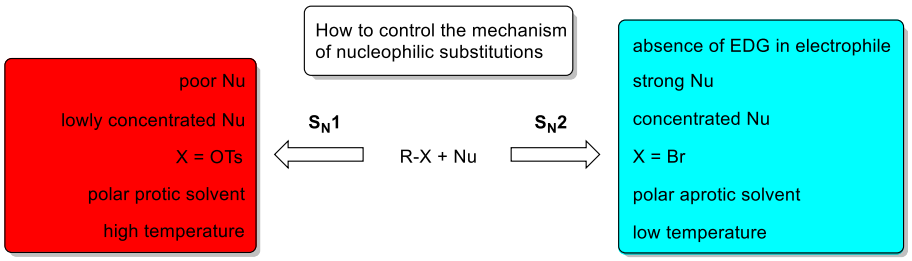

Figure 20. How to control the mechanism of nucleophilic substitutions. Factors that favour S_N1 are on the left (red box), while factors that favour S_N2 are on the right (blue box).

Choosing the correct solvent can also make a huge difference, as protic dipolar solvents increase S_N1 reaction rates and decrease S_N2 reaction rates when compared to aprotic dipolar solvents.
Temperature had a minor impact on the S_N1/S_N2 ratio, however a small shift of selectivity towards the S_N2 mechanism could be demonstrated at lower temperatures. Furthermore, we could show that the assistance of a nucleophile reduces the enthalpic activation barrier of a nucleophilic substitution while also increasing the entropic activation barrier, when comparing S_N1 and S_N2 mechanisms.
After all it is the systematic application of all these factors that allows the arbitrary switch from an S_N1 mechanism to an S_N2 mechanism, and *vice versa*. Though only secondary, benzylic carbons were investigated in this work, it can be expected that these results will be applicable in a much broader context. Also, we could show that bromides react *via* lower intrinsic barriers than tosylates in nucleophilic substitutions though bromide is the thermodynamically less favorable leaving group. This causes bromide and tosylate to be similarly strong leaving groups in S_N2 reactions, where both the intrinsic barrier and thermodynamics are important. In S_N1 reactions on the other hand, thermodynamic aspects become much more and intrinsic barriers less important, which explains why alkyl tosylates are much more reactive than alkyl bromides in S_N1 reactions.

4.4 References

(1) (a) Phan, T. B.; Nolte, C.; Kobayashi, S.; Ofial, A. R.; Mayr, H., *J. Am. Chem. Soc.* **2009,** *131*, 11392−11401. (b) Parker, A., Rates of bimolecular substitution reactions in protic and dipolar aprotic solvents. In *Advances in Physical Organic Chemistry*, Elsevier: 1967; Vol. 5, p 173−235. (c) Pienta, N. J.; Kessler, R. J., *J. Am. Chem. Soc.* **1993,** *115*, 8330−8339. (d) Wang, T.-T.; Iou, Q.-L., *Chem. Eng. J.* **2002,** *87*, 197−206. (e) Meng, Q.; Thibblin, A., *J. Am. Chem. Soc.* **1995,** *117*, 9399−9407. (f) Westaway, K. C.; Ali, S. F., *Can. J. Chem.* **1979,** *57*, 1354−1367. (g) Vlasov, V. M., *J. Phys. Org. Chem.* **2010,** *23*, 468−476. (h) Katritzky, A. R.; Musumarra, G., *Chem. Soc. Rev.* **1984,** *13*, 47−68. (i) Bentley, T.; Choi, H.; Koo, I. S.; Kevill, D. N., *J. Phys. Org. Chem.* **2017,** *30*, e3585. (j) Xie, J.; Hase, W. L., *Science* **2016,** *352*, 32−33. (k) Stei, M.; Carrascosa, E.; Kainz, M. A.; Kelkar, A. H.; Meyer, J.; Szabó, I.; Czakó, G.; Wester, R., *Nat. Chem.* **2016,** *8*, 151−156. (l) Uggerud, E., *J. Phys. Org. Chem.* **2006,** *19*, 461−466. (m) Liu, X.; Zhang, J.; Yang, L.; Hase, W. L., *J. Am. Chem. Soc.* **2018,** *140*, 10995−11005. (n) Bento, A. P.; Bickelhaupt, F. M., *J. Org. Chem.* **2008,** *73*, 7290−7299. (o) Fernández, I.; Frenking, G.; Uggerud, E., *Chem. Eur. J.* **2009,** *15*, 2166−2175. (p) Kim, Y.; Cramer, C. J.; Truhlar, D. G., *J. Phys. Chem. A* **2009,** *113*, 9109−9114.

(2) Smith, M. B.; March, J., March's Advanced Organic Chemistry (6th ed.). John Wiley & Sons, Inc.: Hoboken, New Jersey, 2007; p 425−443.

(3) Pavez, P.; Millán, D.; Morales, J.; Rojas, M.; Céspedes, D.; Santos, J. G., *Org. Biomol. Chem.* **2016,** *14*, 1421-1427.

(4) (a) Alexander, R.; Ko, E. C. F.; Parker, A. J.; Broxton, T. J., *J. Am. Chem. Soc.* **1968,** *90*, 5049−5069. (b) Haberfield, P.; Nudelman, A.; Bloom, A.; Romm, R.; Ginsberg, H., *J. Org. Chem.* **1971,** *36*, 1792−1795. (c) Mizue, F.; Toshihiro, S.; Ken-ichi, Y.; Yoshihiro, S.; Mutsuo, G.; Hong, K. S.; Yutaka, T.; Zvi, R.; Yuho, T., *Bull. Chem. Soc. Jpn.* **1995,** *68*, 2619−2628. (d) Streidl, N.; Mayr, H., *Eur. J. Org. Chem.* **2011**, *2011*, 2498−2506. (e) Streidl, N.; Denegri, B.; Kronja, O.; Mayr, H., *Acc. Chem. Res.* **2010,** *43*, 1537−1549.

(5) (a) Hoffmann, H. M. R., *J. Chem. Soc.* **1965**, 6753−6761. (b) Hoffmann, H. M. R., *J. Chem. Soc.* **1965**, 6762−6769.

(6) (a) Yutaka, T.; Mizue, F.; Yuho, T., *Bull. Chem. Soc. Jpn.* **1990,** *63*, 856−866. (b) Yoh, S.-D.; Tsuno, Y.; Fujio, M.; Sawada, M.; Yukawa, Y., *J. Chem. Soc., Perkin Trans. 2* **1989**, 7−13.

(7) Smith, M. B.; March, J., March's Advanced Organic Chemistry (6th ed.). John Wiley & Sons, Inc.: Hoboken, New Jersey, 2007; p 216−219.

(8) Streidl, N.; Antipova, A.; Mayr, H., *J. Org. Chem.* **2009,** *74*, 7328−7334.

(9) Minegishi, S.; Kobayashi, S.; Mayr, H., *J. Am. Chem. Soc.* **2004,** *126*, 5174−5181.

(10) Kanzian, T.; Nigst, T. A.; Maier, A.; Pichl, S.; Mayr, H., *Eur. J. Org. Chem.* **2009,** *2009*, 6379−6385.

(11) Mayr, H.; Ofial, A. R.; Schimmel, H., *Macromolecules* **2005,** *38*, 33−40.

(12) A database for reactivity parameters *E*, *N*,and s_N is freely accessible via http://www.cup.lmu.de/oc/mayr/DBintro.html.

(13) Lim, C.; Kim, S.-H.; Yoh, S.-D.; Fujio, M.; Tsuno, Y., *Tetrahedron Lett.* **1997,** *38*, 3243−3246.

(14) Denegri, B.; Ofial, A. R.; Jurić, S.; Streiter, A.; Kronja, O.; Mayr, H., *Chem. Eur. J.* **2006,** *12*, 1657−1666.

(15) Kim, S. H.; Yoh, S.-D.; Lim, C.; Mishima, M.; Fujio, M.; Tsuno, Y., *J. Phys. Org. Chem.* **1998,** *11*, 254−260.

(16) Kim, S.-H.; Yoh, S.-D.; Fujio, M.; Imahori, H.; Mishima, M.; Tsuno, Y., *Bull. Korean Chem. Soc.* **1995,** *16*, 760−763.

(17) (a) Gleave, J. L.; Hughes, E. D.; Ingold, C. K., *J. Chem. Soc.* **1935**, 236−244. (b) Hughes, E. D.; Ingold, C. K., *J. Chem. Soc.* **1935**, 244−255.

(18) Reichardt, C.; Welton, T., *Solvents and solvent effects in organic chemistry*. John Wiley & Sons: 2011.

(19) Brotzel, F.; Chu, Y. C.; Mayr, H., *J. Org. Chem.* **2007,** *72*, 3679−3688.

(20) Phan, T. B.; Breugst, M.; Mayr, H., *Angew. Chem., Int. Ed.* **2006,** *45*, 3869−3874.

(21) Abraham, M. H., *J. Chem. Soc. B.* **1971**, 299−308.

(22) Reinheimer, J. D.; Harley, J. D.; Meyers, W. W., *J. Org. Chem.* **1963,** *28*, 1575−1579.

(23) (a) Grunwald, E.; Winstein, S., *J. Am. Chem. Soc.* **1948,** *70*, 846−854. (b) Fainberg, A. H.; Winstein, S., *J. Am. Chem. Soc.* **1956,** *78*, 2770−2777.

(24) Coetzee, J. F.; Padmanabhan, G. R., *J. Am. Chem. Soc.* **1965,** *87*, 5005−5010.

(25) Baidya, M.; Kobayashi, S.; Brotzel, F.; Schmidhammer, U.; Riedle, E.; Mayr, H., *Angew. Chem., Int. Ed.* **2007,** *46*, 6176−6179.

(26) Timofeeva, D. S.; Ofial, A. R.; Mayr, H., *J. Am. Chem. Soc.* **2018,** *140*, 11474−11486.

(27) Eyring, H., *J. Chem. Phys.* **1935,** *3*, 107−115.

(28) (a) Fry, J. L.; Lancelot, C. J.; Lam, L. K.; Harris, J. M.; Bingham, R. C.; Raber, D. J.; Hall, R. E.; Schleyer, P. v. R., *J. Am. Chem. Soc.* **1970,** *92*, 2538−2540. (b) Carey, F. A.; Sundberg, R. J., Advanced organic chemistry: part A: structure and mechanisms (5th ed.). Springer Science & Business Media: 2007; p 389−405.

(29) DePuy, C. H.; Bishop, C. A., *J. Am. Chem. Soc.* **1960,** *82*, 2532−2535.

(30) Denegri, B.; Streiter, A.; Jurić, S.; Ofial, A. R.; Kronja, O.; Mayr, H., *Chem. Eur. J.* **2006,** *12*, 1648−1656.

(31) (a) Noyce, D. S.; Virgilio, J. A., *J. Org. Chem.* **1972,** *37*, 2643−2647. (b) Carey, F. A.; Sundberg, R. J., Advanced organic chemistry: part A: structure and mechanisms (5th ed.). Springer Science & Business Media: 2007; p 414.

(32) Bordwell, F. G.; Branca, J. C.; Cripe, T. A., *Isr. J. Chem.* **1985,** *26*, 357−366.

(33) Swain, C. G.; Scott, C. B., *J. Am. Chem. Soc.* **1953,** *75*, 141−147.

(34) Pearson, R. G.; Sobel, H. R.; Songstad, J., *J. Am. Chem. Soc.* **1968,** *90*, 319−326.

(35) (a) Robinson, R. A.; Stokes, R. H., *Electrolyte solutions*. Dover Publications Inc.: 2002. (b) Morris, D. F. C., *Tetrahedron* **1958,** *4*, 425−429.

(36) (a) Marcus, R. A., *Annu. Rev. Phys. Chem.* **1964,** *15*, 155−196. (b) Marcus, R. A., *J. Phys. Chem.* **1968,** *72*, 891−899. (c) Marcus, R. A., *J. Am. Chem. Soc.* **1969,** *91*, 7224−7225. (d) Albery, W. J.; Kreevoy, M. M., Methyl Transfer Reactions. In *Advances in Physical Organic Chemistry*, Gold, V.; Bethell, D., Eds. Academic Press: 1978; Vol. 16, p 87−157. (e) Albery, W. J., *Annu. Rev. Phys. Chem.*

1980, *31*, 227−263. (f) Marcus, R. A., *Pure Appl. Chem.* **1997,** *69*, 13−30. (g) Marcus, R. A., *Angew. Chem., Int. Ed.* **1993,** *32*, 1111−1121.

(37) (a) Hoz, S.; Basch, H.; Wolk, J. L.; Hoz, T.; Rozental, E., *J. Am. Chem. Soc.* **1999,** *121*, 7724-7725. (b) Hoz, S.; Basch, H.; Wolk, J. L.; Hoz, T.; Rozental, E., *J. Am. Chem. Soc.* **1999,** *121*, 7724−7725.

(38) Yoh, S. D.; Cheong, D. Y.; Lee, C. H.; Kim, S. H.; Park, J. H.; Fujio, M.; Tsuno, Y., *J. Phys. Org. Chem.* **2001,** *14*, 123−130.

(39) Yoh, S.-D.; Lee, M.-K.; Son, K.-J.; Cheong, D.-Y.; Han, I.-S.; Shim, K.-T., *Bull. Korean Chem. Soc.* **1999,** *20*, 466−468.

(40) (a) Gaussian 16, Revision A.03, Frisch, M. J.; Trucks, G. W.; Schlegel, H. B.; Scuseria, G. E.; Robb, M. A.; Cheeseman, J. R.; Scalmani, G.; Barone, V.; Petersson, G. A.; Nakatsuji, H.; Li, X.; Caricato, M.; Marenich, A. V.; Bloino, J.; Janesko, B. G.; Gomperts, R.; Mennucci, B.; Hratchian, H. P.; Ortiz, J. V.; Izmaylov, A. F.; Sonnenberg, J. L.; Williams−Young, D.; Ding, F.; Lipparini, F.; Egidi, F.; Goings, J.; Peng, B.; Petrone, A.; Henderson, T.; Ranasinghe, D.; Zakrzewski, V. G.; Gao, J.; Rega, N.; Zheng, G.; Liang, W.; Hada, M.; Ehara, M.; Toyota, K.; Fukuda, R.; Hasegawa, J.; Ishida, M.; Nakajima, T.; Honda, Y.; Kitao, O.; Nakai, H.; Vreven, T.; Throssell, K.; Montgomery, J. A., Jr.; Peralta, J. E.; Ogliaro, F.; Bearpark, M. J.; Heyd, J. J.; Brothers, E. N.; Kudin, K. N.; Staroverov, V. N.; Keith, T. A.; Kobayashi, R.; Normand, J.; Raghavachari, K.; Rendell, A. P.; Burant, J. C.; Iyengar, S. S.; Tomasi, J.; Cossi, M.; Millam, J. M.; Klene, M.; Adamo, C.; Cammi, R.; Ochterski, J. W.; Martin, R. L.; Morokuma, K.; Farkas, O.; Foresman, J. B.; Fox, D. J. Gaussian, Inc., Wallingford CT, 2016. (b) Haoyu, S. Y.; He, X.; Li, S. L.; Truhlar, D. G., *Chem. Sci.* **2016,** *7*, 5032−5051.

(41) Lee, I.; Kim, H. Y.; Kang, H. K.; Lee, H. W., *J. Org. Chem.* **1988,** *53*, 2678−2683.

(42) Liu, K.-T.; Duann, Y.-F.; Hou, S.-J., *J. Chem. Soc., Perkin Trans. 2* **1998**, 2181−2186.

(43) Liu, K. T.; Chang, L. W.; Yu, D. G.; Chen, P. S.; Fan, J. T., *J. Phys. Org. Chem.* **1997,** *10*, 879−884.

(44) Coates, R. M.; Chen, J. P., *Tetrahedron Lett.* **1969,** *10*, 2705−2708.

(45) Lee, J. H.; Yeo, S. D.; Jeong, D. Y.; Kim, S. H.; Park, J. H., *Bull. Korean Chem. Soc.* **2000,** *21*, 1005−1010.

4.2 Experimental Section

4.2.1 General

Chemicals

Commercial reagents were used without further purification. Deuterated solvents ($CDCl_3$) were obtained and used from EurIsotop. Silica gel plates with a F-254 fluorescence indicator were obtained from Merck and used for thin-layer chromatography. Flash column chromatography was performed with Merck silica gel 60 (0.040–0.063 mm) and distilled solvents.

Methanol and acetonitrile with HPLC grade quality were purchased from VWR.

Amines were purchased from the following companies: DABCO (**9**, >99%), pyrrolidine (**10**, 99%) and propylamine (**13**, 98%) from Sigma-Aldrich. Piperidine (**11**, >96%) from Fluka. Morpholine (**12**, 99%) from ABCR. Pyrrolidine was distilled before use, the other amines were used without further purification. Triethylamine (99%+) from AppliChem. BuI (99%, Aldrich-Chemie), BuOTs (97%, ABCR), BuBr (99%, Sigma-Aldrich) and BuCl (99%, Merck) were also purchased.

Methods

A 400 MHz nuclear magnetic resonance (NMR) spectrometer was used to acquire spectra for ^{1}H and ^{13}C. ^{13}C-NMR were acquired with broad band proton decoupling. Abbreviations for NMR-data: s = singlet, d = doublet, t = triplet, q = quartet, quint = quintet, h = hextet, m = multiplet. Chemical shifts are reported as parts per million (ppm). The internal reference was set to the residual signals of $CDCl_3$ (δ_H = 7.26 ppm, δ_C = 77.16 ppm).[1]

A Thermo Finnigan LTQ FT Ultra Fourier transform ion cyclotron resonance, a Q-Exactive GC Orbitrap, a Finnigan MAT 95 or a Finnigan MAT 90 GC/MS were used to record high-resolution mass spectra (HRMS). Ionization of the samples was done by either electron ionization (EI) or electron spray ionization (ESI).

4.2.2 Synthesis

5-OH: 1-(2,3-dihydrobenzofuran-5-yl)ethan-1-ol:

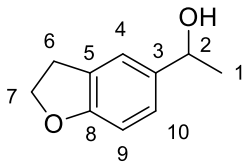

5-OH

1-(2,3-dihydrobenzofuran-5-yl)ethan-1-one (111 mg, 0.686 mmol, 1 eq.) was dissolved in methanol (3 mL) and $NaBH_4$ (31.2 mg, 0.823 mmol, 1.2 eq.) added at 0 °C. The reaction mixture was subsequently stirred for 4 h at 0 °C. The solvent was removed under reduced pressure, diluted with diethylether (10 mL) and washed two times with water (2 × 10 mL). The organic phase was dried over $MgSO_4$. The resulting product was a colorless liquid (111 mg, 0.679 mmol, 99%) and used without further purification.

^{1}H NMR (400 MHz, $CDCl_3$): δ = 7.26 (s, 1H, 4-H), 7.12 (d, *J* = 10.0 Hz, 1H, 10-H), 6.76 (d, *J* = 8.2 Hz, 1H, 8-H), 4.85 (q, *J* = 6.4 Hz, 1H, 2-H), 4.58 (t, *J* = 8.7 Hz, 2H, 7-H), 3.22 (t, *J* = 8.6 Hz, 2H, 6-H), 2.02 (s, 1H, 2-OH), 1.50 (d, *J* = 6.4 Hz, 3H, 1-H).

^{13}C{^{1}H} NMR (101 MHz, $CDCl_3$): δ = 159.51 (C_q, C-8), 138.14 (C_q, C-3), 127.23 (C_q, C-5), 125.42 (C_{Ar}), 122.22 (C_{Ar}), 108.97 (CH, C-9), 71.32 (CO), 70.24 (CO), 29.72 (CH_2, C-6), 25.14 (CH_3, C-1).

HRMS (EI): 164.0831 found for $C_{10}H_{12}O_2^{+\cdot}$ (calculated: 162.0832).

8-OH: (E)-1,3-bis(3,5-difluorophenyl)prop-2-en-1-ol

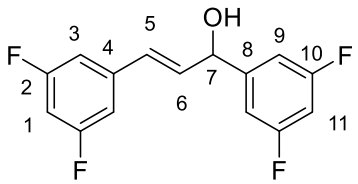

8-OH

1-bromo-3,5-difluorobenzene (0.114 g, 0.595 mmol, 1 eq.) was dissolved under dry conditions in dry THF (4 mL) and then a 1.2 M *s*BuMgCl · LiCl solution (0.496 mL, 0.595 mmol, 1 eq.) in THF was slowly added at 0 °C. The resulting solution was stirred for 2 h and then cooled to −78 °C. (E)-3-(3,5-difluorophenyl)acrylaldehyde (0.100 g, 0.595 mmol, 1 eq.) was dissolved in dry THF (1 mL) and then

added dropwise at −78 °C. The reaction mixture was then stirred for another 4 h at −78 °C and then slowly allowed to reach room temperature overnight. The solvent was reduced under reduced pressure and then the reaction mixture was diluted with diethylether (40 mL) and washed two times with water (2 × 40 mL). The organic phase was then purified with flash column chromatography (7.5% ethylacetate in pentane). The resulting product was a colorless liquid (0.123 g, 0.434 mmol, 73%).

^{1}H NMR (400 MHz, $CDCl_3$): δ = 6.95 (d, *J* = 6.2 Hz, 2H, 3-H, 9-H), 6.89 (d, *J* = 6.6 Hz, 2H, 3-H, 9-H),, 6.77 – 6.68 (m, 2H, 1-H, 11-H), 6.63 (d, *J* = 15.8 Hz, 1H, 5-H), 6.30 (dd, *J* = 15.8, 6.4 Hz, 1H, 6-H), 5.38 – 5.35 (m, 1H, 7-H), 2.11 (d, *J* = 3.5 Hz, 1H, 7-OH).

The spectrum is in agreement with the literature[2]

General procedure 1 (GP1): for the synthesis of benzyl bromides (1-Br, 2-Br, 3-Br, 4-Br, 5-Br, 6-Br, 7-Br, 8-Br)

Synthesis according to the modified procedure in ref.[3]

The corresponding benzyl alcohol (2 mmol, 1.0 eq.) was dissolved in 6 mL toluene and cooled to 0 °C. Then PBr_3 (0.650 g, 2.4 mmol, 1.2 eq.) was added. The reaction mixture was stirred for 4 h at 0 °C. Subsequently, the reaction mixture was washed with water (2 × 6 mL) quickly to avoid prolonged exposure of the product to water. The organic phase was then filtered through a Na_2SO_4 plug and the plug rinsed with diethylether. The solvent was removed under reduced pressure. The resulting products were stored in a freezer (T=−20 °C) under argon to avoid decomposition and used without further purification.

1-Br: (1-bromoethyl)benzene

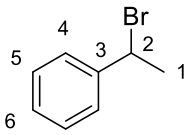

1-Br

Synthesis according to GP1: colorless liquid (344 mg, 1.86 mmol, 93%)

^{1}H NMR (400 MHz, $CDCl_3$): δ = 7.46 – 7.43 (m, 2H, 5-H), 7.37 – 7.27 (m, 3H, 6-H, 4-H), 5.22 (q, *J* = 6.9 Hz, 1H, 2-H), 2.06 (d, *J* = 6.9 Hz, 3H, 1-H).

The spectrum is in agreement with the literature[4]

2-Br: 1-(1-bromoethyl)-4-methylbenzene

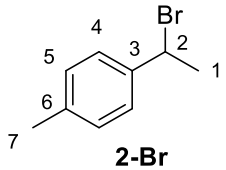

2-Br

Synthesis according to GP1: colorless liquid (366 mg, 1.84 mmol, 92%)

^{1}H NMR (400 MHz, $CDCl_3$): δ = 7.34 (d, *J* = 8.1 Hz, 2H, 4-H), 7.15 (d, *J* = 8.0 Hz, 2H, 5-H), 5.22 (q, *J* = 6.9 Hz, 1H, 2-H), 2.34 (s, 3H, 7-H), 2.04 (d, *J* = 6.9 Hz, 3H, 1-H).

The spectrum is in agreement with the literature[5]

3-Br: 5-(1-bromoethyl)-2,3-dihydro-1*H*-indene

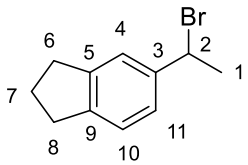

3-Br

Synthesis according to GP1: colorless liquid (410 mg, 1.83 mmol, 91%)

^{1}H NMR (400 MHz, $CDCl_3$): δ = 7.32 (s, 1H, 4-H), 7.23 – 7.16 (m, 2H, 10-H, 11-H), 5.24 (q, *J* = 6.9 Hz, 1H, 2-H), 2.92 – 2.86 (m, 4H, 6-H, 8-H), 2.12 – 2.04 (m, 2H, 7-H), 2.05 (d, *J* = 7.0 Hz, 3H, 1-H).

^{13}C{^{1}H} NMR (101 MHz, $CDCl_3$): δ = 144.84 (C_q, C-5, C-9), 144.79 (C_q, C-5, C-9), 141.25 (C_q, C-3) , 124.80 (CH, C-4, C-10), 124.47 (CH, C-4, C-10), 122.74 (CH, C-11), 50.50 (CH, C-2), 32.75 (CH_2, C-6, C-8), 32.64 (CH_2, C-6, C-8), 26.99 (CH_3, C-1), 25.47 (CH_2, C-7).

HRMS (EI): 144.0934 found for $C_{11}H_{12}^{+\cdot}$ (calculated: 144.0933). Only the elimination product is found.

4-Br: 1-(1-bromoethyl)-4-methoxybenzene

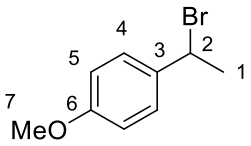

4-Br

Synthesis according to GP1: colorless liquid (386 mg, 1.80 mmol, 90%)

^{1}H NMR (400 MHz, $CDCl_3$): δ = 7.38 (d, *J* = 8.7 Hz, 2H, 5-H), 6.87 (d, *J* = 8.6 Hz, 2H, 4-H), 5.25 (q, *J* = 6.9 Hz, 1H, 2-H), 3.81 (s, 3H, 7-H), 2.05 (d, *J* = 6.9 Hz, 3H, 1-H).

The spectrum is in agreement with the literature.[5]

5-Br: 5-(1-bromoethyl)-2,3-dihydrobenzofuran

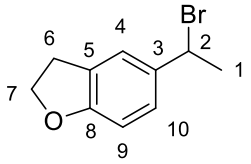

5-Br

Synthesis according to GP1: yellowish liquid (418 mg, 1.84 mmol, 92%)

^{1}H NMR (400 MHz, $CDCl_3$): δ = 7.31 (s, 1H, 4-H), 7.18 (d, *J* = 7.9 Hz, 1H, 10-H), 6.73 (d, *J* = 8.3 Hz, 1H, 9-H), 5.26 (q, *J* = 6.9 Hz, 1H, 2-H), 4.58 (t, *J* = 8.6 Hz, 2H, 7-H), 3.21 (t, *J* = 8.7 Hz, 2H, 6-H), 2.05 (d, *J* = 6.9 Hz, 3H, 1-H).

^{13}C{^{1}H} NMR (101 MHz, $CDCl_3$): δ = 160.23 (C_q, C-8), 135.51 (C_q, C-3), 127.62 (C_q, C-5), 126.92 (CH, C-4, C-10), 123.64 (CH, C-4, C-10), 109.15 (CH, C-9), 71.55 (CH_2, C-7), 50.89 (CH, C-2), 29.57 (CH_2, C-6), 27.08 (CH_3, C-1).

HRMS (EI): 146.0726 found for $C_{10}H_{11}O^{+\cdot}$ (calculated: 146.0726). Only the elimination product is found.

6-Br: (bromomethylene)dibenzene

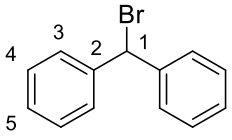

6-Br

Synthesis according to GP1: colorless liquid (466 mg, 1.88 mmol, 94%)

^{1}H NMR (400 MHz, $CDCl_3$): δ = 7.46 (d, *J* = 7.2 Hz, 4H), 7.36 – 7.28 (m, 6H), 6.29 (s, 1H, 1-H).

The spectrum is in agreement with the literature.[6]

7-Br: 4,4'-(bromomethylene)bis(methylbenzene)

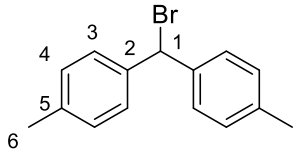

7-Br

Synthesis according to GP1: yellowish liquid (520 mg, 1.89 mmol, 95%)

^{1}H NMR (400 MHz, $CDCl_3$): δ = 7.35 (d, *J* = 8.1 Hz, 2H, 4-H), 7.14 (d, *J* = 8.0 Hz, 2H, 3-H), 6.27 (s, 1H, 1-H), 2.34 (s, 6H, 6-H).

The spectrum is in agreement with the literature.[6]

8-Br: (E)-5,5'-(3-bromoprop-1-ene-1,3-diyl)bis(1,3-difluorobenzene)

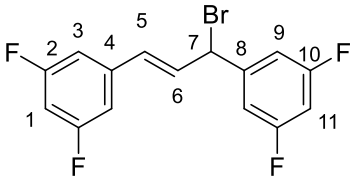

8-Br

Synthesis according to GP1 (1 mmol scale): colorless liquid (317 mg, 0.92 mmol, 92%)

^{1}H NMR (400 MHz, $CDCl_3$): δ = 7.02 (dd, *J* = 7.9 Hz, 2.2 Hz, 2H, 9-H), 6.92 (dd, *J* = 8.4 Hz, 2.1 Hz, 2H, 3-H), 6.80 – 6.71 (m, 2H,1-H, 11-H), 6.58 (dd, *J* = 15.5 Hz, 8.0 Hz, 1H, 6-H), 6.52 (d, *J* = 15.5 Hz, 1H, 5-H), 5.68 (d, *J* = 8.0 Hz, 1H, 7-H).

^{13}C{^{1}H} NMR (101 MHz, $CDCl_3$): δ = 163.37 (dd, J_{CF} = 249 Hz, 12.8 Hz, C-10), 163.13 (dd, J_{CF} = 250 Hz, 12.9 Hz, C-2), 143.64 (t, J_{CF} = 9.2 Hz, C-8), 138.84 (t, J_{CF} = 9.5 Hz, 4-C), 131.01 (s, C-5), 130.76 (s, C-6), 110.99 (d, J_{CF} = 26.3 Hz, C-9), 109.82 (d, J_{CF} = 25.0 Hz, C-3), 104.34 (t, J_{CF} = 22.0 Hz, C-11), 104.02 (t, J_{CF} = 22.3 Hz, C-1), 51.59 (s, C-7).

The spectra are in agreement with the literature.[7]

1-(bromo(phenyl)methyl)-4-methylbenzene:

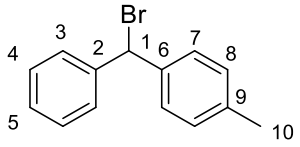

Synthesis according to GP1: colorless liquid (490 mg, 1.88 mmol, 94%)

^{1}H NMR (400 MHz, $CDCl_3$): δ = 7.47 (d, *J* = 7.2 Hz, 2H, 7-H), 7.36 – 7.32 (m, 4H, 3-H, 4-H), 7.29 – 7.26 (m, 1H. 5-H), 7.15 (d, *J* = 8.0 Hz, 2H, 8-H), 6.28 (s, 1H), 2.34 (s, 3H, 10-H).

The spectrum is in agreement with the literature.[6]

General procedure 2 (GP2) for the synthesis of benzyl chlorides (2-Cl and 8-Cl)

Synthesis according to the modified procedure in ref.[8]

The corresponding benzyl alcohol (2 mmol, 1.0 eq.) was dissolved dichloromethane (6 mL) and cooled to 0 °C. Then $SOCl_2$ (0.238 g, 2.8 mmol, 1.4 eq.) was added. The reaction mixture was stirred for 4 h at 0 °C. The reaction mixture was then washed with water (2 × 6 mL) in a short amount of time. The organic phase was then filtered through a Na_2SO_4 plug, the plug rinsed with dichloromethane and the solvent removed under reduced pressure. The resulting products were stored in a freezer (T=−20 °C) under argon to avoid decomposition and used without further purification.

2-Cl: 1-(1-chloroethyl)-4-methylbenzene

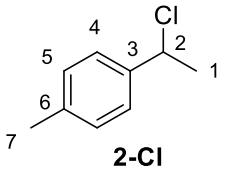

2-Cl

Synthesis according to GP2: colorless liquid (288 mg, 1.86 mmol, 93%)

^{1}H NMR (400 MHz, $CDCl_3$): δ = 7.32 (d, *J* = 8.1 Hz, 2H, 4-H), 7.17 (d, *J* = 8.0 Hz, 2H, 5-H), 5.09 (q, *J* = 6.8 Hz, 1H, 2-H), 2.35 (s, 3H, 7-H), 1.85 (d, *J* = 6.8 Hz, 3H, 1-H).

^{13}C{^{1}H} NMR (101 MHz, $CDCl_3$): δ = 140.08 (C_q, C-3) 138.26 (C_q, C-6), 129.43 (CH, C-4), 126.56 (CH, C-5), 58.95 (CH, C-2), 26.60 (CH_3, C-1), 21.27 (CH_3, C-7).

The spectrum is in agreement with the literature.[9]

8-Cl: (E)-5,5'-(3-chloroprop-1-ene-1,3-diyl)bis(1,3-difluorobenzene)

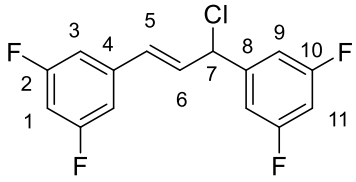

8-Cl

Synthesis according to GP2 (1 mmol scale): colorless liquid (274 mg, 0.91 mmol, 91%)

^{1}H NMR (400 MHz, $CDCl_3$): δ = 7.00 (d, *J* = 5.9 Hz, 2H, 3-H), 6.91 (d, *J* = 6.3 Hz, 2H, 9-H), 6.79 (t, *J* = 8.8 Hz, 1H, 11-H), 6.74 (t, *J* = 8.8 Hz, 1H, 1-H), 6.57 (d, *J* = 15.6 Hz, 1H, 5-H), 6.41 (dd, *J* = 15.6 Hz, 7.7 Hz, 1H, 6-H), 5.54 (d, *J* = 7.6 Hz, 1H, 7-H).

^{13}C{^{1}H} NMR (101 MHz, $CDCl_3$): δ = 163.40 (dd, J_{CF} = 249.0 Hz, 13.6 Hz, CF, C-10), 163.20 (dd, J_{CF} = 251.1 Hz, 12.0 Hz, CF, C-2), 143.50 (t, J_{CF} = 8.8 Hz, C_q, C-8), 138.99 – 138.92 (m, C_q,), 131.10 (s, CH, C-5), 130.53 (s, CH, C-6), 110.82 – 110.46 (m, CH, C-9), 109.94 – 109.64 (m, CH, C-3), 104.28 (t, J_{CF} = 21.3 Hz, CH, C-11), 104.13 – 103.79 (m, CH, C-1) , 61.36 (s, CHCl, C-7).

The spectra are in agreement with the literature.[7]

Synthesis of phenethyl tosylate (1-OTs)

Synthesis according to the modified procedure in ref.[10]

1-Sulfinate (1-phenylethyl 4-methylbenzenesulfinate):

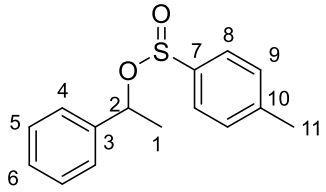

1-Sulfinate

1-phenylethan-1-ol (0.290 g, 2.37 mmol, 1.00 eq.), pyridine (0.255 g, 3.22 mmol, 1.36 eq) and 4-methylbenzenesulfinic chloride (0.500 g, 2.86 mmol, 1.20 eq) were dissolved in diethylether (12 mL) at −70 °C and stirred for 2.5 h without cooling. The reaction mixture was then acidified with 0.1 M HCl (12 mL), washed with with water (12 mL), then with sat. aq. $NaHCO_3$ (12 mL) and then again with water (12 mL). The organic phase was dried over $MgSO_4$. The crude product eluted from the chromatography column (15% Et_2O in pentane) in two fractions (R_f=0.55 and R_f=0.58 in 30% Et_2O in pentane) with a combined mass of 0.490 g (1.79 mmol, 75%, *dr*=1) as a colorless liquid.

1-Sulfinate Diastereomer 1 (1-phenylethyl 4-methylbenzenesulfinate):

^{1}H NMR (400 MHz, $CDCl_3$): δ = 7.55 (d, *J* = 8.2 Hz, 2H, 8-H), 7.30 – 7.23 (m, 5H, H_{Ar}), 7.19 – 7.16 (m, 2H, H_{Ar}), 5.40 (q, *J* = 6.5 Hz, 1H, 2-H), 2.42 (s, 3H, 11-H), 1.70 (d, *J* = 6.6 Hz, 3H, 1-H).

^{13}C{^{1}H} NMR (101 MHz, $CDCl_3$): δ = 142.65 (C_{Ar}), 142.18 (C_{Ar}), 141.61 (C_{Ar}), 129.55 (C_{Ar}), 128.40 (C_{Ar}), 127.97 (C_{Ar}), 126.39 (C_{Ar}), 125.44 (C_{Ar}), 75.58 (CH, C-2), 24.38 (CH_3, C-1), 21.59 (CH_3, C-11).

HRMS (EI): 259.0795 found for $C_{15}H_{15}O_2{}^{32}S^{+\cdot}$ (calculated: 259.0787)

The spectra are in agreement with the literature.[11]

1-Sulfinate Diastereomer 2 (1-phenylethyl 4-methylbenzenesulfinate):

^{1}H NMR (400 MHz, $CDCl_3$): δ = 7.55 (d, *J* = 8.2 Hz, 2H, 8-H), 7.40 – 7.30 (m, 7H, H_{Ar}), 5.45 (q, *J* = 6.6 Hz, 1H, 2-H), 2.42 (s, 3H, 11-H), 1.57 (d, *J* = 6.6 Hz, 3H, 1-H).

^{13}C{^{1}H} NMR (101 MHz, $CDCl_3$): δ = 142.73 (C_q, C-3,C-6, C-7), 142.67 (C_q, C-3,C-6, C-7), 141.78 (C_{Ar}), 129.64 (C_{Ar}), 128.68 (C_{Ar}), 128.32 (C_{Ar}), 126.47 (C_{Ar}), 124.92 (C_{Ar}), 77.13 (CH, C-2), 24.06 (CH_3, C-1), 21.54 (CH_3, C-11).

HRMS (EI): 259.0795 found for $C_{15}H_{15}O_2{}^{32}S^{+\cdot}$ (calculated: 259.0787)

The spectra are in agreement with the literature .[11]

1-OTs: 1-phenylethyl 4-methylbenzenesulfonate

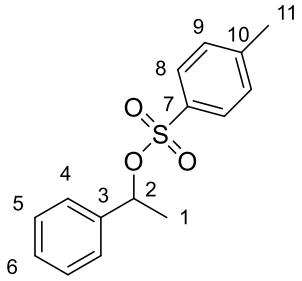

1-OTs

1-sulfinate (0.100 g, 0.384 mmol, 1 eq. mixture of both diastereomers) was dissolved in dichloromethane (2 mL) at 0 °C. *m*CPBA (92.8 mg, 0.538 mmol, 1.4 eq.) was added and stirred for 3 h at 0 °C. The reaction mixture was then quickly washed with an aq. 2 M $NaHCO_3$ solution (2 mL). The organic phase was then filtered through a plug of $MgSO_4$, the plug rinsed with dichloromethane and the solvent removed at 0°C *in vacuo*. The crude product (colorless solid, 80 mg, 0.28 mmol, 72%) was used without further purification. Decomposition at room temperature could be observed with a change in color from colorless to slightly pink and finally to an intense, dark red.

^{1}H NMR (400 MHz, $CDCl_3$, –40 °C): δ = 7.59 (d, *J* = 8.3 Hz, 2H, 8-H), 7.26 – 7.13 (m, 7H, 4-H, 5-H, 6-H, 9-H), 5.50 (q, *J* = 6.6 Hz, 1H, 2-H), 2.38 (s, 3H, 11-H), 1.59 (d, *J* = 6.6 Hz, 3H, 1-H).

^{13}C{^{1}H} NMR (101 MHz, $CDCl_3$, –40 °C): δ = 144.51 (C_q, C-7), 138.76 (C_q, C-10), 133.39 (C_q, C-3), 129.57 (CH, C-4), 128.60 (CH, C-5), 128.46 (CH, C-6), 127.69 (CH, C-8), 126.32 (CH, C-9), 81.47 (CH, C-2), 23.31 (CH_3, C-11), 21.84 (CH_3, C-1).

The spectra are in agreement with the literature.[12]

N-(di-*p*-tolylmethyl)propan-1-amine

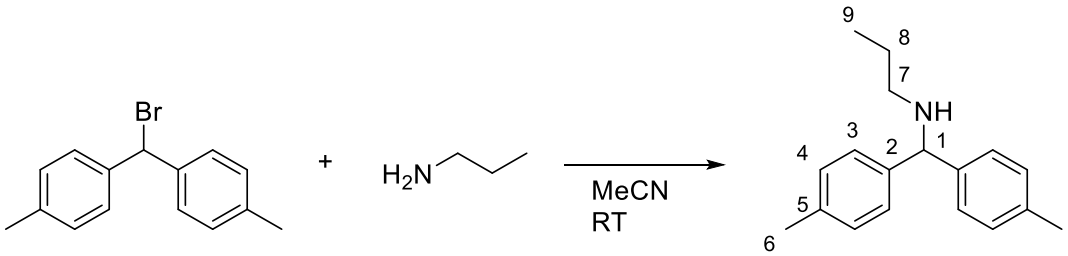

7-Br **13**

7-Br (200 mg, 0.730 mmol, 1 eq.) and **13** (43.2 mg, 0.730 mmol, 1 eq.) were dissolved in 5 mL acetonitrile and stirred for 2 h at RT. Then the reaction mixture was diluted with 30 mL diethylether and washed with sat. aq. Na_2CO_3 solution (30 mL) and water (30 mL). The organic phase was dried over $MgSO_4$ and the solvent removed under reduced pressure. The product was a colorless liquid (176 mg, 0.694 mmol, 95%).

^{1}H NMR (400 MHz, $CDCl_3$): δ = 7.31 (d, *J* = 8.0 Hz, 4H, 4-H), 7.11 (d, *J* = 7.9 Hz, 4H, 3-H), 4.79 (s, 1H, 1-H), 2.57 – 2.53 (m, 2H, 7-H), 2.30 (s, 6H, 6-H), 1.55 (h, *J* = 7.4 Hz, 2H, 8-H), 0.89 (t, *J* = 7.4 Hz, 3H, 9-H).

^{13}C{^{1}H} NMR (101 MHz, $CDCl_3$): δ = 140.76 (C_q, C-2), 136.72 (C_q, C-5), 129.31 (CH, C-4), 127.36 (CH, C-3), 66.96 (CH, C-1), 50.10 (CH_2, C-7), 22.95 (CH_2, C-8), 21.19 (CH_3, C-6), 11.91 (CH_3, C-9).

4.2.3 Kinetics

The development of charge was followed with a (WTW 530) conductometer with a Pt electrode (WTW LTA 1/NS). For rapid kinetics marked with „SF measurement“ a Hi-Tech („HT“) stopped flow conductometer (Hi-Tech SF-61DX2 run by HiTech KinetAssyst2 software) or Applied Photophysics Ltd. („AP“) stopped flow conductometer (SX20/CM with conductivity cell, e-corder 410 and conductivity isoPod run by Pro-Data from eDAQ Pty Ltd.) was used. In all cases the temperature was kept constant (±0.1 °C) with a circulating bath thermostat. For stopped flow kinetics performed in solvent mixtures, one syringe was prepared with the electrophile in acetonitrile and the other syringe with the nucleophile in acetonitrile and methanol. Both syringes were mixed 1:1. For example for a reaction in 20% (v/v) methanol in acetonitrile the electrophile syringe was filled with acetonitrile and the nucleophile syringe with 40% (v/v) methanol in acetonitrile. Nucleophile concentrations were atleast ten times higher than electrophile concentrations to achieve pseudo-first order kinetics. Rate constants were obtained from these kinetics by least squares fitting of the conductance *G* with the equation $G_t = G_0\, e^{kt} + C$. Plots of k_{obs} versus amine concentration gave k_1 and k_2 with the equation $k_{obs} = k_1 + [\text{amine}]\, k_2$. The rate constant k_1 was only taken from the amines which were best suited to give accurate values for k_1. This was the amine with the lowest k_2 and/or the lowest k_{obs}, so k_{obs} would mainly consist of k_1. The relationship of conductance and concentration is not sufficiently linear for protonated amines in acetonitrile without added methanol. As a consequence the kinetic traces are misinterpreted with an overestimated k_{obs} when the traces are not corrected. To correct the kinetics, the charged products were stepwise added into acetonitrile and the conductance recorded. This was done at different amine concentrations, just like in the kinetic experiments, since the amount of ion pairing depends on the amine concentration. Fortunately, the amount of ion pairing can be considered as indepedent oft he employed electrophile, as the product will transfer ist proton and thus charge tot he abundant amine. For this reason the calibration curves were measured by adding aminium chlorides, bromides and tosylates into the corresponding acetonitrile amine solutions at 20 °C. Plotting concentration versus conductance gave a behavior that could be precisely fitted with a second order polynomial. To avoid unneccessary measurements, the parameters a, b and c of the second order polynomial ($aG^2 + bG + c = [\text{salt}]$) were interpolated for some amine concentrations. All kinetics that were corrected in this way are marked.

Kinetics of reactions of phenethylbromide (1-Br)

1-Br and DABCO (**9**) in acetonitrile at 20 °C.

$[\mathbf{1\text{-}Br}]_0$ (mol L^{-1})	**[9]** (mol L^{-1})	k_{obs} (s^{-1})
1.00×10^{-3}	2.00×10^{-2}	6.92×10^{-4}
1.00×10^{-3}	4.00×10^{-2}	1.39×10^{-3}
1.00×10^{-3}	6.00×10^{-2}	2.01×10^{-3}
1.00×10^{-3}	8.00×10^{-2}	2.61×10^{-3}

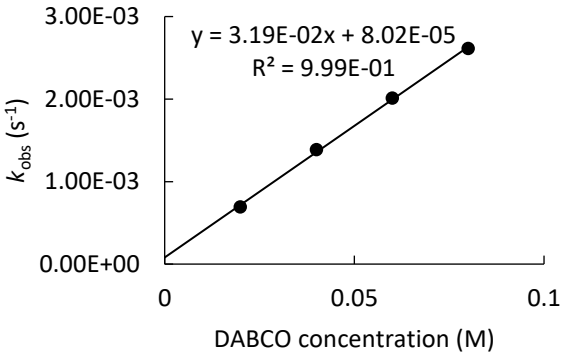

$k_2 = 3.19 \times 10^{-2}$ L mol^{-1} s^{-1}

1-Br and pyrrolidine (**10**) in acetonitrile at 20 °C. Kinetics have been corrected due to ion pairing.

$[\mathbf{1\text{-}Br}]_0$ (mol L^{-1})	**[10]** (mol L^{-1})	k_{obs} (s^{-1})
1.00×10^{-3}	1.00×10^{-1}	8.45×10^{-4}
1.00×10^{-3}	2.00×10^{-1}	1.74×10^{-3}
1.00×10^{-3}	3.00×10^{-1}	2.55×10^{-3}
1.00×10^{-3}	4.00×10^{-1}	3.36×10^{-3}

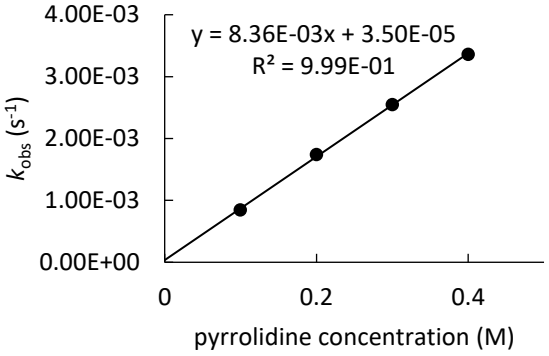

$k_2 = 8.36 \times 10^{-3}$ L mol^{-1} s^{-1}

1-Br and piperidine (**11**) in acetonitrile at 20 °C. Kinetics have been corrected due to ion pairing.

$[\mathbf{1\text{-}Br}]_0$ (mol L^{-1})	**[11]** (mol L^{-1})	k_{obs} (s^{-1})
1.00×10^{-3}	1.00×10^{-1}	5.63×10^{-4}
1.00×10^{-3}	2.00×10^{-1}	1.10×10^{-3}
1.00×10^{-3}	3.00×10^{-1}	2.62×10^{-3}
1.00×10^{-3}	4.00×10^{-1}	3.39×10^{-3}

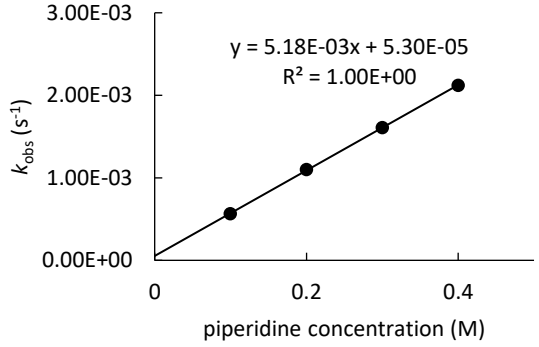

$k_2 = 5.18 \times 10^{-3}$ L mol^{-1} s^{-1}

1-Br and morpholine (**12**) in acetonitrile at 20 °C. Kinetics have been corrected due to ion pairing.

$[\mathbf{1\text{-}Br}]_0$ (mol L^{-1})	**[12]** (mol L^{-1})	k_{obs} (s^{-1})
1.00×10^{-3}	2.00×10^{-1}	2.18×10^{-4}
1.00×10^{-3}	4.00×10^{-1}	4.35×10^{-4}
1.00×10^{-3}	6.00×10^{-1}	7.04×10^{-4}
1.00×10^{-3}	8.00×10^{-1}	9.15×10^{-4}

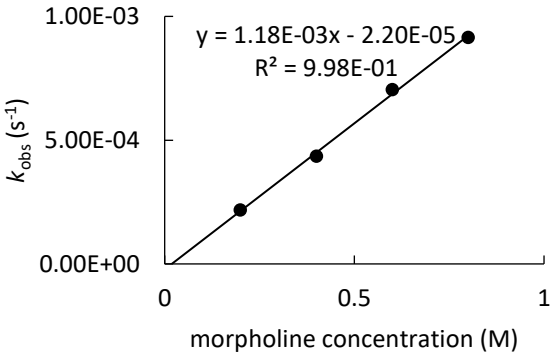

$k_2 = 1.18 \times 10^{-3}$ L mol^{-1} s^{-1}

1-Br and propylamine (**13**) in acetonitrile at 20 °C. Kinetics have been corrected due to ion pairing.

$[\mathbf{1\text{-}Br}]_0$ (mol L^{-1})	**[13]** (mol L^{-1})	k_{obs} (s^{-1})
1.00×10^{-3}	3.00×10^{-1}	1.27×10^{-4}
1.00×10^{-3}	6.00×10^{-1}	2.32×10^{-4}
1.00×10^{-3}	9.00×10^{-1}	3.34×10^{-4}
1.00×10^{-3}	1.20×10^{0}	4.22×10^{-4}

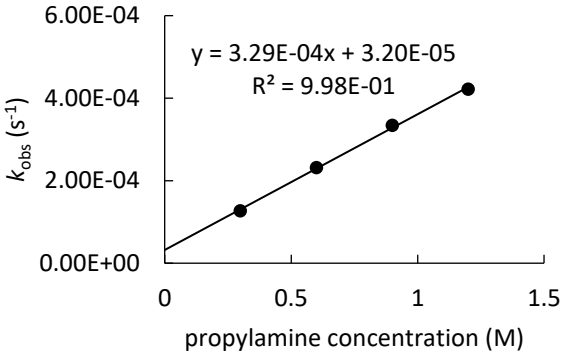

$k_2 = 3.29 \times 10^{-4}$ L mol^{-1} s^{-1}

Kinetics of reactions of 1-OTs: 1-phenethyl tosylate

1-OTs and DABCO (**9**) in 95AN5Tol at 20 °C.

$[\mathbf{1\text{-}OTs}]_0$ (mol L^{-1})	**[9]** (mol L^{-1})	k_{obs} (s^{-1})
1.00×10^{-3}	1.00×10^{-1}	2.45×10^{-3}
1.00×10^{-3}	2.00×10^{-1}	5.07×10^{-3}
1.00×10^{-3}	3.00×10^{-1}	7.46×10^{-3}
1.00×10^{-3}	4.00×10^{-1}	9.83×10^{-3}

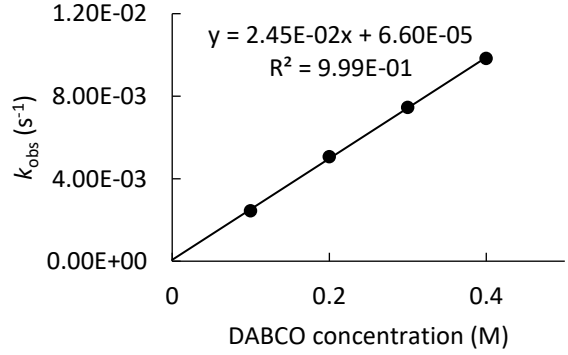

$k_2 = 2.45 \times 10^{-2}$ L mol^{-1} s^{-1}

1-OTs and pyrrolidine (**10**) in 95AN5Tol at 20 °C.

$[\mathbf{1\text{-}OTs}]_0$ (mol L^{-1})	**[10]** (mol L^{-1})	k_{obs} (s^{-1})
1.00×10^{-3}	1.00×10^{-1}	5.53×10^{-4}
1.00×10^{-3}	2.00×10^{-1}	1.12×10^{-3}
1.00×10^{-3}	3.00×10^{-1}	1.69×10^{-3}
1.00×10^{-3}	4.00×10^{-1}	2.19×10^{-3}

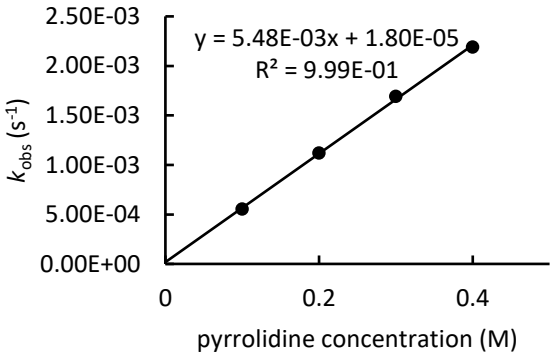

$k_2 = 5.48 \times 10^{-3}$ L mol^{-1} s^{-1}

1-OTs and piperidine (**11**) in 95AN5Tol at 20 °C.

$[\mathbf{1\text{-}OTs}]_0$ (mol L^{-1})	**[11]** (mol L^{-1})	k_{obs} (s^{-1})
1.00×10^{-3}	1.00×10^{-1}	3.82×10^{-4}
1.00×10^{-3}	2.00×10^{-1}	7.56×10^{-4}
1.00×10^{-3}	3.00×10^{-1}	1.11×10^{-3}
1.00×10^{-3}	4.00×10^{-1}	1.40×10^{-3}

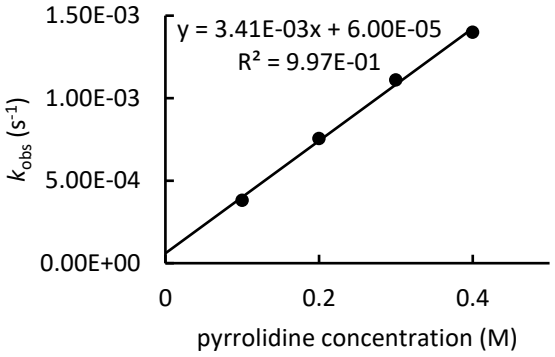

$k_2 = 3.41 \times 10^{-3}$ L mol^{-1} s^{-1}

1-OTs and morpholine (**12**) in 95AN5Tol at 20 °C.

$[\mathbf{1\text{-}OTs}]_0$ (mol L^{-1})	**[12]** (mol L^{-1})	k_{obs} (s^{-1})
1.00×10^{-3}	1.00×10^{-1}	1.16×10^{-4}
1.00×10^{-3}	2.00×10^{-1}	2.20×10^{-4}
1.00×10^{-3}	3.00×10^{-1}	3.49×10^{-4}
1.00×10^{-3}	4.00×10^{-1}	4.69×10^{-4}

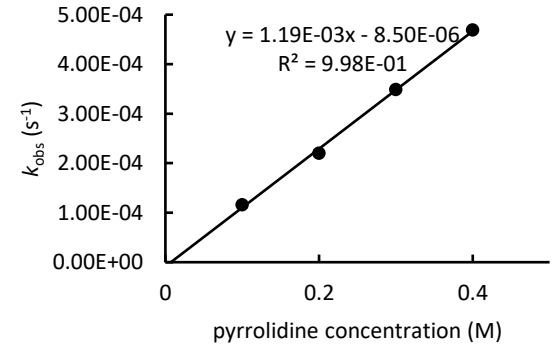

$k_2 = 1.19 \times 10^{-3}$ L mol^{-1} s^{-1}

1-OTs and propylamine (**13**) in 95AN5Tol at 20 °C.

[1-OTs]$_0$ (mol L^{-1})	**[13]** (mol L^{-1})	k_{obs} (s^{-1})
1.00×10^{-3}	3.00×10^{-1}	1.63×10^{-4}
1.00×10^{-3}	6.00×10^{-1}	3.14×10^{-4}
1.00×10^{-3}	9.00×10^{-1}	4.56×10^{-4}
1.00×10^{-3}	1.20×10^{0}	5.90×10^{-4}

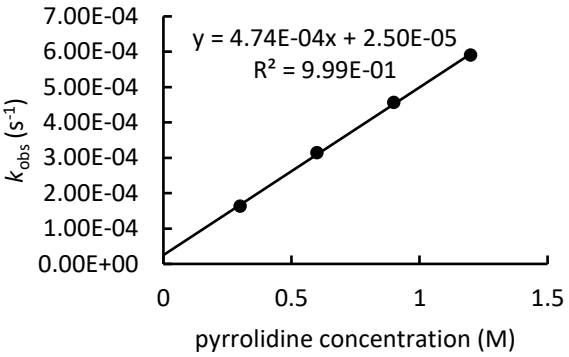

$k_2 = 4.74 \times 10^{-4}$ L mol^{-1} s^{-1}

1-OTs and NEt_3 in 95AN5Tol at 20 °C.

[1-OTs]$_0$ (mol L^{-1})	**[NEt_3]** (mol L^{-1})	k_{obs} (s^{-1})
1.00×10^{-3}	1.00×10^{-1}	1.65×10^{-5}

$k_1 = 1.65 \times 10^{-5}$ s^{-1}

Kinetics of reactions of 2-Br: 1-(1-bromoethyl)-4-methylbenzene

2-Br and DABCO (**9**) in 80AN20M at 20 °C.

[2-Br]$_0$ (mol L^{-1})	**[9]** (mol L^{-1})	k_{obs} (s^{-1})
1.00×10^{-3}	2.00×10^{-2}	5.78×10^{-4}
1.00×10^{-3}	4.00×10^{-2}	9.42×10^{-4}
1.00×10^{-3}	6.00×10^{-2}	1.29×10^{-3}
1.00×10^{-3}	8.00×10^{-2}	1.67×10^{-3}

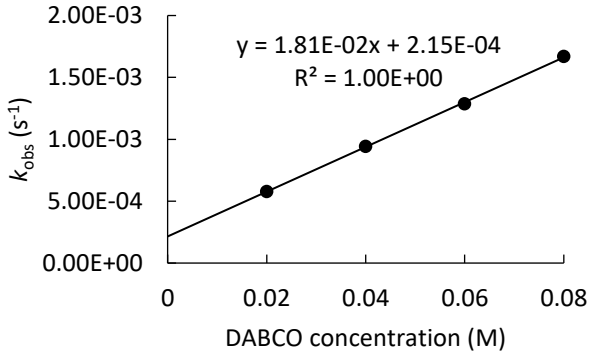

$k_2 = 1.81 \times 10^{-2}$ L mol^{-1} s^{-1}

2-Br and pyrrolidine (**10**) in 80AN20M at 20 °C.

$[\mathbf{2\text{-}Br}]_0$ (mol L^{-1})	**[10]** (mol L^{-1})	k_{obs} (s^{-1})
1.00×10^{-3}	1.00×10^{-1}	5.78×10^{-4}
1.00×10^{-3}	2.00×10^{-1}	8.94×10^{-4}
1.00×10^{-3}	3.00×10^{-1}	1.25×10^{-3}
1.00×10^{-3}	4.00×10^{-1}	1.63×10^{-3}

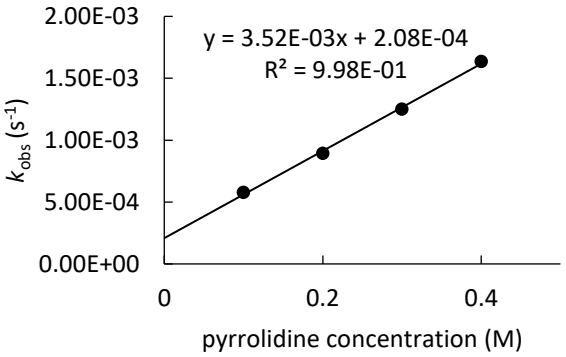

$k_2 = 3.52 \times 10^{-3}$ L mol^{-1} s^{-1}

2-Br and piperidine (**11**) in 80AN20M at 20 °C.

$[\mathbf{2\text{-}Br}]_0$ (mol L^{-1})	**[11]** (mol L^{-1})	k_{obs} (s^{-1})
1.00×10^{-3}	1.00×10^{-1}	5.07×10^{-4}
1.00×10^{-3}	2.00×10^{-1}	7.66×10^{-4}
1.00×10^{-3}	3.00×10^{-1}	1.06×10^{-3}
1.00×10^{-3}	4.00×10^{-1}	1.31×10^{-3}

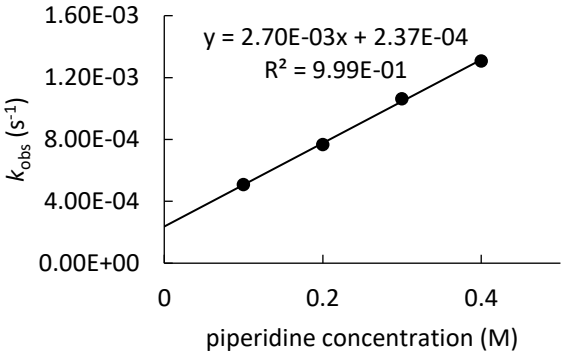

$k_2 = 2.70 \times 10^{-3}$ L mol^{-1} s^{-1} $k_1 = 2.37 \times 10^{-4}$ s^{-1}

2-Br and morpholine (**12**) in 80AN20M at 20 °C.

$[\mathbf{2\text{-}Br}]_0$ (mol L^{-1})	**[12]** (mol L^{-1})	k_{obs} (s^{-1})
1.00×10^{-3}	1.00×10^{-1}	3.91×10^{-4}
1.00×10^{-3}	2.00×10^{-1}	5.61×10^{-4}
1.00×10^{-3}	3.00×10^{-1}	7.15×10^{-4}
1.00×10^{-3}	4.00×10^{-1}	9.09×10^{-4}

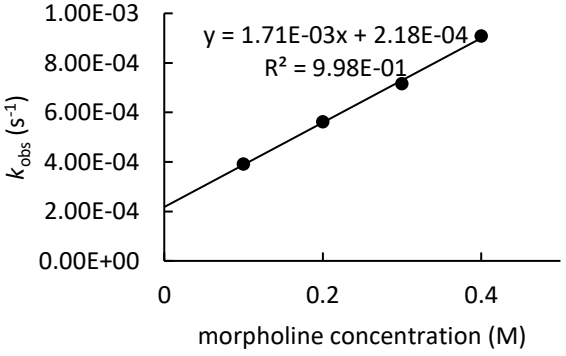

$k_2 = 1.71 \times 10^{-3}$ L mol^{-1} s^{-1}

2-Br and propylamine (**13**) in 80AN20M at 20 °C.

[2-Br]$_0$ (mol L^{-1})	**[13]** (mol L^{-1})	k_{obs} (s^{-1})
1.00×10^{-3}	2.50×10^{-1}	3.26×10^{-4}
1.00×10^{-3}	5.00×10^{-1}	4.51×10^{-4}
1.00×10^{-3}	7.50×10^{-1}	5.90×10^{-4}
1.00×10^{-3}	1.00×10^{0}	7.60×10^{-4}

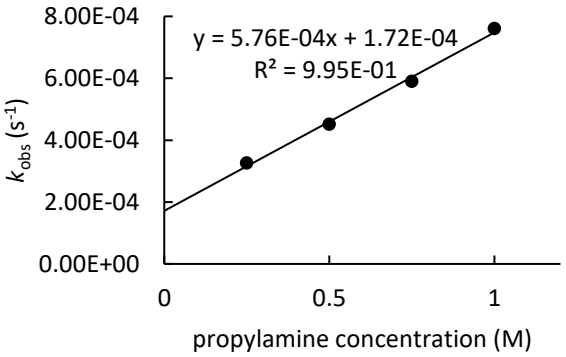

$k_2 = 5.76 \times 10^{-4}$ L mol^{-1} s^{-1}

2-Br and piperidine (**11**) in 50AN50M at 20 °C.

[2-Br]$_0$ (mol L^{-1})	**[11]** (mol L^{-1})	k_{obs} (s^{-1})
1.00×10^{-3}	5.00×10^{-1}	1.37×10^{-3}
1.00×10^{-3}	1.00×10^{0}	1.80×10^{-3}
1.00×10^{-3}	1.50×10^{0}	2.23×10^{-3}
1.00×10^{-3}	2.00×10^{0}	2.66×10^{-3}

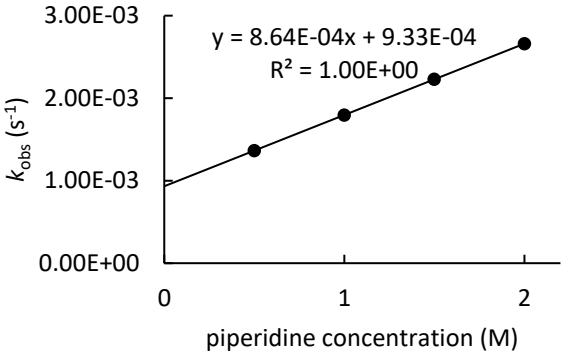

$k_2 = 8.64 \times 10^{-4}$ L mol^{-1} s^{-1}

2-Br and piperidine (**11**) in 60AN40M at 20 °C.

[2-Br]$_0$ (mol L^{-1})	**[11]** (mol L^{-1})	k_{obs} (s^{-1})
1.00×10^{-3}	1.00×10^{-1}	8.96×10^{-4}
1.00×10^{-3}	3.00×10^{-1}	1.11×10^{-3}
1.00×10^{-3}	5.00×10^{-1}	1.34×10^{-3}
1.00×10^{-3}	1.00×10^{0}	2.00×10^{-3}
1.00×10^{-3}	1.50×10^{0}	2.58×10^{-3}

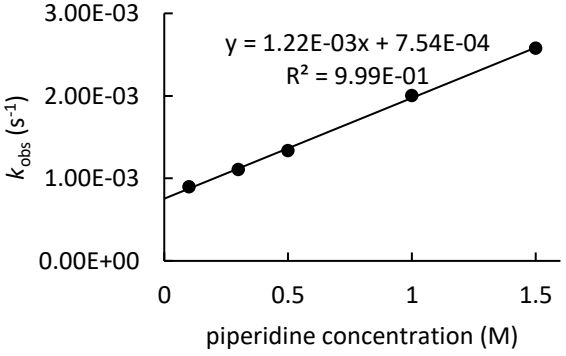

$k_2 = 1.22 \times 10^{-3}$ L mol^{-1} s^{-1}

2-Br and piperidine (**11**) in 70AN30M at 20 °C.

$[\mathbf{2\text{-}Br}]_0$ (mol L^{-1})	**[11]** (mol L^{-1})	k_{obs} (s^{-1})
1.00×10^{-3}	1.00×10^{-1}	6.51×10^{-4}
1.00×10^{-3}	2.00×10^{-1}	8.29×10^{-4}
1.00×10^{-3}	3.00×10^{-1}	1.03×10^{-3}
1.00×10^{-3}	4.00×10^{-1}	1.19×10^{-3}

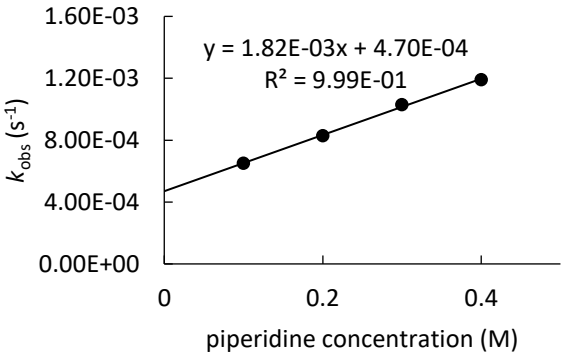

$k_2 = 1.82 \times 10^{-3}$ L mol^{-1} s^{-1}

2-Br and piperidine (**11**) in 90AN10M at 20 °C.

$[\mathbf{2\text{-}Br}]_0$ (mol L^{-1})	**[11]** (mol L^{-1})	k_{obs} (s^{-1})
1.00×10^{-3}	1.00×10^{-1}	5.05×10^{-4}
1.00×10^{-3}	2.00×10^{-1}	9.65×10^{-4}
1.00×10^{-3}	3.00×10^{-1}	1.42×10^{-3}
1.00×10^{-3}	4.00×10^{-1}	1.85×10^{-3}

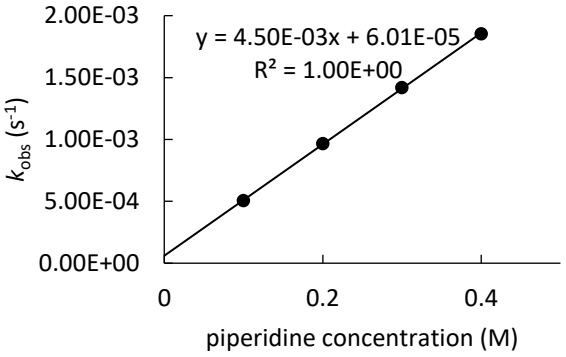

$k_2 = 4.50 \times 10^{-3}$ L mol^{-1} s^{-1}

2-Br and piperidine (**11**) in acetonitrile at 20 °C. Kinetics have been corrected due to ion pairing.

$[\mathbf{2\text{-}Br}]_0$ (mol L^{-1})	**[11]** (mol L^{-1})	k_{obs} (s^{-1})
1.00×10^{-3}	1.00×10^{-1}	1.09×10^{-3}
1.00×10^{-3}	2.00×10^{-1}	2.15×10^{-3}
1.00×10^{-3}	3.00×10^{-1}	3.26×10^{-3}
1.00×10^{-3}	4.00×10^{-1}	4.39×10^{-3}

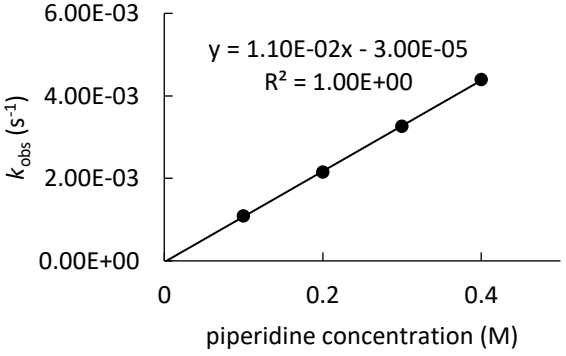

$k_2 = 1.10 \times 10^{-2}$ L mol^{-1} s^{-1}

2-Br and NEt_3 in 50AN50M at 20 °C.

[2-Br]$_0$ (mol L^{-1})	[NEt_3] (mol L^{-1})	k_{obs} (s^{-1})
1.00×10^{-3}	2.00×10^{-2}	1.00×10^{-3}
1.00×10^{-3}	4.00×10^{-2}	1.03×10^{-3}
1.00×10^{-3}	6.00×10^{-2}	9.59×10^{-4}
1.00×10^{-3}	8.00×10^{-2}	9.36×10^{-4}

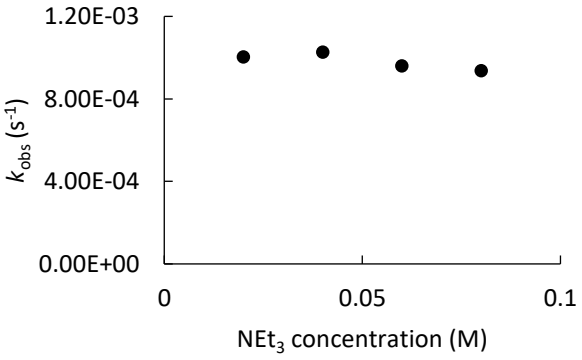

$k_1 = 1.03 \times 10^{-3}$ s^{-1}

2-Br and NEt_3 in 60AN40M at 20 °C.

[2-Br]$_0$ (mol L^{-1})	[NEt_3] (mol L^{-1})	k_{obs} (s^{-1})
1.00×10^{-3}	2.00×10^{-2}	7.28×10^{-4}
1.00×10^{-3}	4.00×10^{-2}	6.90×10^{-4}
1.00×10^{-3}	6.00×10^{-2}	7.09×10^{-4}

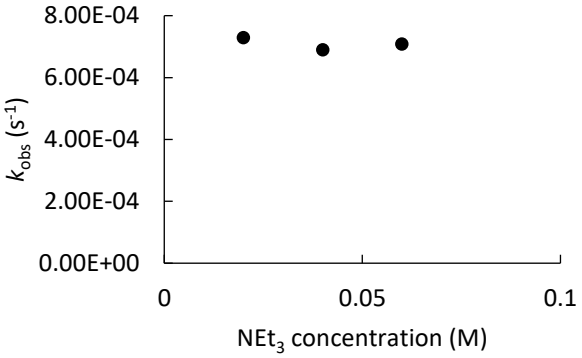

$k_1 = 7.29 \times 10^{-4}$ s^{-1}

2-Br and NEt_3 in 70AN30M at 20 °C.

[2-Br]$_0$ (mol L^{-1})	[NEt_3] (mol L^{-1})	k_{obs} (s^{-1})
1.00×10^{-3}	2.00×10^{-2}	4.50×10^{-4}
1.00×10^{-3}	4.00×10^{-2}	4.47×10^{-4}
1.00×10^{-3}	6.00×10^{-2}	4.42×10^{-4}
1.00×10^{-3}	8.00×10^{-2}	4.26×10^{-4}

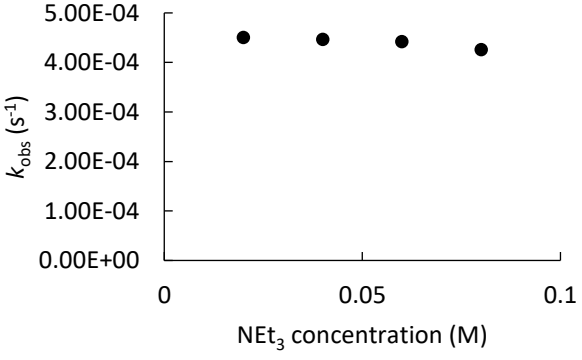

$k_1 = 4.50 \times 10^{-4}$ s^{-1}

2-Br and NEt_3 in 80AN20M at 20 °C.

[2-Br]$_0$ (mol L^{-1})	[NEt_3] (mol L^{-1})	k_{obs} (s^{-1})
1.00×10^{-3}	2.00×10^{-2}	2.15×10^{-4}
1.00×10^{-3}	4.00×10^{-2}	2.12×10^{-4}
1.00×10^{-3}	6.00×10^{-2}	2.14×10^{-4}
1.00×10^{-3}	8.00×10^{-2}	2.16×10^{-4}

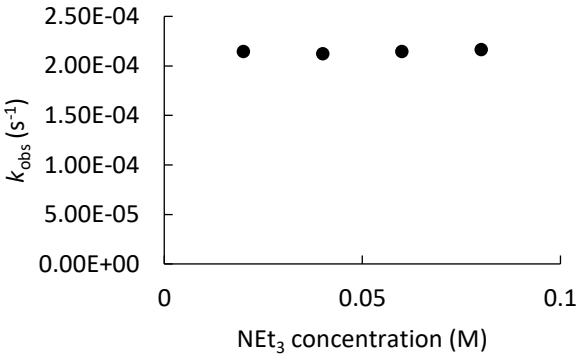

$k_1 = 2.16 \times 10^{-4}$ s^{-1}

2-Br and NEt_3 in 90AN10M at 20 °C.

[2-Br]$_0$ (mol L^{-1})	[NEt_3] (mol L^{-1})	k_{obs} (s^{-1})
1.00×10^{-3}	2.00×10^{-2}	6.88×10^{-5}
1.00×10^{-3}	4.00×10^{-2}	6.53×10^{-5}

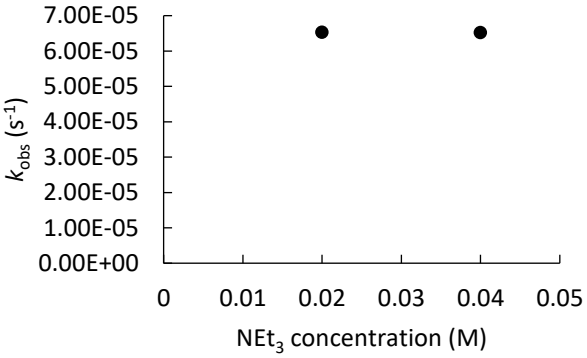

$k_1 = 6.53 \times 10^{-5}$ s^{-1}

2-Br and NEt_3 in acetonitrile at 20 °C.

[2-Br]$_0$ (mol L^{-1})	[NEt_3] (mol L^{-1})	k_{obs} (s^{-1})
1.00×10^{-3}	8.00×10^{-2}	4.83×10^{-6}

$k_1 = 4.83 \times 10^{-6}$ s^{-1}

2-Br and piperidine (**11**) in 80AN20M at 10 °C.

[2-Br]$_0$ (mol L^{-1})	**[11]** (mol L^{-1})	k_{obs} (s^{-1})
1.00×10^{-3}	1.00×10^{-1}	1.94×10^{-4}
1.00×10^{-3}	2.00×10^{-1}	3.12×10^{-4}
1.00×10^{-3}	3.00×10^{-1}	4.23×10^{-4}
1.00×10^{-3}	4.00×10^{-1}	5.42×10^{-4}

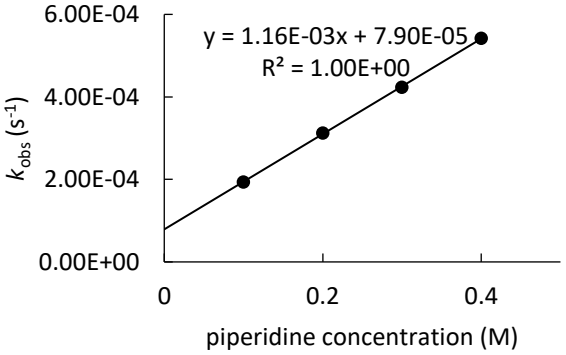

$k_2 = 1.16 \times 10^{-3}$ L mol^{-1} s^{-1} $k_1 = 7.90 \times 10^{-5}$ s^{-1}

2-Br and piperidine (**11**) in 80AN20M at 30 °C.

[2-Br]$_0$ (mol L^{-1})	**[11]** (mol L^{-1})	k_{obs} (s^{-1})
1.00×10^{-3}	1.00×10^{-1}	1.18×10^{-3}
1.00×10^{-3}	2.00×10^{-1}	1.79×10^{-3}
1.00×10^{-3}	3.00×10^{-1}	2.36×10^{-3}
1.00×10^{-3}	4.00×10^{-1}	2.97×10^{-3}

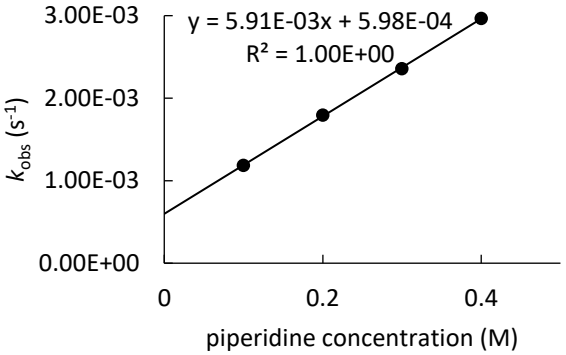

$k_2 = 5.91 \times 10^{-3}$ L mol^{-1} s^{-1} $k_1 = 5.98 \times 10^{-4}$ s^{-1}

2-Br and piperidine (**11**) in 80AN20M at 40 °C.

[2-Br]$_0$ (mol L^{-1})	**[11]** (mol L^{-1})	k_{obs} (s^{-1})
1.00×10^{-3}	1.00×10^{-1}	2.73×10^{-3}
1.00×10^{-3}	2.00×10^{-1}	3.99×10^{-3}
1.00×10^{-3}	3.00×10^{-1}	5.17×10^{-3}
1.00×10^{-3}	4.00×10^{-1}	6.30×10^{-3}

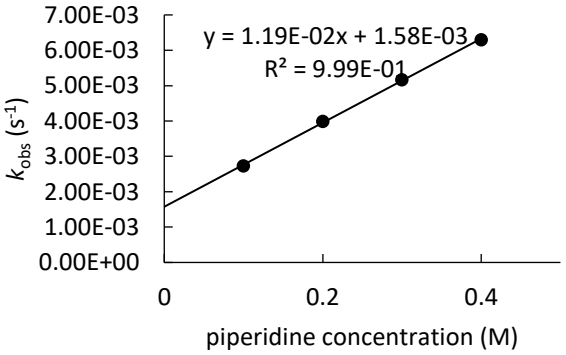

$k_2 = 1.19 \times 10^{-2}$ L mol^{-1} s^{-1} $k_1 = 1.58 \times 10^{-3}$ s^{-1}

2-Br and piperidine (**11**) in 80AN20M at 50 °C.

[2-Br]$_0$ (mol L^{-1})	**[11]** (mol L^{-1})	k_{obs} (s^{-1})
1.00×10^{-3}	1.00×10^{-1}	5.81×10^{-3}
1.00×10^{-3}	2.00×10^{-1}	8.04×10^{-3}
1.00×10^{-3}	3.00×10^{-1}	1.03×10^{-2}
1.00×10^{-3}	4.00×10^{-1}	1.26×10^{-2}

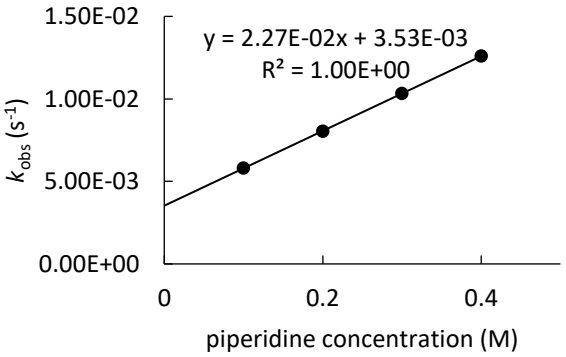

$k_2 = 2.27 \times 10^{-2}$ L mol^{-1} s^{-1} $k_1 = 3.53 \times 10^{-3}$ s^{-1}

Kinetics of reactions of 2-Cl: 1-(1-chloroethyl)-4-methylbenzene

2-Cl and DABCO (**9**) in 80AN20M at 20 °C.

[2-Cl]$_0$ (mol L^{-1})	**[9]** (mol L^{-1})	k_{obs} (s^{-1})
1.00×10^{-3}	1.25×10^{-1}	1.98×10^{-5}
1.00×10^{-3}	2.50×10^{-1}	3.79×10^{-5}
1.00×10^{-3}	3.75×10^{-1}	5.56×10^{-5}
1.00×10^{-3}	5.00×10^{-1}	7.18×10^{-5}

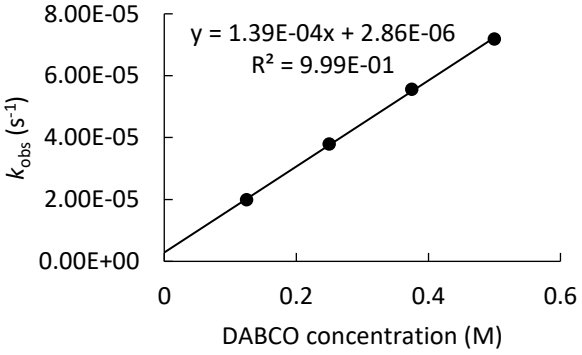

$k_2 = 1.39 \times 10^{-4}$ L mol^{-1} s^{-1}

2-Cl and pyrrolidine (**10**) in 80AN20M at 20 °C.

[2-Cl]$_0$ (mol L^{-1})	**[10]** (mol L^{-1})	k_{obs} (s^{-1})
1.00×10^{-3}	4.00×10^{-1}	1.22×10^{-5}
1.00×10^{-3}	8.00×10^{-1}	2.10×10^{-5}
1.00×10^{-3}	1.20×10^{0}	3.00×10^{-5}
1.00×10^{-3}	1.60×10^{0}	4.08×10^{-5}

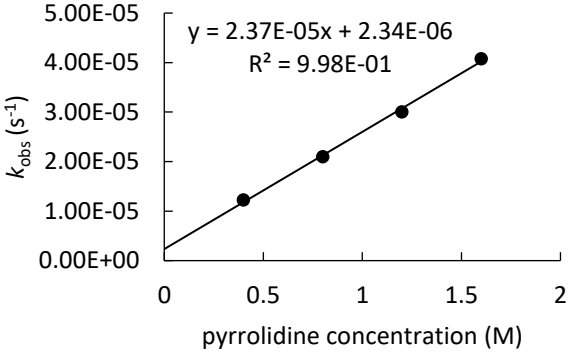

$k_2 = 2.37 \times 10^{-5}$ L mol^{-1} s^{-1}

2-Cl and piperidine (**11**) in 80AN20M at 20 °C.

[2-Cl]$_0$ (mol L^{-1})	**[11]** (mol L^{-1})	k_{obs} (s^{-1})
1.00×10^{-3}	4.00×10^{-1}	1.13×10^{-5}
1.00×10^{-3}	8.00×10^{-1}	1.76×10^{-5}
1.00×10^{-3}	1.20×10^{0}	2.38×10^{-5}
1.00×10^{-3}	1.60×10^{0}	2.93×10^{-5}

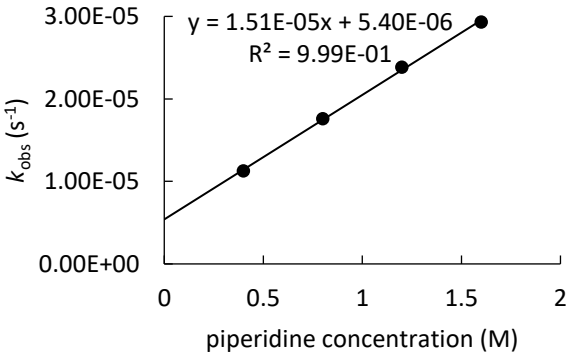

$k_2 = 1.51 \times 10^{-5}$ L mol^{-1} s^{-1}

2-Cl and morpholine (**12**) in 80AN20M at 20 °C.

[2-Cl]$_0$ (mol L^{-1})	**[12]** (mol L^{-1})	k_{obs} (s^{-1})
1.00×10^{-3}	4.00×10^{-1}	8.85×10^{-6}
1.00×10^{-3}	8.00×10^{-1}	1.34×10^{-5}
1.00×10^{-3}	1.20×10^{0}	1.78×10^{-5}
1.00×10^{-3}	1.60×10^{0}	2.25×10^{-5}

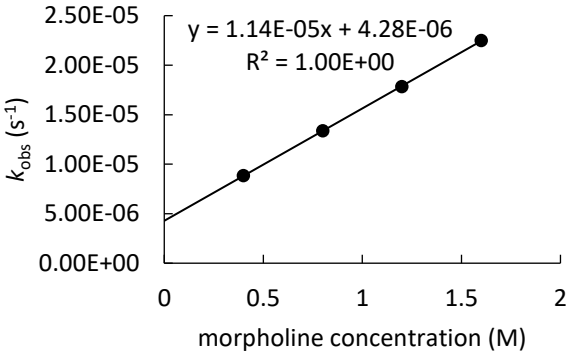

$k_2 = 1.14 \times 10^{-5}$ L mol^{-1} s^{-1} $k_1 = 4.28 \times 10^{-6}$ s^{-1}

Kinetics of reactions of 3-Br: 5-(1-bromoethyl)-2,3-dihydro-1*H*-indene

3-Br and DABCO (**9**) in acetonitrile at 20 °C.

[3-Br]$_0$ (mol L^{-1})	**[9]** (mol L^{-1})	k_{obs} (s^{-1})
1.00×10^{-3}	2.00×10^{-2}	2.19×10^{-3}
1.00×10^{-3}	4.00×10^{-2}	4.28×10^{-3}
1.00×10^{-3}	6.00×10^{-2}	6.47×10^{-3}
1.00×10^{-3}	8.00×10^{-2}	8.75×10^{-3}

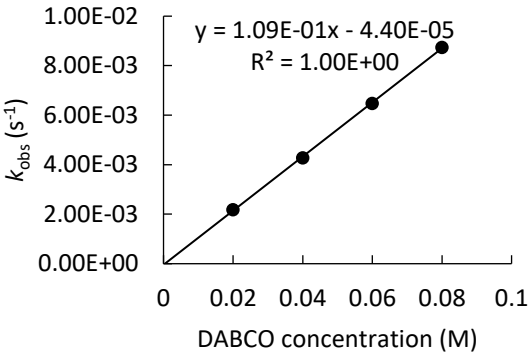

$k_2 = 1.09 \times 10^{-1}$ L mol^{-1} s^{-1}

3-Br and pyrrolidine (**10**) in acetonitrile at 20 °C. Kinetics have been corrected due to ion pairing.

$[\mathbf{3\text{-}Br}]_0$ (mol L^{-1})	**[10]** (mol L^{-1})	k_{obs} (s^{-1})
1.00×10^{-3}	1.00×10^{-1}	2.21×10^{-3}
1.00×10^{-3}	2.00×10^{-1}	4.48×10^{-3}
1.00×10^{-3}	3.00×10^{-1}	6.44×10^{-3}
1.00×10^{-3}	4.00×10^{-1}	8.42×10^{-3}

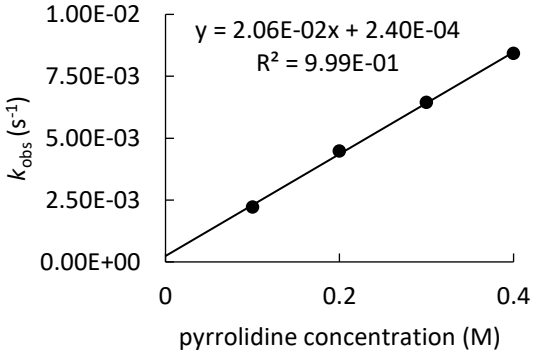

$k_2 = 2.06 \times 10^{-2}$ L mol^{-1} s^{-1}

3-Br and piperidine (**11**) in acetonitrile at 20 °C. Kinetics have been corrected due to ion pairing.

$[\mathbf{3\text{-}Br}]_0$ (mol L^{-1})	**[11]** (mol L^{-1})	k_{obs} (s^{-1})
1.00×10^{-3}	1.00×10^{-1}	1.43×10^{-3}
1.00×10^{-3}	2.00×10^{-1}	2.72×10^{-3}
1.00×10^{-3}	3.00×10^{-1}	4.03×10^{-3}

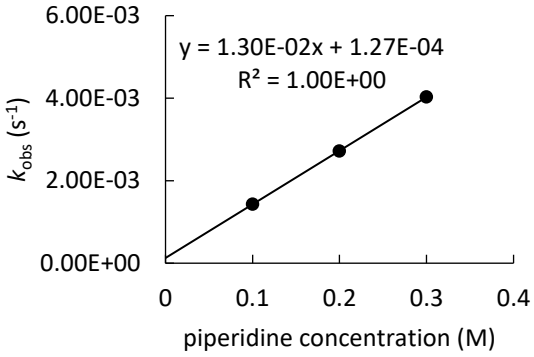

$k_2 = 1.30 \times 10^{-2}$ L mol^{-1} s^{-1}

3-Br and morpholine (**12**) in acetonitrile at 20 °C. Kinetics have been corrected due to ion pairing.

$[\mathbf{3\text{-}Br}]_0$ (mol L^{-1})	**[12]** (mol L^{-1})	k_{obs} (s^{-1})
1.00×10^{-3}	1.00×10^{-1}	3.59×10^{-4}
1.00×10^{-3}	2.00×10^{-1}	7.73×10^{-4}
1.00×10^{-3}	3.00×10^{-1}	1.14×10^{-3}
1.00×10^{-3}	4.00×10^{-1}	1.55×10^{-3}

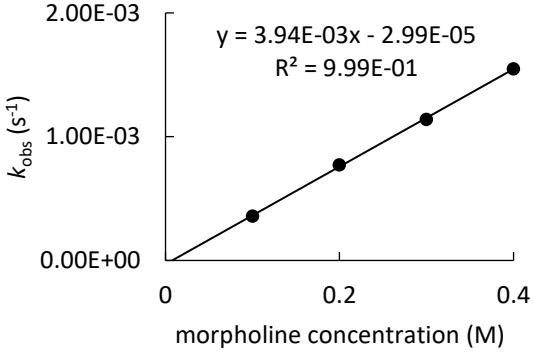

$k_2 = 3.94 \times 10^{-3}$ L mol^{-1} s^{-1}

3-Br and propylamine (**13**) in acetonitrile at 20 °C. Kinetics have been corrected due to ion pairing.

[3-Br]$_0$ (mol L^{-1})	**[13]** (mol L^{-1})	k_{obs} (s^{-1})
1.00×10^{-3}	5.00×10^{-1}	5.69×10^{-4}
1.00×10^{-3}	1.00×10^{0}	1.06×10^{-3}
1.00×10^{-3}	1.50×10^{0}	1.52×10^{-3}
1.00×10^{-3}	2.00×10^{0}	1.93×10^{-3}

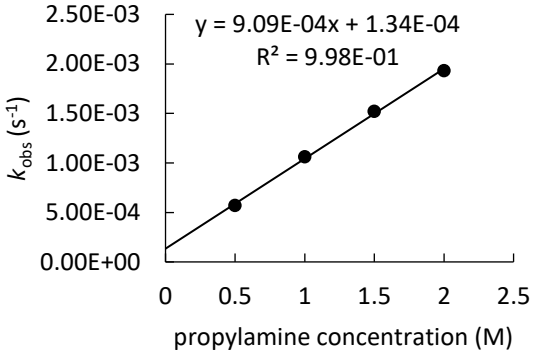

$k_2 = 9.09 \times 10^{-4}$ L mol^{-1} s^{-1}

3-Br and NEt_3 in acetonitrile at 20 °C.

[3-Br]$_0$ (mol L^{-1})	**[NEt_3]** (mol L^{-1})	k_{obs} (s^{-1})
1.00×10^{-3}	4.00×10^{-2}	2.11×10^{-5}

$k_1 = 2.11 \times 10^{-5}$ s^{-1}

Kinetics of reactions of 4-Br: 1-(1-bromoethyl)-4-methoxybenzene

4-Br and DABCO (**9**) in acetonitrile at 20 °C. SF measurement on HT.

[4-Br]$_0$ (mol L^{-1})	**[9]** (mol L^{-1})	k_{obs} (s^{-1})
1.00×10^{-3}	5.00×10^{-2}	2.29×10^{-2}
1.00×10^{-3}	1.00×10^{-1}	4.12×10^{-2}
1.00×10^{-3}	1.50×10^{-1}	6.50×10^{-2}
1.00×10^{-3}	2.00×10^{-1}	8.83×10^{-2}

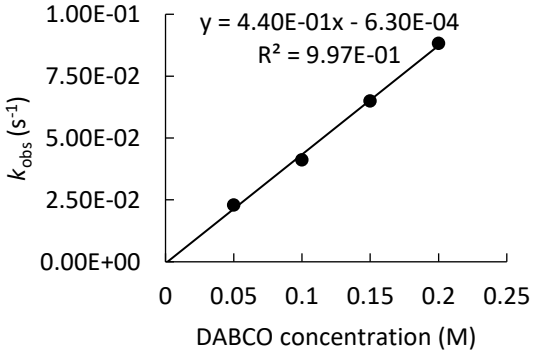

$k_2 = 4.40 \times 10^{-1}$ L mol^{-1} s^{-1}

4-Br and pyrrolidine (**10**) in acetonitrile at 20 °C. SF measurement on HT. Kinetics have been corrected due to ion pairing.

[4-Br]$_0$ (mol L^{-1})	**[10]** (mol L^{-1})	k_{obs} (s^{-1})
1.00×10^{-3}	5.00×10^{-2}	6.22×10^{-3}
1.00×10^{-3}	1.00×10^{-1}	8.48×10^{-3}
1.00×10^{-3}	1.50×10^{-1}	1.15×10^{-2}
1.00×10^{-3}	2.00×10^{-1}	1.48×10^{-2}

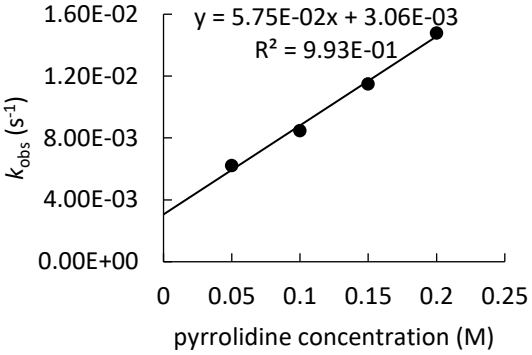

$k_2 = 5.75 \times 10^{-2}$ L mol^{-1} s^{-1}

4-Br and piperidine (**11**) in acetonitrile at 20 °C. SF measurement on HT. Kinetics have been corrected due to ion pairing.

[4-Br]$_0$ (mol L^{-1})	**[11]** (mol L^{-1})	k_{obs} (s^{-1})
1.00×10^{-3}	5.00×10^{-2}	9.02×10^{-3}
1.00×10^{-3}	1.00×10^{-1}	1.09×10^{-2}
1.00×10^{-3}	1.50×10^{-1}	1.34×10^{-2}
1.00×10^{-3}	2.00×10^{-1}	1.67×10^{-2}

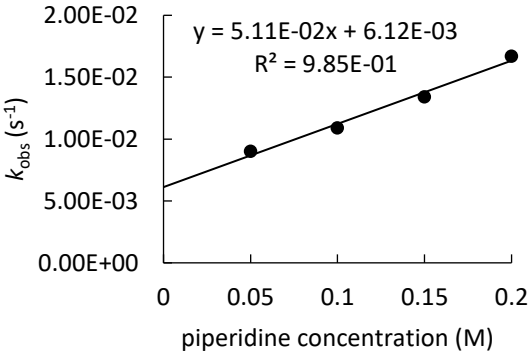

$k_2 = 5.11 \times 10^{-2}$ L mol^{-1} s^{-1}

4-Br and morpholine (**12**) in acetonitrile at 20 °C. SF measurement on HT. Kinetics have been corrected due to ion pairing.

[4-Br]$_0$ (mol L^{-1})	**[12]** (mol L^{-1})	k_{obs} (s^{-1})
1.00×10^{-3}	5.00×10^{-2}	4.47×10^{-3}
1.00×10^{-3}	1.00×10^{-1}	5.48×10^{-3}
1.00×10^{-3}	1.50×10^{-1}	6.48×10^{-3}
1.00×10^{-3}	2.00×10^{-1}	7.35×10^{-3}

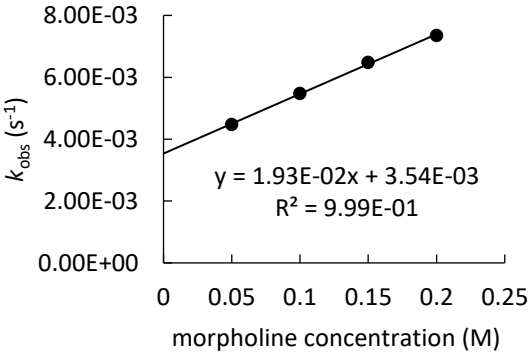

$k_2 = 1.93 \times 10^{-2}$ L mol^{-1} s^{-1}

4-Br and propylamine (**13**) in acetonitrile at 20 °C. SF measurement on HT. Kinetics have been corrected due to ion pairing.

[4-Br]$_0$ (mol L^{-1})	**[13]** (mol L^{-1})	k_{obs} (s^{-1})
1.00×10^{-3}	2.50×10^{-1}	5.55×10^{-3}
1.00×10^{-3}	5.00×10^{-1}	7.41×10^{-3}
1.00×10^{-3}	7.50×10^{-1}	9.17×10^{-3}
1.00×10^{-3}	1.00×10^{0}	1.06×10^{-2}

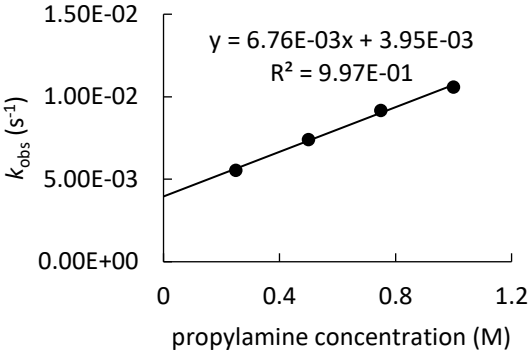

$k_2 = 6.76 \times 10^{-3}$ L mol^{-1} s^{-1} $k_1 = 3.95 \times 10^{-3}$ s^{-1}

Kinetics of reactions of 5-Br: 5-(1-bromoethyl)-2,3-dihydrobenzofuran

5-Br and DABCO (**9**) in 95AN5Tol at 20 °C. SF measurement on AP.

[5-Br]$_0$ (mol L^{-1})	**[9]** (mol L^{-1})	k_{obs} (s^{-1})
1.00×10^{-4}	1.00×10^{-1}	5.15×10^{-1}
1.00×10^{-4}	2.00×10^{-1}	7.17×10^{-1}
1.00×10^{-4}	3.00×10^{-1}	9.47×10^{-1}
1.00×10^{-4}	4.00×10^{-1}	1.15×10^{0}

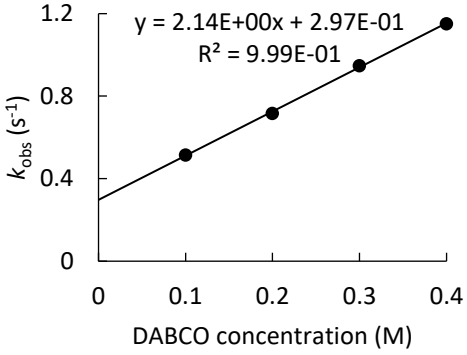

$k_2 = 2.14 \times 10^{0}$ L mol^{-1} s^{-1}

5-Br and pyrrolidine (**10**) in 95AN5Tol at 20 °C. SF measurement on AP.

[5-Br]$_0$ (mol L^{-1})	**[10]** (mol L^{-1})	k_{obs} (s^{-1})
1.00×10^{-4}	1.00×10^{-1}	3.91×10^{-1}
1.00×10^{-4}	2.00×10^{-1}	4.65×10^{-1}
1.00×10^{-4}	3.00×10^{-1}	5.42×10^{-1}
1.00×10^{-4}	4.00×10^{-1}	6.13×10^{-1}

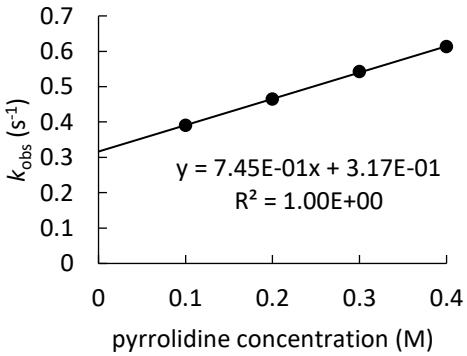

$k_2 = 7.45 \times 10^{-1}$ L mol^{-1} s^{-1}

5-Br and piperidine (**11**) in 95AN5Tol at 20 °C. SF measurement on AP.

$[\mathbf{5\text{-}Br}]_0$ (mol L^{-1})	**[11]** (mol L^{-1})	k_{obs} (s^{-1})
1.00×10^{-4}	1.00×10^{-1}	3.16×10^{-1}
1.00×10^{-4}	2.00×10^{-1}	3.65×10^{-1}
1.00×10^{-4}	3.00×10^{-1}	4.14×10^{-1}
1.00×10^{-4}	4.00×10^{-1}	4.55×10^{-1}

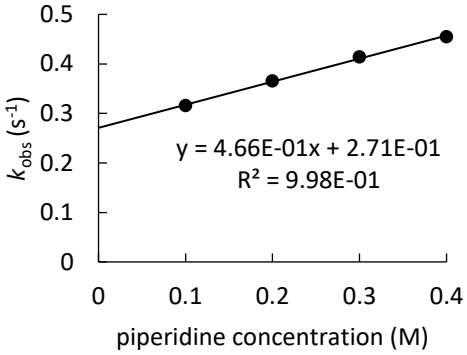

$k_2 = 4.66 \times 10^{-1}$ L mol^{-1} s^{-1} $k_1 = 2.71 \times 10^{-3}$ s^{-1}

Kinetics of reactions of 6-Br: benzhydryl bromide

6-Br and DABCO (**9**) in acetonitrile at 20 °C.

$[\mathbf{6\text{-}Br}]_0$ (mol L^{-1})	**[9]** (mol L^{-1})	k_{obs} (s^{-1})
1.00×10^{-3}	5.00×10^{-2}	1.36×10^{-3}
1.00×10^{-3}	1.00×10^{-1}	2.65×10^{-3}
1.00×10^{-3}	1.50×10^{-1}	3.89×10^{-3}
1.00×10^{-3}	2.00×10^{-1}	5.16×10^{-3}

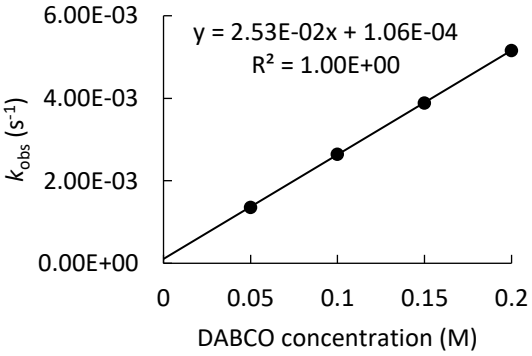

$k_2 = 2.53 \times 10^{-2}$ L mol^{-1} s^{-1}

6-Br and pyrrolidine (**10**) in acetonitrile at 20 °C. Kinetics have been corrected due to ion pairing.

$[\mathbf{6\text{-}Br}]_0$ (mol L^{-1})	**[10]** (mol L^{-1})	k_{obs} (s^{-1})
1.00×10^{-3}	5.00×10^{-2}	3.88×10^{-4}
1.00×10^{-3}	1.00×10^{-1}	7.69×10^{-4}
1.00×10^{-3}	1.50×10^{-1}	1.14×10^{-3}
1.00×10^{-3}	2.00×10^{-1}	1.52×10^{-3}

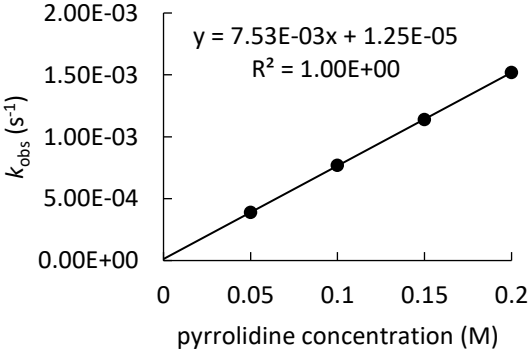

$k_2 = 7.53 \times 10^{-3}$ L mol^{-1} s^{-1}

6-Br and piperidine (**11**) in acetonitrile at 20 °C. Kinetics have been corrected due to ion pairing.

$[\mathbf{6\text{-}Br}]_0$ (mol L^{-1})	**[11]** (mol L^{-1})	k_{obs} (s^{-1})
1.00×10^{-3}	5.00×10^{-2}	2.75×10^{-4}
1.00×10^{-3}	1.00×10^{-1}	5.52×10^{-3}
1.00×10^{-3}	1.50×10^{-1}	8.00×10^{-3}
1.00×10^{-3}	2.00×10^{-1}	1.05×10^{-3}

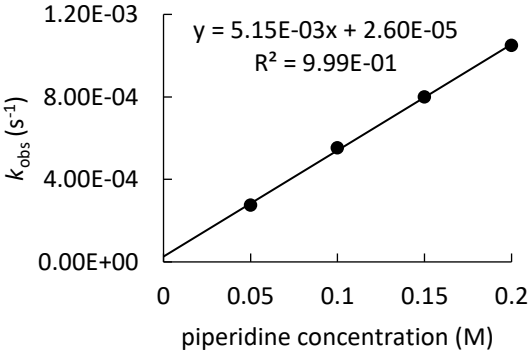

$k_2 = 5.15 \times 10^{-3}$ L mol^{-1} s^{-1}

6-Br and morpholine (**12**) in acetonitrile at 20 °C. Kinetics have been corrected due to ion pairing.

$[\mathbf{6\text{-}Br}]_0$ (mol L^{-1})	**[12]** (mol L^{-1})	k_{obs} (s^{-1})
1.00×10^{-3}	1.00×10^{-1}	1.27×10^{-4}
1.00×10^{-3}	2.00×10^{-1}	2.98×10^{-4}
1.00×10^{-3}	3.00×10^{-1}	4.16×10^{-4}
1.00×10^{-3}	4.00×10^{-1}	5.85×10^{-3}

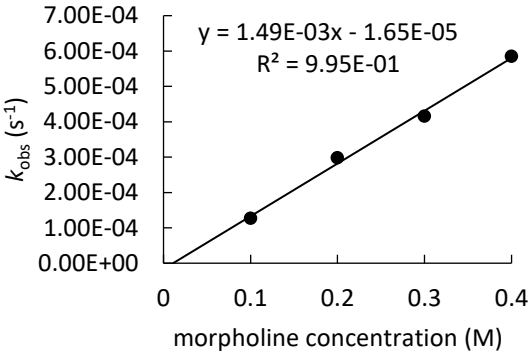

$k_2 = 1.49 \times 10^{-3}$ L mol^{-1} s^{-1}

6-Br and propylamine (**13**) in acetonitrile at 20 °C. Kinetics have been corrected due to ion pairing.

$[\mathbf{6\text{-}Br}]_0$ (mol L^{-1})	**[13]** (mol L^{-1})	k_{obs} (s^{-1})
1.00×10^{-3}	2.00×10^{-1}	8.45×10^{-5}
1.00×10^{-3}	4.00×10^{-1}	1.60×10^{-4}
1.00×10^{-3}	6.00×10^{-1}	2.31×10^{-4}
1.00×10^{-3}	8.00×10^{-1}	2.96×10^{-4}

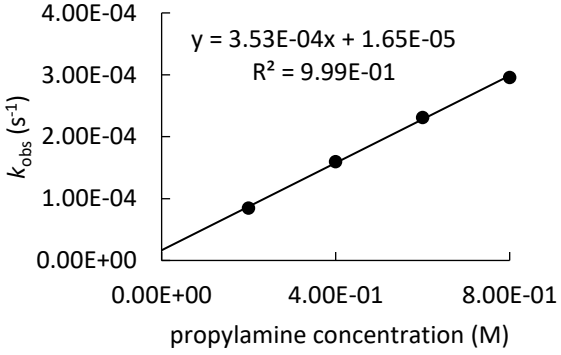

$k_2 = 3.53 \times 10^{-4}$ L mol^{-1} s^{-1}

6-Br and NEt_3 in acetonitrile at 20 °C. With 0.025 M MeOH to suppress reverse reaction.

[6-Br]$_0$ (mol L^{-1})	[NEt_3] (mol L^{-1})	k_{obs} (s^{-1})
1.00×10^{-3}	2.50×10^{-2}	6.92×10^{-6}

$k_1 = 6.92 \times 10^{-6}$ s^{-1}

Kinetics of reactions of 7-Br: 4,4'-dimethylbenzhydryl bromide

7-Br and DABCO (**9**) in acetonitrile at 20 °C.

[7-Br]$_0$ (mol L^{-1})	**[9]** (mol L^{-1})	k_{obs} (s^{-1})
1.00×10^{-3}	4.00×10^{-2}	2.12×10^{-2}
1.00×10^{-3}	8.00×10^{-2}	3.86×10^{-2}
1.00×10^{-3}	1.20×10^{-1}	5.41×10^{-2}
1.00×10^{-3}	1.60×10^{-1}	7.01×10^{-2}

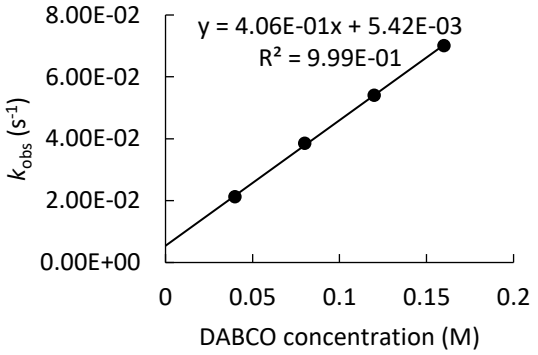

$k_2 = 4.06 \times 10^{-1}$ L mol^{-1} s^{-1}

7-Br and pyrrolidine (**10**) in acetonitrile at 20 °C. Kinetics have been corrected due to ion pairing.

[7-Br]$_0$ (mol L^{-1})	**[10]** (mol L^{-1})	k_{obs} (s^{-1})
1.00×10^{-3}	5.00×10^{-2}	8.54×10^{-3}
1.00×10^{-3}	1.00×10^{-1}	1.30×10^{-2}
1.00×10^{-3}	1.50×10^{-1}	1.75×10^{-2}
1.00×10^{-3}	2.00×10^{-1}	2.30×10^{-2}

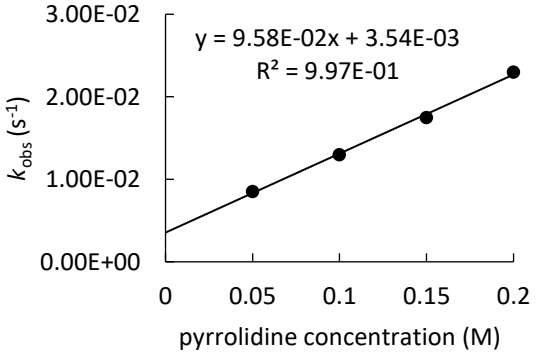

$k_2 = 9.58 \times 10^{-2}$ L mol^{-1} s^{-1}

7-Br and piperidine (**11**) in acetonitrile at 20 °C. Kinetics have been corrected due to ion pairing.

$[\mathbf{7\text{-}Br}]_0$ (mol L^{-1})	**[11]** (mol L^{-1})	k_{obs} (s^{-1})
1.00×10^{-3}	5.00×10^{-2}	7.11×10^{-3}
1.00×10^{-3}	1.00×10^{-1}	1.06×10^{-2}
1.00×10^{-3}	1.50×10^{-1}	1.36×10^{-2}
1.00×10^{-3}	2.00×10^{-1}	1.62×10^{-2}

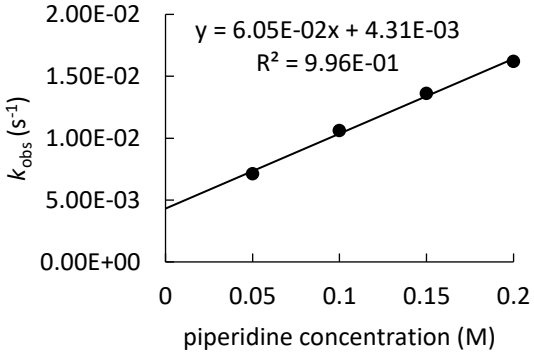

$k_2 = 6.05 \times 10^{-2}$ L mol^{-1} s^{-1} $k_1 = 4.31 \times 10^{-3}$ s^{-1}

7-Br and morpholine (**12**) in acetonitrile at 20 °C. Kinetics have been corrected due to ion pairing.

$[\mathbf{7\text{-}Br}]_0$ (mol L^{-1})	**[12]** (mol L^{-1})	k_{obs} (s^{-1})
1.00×10^{-3}	1.00×10^{-1}	7.73×10^{-3}
1.00×10^{-3}	2.00×10^{-1}	1.19×10^{-2}
1.00×10^{-3}	3.00×10^{-1}	1.52×10^{-2}
1.00×10^{-3}	4.00×10^{-1}	1.83×10^{-2}

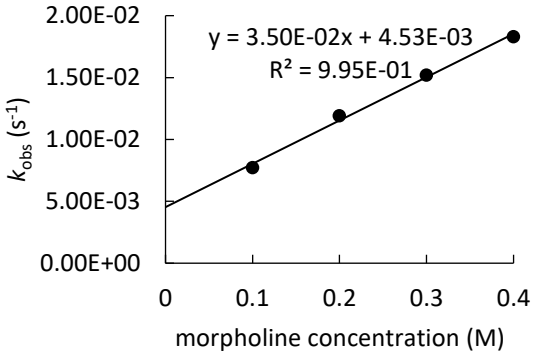

$k_2 = 3.50 \times 10^{-2}$ L mol^{-1} s^{-1}

7-Br and propylamine (**13**) in acetonitrile at 20 °C. Kinetics have been corrected due to ion pairing.

$[\mathbf{7\text{-}Br}]_0$ (mol L^{-1})	**[13]** (mol L^{-1})	k_{obs} (s^{-1})
1.00×10^{-3}	3.00×10^{-1}	1.04×10^{-2}
1.00×10^{-3}	6.00×10^{-1}	1.51×10^{-2}
1.00×10^{-3}	9.00×10^{-1}	1.88×10^{-2}
1.00×10^{-3}	1.20×10^{0}	2.17×10^{-2}

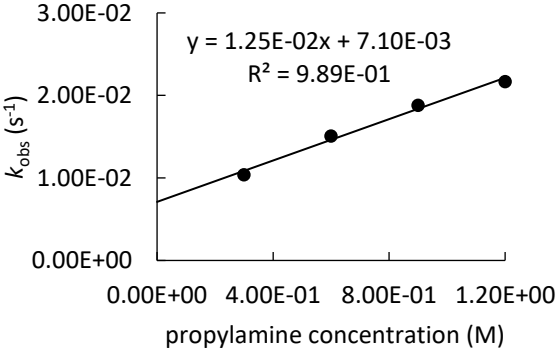

$k_2 = 1.25 \times 10^{-2}$ L mol^{-1} s^{-1}

Kinetics of the reactions of 8-Br: (E)-5,5'-(3-bromoprop-1-ene-1,3-diyl)bis(1,3-difluorobenzene)

8-Br and pyrrolidine (**10**) in 90AN10M at 20 °C. SF measurement on HT.

[8-Br]$_0$ (mol L^{-1})	**[10]** (mol L^{-1})	k_{obs} (s^{-1})
1.00×10^{-3}	1.00×10^{-1}	1.78×10^{-2}
1.00×10^{-3}	2.00×10^{-1}	3.00×10^{-2}
1.00×10^{-3}	3.00×10^{-1}	4.34×10^{-2}
1.00×10^{-3}	4.00×10^{-1}	5.98×10^{-2}

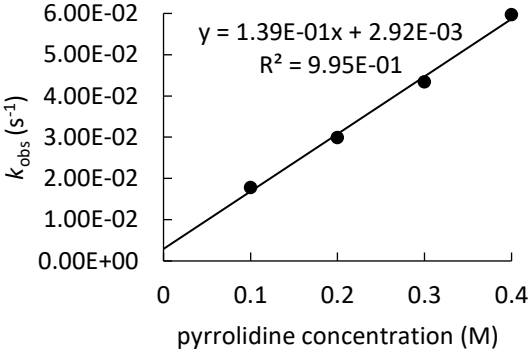

$k_2 = 1.39 \times 10^{-1}$ L mol^{-1} s^{-1}

8-Br and piperidine (**11**) in 90AN10M at 20 °C.

[8-Br]$_0$ (mol L^{-1})	**[11]** (mol L^{-1})	k_{obs} (s^{-1})
1.00×10^{-3}	1.00×10^{-1}	1.63×10^{-2}
1.00×10^{-3}	2.00×10^{-1}	3.08×10^{-2}
1.00×10^{-3}	3.00×10^{-1}	4.61×10^{-2}
1.00×10^{-3}	4.00×10^{-1}	6.24×10^{-2}

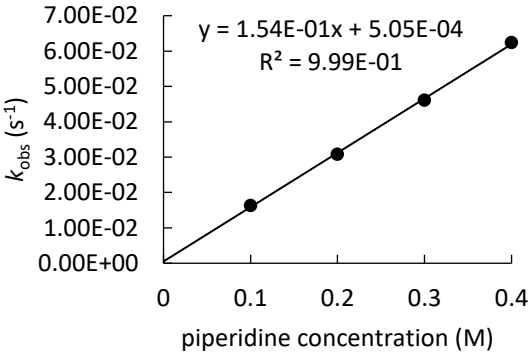

$k_2 = 1.54 \times 10^{-1}$ L mol^{-1} s^{-1}

8-Br and morpholine (**12**) in 90AN10M at 20 °C. SF measurement on HT.

[8-Br]$_0$ (mol L^{-1})	**[12]** (mol L^{-1})	k_{obs} (s^{-1})
1.00×10^{-3}	1.00×10^{-1}	8.02×10^{-3}
1.00×10^{-3}	2.00×10^{-1}	1.31×10^{-2}
1.00×10^{-3}	3.00×10^{-1}	1.84×10^{-2}
1.00×10^{-3}	4.00×10^{-1}	2.36×10^{-2}

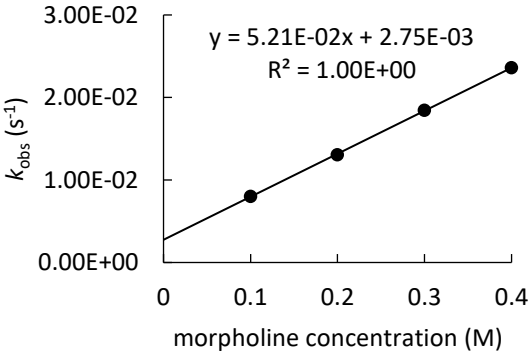

$k_2 = 5.21 \times 10^{-2}$ L mol^{-1} s^{-1}

8-Br and propylamine (**13**) in 90AN10M at 20 °C. SF measurement on HT.

[8-Br]$_0$ (mol L^{-1})	**[13]** (mol L^{-1})	k_{obs} (s^{-1})
1.00×10^{-3}	1.00×10^{-1}	4.21×10^{-3}
1.00×10^{-3}	2.00×10^{-1}	4.85×10^{-3}
1.00×10^{-3}	3.00×10^{-1}	5.53×10^{-3}
1.00×10^{-3}	4.00×10^{-1}	6.30×10^{-3}

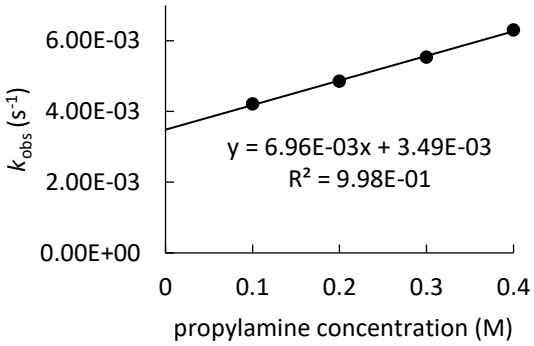

$k_2 = 6.96 \times 10^{-3}$ L mol^{-1} s^{-1}

8-Br and NEt_3 in 90AN10M at 20 °C.

[8-Br]$_0$ (mol L^{-1})	**[NEt$_3$]** (mol L^{-1})	k_{obs} (s^{-1})
1.00×10^{-3}	1.00×10^{-1}	3.29×10^{-3}
1.00×10^{-3}	2.00×10^{-1}	3.26×10^{-3}
1.00×10^{-3}	4.00×10^{-1}	2.88×10^{-3}

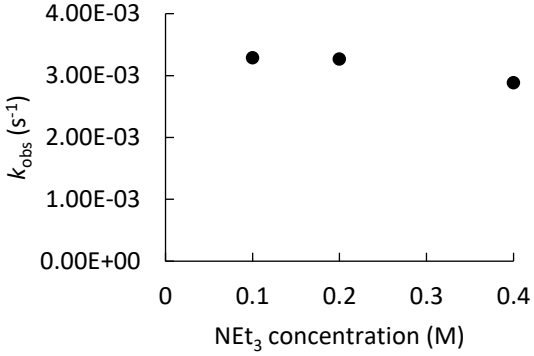

$k_1 = 3.29 \times 10^{-3}$ s^{-1}

8-Br and pyrrolidine (**10**) in 91M9AN at 20 °C.

[8-Br]$_0$ (mol L^{-1})	**[10]** (mol L^{-1})	k_{obs} (s^{-1})
1.00×10^{-3}	1.00×10^{-1}	5.79×10^{-2}
1.00×10^{-3}	2.00×10^{-1}	6.90×10^{-2}
1.00×10^{-3}	3.00×10^{-1}	5.72×10^{-2}
1.00×10^{-3}	4.00×10^{-1}	5.87×10^{-2}

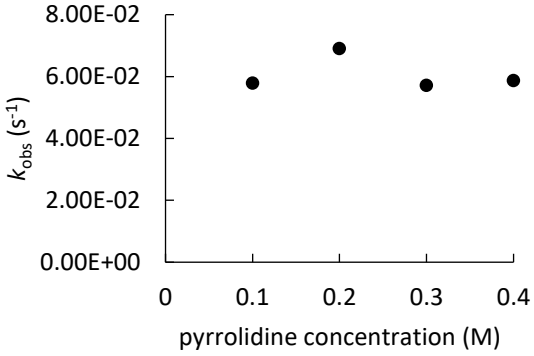

$k_1 = 6.90 \times 10^{-2}$ s^{-1}

8-Br and piperidine (**11**) in 90AN10W at 20 °C.

[8-Br]$_0$ (mol L^{-1})	**[11]** (mol L^{-1})	k_{obs} (s^{-1})
1.00×10^{-3}	1.00×10^{-1}	2.64×10^{-2}
1.00×10^{-3}	2.00×10^{-1}	4.20×10^{-2}
1.00×10^{-3}	3.00×10^{-1}	6.12×10^{-2}
1.00×10^{-3}	4.00×10^{-1}	7.93×10^{-2}

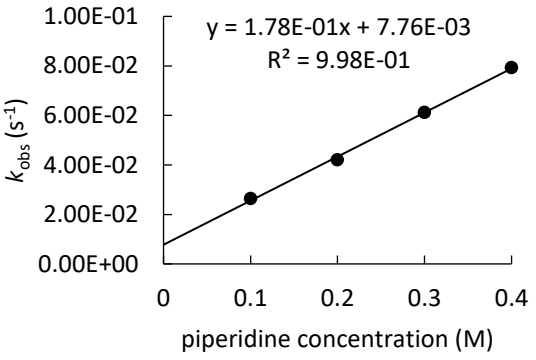

$k_2 = 1.78 \times 10^{-1}$ L mol^{-1} s^{-1}

8-Br and diethanolamine in 90AN10M at 20 °C. SF measurement on HT.

[8-Br]$_0$ mol L^{-1}	**[diethanolamine]** (mol L^{-1})	k_{obs} (s^{-1})
1.00×10^{-3}	1.00×10^{-1}	3.95×10^{-3}
1.00×10^{-3}	2.00×10^{-1}	5.07×10^{-3}
1.00×10^{-3}	3.00×10^{-1}	5.96×10^{-3}
1.00×10^{-3}	4.00×10^{-1}	7.08×10^{-3}

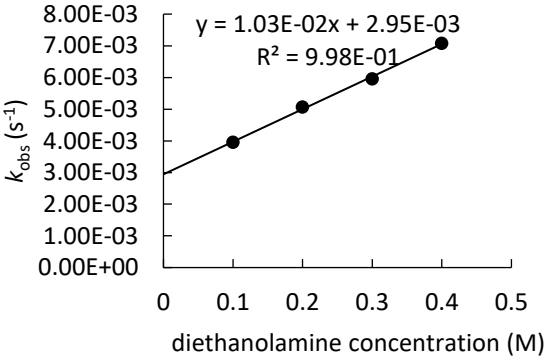

$k_2 = 1.03 \times 10^{-2}$ L mol^{-1} s^{-1}

8-Br and ethanolamine in 90AN10M at 20 °C. SF measurement on HT.

[8-Br]$_0$ (mol L^{-1})	**[ethanolamine]** (mol L^{-1})	k_{obs} (s^{-1})
1.00×10^{-3}	2.00×10^{-1}	3.65×10^{-3}
1.00×10^{-3}	4.00×10^{-1}	4.39×10^{-3}
1.00×10^{-3}	6.00×10^{-1}	4.87×10^{-3}
1.00×10^{-3}	8.00×10^{-1}	5.30×10^{-3}

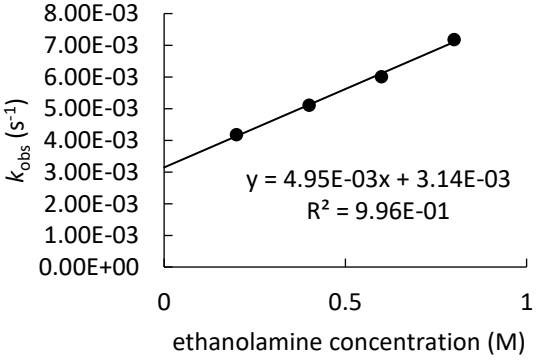

$k_2 = 4.95 \times 10^{-3}$ L mol^{-1} s^{-1}

8-Br and benzylamine in 90AN10M at 20 °C. SF measurement on HT.

[8-Br]$_0$ (mol L^{-1})	**[benzylamine]** (mol L^{-1})	k_{obs} (s^{-1})
1.00×10^{-3}	1.00×10^{-1}	4.09×10^{-3}
1.00×10^{-3}	2.00×10^{-1}	4.51×10^{-3}
1.00×10^{-3}	3.00×10^{-1}	4.85×10^{-3}
1.00×10^{-3}	4.00×10^{-1}	5.27×10^{-3}

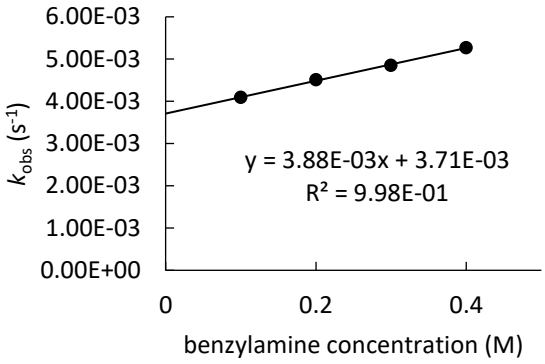

$k_2 = 3.88 \times 10^{-3}$ L mol^{-1} s^{-1}

8-Br and imidazole in 90AN10M at 20 °C. SF measurement on HT.

[8-Br]$_0$ (mol L^{-1})	**[imidazole]** (mol L^{-1})	k_{obs} (s^{-1})
1.00×10^{-3}	2.00×10^{-1}	3.65×10^{-3}
1.00×10^{-3}	4.00×10^{-1}	4.39×10^{-3}
1.00×10^{-3}	6.00×10^{-1}	4.87×10^{-3}
1.00×10^{-3}	8.00×10^{-1}	5.30×10^{-3}

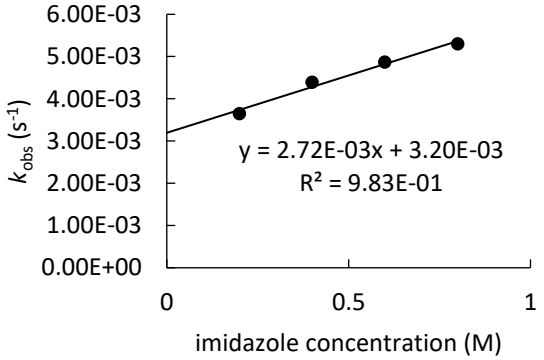

$k_2 = 2.72 \times 10^{-3}$ L mol^{-1} s^{-1}

Kinetics of reactions of 8-Cl: (E)-5,5'-(3-chloroprop-1-ene-1,3-diyl)bis(1,3-difluorobenzene)

8-Cl and pyrrolidine (**10**) in 90AN10M at 20 °C.

[8-Cl]$_0$ (mol L^{-1})	**[10]** (mol L^{-1})	k_{obs} (s^{-1})
1.00×10^{-3}	1.00×10^{-1}	1.58×10^{-4}
1.00×10^{-3}	2.00×10^{-1}	1.75×10^{-4}
1.00×10^{-3}	3.00×10^{-1}	2.03×10^{-4}
1.00×10^{-3}	4.00×10^{-1}	2.36×10^{-4}

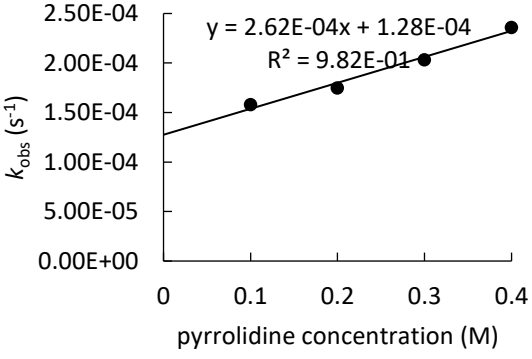

$k_2 = 2.62 \times 10^{-4}$ L mol^{-1} s^{-1}

8-Cl and piperidine (**11**) in 90AN10M at 20 °C.

[8-Cl]$_0$ (mol L^{-1})	**[11]** (mol L^{-1})	k_{obs} (s^{-1})
1.00×10^{-3}	1.00×10^{-1}	1.90×10^{-4}
1.00×10^{-3}	2.00×10^{-1}	2.20×10^{-4}
1.00×10^{-3}	3.00×10^{-1}	2.50×10^{-4}
1.00×10^{-3}	4.00×10^{-1}	2.83×10^{-4}

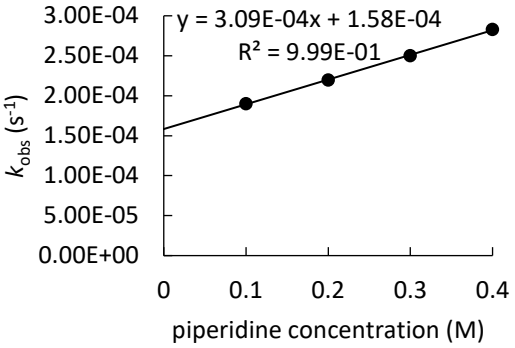

$k_2 = 3.09 \times 10^{-4}$ L mol^{-1} s^{-1}

8-Cl and morpholine (**12**) in 90AN10M at 20 °C.

[8-Cl]$_0$ (mol L^{-1})	**[12]** (mol L^{-1})	k_{obs} (s^{-1})
1.00×10^{-3}	1.00×10^{-1}	1.45×10^{-4}
1.00×10^{-3}	2.00×10^{-1}	1.81×10^{-4}
1.00×10^{-3}	3.00×10^{-1}	1.97×10^{-4}
1.00×10^{-3}	4.00×10^{-1}	2.18×10^{-4}

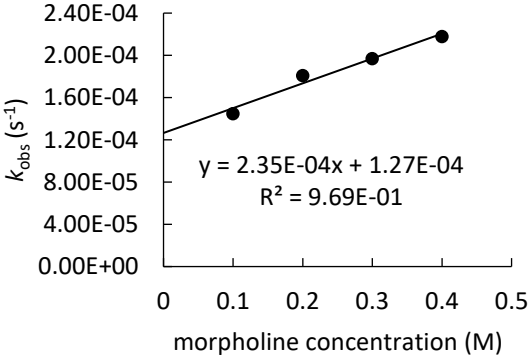

$k_2 = 2.35 \times 10^{-4}$ L mol^{-1} s^{-1}

8-Cl and diethanolamine in 90AN10M at 20 °C.

[8-Cl]$_0$ (mol L^{-1})	**[diethanolamine]** (mol L^{-1})	k_{obs} (s^{-1})
1.00×10^{-3}	1.20×10^{-1}	1.35×10^{-4}
1.00×10^{-3}	2.00×10^{-1}	1.58×10^{-4}
1.00×10^{-3}	3.00×10^{-1}	1.84×10^{-4}
1.00×10^{-3}	4.00×10^{-1}	2.12×10^{-4}

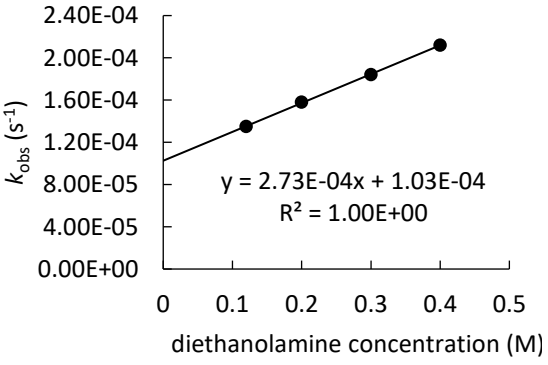

$k_2 = 2.73 \times 10^{-4}$ L mol^{-1} s^{-1}

8-Cl and ethanolamine in 90AN10M at 20 °C.

[8-Cl]$_0$ (mol L^{-1})	**[ethanolamine]** (mol L^{-1})	k_{obs} (s^{-1})
1.00×10^{-3}	1.00×10^{-1}	1.33×10^{-4}
1.00×10^{-3}	2.00×10^{-1}	1.40×10^{-4}
1.00×10^{-3}	3.00×10^{-1}	1.52×10^{-4}
1.00×10^{-3}	4.00×10^{-1}	1.57×10^{-4}

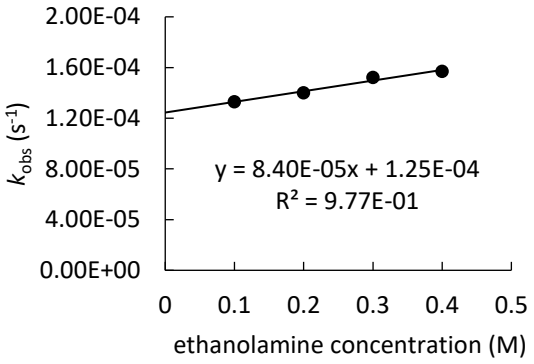

$k_2 = 8.40 \times 10^{-5}$ L mol^{-1} s^{-1}

8-Cl and benzylamine in 90AN10M at 20 °C.

[8-Cl]$_0$ (mol L^{-1})	**[benzylamine]** (mol L^{-1})	k_{obs} (s^{-1})
1.00×10^{-3}	2.00×10^{-1}	1.38×10^{-4}
1.00×10^{-3}	4.00×10^{-1}	1.41×10^{-4}
1.00×10^{-3}	6.00×10^{-1}	1.45×10^{-4}
1.00×10^{-3}	8.00×10^{-1}	1.50×10^{-4}

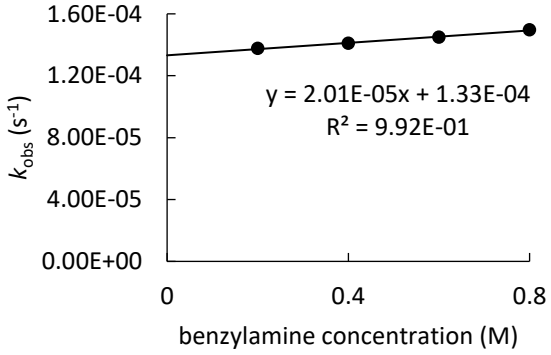

$k_2 = 2.01 \times 10^{-5}$ L mol^{-1} s^{-1} $k_1 = 1.33 \times 10^{-4}$ L mol^{-1} s^{-1}

8-Cl and imidazole in 90AN10M at 20 °C.

[8-Cl]$_0$ (mol L^{-1})	**[imidazole]** (mol L^{-1})	k_{obs} (s^{-1})
1.00×10^{-3}	2.00×10^{-1}	1.41×10^{-4}
1.00×10^{-3}	3.00×10^{-1}	1.45×10^{-4}
1.00×10^{-3}	4.00×10^{-1}	1.50×10^{-4}

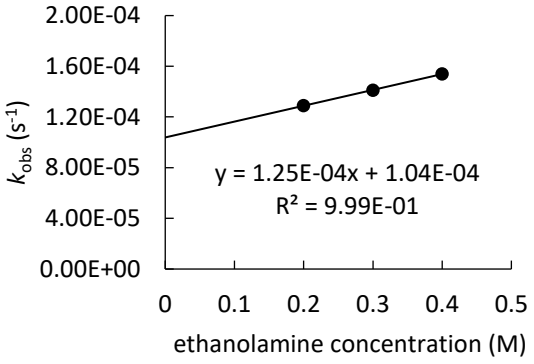

$k_2 = 1.25 \times 10^{-4}$ L mol^{-1} s^{-1}

4-methylbenzhydryl bromide

and propylamine in acetonitrile at 20 °C. Kinetics have been corrected due to ion pairing.

[TolCHBrPh]$_0$ (mol L^{-1})	**[13]** (mol L^{-1})	k_{obs} (s^{-1})
1.00×10^{-3}	2.15×10^{-2}	2.07×10^{-4}
1.00×10^{-3}	3.88×10^{-2}	2.35×10^{-4}
1.00×10^{-3}	5.93×10^{-2}	2.64×10^{-4}
1.00×10^{-3}	8.07×10^{-2}	3.01×10^{-4}

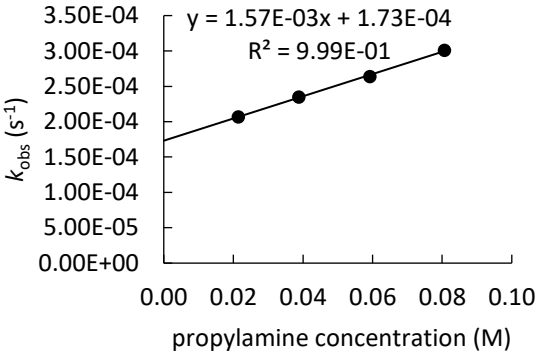

$k_2 = 1.57 \times 10^{-3}$ L mol^{-1} s^{-1} $k_1 = 1.73 \times 10^{-4}$ s^{-1}

Kinetics of reactions of butyl chloride:

Bu-Cl and DABCO (**9**) in acetonitrile at 20 °C.

[Bu-Cl]$_0$ (mol L^{-1})	**[9]** (mol L^{-1})	k_{obs} (s^{-1})
1.00×10^{-3}	3.00×10^{-1}	4.65×10^{-6}
1.00×10^{-3}	9.00×10^{-1}	1.05×10^{-5}
1.00×10^{-3}	1.20×10^{0}	1.43×10^{-5}

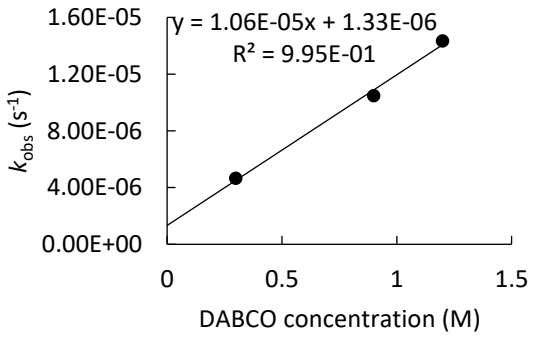

$k_2 = 1.06 \times 10^{-5}$ L mol^{-1} s^{-1}

Kinetics of reactions of butyl bromide:

Bu-Br and DABCO (**9**) in acetonitrile at 20 °C.

[Bu-Br]$_0$ (mol L^{-1})	**[9]** (mol L^{-1})	k_{obs} (s^{-1})
1.00×10^{-3}	1.00×10^{-1}	1.72×10^{-4}
1.00×10^{-3}	2.00×10^{-1}	3.55×10^{-4}
1.00×10^{-3}	3.33×10^{-1}	5.84×10^{-4}
1.00×10^{-3}	4.00×10^{-1}	7.04×10^{-4}

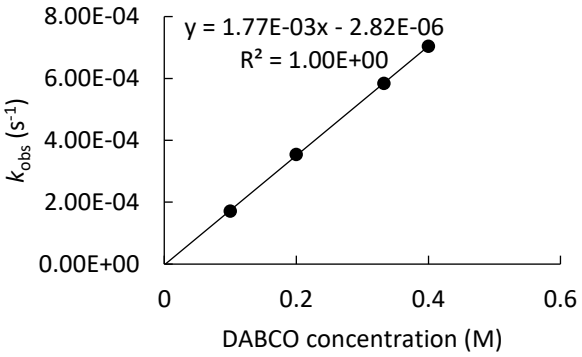

$k_2 = 1.77 \times 10^{-3}$ L mol^{-1} s^{-1}

Bu-Br and piperidine (**11**) in acetonitrile at 20 °C. Kinetics have been corrected due to ion pairing.

$[\textbf{Bu-Br}]_0$ (mol L^{-1})	**[11]** (mol L^{-1})	k_{obs} (s^{-1})
1.00×10^{-3}	2.00×10^{-1}	1.22×10^{-4}
1.00×10^{-3}	4.00×10^{-1}	2.36×10^{-4}
1.00×10^{-3}	6.00×10^{-1}	3.48×10^{-4}
1.00×10^{-3}	8.00×10^{-1}	4.57×10^{-4}

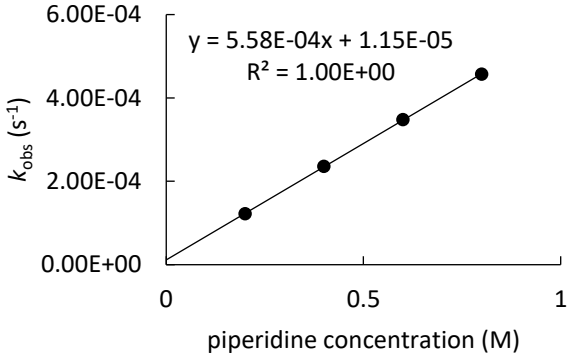

$k_2 = 5.58 \times 10^{-4}$ L mol^{-1} s^{-1}

Bu-Br and morpholine (**12**) in acetonitrile at 20 °C. Kinetics have been corrected due to ion pairing.

$[\textbf{Bu-Br}]_0$ (mol L^{-1})	**[12]** (mol L^{-1})	k_{obs} (s^{-1})
1.00×10^{-3}	2.00×10^{-1}	2.01×10^{-5}
1.00×10^{-3}	4.00×10^{-1}	3.66×10^{-5}
1.00×10^{-3}	6.00×10^{-1}	5.51×10^{-5}
1.00×10^{-3}	8.00×10^{-1}	7.13×10^{-5}

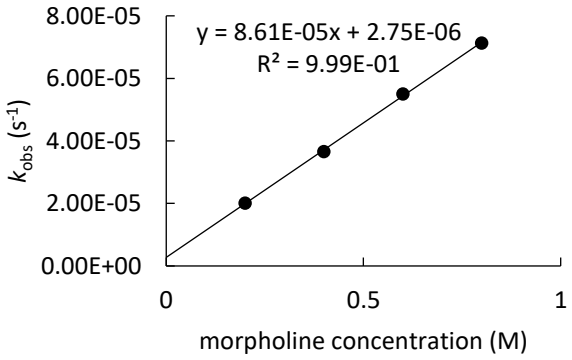

$k_2 = 8.61 \times 10^{-5}$ L mol^{-1} s^{-1}

Kinetics of reactions of butyl iodide:

Bu-I and DABCO (**9**) in acetonitrile at 20 °C.

$[\textbf{Bu-I}]_0$ (mol L^{-1})	**[9]** (mol L^{-1})	k_{obs} (s^{-1})
1.00×10^{-3}	2.50×10^{-2}	2.39×10^{-4}
1.00×10^{-3}	5.00×10^{-2}	4.83×10^{-4}
1.00×10^{-3}	7.50×10^{-2}	7.27×10^{-4}
1.00×10^{-3}	1.00×10^{-1}	9.48×10^{-4}

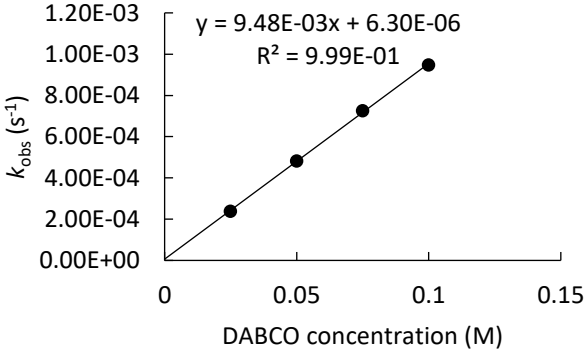

$k_2 = 9.48 \times 10^{-3}$ L mol^{-1} s^{-1}

Bu-I and piperidine (**11**) in acetonitrile at 20 °C.

$[\textbf{Bu-I}]_0$ (mol L^{-1})	**[11]** (mol L^{-1})	k_{obs} (s^{-1})
1.00×10^{-3}	4.00×10^{-2}	1.15×10^{-4}
1.00×10^{-3}	8.00×10^{-2}	2.27×10^{-4}
1.00×10^{-3}	1.20×10^{-1}	3.39×10^{-4}
1.00×10^{-3}	1.60×10^{-1}	4.51×10^{-4}

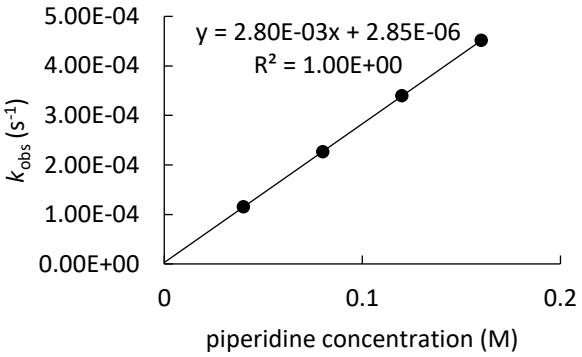

$k_2 = 2.80 \times 10^{-3}$ L mol^{-1} s^{-1}

Bu-I and morpholine (**12**) in acetonitrile at 20 °C.

$[\textbf{Bu-I}]_0$ (mol L^{-1})	**[12]** (mol L^{-1})	k_{obs} (s^{-1})
1.00×10^{-3}	1.00×10^{-1}	4.60×10^{-5}
1.00×10^{-3}	2.00×10^{-1}	9.73×10^{-5}
1.00×10^{-3}	3.00×10^{-1}	1.41×10^{-4}
1.00×10^{-3}	4.00×10^{-1}	1.91×10^{-4}

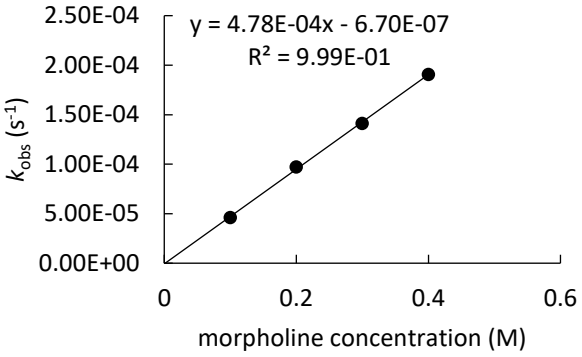

$k_2 = 4.78 \times 10^{-4}$ L mol^{-1} s^{-1}

Kinetics of reactions of butyl tosylate:

Bu-OTs and DABCO (**9**) in acetonitrile at 20 °C.

$[\textbf{Bu-OTs}]_0$ (mol L^{-1})	**[9]** (mol L^{-1})	k_{obs} (s^{-1})
1.00×10^{-3}	5.00×10^{-2}	3.75×10^{-5}
1.00×10^{-3}	1.00×10^{-1}	7.19×10^{-5}
1.00×10^{-3}	1.50×10^{-1}	1.13×10^{-4}
1.00×10^{-3}	2.00×10^{-1}	1.46×10^{-4}

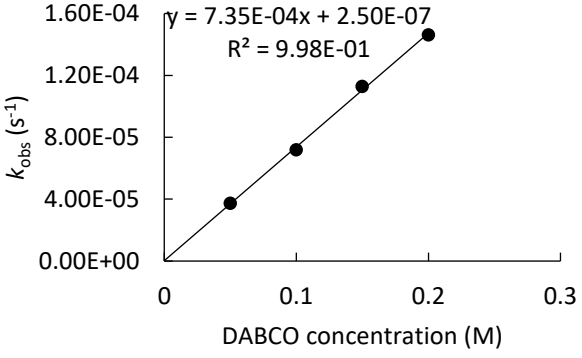

$k_2 = 7.35 \times 10^{-4}$ L mol^{-1} s^{-1}

Bu-OTs and piperidine (**11**) in acetonitrile at 20 °C.

[Bu-OTs]$_0$ (mol L^{-1})	**[11]** (mol L^{-1})	k_{obs} (s^{-1})
1.00×10^{-3}	2.00×10^{-1}	3.80×10^{-5}
1.00×10^{-3}	4.00×10^{-1}	7.34×10^{-5}
1.00×10^{-3}	6.00×10^{-1}	1.16×10^{-4}
1.00×10^{-3}	8.00×10^{-1}	1.51×10^{-4}

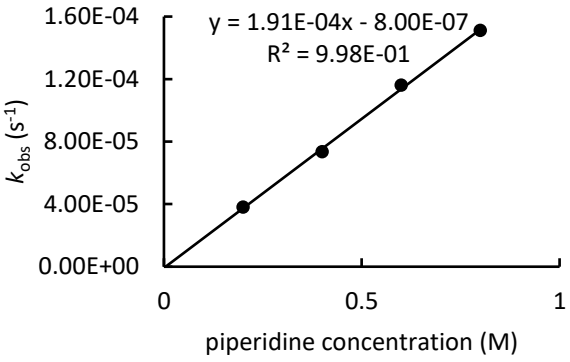

$k_2 = 1.91 \times 10^{-4}$ L mol^{-1} s^{-1}

Bu-OTs and morpholine (**12**) in acetonitrile at 20 °C.

[Bu-OTs]$_0$ (mol L^{-1})	**[12]** (mol L^{-1})	k_{obs} (s^{-1})
1.00×10^{-3}	4.00×10^{-1}	1.14×10^{-5}
1.00×10^{-3}	6.00×10^{-1}	1.79×10^{-5}
1.00×10^{-3}	8.00×10^{-1}	2.47×10^{-5}

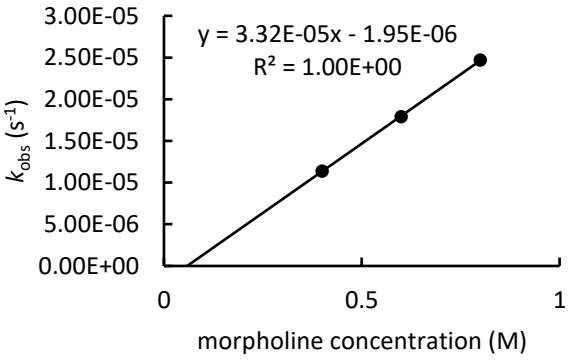

$k_2 = 3.32 \times 10^{-5}$ L mol^{-1} s^{-1}

4.2.4 Correction of ion pairing effects on conductance

To correct the non-linear behavior of conductance versus concentration, the curved relationship was monitored and fitted with a second order polynomial. The aminium halide or tosylate salts were added into acetonitrile and the corresponding amine at the desired amine concentrations at 20 °C. The secondary aminium salts are the primary conducting product of the Menschutkin reaction, since the amines are always in at least 9-fold and regularly even higher excess and slightly more basic (pK_{aH} of piperidine (**11**) in acetonitrile: 19.35 and 18.25 for *N*-methyl-piperidine[13]). This causes them to be the protonated, charged species and not the actual reaction product of electrophile and amine. Propylamine (**13**), the only investigated primary amine, which becomes more basic after alkylation (pK_{aH} of propylamine (**13**) in acetonitrile: 18.42 and 18.92 for *N*-methyl-propylamine[14]), was treated in the same way due to an even higher excess in propylamine in comparison to the Menschutkin product.

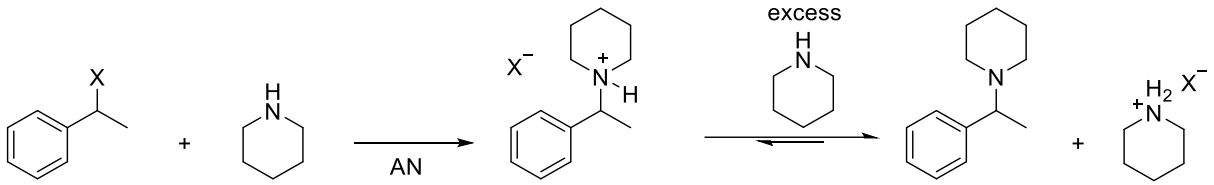

Scheme 1. Menschutkin reaction of amines with alkyl halides or tosylates in acetonitrile in the presence of excess amine.

This fact simplified the acquisition of the correction polynomial, as not every product needed to be investigated, but only the secondary and primary amines and their hydro halide and tosylate salts in acetonitrile at 20 °C. These salts were added in small portions as acetonitrile solutions to the corresponding amine in acetonitrile and the resulting conductance recorded. Concentration was plotted versus conductance, as the data could be fitted much more accurately with a second order polynomial. This second order polynomial was then applied to the kinetic traces, to correct for the curvature in the conductance/concentration relationship. For all systems that exhibited significant curvature, the parameters a, b, and c of the second-order polynomial $y=ax^2+bx+c$ were summarized in tables and the parameters employed to correct the kinetic conductance traces.

Conductance of 1-(1-(4-methoxyphenyl)ethyl)-1,4-diazabicyclo[2.2.2]octan-1-ium bromide (14d) in acetonitrile.

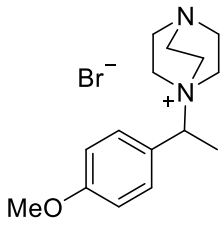

14d

14d and DABCO (**9**, 0.02 M) in acetonitrile at 20 °C.

[14d] (mol L^{-1})	*G* (μS)
0	0.003
4.412×10^{-5}	0.036
1.102×10^{-4}	0.113
2.199×10^{-4}	0.212
3.292×10^{-4}	0.306
4.381×10^{-4}	0.410
5.465×10^{-4}	0.503
6.545×10^{-4}	0.601
1.082×10^{-3}	0.939
1.504×10^{-3}	1.269
1.918×10^{-3}	1.573
2.326×10^{-3}	1.871

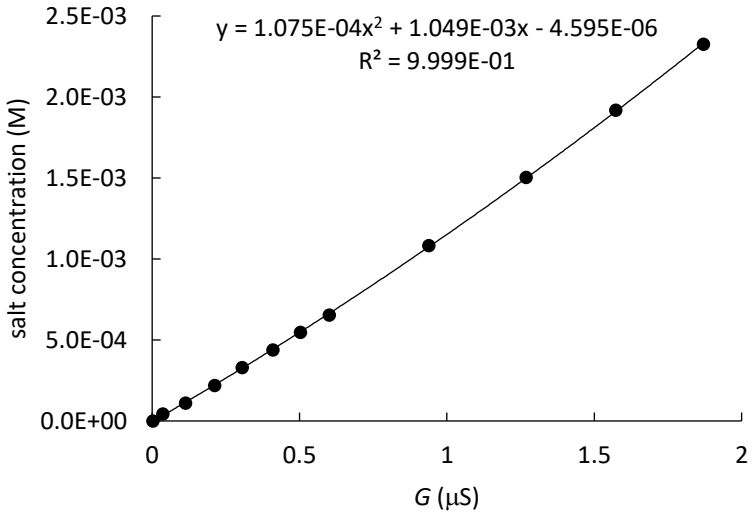

14d and DABCO (**9**, 0.1 M) in acetonitrile at 20 °C.

[14d] (mol L^{-1})	*G* (μS)
0	0.006
4.412×10^{-5}	0.051
1.102×10^{-4}	0.106
2.199×10^{-4}	0.208
3.292×10^{-4}	0.306
4.381×10^{-4}	0.404
5.465×10^{-4}	0.491
6.545×10^{-4}	0.584
1.082×10^{-3}	0.924
1.504×10^{-3}	1.247
1.918×10^{-3}	1.559
2.326×10^{-3}	1.853

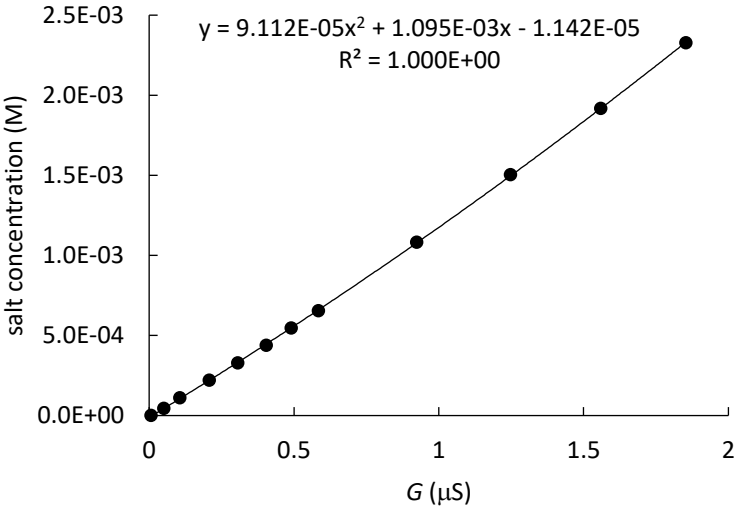

14d and DABCO (**9**, 0.4 M) in acetonitrile at 20 °C.

[14d] (mol L^{-1})	*G* (μS)
0	0.006
4.412×10^{-5}	0.056
1.102×10^{-4}	0.109
2.199×10^{-4}	0.206
3.292×10^{-4}	0.308
4.381×10^{-4}	0.397
5.465×10^{-4}	0.485
6.545×10^{-4}	0.575
1.082×10^{-3}	0.908
1.504×10^{-3}	1.207
1.918×10^{-3}	1.520
2.326×10^{-3}	1.794

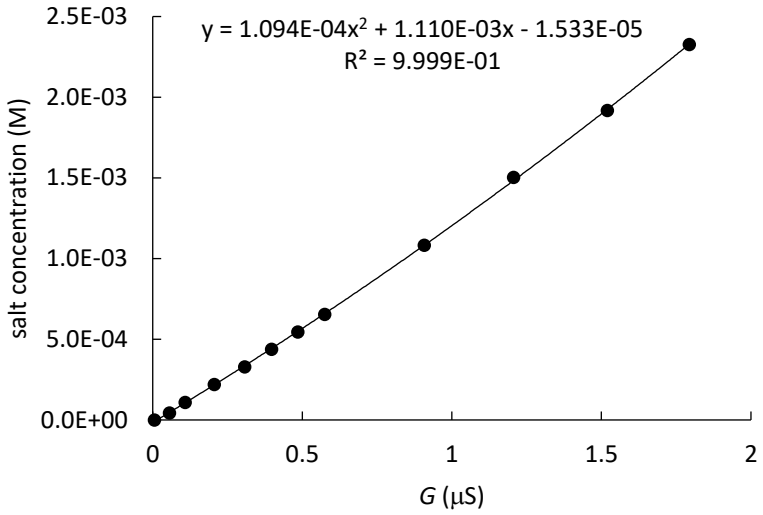

14d and DABCO (**9**, 1.2 M) in acetonitrile at 20 °C.

[14d] (mol L^{-1})	*G* (μS)
0	0.014
4.412×10^{-5}	0.054
1.102×10^{-4}	0.110
2.199×10^{-4}	0.197
3.292×10^{-4}	0.274
4.381×10^{-4}	0.357
5.465×10^{-4}	0.438
6.545×10^{-4}	0.514
8.693×10^{-4}	0.663
1.082×10^{-3}	0.806
1.294×10^{-3}	0.945
1.504×10^{-3}	1.088
1.712×10^{-3}	1.217
1.918×10^{-3}	1.349
2.123×10^{-3}	1.473
2.326×10^{-3}	1.592
2.528×10^{-3}	1.721

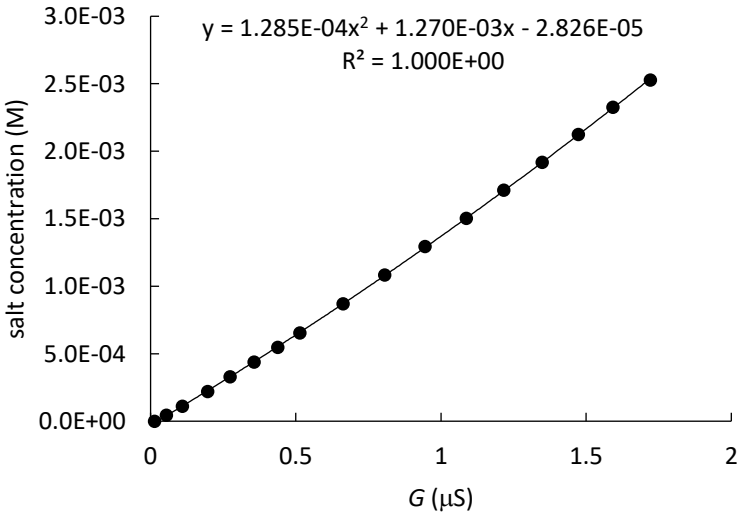

Conductance of pyrrolidinium bromide (10·HBr) in acetonitrile.

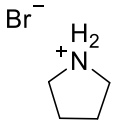

10·HBr

10·HBr and pyrrolidine (**10**, 0.05 M) in acetonitrile at 20 °C.

[10·HBr] (mol L^{-1})	*G* (μS)
0	0.011
3.892×10^{-5}	0.045
9.717×10^{-5}	0.102
1.939×10^{-4}	0.188
2.903×10^{-4}	0.277
3.863×10^{-4}	0.345
4.820×10^{-4}	0.404
5.772×10^{-4}	0.472
9.545×10^{-4}	0.688
1.326×10^{-3}	0.879
1.692×10^{-3}	1.033
2.052×10^{-3}	1.177
2.406×10^{-3}	1.312
2.755×10^{-3}	1.433
3.099×10^{-3}	1.547
3.438×10^{-3}	1.652

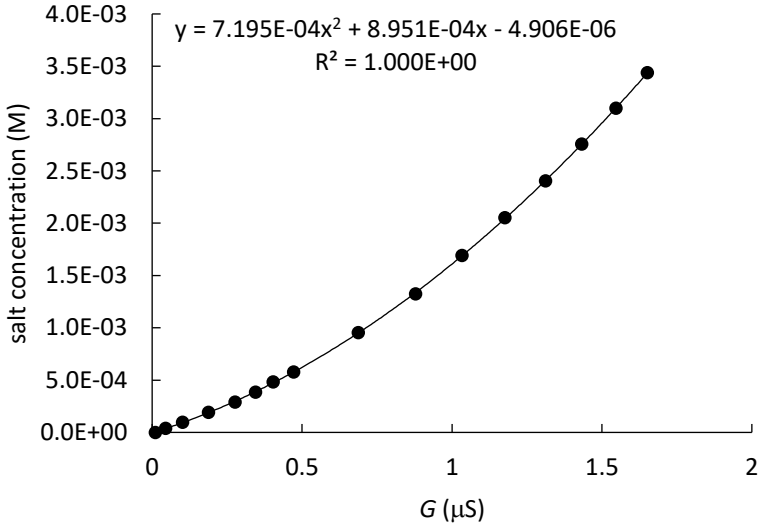

10·HBr and pyrrolidine (**10**, 0.1 M) in acetonitrile at 20 °C.

[10·HBr] (mol L^{-1})	*G* (μS)
0	0.009
3.893×10^{-5}	0.037
9.721×10^{-5}	0.101
1.940×10^{-4}	0.192
2.905×10^{-4}	0.272
3.865×10^{-4}	0.354
4.822×10^{-4}	0.429
5.775×10^{-4}	0.492
9.549×10^{-4}	0.735

1.326×10^{-3}	0.941
1.692×10^{-3}	1.120
2.052×10^{-3}	1.284
2.407×10^{-3}	1.423
2.757×10^{-3}	1.563
3.101×10^{-3}	1.687
3.440×10^{-3}	1.801

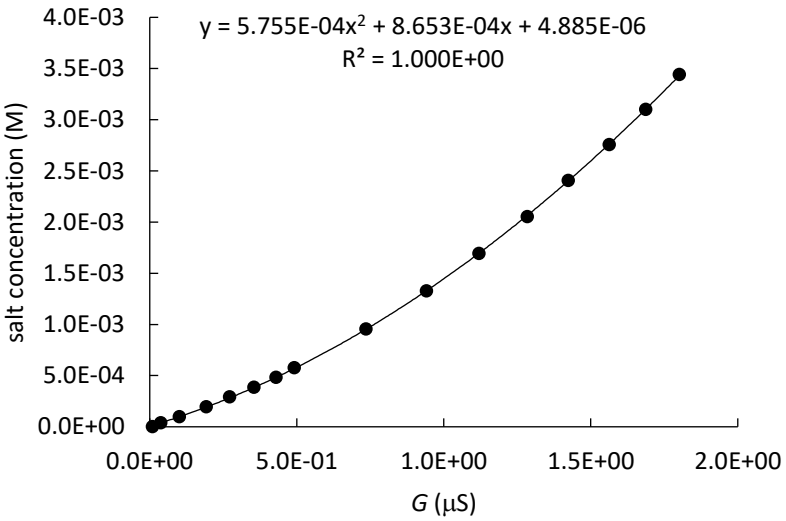

10·HBr and pyrrolidine (**10**, 0.15 M) in acetonitrile at 20 °C.

[10·HBr] (mol L^{-1})	*G* (μS)
0	0.015
3.893×10^{-5}	0.054
9.721×10^{-5}	0.112
1.940×10^{-4}	0.203
2.905×10^{-4}	0.289
3.865×10^{-4}	0.367
4.822×10^{-4}	0.439
5.775×10^{-4}	0.508
9.549×10^{-4}	0.754
1.326×10^{-3}	0.970
1.692×10^{-3}	1.164
2.052×10^{-3}	1.327
2.407×10^{-3}	1.489
2.757×10^{-3}	1.630
3.101×10^{-3}	1.766
3.440×10^{-3}	1.894

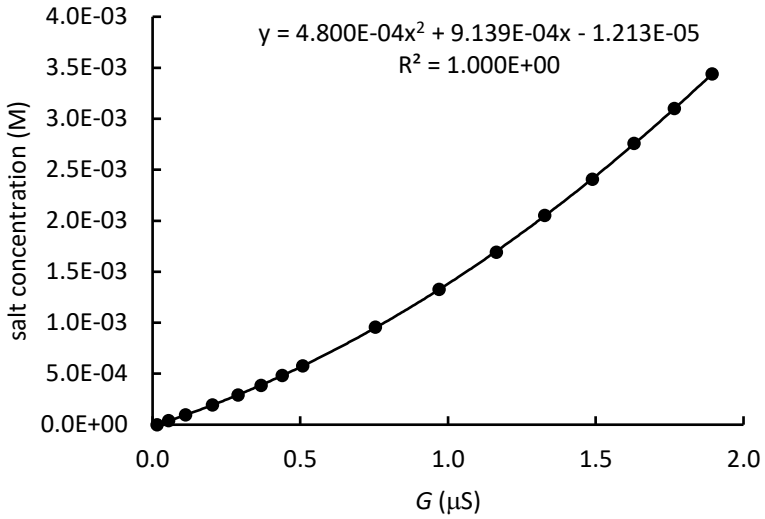

10·HBr and pyrrolidine (**10**, 0.2 M) in acetonitrile at 20 °C.

[10·HBr] (mol L^{-1})	*G* (μS)
0	0.017
3.892×10^{-5}	0.054
9.717×10^{-5}	0.113
1.939×10^{-4}	0.204
2.903×10^{-4}	0.285
3.863×10^{-4}	0.369
4.820×10^{-4}	0.444
5.772×10^{-4}	0.513
9.545×10^{-4}	0.767
1.326×10^{-3}	0.991
1.692×10^{-3}	1.191
2.052×10^{-3}	1.379
2.406×10^{-3}	1.543
2.755×10^{-3}	1.695
3.099×10^{-3}	1.842

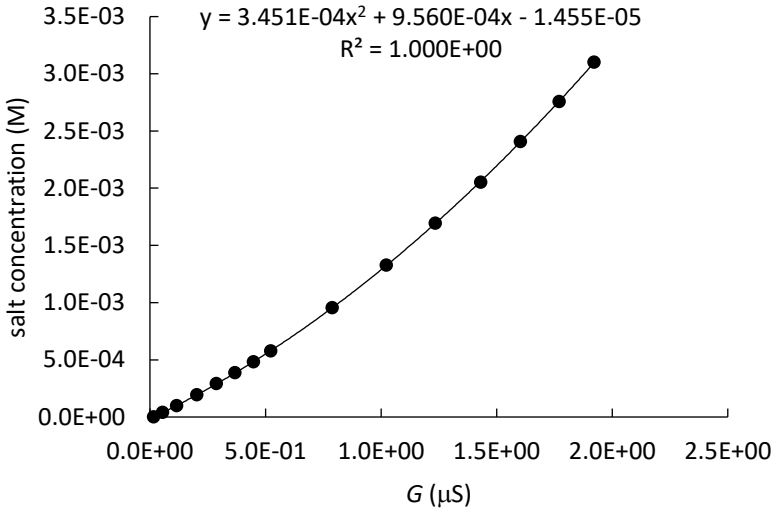

10·HBr and pyrrolidine (**10**, 0.3 M) in acetonitrile at 20 °C.

[10·HBr] (mol L^{-1})	*G* (μS)
0	0.016
3.893×10^{-5}	0.055
9.721×10^{-5}	0.115
1.940×10^{-4}	0.202
2.905×10^{-4}	0.287
3.865×10^{-4}	0.368
4.822×10^{-4}	0.448
5.775×10^{-4}	0.523
9.549×10^{-4}	0.788
1.326×10^{-3}	1.023
1.692×10^{-3}	1.234
2.052×10^{-3}	1.431
2.407×10^{-3}	1.603
2.757×10^{-3}	1.770
3.101×10^{-3}	1.922

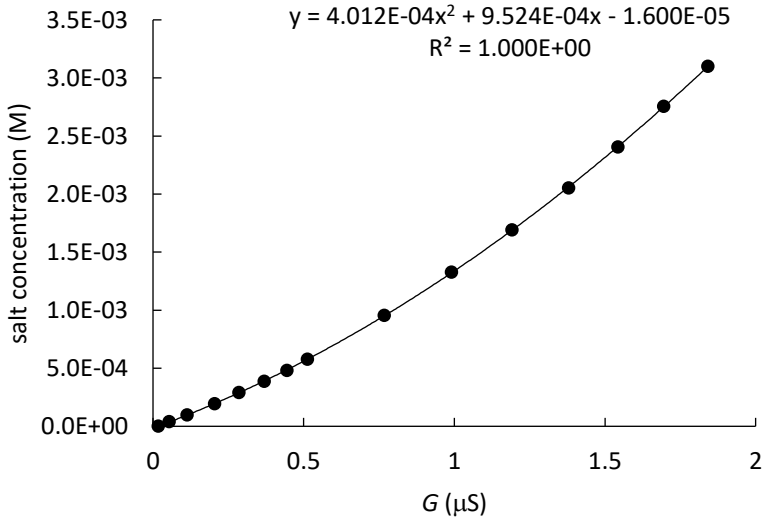

10·HBr and pyrrolidine (**10**, 0.4 M) in acetonitrile at 20 °C.

[10·HBr] (mol L^{-1})	*G* (μS)
0	0.023
3.892×10^{-5}	0.052
9.717×10^{-5}	0.110
1.939×10^{-4}	0.202
2.903×10^{-4}	0.293
3.863×10^{-4}	0.372
4.820×10^{-4}	0.456
5.772×10^{-4}	0.534
9.545×10^{-4}	0.813
1.326×10^{-3}	1.054
1.692×10^{-3}	1.271
2.052×10^{-3}	1.481
2.406×10^{-3}	1.666
2.755×10^{-3}	1.838
3.099×10^{-3}	1.999

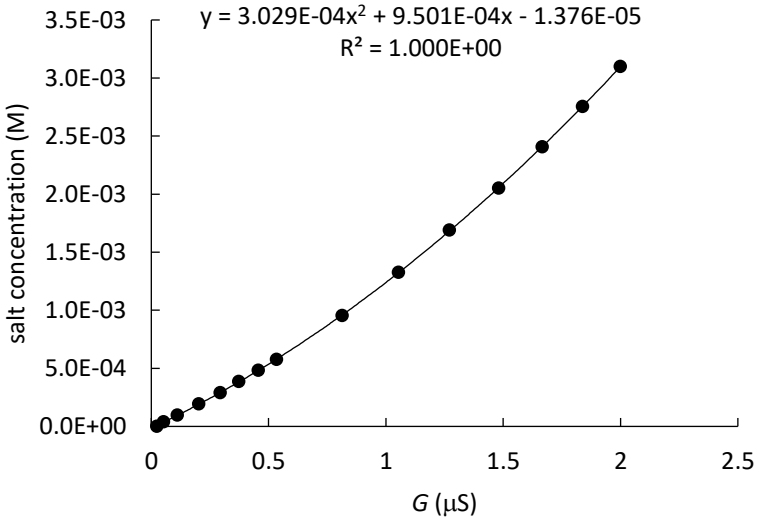

10·HBr in acetonitrile and methanol (90:10 v/v) at 20 °C.

[10·HBr] (mol L^{-1})	*G* (μS)
0	0.019
3.892×10^{-5}	0.063
9.717×10^{-5}	0.127
1.939×10^{-4}	0.234
2.903×10^{-4}	0.330
3.863×10^{-4}	0.425
4.820×10^{-4}	0.523
5.772×10^{-4}	0.616
9.583×10^{-4}	0.965
1.336×10^{-3}	1.280
1.711×10^{-3}	1.584
2.084×10^{-3}	1.850

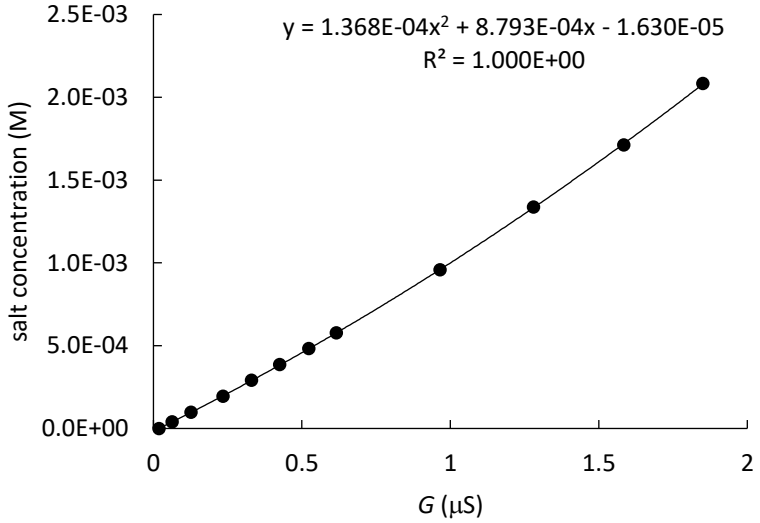

10·HBr in acetonitrile and methanol (80:20 v/v) at 20 °C.

[10·HBr] (mol L^{-1})	*G* (μS)
0	0.017
3.892×10^{-5}	0.063
9.717×10^{-5}	0.123
1.939×10^{-4}	0.234
2.903×10^{-4}	0.331
3.863×10^{-4}	0.427
4.820×10^{-4}	0.528
5.772×10^{-4}	0.623
9.583×10^{-4}	0.990
1.336×10^{-3}	1.327
1.711×10^{-3}	1.657
2.084×10^{-3}	1.965

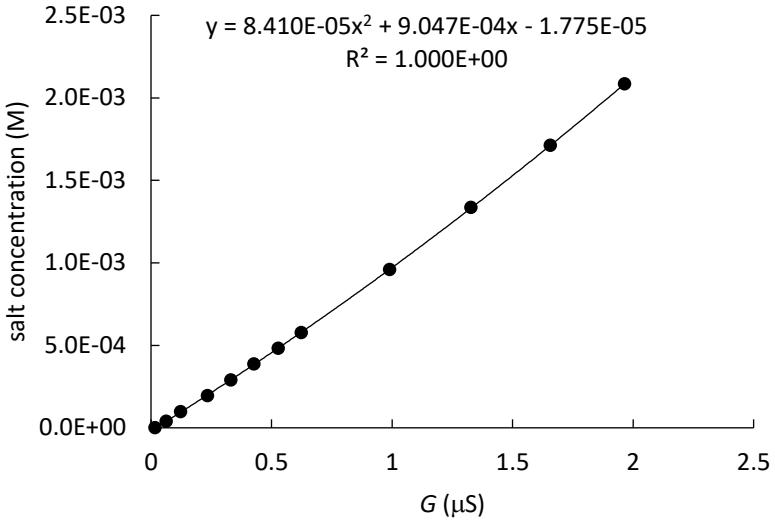

For pyrrolidinium hydrobromides (**10·HBr**) the employed, second order polynomials ($y=ax^2+bx+c$) for correction have three different parameters a, b and c. These are summarized in the table below

Parameters a, b and c for **10·HBr** in pyrrolidine (**10**) in acetonitrile at 20 °C.

[10], (mol L^{-1})	a	b	c
0.05	7.195×10^{-4}	8.951×10^{-4}	-4.906×10^{-6}
0.15	4.800×10^{-4}	9.139×10^{-4}	-1.213×10^{-5}
0.2	4.012×10^{-4}	9.524×10^{-4}	-1.600×10^{-5}
0.3	3.451×10^{-4}	9.560×10^{-4}	-1.455×10^{-5}
0.4	3.029×10^{-4}	9.501×10^{-4}	-1.376×10^{-5}

Conductance of piperidinium bromide (11·HBr) and the bromide salts 4-11-Br and 7-11-Br in acetonitrile.

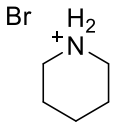

11·HBr

11·HBr and piperidine (**11**, 0.05 M) in acetonitrile at 20 °C.

[11·HBr] (mol L^{-1})	*G* (μS)
0	0.011
3.320×10^{-5}	0.044
8.289×10^{-5}	0.092
1.655×10^{-4}	0.162
2.477×10^{-4}	0.225
3.296×10^{-4}	0.284
4.112×10^{-4}	0.335
4.925×10^{-4}	0.383
8.143×10^{-4}	0.560
1.131×10^{-3}	0.710
1.443×10^{-3}	0.840
1.750×10^{-3}	0.959
2.053×10^{-3}	1.057
2.351×10^{-3}	1.154
2.644×10^{-3}	1.250
2.933×10^{-3}	1.330

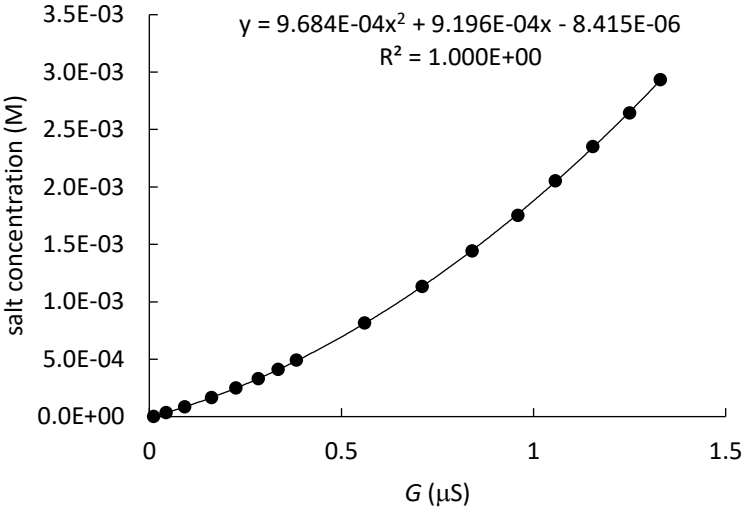

11·HBr and piperidine (**11**, 0.1 M) in acetonitrile at 20 °C.

[11·HBr] (mol L^{-1})	*G* (μS)
0	0.018
3.320×10^{-5}	0.047
8.289×10^{-5}	0.096
1.655×10^{-4}	0.161
2.477×10^{-4}	0.228
3.296×10^{-4}	0.286
4.112×10^{-4}	0.342
4.925×10^{-4}	0.396
8.143×10^{-4}	0.583
1.131×10^{-3}	0.743
1.443×10^{-3}	0.884
1.750×10^{-3}	1.010
2.053×10^{-3}	1.123
2.351×10^{-3}	1.229
2.644×10^{-3}	1.331
2.933×10^{-3}	1.425

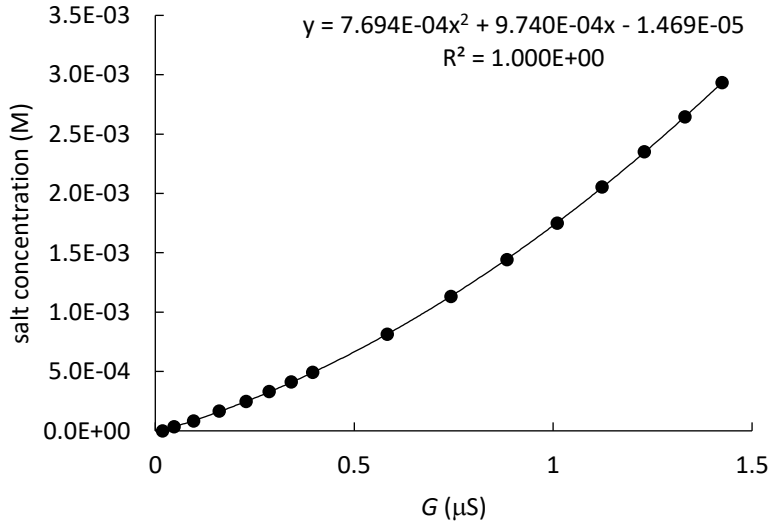

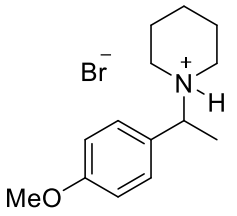

14b

14b and piperidine (**11**, 0.1 M) in acetonitrile at 20 °C.

[14b] (mol L^{-1})	*G* (μS)
0	0.021
3.446×10^{-5}	0.047
8.605×10^{-5}	0.092
1.718×10^{-4}	0.162
2.571×10^{-4}	0.225
3.421×10^{-4}	0.276
4.268×10^{-4}	0.332
5.112×10^{-4}	0.383
8.451×10^{-4}	0.560
1.174×10^{-3}	0.713
1.497×10^{-3}	0.854
1.816×10^{-3}	0.967
2.130×10^{-3}	1.081
2.439×10^{-3}	1.187
2.744×10^{-3}	1.284
3.043×10^{-3}	1.371

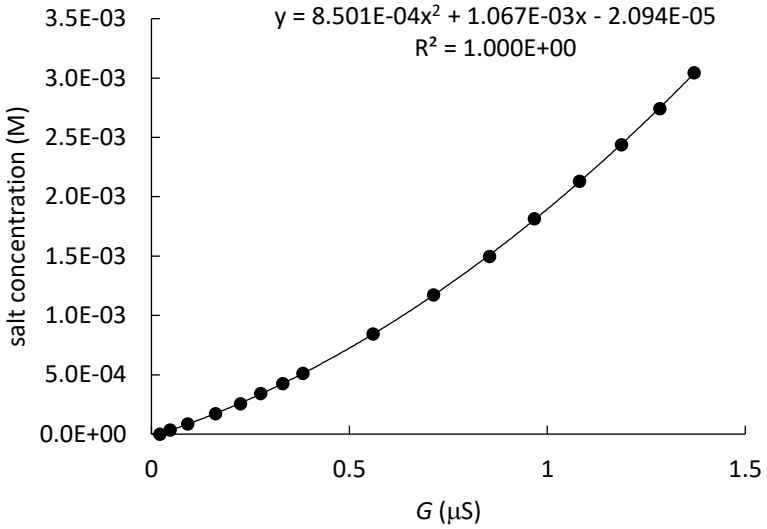

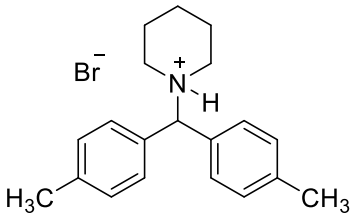

14c

14c and piperidine (**11**, 0.1 M) in acetonitrile at 20 °C.

[14c] (mol L^{-1})	*G* (μS)
0	0.021
1.075×10^{-4}	0.105
2.145×10^{-4}	0.195
3.211×10^{-4}	0.297
4.273×10^{-4}	0.376
5.331×10^{-4}	0.457
6.384×10^{-4}	0.523
8.480×10^{-4}	0.657
1.056×10^{-3}	0.768
1.262×10^{-3}	0.868
1.467×10^{-3}	0.961
1.670×10^{-3}	1.053
1.872×10^{-3}	1.135
2.072×10^{-3}	1.216
2.467×10^{-3}	1.368
2.857×10^{-3}	1.497
3.240×10^{-3}	1.624

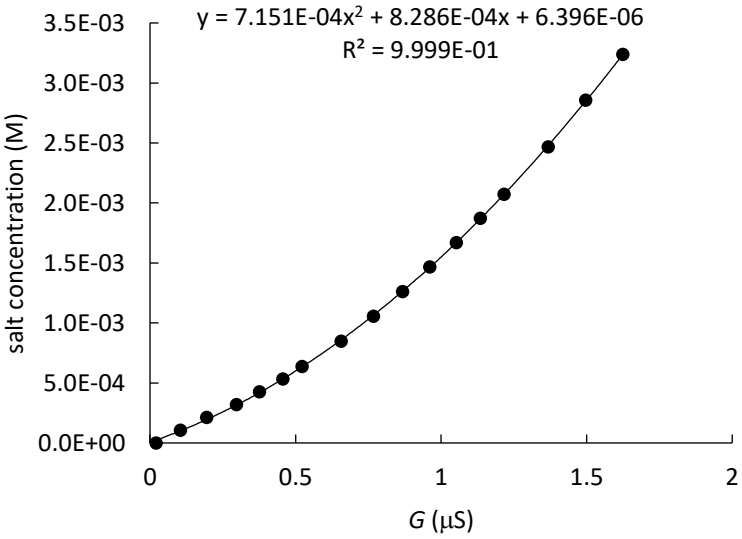

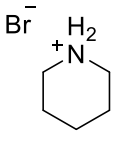

11·HBr

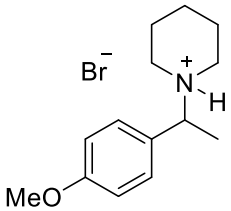

14b

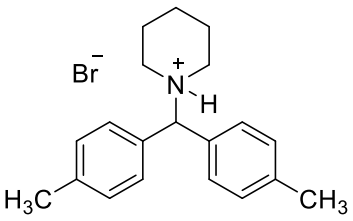

14c

Overlay of the plots of **11·HBr**, **14b** and **14c** (in acetonitrile, 0.1 M piperidine (**11**) at 20 °C). As stated before, the effect of the electrophile is negligible as demonstrated by the graph below. Deviations are attributed to experimental error.

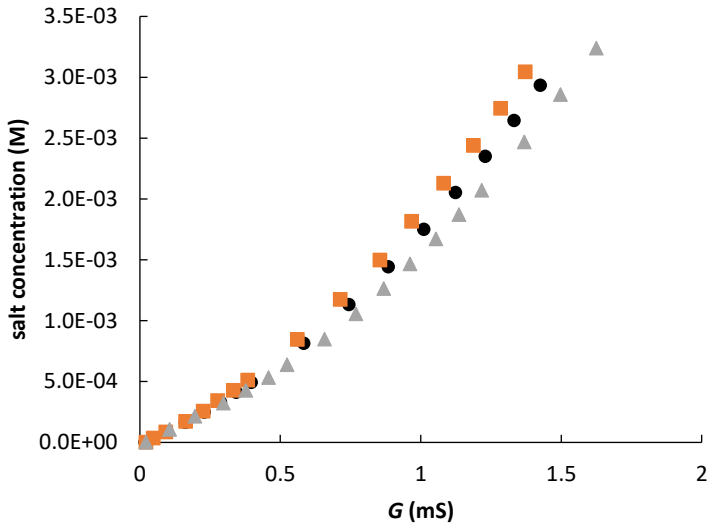

Orange squares: **14b**
Black dots: **11·HBr**
Grey triangles: **14c**

11·HBr and piperidine (**11**, 0.2 M) in acetonitrile at 20 °C.

[11·HBr] (mol L^{-1})	*G* (μS)
0	0.028
3.320×10^{-5}	0.051
8.289×10^{-5}	0.098
1.655×10^{-4}	0.170
2.477×10^{-4}	0.238
3.296×10^{-4}	0.299
4.112×10^{-4}	0.355
4.925×10^{-4}	0.412
8.143×10^{-4}	0.611
1.131×10^{-3}	0.780
1.443×10^{-3}	0.933
1.750×10^{-3}	1.070
2.053×10^{-3}	1.191
2.351×10^{-3}	1.309
2.644×10^{-3}	1.417
2.933×10^{-3}	1.512

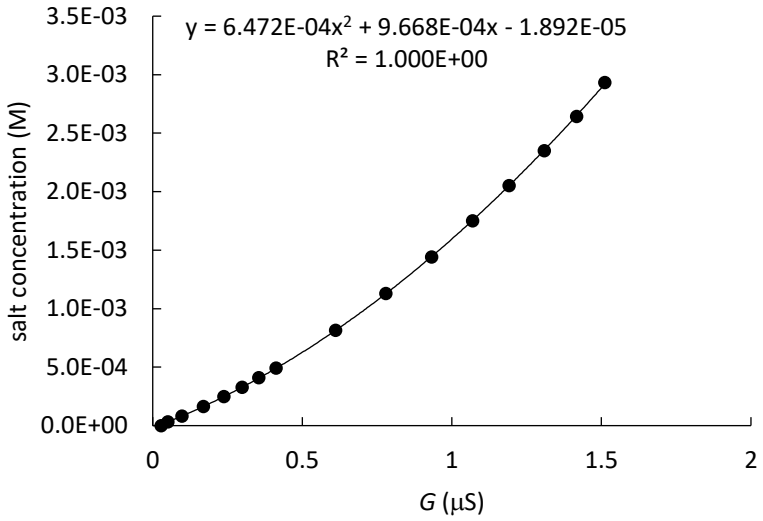

11·HBr and piperidine (**11**, 0.8 M) in acetonitrile at 20 °C.

[11·HBr] (mol L^{-1})	*G* (μS)
0	0.062
3.320×10^{-5}	0.087
8.289×10^{-5}	0.119
1.655×10^{-4}	0.195
2.477×10^{-4}	0.256
3.296×10^{-4}	0.319
4.112×10^{-4}	0.374
4.925×10^{-4}	0.438
8.143×10^{-4}	0.646
1.131×10^{-3}	0.826
1.443×10^{-3}	1.002
1.750×10^{-3}	1.154
2.053×10^{-3}	1.298
2.351×10^{-3}	1.432
2.644×10^{-3}	1.558
2.933×10^{-3}	1.681

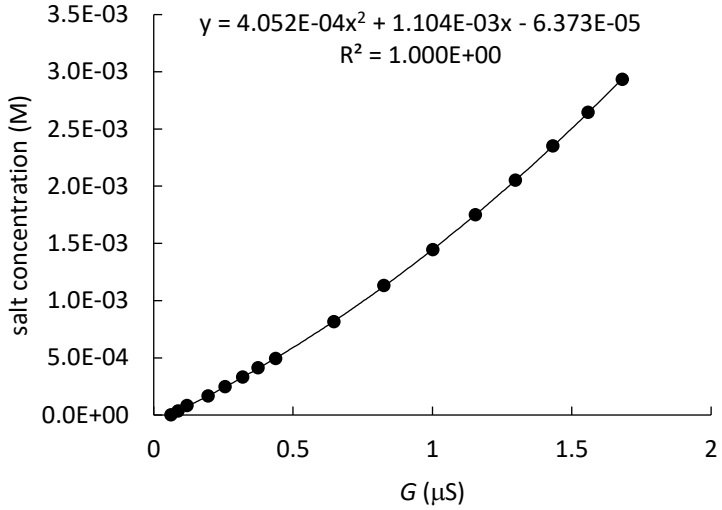

For piperidinium hydrobromides (**11·HBr**) not all necessary piperidine concentrations had to be experimentally determined, as the remaining could be interpolated with the following plots. The employed, second order polynomials ($y=ax^2+bx+c$) have three different parameters a, b and c. Parameter a and b could be interpolated with a linear correlation of the plot of the logarithm of the piperidine concentration versus a or b respectively. Parameter c could be interpolated by a linear correlation of the plot of the piperidine concentration versus c. The resulting linear correlations were used to calculate the interpolated parameters.

Parameters a, b and c for **11·HBr** in piperidine (**11**) in acetonitrile at 20 °C.

[11] (mol L^{-1})	log **[11]**	a	b	c	Interpolated?
0.05	-1.301	9.684×10^{-4}	9.196×10^{-4}	-8.415×10^{-6}	No
0.1	-1.000	7.694×10^{-4}	9.740×10^{-4}	-1.469×10^{-5}	No
0.2	-0.6990	6.472×10^{-4}	9.668×10^{-4}	-1.892×10^{-5}	No
0.8	-0.09691	4.052×10^{-4}	1.104×10^{-3}	-6.373×10^{-5}	No
0.15		7.201×10^{-4}	9.843×10^{-4}	-1.646×10^{-5}	Yes
0.3		5.832×10^{-4}	1.028×10^{-3}	-2.735×10^{-5}	Yes
0.4		5.263×10^{-4}	1.047×10^{-3}	-3.460×10^{-5}	Yes
0.6		4.462×10^{-4}	1.072×10^{-3}	-4.911×10^{-5}	Yes

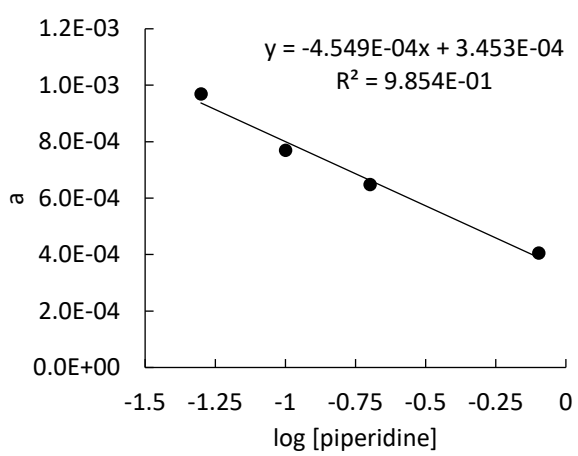

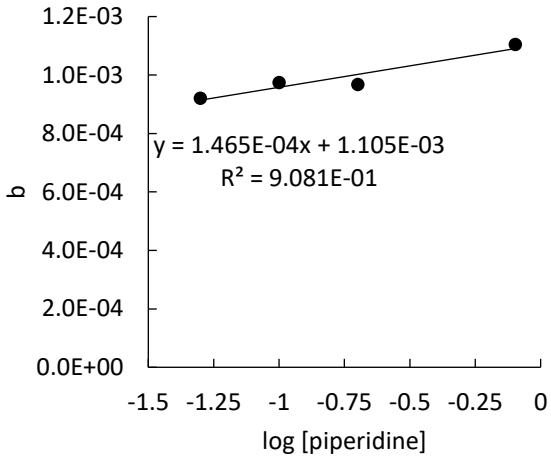

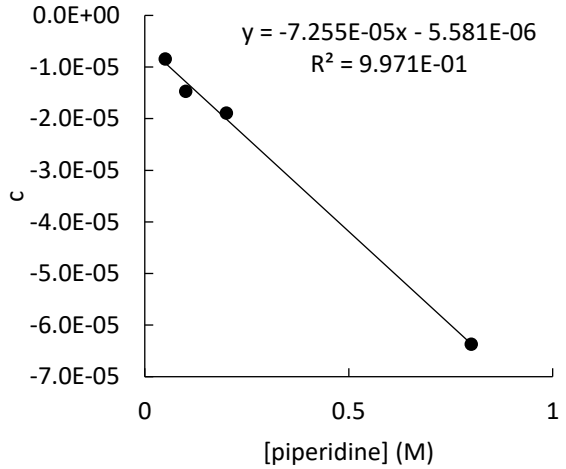

Conductance of morpholinium bromide (12·HBr) in acetonitrile.

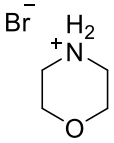

12·HBr

12·HBr and morpholine (**12**, 0.05 M) in acetonitrile at 20 °C.

[12·HBr] (mol L^{-1})	*G* (μS)
0	0.006
3.574×10^{-5}	0.030
8.916×10^{-5}	0.073
1.776×10^{-4}	0.152
2.654×10^{-4}	0.209
3.524×10^{-4}	0.256
4.388×10^{-4}	0.301
5.245×10^{-4}	0.339
8.608×10^{-4}	0.469
1.187×10^{-3}	0.581

1.503×10^{-3}	0.663
1.810×10^{-3}	0.747
2.108×10^{-3}	0.809
2.398×10^{-3}	0.878
2.679×10^{-3}	0.932
2.952×10^{-3}	0.982

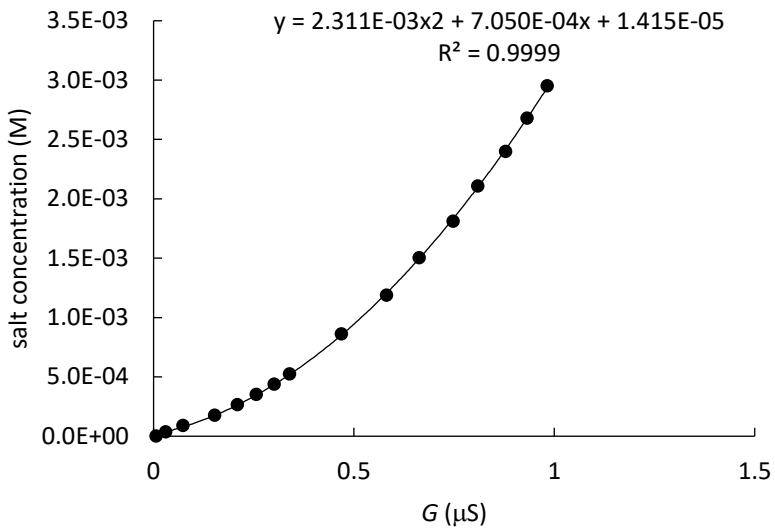

12·HBr and morpholine (**12**, 0.1 M) in acetonitrile at 20 °C.

[12·HBr] (mol L^{-1})	G (μS)
0	0.008
2.077×10^{-5}	0.027
5.179×10^{-5}	0.060
1.032×10^{-4}	0.106
1.542×10^{-4}	0.144
2.047×10^{-4}	0.184
2.549×10^{-4}	0.218
3.047×10^{-4}	0.248
5.000×10^{-4}	0.352
6.894×10^{-4}	0.440
8.731×10^{-4}	0.512
1.051×10^{-3}	0.578
1.225×10^{-3}	0.639
1.556×10^{-3}	0.737
1.870×10^{-3}	0.826
2.167×10^{-3}	0.902

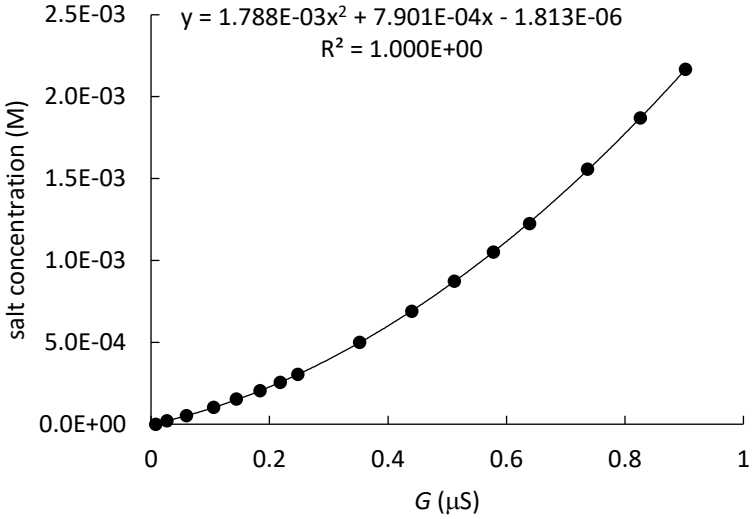

12·HBr and morpholine (**12**, 0.2 M) in acetonitrile at 20 °C.

[12·HBr] (mol L^{-1})	*G* (μS)
0	0.007
3.574×10^{-5}	0.037
8.916×10^{-5}	0.082
1.776×10^{-4}	0.146
2.654×10^{-4}	0.197
3.524×10^{-4}	0.248
4.388×10^{-4}	0.292
5.245×10^{-4}	0.329
8.608×10^{-4}	0.468
1.187×10^{-3}	0.583
1.503×10^{-3}	0.681
1.810×10^{-3}	0.763
2.108×10^{-3}	0.841
2.398×10^{-3}	0.909
2.679×10^{-3}	0.967
2.952×10^{-3}	1.031

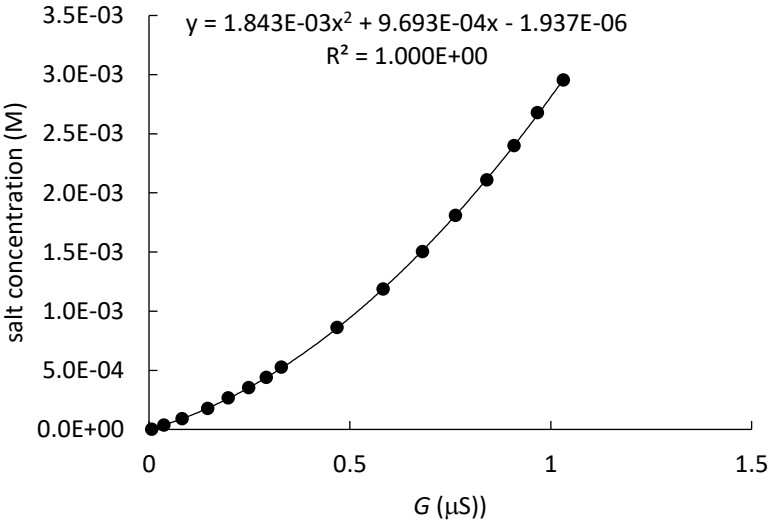

12·HBr and morpholine (**12**, 0.4 M) in acetonitrile at 20 °C.

[12·HBr] (mol L^{-1})	*G* (μS)
0	0.009
3.574×10^{-5}	0.043
8.916×10^{-5}	0.092
1.776×10^{-4}	0.161
2.654×10^{-4}	0.219
3.524×10^{-4}	0.270
4.388×10^{-4}	0.309
5.245×10^{-4}	0.350
8.608×10^{-4}	0.504
1.187×10^{-3}	0.609
1.503×10^{-3}	0.739
1.810×10^{-3}	0.815
2.108×10^{-3}	0.883
2.398×10^{-3}	0.979
2.679×10^{-3}	1.040
2.952×10^{-3}	1.100

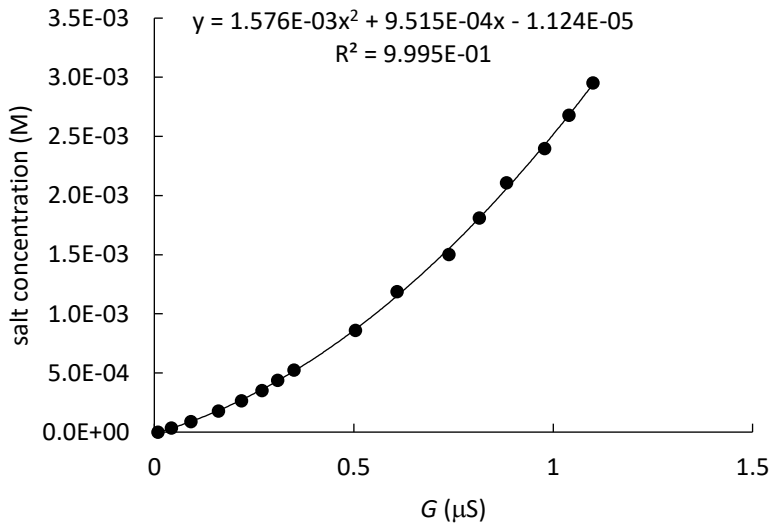

12·HBr and morpholine (**12**, 0.6 M) in acetonitrile at 20 °C.

[12·HBr] (mol L^{-1})	*G* (μS)
0	0.011
2.077×10^{-5}	0.032
5.179×10^{-5}	0.064
1.032×10^{-4}	0.108
1.542×10^{-4}	0.148
2.047×10^{-4}	0.190
2.549×10^{-4}	0.229
3.047×10^{-4}	0.259
5.000×10^{-4}	0.373
8.731×10^{-4}	0.557
1.225×10^{-3}	0.702
1.556×10^{-3}	0.824
1.870×10^{-3}	0.930
2.094×10^{-3}	0.991

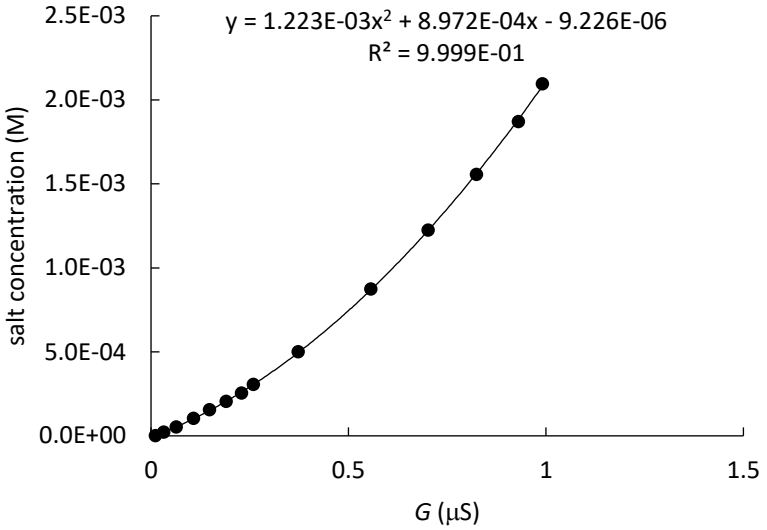

12·HBr and morpholine (**12**, 0.8 M) in acetonitrile at 20 °C.

[12·HBr] (mol L^{-1})	*G* (μS)
0	0.014
3.574×10^{-5}	0.037
8.916×10^{-5}	0.086
1.776×10^{-4}	0.150
2.654×10^{-4}	0.204
3.524×10^{-4}	0.264
4.388×10^{-4}	0.308
5.245×10^{-4}	0.348
8.608×10^{-4}	0.528
1.187×10^{-3}	0.655
1.503×10^{-3}	0.766
1.810×10^{-3}	0.860
2.108×10^{-3}	0.944
2.398×10^{-3}	1.018
2.679×10^{-3}	1.090
2.952×10^{-3}	1.148

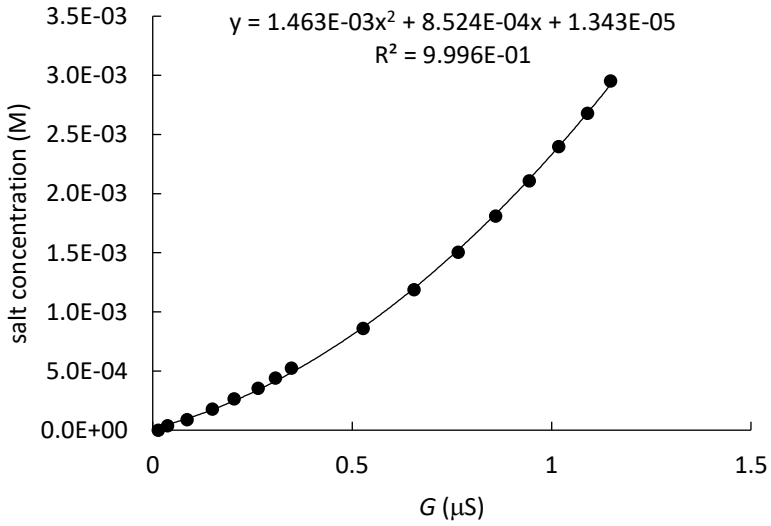

For morpholinium hydrobromides (**12·HBr**) not all necessary piperidine concentrations had to be experimentally determined, as the remaining could be interpolated with the following plots. The employed, second order polynomials ($y=ax^2+bx+c$) have three different parameters a, b and c. Parameter a could be interpolated with a linear correlation of the plot of logarithm of the morpholine concentration versus a respectively. Parameter b was obtained from a plot of b versus the logarithm of the morpholine concentration. A linear correlation was not observed in this case, but a second order polynomial could be used to describe the relationship sufficiently instead. Parameter c could not be interpolated by plotting the piperidine concentration versus c in this case. Since parameter c is 2-3 orders of magnitude smaller than parameters a and b and has no influence on the shape/curvature of the second order polynomial, other than the location of the intercept. An inferior method of interpolation was thus deemed acceptable and a linear correlation with the 2 adjacent data points only employed. So parameter c for a 0.15 M morpoline concentration was interpolated from the experimentally obtained parameters c of a 0.1 M and a 0.2 M morpholine concentration. The same method was applied for a 0.3 M concentration and the experimentally obtained data points of a 0.2 M and a 0.4 M morpholine concentration.

Parameters a, b and c for **12·HBr** in morpholine (**12**) in acetonitrile at 20 °C.

[12] (mol L^{-1})	log **[12]**	a	b	c	Interpolated?
0.05	−1.301	2.311×10^{-3}	7.050×10^{-4}	1.415×10^{-5}	No
0.1	−1.000	2.055×10^{-3}	9.080×10^{-4}	-2.083×10^{-6}	No
0.2	−0.6990	1.843×10^{-3}	9.693×10^{-4}	-1.937×10^{-6}	No
0.4	−0.3979	1.576×10^{-3}	9.515×10^{-4}	-1.124×10^{-5}	No
0.6	−0.2218	1.406×10^{-3}	1.031×10^{-3}	-1.060×10^{-5}	No
0.8	−0.09691	1.463×10^{-3}	8.524×10^{-4}	1.343×10^{-5}	No
0.15		1.931×10^{-3}	9.594×10^{-4}	-2.010×10^{-6}	Yes
0.3		1.703×10^{-3}	9.982×10^{-4}	-6.589×10^{-6}	Yes

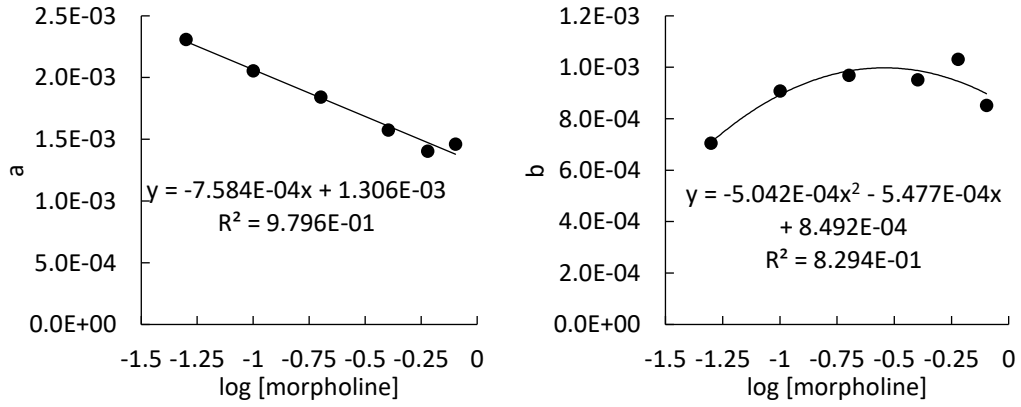

Conductance of propylaminium bromide (13·HBr) in acetonitrile.

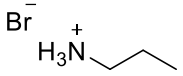

13·HBr

13·HBr and propylamine (**13**, 0.001 M) in acetonitrile at 20 °C.

[13·HBr] (mol L^{-1})	*G* (μS)
0	0.013
3.997×10^{-5}	0.054
9.980×10^{-5}	0.100
1.992×10^{-4}	0.174
2.982×10^{-4}	0.244
3.968×10^{-4}	0.309
4.950×10^{-4}	0.365
5.929×10^{-4}	0.422
9.804×10^{-4}	0.621
1.362×10^{-3}	0.790
1.737×10^{-3}	0.936
2.107×10^{-3}	1.063
2.471×10^{-3}	1.186
2.830×10^{-3}	1.290
3.184×10^{-3}	1.391
3.532×10^{-3}	1.482

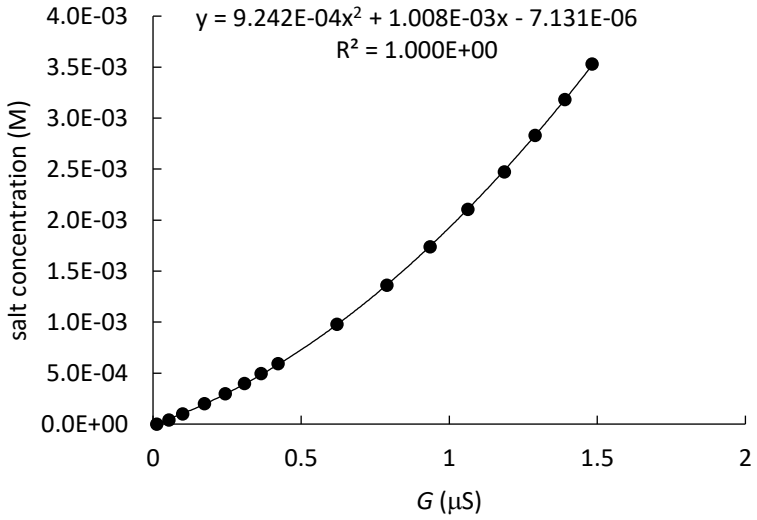

13·HBr and propylamine (**13**, 0.2 M) in acetonitrile at 20 °C.

[13·HBr] (mol L^{-1})	*G* (μS)
0	0.068
3.997×10^{-5}	0.097
9.980×10^{-5}	0.145
1.992×10^{-4}	0.225
2.982×10^{-4}	0.290
3.968×10^{-4}	0.359
4.950×10^{-4}	0.433
5.929×10^{-4}	0.492
9.804×10^{-4}	0.728

1.362×10^{-3}	0.935
1.737×10^{-3}	1.119
2.107×10^{-3}	1.294
2.471×10^{-3}	1.450
2.830×10^{-3}	1.596
3.184×10^{-3}	1.729
3.532×10^{-3}	1.850

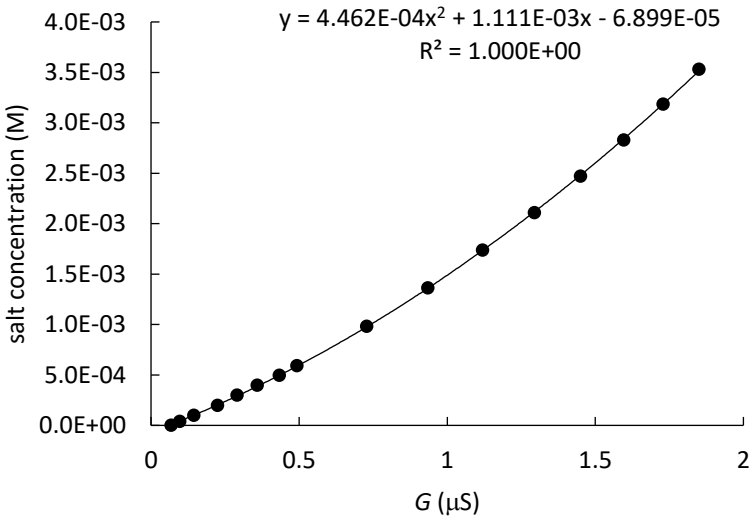

13·HBr and propylamine (**13**, 0.5 M) in acetonitrile at 20 °C.

[13·HBr] (mol L^{-1})	*G* (μS)
0	0.145
3.997×10^{-5}	0.174
9.980×10^{-5}	0.215
1.992×10^{-4}	0.289
2.982×10^{-4}	0.361
3.968×10^{-4}	0.436
4.950×10^{-4}	0.497
5.929×10^{-4}	0.567
9.804×10^{-4}	0.804
1.362×10^{-3}	1.018
1.737×10^{-3}	1.215
2.107×10^{-3}	1.397
2.471×10^{-3}	1.571
2.830×10^{-3}	1.733
3.184×10^{-3}	1.885

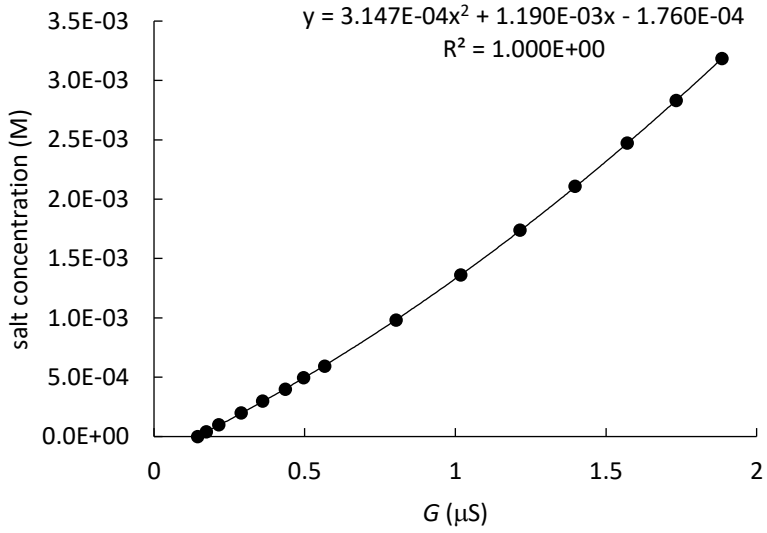

13·HBr and propylamine (**13**, 1.0 M) in acetonitrile at 20 °C.

[13·HBr] (mol L^{-1})	*G* (μS)
0	0.262
3.997×10^{-5}	0.287
9.980×10^{-5}	0.331
1.992×10^{-4}	0.396
2.982×10^{-4}	0.465
3.968×10^{-4}	0.530
4.950×10^{-4}	0.597
5.929×10^{-4}	0.656
9.843×10^{-4}	0.895
1.373×10^{-3}	1.112
1.758×10^{-3}	1.320
2.140×10^{-3}	1.506
2.519×10^{-3}	1.685
2.896×10^{-3}	1.859

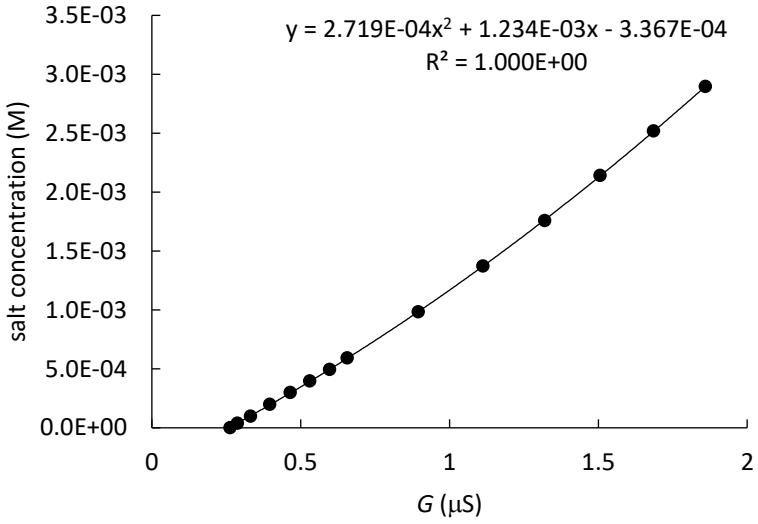

13·HBr and propylamine (**13**, 2.0 M) in acetonitrile at 20 °C.

[13·HBr] (mol L^{-1})	*G* (μS)
0	0.464
3.997×10^{-5}	0.492
9.980×10^{-5}	0.530
1.992×10^{-4}	0.595
2.982×10^{-4}	0.658
3.968×10^{-4}	0.724
4.950×10^{-4}	0.773
5.929×10^{-4}	0.829
9.843×10^{-4}	1.059
1.373×10^{-3}	1.261
1.758×10^{-3}	1.466
2.140×10^{-3}	1.653
2.519×10^{-3}	1.831

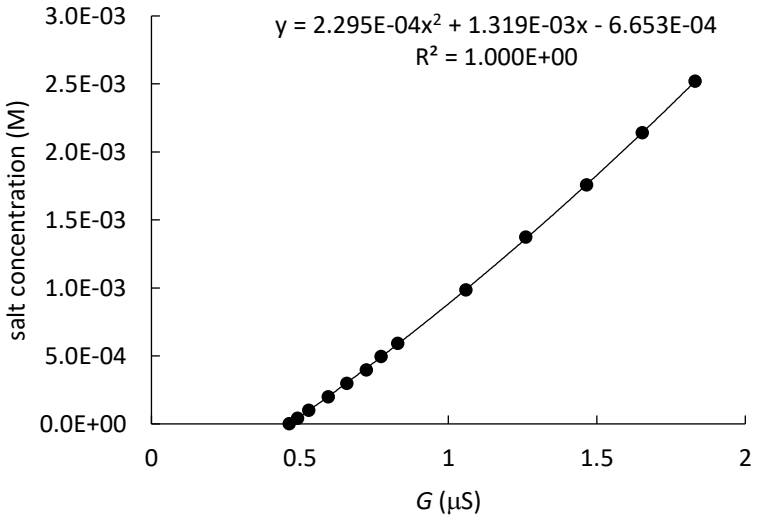

For propylaminium hydrobromides (**13·HBr**) not all necessary propylamine concentrations had to be experimentally determined, as the remaining could be interpolated with the following plots. The employed, second order polynomials ($y=ax^2+bx+c$) have three different parameters a, b and c. Parameter a and b could be interpolated with a linear correlation of the plot of the logarithm of the propylamine concentration versus a or b respectively. Parameter c could be interpolated by a linear correlation of the plot of the propylamine concentration versus c. The resulting linear correlations were used to calculate the interpolated parameters.

Parameters a, b and c for **13·HBr** in propylamine (**13**) in acetonitrile at 20 °C.

[13] (mol L^{-1})	log **[13]**	a	b	c	Interpolated?
0.001	−3.000	9.684×10^{-4}	9.196×10^{-4}	-8.415×10^{-6}	No
0.2	−0.6990	7.694×10^{-4}	9.740×10^{-4}	-1.469×10^{-5}	No
0.5	−0.3010	6.472×10^{-4}	9.668×10^{-4}	-1.892×10^{-5}	No
1.0	0.000	4.052×10^{-4}	1.104×10^{-3}	-6.373×10^{-5}	No
2.0	0.3010	7.201×10^{-4}	9.843×10^{-4}	-1.646×10^{-5}	No
0.02		6.438×10^{-4}	9.063×10^{-4}	-1.340×10^{-5}	Yes
0.04		5.790×10^{-4}	9.670×10^{-4}	-2.000×10^{-5}	Yes
0.06		5.411×10^{-4}	1.003×10^{-3}	-2.659×10^{-5}	Yes
0.08		5.142×10^{-4}	1.028×10^{-3}	-3.319×10^{-5}	Yes
0.25		4.076×10^{-4}	1.128×10^{-3}	-8.924×10^{-5}	Yes
0.3		3.906×10^{-4}	1.144×10^{-3}	-1.057×10^{-4}	Yes
0.4		3.637×10^{-4}	1.169×10^{-3}	-1.387×10^{-4}	Yes
0.6		3.258×10^{-4}	1.204×10^{-3}	-2.046×10^{-4}	Yes
0.75		3.049×10^{-4}	1.224×10^{-3}	-2.541×10^{-4}	Yes
0.8		2.989×10^{-4}	1.229×10^{-3}	-2.706×10^{-4}	Yes
0.9		2.879×10^{-4}	1.240×10^{-3}	-3.035×10^{-4}	Yes
1.2		2.610×10^{-4}	1.265×10^{-3}	-4.025×10^{-4}	Yes
1.5		2.401×10^{-4}	1.285×10^{-3}	-5.014×10^{-4}	Yes

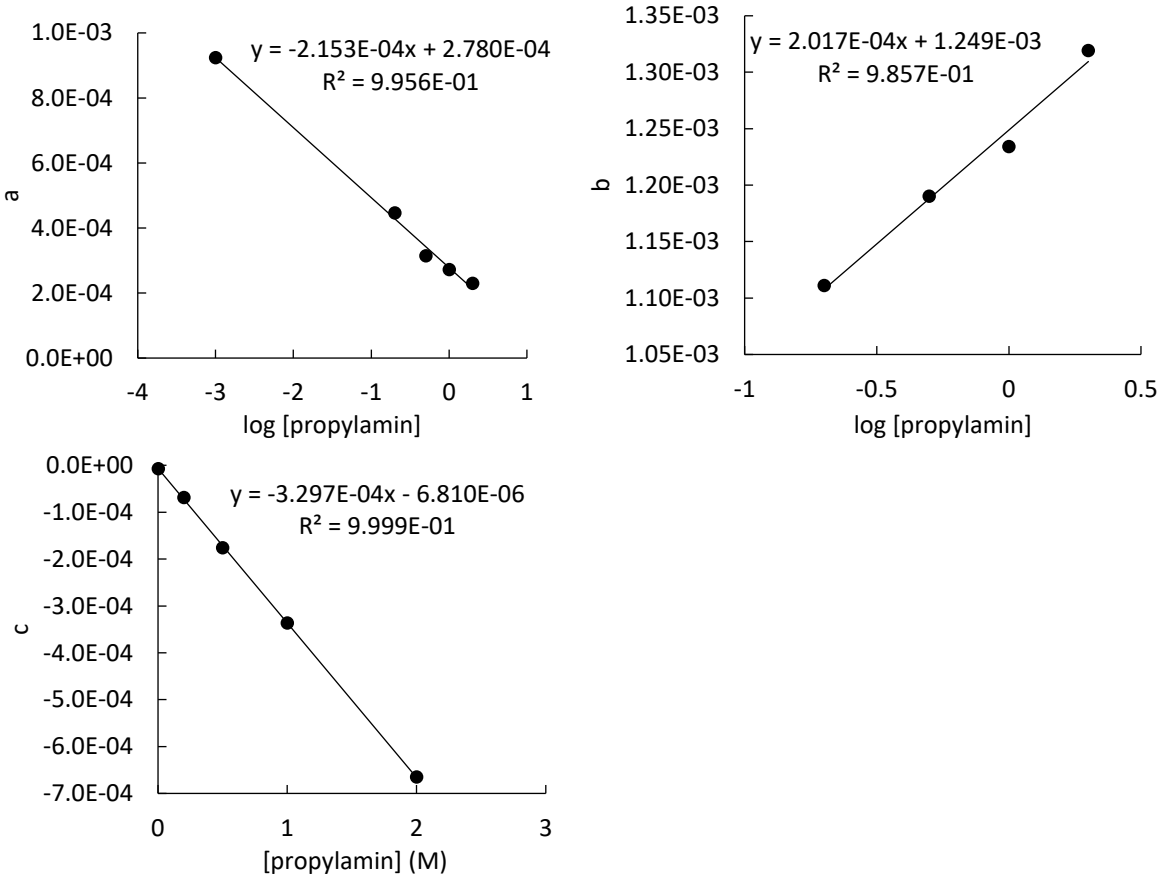

Conductance of *N*,*N*,*N*-triethyl-1-(4-methoxyphenyl)ethan-1-aminium bromide (14e) in acetonitrile.

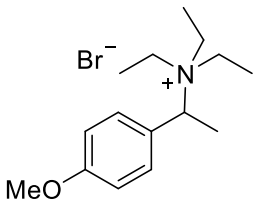

14e

14e and NEt_3 (0.025 M) in acetonitrile at 20 °C.

[14e] (mol L^{-1})	*G* (μS)
0	0.006
3.137×10^{-5}	0.042
7.832×10^{-5}	0.076
1.563×10^{-4}	0.135
2.340×10^{-4}	0.188
3.114×10^{-4}	0.237
3.885×10^{-4}	0.283
4.653×10^{-4}	0.326

7.694×10^{-4}	0.489
1.069×10^{-3}	0.632
1.364×10^{-3}	0.766
1.654×10^{-3}	0.897
1.940×10^{-3}	1.021
2.221×10^{-3}	1.135
2.498×10^{-3}	1.251
2.772×10^{-3}	1.361

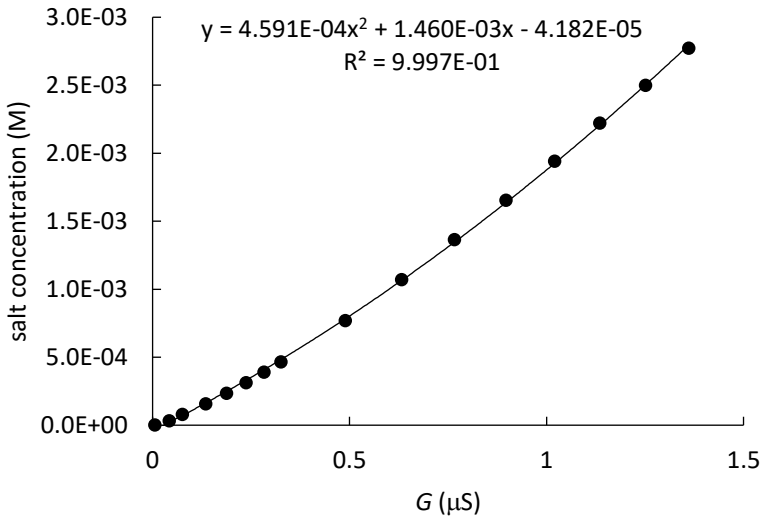

14e and NEt_3 (0.04 M) in acetonitrile at 20 °C.

[14e] (mol L^{-1})	*G* (μS)
0	0.01
3.137×10^{-5}	0.038
7.832×10^{-5}	0.08
1.563×10^{-4}	0.139
2.340×10^{-4}	0.189
3.114×10^{-4}	0.242
3.885×10^{-4}	0.283
4.653×10^{-4}	0.331
7.694×10^{-4}	0.488
1.069×10^{-3}	0.633
1.364×10^{-3}	0.772
1.654×10^{-3}	0.9
1.940×10^{-3}	1.027
2.221×10^{-3}	1.137
2.498×10^{-3}	1.254
2.772×10^{-3}	1.364

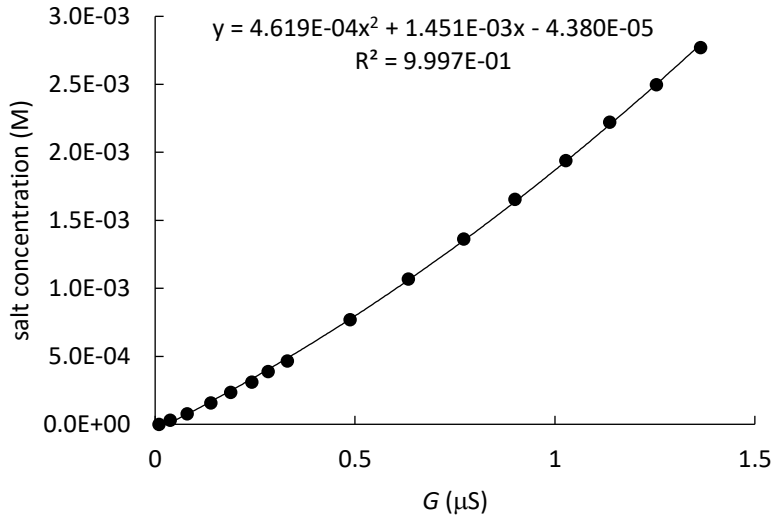

14e and NEt_3 (0.1 M) in acetonitrile at 20 °C.

[14e] (mol L^{-1})	*G* (μS)
0	0.017
3.137×10^{-5}	0.044
7.832×10^{-5}	0.085
1.563×10^{-4}	0.143
2.340×10^{-4}	0.191
3.114×10^{-4}	0.238
3.885×10^{-4}	0.286
4.653×10^{-4}	0.327
7.694×10^{-4}	0.483
1.069×10^{-3}	0.627
1.364×10^{-3}	0.765
1.654×10^{-3}	0.895
1.940×10^{-3}	1.019
2.221×10^{-3}	1.131
2.498×10^{-3}	1.242
2.772×10^{-3}	1.354

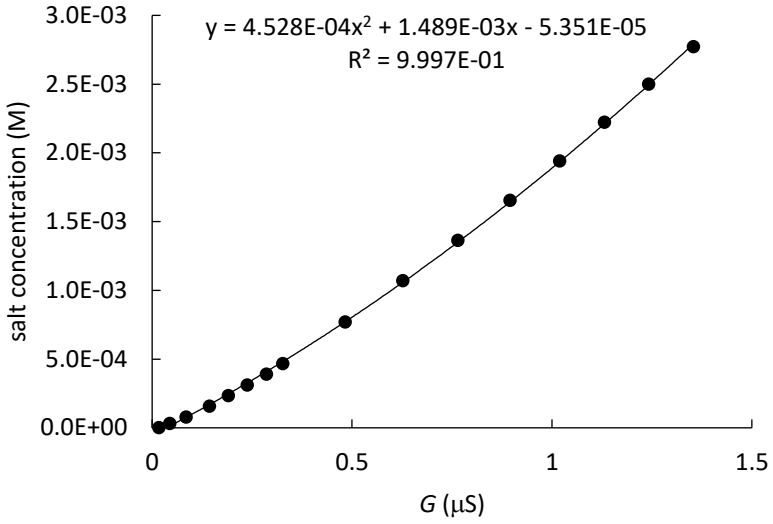

Conductance of 1,4-diazabicyclo[2.2.2]octan-1-ium chloride (9·HCl) in acetonitrile/methanol solutions.

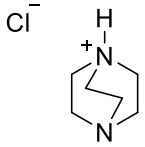

9·HCl

9·HCl and methanol (10% (v/v)) in acetonitrile at 20 °C.

[9·HCl] (mol L^{-1})	*G* (μS)
0	0.012
4.162×10^{-5}	0.051
1.039×10^{-4}	0.113
2.075×10^{-4}	0.216
3.106×10^{-4}	0.307
4.133×10^{-4}	0.385
5.155×10^{-4}	0.468
6.174×10^{-4}	0.548
1.021×10^{-3}	0.823
1.418×10^{-3}	1.070
1.809×10^{-3}	1.300
2.195×10^{-3}	1.507
2.574×10^{-3}	1.698
2.947×10^{-3}	1.875

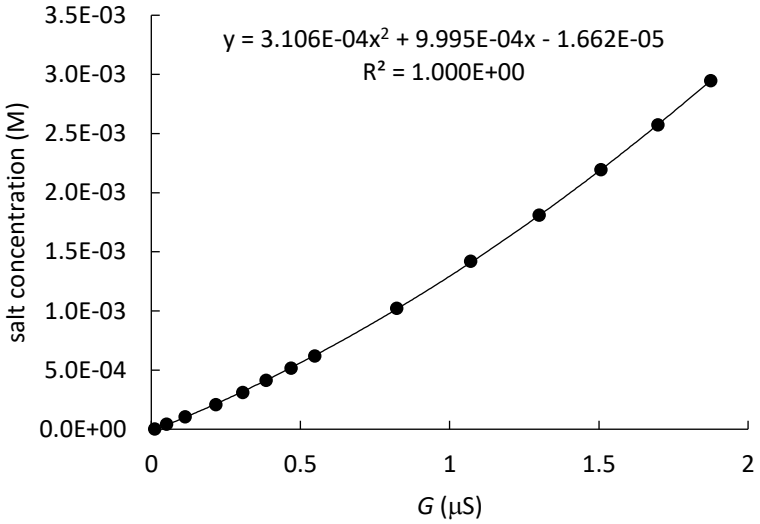

9·HCl and methanol (20% (v/v)) in acetonitrile at 20 °C.

[9·HCl] (mol L^{-1})	*G* (μS)
0	0.011
4.162×10^{-5}	0.052
1.039×10^{-4}	0.117
2.075×10^{-4}	0.212
3.106×10^{-4}	0.304
4.133×10^{-4}	0.393
5.155×10^{-4}	0.489
6.174×10^{-4}	0.573
1.021×10^{-3}	0.899
1.418×10^{-3}	1.199
1.809×10^{-3}	1.478
2.195×10^{-3}	1.744

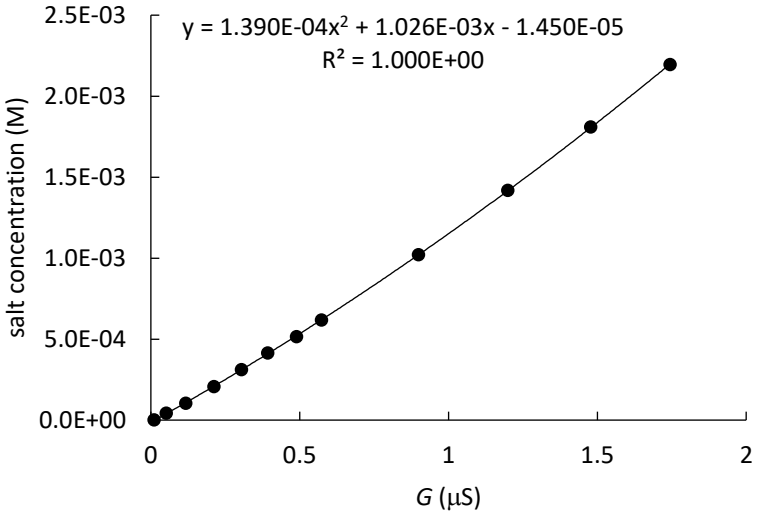

Conductance of pyrrolidinium chloride (10·HCl) in acetonitrile/methanol solutions.

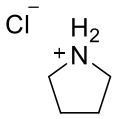

10·HCl

10·HCl and methanol (10% (v/v)) in acetonitrile at 20 °C.

[10·HCl] (mol L^{-1})	*G* (μS)
0	0.013
4.049×10^{-5}	0.054
1.011×10^{-4}	0.119
2.018×10^{-4}	0.221
3.021×10^{-4}	0.317
4.019×10^{-4}	0.412
5.014×10^{-4}	0.497
6.005×10^{-4}	0.584
9.933×10^{-4}	0.894
1.380×10^{-3}	1.175
1.761×10^{-3}	1.429
2.136×10^{-3}	1.664
2.505×10^{-3}	1.883

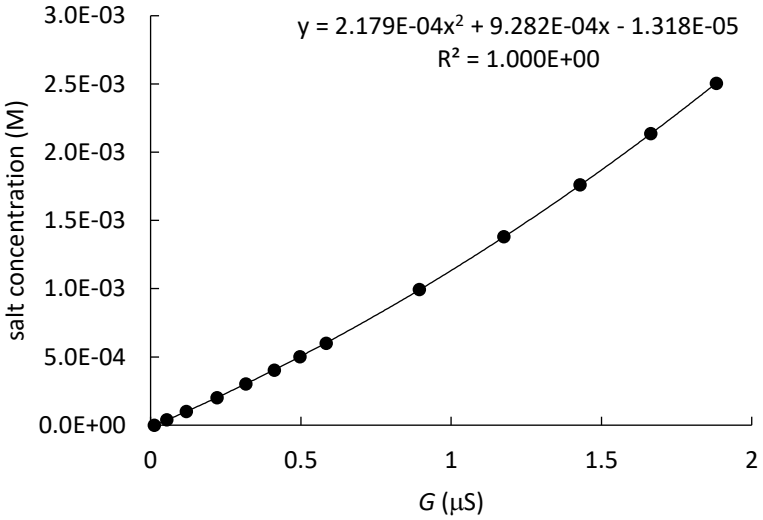

10·HCl and methanol (20% (v/v)) in acetonitrile at 20 °C.

[10·HCl] (mol L^{-1})	*G* (μS)
0	0.012
4.049×10^{-5}	0.055
1.011×10^{-4}	0.121
2.018×10^{-4}	0.227
3.021×10^{-4}	0.320
4.019×10^{-4}	0.423
5.014×10^{-4}	0.513
6.005×10^{-4}	0.607
9.933×10^{-4}	0.951
1.380×10^{-3}	1.272
1.761×10^{-3}	1.582
2.136×10^{-3}	1.869

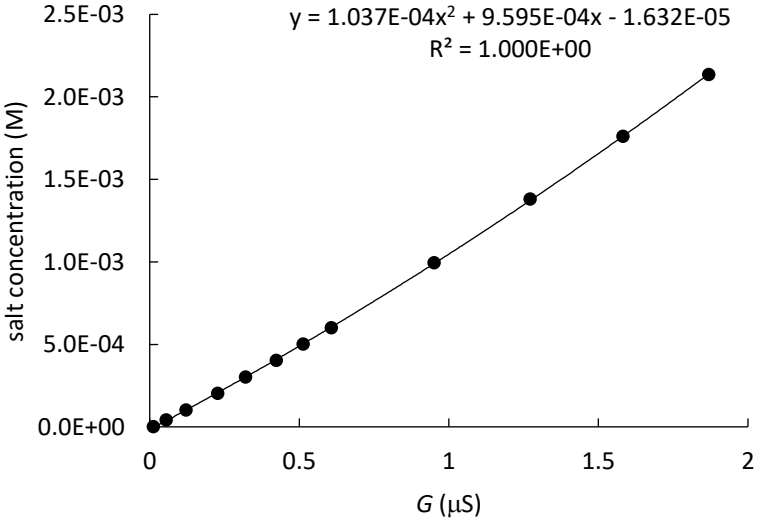

Conductance of piperidinium chloride (11·HCl) in acetonitrile/methanol solutions.

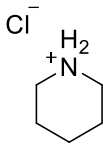

11·HCl

11·HCl and methanol (10% (v/v)) in acetonitrile at 20 °C.

[11·HCl] (mol L^{-1})	*G* (μS)
0	0.012
3.997×10^{-5}	0.051
9.980×10^{-5}	0.126
1.992×10^{-4}	0.221
2.982×10^{-4}	0.316
3.968×10^{-4}	0.399
4.950×10^{-4}	0.494
5.929×10^{-4}	0.565
9.804×10^{-4}	0.873
1.362×10^{-3}	1.145
1.737×10^{-3}	1.395
2.107×10^{-3}	1.626
2.471×10^{-3}	1.838

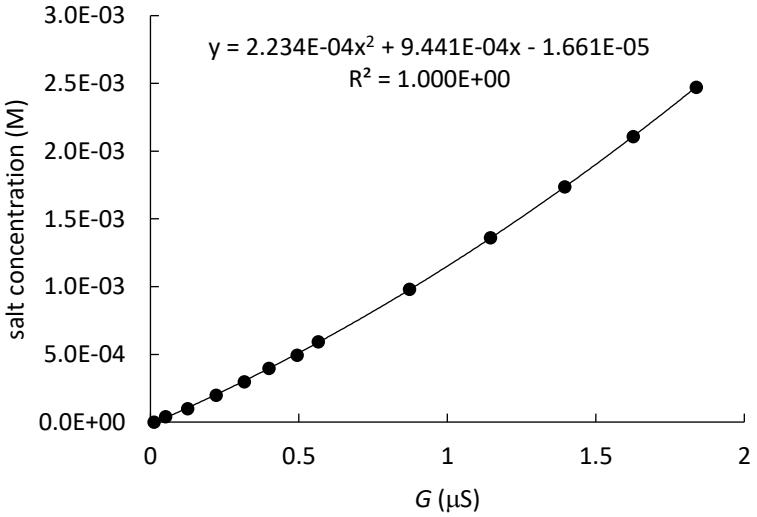

11·HCl and methanol (20% (v/v)) in acetonitrile at 20 °C.

[11·HCl] (mol L^{-1})	*G* (μS)
0	0.011
3.997×10^{-5}	0.052
9.980×10^{-5}	0.115
1.992×10^{-4}	0.220
2.982×10^{-4}	0.315
3.968×10^{-4}	0.414
4.950×10^{-4}	0.501
5.929×10^{-4}	0.591
9.804×10^{-4}	0.936
1.362×10^{-3}	1.249
1.737×10^{-3}	1.543
2.107×10^{-3}	1.827

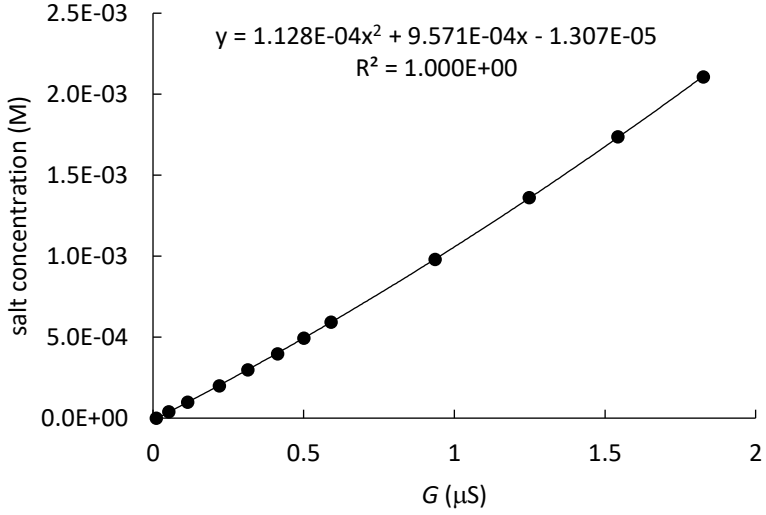

Conductance of morpholinium chloride (12·HCl) in acetonitrile/methanol solutions.

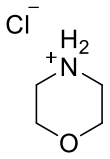

12·HCl

12·HCl and methanol (10% (v/v)) in acetonitrile at 20 °C.

[12·HCl] (mol L^{-1})	*G* (μS)
0	0.011
3.997×10^{-5}	0.049
9.980×10^{-5}	0.103
1.992×10^{-4}	0.193
2.982×10^{-4}	0.282
3.968×10^{-4}	0.361
4.950×10^{-4}	0.435
5.929×10^{-4}	0.506
9.804×10^{-4}	0.772
1.362×10^{-3}	1.004
1.737×10^{-3}	1.215
2.107×10^{-3}	1.401
2.471×10^{-3}	1.579
2.830×10^{-3}	1.742
3.184×10^{-3}	1.899

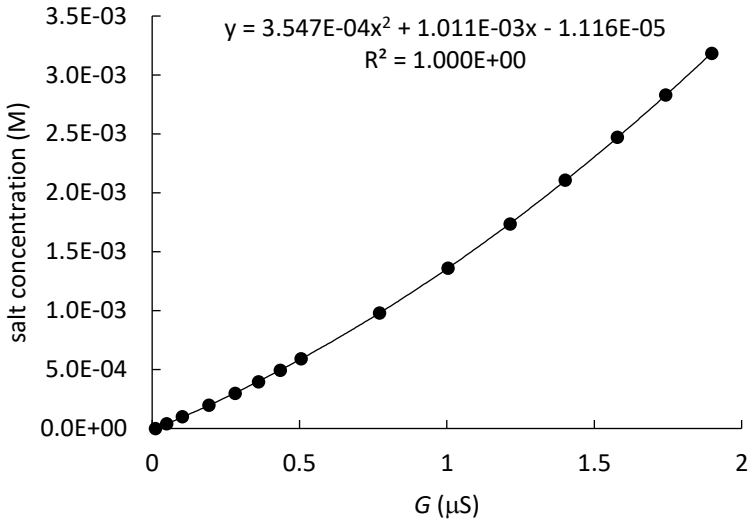

12·HCl and methanol (20% (v/v)) in acetonitrile at 20 °C.

[12·HCl] (mol L^{-1})	*G* (μS)
0	0.013
3.997×10^{-5}	0.042
9.980×10^{-5}	0.106
1.992×10^{-4}	0.199
2.982×10^{-4}	0.290

3.968×10^{-4}	0.383
4.950×10^{-4}	0.462
5.929×10^{-4}	0.550
9.804×10^{-4}	0.855
1.362×10^{-3}	1.145
1.737×10^{-3}	1.409
2.107×10^{-3}	1.653
2.471×10^{-3}	1.885

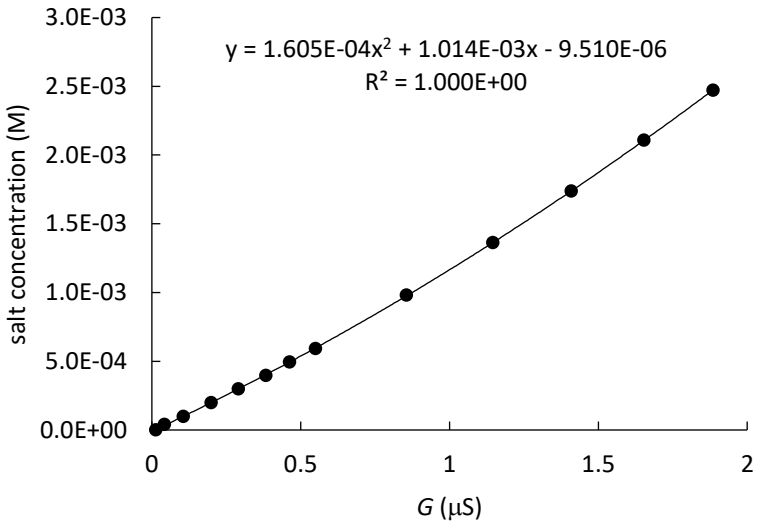

Conductance of propylaminium chloride (13·HCl) in acetonitrile/methanol solutions.

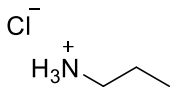

13·HCl

13·HCl and methanol (10% (v/v)) in acetonitrile at 20 °C.

[13·HCl] (mol L^{-1})	*G* (μS)
0	0.011
4.638×10^{-5}	0.059
1.158×10^{-4}	0.129
2.312×10^{-4}	0.238
3.460×10^{-4}	0.342
4.605×10^{-4}	0.444
5.745×10^{-4}	0.545
6.880×10^{-4}	0.644
1.138×10^{-3}	0.997
1.580×10^{-3}	1.317
2.016×10^{-3}	1.604
2.445×10^{-3}	1.872

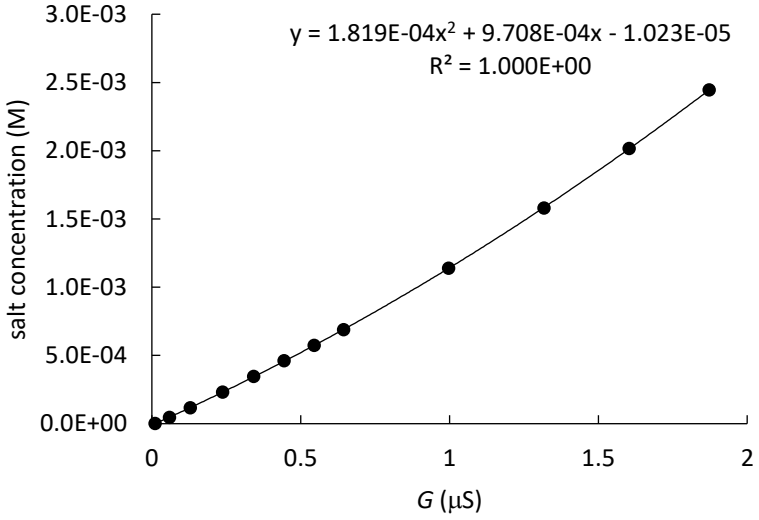

13·HCl and methanol (20% (v/v)) in acetonitrile at 20 °C.

[13·HCl] (mol L^{-1})	*G* (μS)
0	0.015
4.638×10^{-5}	0.061
1.158×10^{-4}	0.140
2.312×10^{-4}	0.255
3.460×10^{-4}	0.359
4.605×10^{-4}	0.465
5.745×10^{-4}	0.563
6.880×10^{-4}	0.666
1.138×10^{-3}	1.050
1.580×10^{-3}	1.394
2.016×10^{-3}	1.729

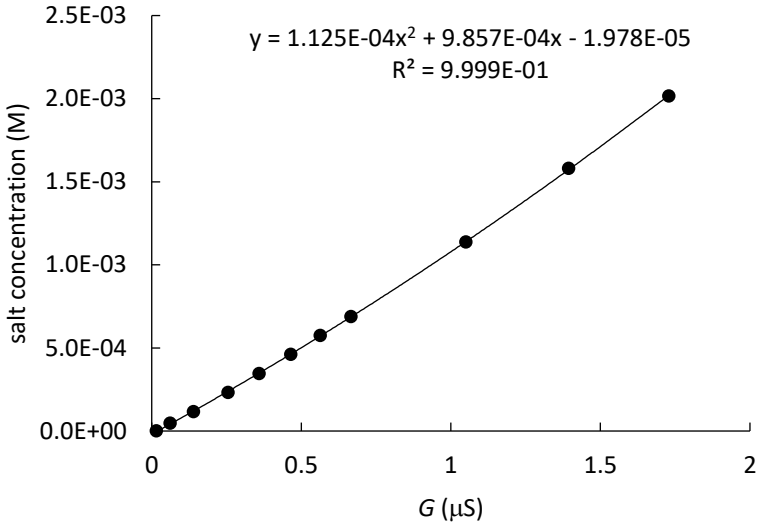

Conductance of triethylaminium chloride ($HNEt_3Cl$) in acetonitrile/methanol solutions.

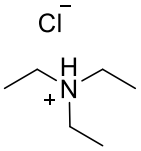

$HNEt_3Cl$

$HNEt_3Cl$ and methanol (10% (v/v)) in acetonitrile at 20 °C.

[$HNEt_3Cl$] (mol L^{-1})	*G* (μS)
0	0.012
4.855×10^{-5}	0.054
1.212×10^{-4}	0.114
2.420×10^{-4}	0.222
3.623×10^{-4}	0.314
4.821×10^{-4}	0.408
6.014×10^{-4}	0.491
7.202×10^{-4}	0.571
1.191×10^{-3}	0.854
1.654×10^{-3}	1.108
2.111×10^{-3}	1.339
2.560×10^{-3}	1.552
3.002×10^{-3}	1.737

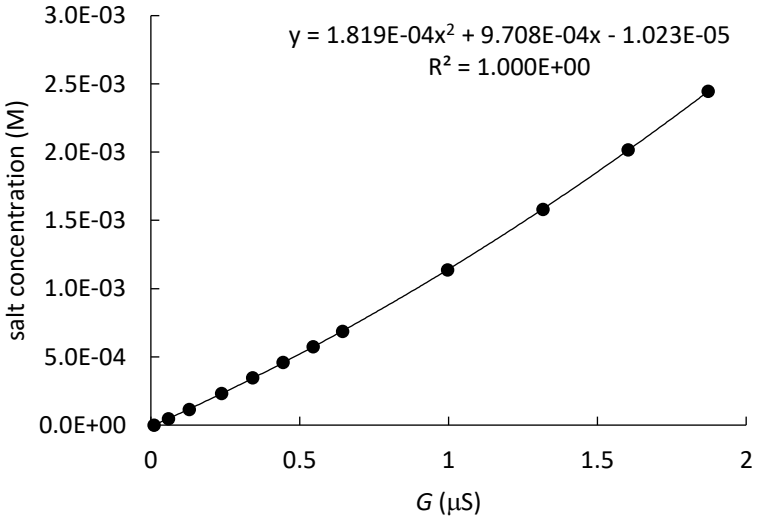

$HNEt_3Cl$ and methanol (20% (v/v)) in acetonitrile at 20 °C.

[$HNEt_3Cl$], (mol L^{-1})	*G* (μS)
0	0.013
4.855×10^{-5}	0.057
1.212×10^{-4}	0.135
2.420×10^{-4}	0.246
3.623×10^{-4}	0.355
4.821×10^{-4}	0.472
6.014×10^{-4}	0.570
7.202×10^{-4}	0.675
1.191×10^{-3}	1.046
1.654×10^{-3}	1.385
2.111×10^{-3}	1.698

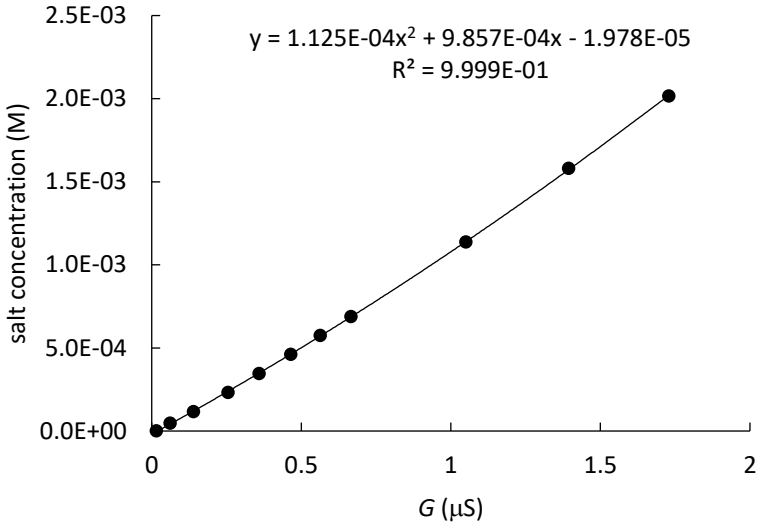

Conductance of pyrrolidinium tosylate (10·HOTs) in acetonitrile.

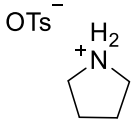

10·HOTs

10·HOTs and pyrrolidine (**10**, 0.1 M) in acetonitrile at 20 °C.

[10·HOTs] (mol L^{-1})	*G* (μS)
0	0.013
3.946×10^{-5}	0.047
9.854×10^{-5}	0.097
1.967×10^{-4}	0.181
2.945×10^{-4}	0.253
3.918×10^{-4}	0.326
4.888×10^{-4}	0.393
5.854×10^{-4}	0.463
9.680×10^{-4}	0.688
1.345×10^{-3}	0.893
1.716×10^{-3}	1.073
2.081×10^{-3}	1.232
2.440×10^{-3}	1.381
2.795×10^{-3}	1.517
3.143×10^{-3}	1.648
3.487×10^{-3}	1.763

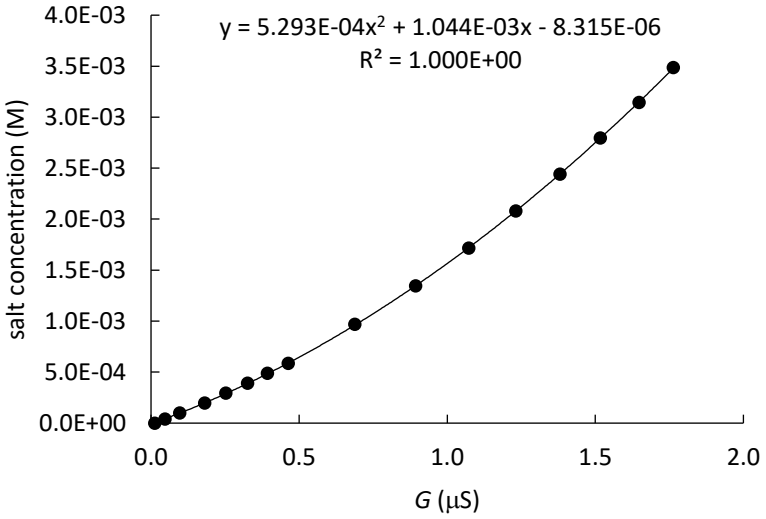

10·HOTs and pyrrolidine (**10**, 0.2 M) in acetonitrile at 20 °C.

[10·HOTs] (mol L^{-1})	*G* (μS)
0	0.014
3.946×10^{-5}	0.043
9.854×10^{-5}	0.094
1.967×10^{-4}	0.180
2.945×10^{-4}	0.253
3.918×10^{-4}	0.332
4.888×10^{-4}	0.398

5.854×10^{-4}	0.474
9.680×10^{-4}	0.714
1.345×10^{-3}	0.937
1.716×10^{-3}	1.137
2.081×10^{-3}	1.313
2.440×10^{-3}	1.478
2.795×10^{-3}	1.634
3.143×10^{-3}	1.780

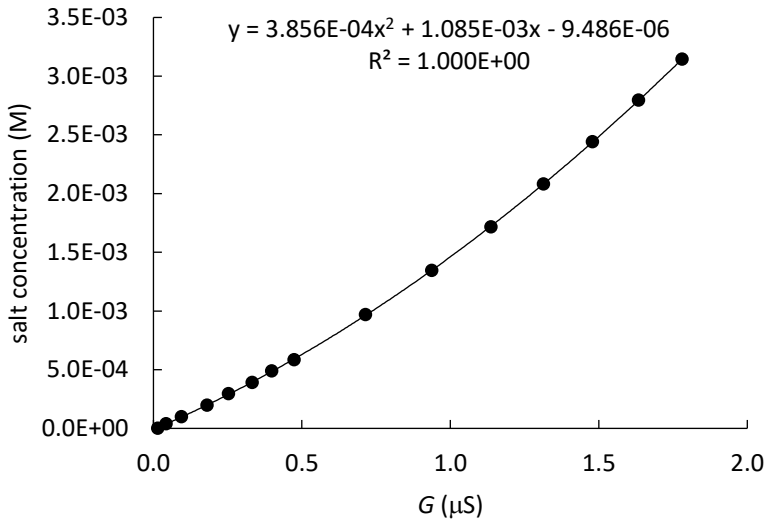

10·HOTs and pyrrolidine (**10**, 0.3 M) in acetonitrile at 20 °C.

[10·HOTs] (mol L^{-1})	*G* (μS)
0	0.018
3.946×10^{-5}	0.047
9.854×10^{-5}	0.098
1.967×10^{-4}	0.179
2.945×10^{-4}	0.260
3.918×10^{-4}	0.336
4.888×10^{-4}	0.408
5.854×10^{-4}	0.477
9.680×10^{-4}	0.729
1.345×10^{-3}	0.961
1.716×10^{-3}	1.167
2.081×10^{-3}	1.355
2.440×10^{-3}	1.532
2.795×10^{-3}	1.700
3.143×10^{-3}	1.852

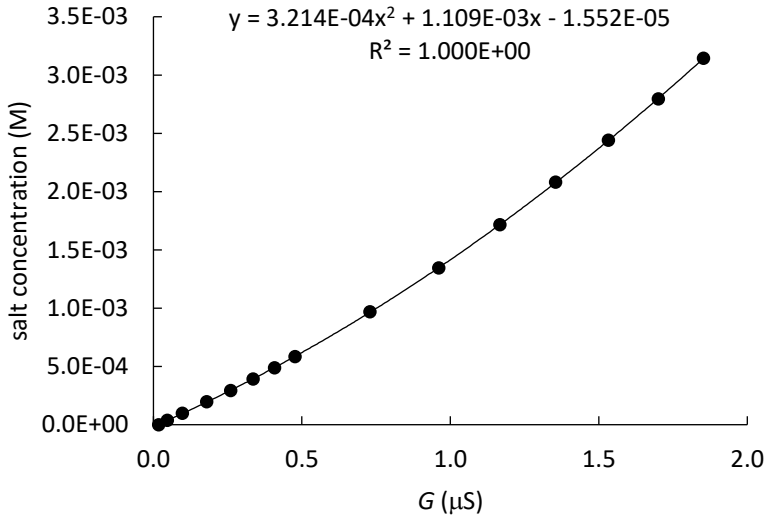

10·HOTs and pyrrolidine (**10**, 0.4 M) in acetonitrile at 20 °C.

[10·HOTs] (mol L^{-1})	*G* (μS)
0	0.019
3.946×10^{-5}	0.049
9.854×10^{-5}	0.098
1.967×10^{-4}	0.181
2.945×10^{-4}	0.264
3.918×10^{-4}	0.340
4.888×10^{-4}	0.412
5.854×10^{-4}	0.483
9.680×10^{-4}	0.741
1.345×10^{-3}	0.979
1.716×10^{-3}	1.192
2.081×10^{-3}	1.389
2.440×10^{-3}	1.573
2.795×10^{-3}	1.746
3.143×10^{-3}	1.905

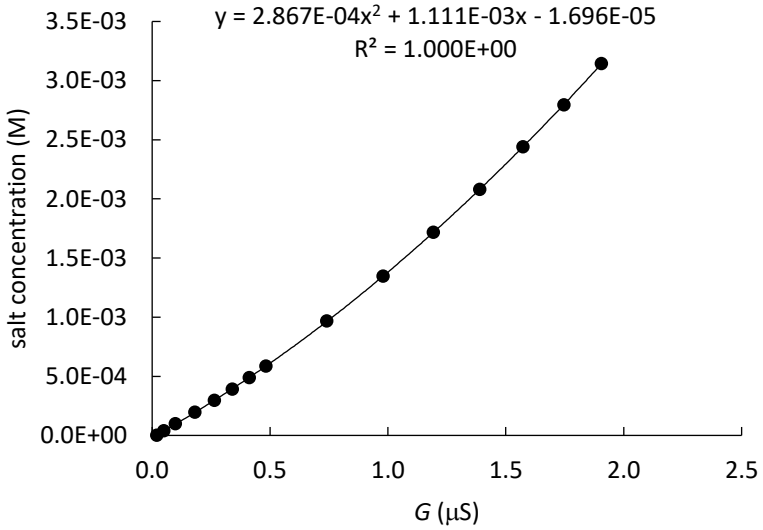

For pyrrolidinium tosylates (**10·HOTs**) the employed, second order polynomials ($y=ax^2+bx+c$) for correction have three different parameters a, b and c. These are summarized in the table below

Parameters a, b and c for **10·HOTs** in pyrrolidine (**10**) in acetonitrile at 20 °C.

[10] (mol L^{-1})	a	b	c
0.1	5.293×10^{-4}	1.044×10^{-3}	-8.315×10^{-6}
0.2	3.856×10^{-4}	1.085×10^{-3}	-9.486×10^{-6}
0.3	3.214×10^{-4}	1.109×10^{-3}	-1.552×10^{-5}
0.4	2.867×10^{-4}	1.111×10^{-3}	-1.696×10^{-5}

Conductance of piperidinium tosylate (11·HOTs) in acetonitrile.

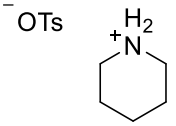

11·HOTs

11·HOTs and piperidine (**11**, 0.1 M) in acetonitrile at 20 °C.

[11·HOTs] (mol L^{-1})	*G* (μS)
0	0.015
3.946×10^{-5}	0.049
9.854×10^{-5}	0.094
1.967×10^{-4}	0.174
2.945×10^{-4}	0.238
3.918×10^{-4}	0.303
4.888×10^{-4}	0.359
5.854×10^{-4}	0.415
9.680×10^{-4}	0.604
1.345×10^{-3}	0.769
1.716×10^{-3}	0.918
2.081×10^{-3}	1.048
2.440×10^{-3}	1.165
2.795×10^{-3}	1.271
3.143×10^{-3}	1.372
3.487×10^{-3}	1.468
3.826×10^{-3}	1.554
4.159×10^{-3}	1.643
4.488×10^{-3}	1.717
4.812×10^{-3}	1.797

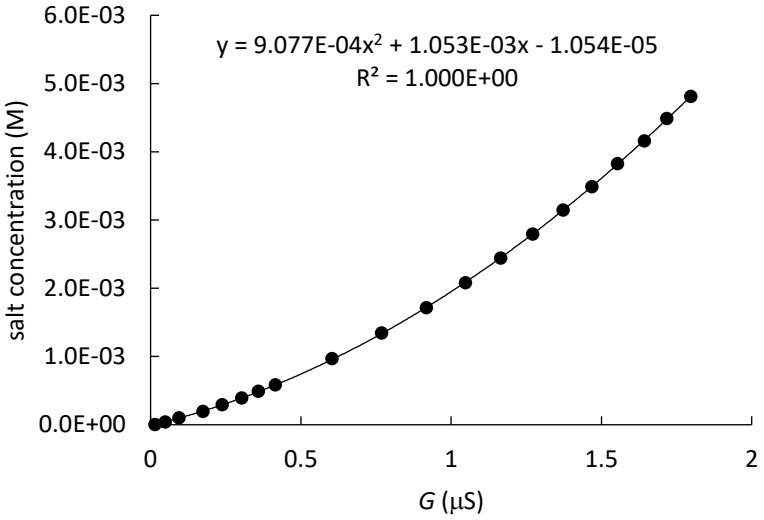

11·HOTs and piperidine (**11**, 0.2 M) in acetonitrile at 20 °C.

[11·HOTs] (mol L^{-1})	*G* (μS)
0	0.023
3.946×10^{-5}	0.051
9.854×10^{-5}	0.104
1.967×10^{-4}	0.172
2.945×10^{-4}	0.240

3.918×10^{-4}	0.303
4.888×10^{-4}	0.361
5.854×10^{-4}	0.423
9.680×10^{-4}	0.623
1.345×10^{-3}	0.801
1.716×10^{-3}	0.959
2.081×10^{-3}	1.100
2.440×10^{-3}	1.229
2.795×10^{-3}	1.348
3.143×10^{-3}	1.460
3.487×10^{-3}	1.563

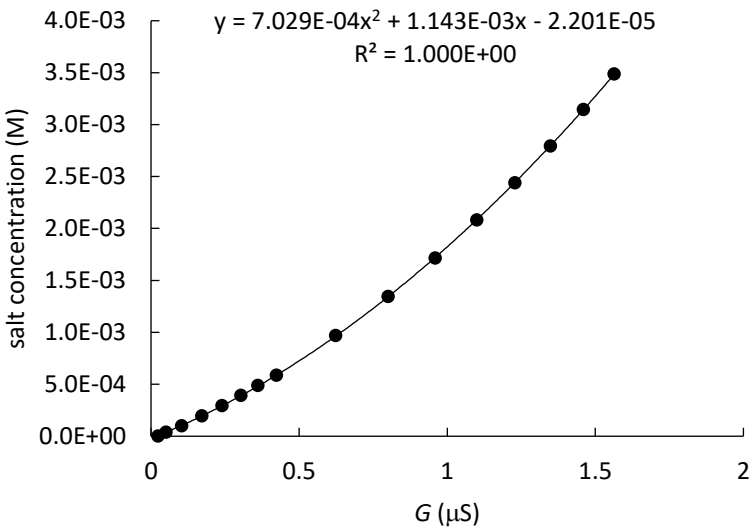

11·HOTs and piperidine (**11**, 0.4 M) in acetonitrile at 20 °C.

[11·HOTs] (mol L^{-1})	*G* (μS)
0	0.039
3.946×10^{-5}	0.063
9.854×10^{-5}	0.115
1.967×10^{-4}	0.182
2.945×10^{-4}	0.249
3.918×10^{-4}	0.312
4.888×10^{-4}	0.366
5.854×10^{-4}	0.428
9.680×10^{-4}	0.638
1.345×10^{-3}	0.821
1.716×10^{-3}	0.995
2.081×10^{-3}	1.147
2.440×10^{-3}	1.284
2.795×10^{-3}	1.415
3.143×10^{-3}	1.540
3.487×10^{-3}	1.652

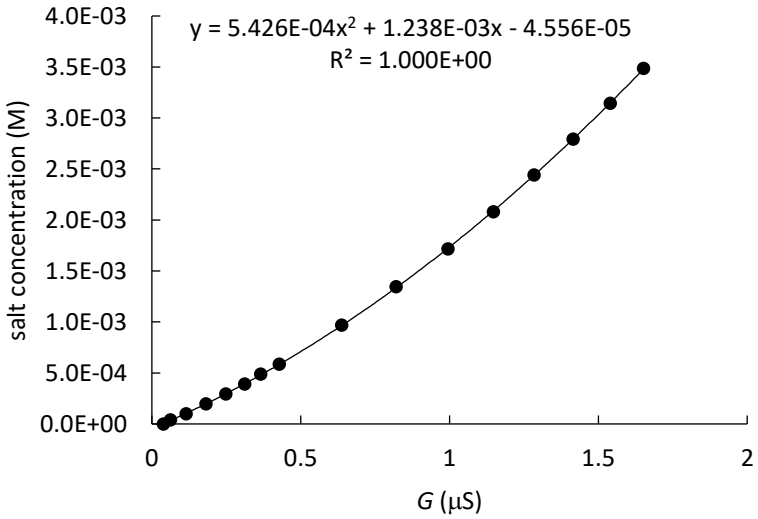

11·HOTs and piperidine (**11**, 0.4 M) in acetonitrile at 20 °C.

[11·HOTs] (mol L^{-1})	*G* (μS)
0	0.060
3.946×10^{-5}	0.087
9.854×10^{-5}	0.127
1.967×10^{-4}	0.197
2.945×10^{-4}	0.265
3.918×10^{-4}	0.322
4.888×10^{-4}	0.382
5.854×10^{-4}	0.438
9.680×10^{-4}	0.652
1.345×10^{-3}	0.846
1.716×10^{-3}	1.020
2.081×10^{-3}	1.177
2.440×10^{-3}	1.324
2.795×10^{-3}	1.458
3.143×10^{-3}	1.590
3.487×10^{-3}	1.711

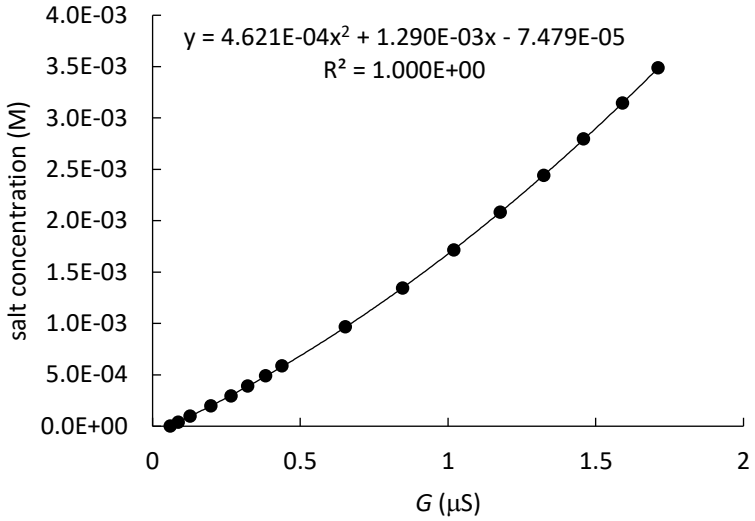

For piperidinium tosylates (**11·HOTs**) not all necessary piperidine concentrations had to be experimentally determined, as the remaining could be interpolated with the following plots. The employed, second order polynomials ($y=ax^2+bx+c$) have three different parameters a, b and c. Parameter a and b could be interpolated with a linear correlation of the plot of the logarithm of the piperidine concentration versus a or b respectively. Parameter c could be interpolated by a linear correlation of the plot of the piperidine concentration versus c. The resulting linear correlations were used to calculate the interpolated parameters.

Parameters a, b and c for **11·HOTs** in piperidine (**11**) in acetonitrile at 20 °C.

[11] (mol L^{-1})	log **[11]**	a	b	c	Interpolated?
0.1	−1.000	9.077×10^{-4}	1.053×10^{-3}	-1.054×10^{-5}	No
0.2	−0.6990	7.029×10^{-4}	1.143×10^{-3}	-2.201×10^{-5}	No
0.4	−0.3979	5.426×10^{-4}	1.238×10^{-3}	-4.556×10^{-5}	No
0.8	−0.09691	4.621×10^{-4}	1.290×10^{-3}	-7.479×10^{-5}	No
0.3		6.409×10^{-4}	1.190×10^{-3}	-3.138×10^{-5}	Yes
0.6		4.913×10^{-4}	1.271×10^{-3}	-5.868×10^{-5}	Yes

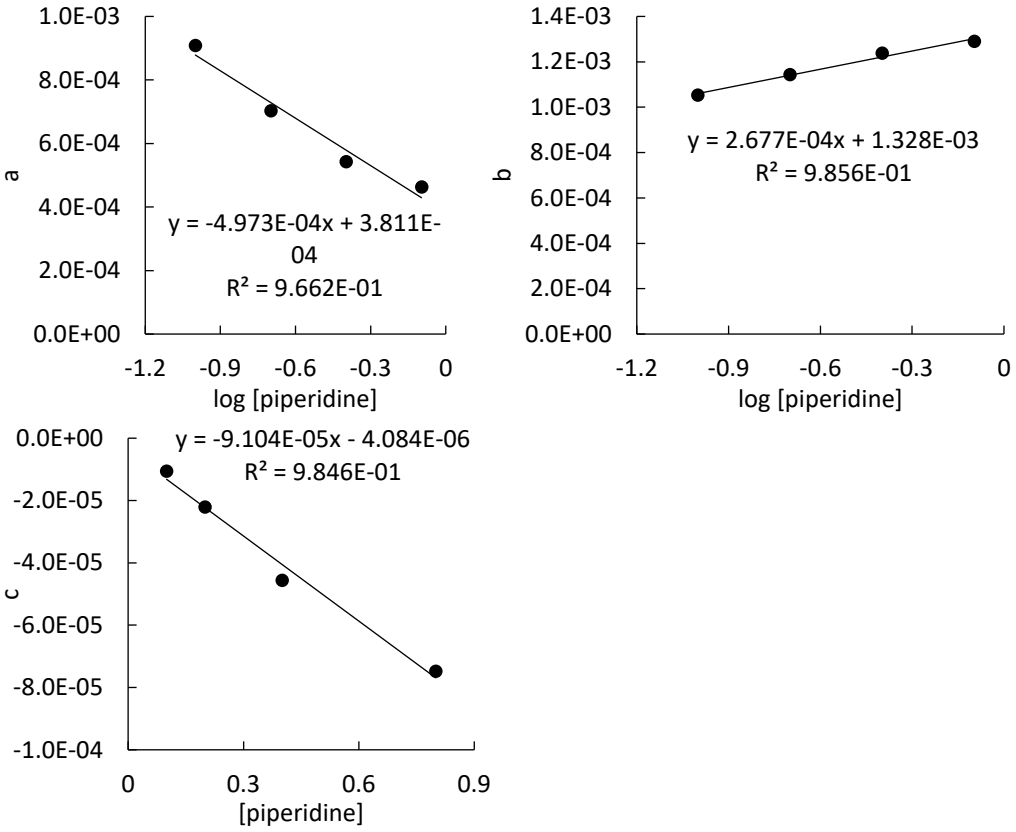

Conductance of morpholinium tosylate (12·HOTs) in acetonitrile.

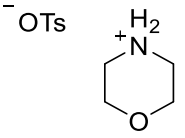

12·HOTs

12·HOTs and morpholine (**12**, 0.1 M) in acetonitrile at 20 °C.

[12·HOTs] (mol L^{-1})	G (μS)
0	0.004
3.946×10^{-5}	0.039
9.854×10^{-5}	0.080
1.967×10^{-4}	0.139
2.945×10^{-4}	0.188
3.918×10^{-4}	0.237
4.888×10^{-4}	0.276
5.854×10^{-4}	0.313
9.680×10^{-4}	0.444

1.345×10^{-3}	0.546
1.716×10^{-3}	0.642
2.081×10^{-3}	0.722
2.440×10^{-3}	0.800
2.795×10^{-3}	0.867
3.143×10^{-3}	0.925
3.487×10^{-3}	0.983
3.826×10^{-3}	1.036
4.159×10^{-3}	1.090
4.488×10^{-3}	1.139
4.812×10^{-3}	1.182
5.132×10^{-3}	1.227

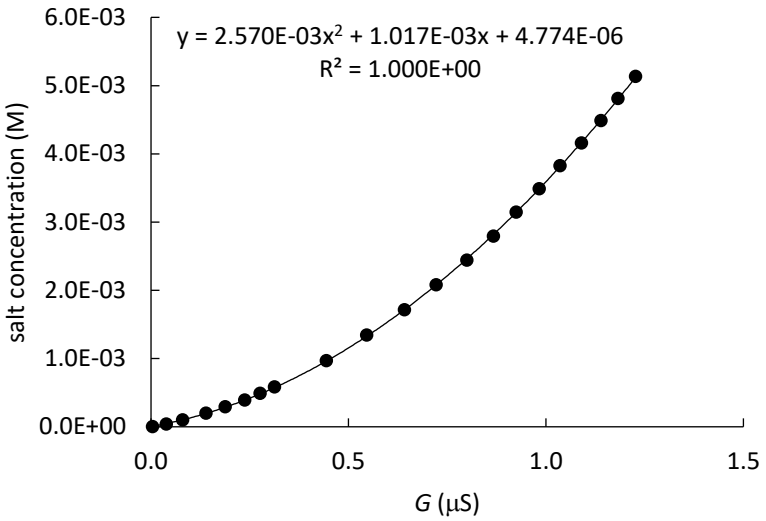

12·HOTs and morpholine (**12**, 0.2 M) in acetonitrile at 20 °C.

[12·HOTs] (mol L^{-1})	*G* (μS)
0	0.005
3.946×10^{-5}	0.035
9.854×10^{-5}	0.086
1.967×10^{-4}	0.146
2.945×10^{-4}	0.195
3.918×10^{-4}	0.244
4.888×10^{-4}	0.287
5.854×10^{-4}	0.326
9.680×10^{-4}	0.460
1.345×10^{-3}	0.569
1.716×10^{-3}	0.666
2.081×10^{-3}	0.757
2.440×10^{-3}	0.831
2.795×10^{-3}	0.903
3.143×10^{-3}	0.973
3.487×10^{-3}	1.028
3.826×10^{-3}	1.088
4.159×10^{-3}	1.144
4.488×10^{-3}	1.195
4.812×10^{-3}	1.246
5.132×10^{-3}	1.292

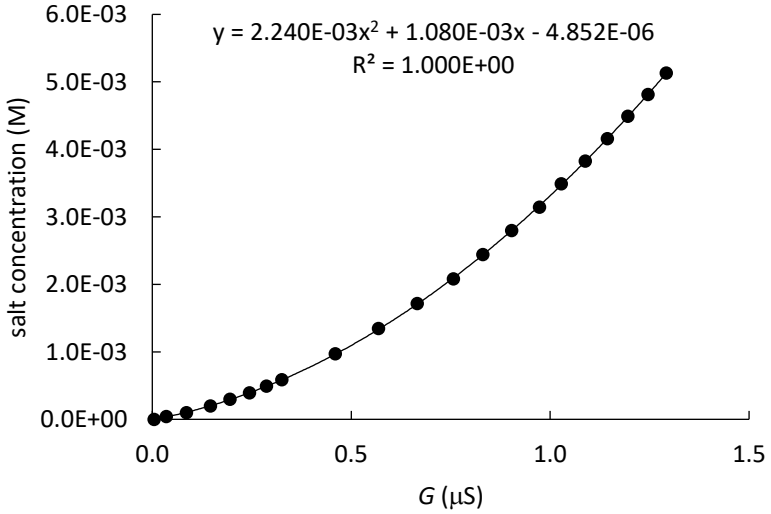

12·HOTs and morpholine (**12**, 0.3 M) in acetonitrile at 20 °C.

[12·HOTs] (mol L^{-1})	*G* (μS)
0	0.006
3.946×10^{-5}	0.035
9.854×10^{-5}	0.076
1.967×10^{-4}	0.142
2.945×10^{-4}	0.191
3.918×10^{-4}	0.240
4.888×10^{-4}	0.277
5.854×10^{-4}	0.322
9.680×10^{-4}	0.460
1.345×10^{-3}	0.580
1.716×10^{-3}	0.677
2.081×10^{-3}	0.765
2.440×10^{-3}	0.845
2.795×10^{-3}	0.927
3.143×10^{-3}	0.992
3.487×10^{-3}	1.058
3.826×10^{-3}	1.121
4.159×10^{-3}	1.174
4.488×10^{-3}	1.230
4.812×10^{-3}	1.280
5.132×10^{-3}	1.326

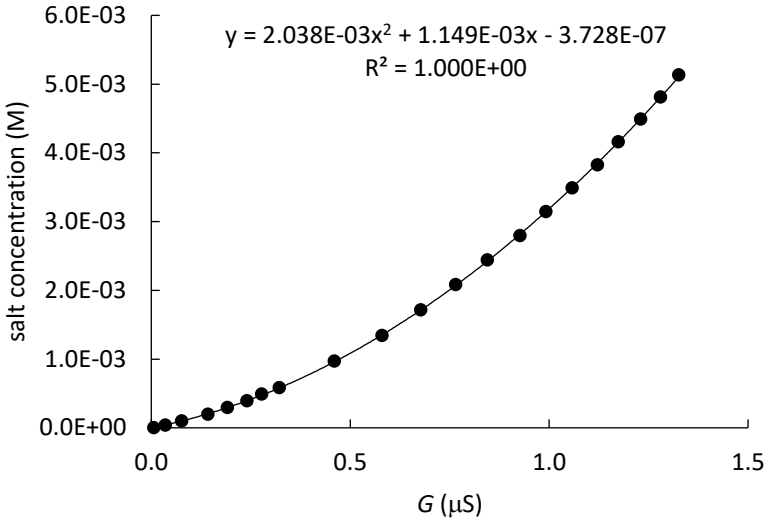

12·HOTs and morpholine (**12**, 0.4 M) in acetonitrile at 20 °C.

[12·HOTs] (mol L^{-1})	*G* (μS)
0	0.012
3.946×10^{-5}	0.032
9.854×10^{-5}	0.079
1.967×10^{-4}	0.137
2.945×10^{-4}	0.191
3.918×10^{-4}	0.237
4.888×10^{-4}	0.282
5.854×10^{-4}	0.327
9.680×10^{-4}	0.471

1.345×10^{-3}	0.585
1.716×10^{-3}	0.687
2.081×10^{-3}	0.779
2.440×10^{-3}	0.863
2.795×10^{-3}	0.942
3.143×10^{-3}	1.014
3.487×10^{-3}	1.077
3.826×10^{-3}	1.140
4.159×10^{-3}	1.199
4.488×10^{-3}	1.257
4.812×10^{-3}	1.310
5.132×10^{-3}	1.362

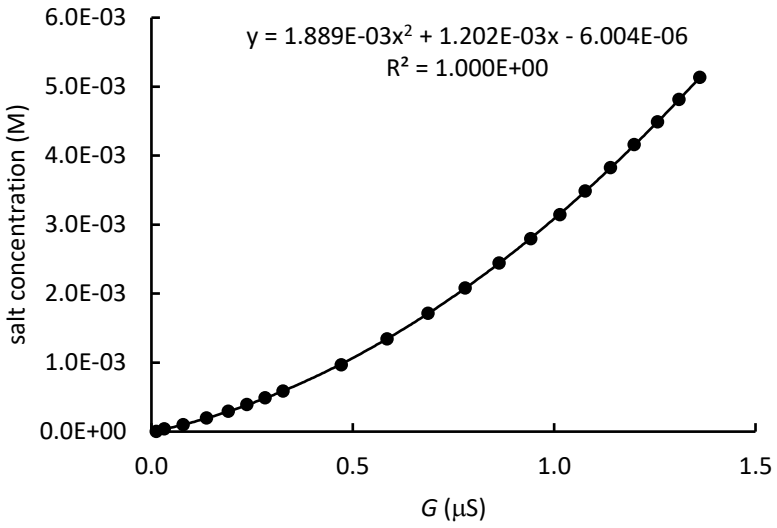

12·HOTs and morpholine (**12**, 0.6 M) in acetonitrile at 20 °C.

[12·HOTs] (mol L^{-1})	G (μS)
0	0.011
3.946×10^{-5}	0.035
9.854×10^{-5}	0.080
1.967×10^{-4}	0.140
2.945×10^{-4}	0.191
3.918×10^{-4}	0.241
4.888×10^{-4}	0.285
5.854×10^{-4}	0.330
9.680×10^{-4}	0.474
1.345×10^{-3}	0.591
1.716×10^{-3}	0.702
2.081×10^{-3}	0.794
2.440×10^{-3}	0.882
2.795×10^{-3}	0.963
3.143×10^{-3}	1.034
3.487×10^{-3}	1.102
3.826×10^{-3}	1.170
4.159×10^{-3}	1.232
4.488×10^{-3}	1.293
4.812×10^{-3}	1.346
5.132×10^{-3}	1.396

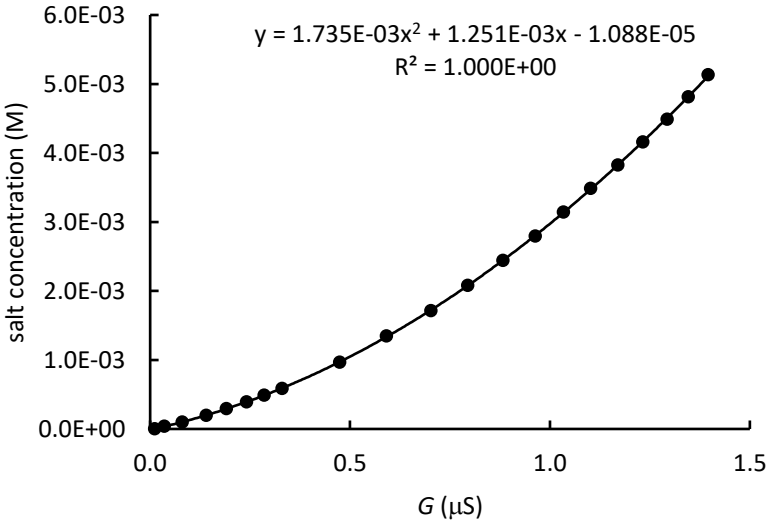

12·HOTs and morpholine (**12**, 0.6 M) in acetonitrile at 20 °C.

[12·HOTs] (mol L^{-1})	*G* (μS)
0	0.013
3.946×10^{-5}	0.034
9.854×10^{-5}	0.074
1.967×10^{-4}	0.139
2.945×10^{-4}	0.189
3.918×10^{-4}	0.234
4.888×10^{-4}	0.282
5.854×10^{-4}	0.321
9.680×10^{-4}	0.472
1.345×10^{-3}	0.592
1.716×10^{-3}	0.697
2.081×10^{-3}	0.798
2.440×10^{-3}	0.884
2.795×10^{-3}	0.963
3.143×10^{-3}	1.039
3.487×10^{-3}	1.108
3.826×10^{-3}	1.172
4.159×10^{-3}	1.237
4.488×10^{-3}	1.297
4.812×10^{-3}	1.354
5.132×10^{-3}	1.406

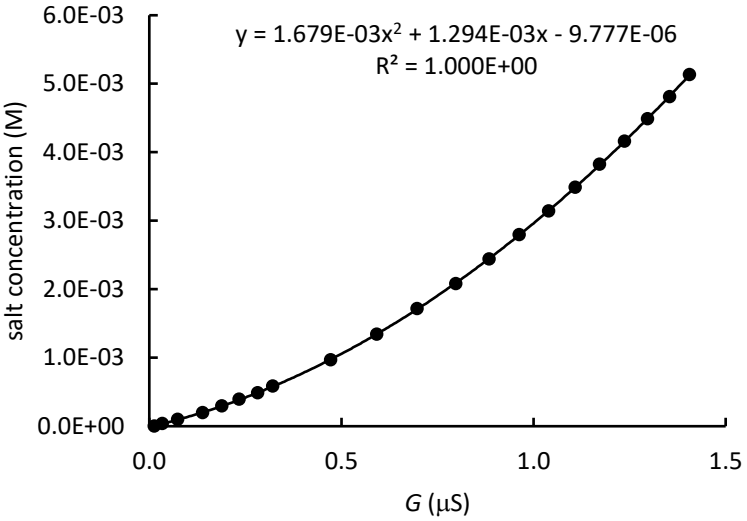

For morpholinium tosylates (**12·HOTs**) the employed, second order polynomials ($y=ax^2+bx+c$) for correction have three different parameters a, b and c. These are summarized in the table below

Parameters a, b and c for **12·HOTs** in morpholine (**12**) in acetonitrile at 20 °C.

[12] (mol L^{-1})	a	b	c
0.1	2.570×10^{-3}	1.017×10^{-3}	4.774×10^{-6}
0.2	2.240×10^{-3}	1.080×10^{-3}	-4.852×10^{-6}
0.3	2.04×10^{-3}	1.15×10^{-3}	-3.73×10^{-7}
0.4	1.889×10^{-3}	1.202×10^{-3}	-6.004×10^{-6}
0.6	1.735×10^{-3}	1.251×10^{-3}	-1.088×10^{-5}
0.8	1.679×10^{-3}	1.294×10^{-3}	-9.777×10^{-6}

Conductance of propylaminium tosylate (13·HOTs) in acetonitrile.

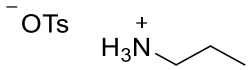

13·HOTs

13·HOTs and morpholine (**13**, 0.3 M) in acetonitrile at 20 °C.

[13·HOTs] (mol L^{-1})	*G* (μS)
3.946×10^{-5}	0.117
9.854×10^{-5}	0.165
1.967×10^{-4}	0.231
2.945×10^{-4}	0.298
3.918×10^{-4}	0.361
4.888×10^{-4}	0.428
5.854×10^{-4}	0.486
9.680×10^{-4}	0.691
1.345×10^{-3}	0.894
1.716×10^{-3}	1.064
2.081×10^{-3}	1.221
2.440×10^{-3}	1.369
2.795×10^{-3}	1.507
3.143×10^{-3}	1.632
3.487×10^{-3}	1.754

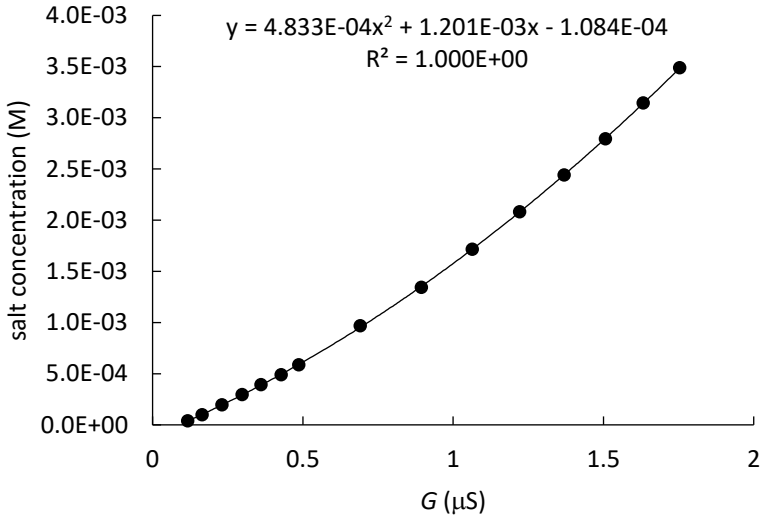

13·HOTs and morpholine (**13**, 0.6 M) in acetonitrile at 20 °C.

[13·HOTs] (mol L^{-1})	*G* (μS)
0	0.162
3.946×10^{-5}	0.189
9.854×10^{-5}	0.233
1.967×10^{-4}	0.302
2.945×10^{-4}	0.364
3.918×10^{-4}	0.428
4.888×10^{-4}	0.487
5.854×10^{-4}	0.544
9.680×10^{-4}	0.762

1.345×10^{-3}	0.964
1.716×10^{-3}	1.146
2.081×10^{-3}	1.314
2.440×10^{-3}	1.470
2.795×10^{-3}	1.619
3.143×10^{-3}	1.752
3.487×10^{-3}	1.882

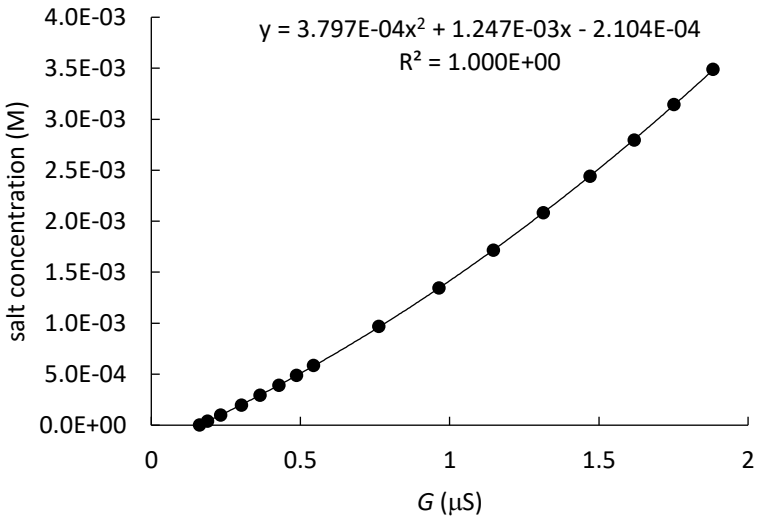

13·HOTs and morpholine (**13**, 0.9 M) in acetonitrile at 20 °C.

[13·HOTs] (mol L^{-1})	*G* (μS)
0	0.236
3.946×10^{-5}	0.261
9.854×10^{-5}	0.296
1.967×10^{-4}	0.357
2.945×10^{-4}	0.422
3.918×10^{-4}	0.481
4.888×10^{-4}	0.538
5.854×10^{-4}	0.601
9.680×10^{-4}	0.824
1.345×10^{-3}	1.022
1.716×10^{-3}	1.203
2.081×10^{-3}	1.385
2.440×10^{-3}	1.544
2.795×10^{-3}	1.693
3.143×10^{-3}	1.840

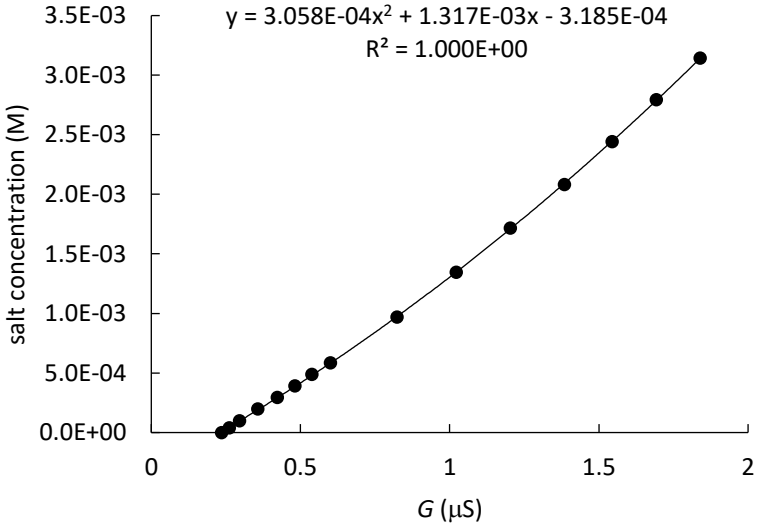

13·HOTs and morpholine (**13**, 1.2 M) in acetonitrile at 20 °C.

[13·HOTs] (mol L^{-1})	*G* (μS)
0	0.310
3.946×10^{-5}	0.333
9.854×10^{-5}	0.378
1.967×10^{-4}	0.437
2.945×10^{-4}	0.496
3.918×10^{-4}	0.554
4.888×10^{-4}	0.612
5.854×10^{-4}	0.664
9.680×10^{-4}	0.883
1.345×10^{-3}	1.083
1.716×10^{-3}	1.264
2.081×10^{-3}	1.437
2.440×10^{-3}	1.601
2.795×10^{-3}	1.756
3.143×10^{-3}	1.897

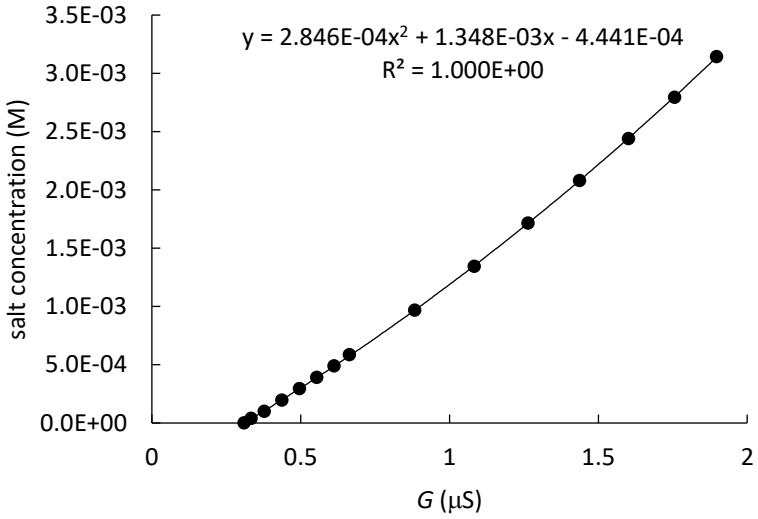

For propylaminium tosylates (**13·HOTs**) the employed, second order polynomials ($y=ax^2+bx+c$) for correction have three different parameters a, b and c. These are summarized in the table below.

Parameters a, b and c for **13·HOTs** in propylamine (**13**) in acetonitrile at 20 °C.

[13] (mol L^{-1})	a	b	c
0.3	4.833×10^{-4}	1.201×10^{-3}	-1.084×10^{-4}
0.6	3.797×10^{-4}	1.247×10^{-3}	-2.104×10^{-4}
0.9	3.058×10^{-4}	1.317×10^{-3}	-3.185×10^{-4}
1.2	2.846×10^{-4}	1.348×10^{-3}	-4.441×10^{-4}

4.2.5 Copies of NMR Spectra

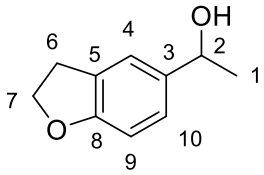

5-OH

^{1}H NMR (400 MHz), $CDCl_3$

$^{13}C\{^1H\}$ NMR (101 MHz), $CDCl_3$

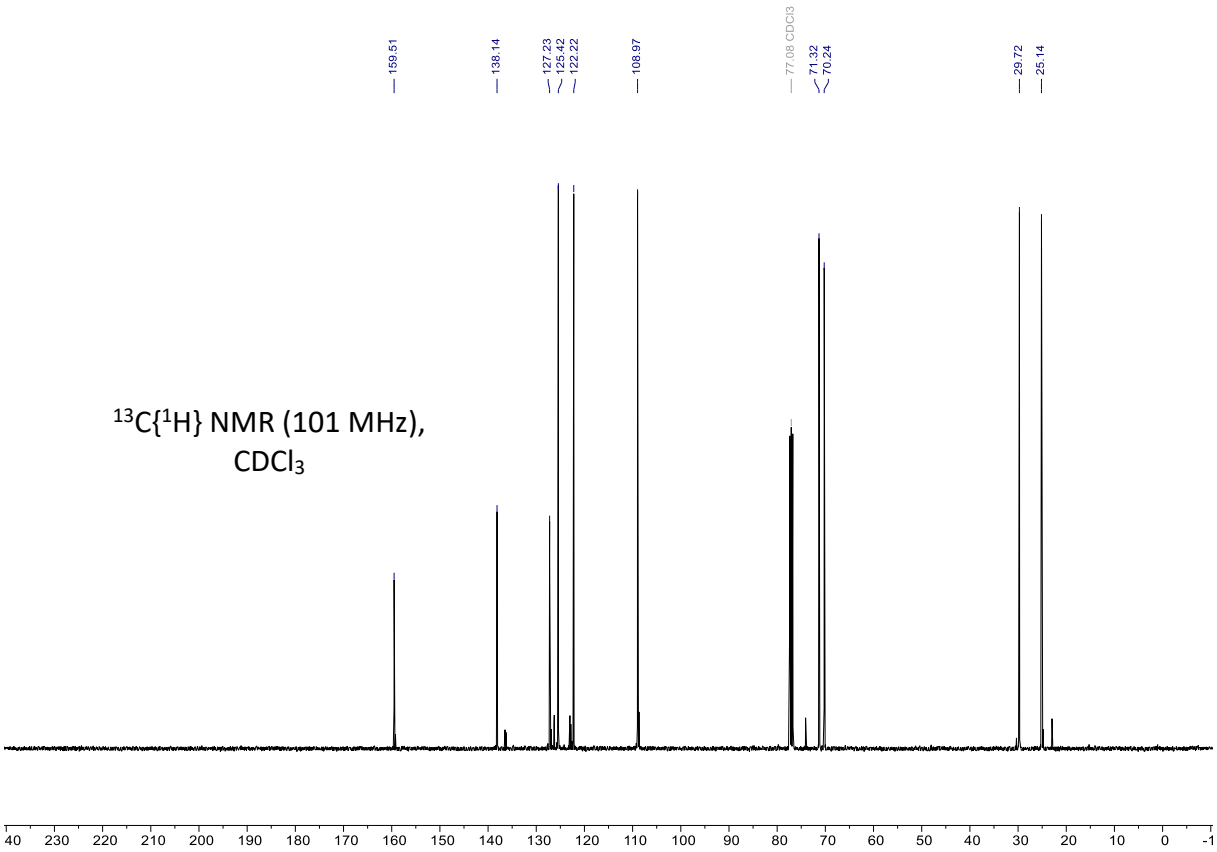

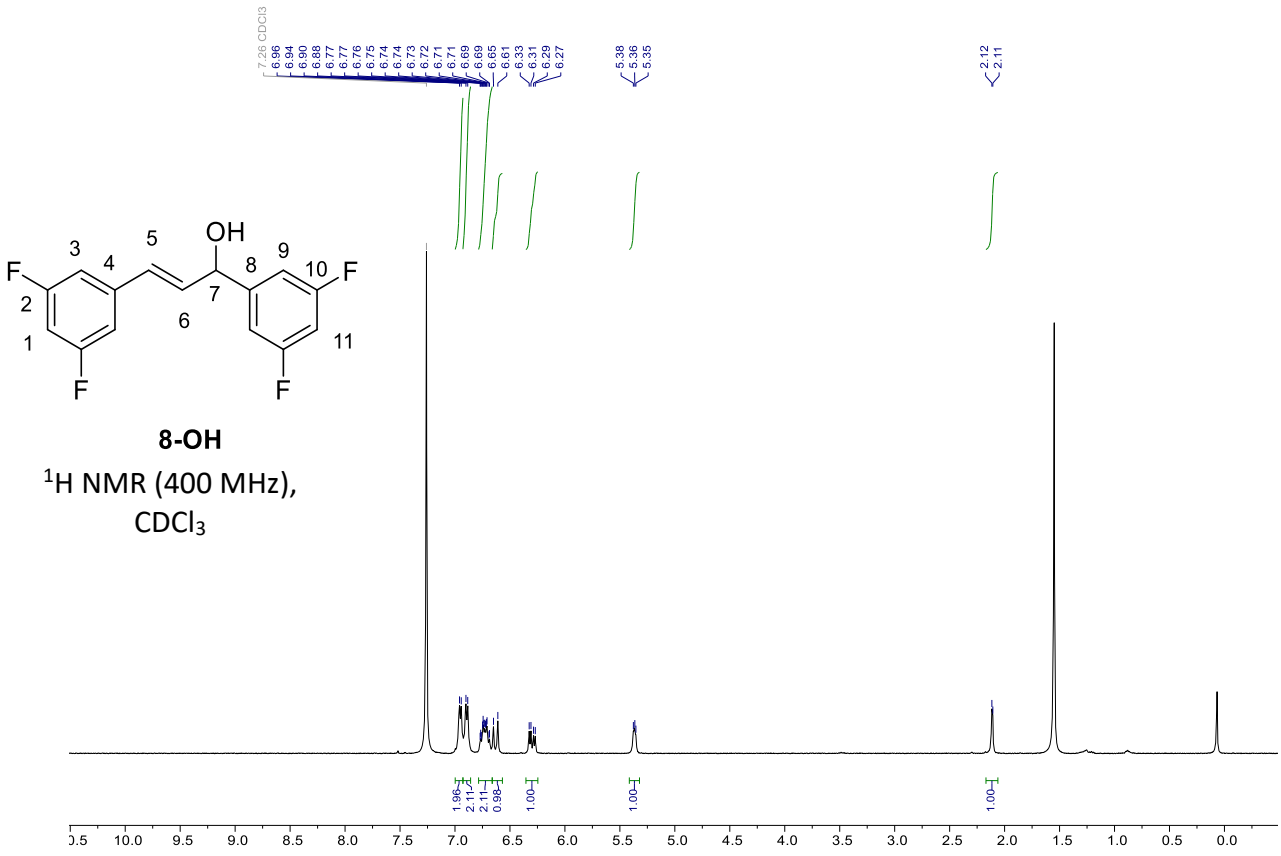

8-OH

^{1}H NMR (400 MHz), $CDCl_3$

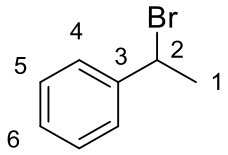

1-Br

^{1}H NMR (400 MHz), $CDCl_3$

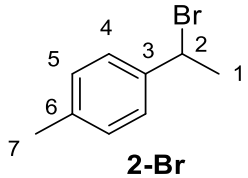

2-Br

^{1}H NMR (400 MHz), $CDCl_3$

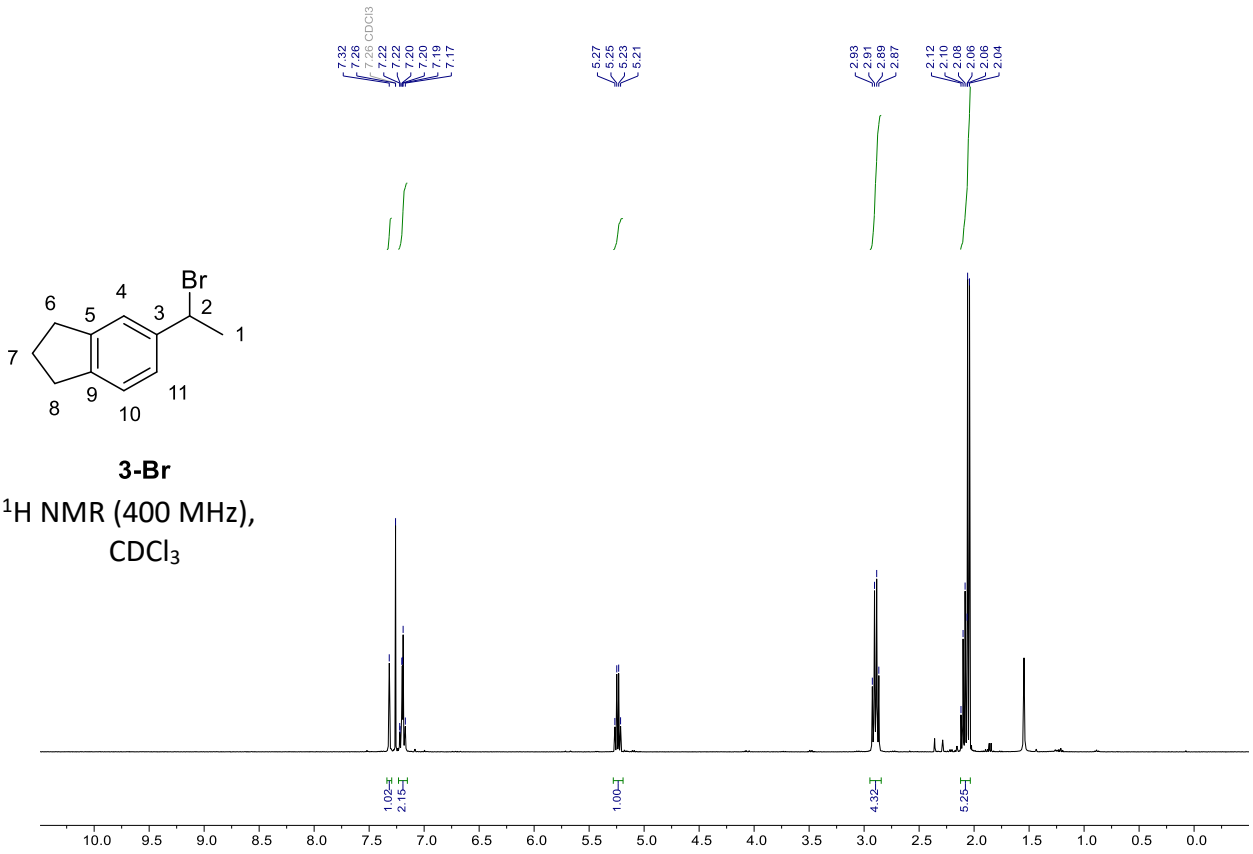

3-Br

^{1}H NMR (400 MHz), $CDCl_3$

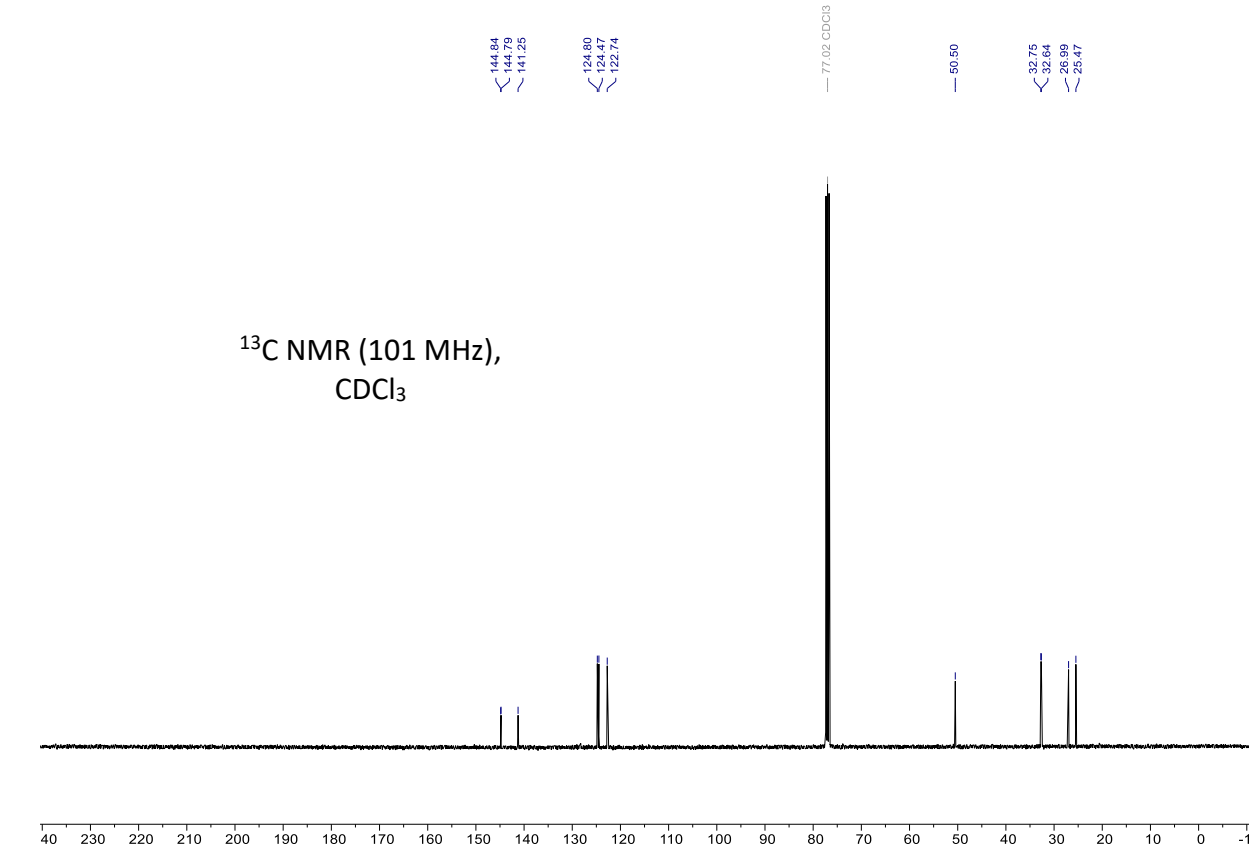

^{13}C NMR (101 MHz), $CDCl_3$

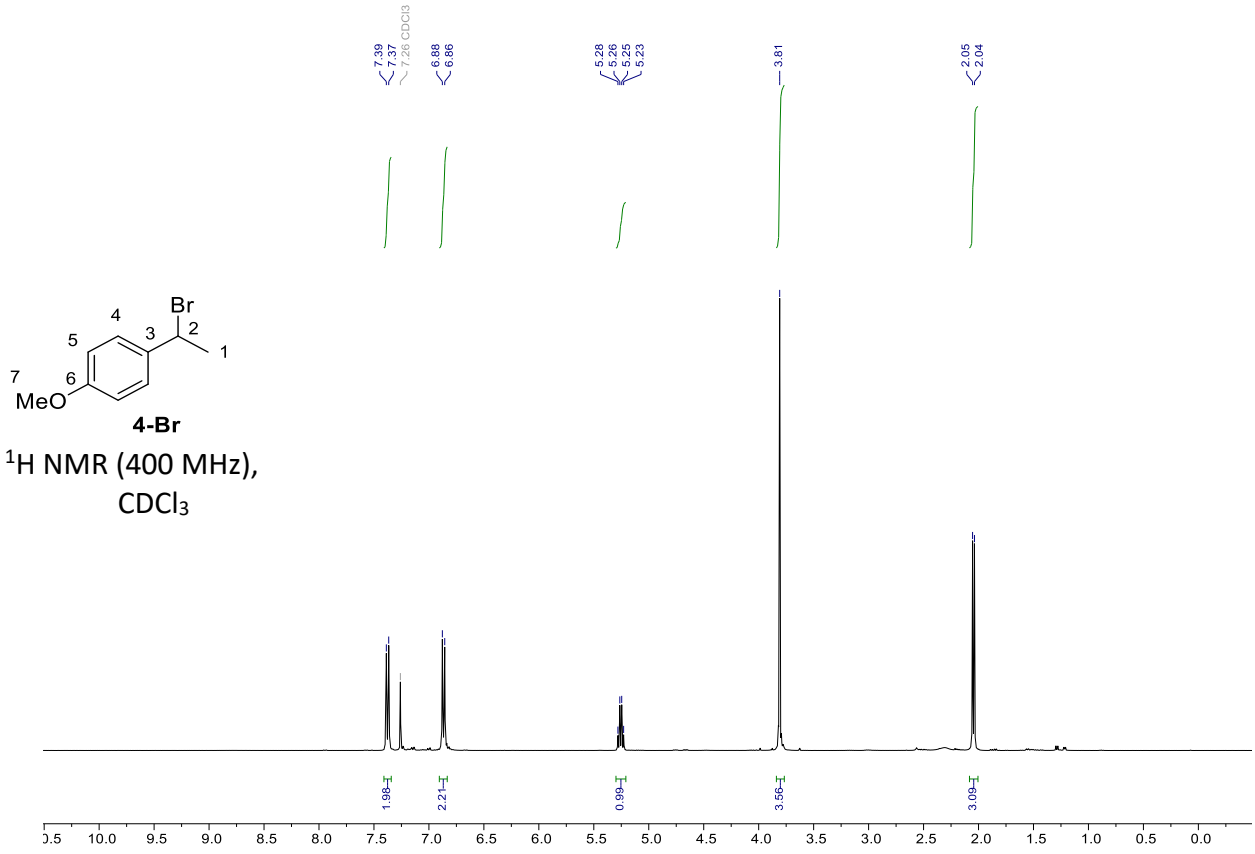

4-Br

^{1}H NMR (400 MHz), $CDCl_3$

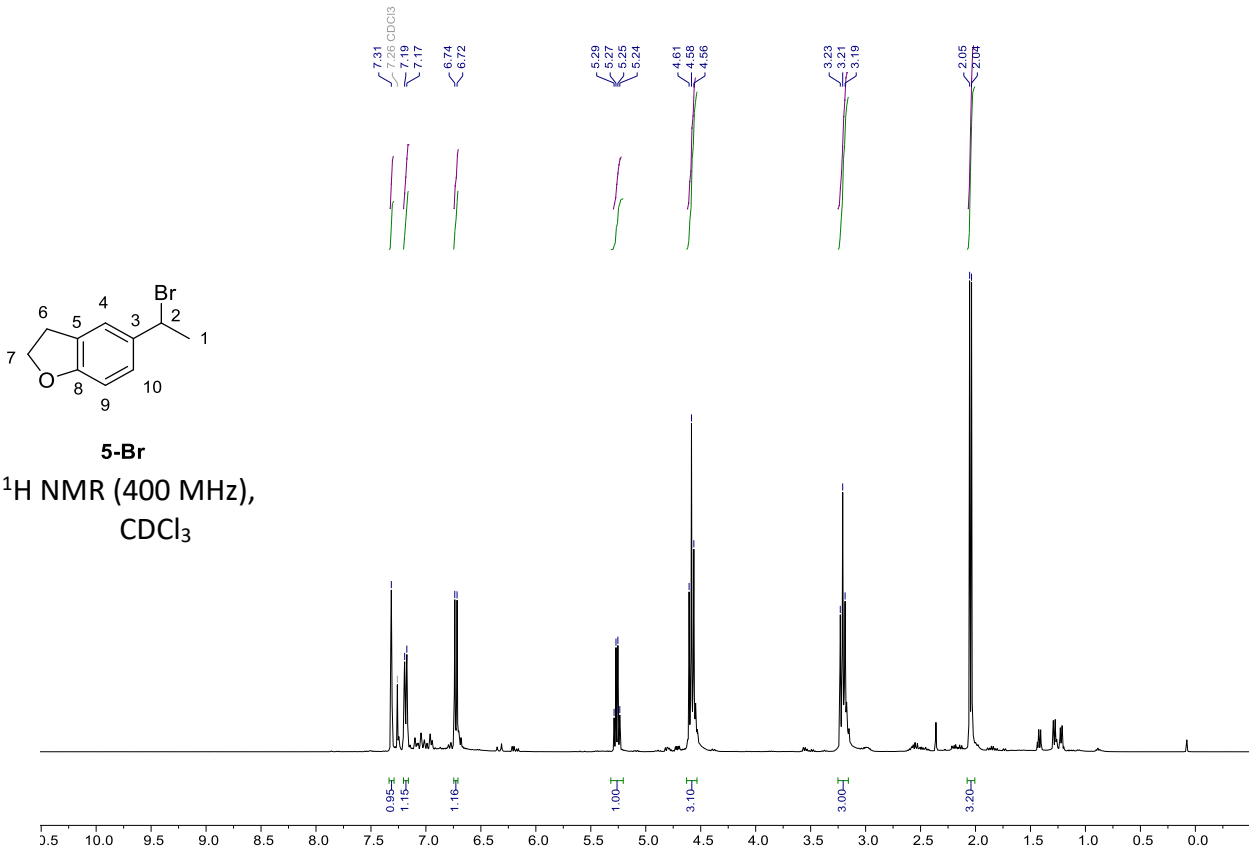

5-Br

^{1}H NMR (400 MHz), $CDCl_3$

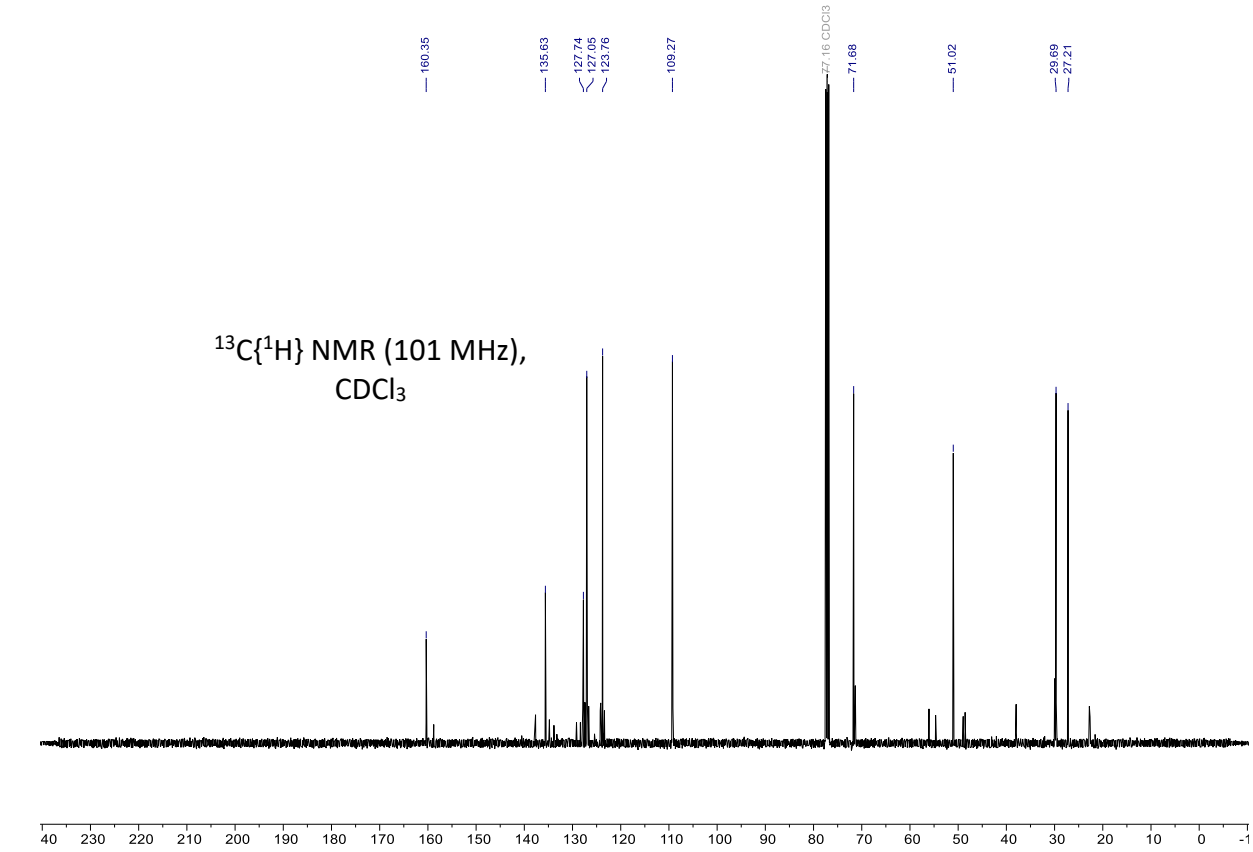

$^{13}C\{^1H\}$ NMR (101 MHz), $CDCl_3$

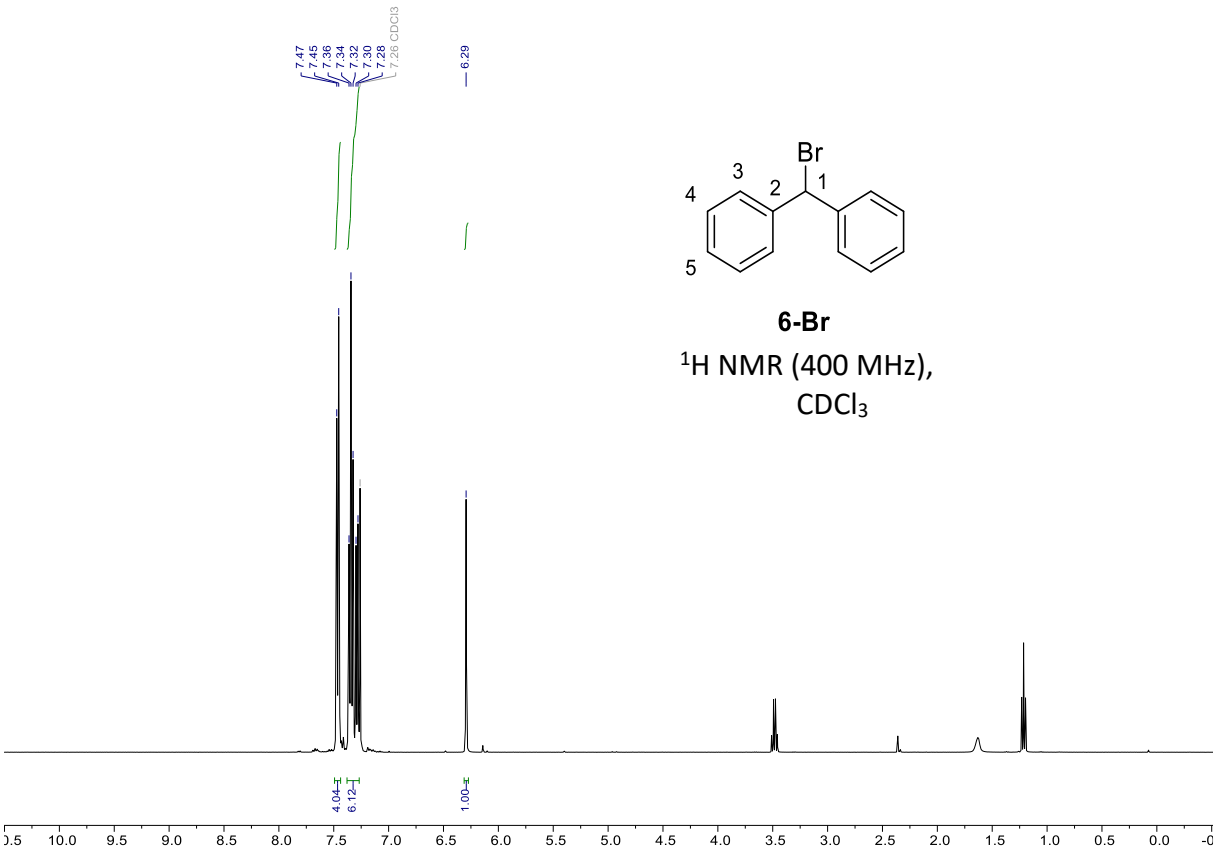

6-Br

^{1}H NMR (400 MHz), $CDCl_3$

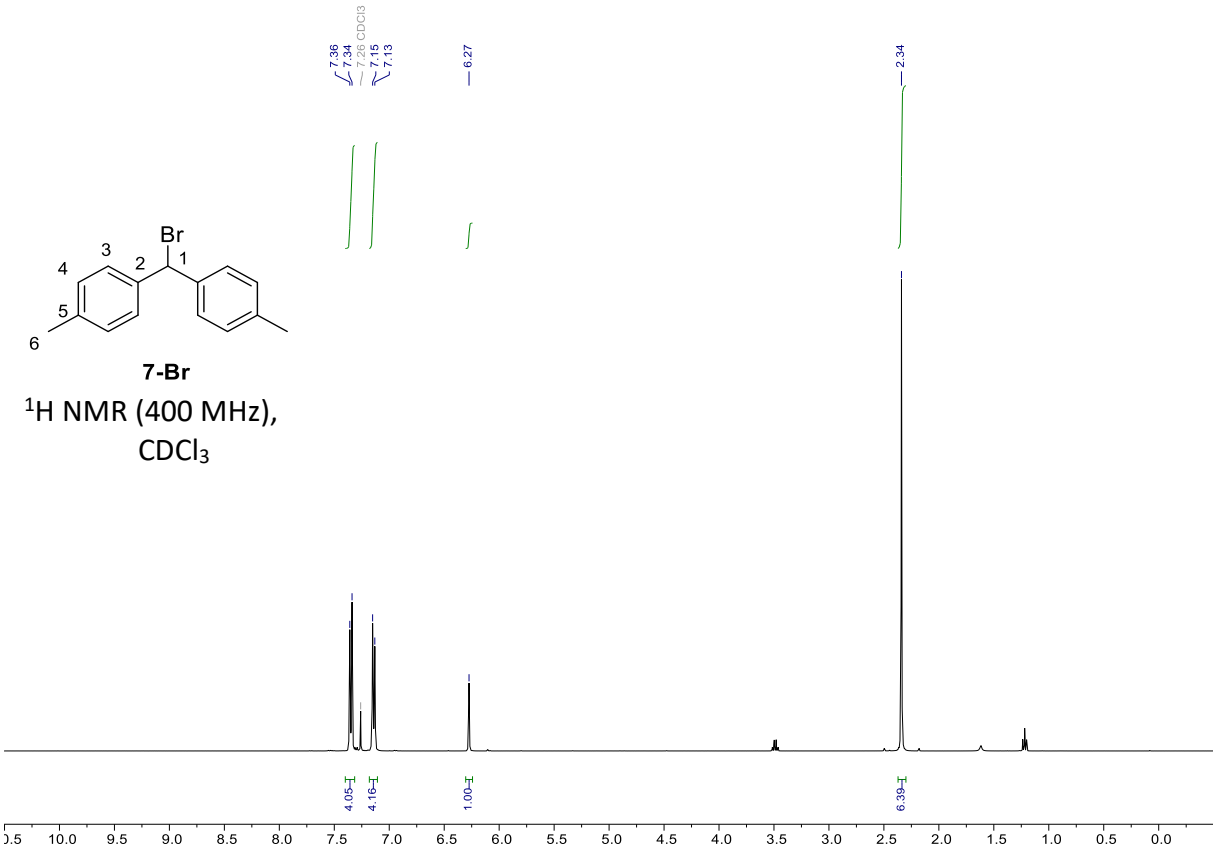

7-Br

^{1}H NMR (400 MHz), $CDCl_3$

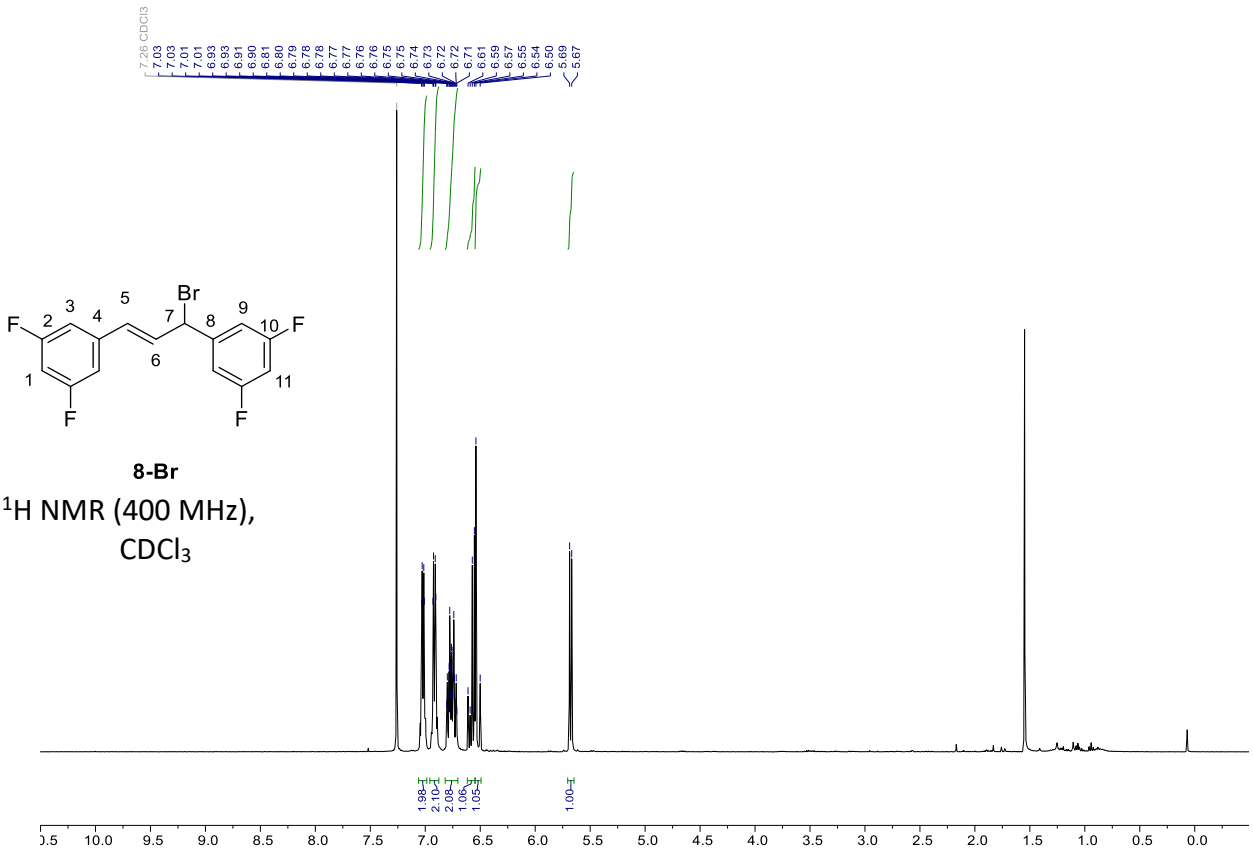

8-Br

^{1}H NMR (400 MHz), $CDCl_3$

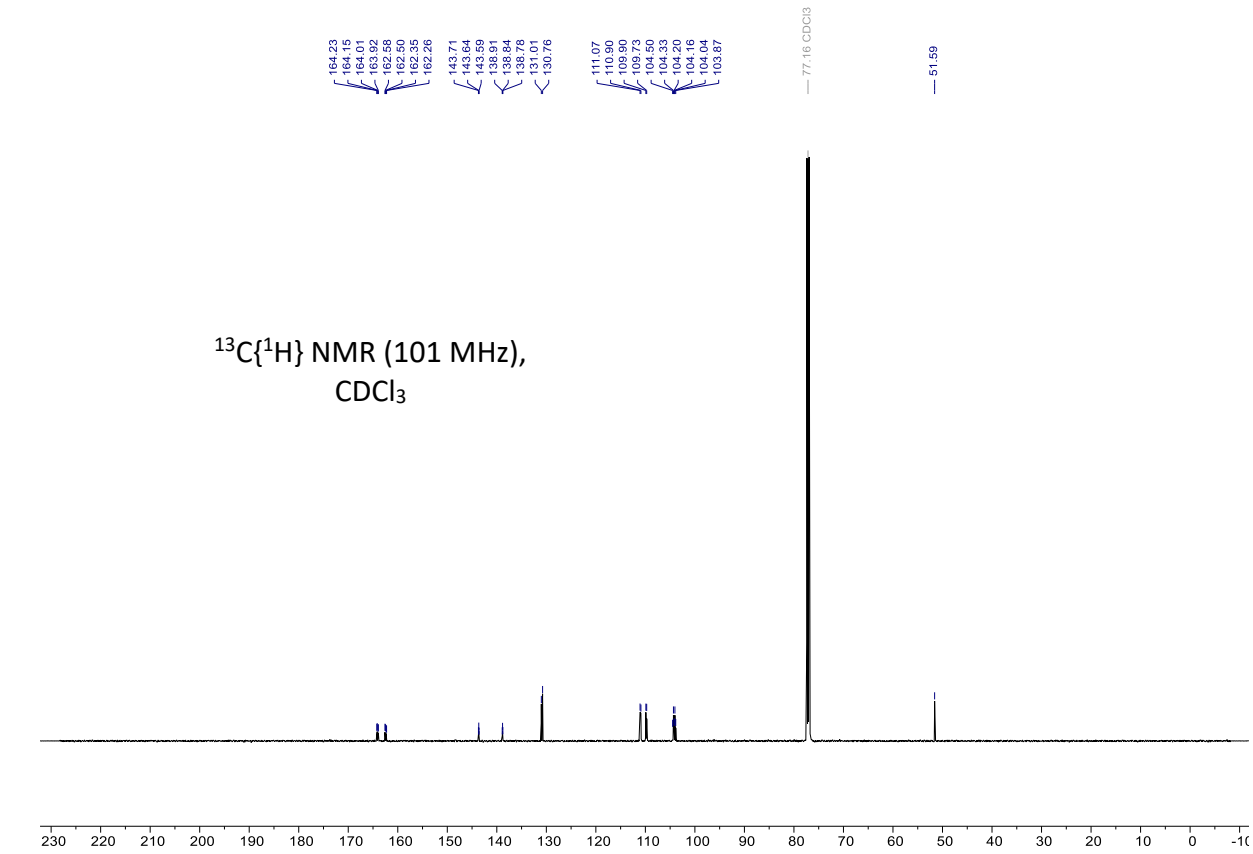

$^{13}C\{^1H\}$ NMR (101 MHz), $CDCl_3$

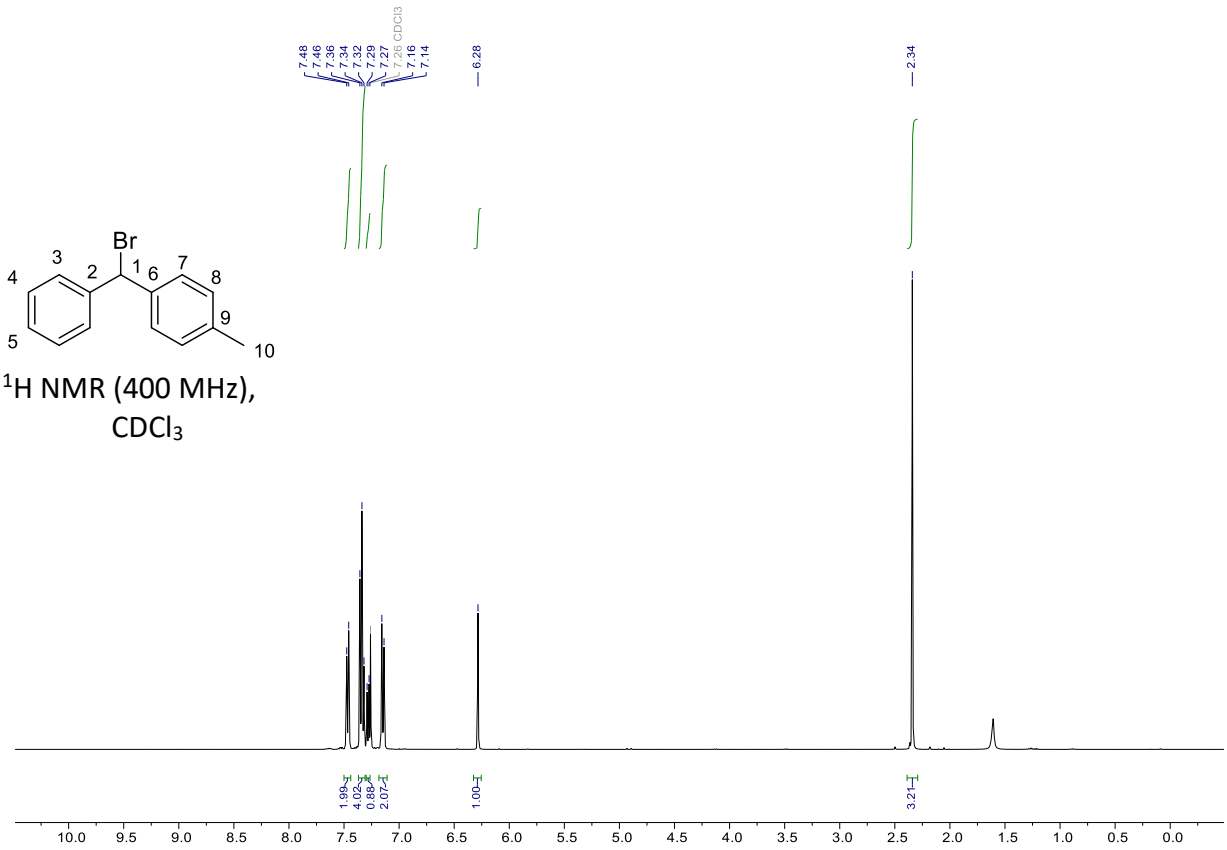

^{1}H NMR (400 MHz), $CDCl_3$

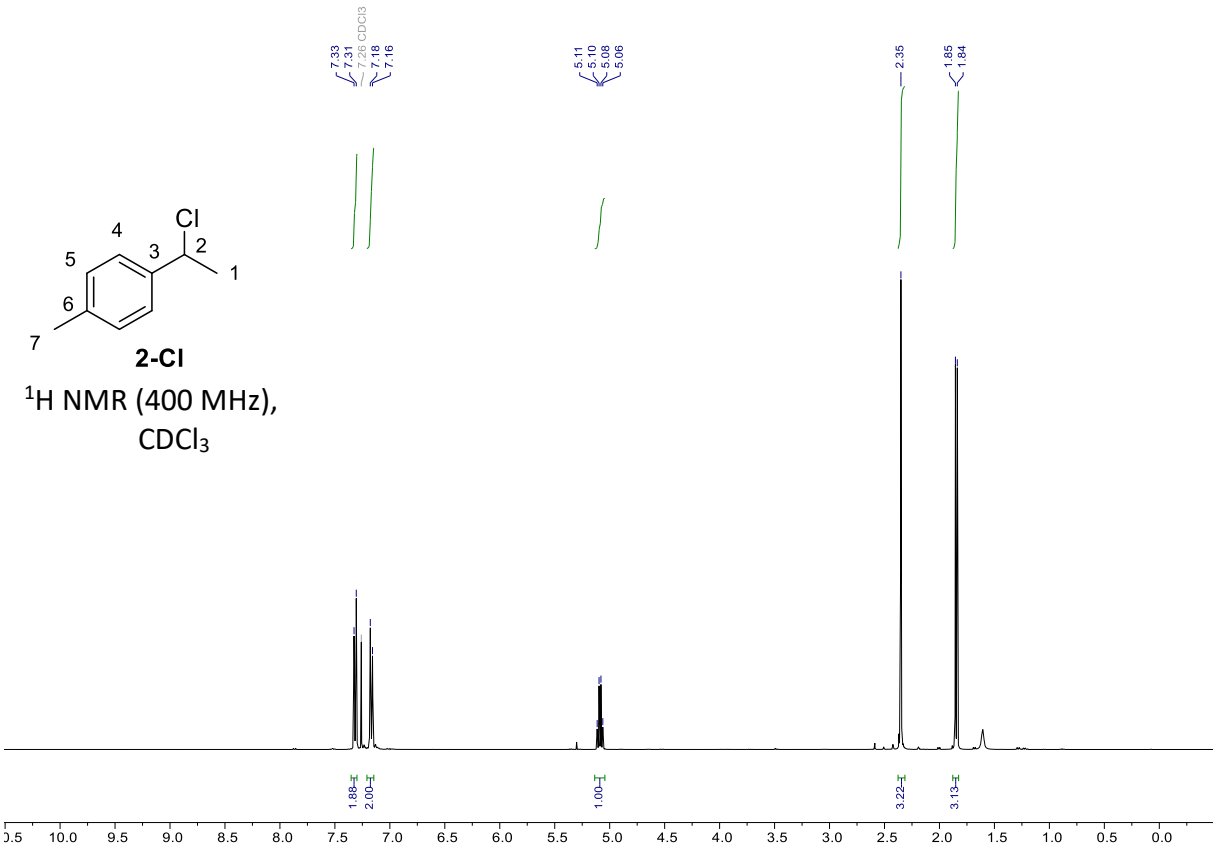

2-Cl

^{1}H NMR (400 MHz), $CDCl_3$

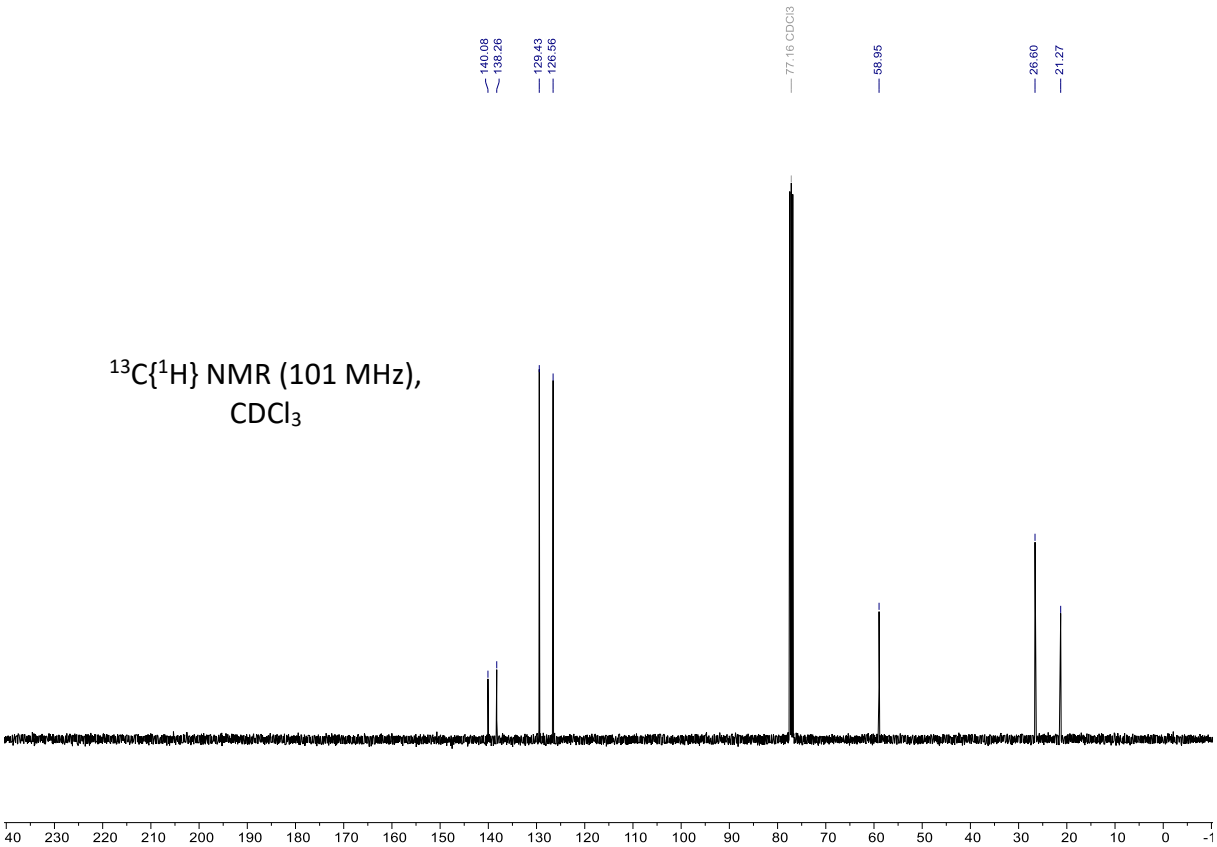

$^{13}C\{^1H\}$ NMR (101 MHz), $CDCl_3$

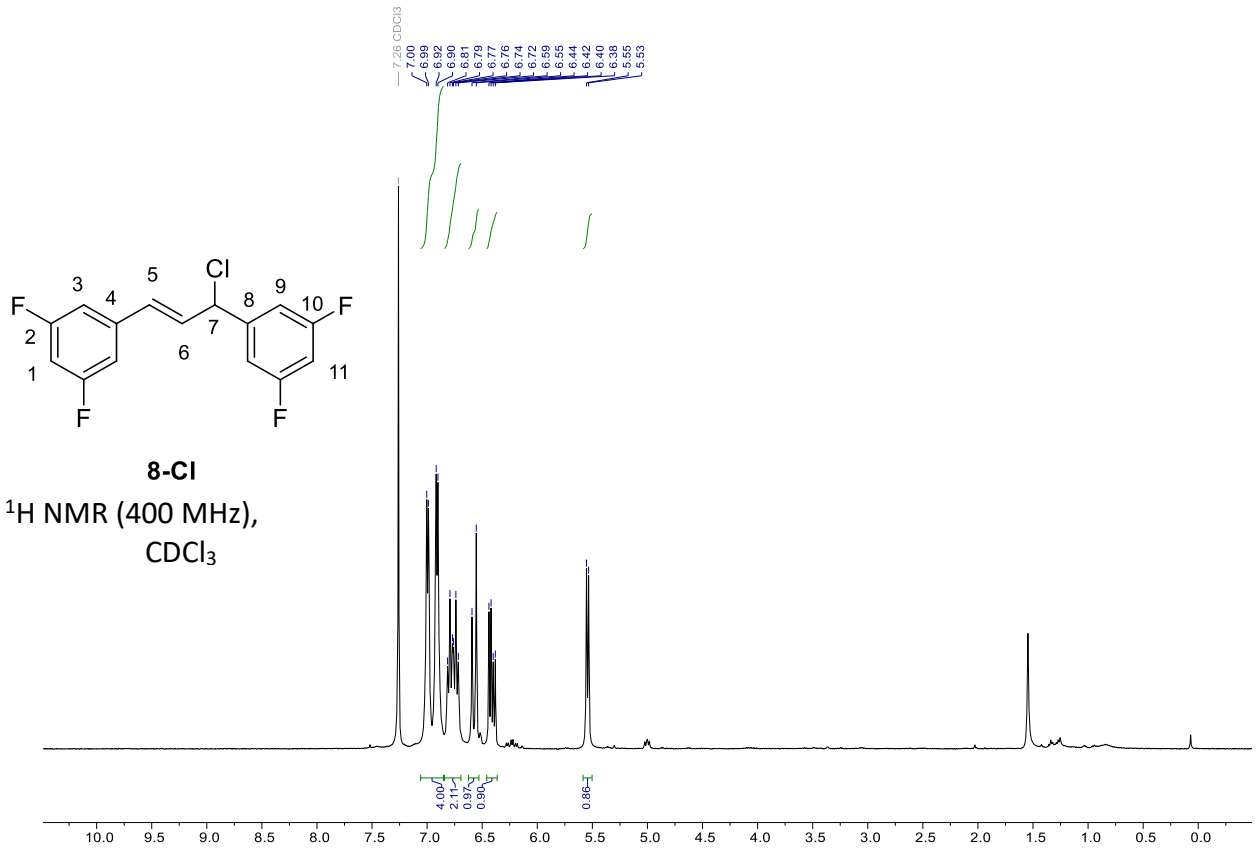

8-Cl

^{1}H NMR (400 MHz), $CDCl_3$

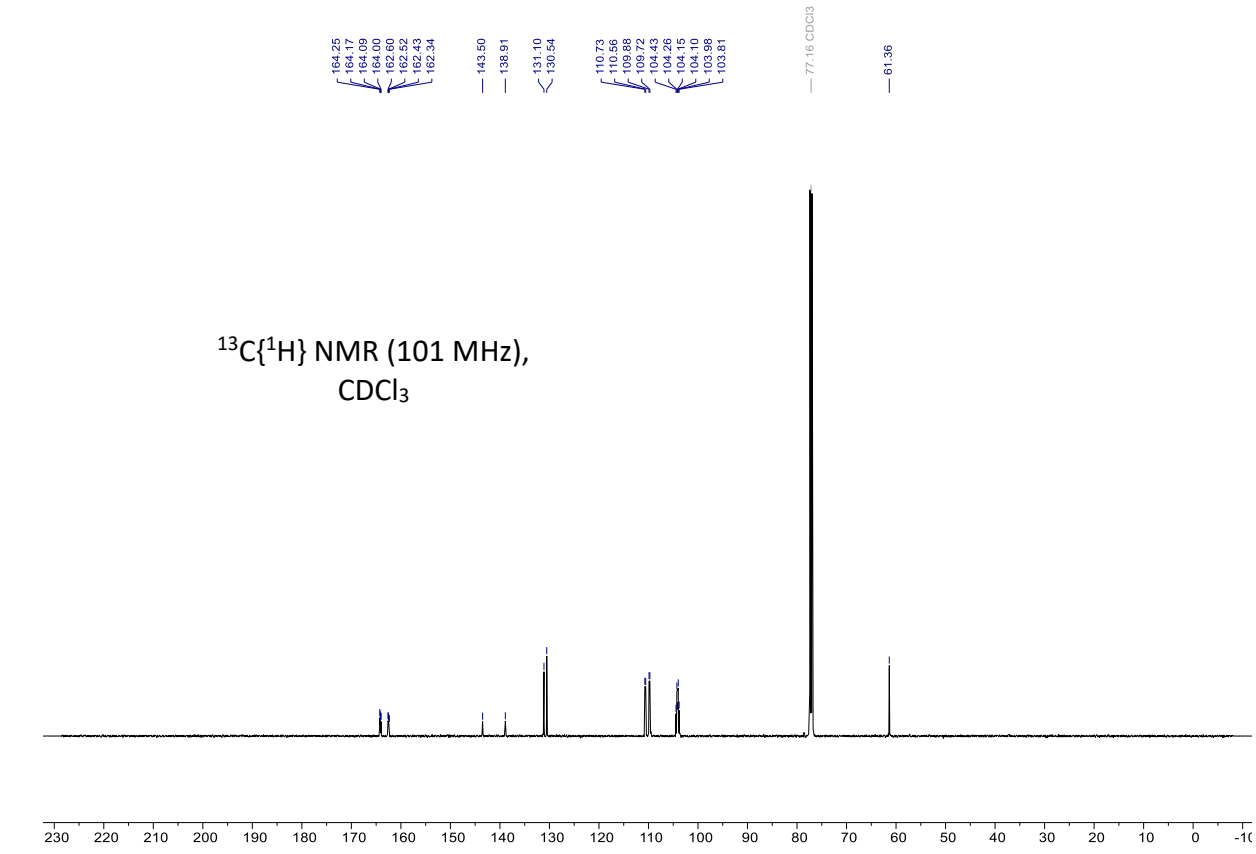

$^{13}C\{^1H\}$ NMR (101 MHz), $CDCl_3$

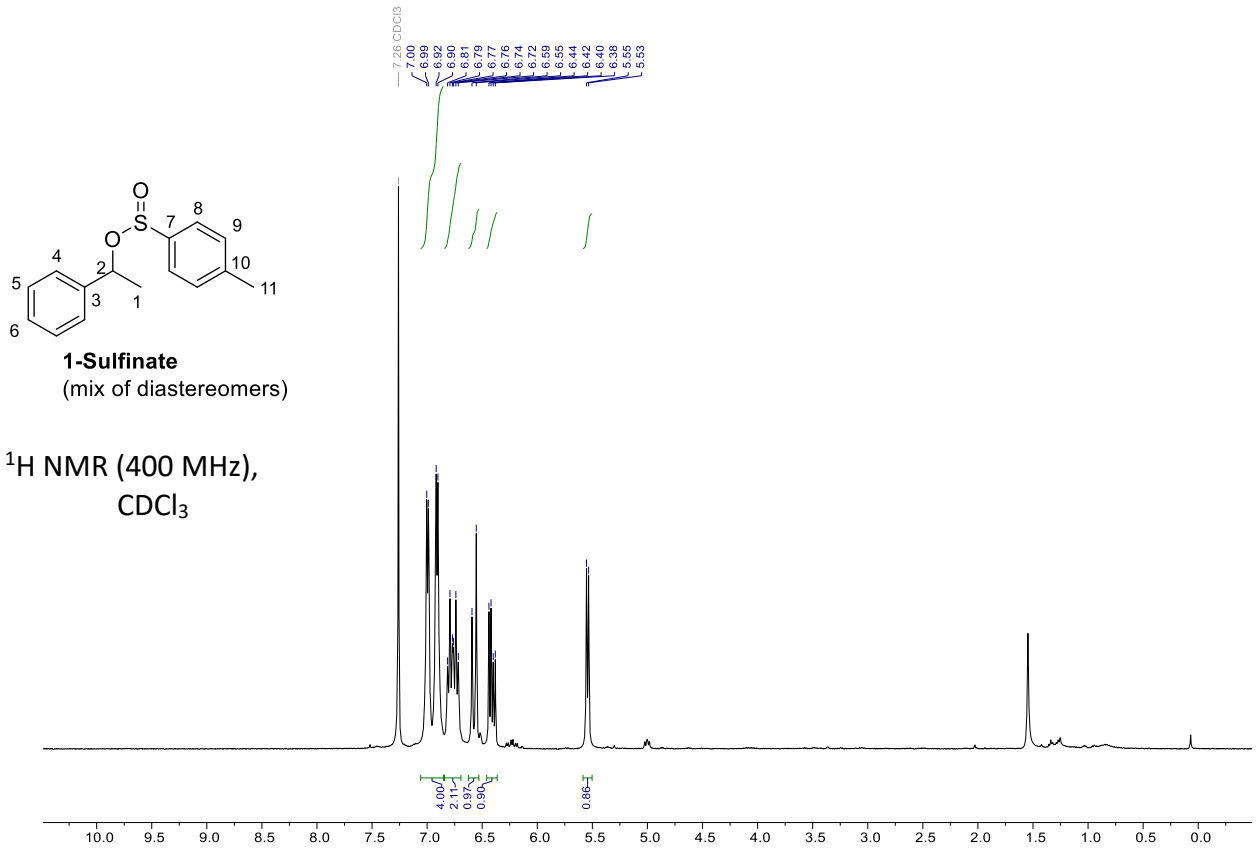

1-Sulfinate
(mix of diastereomers)

^{1}H NMR (400 MHz), $CDCl_3$

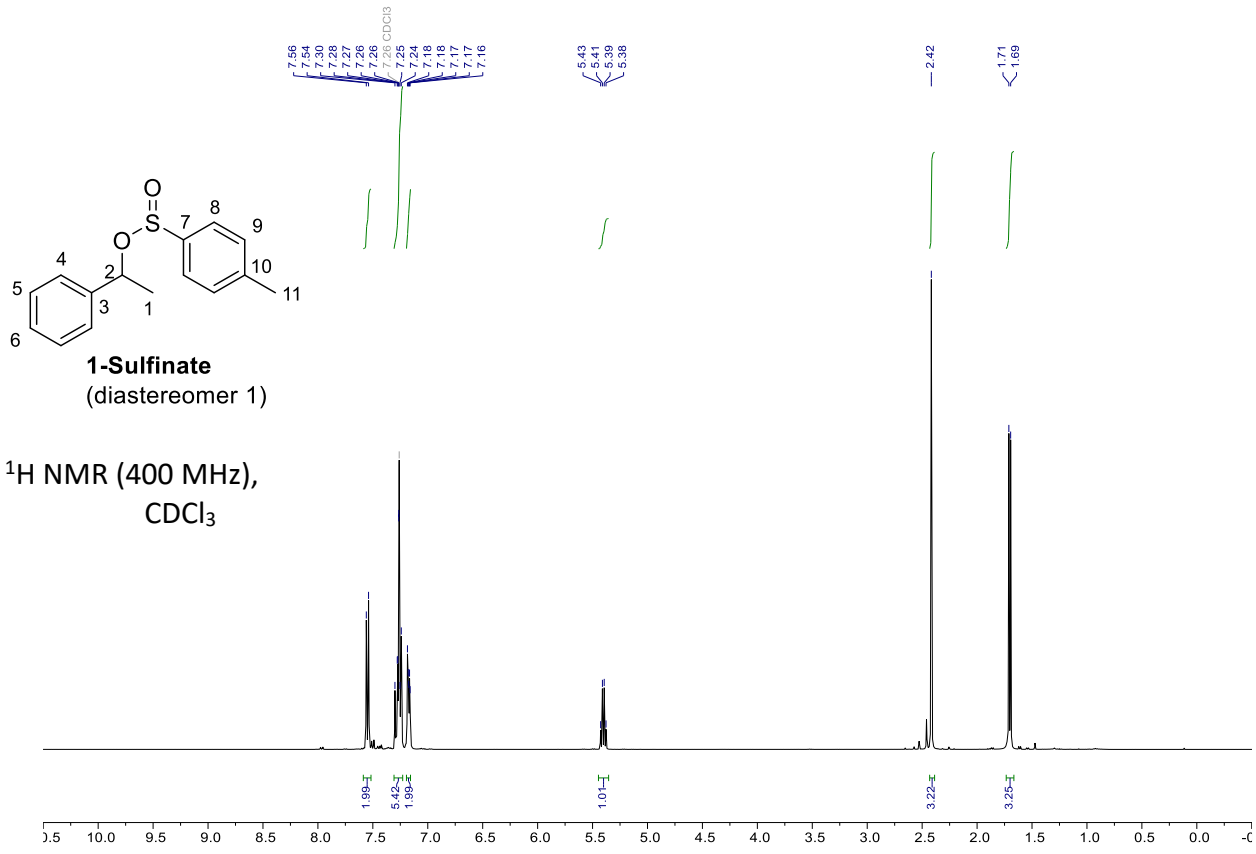

1-Sulfinate
(diastereomer 1)

^{1}H NMR (400 MHz), $CDCl_3$

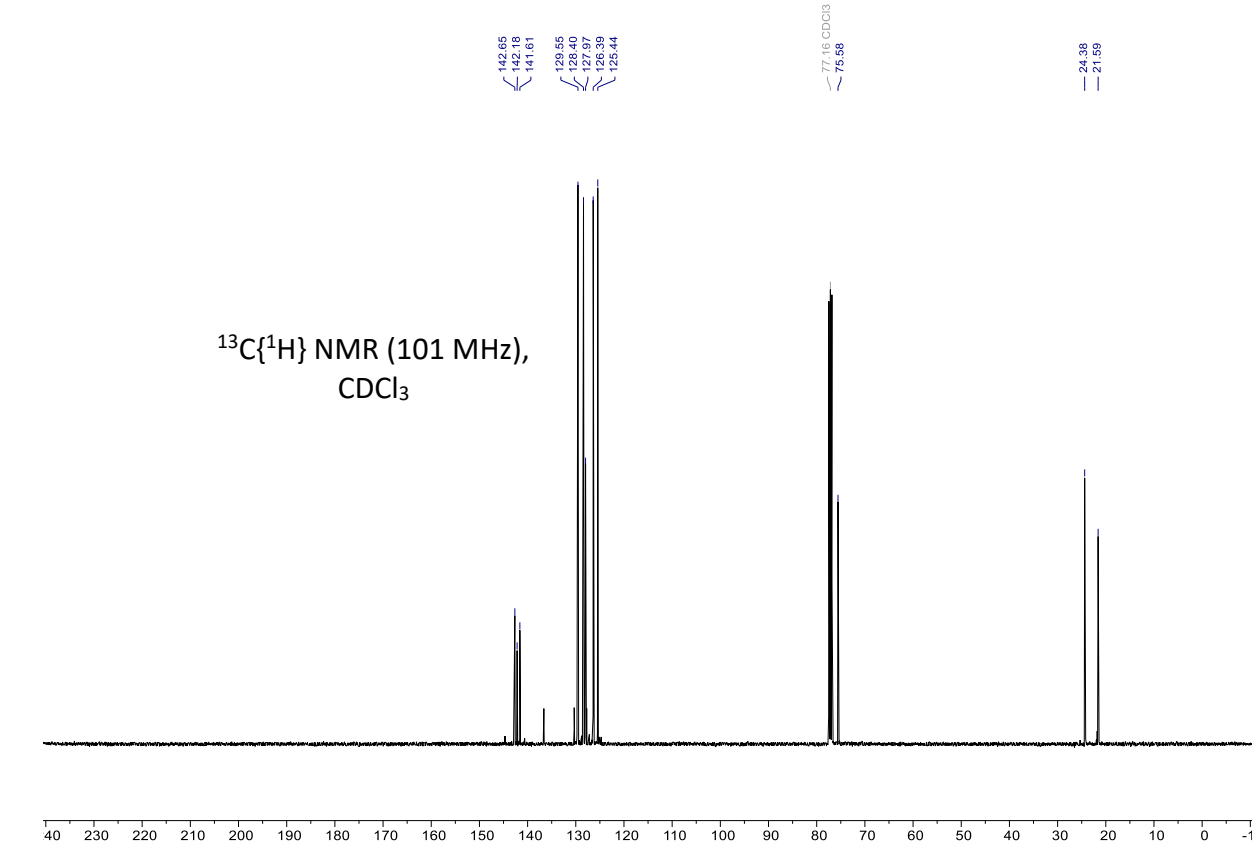

$^{13}C\{^1H\}$ NMR (101 MHz), $CDCl_3$

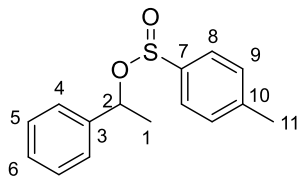

1-Sulfinate
(diastereomer 2)

^{1}H NMR (400 MHz), $CDCl_3$

$^{13}C\{^1H\}$ NMR (101 MHz), $CDCl_3$

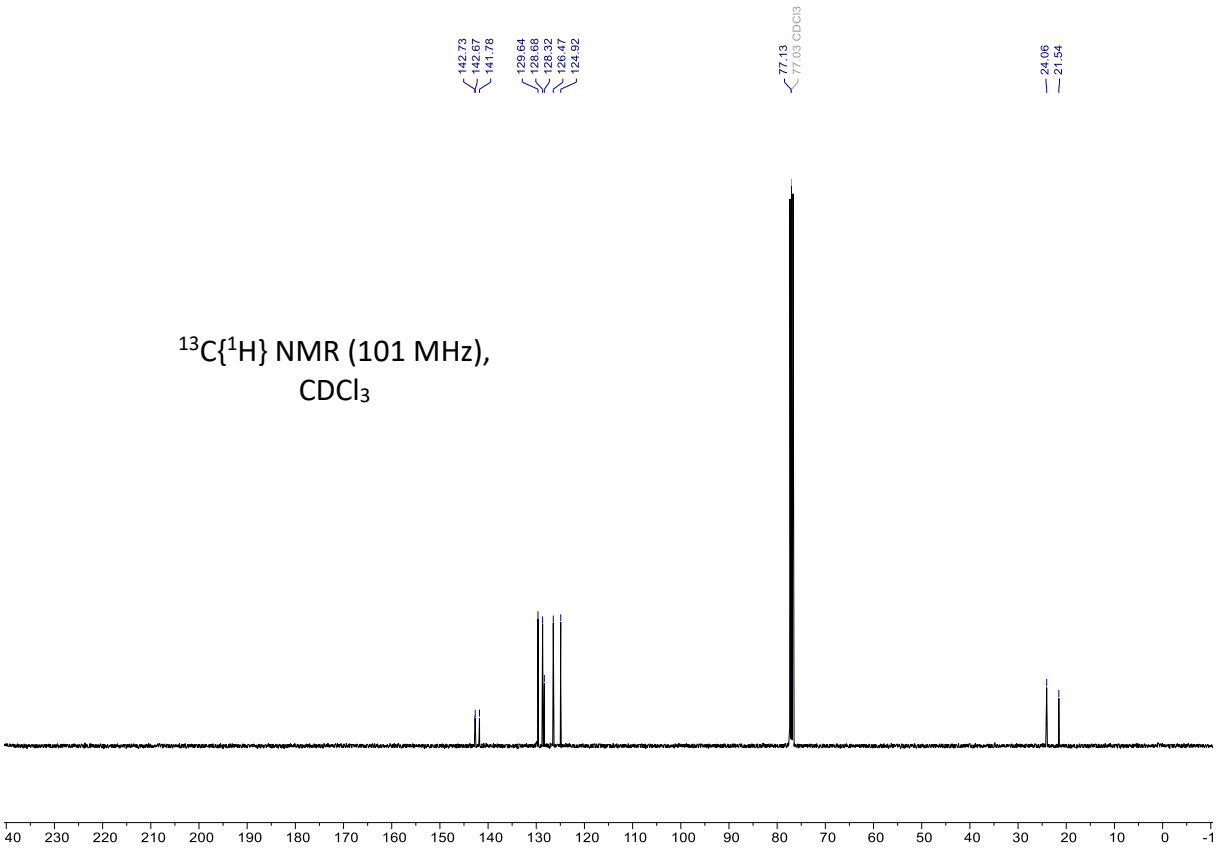

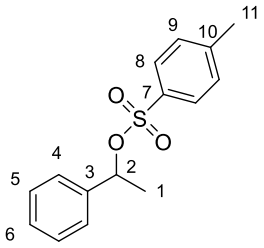

1-OTs

^{1}H NMR (400 MHz), $CDCl_3$

$^{13}C\{^1H\}$ NMR (101 MHz), $CDCl_3$

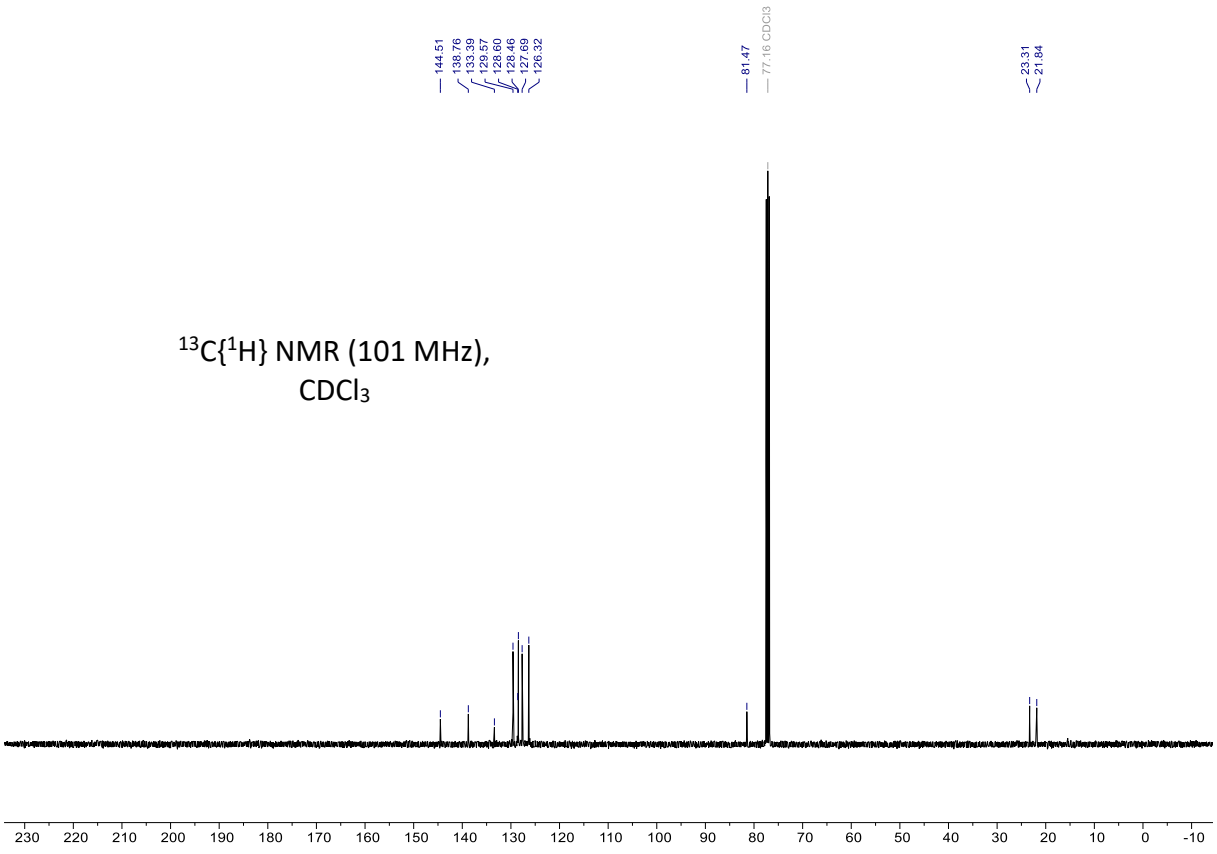

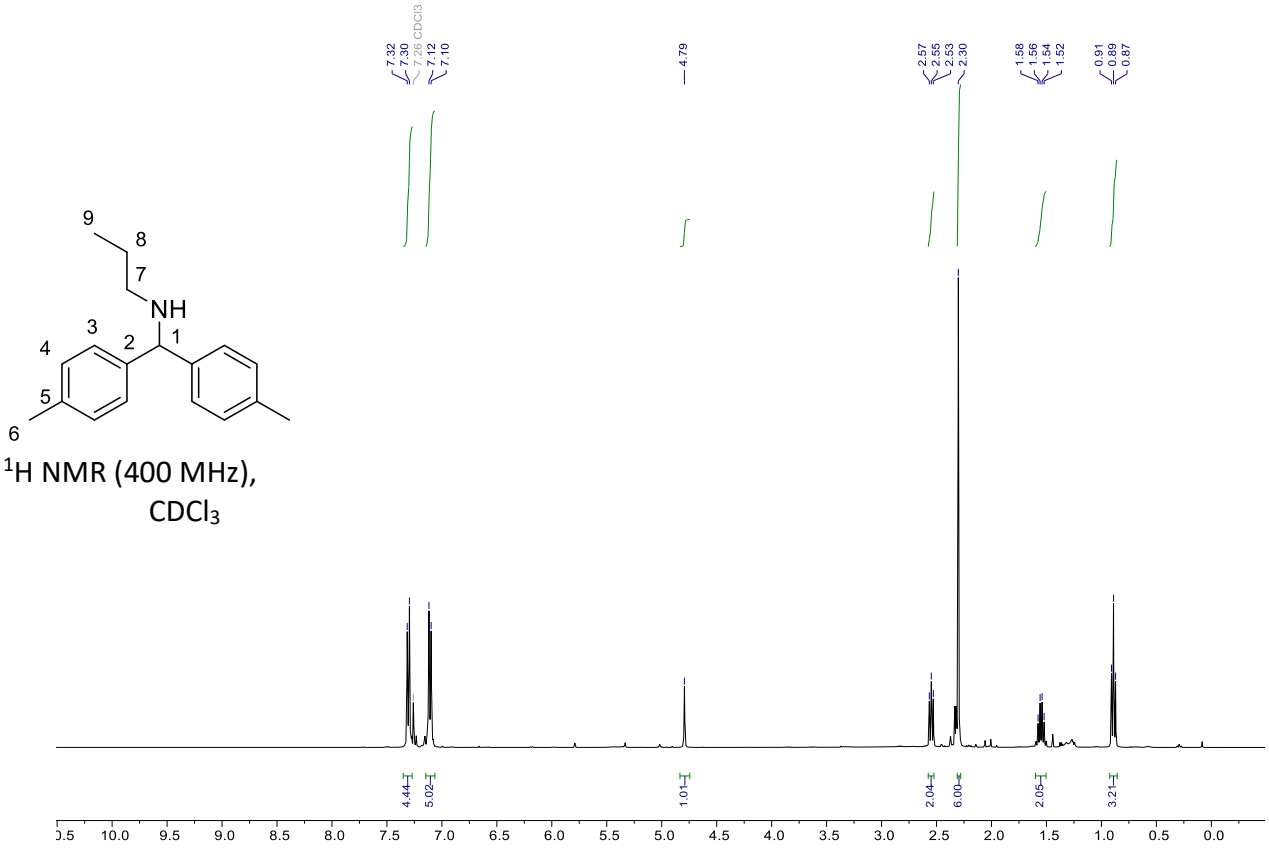

^{1}H NMR (400 MHz), $CDCl_3$

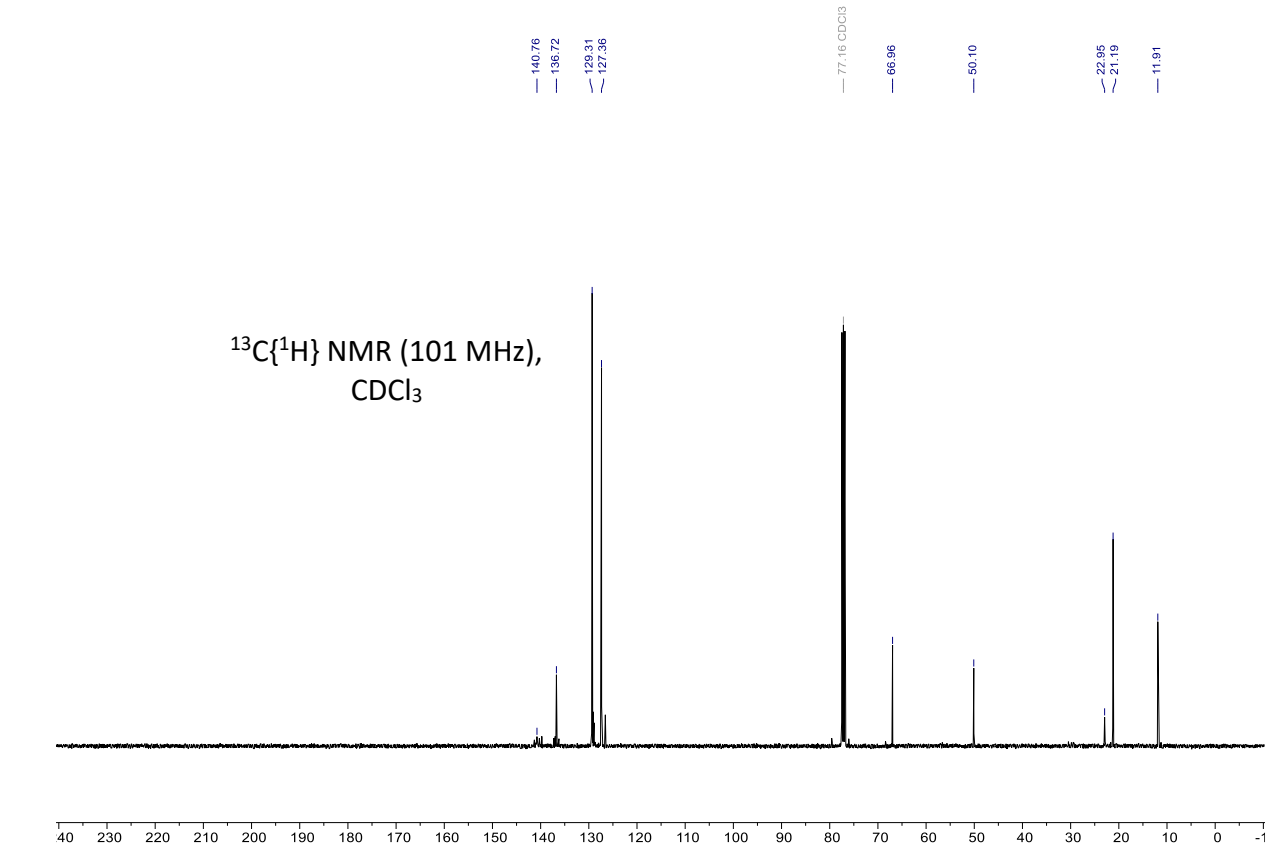

$^{13}C\{^1H\}$ NMR (101 MHz), $CDCl_3$

4.2.6 References

(1) Fulmer, G. R.; Miller, A. J. M.; Sherden, N. H.; Gottlieb, H. E.; Nudelman, A.; Stoltz, B. M.; Bercaw, J. E.; Goldberg, K. I., *Organometallics* **2010,** *29*, 2176−2179.

(2) Troshin, K.; Schindele, C.; Mayr, H., *J. Org. Chem.* **2011,** *76*, 9391−9408.

(3) Psiorz, M.; Schmid, R., *Chem. Ber.* **1987,** *120*, 1825−1828.

(4) Denton, R. M.; An, J.; Adeniran, B.; Blake, A. J.; Lewis, W.; Poulton, A. M., *J. Org. Chem.* **2011,** *76*, 6749−6767.

(5) Holz, J.; Pfeffer, C.; Zuo, H.; Beierlein, D.; Richter, G.; Klemm, E.; Peters, R., *Angew. Chem., Int. Ed.* **2019,** *58*, 10330−10334.

(6) Denegri, B.; Streiter, A.; Jurić, S.; Ofial, A. R.; Kronja, O.; Mayr, H., *Chem. Eur. J.* **2006,** *12*, 1648−1656.

(7) Troshin, K.; Mayr, H., *J. Org. Chem.* **2013,** *78*, 2649−2660.

(8) Iwamoto, H.; Endo, K.; Ozawa, Y.; Watanabe, Y.; Kubota, K.; Imamoto, T.; Ito, H., *Angew. Chem., Int. Ed.* **2019,** *58*, 11112−11117.

(9) Kiyokawa, K.; Yasuda, M.; Baba, A., *Org. Lett.* **2010,** *12*, 1520−1523.

(10) Coates, R. M.; Chen, J. P., *Tetrahedron Lett.* **1969,** *10*, 2705−2708.

(11) Ji, Y.-Z.; Li, H.-J.; Zhang, J.-Y.; Wu, Y.-C., *Eur. J. Org. Chem.* **2019,** *2019*, 1846−1855.

(12) Lee, J. H.; Yeo, S. D.; Jeong, D. Y.; Kim, S. H.; Park, J. H., *Bull. Korean Chem. Soc.* **2000,** *21*, 1005−1010.

(13) Tshepelevitsh, S.; Kütt, A.; Lõkov, M.; Kaljurand, I.; Saame, J.; Heering, A.; Plieger, P. G.; Vianello, R.; Leito, I., *Eur. J. Org. Chem.* **2019,** *2019*, 6735−6748.

(14) Rõõm, E.-I.; Kütt, A.; Kaljurand, I.; Koppel, I.; Leito, I.; Koppel, I. A.; Mishima, M.; Goto, K.; Miyahara, Y., *Chem. Eur. J.* **2007,** *13*, 7631−7643.

Chapter 5. Effects of the Diffusion Limit on the Mayr-Kronja Equation

5.1 Dynamics of the Dimethyl Sulfide Exchange of (1,3-Diphenylallyl)dimethylsulfonium Ions

P. M. Jüstel, P. Rovó, H. Mayr, A. R. Ofial, *J Phys Org Chem* **2021**, e4270.
https://doi.org/10.1002/poc.4270

Author Contributions

Patrick M. Jüstel performed all experiments. The manuscript of Chapter 5.1 was written jointly by Patrick M. Jüstel, Petra Rovó, Herbert Mayr and Armin R. Ofial. The manuscript of Chapter 5.2 was written by Patrick M. Jüstel.

5.1 Dynamics of the Dimethyl Sulfide Exchange of (1,3-Diphenylallyl)dimethylsulfonium Ions

Received: 4 June 2021 | Revised: 14 July 2021 | Accepted: 18 July 2021

DOI: 10.1002/poc.4270

SPECIAL ISSUE ARTICLE

Journal of Physical Organic Chemistry WILEY

Dynamics of the dimethyl sulfide exchange of (1,3-diphenylallyl)dimethylsulfonium ions

Patrick M. Jüstel | **Petra Rovó** | **Herbert Mayr** | **Armin R. Ofial**

Department Chemie, Ludwig-Maximilians-Universität München, Munich, Germany

Correspondence
Armin R. Ofial, Department Chemie, Ludwig-Maximilians-Universität München, Butenandtstr. 5-13, 81377 Munich, Germany.
Email: ofial@lmu.de

In admiration of Professor Barry K. Carpenter's fundamental contributions to Physical Organic Chemistry

Abstract

The dynamics of the allylic rearrangement of the (1,3-diphenylallyl) dimethylsulfonium ion in CD_2Cl_2, which proceeds via intermediate 1,3-diphenylallyl cations, has been investigated by variable temperature ^1H NMR spectroscopy. At low temperature, the three allylic protons give rise to an AMX system, and the two diastereotopic *S*-methyl groups resonate at different frequencies. At higher temperature, an AX_2 system for the allylic protons and a single signal for the *S*-methyl groups are observed. The resulting exchange rate constant of (364 ± 2) s^{-1} at 25°C, which corresponds to the rate of the heterolytic cleavage of the C–S bond, was used to explore the range of validity of the linear free energy relationship $\log k_{het}(25°C) = s_f\ (N_f + E_f)$, which describes the rates of heterolytic cleavages by the electrofugality parameter E_f and the solvent-dependent nucleofuge-specific parameters N_f and s_f. The observed rate constant corroborates a previous conclusion that two different sets of N_f and s_f parameters may exist for the same nucleofuge. Knowledge of whether the reverse bond-forming reaction occurs under activation or under diffusion control is crucial for the choice of the appropriate set of nucleofugality parameters.

KEYWORDS

chalcogenides, heterolysis, kinetics, line shape analysis, linear free energy relationships

1 | INTRODUCTION

Dialkyl sulfides are strong nucleophiles, comparable with pyridine and *N*-methylimidazole.[1] On the other hand, dialkyl sulfides are much weaker Lewis bases than these *N*-heterocycles, which makes their Lewis adducts with carbocations R^+ less stable than those generated by reactions of R^+ with *N*-heterocycles of comparable nucleophilicity.[1,2] The combination of both properties, low intrinsic barriers and weak Lewis basicities, gives also rise to the high speed of the reverse reactions, that is, the fast heterolytic scissions of sulfonium ions.[1,3–5] In other words, dialkyl sulfides are characterized by high nucleophilicity as well as by high nucleofugality (leaving group ability),[1] which explains their ability to act as organocatalysts.[6–11]

Recently, we derived rate constants k_{het} for the carbon–sulfur bond cleavage of dialkyl (diarylmethyl)sulfonium ions ($Ar_2CH–^+SR_2$) from the ratio k_f/K, where k_f is the second-order rate constant for the reaction of

benzhydrylium ions with dialkyl sulfides (Equation 1) and K ($= k_f/k_{het}$) is the equilibrium constant for the corresponding reaction in dichloromethane.[1]

$$Ar_2CH^+ + SR_2 \underset{k_{het}}{\overset{k_f}{\rightleftharpoons}} Ar_2CH\text{-}\overset{+}{S}R_2 \quad (1)$$

It has been reported that the rates of S_N1 reactions can generally be calculated by Equation (2), where E_f represents an solvent-independent electrofugality parameter for the carbocation and the solvent-specific parameters N_f and s_f characterize the nucleofuges.[12–14]

$$\log k_{het}(25^oC) = s_f(E_f + N_f) \quad (2)$$

When trying to quantify N_f and s_f of these dialkyl sulfides in the common way by plotting the rate constants of the heterolytic cleavages (k_{het} in CH_2Cl_2) of alkoxy-substituted benzhydrylsulfonium ions $\mathbf{1}^+$ against the corresponding electrofugalities of the benzhydrylium ions, we arrived at nucleofugality parameters N_f for dialkyl sulfides that were more than two orders of magnitude larger than those previously derived by Jurić, Denegri, and Kronja from solvolysis rates of unsubstituted and halogen-substituted benzhydrylsulfonium ions $\mathbf{2}^+$.[3–5]

We rationalized this observation by the differences of the transition states of the two reaction series (Figure 1)[1]: The carbocationic character of the benzhydrylium ions is only partially developed in the heterolyses of $\mathbf{1}^+$, which give highly stabilized benzhydrylium ions (Figure 1A). In solvolysis reactions of $\mathbf{2}^+$, which proceed via non-stabilized benzhydrylium ions, carbocationic character is fully developed in the transition state (Figure 1B; subsequent reaction with solvent not drawn).

Because this observation is of fundamental significance for the applicability of Equation (2) to predict absolute heterolysis rate constants of C–X bonds from the electrofugality parameter E_f of carbenium ions and the solvent-dependent nucleofuge-specific parameters N_f and s_f of leaving groups,[13,14] we have now investigated the heterolysis rates of the (1,3-diphenylallyl) dimethylsulfonium ion $\mathbf{4}^+$ by dynamic NMR spectroscopy (DNMR).[15–17]

2 | EXPERIMENTAL

2.1 | 1,3-Diphenylallyl chloride (3)

(*E*)-1,3-Diphenylprop-2-en-1-ol (0.172 g, 0.818 mmol)[18] was dissolved in dichloromethane (3 ml) at 0°C. After adding thionyl chloride (0.136 g, 1.14 mmol, 1.4 equiv), the solution was stirred for 2 h at 0°C. Subsequently, the solvent was removed under reduced pressure. The colorless solid residue (0.186 g, 99%) was analyzed by ^{1}H NMR spectroscopy and used without further purification. ^{1}H NMR (400 MHz, $CDCl_3$)[19]: δ 7.50–7.47 (m, 2 H, Ph), 7.42–7.27 (m, 8 H, Ph), 6.64 (d, J = 15.6 Hz, 1 H, 5-H), 6.53 (dd, J = 15.6, 7.7 Hz, 1 H, 6-H), 5.66 (d, J = 7.7 Hz, 1 H, 7-H); in accord with reported data in ref.[20]

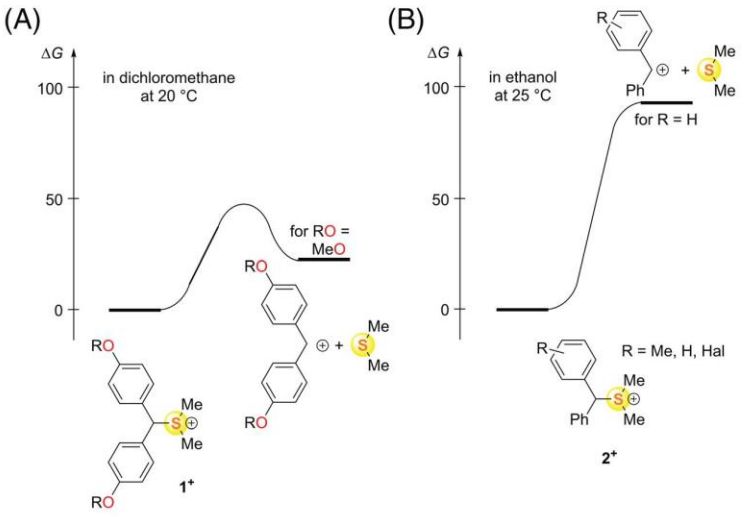

FIGURE 1 Gibbs energy profiles for heterolyses of differently substituted benzhydryldimethylsulfonium ions yielding (A) highly stabilized or (B) non-stabilized benzhydrylium ions

2.2 | Dynamic NMR spectroscopy

2.2.1 | Sample preparation

(1,3-Diphenylallyl)dimethylsulfonium triflate ($\mathbf{4}^+$ TfO^-) was generated by dissolving the allyl chloride **3**, dimethyl sulfide (**5**, 1.5 to 4.5 equiv), and trimethylsilyl triflate (TMSOTf, 1.05 equiv) in CD_2Cl_2. The ^1H NMR spectrum (400 MHz) of the resulting solution at −70°C (Supporting Information) showed the quantitative consumption of **3** and the exclusive formation of $\mathbf{4}^+$ TfO^-: ^1H NMR (400 MHz, −70°C, CD_2Cl_2)[19]: δ 7.59–7.55 (m, 2 H, Ph), 7.48–7.44 (m, 5 H, Ph), 7.35–7.31 (m, 3 H, Ph), 7.09 (d, $J = 15.5$ Hz, 1 H, 5-H), 6.43 (dd, $J = 15.4$, 10.6 Hz, 1 H, 4-H), 5.71 (d, $J = 10.5$ Hz, 1 H, 3-H), 2.95 (s, 3 H, 1-H or 2-H), 2.66 (s, 3 H, 1-H or 2-H), 2.04 (s, 6 H, free Me_2S).

2.2.2 | Temperature-dependent NMR measurements

^1H NMR spectra (400 MHz) of CD_2Cl_2 solutions of $\mathbf{4}^+$ TfO^- and variable amounts of dimethyl sulfide (**5**) were measured at variable temperature (5 K increments). Line shape analysis (LSA) of broadened resonances in the temperature range between −10 and +20°C was performed by manual fitting with simulated spectra generated by the DNMR6 algorithm of the *iNMR* software.[21] The obtained rate constants were analyzed by the Eyring equation (3) to determine the activation parameters $\Delta H^‡$ and $\Delta S^‡$.

$$\ln(k/T) = (-\Delta H^‡/R) \times (1/T) + \ln(k_B/h) + \Delta S^‡/R \quad (3)$$

The activation parameters $\Delta H^‡$ and $\Delta S^‡$ from Equation (3) were used to extrapolate the rate constant k (25°C).

3 | RESULTS

When 1,3-diphenylallyl chloride (**3**) was treated with trimethylsilyl triflate (1.05 equiv) and 3 equivalents of dimethyl sulfide (**5**) in CD_2Cl_2, the ^1H NMR spectra depicted in Figure 2 were obtained. At −70°C, one can assign three resonances to different *S*-methyl groups; two

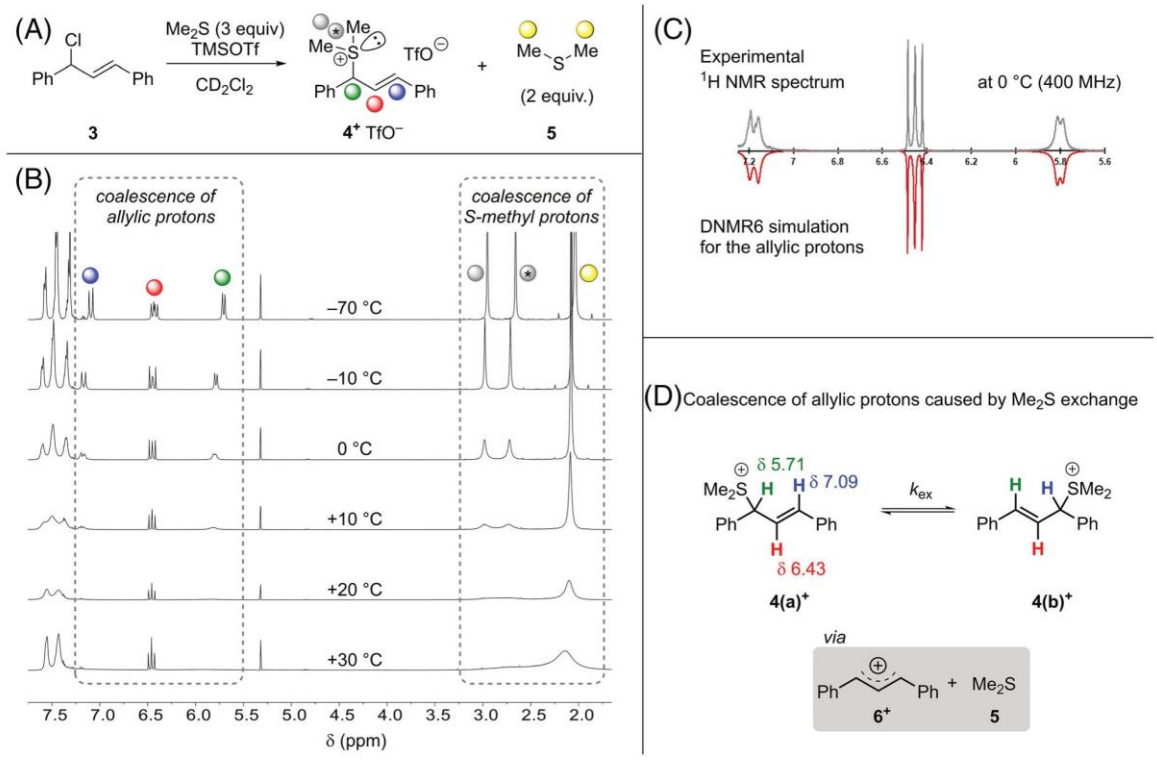

FIGURE 2 (A) Synthesis of $\mathbf{4}^+$ TfO^- with excess Me_2S (**5**). (B) ^1H NMR spectra (400 MHz) of a mixture of $\mathbf{4}^+$ with Me_2S (**5**) (2 equiv) in CD_2Cl_2 at variable temperatures. Protons used for line shape analysis are marked by colored circles. (C) Experimental and simulated ^1H NMR (400 MHz) spectra at 0°C used to determine k_{ex} from resonances of allylic protons. (D) Mutual exchange reaction observed in the DNMR studies of $\mathbf{4}^+/\mathbf{5}$ mixtures in CD_2Cl_2 (chemical shifts refer to −70°C)

of them are the diastereotopic *S*-methyl groups in the sulfonium ion $\mathbf{4}^+$ (δ 2.95 and 2.66 ppm), and one resonance is due to the unbound **5** (δ 2.04 ppm). When raising the temperature, the resonances of the diastereotopic *S*-methyl groups of $\mathbf{4}^+$ and that of external Me_2S (**5**) coalesce. Simultaneously, the AMX pattern of the allylic resonances (marked with green, red, and blue dots in Figure 2) converges into an AX_2 spectrum. At +20 and +30°C, only the well-resolved triplet of the central 2-CH group (red) can be seen, whereas the coalesced signal for 1-H and 3-H protons is still broadened to an extent that it cannot be spotted in Figure 2B.

Because free 1,3-diphenylallyl cations $\mathbf{6}^+$ were not observable in any of the experiments, one can conclude that the equilibrium is always on the side of the sulfonium ions $\mathbf{4}^+$. Consequently, the heterolytic cleavage of the sulfonium ion $\mathbf{4}^+$ must be slower than the recombination of allyl cation $\mathbf{6}^+$ with Me_2S (**5**). Accordingly, the rate of the exchange of the SCH_3 signals as well as that of the allylic protons must be controlled by the heterolysis of $\mathbf{4}^+$. The broadening of the resonances for the diastereotopic *S*-methyl groups in $\mathbf{4}^+$ is coupled with the exchange with Me_2S from the solution, however, and cannot be analyzed straightforwardly. We have, therefore, considered the allylic region of the temperature-dependent ^1H NMR spectra to derive information on the rate of the C–S bond-breaking reaction.

Hence, allylic proton signals of $\mathbf{4}^+$ at δ 7.09, 6.43, and 5.71 ppm were analyzed by LSA (Figure 2C) in the temperature range between −10 and +20°C (5 K increments; only a selection of spectra is shown in Figure 2B). Line broadening of the allylic protons is caused by mutual exchange between $\mathbf{4(a)}^+$ and $\mathbf{4(b)}^+$ (Figure 2D). The frequency of this exchange reaction between sulfonium ions $\mathbf{4}^+$ is described by the temperature-dependent exchange rate constant k_{ex} (s^{-1}).

Analogous DNMR studies of solutions with 3.5, 2.0, or 0.5 equivalents of non-bound Me_2S (**5**) gave almost identical k_{ex} values at each of the investigated temperatures (Table 1). Given that the Me_2S concentration does not influence the rate of the exchange process, the occurrence of S_N2 (or S_N2') mechanisms can be excluded. From the Eyring activation parameters [$\Delta H^{\ddagger} = (69.4 \pm 0.2)$ kJ mol^{-1}, $\Delta S^{\ddagger} = (37.0 \pm 0.7)$ J mol^{-1} K^{-1}] for the combined $k_{ex}(T)$ data of the three independent series of measurements at different Me_2S concentrations, an exchange rate constant $k_{ex}(25°C) = (364 \pm 2)$ s^{-1} was determined. On a molecular level, we assign k_{ex} to the rate constant k_{het} for the heterolytic C–S bond cleavage in $\mathbf{4}^+$ to give Me_2S (**5**) and the allyl cation $\mathbf{6}^+$ as depicted in Figure 2D.

We could not analyze in detail the exchange processes that caused the coalescence phenomena for the *S*-methyl groups. Nevertheless, the broadening of the resonance for the excess Me_2S (**5**) occurs in the same temperature range as the evaluated allyl isomerization, which indicates comparable exchange rates and a significant participation of free Me_2S (**5**) in the dynamics. We, therefore, exclude that intramolecular 1,3-migrations of the Me_2S group in $\mathbf{4}^+$ contribute significantly to the observed exchange reaction.

4 | DISCUSSION

Recently, it was found that heterolysis rate constants for the benzhydryldimethylsulfonium ions $\mathbf{1}^+$ and $\mathbf{2}^+$, in which the electrofugalities of the benzhydryl moieties are varied over a wide range, cannot be described by a single set of nucleofugality parameters N_f and s_f for the Me_2S nucleofuge.[1]

In general, N_f and s_f parameters in Equation (2) describe the leaving group ability of a certain nucleofuge in a certain solvent.[12,14] It has long been known that the leaving group abilities of anionic nucleofuges (e.g., chloride, bromide, and tosylate anions) vary over several orders of magnitude in protic solvents of variable

TABLE 1 Temperature-dependent DNMR exchange rate constants $k_{ex}(T)$ for mixtures of $\mathbf{4}^+$ and Me_2S (**5**) in CD_2Cl_2

	k_{ex} (s^{-1})		
T (°C)	$\mathbf{4}^+ + \mathbf{5}$ (0.5 equiv)[a]	$\mathbf{4}^+ + \mathbf{5}$ (2.0 equiv)[b]	$\mathbf{4}^+ + \mathbf{5}$ (3.5 equiv)[c]
−10	7.7	7.7	7.7
−5	14.3	14.3	14.3
0	26.0	26.0	26.0
+5	46.0	46.0	46.0
+10	76.0	78.0	76.0
+15	132	132	132
+20	225	225	225

[a]Generated by mixing **3** (0.077 mmol), TMSOTf (1 equiv), and Me_2S (**5**, 1.5 equiv) in CD_2Cl_2 (0.7 mL).
[b]Generated by mixing **3** (0.077 mmol), TMSOTf (1 equiv), and Me_2S (**5**, 3.0 equiv) in CD_2Cl_2 (0.7 mL).
[c]Generated by mixing **3** (0.077 mmol), TMSOTf (1 equiv), and Me_2S (**5**, 4.5 equiv) in CD_2Cl_2 (0.7 mL).

composition. Generally, the solvent dependence decreases with decreasing need for anion solvation.[12] Benzhydryldimethylsulfonium ions generate the neutral leaving group Me_2S, and the corresponding solvolysis rate constants have been studied in detail by Kevill and coworkers in 35 solvents.[22] When reactions in the slightly acidic solvent mixtures of fluorinated alcohols (i.e., aq TFE or aq HFIP mixtures) are disregarded, solvolysis rate constants for the $[Ph_2CH\text{-}SMe_2]^+$ ion fluctuated by about one order of magnitude when the solvents were varied from 95/5 dioxane/water mixtures ($k_{solv} = 0.75 \times 10^{-4}$ s^{-1}) to pure methanol ($k_{solv} = 7.88 \times 10^{-4}$ s^{-1}). Destabilization of the reactant ground state of $[Ar_2CH\text{-}SMe_2]^+$ in less polar solvents has been suggested to rationalize why the nucleofugality of Me_2S tends to increase mildly with decreasing solvent polarity in aqueous alcohol mixtures.[3,23]

Figure 3 illustrates the separation of the two data sets reported in ref.[1]: Based on previously reported solvent effects on the carbon–sulfur bond cleavage rates of benzhydryldimethylsulfonium ions,[3,22] it is not surprising that extrapolation of the ethanolysis rate constants of the benzhydryldimethylsulfonium ions **2a**$^+$–**2e**$^+$ on the left does not perfectly merge with the correlation line for the heterolysis rates of the benzhydryldimethylsulfonium ions **1a**$^+$–**1c**$^+$ in dichloromethane on the right. Because the nucleofugalities of neutral leaving groups are only marginally affected by the solvent,[3–5,14,22–24], however, the large separation by almost a factor of thousand could not be due to the fact that the heterolyses of the sulfonium ions **2a**$^+$–**2e**$^+$ were investigated in ethanol but the heterolysis reactions of **1a**$^+$–**1c**$^+$ refer to dichloromethane solution. Rather, this difference was explained by the fact that the solvolysis reactions of sulfonium ions derived from non-stabilized benzhydrylium ions on the left (i.e., **2a**$^+$–**2e**$^+$) proceed via transition states, which equal the separated products, benzhydrylium ions **8a**$^+$–**8e**$^+$ and Me_2S (cf. Figure 1B), whereas in the heterolyses of sulfonium ions derived from alkoxy-substituted benzhydrylium ions **7a**$^+$–**7c**$^+$ on the right (i.e., **1a**$^+$–**1c**$^+$), the benzhydrylium ion character is not yet fully developed in the transition state (cf. Figure 1A). Why does the heterolysis rate constant of **4**$^+$ (with formation of **6**$^+$, $E_f = -0.46$[25]) better match the correlation line defined by the sulfonium ions **2a**$^+$–**2e**$^+$ (deviation by a factor of 7.6) than that of the alkoxy-substituted analogues **1a**$^+$–**1c**$^+$ with similar electrofugalities (deviation by a factor of 1/55)?

One reason might be that Equation (2), which was derived from solvolysis rates of benzhydryl-model compounds, is less reliable when applied to solvolysis reactions that generate structurally different types of carbocations. It has been shown, however, that electrofugality parameters E_f for aryl-substituted carbocations that were calculated from individual solvolysis reactions with different leaving groups in different solvents scatter only slightly around the optimum E_f value (±0.4 at maximum; for the 1-phenylallylium ion: ±0.24).[13] The optimized E_f parameter for carbenium ion **6**$^+$ was obtained from a series of solvolysis kinetics that comprised three

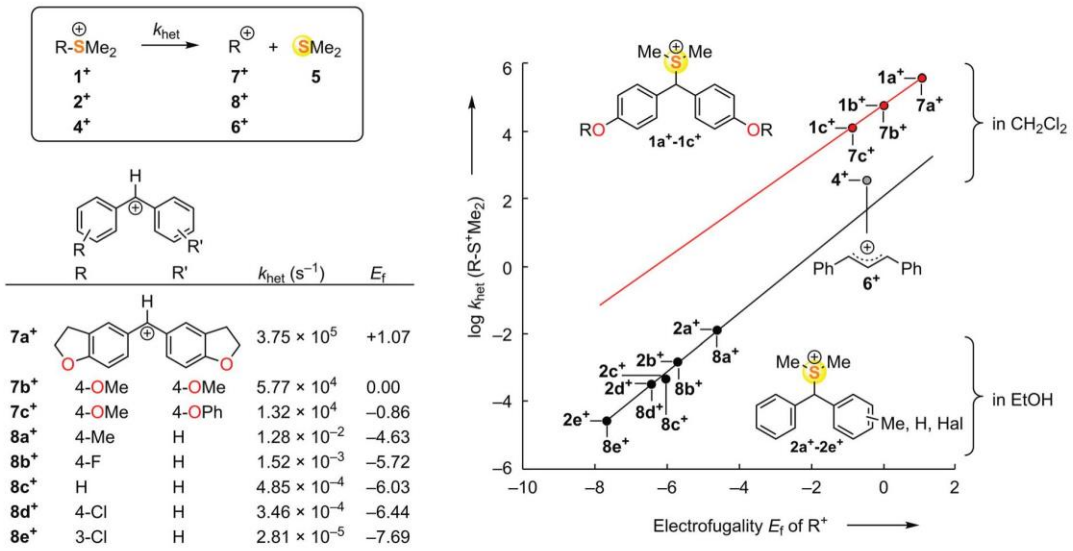

FIGURE 3 Correlation of the heterolysis rate constants of benzhydryldimethylsulfonium ions **1**$^+$ and **2**$^+$ and the (1,3-diphenylallyl) dimethylsulfonium ion **4**$^+$ with the electrofugality parameters E_f of the resulting carbenium ions **6**$^+$, **7**$^+$, and **8**$^+$ (k_{het} at 20 or 25°C from refs.[1,3]; E_f from refs.[14,25])

different leaving groups and seven solvent mixtures and covered an overall reactivity range of more than six orders of magnitude. Nevertheless, none of the individual rate constants deviated more than by a factor of 3.2 from the solvolysis rate constants calculated by Equation (2) and the optimized $E_f = -0.46$.[25]

Notably, the electrophilicity of allyl cation $\mathbf{6}^+$ ($E = 2.70$)[26] is almost 3 orders of magnitude greater than that of $\mathbf{7b}^+$ ($E = 0.0$) though the electrofugalities E_f of these two carbenium ions are very similar (abscissa of Figure 3). From the electrophilicity $E = 2.70$ for $\mathbf{6}^+$ and the recently published nucleophilicity parameters $N = 12.32$, $s_N = 0.72$ for Me_2S (**5**) in dichloromethane,[1] one can calculate (by Equation 4) a second-order rate constant of $k_2 = 6.5 \times 10^{10}$ M^{-1} s^{-1} for the reaction of $\mathbf{6}^+$ with Me_2S, that is, this bond-forming reaction is diffusion-controlled.

$$\log k_2(20°C) = s_N(N + E) \quad (4)$$

Application of the principle of microscopic reversibility leads to the conclusion that the heterolysis of the allylsulfonium ion $\mathbf{4}^+$ proceeds through a transition state that corresponds to the products like the benzhydryl-substituted sulfonium ions $\mathbf{2}^+$ illustrated in Figure 1B, but unlike the sulfonium ions $\mathbf{1}^+$ depicted in Figure 1A. For that reason, the heterolysis rate of the allylsulfonium ion $\mathbf{4}^+$ is better described by the nucleofugality parameters N_f/s_f for Me_2S (**5**) derived from the solvolysis rates of $\mathbf{2}^+$, which form non-stabilized benzhydrylium ions $\mathbf{8}^+$,[3–5,24] than by those determined from the solvolysis rates of $\mathbf{1}^+$, which give stabilized alkoxy-substituted benzhydrylium ions $\mathbf{7}^+$.[1]

5 | CONCLUSIONS

Investigations of the kinetics of numerous bond-forming reactions of carbenium ions with nucleophiles have shown that Equation (4) is well suited for predicting second-order rate constants k_2 (at 20°C), if k_2 is smaller than 10^8 M^{-1} s^{-1}.[27] Equation (4) does not hold for faster reactions, however, where the diffusion rates become dominant.[27,28] Because S_N1 reactions must proceed through the same transition states as the reverse reactions (principle of microscopic reversibility), we had previously reported that the linear correlations between the rate constants of S_N1 reactions and Lewis acidities of the resulting carbenium ions break down when the reverse reactions (reactions of carbocations with the leaving groups) change from diffusion to activation control.[27,29] Only recently we have observed that the switchover from activation to diffusion control of the reverse (bond-forming) reactions also limits the range of validity of Equation (2).[1]

The heterolysis rate constant of the allylsulfonium ion $\mathbf{4}^+$ reported in this work is in line with this interpretation and underlines the role of the rate of the reverse reaction, that is, recombination of the carbocation with the leaving group, for defining the applicability of Equation (2) to describe the heterolytic scission of C–X σ-bonds.

Whereas the limitation of Equation (4), which describes the rate constants of the electrophile nucleophile combinations, can easily be recognized by the fact that calculated rate constants $>10^{10}$ M^{-1} s^{-1} cannot exist because of the diffusion limit (k approx. 10^{10} M^{-1} s^{-1}), the situation is more complex for Equation (2), because its application requires consideration of the reverse reaction.

ACKNOWLEDGEMENTS

We thank Dr. David Stephenson and Claudia Ober for help with the NMR experiments.

DATA AVAILABILITY STATEMENT

Data available on request from the authors.

ORCID

Patrick M. Jüstel https://orcid.org/0000-0002-1857-5916
Petra Rovó https://orcid.org/0000-0001-8729-7326
Herbert Mayr https://orcid.org/0000-0003-0768-5199
Armin R. Ofial https://orcid.org/0000-0002-9600-2793

REFERENCES

[1] B. Maji, X.-H. Duan, P. M. Jüstel, P. A. Byrne, A. R. Ofial, H. Mayr, *Chem. – Eur. J.* **2021**. EarlyView. https://doi.org/10.1002/chem.202100977

[2] H. Mayr, J. Ammer, M. Baidya, B. Maji, T. A. Nigst, A. R. Ofial, T. Singer, *J. Am. Chem. Soc.* **2015**, *137*, 2580.

[3] S. Jurić, B. Denegri, O. Kronja, *J. Org. Chem.* **2010**, *75*, 3851.

[4] S. Jurić, B. Denegri, O. Kronja, *J. Phys. Org. Chem.* **2012**, *25*, 147.

[5] B. Denegri, M. Matić, O. Kronja, *Synthesis* **2017**, *49*, 3422.

[6] R. Okazaki, N. Tokitoh, V. K. Aggarwal, C. L. Winn, *Encyclopedia of Reagents for Organic Synthesis*, Wiley, New York **2006**. https://doi.org/10.1002/047084289X.rd372.pub2

[7] A.-H. Li, L.-X. Dai, V. K. Aggarwal, *Chem. Rev.* **1997**, *97*, 2341.

[8] E. M. McGarrigle, E. L. Myers, O. Illa, M. A. Shaw, S. L. Riches, V. K. Aggarwal, *Chem. Rev.* **2007**, *107*, 5841.

[9] D. Basavaiah, A. J. Rao, T. Satyanarayana, *Chem. Rev.* **2003**, *103*, 811.

[10] D. Basavaiah, B. S. Reddy, S. S. Badsara, *Chem. Rev.* **2010**, *110*, 5447.

[11] D. Basavaiah, R. T. Naganaboina, *New J. Chem.* **2018**, *42*, 14036.

[12] a) B. Denegri, A. Streiter, S. Jurić, A. R. Ofial, O. Kronja, H. Mayr, *Chem. – Eur. J.* **2006**, *12*, 1648; b) B. Denegri, A. Streiter,

S. Jurić, A. R. Ofial, O. Kronja, H. Mayr, *Chem. – Eur. J.* **2006**, *12*, 5415.
[13] B. Denegri, A. R. Ofial, S. Jurić, A. Streiter, O. Kronja, H. Mayr, *Chem. – Eur. J.* **2006**, *12*, 1657.
[14] N. Streidl, B. Denegri, O. Kronja, H. Mayr, *Acc. Chem. Res.* **2010**, *43*, 1537.
[15] D. Darwish, G. Tourigny, *J. Am. Chem. Soc.* **1966**, *88*, 4303.
[16] M. Nakamura, H. Kihara, N. Nakamura, M. Oki, *Org. Magn. Reson.* **1979**, *12*, 702.
[17] D. Darwish, S. H. Hui, R. Tomilson, *J. Am. Chem. Soc.* **1968**, *90*, 5631.
[18] J. M. Dickinson, J. A. Murphy, C. W. Patterson, N. F. Wooster, *J. Chem. Soc. Perkin Trans. 1* **1980**, 1179.
[19] See the Supporting Information for atom labelling.
[20] M. A. Tandiary, Y. Masui, M. Onaka, *Synlett* **2014**, *25*, 2639.
[21] Mestrelab Research, iNMR for Windows (version 6.1.8), http://www.inmr.net, **2018**.
[22] D. N. Kevill, S. W. Anderson, N. H. Ismail, *J. Org. Chem.* **1996**, *61*, 7256.
[23] M. Matić, B. Denegri, S. Jurić, O. Kronja, *Croat. Chem. Acta* **2017**, *90*, 571.
[24] S. Jurić, B. Portolan, O. Kronja, *Croat. Chem. Acta* **2016**, *89*, 65.
[25] K. Troshin, H. Mayr, *J. Org. Chem.* **2013**, *78*, 2649.
[26] K. Troshin, C. Schindele, H. Mayr, *J. Org. Chem.* **2011**, *76*, 9391.
[27] H. Mayr, A. R. Ofial, *Acc. Chem. Res.* **2016**, *49*, 952.
[28] J. Ammer, C. Nolte, H. Mayr, *J. Am. Chem. Soc.* **2012**, *134*, 13902.
[29] H. Mayr, A. R. Ofial, *Pure Appl. Chem.* **2017**, *89*, 729.

SUPPORTING INFORMATION

Additional supporting information may be found online in the Supporting Information section at the end of this article.

How to cite this article: P. M. Jüstel, P. Rovó, H. Mayr, A. R. Ofial, *J Phys Org Chem* **2021**, e4270. https://doi.org/10.1002/poc.4270

5.2 Intrinsic Barriers, an Unsolved Limitation for LFERs

Just recently we have noted that switching from activation control to diffusion control in addition reactions introduces constraints not only for the applicability of the Mayr-Patz equation log $k_2 = s_N$ (N + E) (eq1), but also for the Mayr-Kronja equation log $k_{het} = s_f$ (N_f + E_f) (eq 2) (Chapter 5.1).[1] In Scheme 1 the forward, addition reaction proceeds with the rate constant k_2 and the reverse, heterolysis reaction proceeds with the rate constant k_{het}. These rate constants can be predicted with equations 1 and 2 respectively, if the required electrophile (E) and nucleophile (s_N, N) specific parameters are known (eq1) or the required electrofuge (E_f) and nucleofuge (s_f, N_f) specific parameters are known (eq2). Furthermore, the equilibrium constant of this reaction can be predicted with log $K = LA + LB$ (eq3), where LA is the Lewis acidity parameter of the Lewis acid and LB the Lewis basicity parameter of the Lewis base.

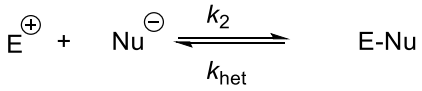

$$\log k_2 = s_N(N + E) \quad \text{(eq1)}$$
$$\log k_{het} = s_f(N_f + E_f) \quad \text{(eq2)}$$
$$\log K = LA + LB \quad \text{(eq3)}$$

Scheme 1: Nucleophilic addition reaction of an anionic nucleophile (Nu) to a carbocation electrophile (E) to form a covalent product (E-Nu).

The three solvent independent electrophile/Lewis acid specific parameters (E, E_f and LA) correlate linearly with each other only in some areas, as shown in Figure 1, but not in other areas. For example, electrophilicity E does no longer correlate linearly with electrofugality E_f when the electrofugality was determined under activation control for the reverse addition reaction in one case and under diffusion control for the reverse addition reaction in another (Figure 1).[2]

Due to the principle of microscopic reversibility, the transition states resemble the carbocations in the case of activation control, while the carbocations are also the transition state itself in the case of diffusion control, as the reaction is without activation barrier in the reverse reaction. We have explained how this results in different sets of s_f and N_f nucleofugality parameters, depending on whether the reverse addition reaction is diffusion-controlled or activation-controlled (Chapter 5.1). Electrofugality E_f stops correlating linearly with electrophilicity E (Figure 1a), when the addition reaction changes from activation control to diffusion control. This border is in between nitrogen and oxygen substituted benzhydrylium ions, due to the nucleofuge combinations that were employed to determine E and E_f. Electrophilicity parameter E, however, appears to correlate linearly with Lewis

acidity parameter *LA* (Figure 1 right), consequently E_f and *LA* also do not correlate linearly (Figure 1c). The explanation why the kinetic parameter *E* correlates with the thermodynamic parameter *LA* while the kinetic parameter E_f does not is simple: no *E* parameters were acquired under diffusion control, as the problem is instantly apparent during the experiment, unlike for similar heterolysis reactions. We have also noted before, that the Mayr-Patz equation log $k_2 = s_N (N + E)$ (eq1) can no longer accurately predict rate constants when the diffusion limit ($k_2 > 2 \times 10^8$ s^{-1} M^{-1}) is approached. In plots of log k_2 versus *E* a characteristic curvature becomes apparent in such cases. This is displayed exemplarily in Figure 2 for the reactions of the chloride anion with benzhydrylium ions in acetonitrile.[3]

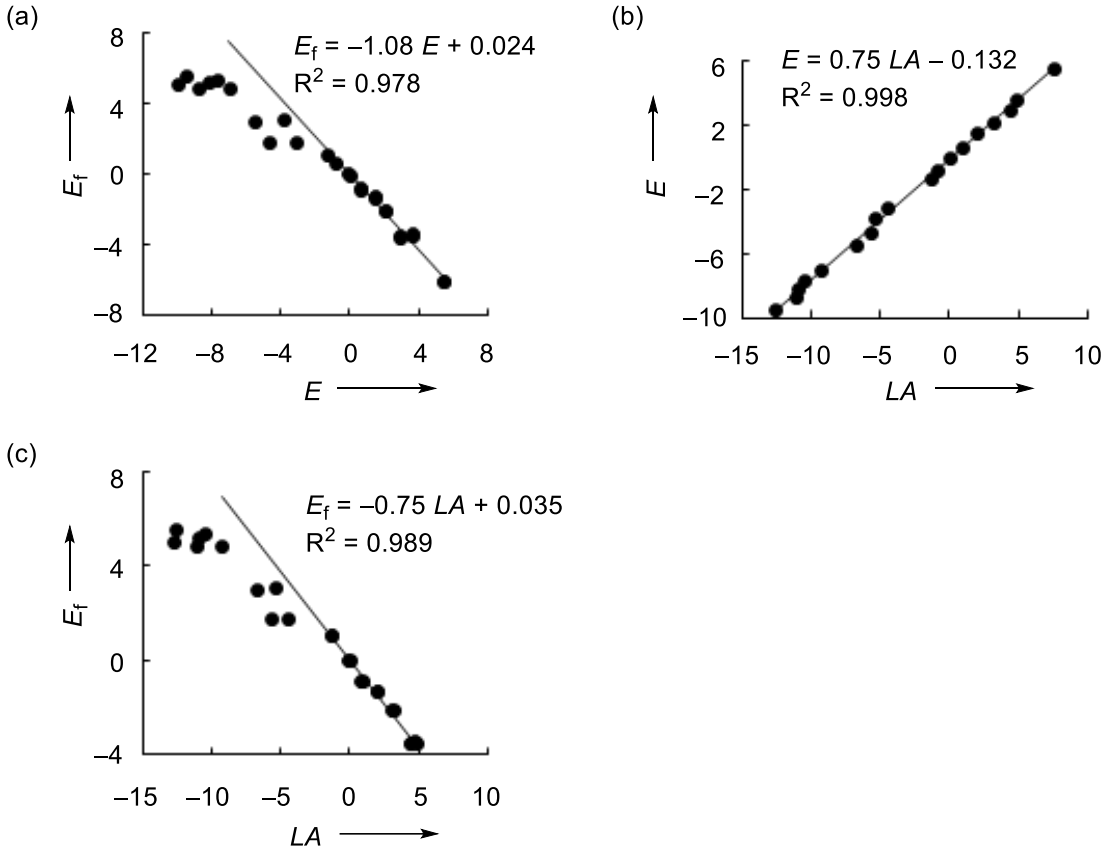

Figure 1: (a) Linear correlation of electrofugality parameter E_f versus electrophilicity parameter *E* of benzhydrylium ions. The borderline, where correlation breaks down, is between the nitrogen and the oxygen substituted benzhydrylium ions. (b) Linear correlation of electrophilicity parameter *E* versus Lewis acidity parameter *LA* of benzhydrylium ions. (c) Linear correlation of electrofugality parameter E_f versus Lewis acidity parameter *LA* of benzhydrylium ions.

Now one might ask, what is the point of these examples, that do not seem connected at all? To answer this question, we first need to ask another question: If heterolysis rate constants can be described with the equation log $k_{het} = s_f (N_f + E_f)$ (eq2), equilibrium constants with log $K = LA + LB$ (eq3) and addition rate constants with log $k_2 = s_N (N + E)$, then what happens when these 3 equations are linked with the equation $K = k_2/k_{het}$ (eq4) and equation 1 breaks down at the diffusion limit?

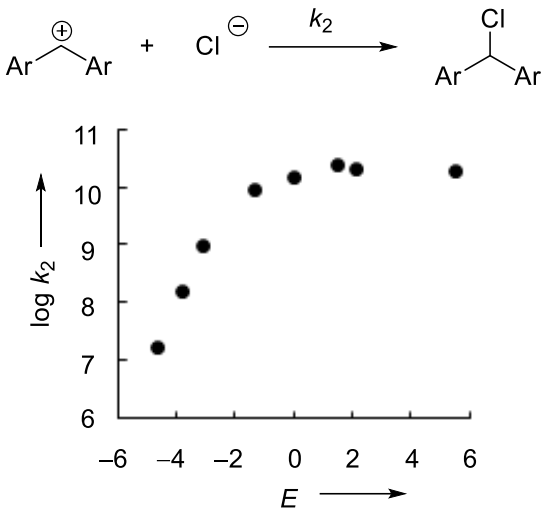

Figure 2: Plot of the logarithmic rate constant k_2 of the reactions of chloride with benzhydrylium ions versus the electrophilicity parameter *E* of the benzhydrylium ions.

Will the prediction of equilibrium constants (eq3) or heterolysis constants (eq2) fail? Or both? To answer this question, equation 4 was plotted for the reaction of the nucleophile/Lewis base chloride with known or calculated data (calculated with eq 1 and 2) for substituted benzhydrylium ions in Figure 3.

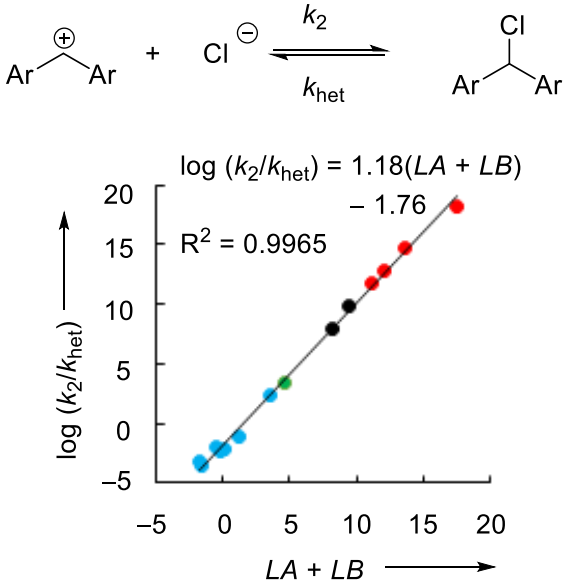

Figure 3: Linear correlation of log (k_2/k_{het}) versus *LA* + *LB* in acetonitrile. Double logarithmic plot of two different ways to predict equilibrium constants. Black dots represent data points with measured rate constants for k_2 and k_{het}. Red dots have reached the diffusion limit (k_2 = const.). The green dot has only an experimentally measured rate constant k_2, k_{het} has been calculated with eq 2. Blue dots consist only of calculated data for k_2 (calculated with eq1) and k_{het} (calculated with eq2). *N*, s_N, N_f, s_f and *LB* of Cl^- are constant. There are only 3 variables in this plot: *E*, E_f, and *LA*. Depiction/axis was chosen this way to show the relation to eq 4. Data is compiled in Table 1.

In Figure 3 the black dots represent data points with experimentally determined k_2 and k_{het}, while the green dot has experimentally determined k_2 but k_{het} has been calculated by eq2 (Table 1). The data of the blue dots consist only of calculated rate constants, by eq1 and eq2 respectively. The red dots are remarkable, because k_2 is constant for these and no longer increasing with stronger electrophiles, due to the diffusion limit (red dots: k_2=2.2×10^{10} M^{-1} s^{-1}). In spite of this fact, the linear correlation still holds for the red dots, which is only possible if k_{het} is also acting differently under diffusion control. The linear correlation works exceptionally well, especially given the fact that a range of 22 orders of magnitude for the equilibrium constants is covered. In theory, since Figure 3 plots essentially log *K* versus log *K*, the linear correlation should go through the origin and have a slope of 1. The intercept different from zero hints at an incorrect *LB* for chloride in acetonitrile.

Table 1. Reactivity parameters for benzhydrylium ions and rate constant with chloride as nucleophile or nucleofuge in MeCN. Black entries are experimentally acquired, green entries are calculated with various methods (see footnote below).

Benzhydrylium ion	k_{het} (25 °C) / s^{-1}	E_f [a]	k_2 (20 °C) / s^{-1} M^{-1}	E [b]	LA(MeCN)[c]	log (k_2/k_{het})
Ph_2	1.08×10^{-8}[d]	-6.03	2.20×10^{10}[e]	5.47	6.62[g]	18.31
Tol_2	4.32×10^{-5}[d]	-3.44	2.20×10^{10}[e]	3.63	2.63[g]	14.71
PopPh	3.34×10^{-5}[d]	-3.52	2.20×10^{10}[e]	2.9		14.82
AniPh	3.60×10^{-3}[i]	-2.09	2.20×10^{10}[h]	2.11	1.12[g]	12.79
AniTol	3.77×10^{-2}[i]	-1.32	2.44×10^{10}[h]	1.48	0.16[g]	11.81
AniPop	1.47×10^{-1}[i]	-0.86		0.61		
Ani_2	2.40[i]	0	1.50×10^{10}[h]	0	-1.6[g]	9.80
FurAni	1.70×10^{1}[i]	0.61		-0.81	-2.57[g]	
Fur_2	9.51×10^{1}[i]	1.07	9.39×10^{9}[h]	-1.36	-2.73[g]	7.99
Pfa_2	8.04×10^{2}[d]	1.79	9.70×10^{8}[h]	-3.14		6.08
Mfa_2	5.86×10^{4}[d]	3.13	1.61×10^{8}[h]	-3.85	-6.33[g]	3.44
Dpa_2	7.78×10^{2}[d]	1.78	1.76×10^{7}[h]	-4.72		4.35
$Morph_2$	4.25×10^{4}[d]	3.03	1.00×10^{7}[f]	-5.53	-7.52	2.37
Dma_2	1.40×10^{7}[d]	4.84	1.28×10^{6}[f]	-7.02	-9.82	-1.04
Pyr_2	7.14×10^{7}[d]	5.35	5.08×10^{5}[f]	-7.69	-10.83	-2.15
Thq_2	4.71×10^{7}[d]	5.22	2.44×10^{5}[f]	-8.22	-11.27	-2.28
Ind_2	1.35×10^{7}[d]	4.83	1.16×10^{5}[f]	-8.76	-11.46	-2.07
Jul_2	1.64×10^{8}[d]	5.61	4.47×10^{4}[f]	-9.45	-12.61	-3.56
Lil_2	2.73×10^{7}[d]	5.05	1.98×10^{4}[f]	-10.04	-12.76	-3.14

[a] from ref[4] [b] from ref[5] [c] from ref[2a] [d] Calculated with equation 2 (log k_{het} = s_f (N_f + E_f)), N_f=0.3, s_f =1.39 for Chloride in MeCN [e] rate constant assumed to equal the rate constant of AniPh (strongest electrophile measured) with chloride [f] Calculated with equation 1 (log k_2 = s_N (N + E)), N=17.2, s_N =0.6 for Chloride in MeCN. Due to lack of nucleophilicity parameters in CH_2Cl_2, parameters gained in MeCN were used instead. Error is most likely small and systematic. [g] calculated from methyl anion affinities [h] from ref[3] [i] from ref[6]

This is not surprising, as this value was not deemed overly accurate before and might now be changed from *LA* = 11 to *LA* = 9.5. For the slope the only solution would be to introduce another factor into eq 3, which we deem not necessary since the deviation from 1 is only minor. Also, this might be an artifact due to the calculated values (blue and green dots in Figure 3) and not actually represent the true equilibrium constants.

But now to answer the pending question: Figure 3 shows, that the diffusion limit has no effect on the prediction of equilibrium constants, because while the addition rate constants k_2 can no longer increase with stronger electrophiles after the diffusion limit is reached (red points), the heterolysis rate constants also change their behavior accordingly. This is also what is observed in Figure 1: electrophilicity *E* and electrofugality E_f do only correlate linearly up to a certain degree. Interestingly, and much to our surprise the curvature of Figure 1 and Figure 2 are canceled out exactly by the invariable k_2 under diffusion control in Figure 3. This is not only true in acetonitrile, but also holds true for chloride in dichloromethane (Figure 4).

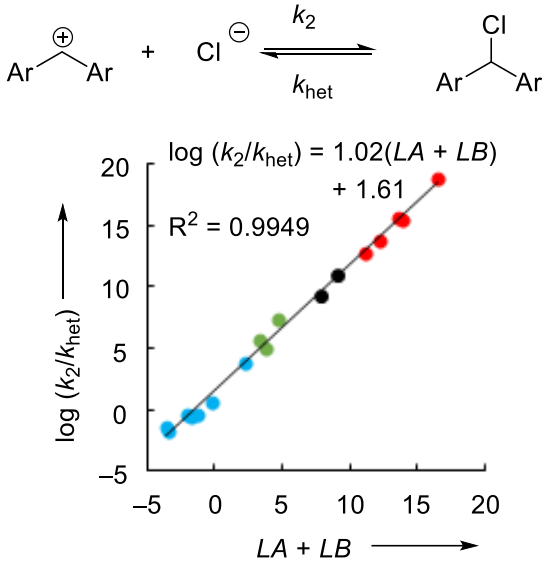

Figure 4: Linear correlation of log (k_2/k_{het}) versus *LA* + *LB* in dichloromethane. Double logarithmic plot of 2 different ways to predict equilibrium constants. Due to the lack of rate constants k_2 in dichloromethane, rate constants in acetonitrile have been used instead. Black dots represent data points with measured rate constants for *k* and k_{het}. Red dots have reached the diffusion limit (k_2 = const.). The green dots have only experimentally measured rate constants k_2, k_{het} has been calculated with eq 2. Blue dots consist only of calculated data for k_2 (calculated with eq1) and k_{het} (calculated with eq2). *LB* is constant. Data is compiled in Table 2.

The linear correlation in Figure 4 is still excellent, even despite the fact that rate constants k_2 acquired in acetonitrile have been used due to the lack of such data in dichloromethane. The error introduced in this way should be small and systematic due to the similarity of the polar aprotic solvents acetonitrile and dichloromethane. Here the slope is negligibly deviating from 1, but this can be attributed to error.

The intercept however is again different from zero, but this is likely due to rate constants k_2 in acetonitrile being used instead of (the non-existent) rate constants in dichloromethane.

Table 2. Reactivity parameters for benzhydrylium ions and rate constant with chloride as nucleophile or nucleofuge in CH_2Cl_2. Black entries are experimentally acquired, green entries are calculated with various methods (see footnote below).

Benzhydrylium ion	k_{het} (25 °C) / s^{-1}	E_f [a]	k_2 (20 °C) / s^{-1} M^{-1}	E [b]	$LA(CH_2Cl_2)$[c]	log (k_2/k_{het})
Ph_2	3.56×10^{-9}[d]	-6.03	2.20×10^{10}[e]	5.47	7.46[g]	18.79
Tol_2	7.37×10^{-6}[d]	-3.44	2.20×10^{10}[e]	3.63	4.82	15.48
PopPh	5.82×10^{-6}[d]	-3.52	2.20×10^{10}[e]	2.9	4.42	15.58
AniPh	3.94×10^{-4}[d]	-2.09	2.20×10^{10}[h]	2.11	3.1	13.75
AniTol	4.00×10^{-3}[i]	-1.32	2.44×10^{10}[h]	1.48	2.0	12.79
AniPop	1.54×10^{-2}[i]	-0.86		0.61	0.9	
Ani_2	2.72×10^{-1}[i]	0	1.50×10^{10}[h]	0	0	10.94
FurAni	1.02[i]	0.61		-0.81		
Fur_2	4.84[i]	1.07	9.39×10^{9}[h]	-1.36	-1.29	9.29
Pfa_2	3.64×10^{1}[d]	1.79	9.70×10^{8}[h]	-3.14	-4.47	7.43
Mfa_2	1.89×10^{3}[d]	3.13	1.61×10^{8}[h]	-3.85	-5.39	4.93
Dpa_2	3.54×10^{1}[d]	1.78	1.76×10^{7}[h]	-4.72	-5.72	5.70
$Morph_2$	1.41×10^{3}[d]	3.03	1.00×10^{7}[f]	-5.53	-6.82	3.85
Dma_2	2.92×10^{5}[d]	4.84	1.28×10^{6}[f]	-7.02	-9.3	0.64
Pyr_2	1.31×10^{6}[d]	5.35	5.08×10^{5}[f]	-7.69	-10.46	-0.41
Thq_2	8.95×10^{5}[d]	5.22	2.44×10^{5}[f]	-8.22	-10.92	-0.56
Ind_2	2.84×10^{5}[d]	4.83	1.16×10^{5}[f]	-8.76	-11.16	-0.39
Jul_2	2.83×10^{6}[d]	5.61	4.47×10^{4}[f]	-9.45	-12.62	-1.80
Lil_2	5.43×10^{5}[d]	5.05	1.98×10^{4}[f]	-10.04	-12.76	-1.44

[a] from ref[4] [b] from ref[5] [c] from ref[2a] [d] Calculated with equation 2 (log $k_{het} = s_f (N_f + E_f)$), N_f=-0.57, s_f =1.28 for Chloride in CH_2Cl_2 [e] rate constant assumed to equal the rate constant of AniPh (strongest electrophile measured) with chloride [f] Calculated with equation 1 (log $k_2 = s_N (N + E)$), N=17.2, s_N =0.6 for Chloride in MeCN. Due to lack of nucleophilicity parameters in CH_2Cl_2, parameters gained in MeCN were used instead. Error is most likely small and systematic. [g] extrapolated from Figure 1 top right [h] rate constants measured in MeCN, error is most likely small and systematic. Data from ref[3] [i] from ref[6]

The linear correlations depicted in Figure 3 and 4 in combination with the available data on benzhydrylium ions (E, E_f and LA parameters) now enable to determine an estimate for LB with s_N/N and s_f/N_f. Eq1 and eq2 only predict accurate rate constants, when the addition reaction remains below the diffusion limit. Eq2 can predict rate constants, when the addition reaction has exceeded below the diffusion limit, but a different set of fugality parameters are required to do this (Chapter 5.1). For addition reactions, only activation-controlled reactions are of interest, as the prediction of rate constants at the diffusion limit is pointless. For heterolysis reactions, often both types (activation and

diffusion controlled) of reverse addition reactions are of interest. This arises the question, what is the difference in heterolysis reactions between an activation-controlled and a diffusion-controlled reverse addition reaction? And why does one obtain different sets of linear correlations depending on activation of diffusion control (Chapter 5.1)?

As mentioned before, the transition state is becoming ever more like the two separated species, carbocation and halide ion in this case, when approaching the diffusion limit. According to Marcus theory, up to the diffusion limit the activation barrier ($\Delta G^{\ddagger}$) can be described by the intrinsic barrier ($\Delta G_0^{\ddagger}$) and the free Gibbs energy (ΔG^0, eq 5).

$$\Delta G^{\ddagger} = \Delta G_0^{\ddagger} + 0.5\ \Delta G^0 + (\Delta G^0)^2/16\Delta G_0^{\ddagger} \quad \text{(equation 5)}$$

Importantly, the influence of the intrinsic barrier on the activation barrier becomes minimal and constant once the diffusion limit is reached (Figure 5). At that point the activation barrier ($\Delta G^{\ddagger}_{het}$) for the heterolysis reaction equals ΔG^0 in approximation because of the principle of microscopic reversibility. This is the effect, that causes the bend in the linear correlations of E_f versus *E* and *LA* (Figure 1) and the different N_f and s_f parameters determined for dimethyl sulfide. In other words, the intrinsic barrier becomes irrelevant once the diffusion limit for addition reactions is reached and thus LFER work only up to the diffusion limit (activation controlled reactions) and past the diffusion limit (diffusion controlled reactions), but cannot cross over. There is no sharp boundary in between, but a transition region. This insight can also be gained from Figure 1. If electrophilicity *E*, that is kinetics, correlates linearly with Lewis acidity *LA*, that is thermodynamics, then the logarithm of addition rate constants correlate linearly with the logarithm of equilibrium constants as a consequence. This in turn results in the linear correlation of $\Delta G^{\ddagger}$ and ΔG^0. If $\Delta G^{\ddagger}$ and ΔG^0 correlate linearly, then the intrinsic barriers $\Delta G_0^{\ddagger}$ either do not change at all or increase/decrease proportionally to the Gibbs reaction energy ΔG^0. We consider the latter more likely for activation-controlled reactions. Consequently, electrofugality E_f also must correlate with *LA* due to equal ΔG^0 and $\Delta G_0^{\ddagger}$ (principle of microscopic reversibility) just like in the aforementioned case. As was demonstrated in Chapter 5.1, linear correlations for heterolysis reactions are possible, even if the addition reactions are diffusion controlled. Figure 1 shows the effect of the transition from activation to diffusion control on correlations.

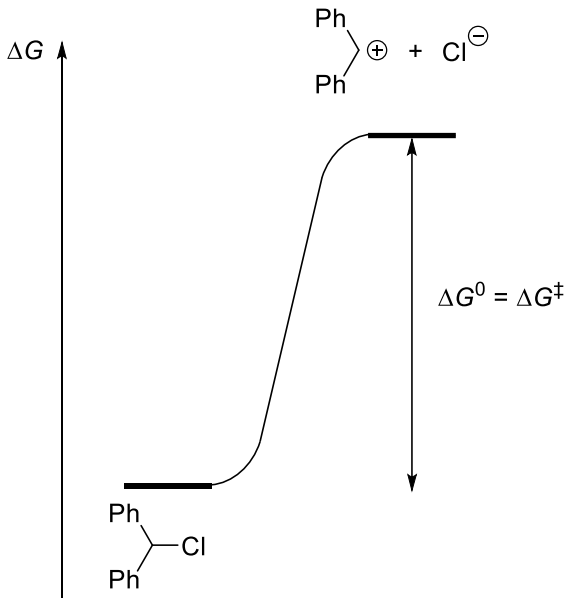

Figure 5: Qualitative energy diagram of the heterolysis of benzhydryl chloride. The reverse recombination reaction is barrierless and thus diffusion-controlled. As a consequence: $\Delta G^0 = \Delta G^{\ddagger}$.

Conclusion

As the diffusion limit in addition reactions is approached, the effect of intrinsic barriers ($\Delta\Delta G_0^{\ddagger}$) becomes minimal. At the diffusion limit, the Mayr-Patz equation (eq1) loses its predictive power. At the same time, almost unnoticed, the reverse heterolysis reactions are equally affected: Since the intrinsic barrier is equal in both directions of the reaction, its contribution to heterolysis reactions becomes negligible at this point. From here on (for larger *E*/*LA*), E_f does have a different correlation line with *LA*, because adding stronger electron withdrawing groups to a benzhydrylium ion (i.e. increasing *E* and *LA*) now only increases ΔG^0 and the contribution of the intrinsic barrier is rendered irrelevant. To put it in a nutshell: for activation-controlled reactions LFERs have to take changes of the Gibbs reaction energy ($\Delta\Delta G^0$) and changes to intrinsic barriers ($\Delta\Delta G_0^{\ddagger}$) into account, while for diffusion-controlled reactions LFERs only have to take changes to the Gibbs reaction energy ($\Delta\Delta G^0$) into account (Figure 5), resulting in 2 separate linear correlations. Also we could show that the problem we described in earlier studies[1] (Chapter 5.1) is a structural problem and not specific to the investigated case.

Now one could assume, that equilibrium constants are also affected at this point and LFERs would have trouble predicting equilibrium constants beyond the diffusion limit. Interestingly, one variable (k_2) in equation 4 ($K = k_2/k_{het}$) becoming a constant does not influence the linear correlation (Figure 3 and 4), because k_{het} is exactly compensating this change. This also tells us, that nucleofugality parameters s_f/N_f only change, once plots of log k_2 versus *E* start becoming curved (Figure 2) due to the diffusion limit

and not before. The plot in Figure 3 would also allow to calculate the change in heterolysis reactions if all parameters from equations 1, 2 and 3 are known, as well as the rate limit induced by diffusion. Since these parameters are all known only in rare cases and the resulting equation would be quite unwieldy, we do not consider this as useful for predicting rate constants.

Intrinsic barriers being the cause of the problem is also the reason why Figure 3 and 4 show excellent linear correlation, despite the bends in the linear correlations of Figure 1. Since Figure 3 and 4 actually plot log *K* against log *K*, intrinsic barriers are irrelevant to this type of plot and only thermodynamic effects matter.

5.2.1 References

(1) Maji, B.; Duan, X.-H.; Jüstel, P. M.; Byrne, P. A.; Ofial, A. R.; Mayr, H., *Chem. Eur. J.* **2021**, Accepted Article (doi: 10.1002/chem.202100977).

(2) (a) Mayr, H.; Ofial, A. R., *Acc. Chem. Res.* **2016,** *49*, 952−965. (b) Mayr, H.; Ofial, A. R., *Pure Appl. Chem.* **2017,** *89*, 729−744.

(3) Minegishi, S.; Loos, R.; Kobayashi, S.; Mayr, H., *J. Am. Chem. Soc.* **2005,** *127*, 2641−2649.

(4) Streidl, N.; Denegri, B.; Kronja, O.; Mayr, H., *Acc. Chem. Res.* **2010,** *43*, 1537−1549.

(5) A database for reactivity parameters *E*, *N*,and s_N is freely accessible via http://www.cup.lmu.de/oc/mayr/DBintro.html.

(6) Streidl, N.; Mayr, H., *Eur. J. Org. Chem.* **2011,** *2011*, 2498−2506.

5.3 Supporting Information

5.3.1 General

Chemicals

(*E*)-1,3-Diphenyl-2-propen-1-ol was obtained by reduction of chalcone with $NaBH_4$ in methanol according to a reported procedure.[1] This allyl alcohol was used to prepare 1,3-diphenylallyl chloride (**3**) as described in the main text. Dimethylsulfide (**5**) was purchased from Sigma-Aldrich (>99%). Trimethylsilyl triflate was purchased from Fluka (>98%). Thionyl chloride was purchased from Merck (>99%). $CDCl_3$ and CD_2Cl_2 were obtained from EurIsotop.

Analytics

A 400 MHz nuclear magnetic resonance (NMR) spectrometer was used to acquire ^{1}H NMR spectra. Abbreviations used for reporting NMR data: s = singlet, d = doublet, m = multiplet, br = broad. Chemical shifts are denoted as parts per million (ppm). The internal reference was set to the residual signals of CD_2Cl_2 (δ_H = 5.32 ppm, δ_C = 54.00 ppm) and $CDCl_3$ (δ_H = 7.26 ppm, δ_C = 77.16 ppm).[2]

Dynamic NMR spectroscopy

The ^{1}H NMR spectra (400 MHz) were recorded at different temperatures (± 1 K) and fitted manually with simulated spectra of the DNMR6 algorithm as part of the *iNMR* software.[3] The obtained rate constants were converted into activation parameters according to the Eyring equation:

$$\ln (k/T) = (-\Delta H^{\ddagger}/R) \times (1/T) + \ln (k_B/h) + \Delta S^{\ddagger}/R \quad \text{(Eyring equation)}$$

with k = rate constant (in s^{-1})
R = gas constant
k_B = Boltzmann constant
h = Planck constant
T = temperature (in K)
$\Delta H^{\ddagger}$ = activation enthalpy (in kJ mol^{-1})
$\Delta S^{\ddagger}$ = activation entropy (in J mol^{-1} K^{-1})

5.3.2 Dynamics of the Me_2S Exchange at the Trialkylsulfonium ion 4^+

Generation of the Sulfonium Triflate 4^+ TfO^- in CD_2Cl_2 Solution

1,3-Diphenylallyl chloride **3** (1 equiv.), dimethylsulfide **5** (>1 equiv.), and trimethylsilyl triflate (TMSOTf, 1.05 equiv.) were dissolved in CD_2Cl_2.

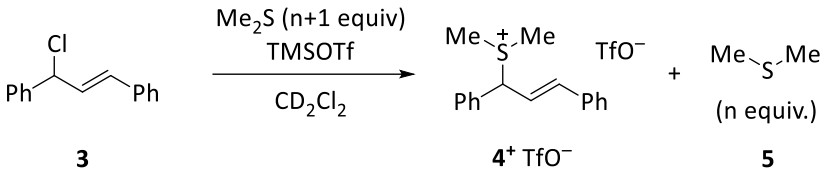

3 **4^+ TfO^-** **5**

The ^1H NMR spectrum (400 MHz) acquired at –70 °C showed the quantitative consumption of **3** and the exclusive formation of the trialkylsulfonium triflate **4^+**·TfO^-.

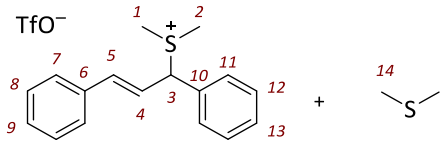

4^+·TfO^- **5**

^1H NMR (400 MHz, –70 °C, CD_2Cl_2): δ 7.59–7.55 (m, 2 H, Ph), 7.48–7.44 (m, 5 H, Ph), 7.35–7.31 (m, 3 H, Ph), 7.09 (d, *J* = 15.5 Hz, 1 H, 5-H), 6.43 (dd, *J* = 15.4, 10.6 Hz, 1 H, 4-H), 5.71 (d, *J* = 10.5 Hz, 1 H, 3-H), 2.95 (s, 3 H, 1-H or 2-H), 2.66 (s, 3 H, 1-H or 2-H), 2.04 (s, 6 H, 14-H, 2.4 equiv Me_2S).

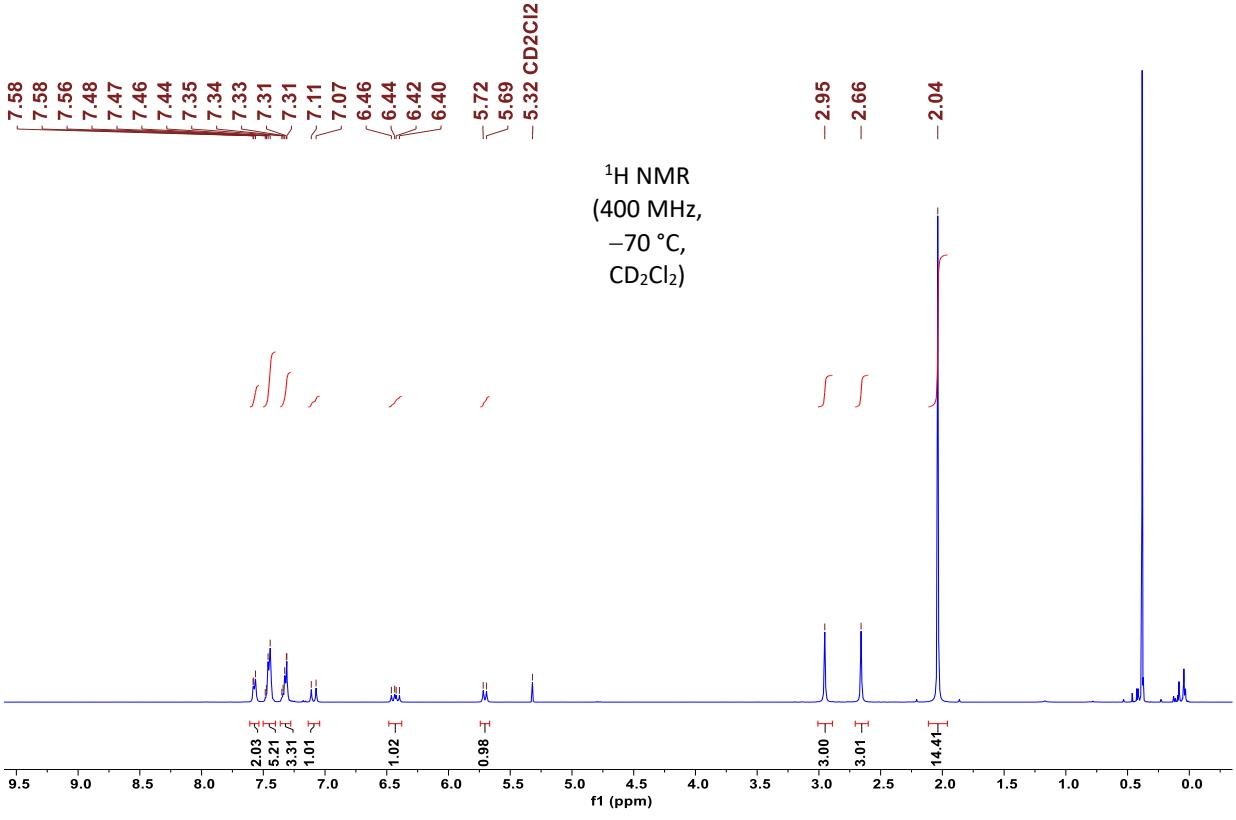

Dynamic NMR Studies

Samples, prepared as described above, were used to acquire ^{1}H NMR spectra (400 MHz) at variable temperature. Line shape analysis of broadened resonances in the temperature range between –10 and +20 °C was performed by manual fitting with simulated spectra generated by the DNMR6 algorithm of *iNMR* software.[3]

Determined exchange rate constants $k_{ex}(T)$ are gathered in Table1 (main text).

Eyring activation parameters were determined by applying the combined set of temperature-dependent rate constants k_{ex} (s^{-1}) in the Eyring equation. Figure S1 shows the resulting Eyring plot for the data in Table 1, which comprises the exchange rate constants k_{ex} for the three different **4**$^+$·TfO^-/**5** mixtures in CD_2Cl_2 at seven temperatures.

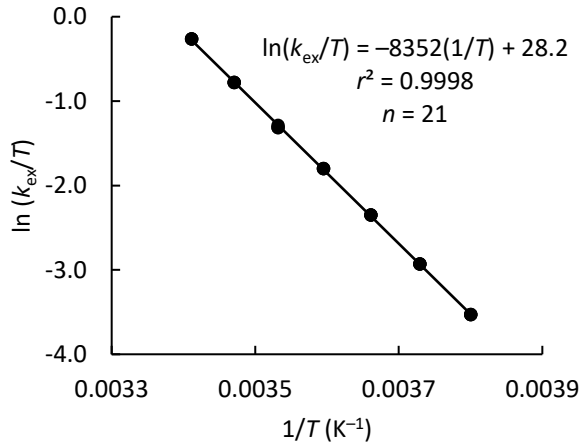

Figure S1. Eyring plot for the combined $k_{ex}(T)$ from Table 1.

5.3.3 ^{1}H NMR spectrum of 3

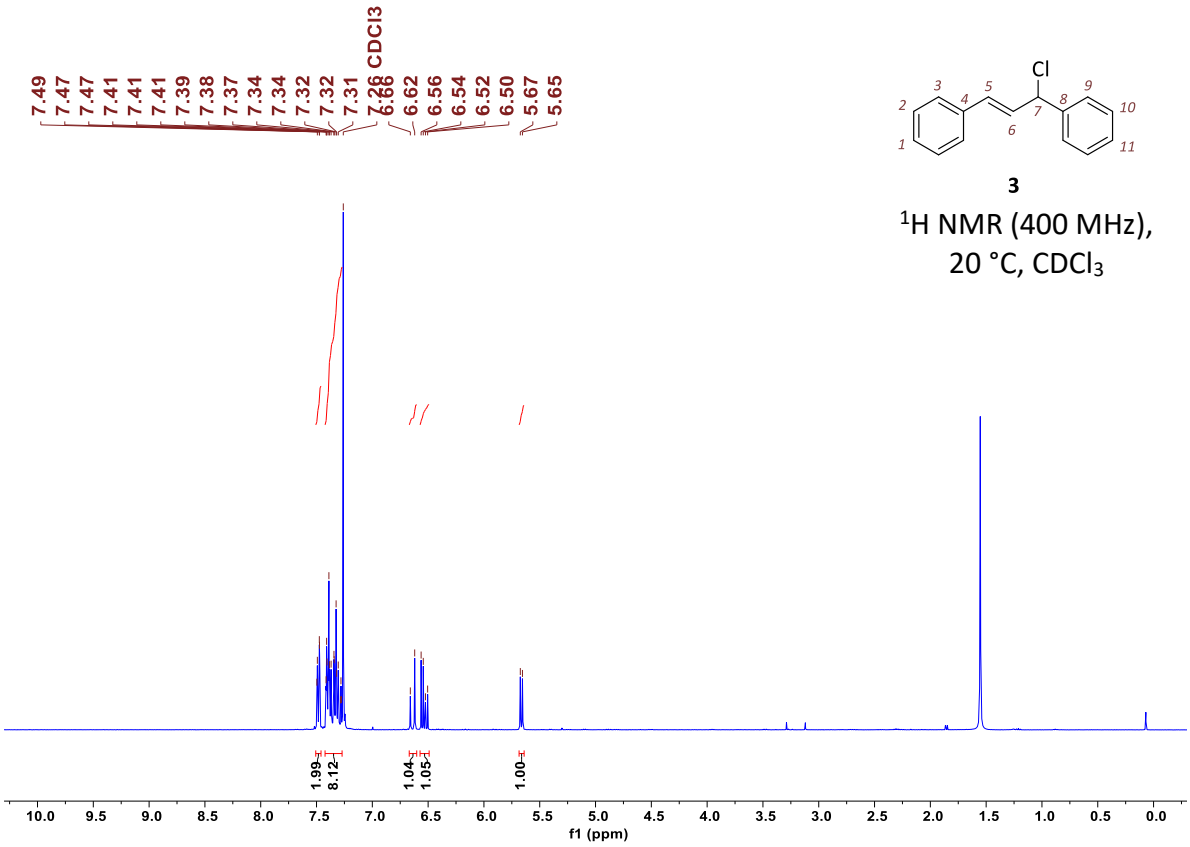

5.3.4 References

(1) Dickinson, J. M.; Murphy, J. A.; Patterson, C. W.; Wooster, N. F., *J. Chem. Soc. Perkin Trans. 1* **1990**, 1179-1184.

(2) Fulmer, G. R.; Miller, A. J. M.; Sherden, N. H.; Gottlieb, H. E.; Nudelman, A.; Stoltz, B. M.; Bercaw, J. E.; Goldberg, K. I., *Organometallics* **2010,** *29*, 2176−2179.

(3) *iNMR for Windows* (version 6.1.8, http://www.inmr.net), Mestrelab Research, 2018.